What Radiology Residents Need to Know
Series Editor: Ronald L. Eisenberg

Tara Catanzano *Editor*

What Radiology Residents Need to Know: Abdominal Radiology

MOREMEDIA

Springer

What Radiology Residents Need to Know

Series Editor
Ronald L. Eisenberg, Harvard University, Boston, MA, USA

The books in the *What Radiology Residents Need to Know* series act as an introduction to radiology, specifically designed for the needs of residents on their first rotation in a specific subspecialty. Radiology residents are asked to learn significant amounts of information at a fast and unrelenting space. The current available literature for residents, though, is dense and includes more information than they can easily digest, while the number, variety, and quality of images is often limited. This forces residents to turn to quick searches on the internet to seek out information that often is not at their exact level of knowledge and leaves gaps in their learning. *What Radiology Residents Need to Know* answers resident needs for each radiology rotation, presenting the material in bullet fashion and dividing it into convenient sub-units, such as introductory clinical information followed by "imaging findings" and, when appropriate, "management." In most cases, an individual pathological condition is presented in one page or less, allowing residents to quickly review the essential information on a specific pattern or disease. Books in the *What Radiology Residents Need to Know* series contain a large number of high-quality images, as well as a downloadable set of additional images that give readers a comprehensive library of illustrations. With both readable text and a broad spectrum of images, the books in the *What Radiology Residents Need to Know* series serve as an ideal guide for radiology residents.

Tara Catanzano
Editor

What Radiology Residents Need to Know: Abdominal Radiology

Springer

Editor
Tara Catanzano
Department of Radiology
UMass Chan-Baystate
Springfield, MA, USA

ISSN 2662-9569 ISSN 2662-9577 (electronic)
What Radiology Residents Need to Know
ISBN 978-3-031-76623-7 ISBN 978-3-031-76624-4 (eBook)
https://doi.org/10.1007/978-3-031-76624-4

© The Editor(s) (if applicable) and The Author(s), under exclusive license to Springer Nature Switzerland AG 2024

This work is subject to copyright. All rights are solely and exclusively licensed by the Publisher, whether the whole or part of the material is concerned, specifically the rights of translation, reprinting, reuse of illustrations, recitation, broadcasting, reproduction on microfilms or in any other physical way, and transmission or information storage and retrieval, electronic adaptation, computer software, or by similar or dissimilar methodology now known or hereafter developed.
The use of general descriptive names, registered names, trademarks, service marks, etc. in this publication does not imply, even in the absence of a specific statement, that such names are exempt from the relevant protective laws and regulations and therefore free for general use.
The publisher, the authors and the editors are safe to assume that the advice and information in this book are believed to be true and accurate at the date of publication. Neither the publisher nor the authors or the editors give a warranty, expressed or implied, with respect to the material contained herein or for any errors or omissions that may have been made. The publisher remains neutral with regard to jurisdictional claims in published maps and institutional affiliations.

This Springer imprint is published by the registered company Springer Nature Switzerland AG
The registered company address is: Gewerbestrasse 11, 6330 Cham, Switzerland

If disposing of this product, please recycle the paper.

Thank you to my husband Brian for your patience and willingness to solo parent human and furbabies while this book was in development. To my tennis teen (Logan) and my Irish dancer (Shae), all my love and gratitude.

Contents

1 Abdominal Imaging Techniques 1
Tara Catanzano

2 Developing a Search Pattern 35
Mary Woodruff, Sunil Jeph, and Robert Panico

3 Hepatobiliary Imaging 61
Matthew E. Maeder and Vidal A. Villela

4 Pancreas 87
Brennan Morrison and Emily Van Antwerp

5 Spleen 117
Christine Boatright

6 Adrenal Imaging 145
Anugayathri Jawahar

7 Genitourinary Diseases 169
Andrew Wentland

8 Gastric Disorders 217
Tara Catanzano

9 Small Bowel Imaging 253
Edward Lawrence

10 The Colon and Appendix 299
Anugayathri Jawahar

11 Artificial Intelligence (AI) in Abdominal Imaging 347
Florence X. Doo

Index 361

Contributors

Christine Boatright, MD Department of Radiology, University of Kansas Medical Center, Kansas City, KS, USA

Tara Catanzano Department of Radiology, UMass Chan-Baystate, Springfield, MA, USA

Department of Radiology, University of Massachusetts Chan Med, Suffield, CT, USA

Florence X. Doo, MD, MA Department of Diagnostic Radiology and Nuclear Medicine, University of Maryland School of Medicine, Baltimore, MD, USA

University of Maryland-Institute for Health Computing (UM-IHC), University of Maryland, North Bethesda, MD, USA

Anugayathri Jawahar Department of Radiology, Northwestern University-Feinberg School of Medicine, Chicago, IL, USA

Sunil Jeph Department of Radiology, Cooper University Hospital, Camden, NJ, USA

Edward Lawrence Department of Radiology, University of Wisconsin-Madison School of Medicine and Public Health, Madison, WI, USA

Department of Radiology, University of Galway, Galway, Ireland

Matthew E. Maeder Geisel School of Medicine at Dartmouth, Hanover, NH, USA

Dartmouth-Hitchcock Medical Center, Lebanon, NH, USA

Brennan Morrison UMass Chan Medical School-Baystate, Springfield, MA, USA

Robert Panico Department of Radiology, Cooper University Hospital, Camden, NJ, USA

Emily Van Antwerp UMass Chan Medical School-Baystate, Springfield, MA, USA

Vidal A. Villela Dartmouth-Hitchcock Medical Center, Lebanon, NH, USA

Andrew Wentland, MD, PhD Department of Radiology, University of Wisconsin School of Medicine and Public Health, Madison, WI, USA

Department of Medical Physics, University of Wisconsin School of Medicine and Public Health, Madison, WI, USA

Department of Biomedical Engineering, University of Wisconsin School of Medicine and Public Health, Madison, WI, USA

Mary Woodruff Department of Radiology, Cooper University Hospital, Camden, NJ, USA

Abdominal Imaging Techniques

1

Tara Catanzano

Imaging Modalities Available for Abdominal Imaging

- There are five major imaging modalities consistently used in the assessment of the abdomen.
- The modalities include plain films (PFs), fluoroscopy, ultrasound (US), computed tomography (CT), and magnetic resonance imaging (MRI).
- Each modality has its own role in the assessment and diagnosis of abdominal disorders. These will be discussed in detail below.

Plain Films

General Considerations

- Both single-view and two- or three-view images can be obtained for different reasons.
- Single views are typically obtained in the AP technique and can be obtained with the patient in a supine or erect position (see Figs. 1.1 and 1.2).
- Two-view abdominal films can be obtained as erect and supine views (see Figs. 1.3 and 1.4) or supine and decubitus views (see Figs. 1.5 and 1.6).

Supplementary Information The online version contains supplementary material available at https://doi.org/10.1007/978-3-031-76624-4_1.

T. Catanzano (✉)
Department of Radiology, UMass Chan-Baystate, Springfield, MA, USA
e-mail: Tara.Catanzano@baystatehealth.org; Tara.catanzano@bhs.org

© The Author(s), under exclusive license to Springer Nature Switzerland AG 2024

T. Catanzano (ed.), *What Radiology Residents Need to Know: Abdominal Radiology*, What Radiology Residents Need to Know,
https://doi.org/10.1007/978-3-031-76624-4_1

Fig. 1.1 Supine abdominal X-ray demonstrating dilated small bowel loops. Note the skin staples in the right upper quadrant from recent surgery

Fig. 1.2 Erect abdominal X-ray in the same patient as Fig. 1.1 demonstrating air fluid levels in the dilated small bowel loops

Fig. 1.3 Erect radiograph of the abdomen demonstrating air fluid levels within dilated small bowel loops in this patient with a small bowel obstruction

Fig. 1.4 Supine radiograph of the abdomen demonstrating a normal bowel gas pattern. Note the right femoral venous access line

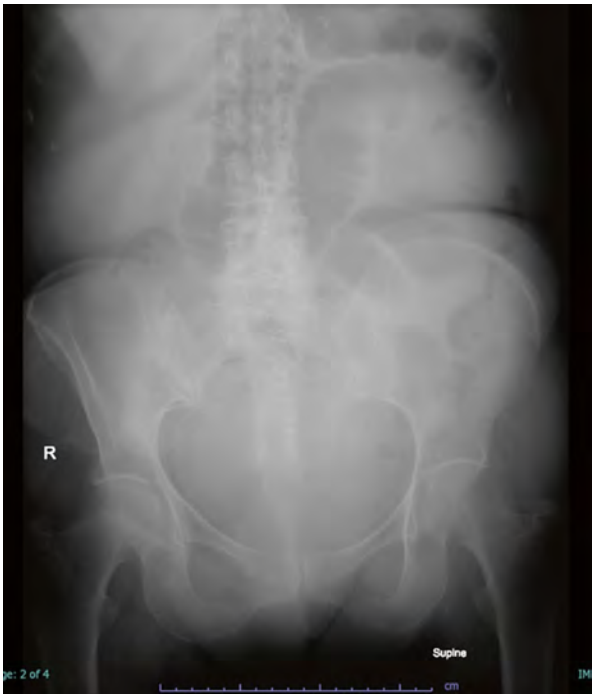

Fig. 1.5 Supine radiograph of the abdomen demonstrating air in the small bowel and colon. Note the skin staples in this postoperative patient

Fig. 1.6 Decubitus view of the abdomen. Note that air fluid levels are visible in the bowel on decubitus views due to the tangential X-ray beam. An enteric tube is located within the stomach

- "Three-view" or acute abdominal series involves a two-view abdominal series (see above) with the addition of a chest X-ray. This increases sensitivity for subdiaphragmatic-free air (see Fig. e1.1) and also lower-lobe pneumonias, which can cause referred abdominal pain (see Fig. e1.2).

Pros

- Plain films are often the first imaging modality used for the assessment of the abdomen due to the fact that they are low cost and easily accessible.
- They can be performed on stationary or portable equipment. Portable X-rays are obtained at the bedside and can be used for acutely ill or immobile patients.
- They have a low radiation dose.
- They are rapidly acquired and quickly processed, particularly with current digital technology.
- A variety of disorders can be identified on plain films, including life-threatening conditions such as pneumoperitoneum (see Figs. 1.7 and e1.3).
- Malpositioned catheters can be rapidly identified (see Figs. 1.8 and e1.4).

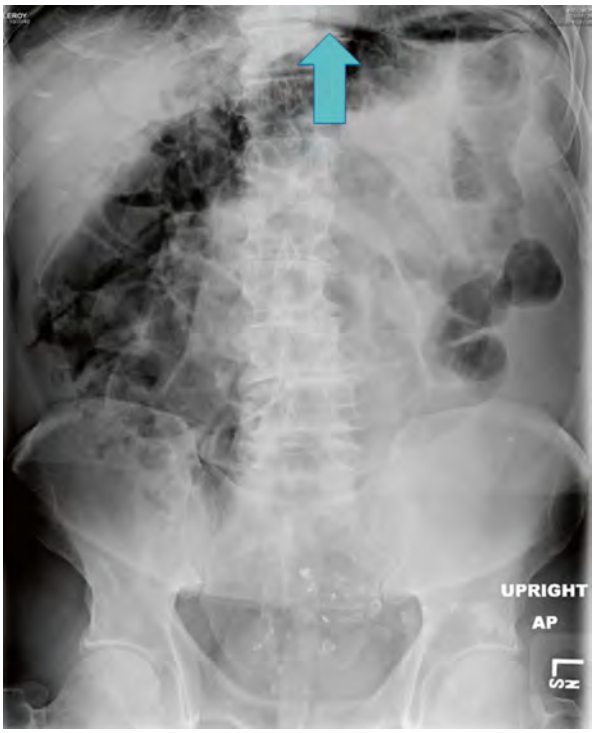

Fig. 1.7 Upright view of the abdomen demonstrating pneumoperitoneum (arrow)

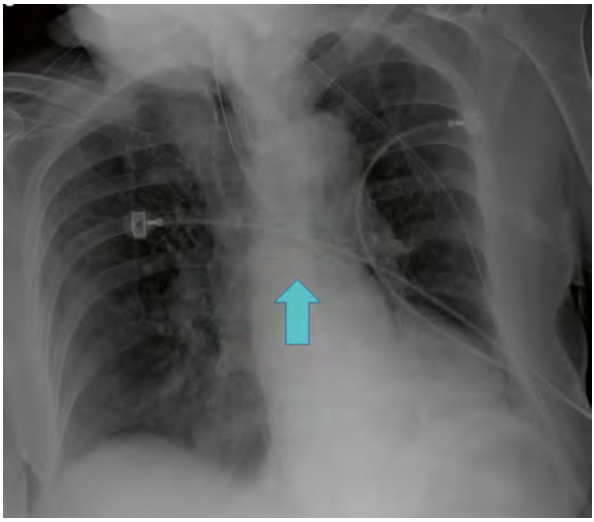

Fig. 1.8 Chest radiograph performed for assessment of enteric tube positioning demonstrates a malpositioned tube in the left mainstem bronchus (arrow)

Cons

- Plain films have a low sensitivity and specificity for diagnosing abnormalities.
- Films are often limited in patients who cannot be adequately positioned (see Figs. 1.9, 1.10, and e1.5) and who are obese (Figs. 1.11, 1.12, and e1.6).
- Catheters can be difficult to identify on plain films in obese patients (see Fig. 1.13).
- The retroperitoneal structures are particularly poorly evaluated on plain films (see Figs. 1.14, 1.15, and 1.16).
- Single views of the abdomen are often insufficient for the evaluation of bowel pathology and pneumoperitoneum.
- High-grade bowel obstructions can be missed on plain film when there is no intraluminal air (see Figs. 1.17 and 1.18).
- While renal and ureteral stones can be seen on abdominal X-rays (see Fig. 1.19), associated renal obstruction cannot typically be diagnosed.

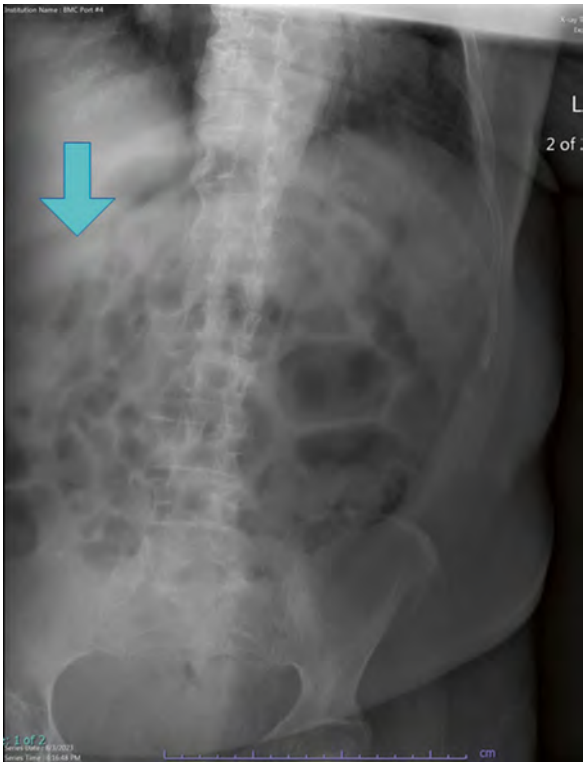

Fig. 1.9 Supine abdominal radiograph is unable to image the entire abdomen due to patient girth and clinical status. Note the long exposures required to penetrate patients of size often result in motion artifacts such as in the bowel in this case (arrow)

Fig. 1.10 Supine abdominal radiograph in an ill, poorly positioned patient is unable to image the entire abdomen. The lung bases should be included to identify lower lobe pneumonias that may be a cause of abdominal pain. These are excluded in this limited examination

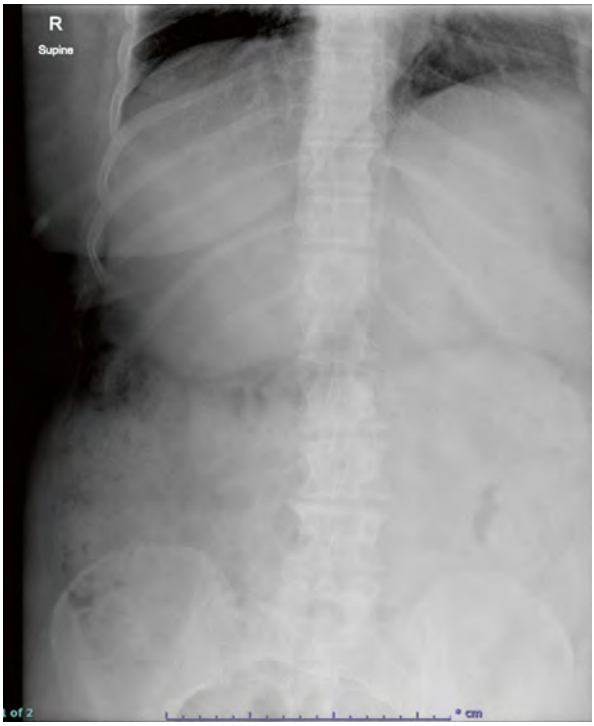

Fig. 1.11 Supine abdominal radiograph in a patient of size. Note that the entire abdomen can not be imaged on one film and that the film is underpenetrated due to patient size

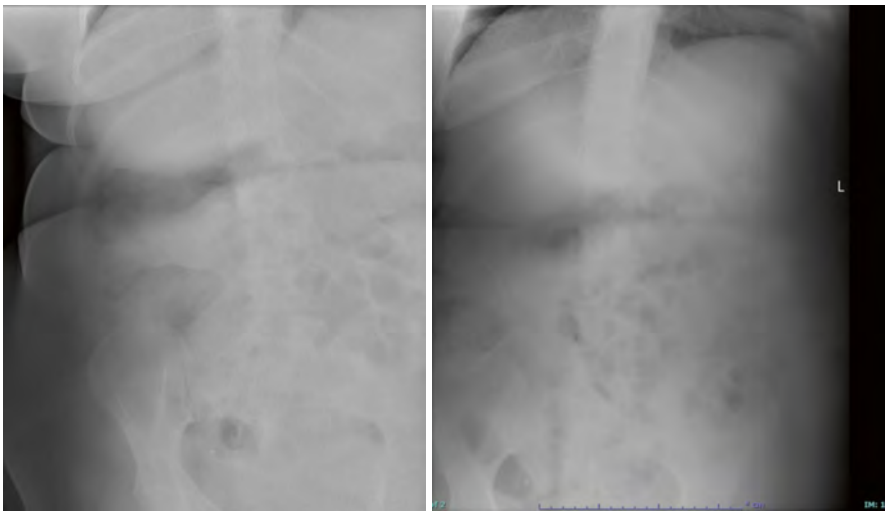

Fig. 1.12 Two views from a patient of size demonstrating inability to include the entire abdomen on a single image and underpenetration due to size

Fig. 1.13 Supine view of the lower pelvis in a patient of size (note the pannus over the left hip). The arrow indicates a urinary catheter which can not be adequately seen due to patient size

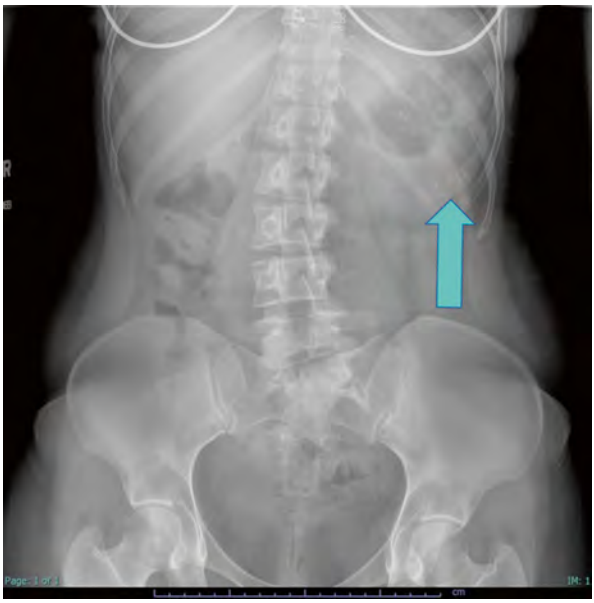

Fig. 1.14 A supine view of the abdomen demonstrates the difficulty in visualizing retroperitoneal structures on radiographs. The arrow indicates calcifications within the left kidney which are much better seen on CT

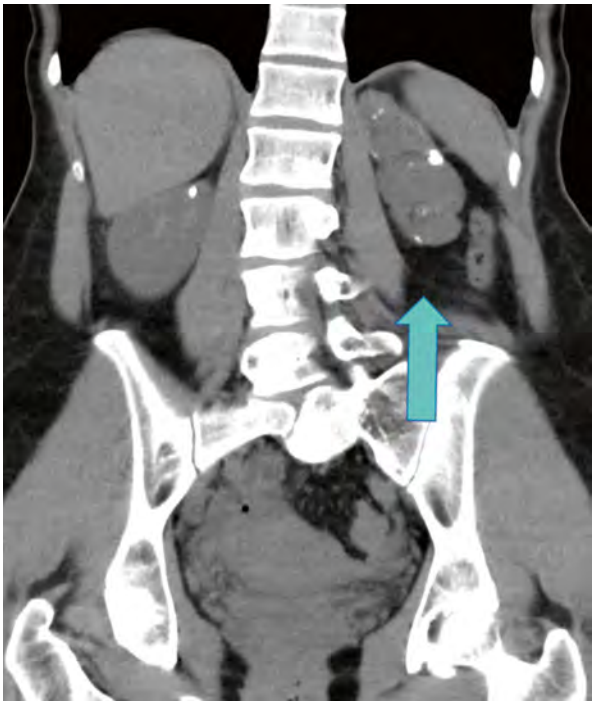

Fig. 1.15 Coronal CT image simulating the plane acquired on abdominal radiographs. Note how well the renal calculi are visualized (arrow)

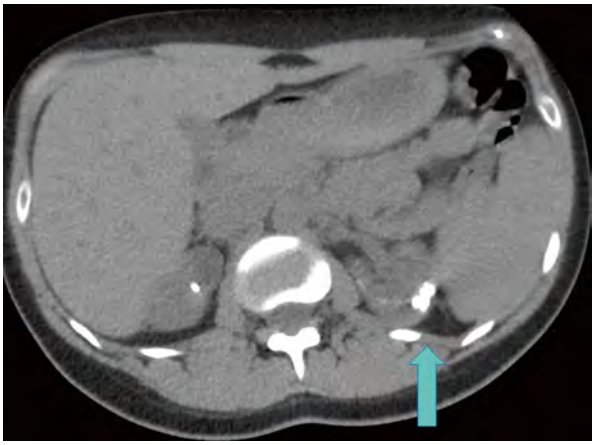

Fig. 1.16 Axial CT image in the same patient as Figs. 1.14 and 1.15 demonstrating the now well visualized left renal calculi (arrow)

Fig. 1.17 Supine view from a CT scout image demonstrates a disorganized bowel gas pattern with a few prominent small bowel loops in the right abdomen, but not highly suspicious for a small bowel obstruction

Fig. 1.18 Axial CT image from the same patient as Fig. 1.23 demonstrates markedly dilated, fluid filled small bowel loops which were not visible on the abdominal film due to complete filling with fluid and lack of a tangential image

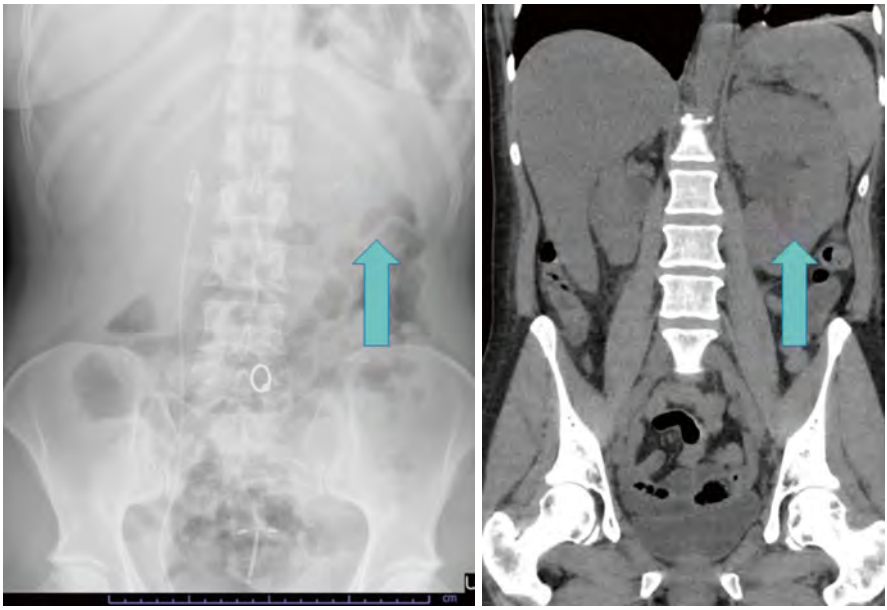

Fig. 1.19 Abdominal radiograph demonstrates renal stones (arrow), however, cannot identify the renal obstruction that is seen on the corresponding CT (arrow; right image)

Fluoroscopy

General Considerations

- Fluoroscopy is sometimes considered "lumenography" as the lumen of the bowel is assessed by administering enteric contrast to outline the structures.
- Contrast can be administered orally or through indwelling catheters (enteric tubes, gastric or gastro-duodenal tubes, rectal catheters; see Figs. 1.20, 1.21, e1.7, and e1.8).
- Rarely, contrast reactions can occur in patients with a history of allergy.
- The type of contrast material used depends on the indication for the study. Water-soluble contrast is used when there is a risk of a perforated viscus since barium will contaminate and complicate the surgical field.
- Water-soluble contrast material should not be used if there is a concern of aspiration since the hyperosmolar contrast can cause pulmonary edema (Fig. 1.22).
- Studies can be performed as single- or double-contrast examinations.
- Single-contrast examinations involve the administration of positive contrast material only (see Fig. 1.23).
- Double-contrast examinations involve the administration of oral contrast and an effervescent agent. This allows the mucosa of the bowel to be evaluated (see Fig. 1.24).

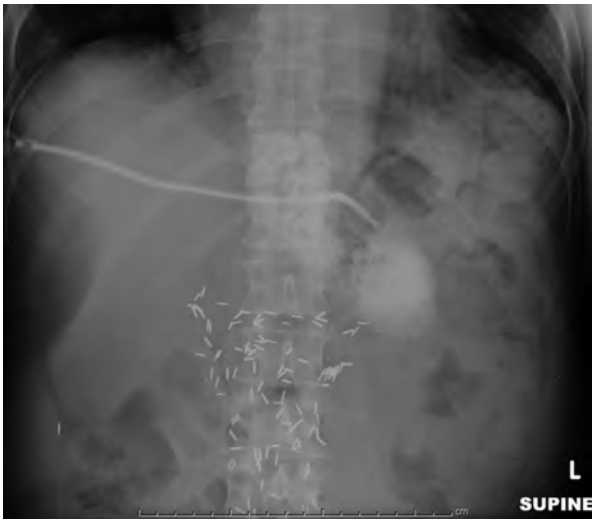

Fig. 1.20 Image obtained after injection of an indwelling gastrostomy tube. Contrast is seen the opacify a structure in the left upper quadrant

Fig. 1.21 Image obtained after injection of a malpositioned gastrostomy tube. Note the free spillage on contrast into the peritoneum, outlining bowel loops

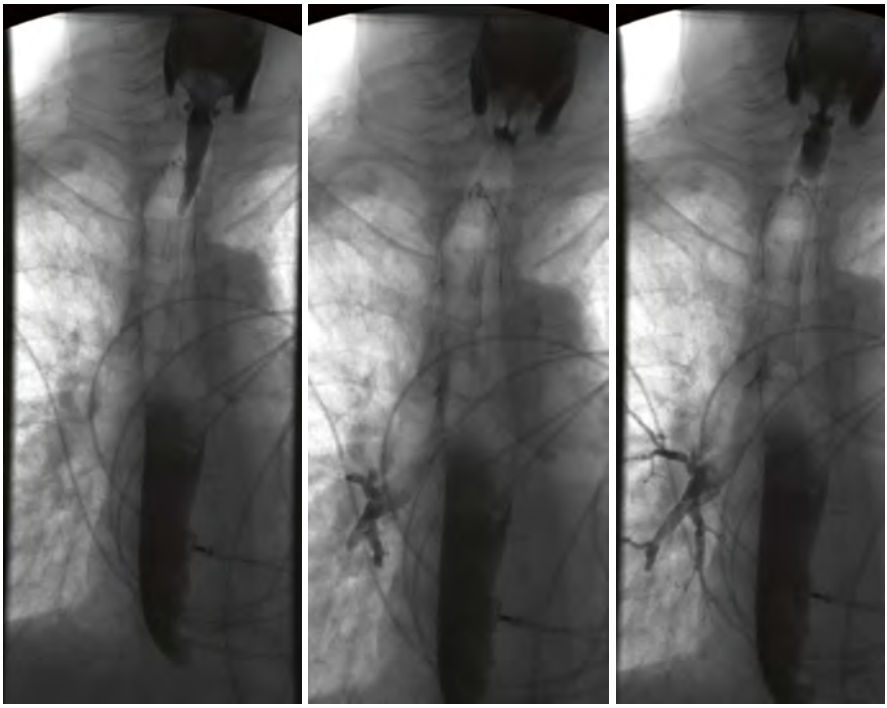

Fig. 1.22 Double contrast esophogram demonstrates aspiration into the right tracheobronchial tree

- Fluoroscopy for nonacute conditions such as ulcer disease is less frequently used in current practice and has been largely supplanted by endoscopy procedural techniques.

Pros

- Low-cost, low-radiation modality.
- Easily accessible for patients who can be moved to the fluoroscopy suite.
- There are multiple methods to administer contrast including oral, syringe, and catheter-based routes.
- Can rapidly make critical diagnoses such as bile leaks on fluoro-guided ERCP (see Fig. 1.25), perforations (see Fig. 1.26), and sites of obstruction and volvulus (see Fig. e1.9).
- In pediatric patients, fluoroscopic procedures can be therapeutic in conditions such as intussusception, where air or contrast can be used under fluoroscopy to reduce the intussusception.
- Difficult-to-place enteric catheters (e.g., NG, NJ tubes) can be placed under direct visualization with fluoroscopy, resulting in a more accurate placement.

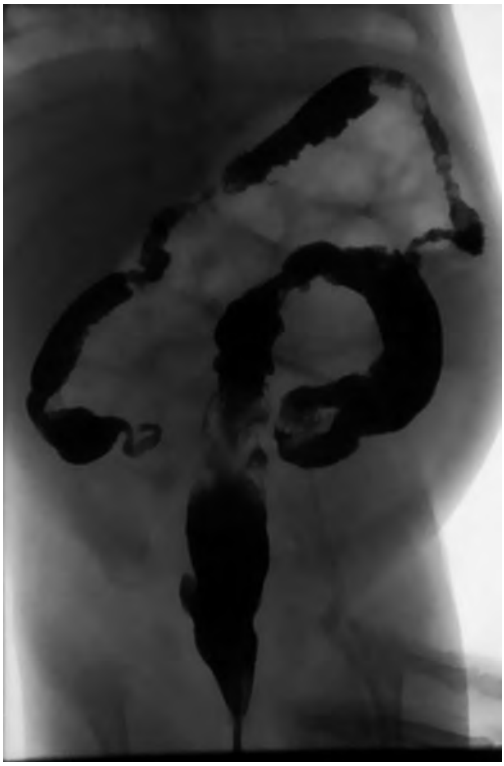

Fig. 1.23 Single contrast barium enema demonstrates a "lumen" view of the colon. Note the lack of mucosal detail on this single contract technique

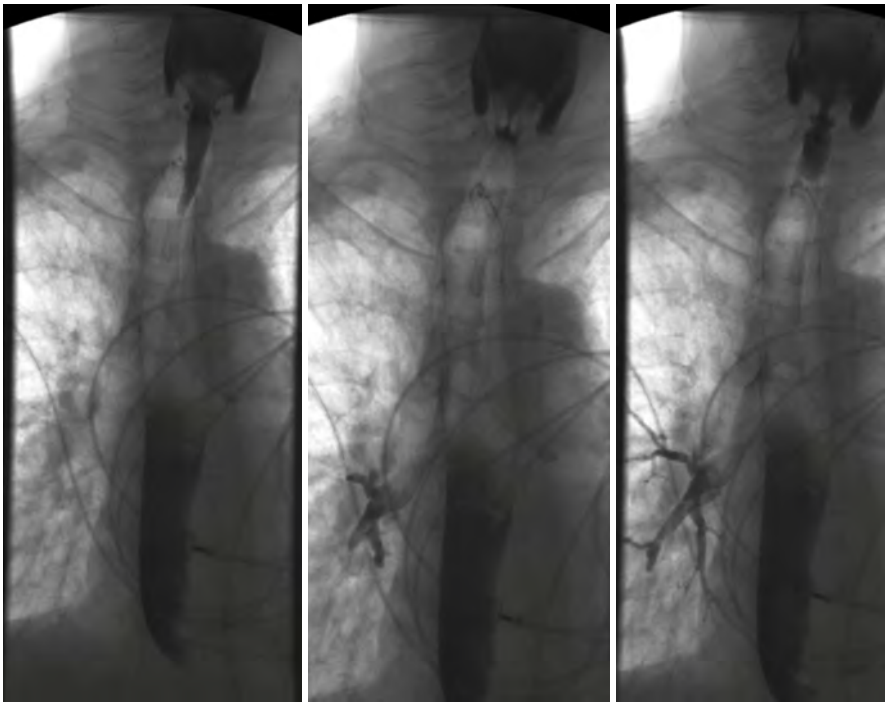

Fig. 1.24 Double contrast esophogram with contrast coating the mucosal lining and outlined by air and the lumen distended with contrast. Note the incidental contrast aspiration into the right tracheobronchial tree

Cons

- Cannot be performed at the bedside for patients who cannot be brought to the imaging suite.
- Procedures are difficult to perform on very ill patients and those with limited mobility.
- There are weight limits to fluoroscopy tables, which can be challenging in bariatric centers where patients may be above the maximum weight limit.
- In obese patients, subtle findings can be difficult to make due to limited resolution and difficulties with patient positioning.
- Patients in whom contrast administration is difficult may have suboptimal or nondiagnostic examinations.

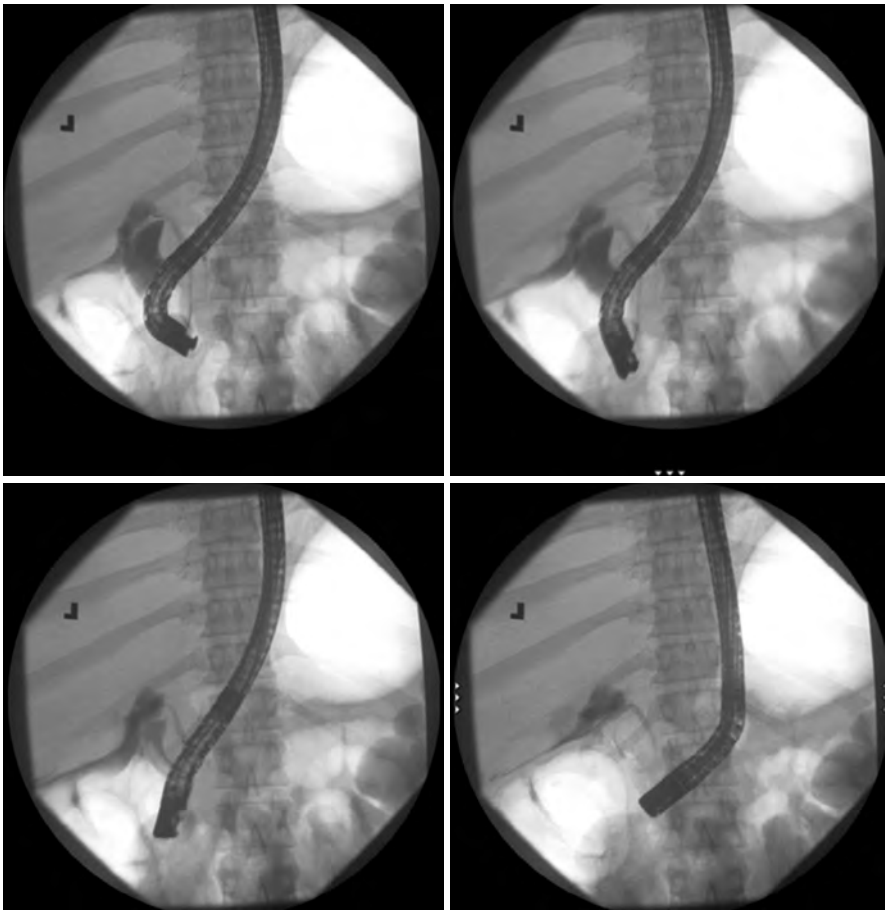

Fig. 1.25 Fluoroscopic images obtained during an ERCP demonstrate contrast leakage from the injected common bile duct, consistent with bile duct injury

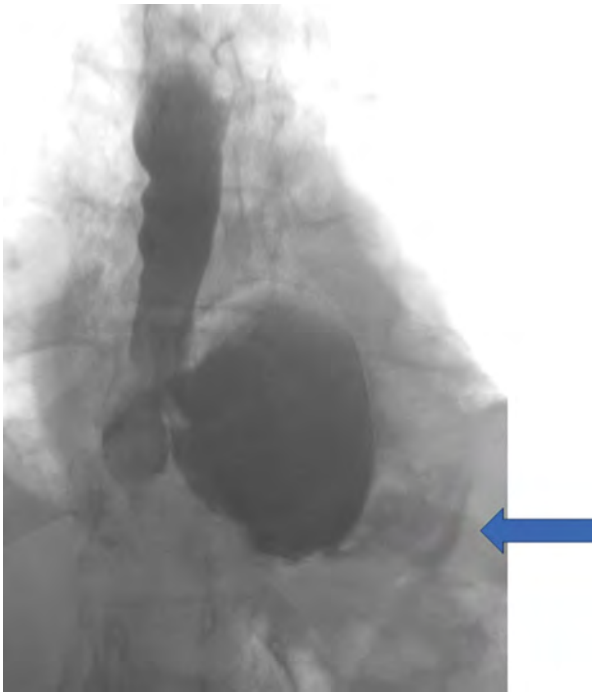

Fig. 1.26 Images obtained during an upper GI examination demonstrate contrast leakage from a gastric perforation (arrow)

Ultrasound

General Considerations

- Ultrasound is one of the main workhorses of abdominal imaging.
- Ultrasound is typically performed without contrast, but modern advances have led to the development of intravascular microbubble contrast agents that can be used for real-time problem-solving indications such as the assessment of liver masses, renal masses, and bowel abnormalities.
- Ultrasound is well suited for the evaluation of acute conditions and can also be used for lesion detection and characterization in chronic conditions.

Pros

- Cost-effective imaging modality, leading to easy access in many clinical settings.
- Ultrasound does not use ionizing radiation.
- Portable technology allows for bedside imaging in acutely ill patients.
- Good for differentiation between cystic and solid lesions (Figs. 1.27 and 1.28).

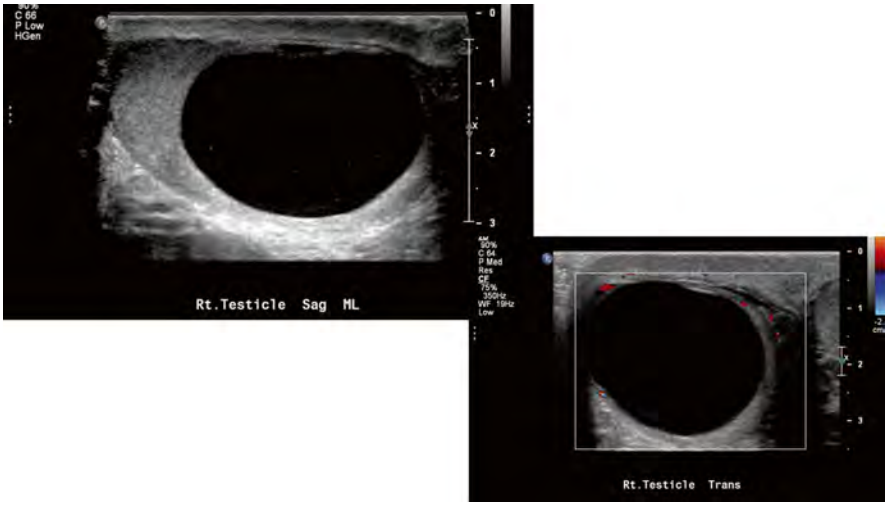

Fig. 1.27 Ultrasound image of the right testicle demonstrating an anechoic, circumscribed, avascular cyst in the testis. Note the through transmission of the ultrasound beam

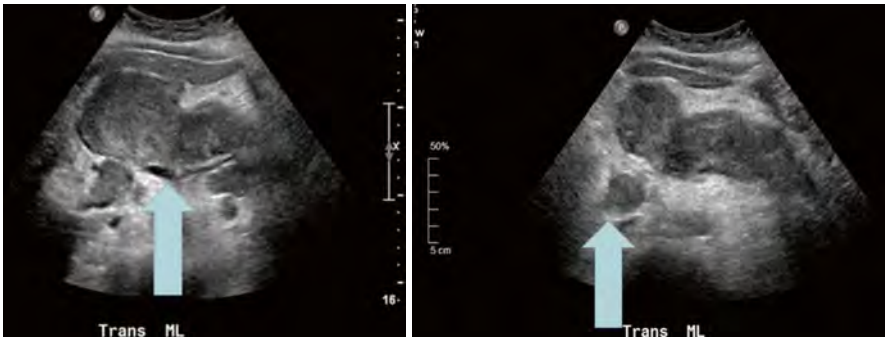

Fig. 1.28 Ultrasound image of a patient with a solid pancreatic mass. Note the heterogeneous and predominantly hypoechoic mass-like areas throughout the pancreas (arrows)

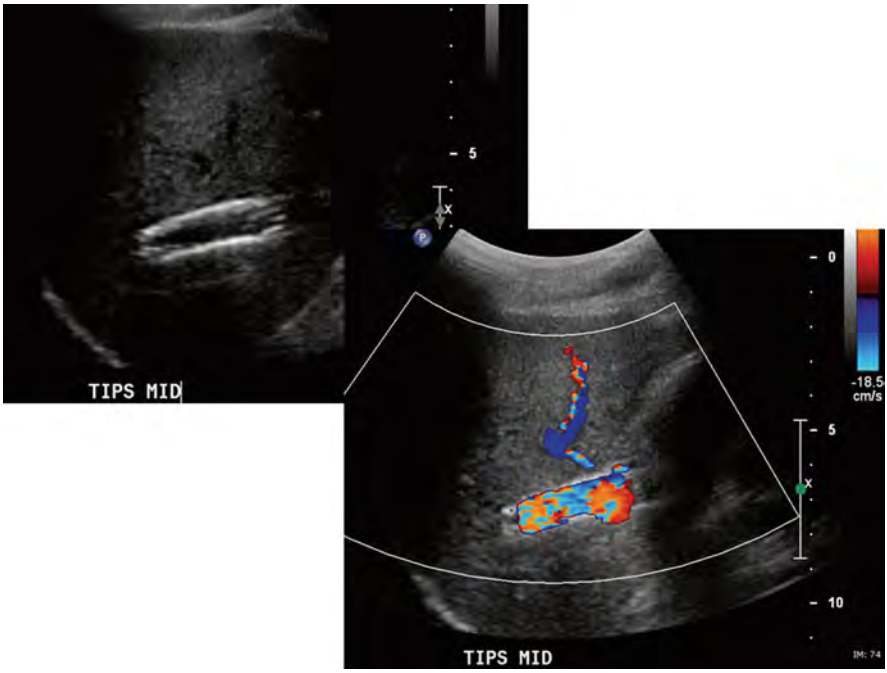

Fig. 1.29 Grayscale and color Doppler images demonstrating the appearance of a TIPS shunt on ultrasound

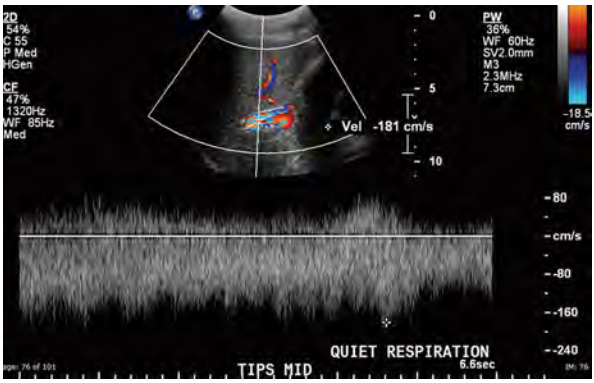

Fig. 1.30 Spectral Doppler ultrasound image demonstrating the waveform in this patent TIPS shunt

- Improvements in technology are increasing the value and capability of ultrasound.
- Ultrasound can be used to guide percutaneous procedures such as biopsy, fluid collection drainage, nephrostomy tube placement, etc.
- Because of the real-time nature of ultrasound and the ability to detect and assess blood flow, ultrasound is an excellent modality to assess vascular abnormalities and vascular supply to the organs. For example, TIPS shunts can be well evaluated with ultrasound (see Figs. 1.29, 1.30, and e1.10).

Cons

- Ultrasound is very operator dependent, often requiring a radiologist to be available to review scanning in real time.
- Ultrasound can be limited in obese patients, COPD patients, patients unable to comply with breath-hold instructions, and patients who cannot be positioned for the examination.
- Air prevents penetration of the ultrasound beam, particularly when attempting to evaluate the pancreas.
- There is a limited role of ultrasound in the evaluation of the bowel. With the advent of microbubble contrast agents, bowel pathology can be more readily assessed.
- Artifacts can lead to diagnostic errors. Each examination should be optimized by the sonographer to minimize the risk of artifacts mimicking disease.
- Tortuous, heavily calcified or small vessels can be difficult to assess, for example, in patients with cirrhosis in whom assessment of hepatic and portal vein patency requires assessment (Figs. 1.31 and e1.11).

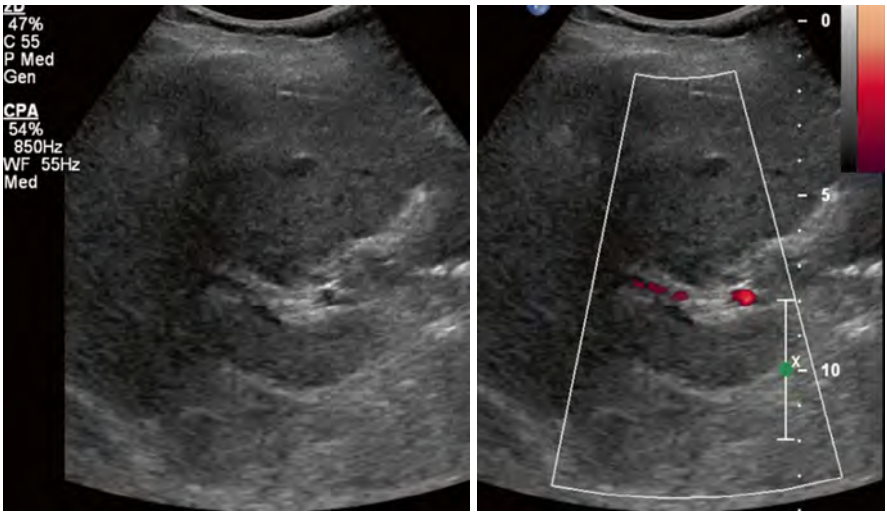

Fig. 1.31 Ultrasound image of a patient with cirrhosis. Note how difficult it is to visualize and interrogate the small vessels commonly seen in this fibrotic condition

Computed Tomography

General Considerations

- CT is the workhorse for the evaluation of patients with abdominal complaints.
- There are a variety of techniques and protocols that can be used to evaluate different pathologies and organ systems in the abdomen. These include liver mass (Figs. 1.32, 1.33, and 1.34) and renal mass protocols, renal stone protocols (Fig. 1.35), and enterography (see Figs. 1.35 and e1.12), among others.
- Studies can be performed with or without oral contrast, depending on the indication (Figs. 1.36 and 1.37).
- Studies can be performed with or without intravenous contrast, depending on the indication (see Figs. 1.38 and 1.39).
- Most patients are candidates for CT, although morbidly obese patients may not fit into the scanner or may outstrip the table weight limit.

Pros

- Rapid image acquisition.
- Ubiquitous in healthcare settings.
- High sensitivity and specificity.
- Excellent contrast resolution.
- All organ systems can be assessed simultaneously in one examination. This allows for the assessment of organ-based pathology in a systematic way.

Fig. 1.32 CT of the liver without intravenous contrast as part of a liver mass protocol. Oral contrast was administered although is not standard practice

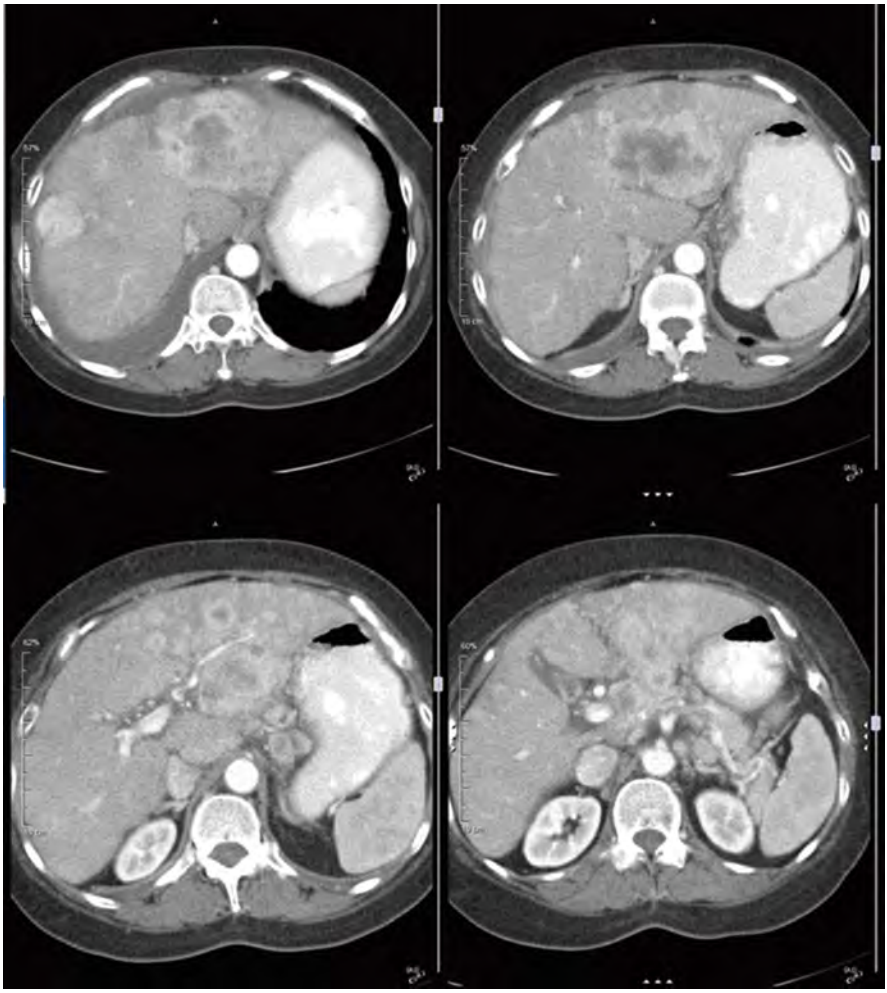

Fig. 1.33 Multiple images from the late arterial phase of a liver mass protocol CT demonstrating hypervascular masses

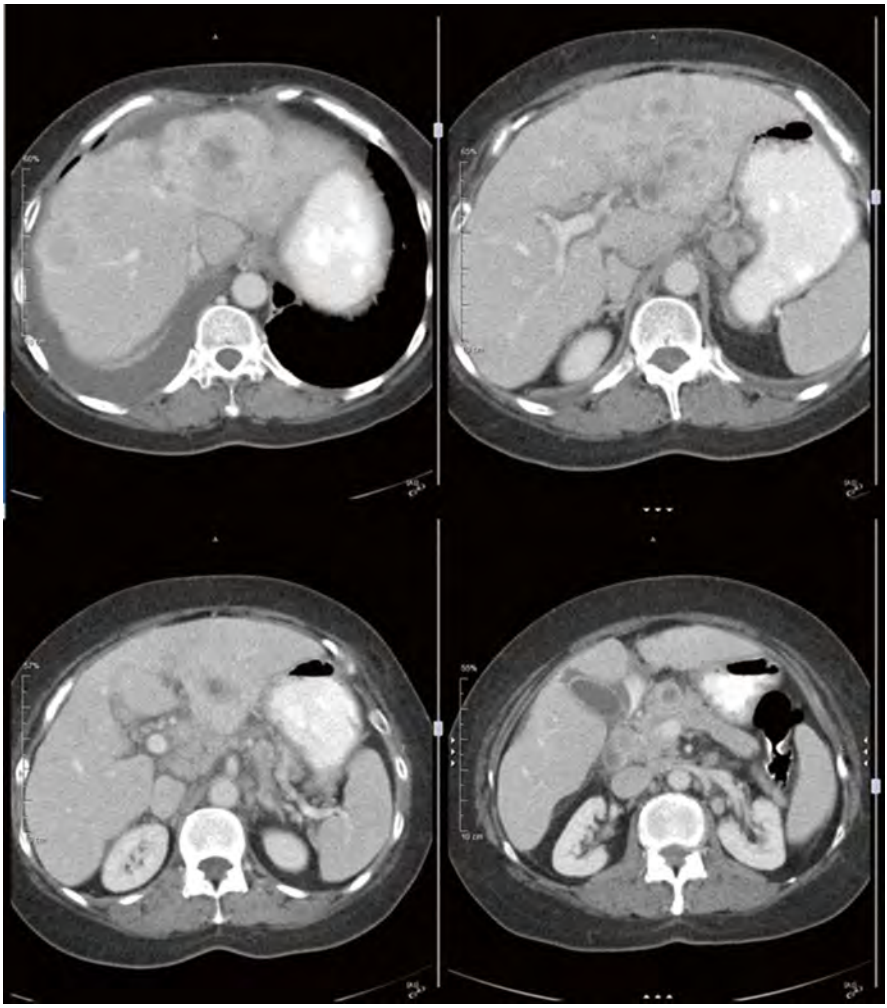

Fig. 1.34 Multiple images from the portalvenous phase of the liver mass protocol shown in Fig. 1.33. Note that the masses are becoming similar in density to the surrounding normal liver, making detection and measurement more difficult

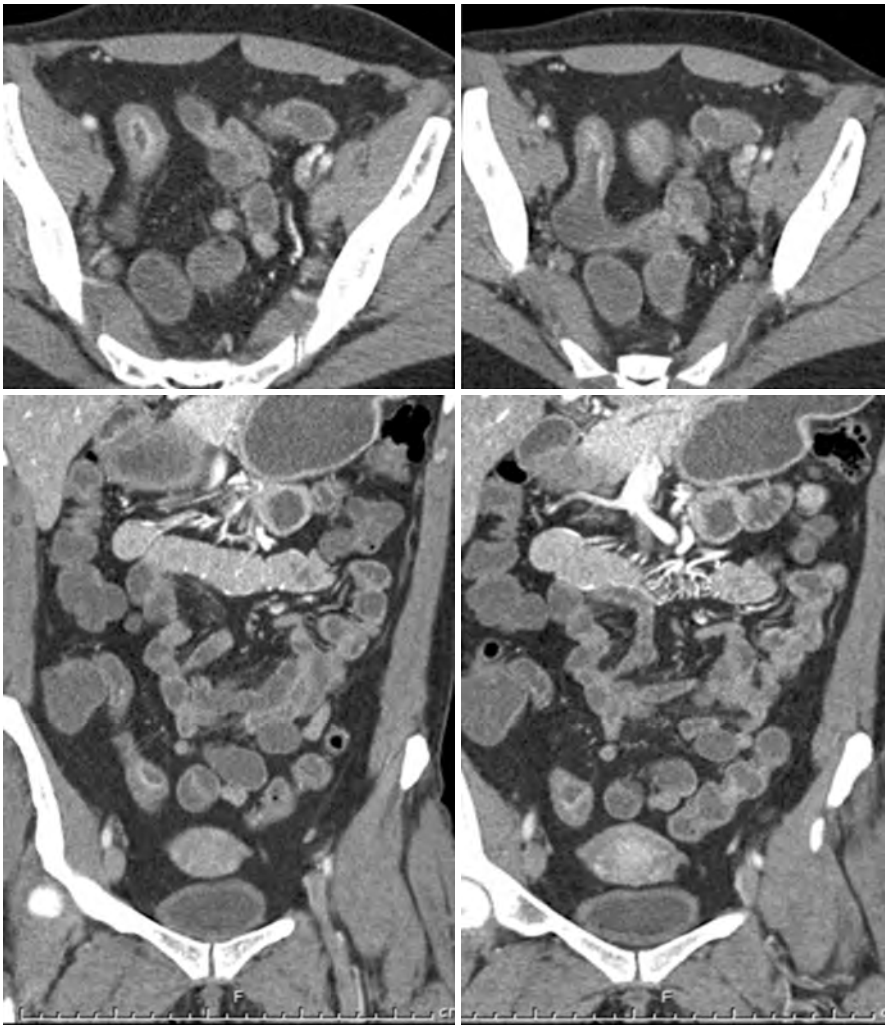

Fig. 1.35 CT enterography. Axial (top row) and coronal (bottom row) images using a CT enterography protocol. Note the fluid in the bowel lumen

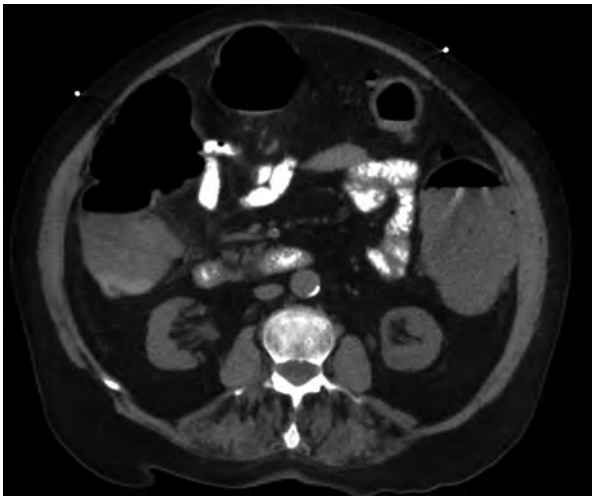

Fig. 1.36 CT of the abdomen with oral and without intravenous contrast. Note the high attenuation positive oral contrast in the small bowel and lack of contrast enhancement of the kidneys

Fig. 1.37 CT of the abdomen with intravenous and without oral contrast. Note the lack of high density positive oral contrast in the bowel and the enhancement of the kidneys

Fig. 1.38 CT of the abdomen without oral or intravenous contrast. Note the absence of enteric and intravenous contrast

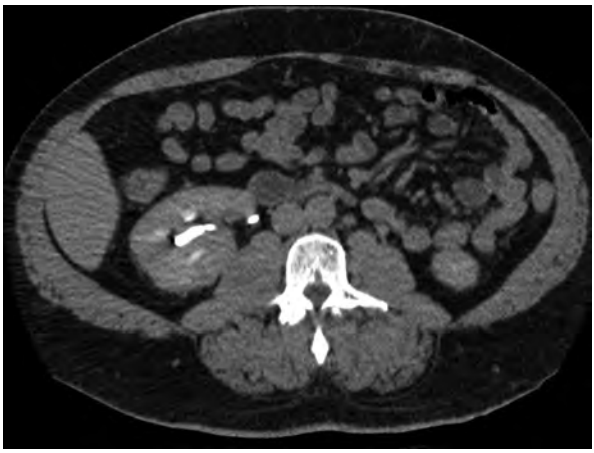

Fig. 1.39 CT of the abdomen with intravenous and without oral contrast. Note the excretion of intravenous contrast into the right renal collecting system on this delayed phase. There is no high density enteric contrast in the bowel

Cons

- CT is a significant source of ionizing medical radiation. Attention must be paid to the dose used and how many CT examinations patients undergo over time.
- Both thin and obese patients may have study limitations. Thin/cachectic patients often lack intraperitoneal and retroperitoneal fat that can make certain diagnoses (such as nephroureterolithiasis) difficult.
- Obese patients may not fit into the scanner (related to body circumference), or may outstrip table weight limits and thus cannot be scanned. If scanned, significant artifact can occur if portions of the body touch the gantry (see Fig. 1.40).
- If patients cannot receive oral contrast, or intravenous contrast, or both, studies can be limited for certain diagnoses. This is particularly true for trauma and oncology patients in whom intravenous contrast cannot be administered.
- Metal causes artifacts and can make evaluation of adjacent structures challenging. Newer techniques can minimize the impact but are not perfect. Causes of metal artifact include embolization coils, metal enteric tube tips, joint replacements, and surgical clips.
- Like ultrasound, air can cause significant artifact, particularly if the patient is moving during image acquisition. This can limit the evaluation of the bowel and adjacent structures.
- Patient movement during a CT examination can render an exam uninterpretable (see Fig. 1.41).
- Enteric barium should not be used if there is a concern for bowel perforation since it will contaminate the surgical field. Water-soluble enteric contrast is, therefore, typically used in most or all cases of suspected acute abdominal/bowel pathology.

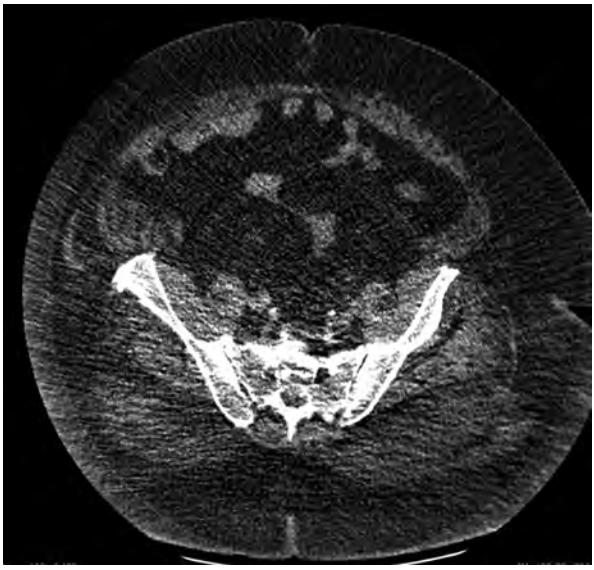

Fig. 1.40 CT of the abdomen in an obese patient. Note the extensive artifact related to the abdomen touching the sides of the scanner. This degrades image quality

Fig. 1.41 CT of the abdomen degraded by patient motion artifact. Note the blurring of the bowel with high density artifacts at the air-filled bowel margin. Note also the motion artifact around both kidneys

- In patients with renal insufficiency, intravenous contrast may result in acute kidney injury and should be avoided when possible.
- Intravenous contrast can cause allergies, including anaphylaxis. Prior contrast reaction history and risk factors for contrast reaction should be taken into consideration and a premedication protocol considered if intravenous contrast cannot be avoided.

Magnetic Resonance Imaging

General Considerations

- MR is typically a problem-solving tool for abdominal indications, although it can occasionally be used for primary diagnosis such as appendicitis in pregnancy.
- There are a variety of techniques and protocols that can be used to evaluate different pathologies and organ systems in the abdomen. These include liver mass (Fig. 1.42), renal mass protocols (Fig. 1.43), MRCPs (Fig. 1.44), and enterography, among others.
- Studies can be performed with or without intravenous contrast, although most MR examinations are performed both without and with intravenous contrast.
- Enteric contrast is not typically administered, although it may be on occasion. The one notable enteric material that is given for MR enterography is a hyperosmolar agent that is used to distend the bowel.
- Patient selection is critical for MR examinations and includes contraindications for MR examinations.
- Contraindications for MR examinations include non-MR-compatible cardiac pacing devices, recent stent placement, and orbital foreign bodies. It is important

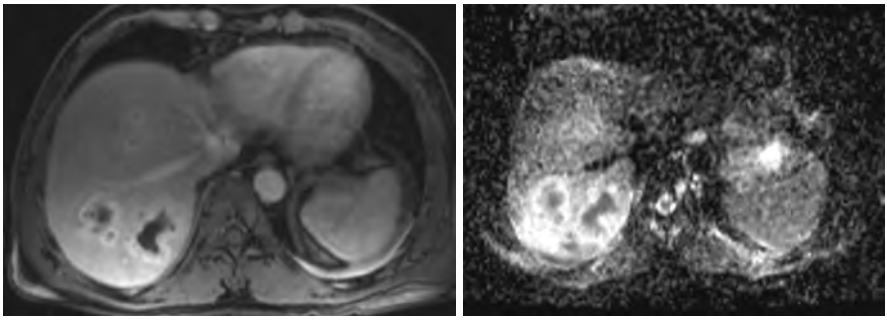

Fig. 1.42 Liver mass protocol MRI. Shown are contrast enhanced T1 weighted image (left) and diffusion weighted image (right). Both images show a neoplasm in the right hepatic lobe

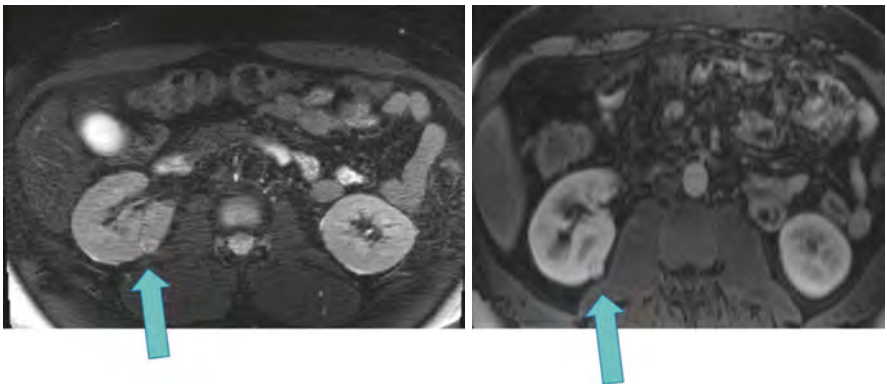

Fig. 1.43 Renal mass protocol MR with T2 weighted image (left) and T1 weighted post contrast image (right) demonstrating an enhancing right renal neoplasm (arrows)

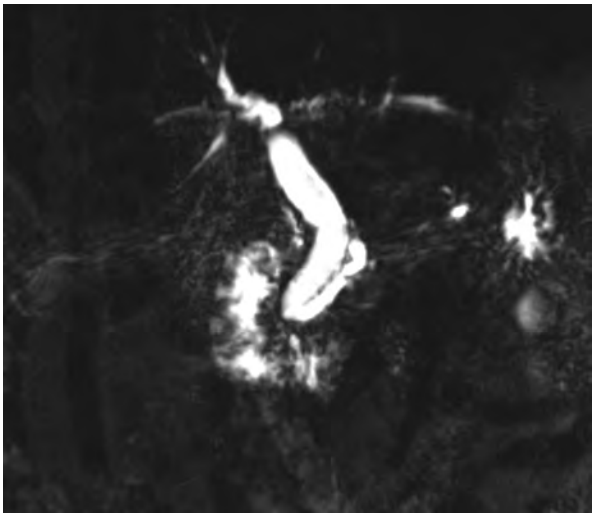

Fig. 1.44 Coronal thick slab 3-D MRCP image. Note that fluid (bile) is T2 bright

to familiarize yourself with institutional contraindications for MR examinations.
- Patient body habitus must be taken into consideration, particularly for obese patients.
- Patients with claustrophobia may be poor candidates for MR examinations due to the small tunnel.
- Altered mental status (e.g., dementia), difficulty hearing, inability to follow commands, and difficulty with holding breath can render examinations nondiagnostic.
- MR is limited by the length of time needed for each sequence, the number of different sequences required, and the need for multiple or prolonged periods of breath-holding.

Pros

- No ionizing radiation.
- MR has excellent spatial and contrast resolution, far superior to CT.
- Very detailed evaluation of small body parts and superficial and deep structures because of its superior resolution capabilities.
- Excellent problem-solving tool due to the multiple sequences and information on tissue characteristics it can obtain.
- The lack of radiation allows the patient to be scanned many times and in different phases of contrast enhancement.
- Dynamic perfusion/enhancement information allows for better lesion characterization.
- No specific fetal risks, unlike CT. Intravenous contrast is contraindicated.

Cons

- Long scan times.
- Patients need to remain immobile throughout the study.
- High risk for artifact related to motion, patient size, and patient compliance with instructions.
- Less available for urgent/emergent studies because of long scan times.
- Not sensitive to the detection of free air, limiting utility in the acute abdomen.
- Field of view and body region to be imaged are limited due to the properties of MR.

Choosing the Right Study: Central Tenants

- Understanding the clinical question for a patient allows you to select the optimal modality and protocol.

- Review the history and indication for each examination and make sure the correct study is ordered.
- Confirm that there are no contraindications or significant limitations to performing a study as ordered.
- Suggest alternative modalities or techniques if the request is not appropriate for the patient.
- Review patient factors to determine if they are a good modality candidate—technologists can assist with this assessment.
- Always strive for the *right study* the first time.
- Optimize protocols to answer the question posed, that is, choose the right protocol and administer intravenous and/or oral contrast when appropriate.
- Continually monitor and assess scan quality and work with the department on areas for improvement.
- Do no harm! Seek out risk factors for, or known contrast reaction history and address immediately.

The ACR (American College of Radiology) Appropriateness Criteria

- A full discussion is beyond the scope of this text.
- The American College of Radiology convenes expert panels to determine what studies are appropriate for what conditions.
- These criteria are evidence based and derived by consensus of the expert panels.
- The criteria are reviewed cyclically to ensure up-to-date research is used to make recommendations.
- It is important to be aware of these criteria and to have easy access to the information.
- The criteria can be shared with referring or ordering providers to achieve consensus on an examination for a particular patient.
- The appropriateness criteria are freely available on the ACR website (www.acr.org).

Templated Reporting

- More institutions and academic societies are moving away from free-text, traditional dictation reports.
- Standardized (templated) reports are becoming standard of care to improve communication of findings, allow data mining from reports, and ensure that pertinent positive and negative findings are included.
- These standardized reports often contain drop-down menus/pick lists that incorporate follow-up management recommendations.
- They improve standardization of practice across a system.

- The report templates can act as a guide of pertinent positive and negative findings to include in a report.
- Useful for high-end imaging where there are specific details that must be included in a report, for example, rectal cancer staging.
- Can improve workflows by reporting shortcuts for negative examinations.
- Caution must be taken to remove portions of the normal templates when there is a relevant finding.

Further Readings

1. Hertzberg BS, Middleton WD. Ultrasound: the requisites. Elsevier Health Sciences; 2015.
2. Boland G. Gastrointestinal imaging: the requisites. 4th ed. Elsevier Health Sciences; 2013.
3. Webb RW, Brant WE, Major NM. Fundamentals of body CT. 5th ed. Elsevier Health Sciences; 2019.
4. Roth CG, Naringrekar H, Deshmukh S. Fundamentals of body MRI (fundamentals of radiology). 2nd ed. Elsevier Health Sciences; 2016.
5. Catanzano TM. How to think like a radiologist: ordering imaging studies. Cambridge University Press; 2008.

Developing a Search Pattern

2

Mary Woodruff, Sunil Jeph, and Robert Panico

Key Points

- Developing a reliable search pattern for each imaging modality is key to the success of a radiologist. This chapter offers suggested search patterns for plain film radiographs, fluoroscopic studies, ultrasound, CT, and MRI examinations of the abdomen.
- This search pattern is developed over years and continues to evolve throughout a radiologist's career. Early in training this is a flexible construct.
- A new resident should explore different approaches and experiment with their own unique pattern. Attending physicians and structured dictation templates may guide this process.
- Early in training, "misses" can be key drivers to ensure critical findings are not overlooked in future exams.
- Missed findings are the number one reason for medical errors in radiology [1], and a well-developed search pattern will ensure a thorough evaluation of each patient.

M. Woodruff (✉) · S. Jeph · R. Panico
Department of Radiology, Cooper University Hospital, Camden, NJ, USA
e-mail: woodruff-mary@cooperhealth.edu; jeph-sunil@cooperhealth.edu; panico-robert@cooperhealth.edu

© The Author(s), under exclusive license to Springer Nature Switzerland AG 2024

T. Catanzano (ed.), *What Radiology Residents Need to Know: Abdominal Radiology*, What Radiology Residents Need to Know,
https://doi.org/10.1007/978-3-031-76624-4_2

Abdominal Plain Film

A plain film offers a quick overview of the abdomen. Usually ordered to rule out a bowel obstruction, it can provide valuable information to the clinician within its limitations.

- Quality improvement/quality control (QI/QC)
  - Confirm you are looking at the correct patient and correct study.
  - Common views include supine, erect, and lateral decubitus views.
  - Confirm the appropriate anatomy is fully imaged with appropriate exposure.
  - Consider the indication for the study and the clinical question.
- Identify the presence and positioning of any visible lines, tubes, and other foreign bodies.
  - Most of these will have at least some radiopaque component that will be identifiable.
  - Confirm they are in the correct region.
  - If they are not in the expected location, suggest where they may have migrated.
  - It is important to promptly report misplaced lines to the care team.
- Check for free intraperitoneal air.
  - This can be a sign of perforated bowel and should raise immediate concern.
  - However, this can also commonly be seen in the postsurgical setting as the abdomen may have been insufflated during the surgery.
  - In an erect film, this will appear as a lucency below the hemidiaphragms (Fig. 2.1).
  - In a lateral decubitus film, free air will rise.

Fig. 2.1 Abdominal radiograph: Erect radiograph of the abdomen demonstrating a curvilinear lucency under the right hemidiaphragm representing free intraperitoneal air

Fig. 2.2 Abdominal radiograph: The contours of the liver, spleen, kidneys and psoas muscles may be outlined

- Evaluate the bowel gas pattern.
  - Check for normal situs; the gastric bubble should be on the left.
  - Observe the distribution of the bowel gas in the abdomen.
  - Scattered air will be seen in the small and large bowel.
  - Dilated or displaced bowel can be concerning for obstruction or mass.
  - Stool can be seen in the colon; assess the stool burden.
- Depending on the technique, the outline of some abdominal organs can be seen as smooth curves.
  - The liver, kidney, and spleen may be outlined (Fig. 2.2).
  - The bilateral psoas muscles may be seen.
  - Loss of these fat planes may suggest active inflammation as the fat becomes abnormal.
- Check the osseous structures.
  - The inferior ribs, spine, pelvis, and proximal femora should be evaluated for lesions, degenerative changes, and fractures.
- Identify any calcifications.
  - Gallstones, renal stones, appendicoliths, atherosclerotic calcifications, or venous phleboliths may be identified (Fig. 2.3).
- After an initial assessment of the abdomen, again review the area of concern, confirming the clinical question has been answered within the limitations of the study.

Fig. 2.3 Abdominal radiograph: Note the vascular calcifications, or phleboliths, in the pelvis

Fluoroscopy

- In fluoroscopy, the radiologist captures the images in real time.
- A combination of exposures/still images and cines/videos may be collected during the exam.
- Single-contrast exams utilize only one contrast solution for the exam, usually water-soluble or barium contrast solution.
- Depending on the study, contrast is either ingested orally or administered rectally.
- Double-contrast exams use air as the second medium.
- In an upper GI exam, the gas is produced with swallowed effervescent crystals.
- In a barium enema, air is administered into the colon via a pneumatic pump.

Esophagram/Upper GI/Small Bowel

- Esophagus
  - The esophagus should be relatively featureless with a smooth contour and uniform distention (Fig. 2.4).
  - Check for normal motility and the primary peristaltic stripping wave in cine clips.
  - The gastroesophageal junction should be below the level of the diaphragm.
  - Swallowed contrast should only travel antegrade through the gastroesophageal junction and not reflux back into the esophagus.
- Stomach
  - The stomach should be smooth in contour (Fig. 2.5).

Fig. 2.4 Fluoroscopic exposure: Double contrast fluoroscopic exposure of the esophagus. The esophagus is distended with uniform smooth mucosa

Fig. 2.5 Fluoroscopic exposure: Double contrast fluoroscopic exposure of the stomach. The stomach has uniform rugal folds and a smooth contour

  - The gastric rugae should be uniform in size.
  - Evaluate for irregular folds and protruding or depressed lesions.
- Duodenum/small bowel
  - Ensure normal developmental rotation of the bowel (Fig. 2.6).
  - Normal rotation refers to the c-loop of the duodenum with the duodenal-jejunal junction located to the left of the spine at the level of the duodenal bulb (Fig. 2.7).

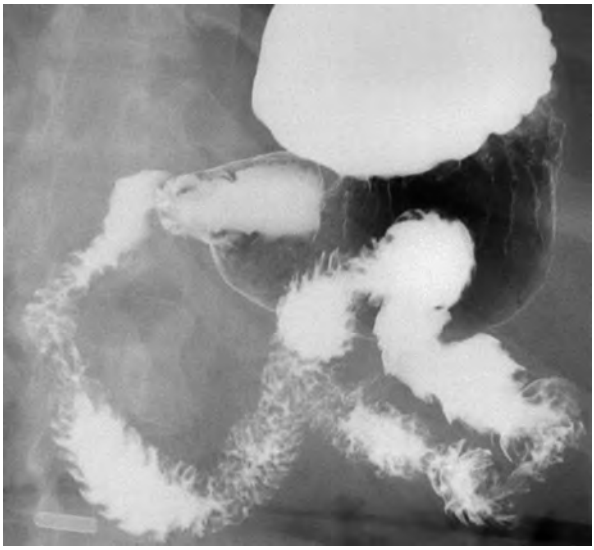

Fig. 2.6 Fluoroscopic exposure: Double contrast fluoroscopic exposure of the proximal duodenum. The C loop of the duodenum crosses the midline in normal situs

Fig. 2.7 Fluoroscopic exposure: Fluoroscopic exposure of the small bowel. Note the normal small bowel mucosal folds and central distribution in the abdomen

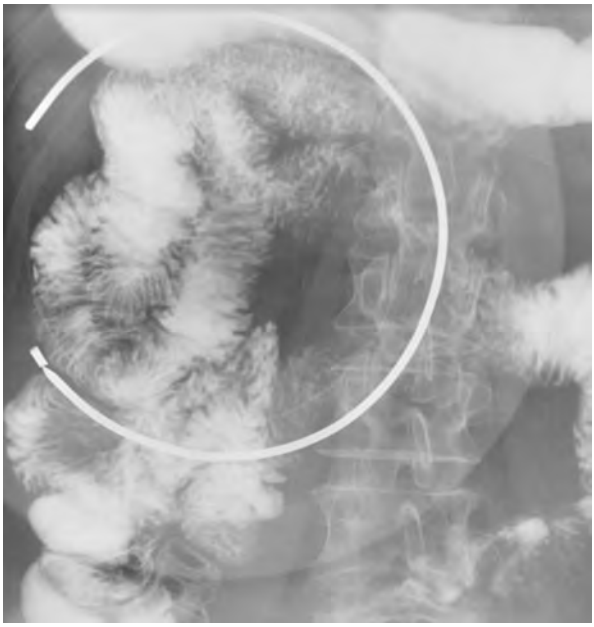

Fig. 2.8 Fluoroscopic exposure: Fluoroscopic exposure of the small bowel. For a magnified spot compression view, a paddle may be used to compress loops of bowel for a more detailed view of a specific region

- The small bowel folds are thin and closely placed and circumferential (valvulae conniventes) and should be uniform (Fig. 2.8).
- Contrast should pass easily through the small bowel and to the ileocecal valve without stricture or obstruction.
- Normal small bowel transit time range is 30–120 min.

Barium Enema

- Colon
  - The colonic folds are widely spaced and are not circumferential (haustral folds).
  - Assess for stricture, obstruction, or volvulus.
  - Identify any masses or polyps.

Ultrasound

- Ultrasound examination of the abdomen is an inexpensive and safe exam that offers a substantial amount of information.
- These exams may be limited secondary to bowel gas obscuring the field of view and patient body habitus.
- Quality improvement/quality control (QI/QC)
  - Confirm you are looking at the correct patient and correct study.

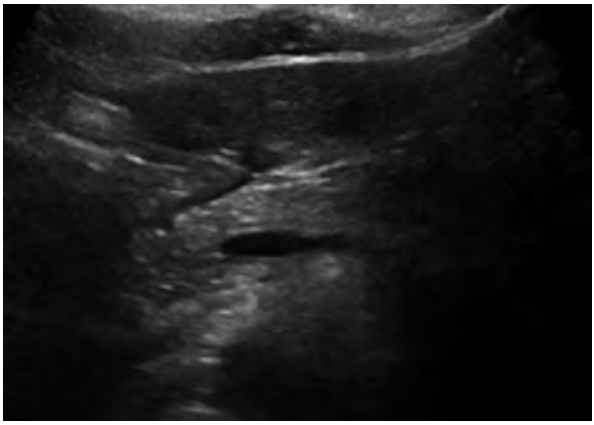

Fig. 2.9 Ultrasound of the pancreas. The pancreatic head and proximal body are homogeneous in echotexture

  - Confirm the appropriate anatomy is fully imaged.
  - Consider the indication for the study and clinical question.
- Pancreas
  - Only the pancreatic head and proximal body can be evaluated by ultrasound based on the anatomic positioning in the abdomen.
  - Occasionally the tail can be seen by using the spleen as a window.
  - It should be smooth in contour with a homogeneous echotexture (Fig. 2.9).
  - The main pancreatic duct may be visible and should measure less than 0.3 cm.
- Liver
  - The liver should have a smooth contour with homogeneous echotexture (Fig. 2.10).
  - Normal craniocaudal length is less than 15.5 cm at the midclavicular line.
  - Assess the visibility of the periportal echoes.
  - Check for surface nodularity and masses (Fig. 2.11).
- Gallbladder and biliary tree
  - The gallbladder can measure up to 10 cm in length with a wall thickness of up to 0.3 cm (Fig. 2.12).
  - Assess for stones, polyps, or layering sludge.
  - The common bile duct can measure up to 0.6 cm in a patient with a gallbladder and up to 1 cm in a post-cholecystectomy patient (Fig. 2.13).
  - Measurements of the common bile duct are obtained from inner wall to inner wall to reflect endoscopic measurements.
- Kidneys
  - The kidneys should have a smooth contour with a cortical echogenicity similar or slightly lower than the liver (Fig. 2.14).
  - The cortex should measure at least 2.6 cm in thickness.
  - Assess the collecting system for dilation or hydronephrosis.
  - Note any cysts, masses, or calculi.
- Spleen
  - The spleen should be homogeneous in echotexture with a maximum dimension of 13 cm (Fig. 2.15).

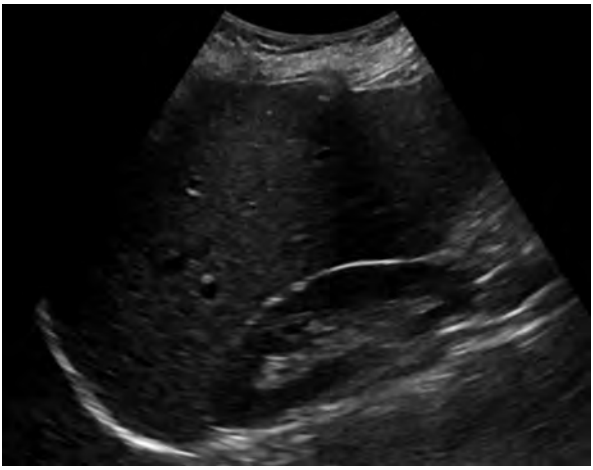

Fig. 2.10 Ultrasound of the liver in long axis. The liver is homogeneous in echotexture with vessels running through the parenchyma and periportal echoes

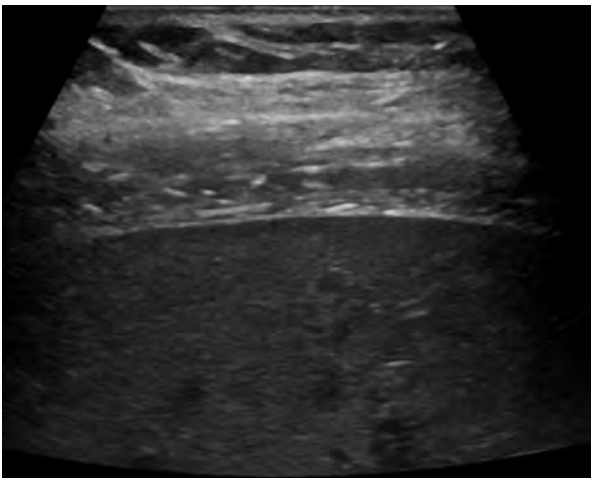

Fig. 2.11 Ultrasound of the liver surface. The surface of the liver is smooth

- Bladder
  - The bladder wall should measure between 0.3 and 0.5 cm in thickness depending on the degree of distension (Fig. 2.16).
  - Using color Doppler, observe the bilateral ureteral jets.
  - There must be urine in the bladder to see the jets since the effect is due to a difference in specific gravity and not flow.
  - Check for trabeculations, internal debris, intraluminal masses, and calcifications.
- Vasculature
  - Assess the main vessels in the abdomen for patency.
  - Ensure appropriate portal venous flow.
  - The abdominal aorta should not exceed 3 cm, anything greater than 3 cm is considered aneurysmal dilation.

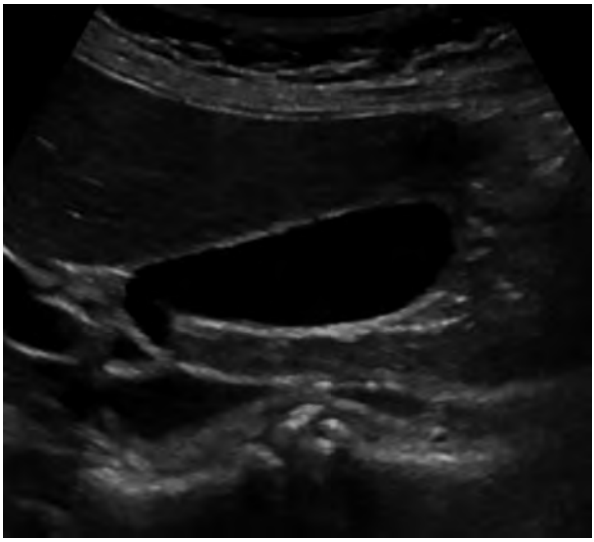

Fig. 2.12 Ultrasound of the gallbladder. The gallbladder is filled with anechoic bile

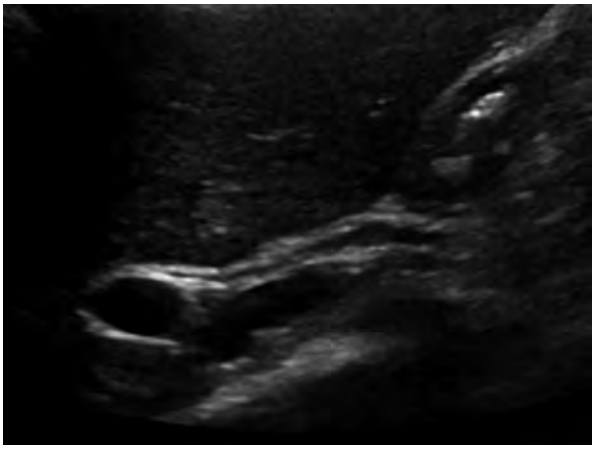

Fig. 2.13 Ultrasound of the biliary tree. The common bile duct is nondilated with smooth contours and no internal debris

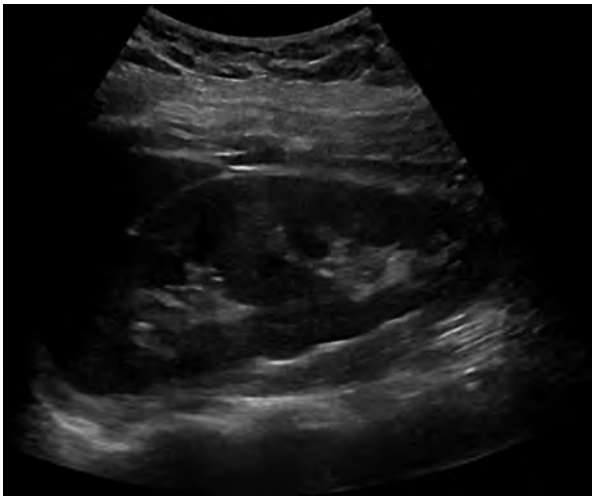

Fig. 2.14 Ultrasound of the kidney in long axis. The kidney has a relatively even cortex with an echogenic fatty hilum

Fig. 2.15 Ultrasound of the spleen. The spleen should be smooth in contour and homogeneous in echotexture

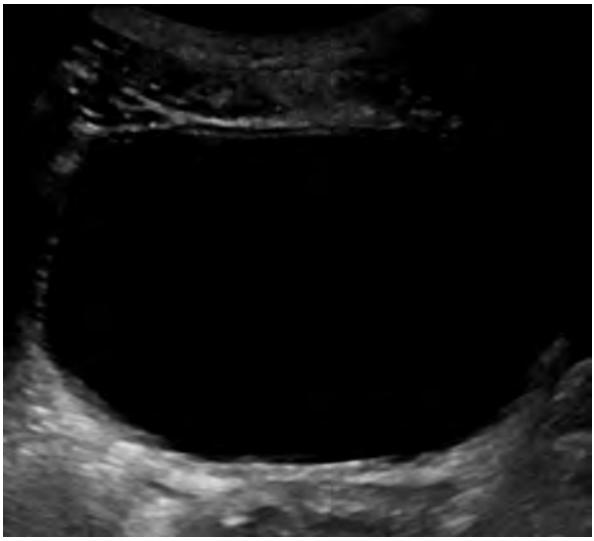

Fig. 2.16 Ultrasound of the urinary bladder. The bladder should be fluid filled and free of debris or trabeculation

CT

- CT is the workhorse of cross-sectional imaging.
- It is quick, accessible, and many times will answer the clinical question.
- Quality improvement/quality control (QI/QC)
  - Confirm you are looking at the correct patient, correct study, and the appropriate anatomy is fully imaged.
  - Check that the study is complete with all sequences in all planes in the imaging jacket.
  - Key contrast phases include arterial phase, portal venous phase, and delayed phases.
  - If contrast was utilized, confirm the appropriate phase of contrast was imaged.
  - Assess the technical quality of the study.
  - Study quality may be degraded by timing of contrast bolus, patient motion artifact, increased patient body habitus, and patient contact with the CT gantry.
  - Consider the indication for the study or clinical question.
- Lower chest
  - Evaluate the lung bases in appropriate lung windows identifying any nodules, parenchymal opacities, and pleural effusions (Fig. 2.17).
  - While in lung windows, scroll through the abdomen briefly to investigate for free intraperitoneal air as it may be more apparent in lung windows.
  - In soft-tissue windows, look at the visualized heart, assessing for cardiomegaly, coronary artery or cardiac valve calcifications and pericardial effusions (Fig. 2.18).
- Liver
  - The liver should be smooth in contour and homogeneous in attenuation (Fig. 2.19).

Fig. 2.17 Axial CT lower chest, lung windows. Confirm the lung bases are free of consolidations, nodules, and effusions

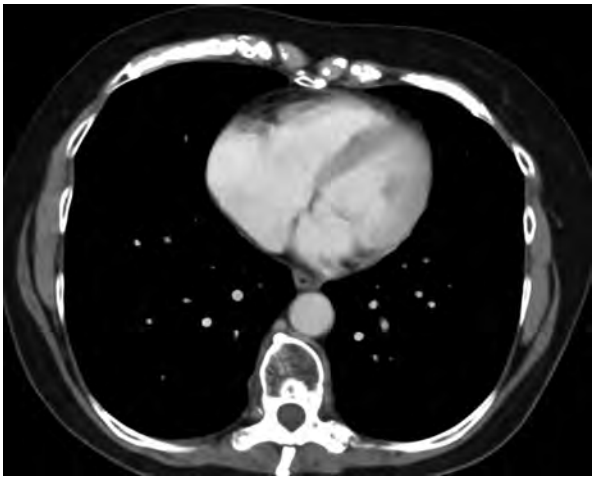

Fig. 2.18 Axial CT lower chest, soft tissue windows. The heart is normal in size without significant pericardial fluid

Fig. 2.19 Axial CT of the liver. The liver is smooth in contour and homogeneous in attenuation

  - The liver should measure less than 15.5 cm at the mid-clavicular line.
  - Identify any focal or diffuse abnormal attenuation.
  - Check for any masses.
- Gallbladder
  - Check if the gallbladder is present (Fig. 2.20).
  - Note anything within the lumen such as stones, sludge, or polyps.
  - Assess wall thickness; the wall should measure less than 0.3 cm.
  - Check for edema or free fluid within the gallbladder fossa.
- Biliary tree
  - The intrahepatic ducts should measure less than 0.2 cm.
  - The common bile duct should be smooth in contour and can measure up to 0.6 cm in a patient with a gallbladder and up to 1 cm in a post-cholecystectomy patient.
  - The coronal plane is particularly useful in assessing the biliary tree (Fig. 2.21).
- Adrenal gland
  - The adrenal glands are small "Y"-shaped organs on top of the kidneys in the axial plane (Fig. 2.22).
  - They should be roughly symmetric.
  - The adrenal glands are typically thin. Look for thickening to suggest hyperplasia.
  - Note any nodules or masses.
- Kidneys
  - The kidneys have a smooth contour and are grossly symmetric in size with the left kidney slightly more cephalad than the right (Fig. 2.23).

Fig. 2.20 Axial CT of the gallbladder. The gallbladder is tucked into the gallbladder fossa of the liver

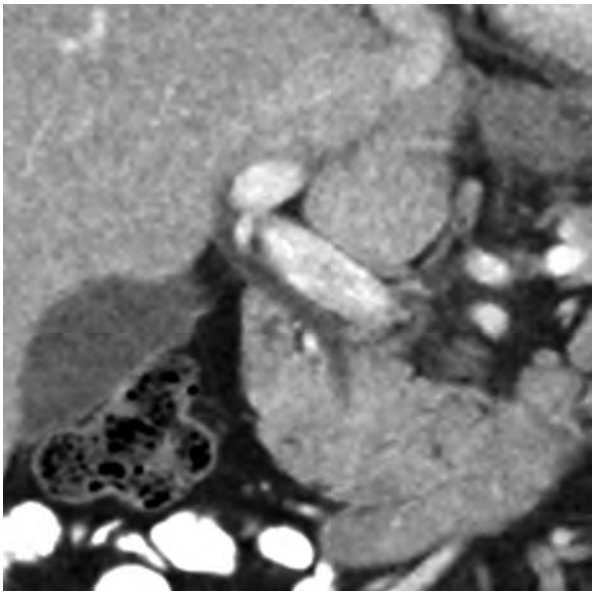

Fig. 2.21 Coronal CT of the common bile duct. The common bile duct can be clearly delineated on the coronal view

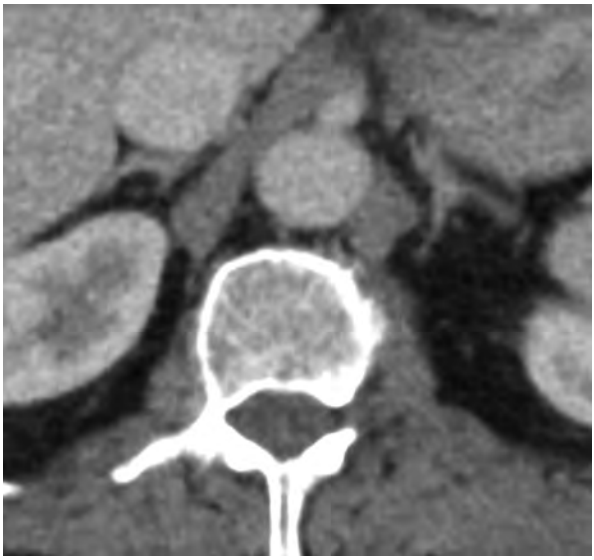

Fig. 2.22 Axial CT of the adrenals. The bilateral adrenal glands can be seen as small "Y" shaped organs over the kidneys

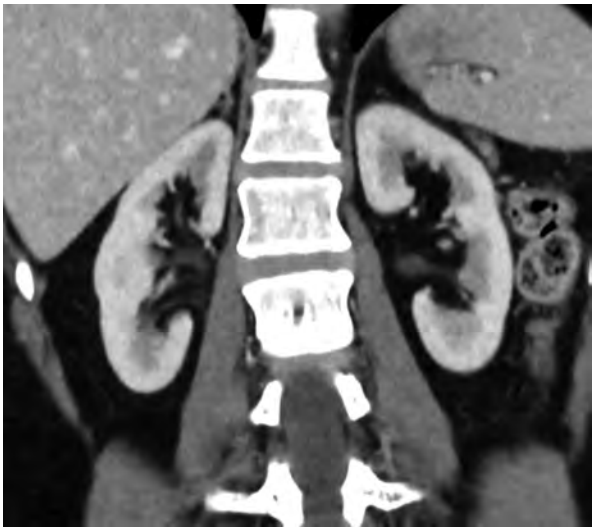

Fig. 2.23 Coronal CT of the kidneys. The right and left kidneys are grossly symmetric in size and enhance homogeneously and symmetrically

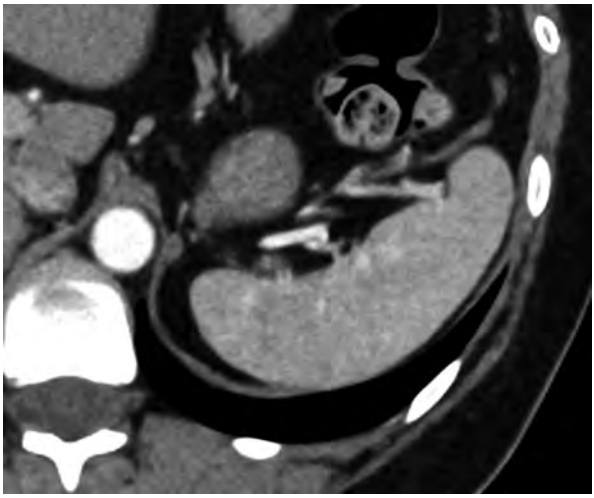

Fig. 2.24 Axial CT of the spleen. The spleen is smooth and homogeneous in attenuation

  - In a contrast-enhanced exam, they should enhance homogeneously and symmetrically.
  - Look for dilation of the collecting system and note the severity.
  - Note any cysts, masses, or calculi.
  - Trace the ureters as they course to the bladder to check for dilation, stones, or masses.
- Spleen
  - The spleen should be smooth and featureless (Fig. 2.24).
  - The spleen should measure less than 13 cm.
  - Accessory splenules may be seen as round soft-tissue masses with the same attenuation as the splenic parenchyma and are usually adjacent to the spleen.

- Pancreas
  - Identify the tail of the pancreas tucked into the splenic hilum and trace backward to the head (Fig. 2.25).
  - The main pancreatic duct can measure up to 0.3 cm.
  - Identify any ductal dilation, masses, calcifications, or peripancreatic edema.
- Bowel
  - Start at the distal esophagus and follow to the stomach.
  - The gastroesophageal junction should be below the diaphragm.
  - Evaluate the stomach.
  - Follow the stomach to the duodenum, evaluating for duodenal diverticulum or masses.
  - Scroll through the small bowel looking for any dilated or thickened loops (Fig. 2.26).
  - Start at either the cecum or the rectum and trace the colon in its entirety to the other end.
    - Observe for uniform enhancement of the mucosa.
    - Look for wall thickening, diverticulosis, and masses.
    - Identify the appendix originating from the cecum, immediately inferior to the ileocecal valve (Fig. 2.27).
    - Consider stool burden.
- Peritoneum
  - Check for free fluid like ascites or blood.
  - Smaller volumes of fluid may collect along the bilateral paracolic gutters and dependent portion of the pelvis.
  - Assess the mesentery.
    - It should be primarily fat studded with vessels and small lymph nodes.
    - Look for focal regions of fat stranding to indicate edema.
    - Assess for haziness, discrete masses, and peritoneal nodules/implants.
- Retroperitoneum
  - Evaluate for masses, implants, and free fluid.
  - Ensure the psoas muscles are symmetric.
- Bladder
  - Evaluate the degree of distension and any focal or diffuse wall thickening.
  - Look for masses, mural nodules, or calcifications.
- GU
  - Male
    - Assess prostate size and evaluate for nodules.
    - The prostate can measure up to 4.8 cm in the transverse dimension.
    - Confirm the seminal vesicles are symmetric.
    - Evaluate the visualized penis and scrotum.
  - Female
    - Identify each ovary.
    - Identify the uterus, cervix, and vaginal canal.
    - Note any cystic or solid masses.
    - The gonadal veins lead directly to the ovary and can be followed to determine if an adnexal mass is ovarian in origin.

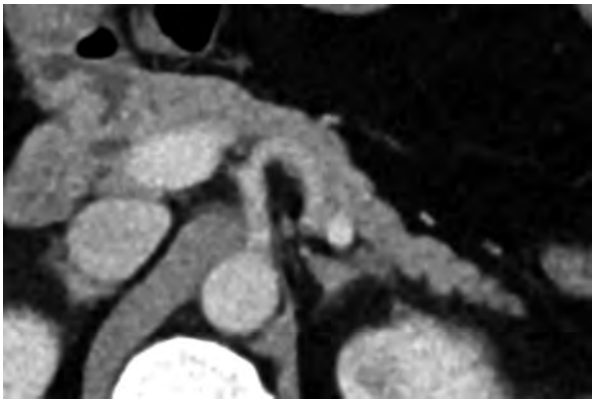

Fig. 2.25 Axial CT of the pancreas. The pancreatic tail and body is smooth and homogenous

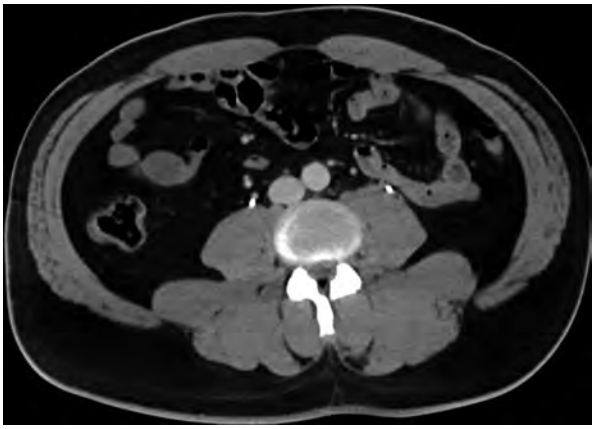

Fig. 2.26 Axial CT small bowel and mesentery. Normal loops of small bowel with clean mesentery primarily consisting of fat studded with vessels

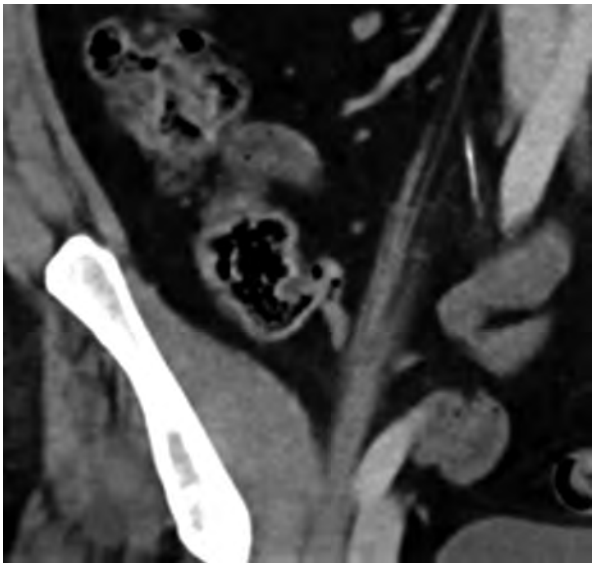

Fig. 2.27 Coronal CT of the appendix. The appendix arises from the cecum just below the level of the ileocecal valve

- Lymph nodes
  - Small scattered lymph nodes can be seen along the main vessels and in the mesentery.
  - Lymph nodes should measure less than 1 cm in short axis.
  - Enlarged lymph nodes may be reactive or concerning for malignancy.
    Pay special attention to the portocaval nodes and para-aortic lymph nodes as these tend to be a common site of metastatic disease.
- Vessels
  - Start with the abdominal aorta and assess the main branches for patency, stenosis, and aneurysmal dilation.
  - Grade any atherosclerosis.
  - Repeat with the venous system.
  - Check the portal vein for patency.
- Bones
  - Evaluate in bone windows.
  - Check the lower ribs, spine, pelvis and proximal femora for fractures, osseous lesions, and degenerative changes.
  - Look at the height and alignment of the vertebral bodies of the thoracolumbar spine in the sagittal plane (Fig. 2.28).
- Abdominal wall and soft tissues
  - Assess for masses, hernias, contusions, or anasarca.

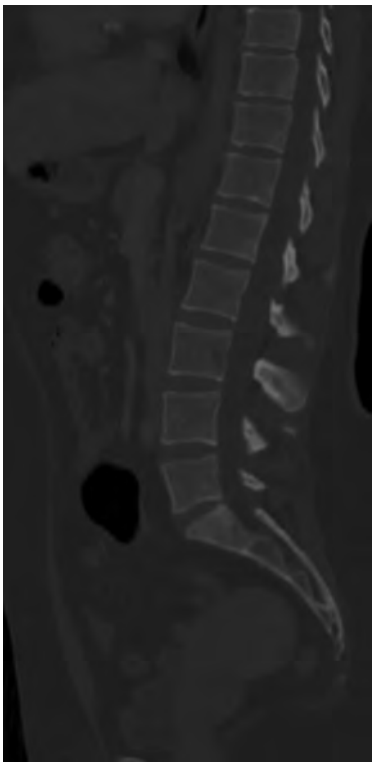

Fig. 2.28 Sagittal CT of the spine, bone windows. The vertebral bodies are aligned with preserved intervertebral disc spaces

MRI

- An MRI of the abdomen is a more specialized and nuanced study.
- Approaching an MRI of the abdomen can initially be an overwhelming task for a new radiology resident.
- In most cases, a patient will have already had a prior cross-sectional exam and there is a specific question to be answered.
- An MRI can shorten the differential if not confirm a diagnosis.
- The search pattern approach to an MRI of the abdomen is generally similar to that of a CT cross-sectional exam with different sequences used to highlight certain anatomy and pathology.
- Of note, individual institutions have different protocols and naming of sequences; this section provides a general framework to consider when approaching an MRI of the abdomen.

HASTE

- HASTE is a heavily weighted T2 sequence.
- This is a key sequence to provide a general overview, usually obtained in both the coronal and axial planes.
- The coronal sequence is usually the largest field of view, including portions of both the chest and pelvis (Fig. 2.29).
- Lungs and lower chest
  - Evaluate for pulmonary masses or nodules (Fig. 2.30).
  - Note that CT is the study of choice to evaluate the lungs.
  - Check for pleural and pericardial effusions.
  - Consider the heart size.
  - The breasts can vary in appearance based on the breast tissue density.
  - Identify any breast masses.
- Liver
  - The liver should have a smooth contour with homogeneous signal intensity (Fig. 2.31).
  - Identify any masses to evaluate on other sequences.
- Spleen
  - The spleen should be smooth with a homogeneous signal intensity (Fig. 2.32).
- Kidneys
  - The renal cortex should be smooth with a homogeneous signal intensity (Fig. 2.33).
  - Identify any lesions to evaluate on other sequences.
  - Assess for dilation of the collecting system.
- Bowel
  - Look for bowel dilation, edema, and masses.

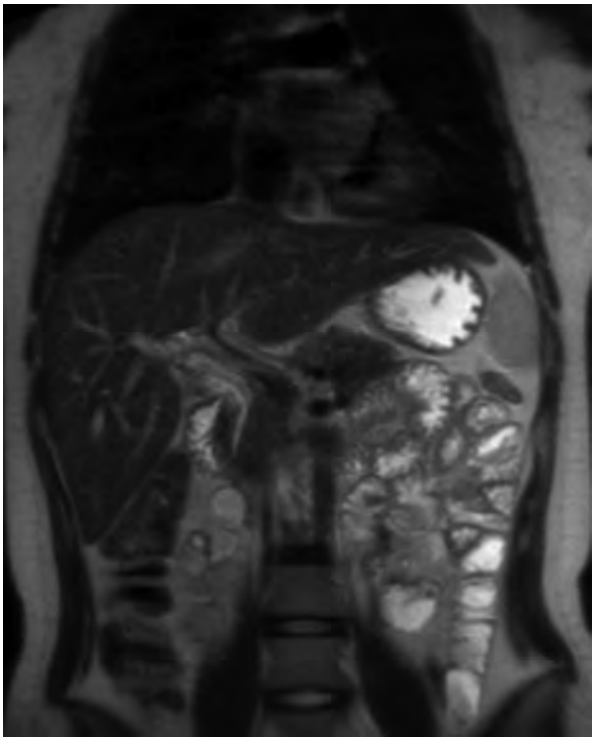

Fig. 2.29 Coronal MRI of the abdomen, HASTE sequence. Note the large field of view with portions of the chest and pelvis included in the image

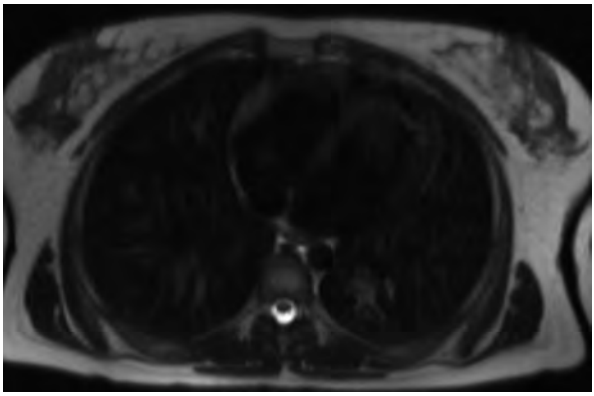

Fig. 2.30 Axial MRI of the lower chest, HASTE sequence. Examine the lung bases, heart, and breast tissue

- Pelvic structures
  - Depending on the field of view, some pelvic structures may be included.
  - Evaluate for pelvic masses.
- Bones
  - The signal intensity of the bones should be homogeneous.
  - Heterogeneity of the bone marrow may be related to degenerative changes or focal lesions, among other etiologies.

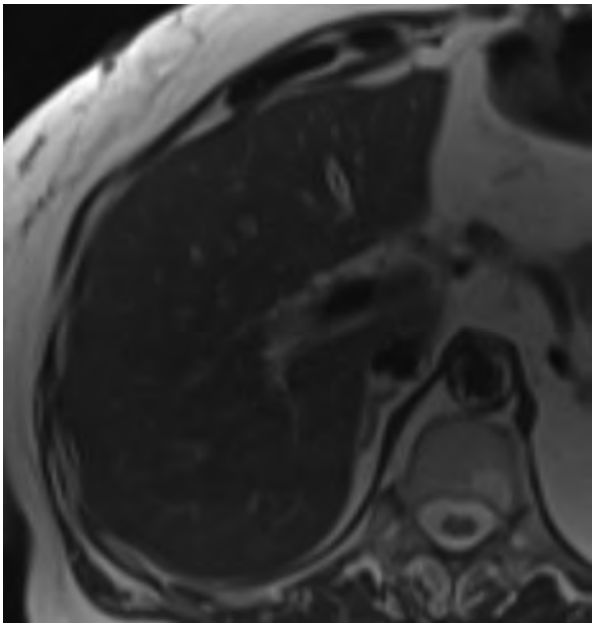

Fig. 2.31 Axial MRI of the liver, HASTE sequence. The liver is smooth in contour and homogeneous in signal intensity

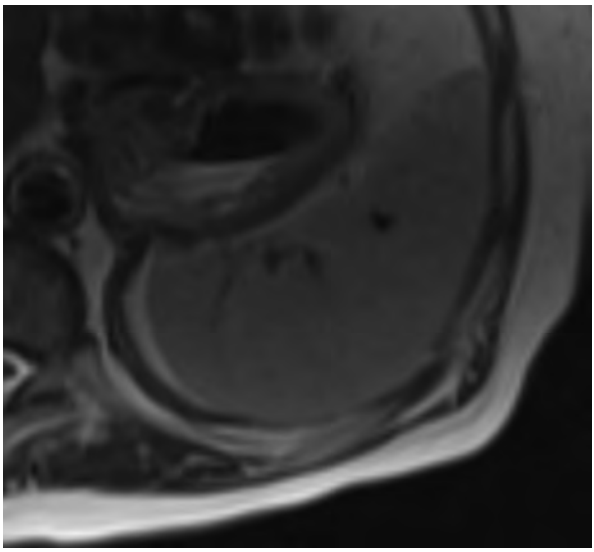

Fig. 2.32 Axial MRI of the spleen, HASTE sequence. The spleen is smooth in contour with homogeneous signal intensity

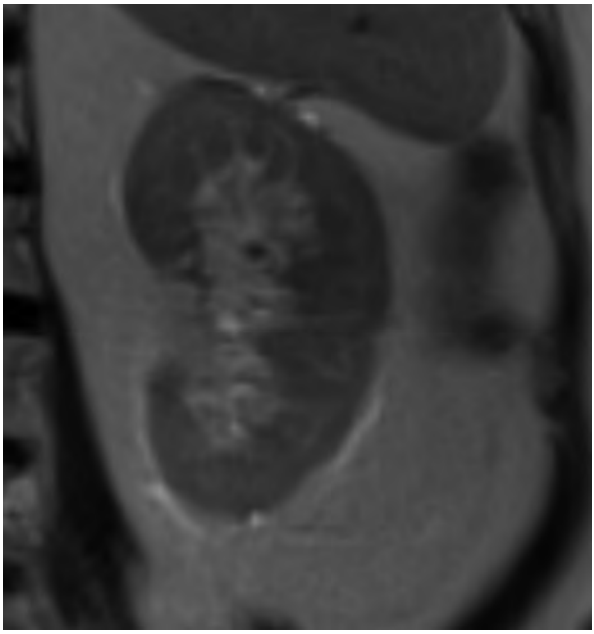

Fig. 2.33 Coronal MRI of the kidney, HASTE sequence. The kidney is smooth in contour

T2 Fat-Saturated (Fat Sat) Sequence

- This can be helpful for evaluating edema and ascites as fluid will have increased signal intensity.

In- and Out-of-Phase Sequences

- This sequence pair evaluates for macroscopic fat.
- On out-of-phase images, fat-containing tissue will have a black outline called india ink artifact (Fig. 2.34).
- On in-phase images, this artifact will null.
  - Loss of signal on out-of-phase imaging is consistent with macroscopic fat (Fig. 2.35).
- This sequence pair is helpful in diagnosing hepatic steatosis, adrenal adenomas, and teratomas among other fat-containing pathologies.

MRCP Sequences

- This is a heavily T2-weighted series of sequences used to evaluate the biliary tree.
- Multiple sequences in multiple planes and angles may be used to capture the complete tree.

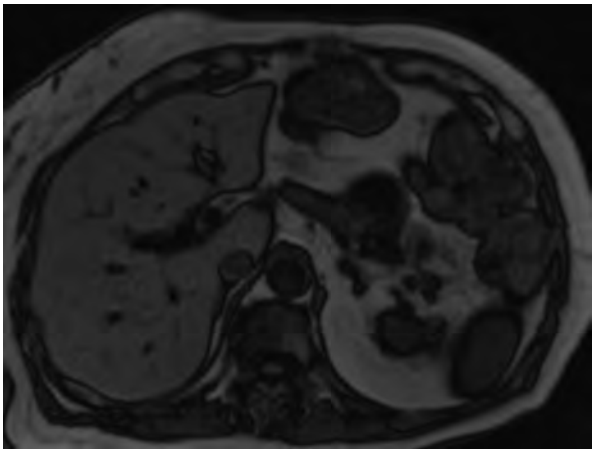

Fig. 2.34 Axial MRI of the abdomen, out-of-phase sequence. Note the india ink artifact around fat-containing organs

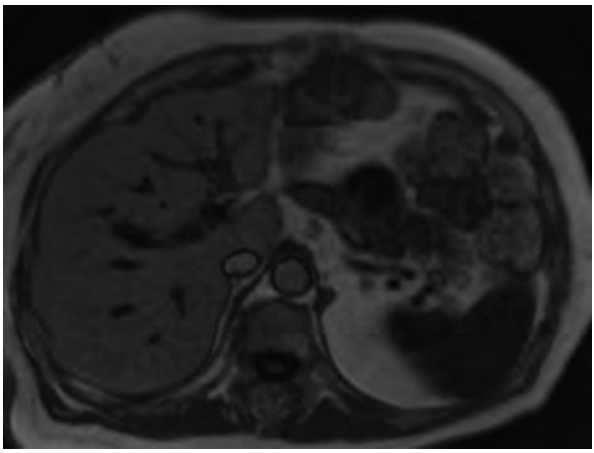

Fig. 2.35 Axial MRI of the abdomen, in-phase sequence. The india ink artifact is nulled

- Follow the common bile duct into the liver, the gallbladder, cystic duct, pancreatic ducts looking for dilation, filling defects, and cystic lesions.

Diffusion

- When assessing a lesion, look for restricted diffusion.
- For a lesion to truly restrict diffusion, there must be a corresponding loss of signal on ADC mapping.
- Hypercellular lesions, abscesses, and many neoplastic lesions will restrict diffusion.

T1 Pre- and Postcontrast Sequences

- Precontrast T1
  - This is the best sequence to evaluate the pancreas as it has a high percentage of fat.
  - Look for blood products, which will appear hyperintense.
  - Look to see anything suggestive of fluid on T2 becomes isodense of T1, suggesting simple fluid.
- Postcontrast sequences usually include an arterial phase, a portal venous phase, and a series of timed delayed sequences.
- Different pathologies have expected patterns of enhancement and washout.
- Of note, contrast is not necessary for the evaluation of rectal cancer.

Conclusion

- Developing a complete and reliable search pattern for each modality of imaging in the abdomen is essential to the success of an early radiologist.
- Again, this is a flexible construct and evolves throughout the radiologist's career.
- This chapter provides a basic framework for each modality to build upon with time and experience.

Reference

1. Bruno M, Walker E, Abujudeh H. Understanding and Confronting Our Mistakes: The Epidemiology of Error in Radiology and Strategies for Error Reduction. Radiographics. 2015;35:1668–76.

Hepatobiliary Imaging

3

Matthew E. Maeder and Vidal A. Villela

- **Hepatobiliary Anatomy**
  - Liver

    The liver is largely covered by peritoneum except for the bare area on the posterior right lobe (Fig. 3.1).

    Peritoneal reflections form a few ligaments, for example, the falciform ligament divides the left lobe into medial and lateral segments.
  - Hepatic blood supply

    Hepatic arteries provide about 20% of blood inflow.

    Most commonly, the right and left hepatic arteries arise from the common hepatic artery (Fig. e3.1).

Supplementary Information The online version contains supplementary material available at https://doi.org/10.1007/978-3-031-76624-4_3.

M. E. Maeder (✉)
Geisel School of Medicine at Dartmouth, Hanover, NH, USA

Dartmouth-Hitchcock Medical Center, Lebanon, NH, USA
e-mail: matthew.e.maeder@hitchcock.org

V. A. Villela
Dartmouth-Hitchcock Medical Center, Lebanon, NH, USA
e-mail: vidal.a.villela@hitchcock.org

© The Author(s), under exclusive license to Springer Nature Switzerland AG 2024

T. Catanzano (ed.), *What Radiology Residents Need to Know: Abdominal Radiology*, What Radiology Residents Need to Know,
https://doi.org/10.1007/978-3-031-76624-4_3

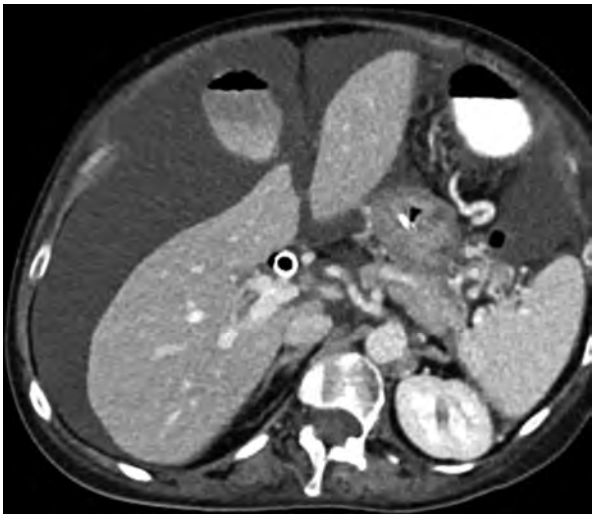

Fig. 3.1 Axial CT image in a patient with ascites. Note the only part of the liver not in contact with peritoneal free fluid is the posterior right lobe, the "bare area" not included in the peritoneal cavity

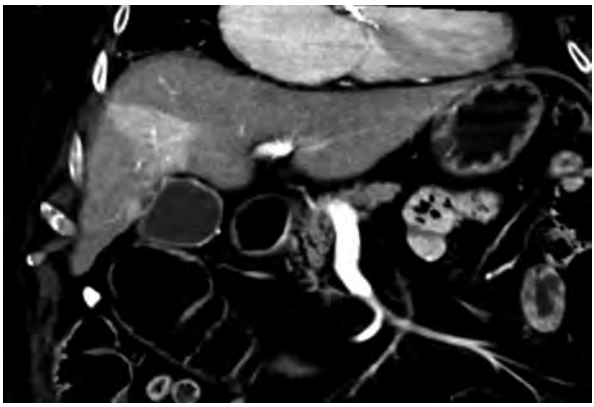

Fig. 3.2 Coronal CT image of the liver. There is a wedge-shaped hyperenhancing portion of the right lobe. Note the nondisplaced, nondistorted hepatic vessels within the area. This is a perfusional abnormality, also referred to as a transient hepatic attenuation difference (THAD)

The main portal vein provides about 80% of blood inflow. It brings blood from the bowel and spleen.

The dual blood supply means hepatic infarcts are extremely rare.

Mismatched arterial/venous blood in one area of the liver will cause altered enhancement, a fairly common observation (see Fig. 3.2).

Blood outflow from the liver is via hepatic veins superiorly toward the IVC.

– Hepatic lobes

Caudate lobe

- This is the smallest lobe.
- Located posteriorly and centrally next to the IVC.

Left lobe

- The left hepatic vein divides the medial and lateral left lobe.

- The falciform ligament is a peritoneal reflection that divides the left lobe to variable degrees; sometimes exactly along the left hepatic vein.

Quadrate lobe
- The least often mentioned lobe; many consider it to be part of the left lobe.
- It is located below the portal vein and sandwiched between the falciform ligament and gallbladder fossa.

Right lobe
- The largest in the majority of the population.
- It is separated from the left lobe by the middle hepatic vein (Cantlie's line), on a line roughly from the IVC to the gallbladder fossa.

– Hepatic segments

Each anatomic segment has its own arterial and portal venous blood supply, hepatic venous, and biliary drainage.
- Couinaud ("*kwee-no*") segments are easy to remember and are the most widely known (see Fig. e3.2).
  - Utilization of segments enables clear reporting and communication with surgeons and interventionalists.
  - Arabic (1–8) and Roman (I–VIII) numerals are both correct and widely used.
  - Segments are divided by hepatic veins and portal veins. This is easiest to learn from images, see below.
- Caudate lobe = segment 1.
- Left lobe = segments 2–4.
  - Segment 2 is on the top of segment 3, both near midline, divided by the entering portal vein.
  - Segments 4A and 4B are between the left hepatic vein and gallbladder fossa/middle hepatic vein.

    4A is on the top of 4B, divided by the entering portal vein.

    The quadrate lobe is essentially segment 4B.
- Right lobe = segments 5–8.
  - The right lobe is posterior to the middle hepatic vein (Cantlie's line).
  - Beginning with segment 5 anteriorly and inferiorly, continue in a circular pattern posteriorly, superiorly, and then anteriorly.

– Biliary system

The biliary system is responsible for collecting bile and delivering it to the intestinal tract.

The largest component is the common bile duct (CBD), between the cystic duct of the gallbladder and the ampulla of Vater.
- Normal CBD diameter is 6 mm or less.
  - Trends higher with age over 60 years and after cholecystectomy.

    Add 1 mm for every decade, so at 70 years think 7 mm, 80 years think 8 mm, and so on.

The common hepatic duct is above the CBD and cystic duct junction.
Right and left hepatic ducts join to form the common hepatic duct in most of the population.

- Gallbladder
  Stores and concentrates bile for ejection into the intestinal tract after eating.
  - The gallbladder backfills with bile when the sphincter of Oddi closes at the ampulla of Vater.

- **Optimal Modalities for the Assessment of the Hepatobiliary System**
  - CT
    This is a rapid and thorough cross-sectional scan able to capture every portion of the liver.
    - CT can evaluate diffuse liver diseases like cirrhosis and steatosis.
    - A limitation of CT is that small lesions under 1 cm may be incompletely characterized, even with multiphasic CT.

    CT is often adequate for evaluating biliary obstruction; however, it is otherwise fairly nonspecific in the biliary tree.
    - Based upon the varied composition of gallstones, approximately 4/5 are not visible on conventional CT.
  - MRI
    MRI is better suited to characterize focal liver findings than CT. Examples to follow in "Focal Liver Lesions" section.
    It takes longer and is more prone to artifacts from motion, metal, and large-volume ascites than CT.
    MRCP
    - Magnetic resonance cholangiopancreatography (MRCP) is a type of MRI study where heavily T2-weighted fluid-sensitive images are acquired to evaluate the biliary tree.
    - The best choice for evaluation of the biliary tree (see Fig. e3.3).
  - Ultrasound
    It is the test of choice for acute gallbladder disease.
    It has the benefits of avoiding ionizing radiation to acquire images and being a portable and inexpensive modality.
    Ultrasound is extremely operator-dependent and is dependent upon patient factors such as body habitus and ability to hold breath.
    Ultrasound can image some of the CBD but not many other bile ducts.
    It is excellent for simple cyst characterization but has low specificity for most solid liver lesions.
    - It can evaluate diffuse liver disease such as cirrhosis and steatosis, and is used for screening cirrhotic livers for solid masses.
    - Ultrasound elastography can quantify the liver's stiffness and correlate with a degree of fibrosis.
  - Nuclear medicine

HIDA

- The workhorse of nuclear medicine hepatobiliary imaging is the hepatobiliary iminodiacetic acid (HIDA) scan. It is also known as hepatobiliary scintigraphy.
- A tracer is injected intravenously and metabolized by the liver and then excreted with bile.
  - The agent is an iminodiacetic acid analog with Technetium-99m attached.
- The study can assess bile concentration and excretion into the biliary tree, gallbladder, and small intestine (see Fig. 3.3).
- It is useful for diagnosing acute cholecystitis, bile duct obstruction, and bile leaks.

PET/CT

- Position emission tomography is usually performed with ^{18}F-fluorodeoxyglucose (FDG) tracer. Newer agents can target somatostatin receptors and prostate-specific membrane antigen and are beyond the scope of this chapter.
- FDG uptake in the liver is normal and fairly homogeneous (see below).
- Lesions above background liver uptake are "hypermetabolic" (Fig. 3.4).
- PET/CT has excellent sensitivity and specificity for metastatic disease for lesions 1 cm and larger. It is less sensitive for smaller lesions.

- **Evaluating Liver Images**
  - US

    First assess liver size and echotexture, then screen for focal findings.

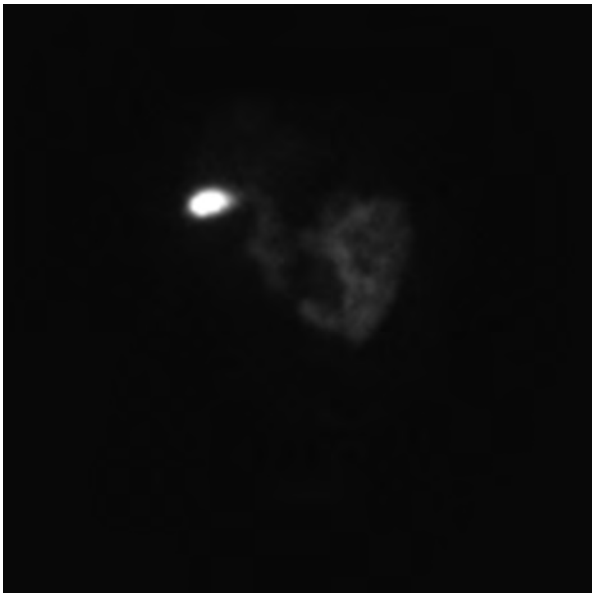

Fig. 3.3 Normal HIDA scan. Tracer is concentrated in the gallbladder and has already passed on to the proximal small bowel

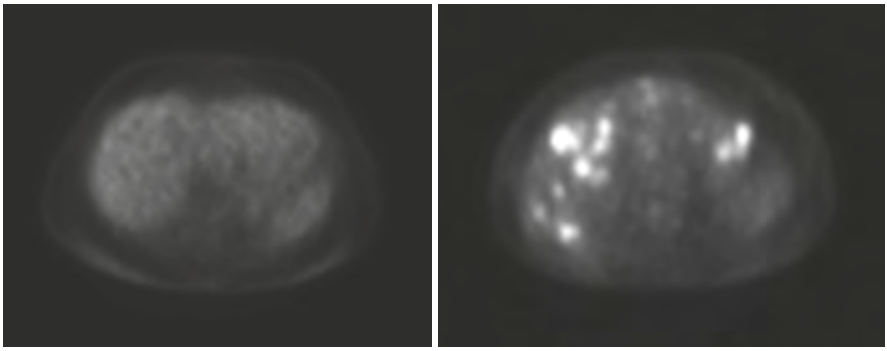

Fig. 3.4 Normal homogeneous liver background uptake on PET scan (left). Lesions with higher FDG uptake are hypermetabolic metastases (right)

- "Normal" craniocaudal liver span varies, most use 16–18 cm when measuring in the vertical right midclavicular line.

US is unable to fully view large and/or fatty livers that prevent sound waves from penetrating deeply.

Ultrasound intravenous contrast does exist, but is not FDA approved in the United States at the time of this publication.

– CT

First assess size, contour, and attenuation.

Most use 18–20 cm as the normal maximum coronal dimension of the right lobe, which is usually not the vertical midclavicular line (see Fig. e3.4).

The liver is commonly scanned in the portal venous phase (60–70 s after IV contrast injection).

- The portal veins should all be visible. Suspect thrombus (or gas) in any dark portal vein branch.

Normal parenchymal attenuation depends on phase. During the portal venous phase, about 80–100 Hounsfield units (HU).

– MRI

A benefit of MRI is that it includes a collection of image sets acquired at different times with different parameters.

First assess size, contour, signal, and enhancement.

T1/T2-weighted images: medium to dark gray parenchymal signal intensity.

- T1/T2 signal does not decrease much with fat suppression unless it is an *extremely* fatty liver (see Fig. 3.5).

Post-gadolinium contrast images: several time points can be rapidly acquired.

- By digitally subtracting a noncontrast image set, enhancement is even more conspicuous.

In- and out-of-phase: A type of T1-weighted imaging. Useful to detect steatosis and iron overload, more about this later.

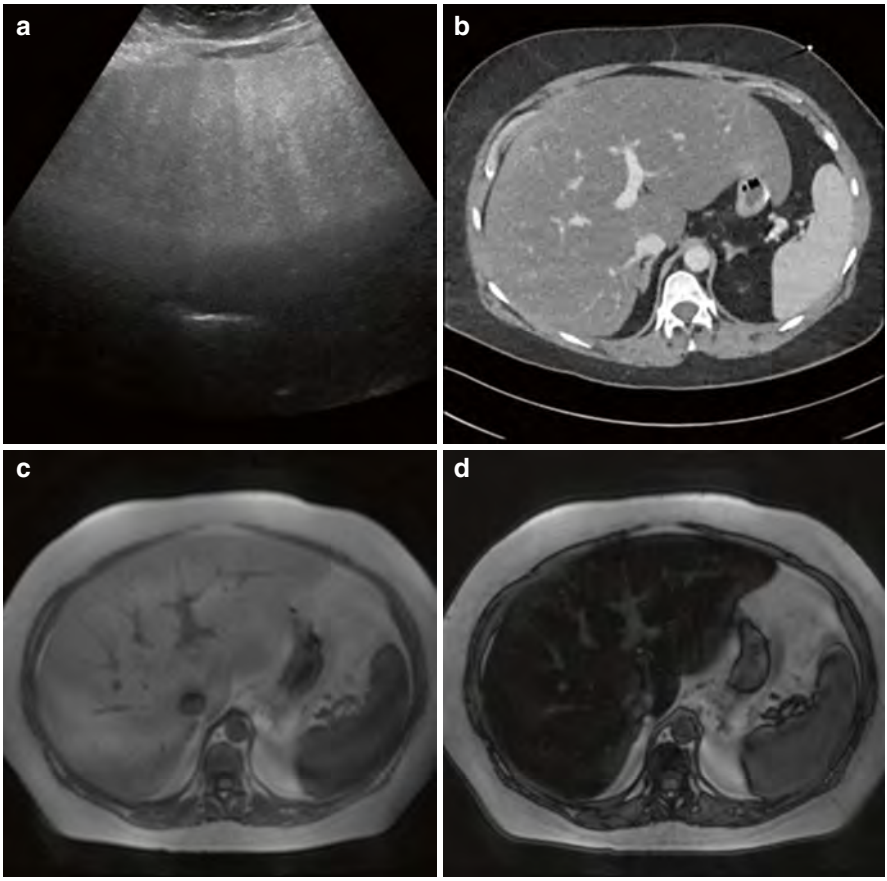

Fig. 3.5 Hepatic steatosis in one patient. (**a**) Ultrasound. The liver is bright due to echogenic fat, which obscures the view as one looks deeper relative to the transducer. (**b**) Portal venous phase CT. Diffuse low liver density (less than approximately 40 HU) is diagnostic of steatosis. (**c**, **d**) MRI in- and out-of-phase sequences. Normal livers will be equal on both images. Excess fat will cause lower signal on out-of-phase

Diffusion-weighted imaging: Exploits the microscopic motion of water in tissues to create signal. Useful to detect and characterize focal findings that prevent water from freely moving. Very prone to artifacts in the abdomen, however.

Focal Liver Lesions

- Hepatic cysts
  - Simple cysts are extremely common. They are found in 5–10% of the population.
  - They look like water on all imaging studies.

    Ultrasound: Cysts are anechoic (black).

    CT: Cysts are low density, less than 20 HU.

    MRI: Cysts are hyperintense (bright) on T2-weighted images. They are generally very dark on T1.

    Biliary hamartomas look identical to cysts and cannot be distinguished, but are usually much smaller than cysts (only a few millimeters).
  - Cysts are benign fluid-filled spaces lined by biliary epithelium. They have no connections to adjacent structures or the biliary tree.
  - Worrisome features include heterogeneity, septations, and nodules (see Fig. 3.6).

    These might suggest a different diagnosis such as biliary cystadenoma and cystadenocarcinoma, metastatic disease.
- Solid liver masses
  - Hemangioma

    Hemangiomas are benign lesions composed of disorganized blood vessels. They can be small, under 2 cm ("flash-filling" or capillary hemangioma) or large, over 10 cm ("giant hemangioma").

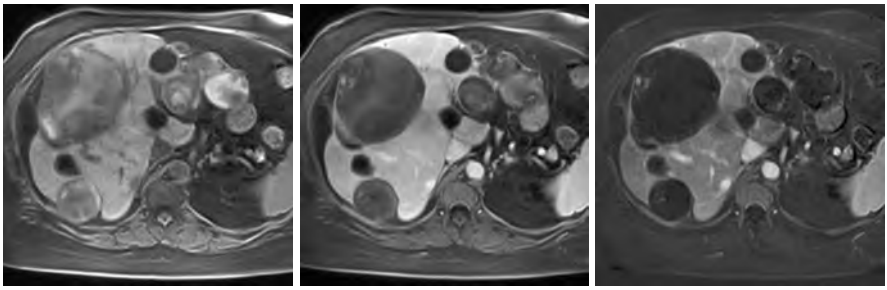

Fig. 3.6 Worrisome cysts. Axial T1-weighted fat-suppressed images of the liver before (left) and after (center) intravenous gadolinium contrast. Many are T1 dark simple cysts. Some are very heterogeneous. The digital subtraction of these two sets (right) helps us see tiny enhancing nodules in some of the cysts

Small hemangiomas may be difficult to characterize based on their contrast enhancement dynamics.

- Flash-filling hemangiomas completely enhance early on.

Discontinuous peripheral nodular enhancement that progressively fills in is pathognomonic (CT or MRI) (see Fig. 3.7).

On noncontrast MRI images, hemangiomas are markedly hyperintense on T2. On US, hemangiomas appear as a focal bright (echogenic) lesion (see Fig. e3.5).

– Focal nodular hyperplasia (FNH)

This is a benign solid lesion composed of normal liver cells in an abnormal configuration.

The cause of FNH is unknown, but may be due to a small vascular occlusion [1].

FNH have been documented to arise in patients receiving chemotherapy, particularly children.

FNH are most common in young women and have been observed to involute over the patient's lifetime.

Imaging

- US
  - The lesion is not visible in 2/3 of cases.
  - If visible, it is similar in echotexture to liver but can have a variable appearance (see Fig. 3.8).
  - The central scar characteristic of an FNH may be visible in larger lesions.
- CT
  - This is a "stealth lesion" on unenhanced CT since it may be equal or slightly lower density to normal liver parenchyma (see Fig. e3.6).
  - On contrast-enhanced CT, it may not be visible or may be slightly hyperattenuating on portal venous phase imaging.

Fig. 3.7 Portal venous CT with anterior liver lesion. A hemangioma can be diagnosed on a single phase when the classic enhancement pattern such as this is encountered. If in doubt, multiphase CT or MRI will increase confidence

Fig. 3.8 Sagittal grayscale US image shows subtle ill-defined brightness in the region of a known FNH in the posterior right lobe, several centimeters in size. Often, an FNH will be identical to the liver around it on US

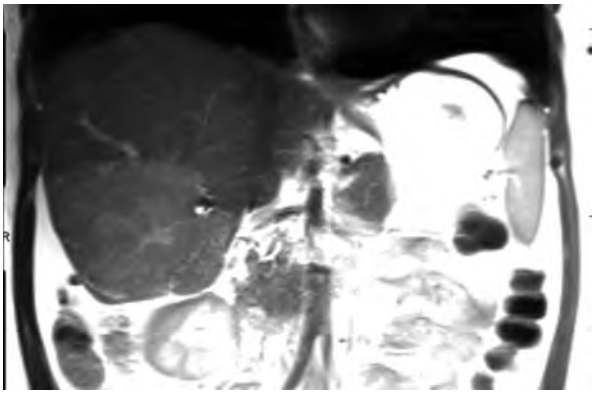

Fig. 3.9 A mildly T2-hyperintense "scar" in the center of a slightly hyperintense FNH on this coronal T2-weighted image of the liver

  - On dedicated liver mass imaging, the lesion is hypervascular on late arterial phase and will equilibrate on portal venous and delayed phases.
- MRI
  - An FNH is slightly darker on T1WI and slightly hyperintense on T2WI compared to normal liver. It will not be as high in T2 signal as a cyst or hemangioma (see Fig. 3.9).
  - A helpful but infrequent feature is a central T2 hyperintense "scar."
  - MR is the test of choice, particularly when using a hepatocyte-specific gadolinium contrast agent (gadoxetate disodium).

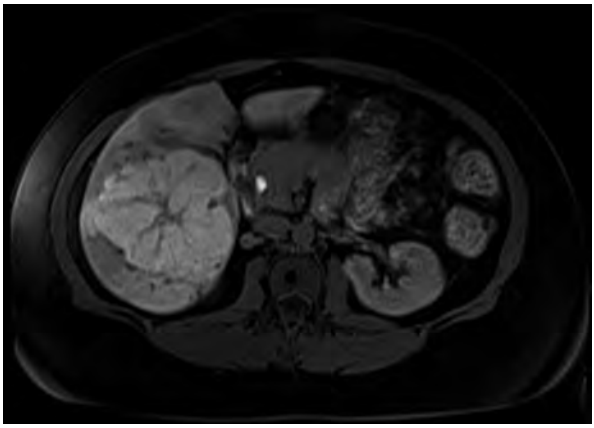

Fig. 3.10 MRI with hepatocyte-specific contrast agent. FNHs contain hepatocytes that are unable to excrete the contrast and will retain the contrast agent for hours. Contrast from the normal liver has been excreted into the CBD and duodenum, seen as bright spots medial to the FNH

  - On hepatocyte phase imaging (20 min after hepatocyte-specific contrast administration), an FNH will characteristically retain the contrast and be hyperintense, although it may occasionally be isointense to the adjacent liver (see Fig. 3.10).
- Adenoma

  This is a rare neoplasm that usually occurs in young women.

  While benign, there is a risk of hemorrhage (16%) and malignant transformation (4%).

  Risks vary with each of the eight known adenoma subtypes.
  - Subtypes are beyond the scope of this chapter but include sonic hedgehog-activated, inflammatory, HNF 1 alpha mutated, beta-catenin mutated [2].
  - Imaging features are not reliable in distinguishing the subtypes.

  General imaging appearances
  - US
    - Nonspecific. Circumscribed, heterogeneous mass with varying levels of echogenicity.
  - CT
    - Nonspecific. Circumscribed lesion with varying levels of density, often isoattenuating to surrounding liver.
  - MRI
    - This is the preferred modality for diagnosis (Fig. e3.7). Suggestive features include

      Microscopic fat, which is seen on in- and out-of-phase images—not fat-suppressed images.
      - The fat will lose signal on out-of-phase images like steatosis, thus will appear darker.

      Mild–moderate T2 hyperintensity.

      There is arterial phase hyperenhancement, which then equilibrates and become isointense at portal venous and later phases.
    - Note: Some subtypes can retain hepatocyte-specific contrast during hepatobiliary phase, enhancing exactly like FNH (see Fig. 3.11) [1].

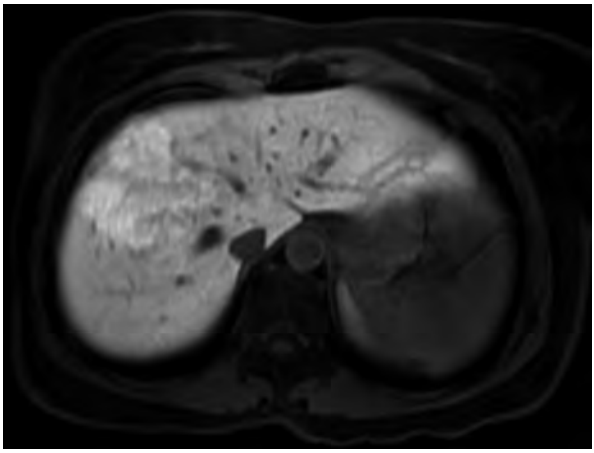

Fig. 3.11 MRI with hepatocyte-specific contrast. This large hyperintense mass surrounded by normal liver was prospectively called FNH. This was an adenoma, biopsy proven

– Metastatic disease

The liver is a common site for metastatic disease, especially from GI, pancreatic, gallbladder, lung, breast, and melanoma primaries.

A large necrotic (or mucinous) metastasis can mimic an abscess, or occasionally a complicated cyst/cystadenoma.

US

- Metastases are variable in echogenicity but are usually darker (hypoechoic) than the surrounding liver.
- Morphology can be cystic/necrotic, solid, circumscribed, ill-defined, or targetoid like a bull's eye (see Fig. e3.8).

CT

- Metastases are variably sized, usually ill-defined and hypoattenuating lesions (see Fig. 3.12).
- Most metastases are seen best on portal venous phase imaging, particularly hypovascular tumors such as adenocarcinoma.
- Hypervascular metastases (e.g., renal cell carcinoma) may be most visible during the late arterial phase (~40 s), so a dual-phase scan is warranted in specific cases.

MRI

- Metastases have variable signal and enhancement characteristics.
- Continuous ring enhancement and washout of a mass help differentiate metastases from hemangiomas and HCC (see Fig. e3.9).
- Hepatocyte-specific contrast agents are sometimes used to completely exclude small metastases. It is particularly sensitive for hypovascular colorectal lesions.
  - Hepatobiliary phase (~20 min after injection) images can detect tiny foci of disease as hypointense spots (metastases contain no hepatocytes).

– Hepatocellular carcinoma (HCC)

HCC is the fifth most common cancer worldwide.

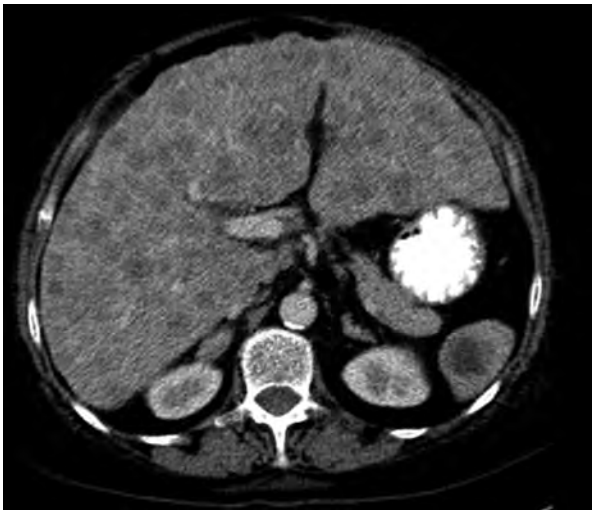

Fig. 3.12 Axial portal venous phase CT image of the same patient displays the burden of metastatic disease in the liver a little more clearly

The incidence is rising in the United States, largely due to nonalcoholic fatty liver disease, which is increasingly referred to as metabolic-associated steatohepatitis (MASH).

The major risk factor is cirrhosis, although it can very rarely arise in a normal liver.

- Screening imaging can be done with US, MRI, or CT or an alternating combination depending upon institutional preference and modality availability.
- On CT and MR, HCCs demonstrate arterial enhancement with washout on delayed phases (see Fig. 3.13).
- LI-RADS is a reporting system to describe the risk of a lesion representing an HCC in a cirrhotic liver.

– Cholangiocarcinoma (CCA)

This is a malignancy arising from bile ducts.

There are different locations that a CCA can arise from which will dictate its imaging appearance.

Hilar CCA (also referred to as Klatskin tumor)

- Ill-defined mass in the biliary hilum obstructing the hepatic bile ducts.
- Due to the fibrous nature of the lesion, the mass will often enhance late.
- There may be associated hepatic perfusion anomalies related to either the biliary obstruction or sinusoidal obstruction.

Distal extrahepatic CCA

- These tumors occur in the common bile duct or ampulla.
- The tumor usually obstructs the biliary tree and less commonly the pancreatic duct.

Intrahepatic CCA

- This tumor can be difficult to differentiate from an infiltrating HCC.

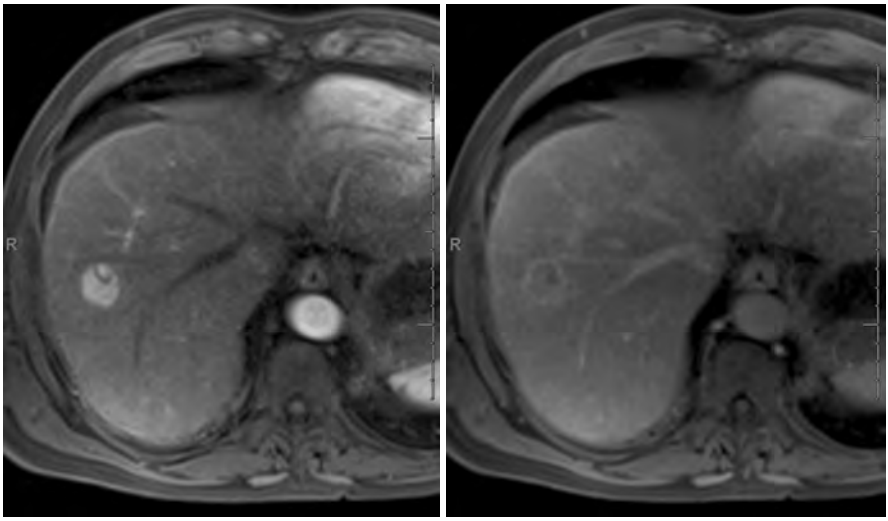

Fig. 3.13 Axial T1 fat-suppressed postcontrast MR images. The hallmark of HCC is arterial phase hyperenhancement (left) followed by contrast washout (right)

- There is an ill-defined mass obstructing peripheral bile ducts and classically shrinking that region of the liver → retraction of the liver contour.
- The capsular retraction, when present, can help differentiate CCA from HCC.

US
- It can be challenging to visualize a mass or capsular retraction.
- Displaced vessels in an area of abnormal echogenicity can suggest the presence of a mass (see Fig. 3.14).

CT
- The mass is often poorly marginated and equal to or higher in attenuation than the liver (see Fig. e3.10).
- There is slow progressive and persistent enhancement due to the fibrous nature of the tumor.
- Capsular retraction may be seen.

MRI
- The mass is often poorly marginated and equal or higher in attenuation than the liver.
- There is slow progressive and persistent enhancement due to the fibrous nature of the tumor (see Figs. 3.15 and 3.16).
- Capsular retraction may be seen.
- The mass is often mildly higher T2 signal than adjacent normal liver.

- **Diffuse Liver Disease**
  - Steatosis

    This is due to excess lipid in hepatocytes.

    It can be diffuse or focal.

Fig. 3.14 Ultrasound image of the central liver with vague increased echogenicity centrally. Some dilated bile ducts can be seen as black dots and lines on the left side of the image

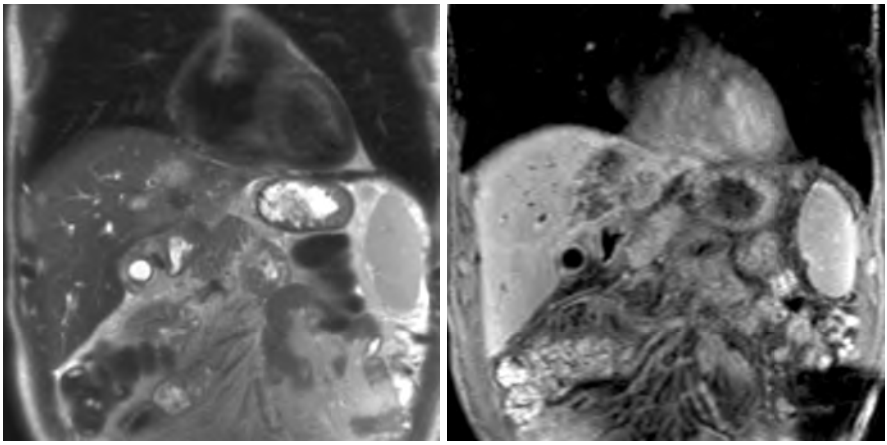

Fig. 3.15 Coronal T2 (left) and T1 fat-suppressed 5 min postcontrast (right) images of the liver. The cholangiocarcinoma in the left lobe is slightly higher T2 signal. Areas of mild and absent enhancement after contrast

Steatosis can develop or resolve slowly over years or rapidly within a month.

Imaging findings were previously demonstrated in Fig. 3.5.

US

- Fat is bright; steatosis is echogenic and "whites out" the liver details.
  - Focal lesions in a fatty liver are extremely difficult to detect as the ultrasound beam can often not penetrate the liver.
- Areas of focal fat (or focal fat sparing) can simulate masses.

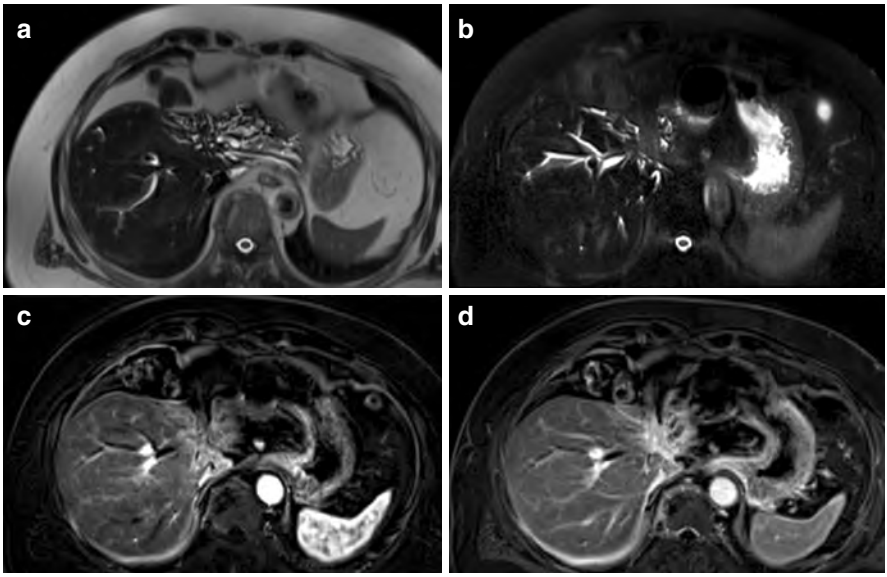

Fig. 3.16 Axial MR images of cholangiocarcinoma. (**a**) T2, dilated bile ducts in the left hepatic lobe with atrophy and capsular retraction. (**b**) T2 fat-suppressed. The mass is barely visible as a dark gray area between the dilated bile ducts. (**c**, **d**) Postcontrast digital subtraction sequences. The mass enhancement increases over time from (**c**) to (**d**)

- One tip to suggest focal fat/fatty sparing is to put on color Doppler—the vessels will course through fat but be displaced by a mass.

CT

- Density values lower than 80 HU on portal venous phase CT (or 40 HU on noncontrast CT). Some use liver density lower than spleen density by 10 HU or more to make the diagnosis.
- Fatty infiltration or sparing are often in the same characteristic locations: anterior to the right portal vein, near the gallbladder fossa, and near the falciform ligament.

MR

- Opposed phase (in and out) gradient echo sequences are the sequence of choice to identify steatosis.
- In a normal liver, both image sets show the same signal. In steatosis, lower signal on out-of-phase images is commonly referred to as dropout (see Fig. 3.5).
  - Another descriptive phrase for this signal loss is phase cancellation artifact.

– Amiodarone toxicity

Amiodarone is an iodine-based anti-arrhythmic.

Patients taking this may have abnormally high attenuation in the liver, with or without hepatic dysfunction or symptoms.

After seeing many normal livers, a hyperattenuating liver (over ~100 HU on portal venous CT) might catch your eye and prompt you to consider this diagnosis (see Fig. e3.11).

– Iron overload

The most common causes of excess liver iron concentration are hereditary hemochromatosis and repeated blood transfusions.

Excessive iron can damage hepatocytes and lead to fibrosis and then cirrhosis.

CT

- Diffuse high attenuation can suggest this diagnosis.
- Other disorders with a similar appearance are amiodarone toxicity, Wilson disease, and gold therapy (e.g., for rheumatoid arthritis).

MRI

- The simplest evaluation is opposed phase sequences.
- The signal characteristics are directly opposite of steatosis: lower signal on *in*-phase.
- There are specific MR sequences that can quantify the amount of iron in a liver but they are not available at all centers.

– Cirrhosis

It is the result of chronic liver damage with necrosis, inflammation, and fibrosis eventually leading to a shrunken and nodular morphology.

- On all modalities, the classic appearance is a small liver with a nodular contour (see Fig. 3.17).
- All lobes may be affected equally. In some patients, the right lobe is the most shrunken and the caudate or left lobes may hypertrophy to compensate.

– Pseudocirrhosis

Any process that mimics cirrhosis by other means [3].

Causes include

- Chemotherapy (any agent).
- Chemotherapy-related ischemia.
- Fibrotic changes from certain liver metastases, breast cancer being a common etiology.

– Liver transplant appearance

A donor liver is placed in the original cavity ("orthotopic liver transplant" or OLT).

It is connected to the common/proper hepatic artery and main portal vein.

The common hepatic duct/common bile ducts are anastomosed.

The donor intrahepatic IVC is anastomosed with the recipient IVC.

Except for a few surgical clips, a transplant liver usually looks like a normal native liver.

- **Gallbladder**

– Anatomy

Blind ending organ

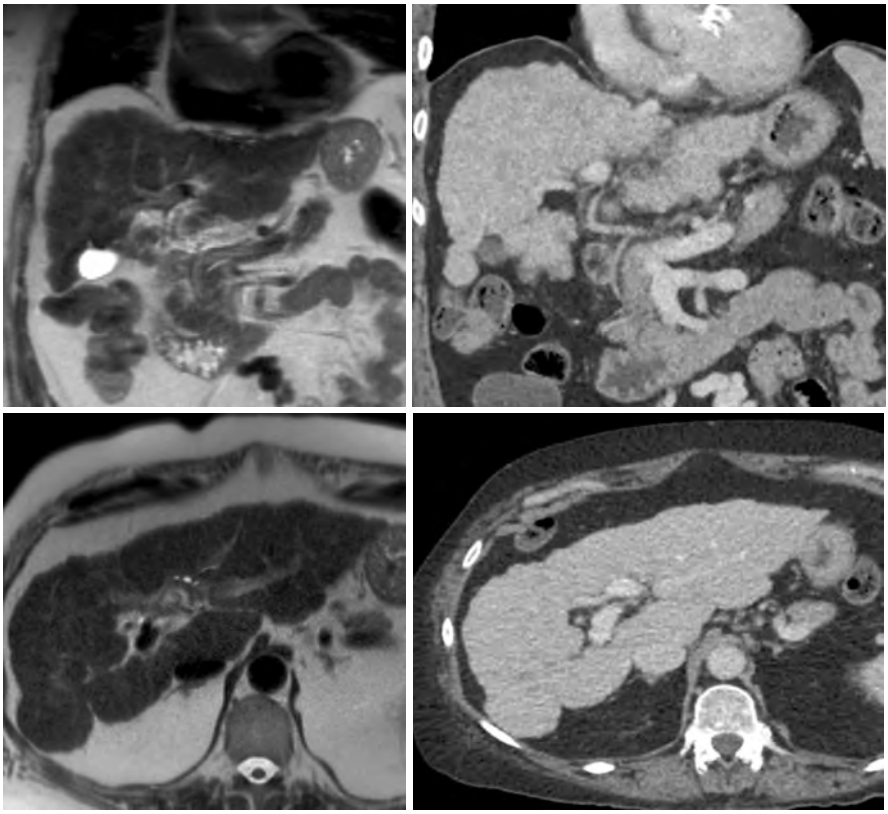

Fig. 3.17 Coronal and axial T2 (left) and coronal and axial CT (right) images of a cirrhotic liver

- Fundus is the blind end, body is in the middle, and neck connects to the cystic duct.
- Cystic duct serves as a single point of entry and exit (see Fig. e3.3).
  - The organ is very small and prone to obstruction.
  - Joins the common hepatic duct to form the common bile duct.

– Cholelithiasis

This is the condition where there is the presence of gallstones without inflammation (see Fig. 3.18).

80% of stones are composed of cholesterol; the remaining 20% have a component of pigment/calcium.

- Ultrasound
  - This is the most sensitive modality for stone detection.
  - Stones appear as mobile echogenic foci with posterior acoustic shadowing.
  - The wall-echo-shadow (WES) sign occurs if the gallbladder is filled with stones and very little liquid bile.

Fig. 3.18 A solitary gallstone in the gallbladder on ultrasound

  - In the WES, the gallbladder may appear as a crescentic echogenic structure that can be difficult to differentiate from the bowel.
- CT
  - Usually only calcified stones will appear as hyperattenuating compared to bile (see Fig. 3.19).
  - Pure cholesterol stones are iso- to hypoattenuating (i.e., routinely invisible).
- MR
  - Cholesterol stones are T1 and T2 dark (see Fig. e3.12).
  - Pigment stones are T1 bright.

– Acute cholecystitis

Etiologies

- Calculous (most common).
  - Gallstone impacted in the GB neck or cystic duct.
- Acalculous (rare).
  - This usually occurs in the critically ill, for example, ICU patients.
  - Contributing factors include bile stasis, gallbladder ischemia, and/or systemic infection. Rarely can be caused by Epstein–Barr virus.

US

- Distended gallbladder with wall thickening (>3 mm), hyperemia on Doppler images, and pericholecystic fluid (see Fig. 3.20) [4].
- A positive sonographic Murphy's sign is the most specific imaging finding of acute cholecystitis.

Fig. 3.19 Axial CT image of the abdomen with a solitary calcified stone in the gallbladder

Fig. 3.20 Ultrasound of acute calculus cholecystitis. Walls are thickened to several millimeters. In this image, a stone lies dependently with a dark acoustic shadow below it

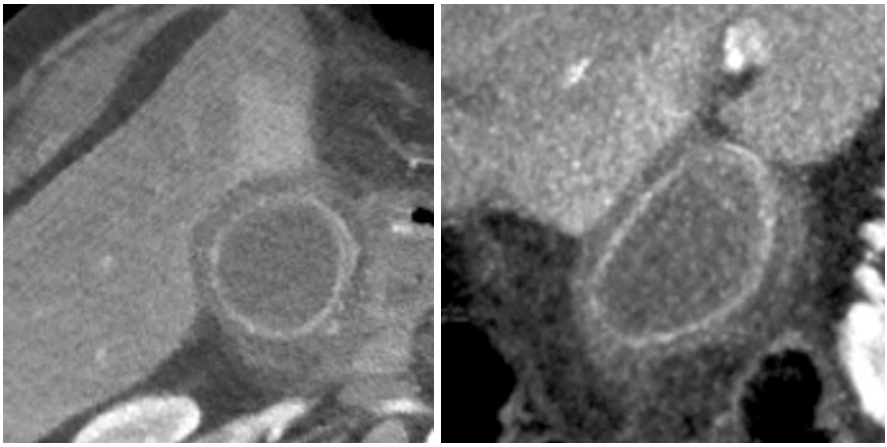

Fig. 3.21 Portal venous axial CT images. Acute cholecystitis without visible cause

  - It is defined as intense pain when the US probe is removed from the gallbladder (it is a peritoneal rebound effect).
  - The presence or absence should always be reported by the sonographer as this is a dynamic, real-time finding.
  - The sign can be unreliable in some patients, for example, if analgesics were given in the acute care setting.

CT

- The findings can be relatively nonspecific in milder cases.
- In more advanced cases, there may be gallbladder distention, wall thickening, mucosal hyperenhancement, pericholecystic fluid and fat stranding, and reactive hyperenhancement of the adjacent liver (see Fig. 3.21).
- If the pericholecystic inflammatory response is advanced, there may be secondary wall thickening of the hepatic flexure of the colon, which can make differentiation from a primary colitis difficult.

MRI

- MRI is generally not the first-line examination, particularly since acutely ill patients have difficulty lying still for the imaging.
- All of the findings seen on CT may be seen on MR, with a higher sensitivity for cholelithiasis and choledocholithiasis.

Nuclear Medicine HIDA scan (cholescintigraphy)

- This study involves injection of a radioisotope that is excreted through bile.
- If the radioisotope fails to accumulate in the gallbladder within 1 h of injection, this suggests an obstructed cystic duct.
- If there is no gallbladder filling at 1 h, follow-up with morphine to constrict the sphincter of Oddi OR continue imaging for 3 additional hours.

Fig. 3.22 Chronic cholecystitis. Coronal CT image displays gallbladder wall thickening, greatest in the neck. There are several small wall calcifications from repeated inflammation

- If radioisotope fails to accumulate gallbladder by 3 h, this is diagnostic of an occluded cystic duct, allowing a diagnosis of acute cholecystitis to be made (see Fig. e3.13).

– Chronic cholecystitis

  This is a chronic inflammatory process, usually associated with cholelithiasis and a component of dysmotility.

  US, CT, and MRI are nonspecific and findings may include stones and wall thickening. The gallbladder may be distended *or* contracted (see Fig. 3.22).

  Nuclear medicine is diagnostic

  - The gallbladder will accumulate radioisotope (unlike acute cholecystitis), but emptying is diminished.
  - An ejection fraction (EF) is calculated after a cholecystokinin analog is administered. An EF <35% is diagnostic.

– Gangrenous cholecystitis

  This is a complication of acute cholecystitis characterized by necrosis.

  US

  - The diagnosis can be difficult to make.
  - Gas within the wall will have an echogenic appearance with dirty posterior acoustic shadowing (similar to bowel).
  - There may be discontinuity in the wall or floating membranes (see Fig. 3.23). This is more easily seen on CT.

  CT

  - Gas within the gallbladder wall.
  - There may be irregular or discontinuous mural enhancement, lack of enhancement, a frank wall defect (perforation), or intraluminal membranes.

– Adenomyomatosis

  Benign mucosal/muscular hyperplasia leading to wall outpouchings (called Rokitansky–Aschoff sinuses) → accumulation of cholesterol-rich material.

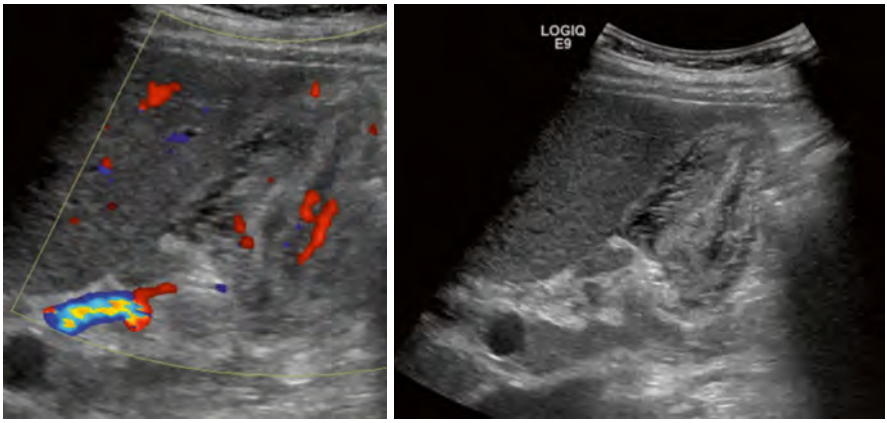

Fig. 3.23 Ultrasound of gangrenous cholecystitis. Markedly thickened gall bladder walls without visible intramural gas. Color Doppler (right) demonstrates large regions of avascularity (no color) in the abnormal gallbladder wall

- These may be diffuse, localized to the fundus, or segmental.

Not to be confused with a different disease of the uterus, adenomyosis. "Uterus" and "adenomyosis" are shorter words than "gallbladder" and "adenomyomatosis," respectively, and go together.

US

- There may be focal or generalized wall thickening with characteristic "ring-down" or "comet-tail" artifact from accumulated cholesterol (see Fig. e3.14).

CT

- There may be nonspecific focal mural thickening.
- Large sinuses can occasionally be seen as focal hypoattenuating wall structures.
- There may be visible cystic changes in the wall or enhancement of the abnormal wall; this may be mistaken for a gallbladder neoplasm.

MRI

- Sinuses have high T2 signal with classic "pearl necklace" appearance of tandem T2 bright foci lining the wall.

– Gallbladder cancer

Primary gallbladder carcinoma.

- This is rare, usually adenocarcinoma.
- There are three morphologies with similar characteristics on US/CT/MRI
  - Mass replacing the gallbladder.
  - Focal or diffuse wall thickening.
  - Intraluminal polypoid tumor.
- Heterogeneous enhancement is seen on contrast-enhanced US, CT, or MR.
- Direct liver spread is common.

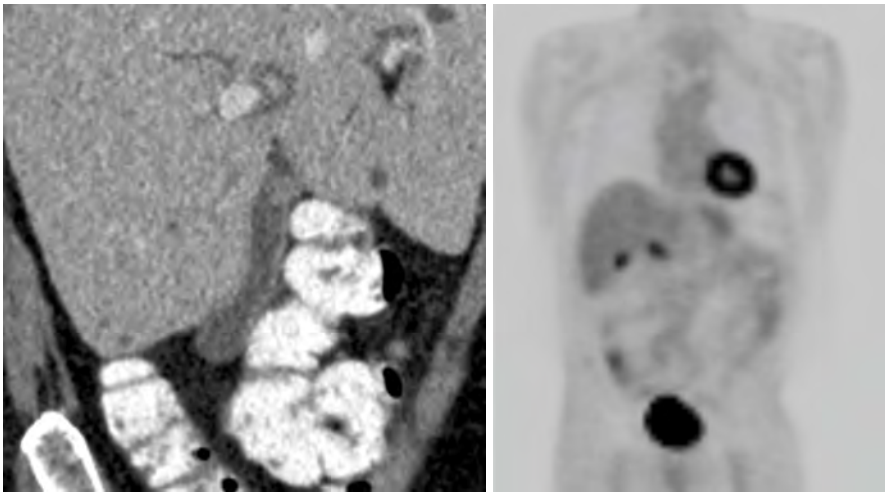

Fig. 3.24 Melanoma metastasis. Solid nodule in the gallbladder neck on portal venous CT (left). PET image confirmed the diagnosis of black, hypermetabolic metastasis in this location (right)

Gallbladder metastases
- These are rare; the most common source is melanoma.
- They present as a single or multiple solid nodule(s) (see Fig. 3.24).

– Gallbladder and cholangiopathy

This general term encompasses many different etiologies with overlapping imaging features.
- There is often stenosis ± dilatation of the bile ducts and biliary wall thickening.
- Use the clinical context to suggest a differential diagnosis.

Etiologies to consider
- AIDS cholangiopathy due to opportunistic infection.
  - For example, cryptosporidium, CMV, Mycobacterium avium-intracellulare.
  - Note: The preferred term for other infectious etiologies is cholangitis, covered later.
- IgG cholangiopathy, an autoimmune disease.
- Chemotherapy.

– Choledocholithiasis

Etiology
- Gallstones passing distally into the bile ducts commonly result in biliary obstruction.

US
- US can detect biliary ductal dilation, but has a poor sensitivity for detecting stones in the bile duct.
- Intrahepatic ducts >2 mm may be seen.
- CBD >6 mm (depends on age and presence or absence of GB).

CT
- Intrahepatic and extrahepatic biliary ductal dilation will be evident.
- Stones may be seen but attenuation is variable. Expect the same composition of stones in the GB and bile ducts.
- Coronal images are helpful to identify stones in the CBD.

MRI/MRCP
- Excellent biliary ductal assessment on T2, stones will manifest as T2-signal voids.

– Cholangiocarcinoma (CCA)

  Previously covered along with intrahepatic CCA.

– Cholangitis

  Bacteria ascend the biliary tract and can result in hepatovenous reflux and bacteremia.
  - Cross-sectional imaging is also used to determine complications, namely abscess formation.

  It is commonly a sequela of biliary obstruction (choledocholithiasis, stricture, malignancy, parasites).

  US
  - Biliary ductal dilation is seen.
  - There may be echogenic purulent material within the ducts.

  CT
  - Dense biliary contents may be present.
  - There are thickened enhancing walls of the bile ducts.

  MRI
  - Thickened enhancing bile duct walls are seen.
  - There is loss of fluid-bright T2 signal of the biliary contents with T1 intermediate signal.
  - Periportal edema is often present.

– Primary sclerosing cholangitis (PSC)

  This is an inflammatory disease associated with IBD.

  Periductal fibrosis results in alternating strictures and stenoses of the intrahepatic *and* extrahepatic bile ducts.

  Ancillary findings include hepatic perfusion abnormalities, segmental atrophy, and cirrhosis.

– Postoperative appearances of cholecystectomy

  Immediate postoperative imaging
  - US: Echogenic fat and small volume fluid in the gallbladder fossa.
  - CT/MRI: Edema and stranding in the gallbladder fossa, small volume pneumoperitoneum (more difficult to detect on MR).
  - A partial cholecystectomy may be performed if the gallbladder is difficult to remove safely, for example, densely adherent to the liver. Clinical history is critical to avoid diagnostic errors in these patients.

  Chronic findings
  - The gallbladder fossa becomes entirely fat-filled.

- Post-cholecystectomy the CBD may become ectatic, sometimes up to 12–15 mm.
  - When the gallbladder is removed, the biliary tree takes over for bile storage and must dilate to hold the extra volume.

Acute complications

- Bile leaks and bilomas: Discrete contained fluid collection (biloma) versus perihepatic fluid spilling into the abdomen/pelvis.
- Acute biliary obstruction: Injury to CBD or hepatic duct with segmental or diffuse biliary ductal dilatation on cross-sectional imaging.

Conclusion

- Hepatobiliary imaging employs many different modalities. There is a wide range of pathology you will see. Collecting a detailed history is essential. The best education is experience, and experience is enhanced with a prepared mind.

References

1. LeGout JD, et al. Focal nodular hyperplasia and focal nodular hyperplasia–like lesions. Radiographics. 2022;42(4):1043–61.
2. Tse JR, et al. Hepatocellular adenomas: molecular basis and multimodality imaging update. Radiographics. 2023;43(3):e220134.
3. Adike A, Karlin N, Menias C, Carey EJ. Pseudocirrhosis: a case series and literature review. Case Rep Gastroenterol. 2016;10(2):381–91. https://doi.org/10.1159/000448066.
4. O'Connor OJ, Maher MM. Imaging of cholecystitis. Am J Roentgenol. 2011;196(4):W367.

Pancreas

4

Brennan Morrison and Emily Van Antwerp

Basic Anatomy/Function

- The pancreas is a unique midline retroperitoneal gland with both endocrine and exocrine functions.
  - Endocrine functions: secretion of insulin, glucagon, and somatostatin.
  - Exocrine functions: production of digestive enzymes.
- The structure consists of the uncinate process, head, body, and tail.
- The main duct spans the length of the pancreas from the tail to the ampulla of Vater, near the head, and joins the common bile duct.

The main pancreatic duct drains to the major papilla (ampulla of Vater) via the duct of Wirsung and to the minor papilla via the duct of Santorini.

Normal Appearance on Imaging Modalities

- Ultrasound
  - The normal pancreas has a variable appearance on ultrasound (Figs. 4.1 and 4.2).

    Typically, it is hypoechoic, but fatty replacement with age results in increasing echogenicity.
  - Normal pancreatic echogenicity should be greater than that of the normal liver.

Supplementary Information The online version contains supplementary material available at https://doi.org/10.1007/978-3-031-76624-4_4.

B. Morrison (✉) · E. Van Antwerp
UMass Chan Medical School-Baystate, Springfield, MA, USA
e-mail: Brennan.Morrison@baystatehealth.org; Emily.VanAntwerp@baystatehealth.org

© The Author(s), under exclusive license to Springer Nature Switzerland AG 2024

T. Catanzano (ed.), *What Radiology Residents Need to Know: Abdominal Radiology*, What Radiology Residents Need to Know,
https://doi.org/10.1007/978-3-031-76624-4_4

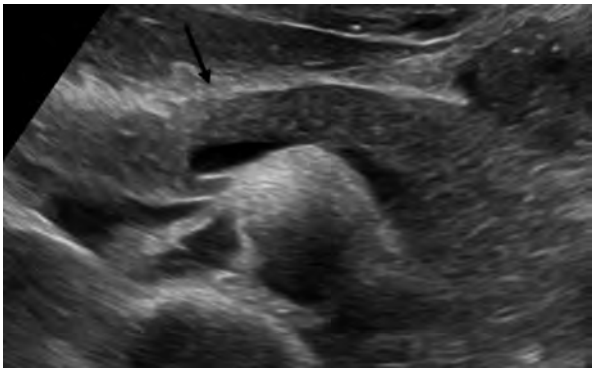

Fig. 4.1 Sagittal ultrasound demonstrating normal pancreas (arrow)

Fig. 4.2 Sagittal ultrasound demonstrating head (left arrow) and body of pancreas (right arrow)

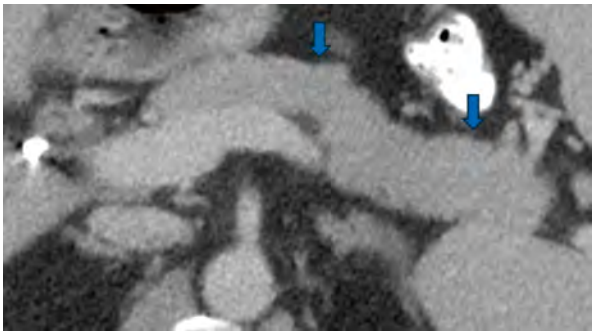

Fig. 4.3 Axial contrast enhanced CT demonstrating a normal pancreatic body (left arrow) and tail (right arrow)

  - Examination with ultrasound is frequently limited by overlying bowel gas or body habitus.
- CT
  - Contrast-enhanced CT is the modality of choice for evaluation of the pancreas (Figs. 4.3 and e4.1).
  - A specific pancreatic protocol (with and without intravenous contrast) may further differentiate abnormal pathologies.

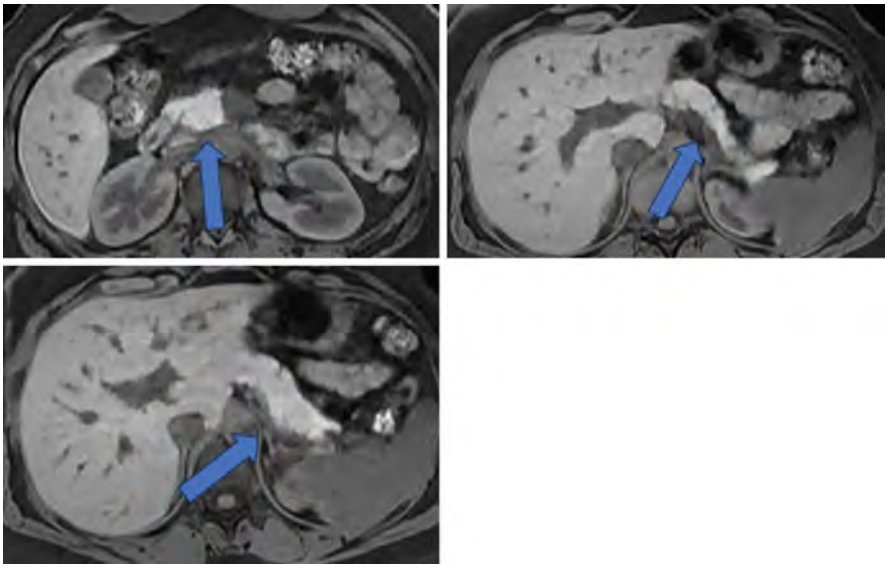

Fig. 4.4 Axial T1 weighted MRI demonstrating a normal pancreas with signal greater than or equal to the liver

- MRI/MRCP/ERCP
  - MRI is useful for evaluating the pancreatic duct for anomalies.
    Further assessment with MCRP provides greater anatomical detail, while ERCP is utilized for therapeutic intervention [1].
  - The normal pancreas should be the brightest organ on non-contrast-enhanced T1-weighted sequences (Fig. 4.4).
    Normal T1 signal intensity should be greater than or equal to that of the liver.
    T1-weighted imaging is ideal for the identification of masses and focal pancreatitis.
  - Variable signal on T2-weighted imaging with normal parenchyma demonstrating low to intermediate signal.
    Excellent for the identification of cystic lesions.
  - The parenchyma will demonstrate homogeneous contrast enhancement.
  - MRCP utilizes heavily T2-weighted sequences to optimize visualization of the ducts and adjacent biliary system compared to surrounding nonfluid-filled soft tissue.
    A normal MRCP demonstrates a continuous, normal caliber duct without filling defects (Fig. 4.5).
- Embryology and "abnormal" anatomy/congenital anomalies
  - The normal pancreas results from the fusion of the ventral and dorsal buds of the embryologic foregut.
  - Once fused, the pancreas lies to the left of the duodenum.

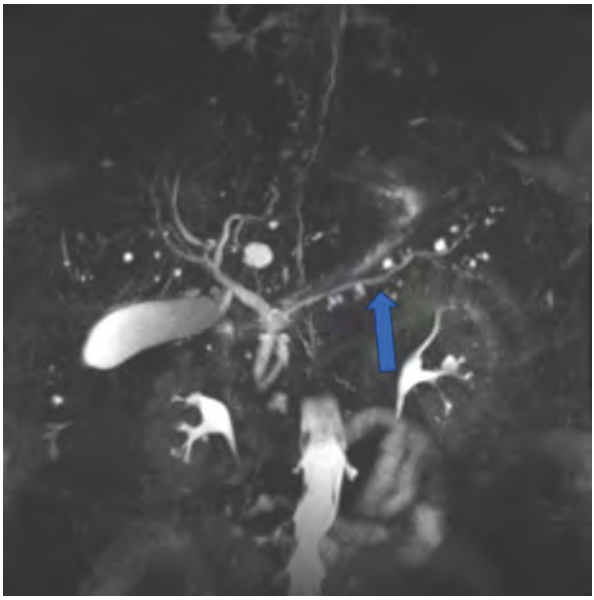

Fig. 4.5 Normal pancreas MRCP, arrow on pancreatic duct. Note the multiple T2 hyperintense cysts in the liver and pancreas

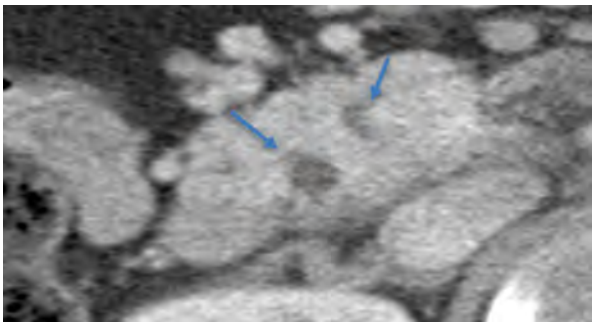

Fig. 4.6 Axial contrast enhanced CT demonstrating two distinct ducts (right and left arrows)

- The normal proximal dorsal duct of Santorini and the Ventral duct of Wirsung fuse to form the main pancreatic duct.
- The distal dorsal duct typically regresses.
- Pancreas divisum

  The most common developmental variation of the pancreatic duct resulting from the failed fusion of the ventral duct and dorsal duct, thus a single pancreatic duct is not formed.
  - Dorsal duct drains to the minor papilla; ventral duct drains to major papilla.
  - CT
    - Two distinct, noncommunicating ducts (Figs. 4.6 and 4.7).

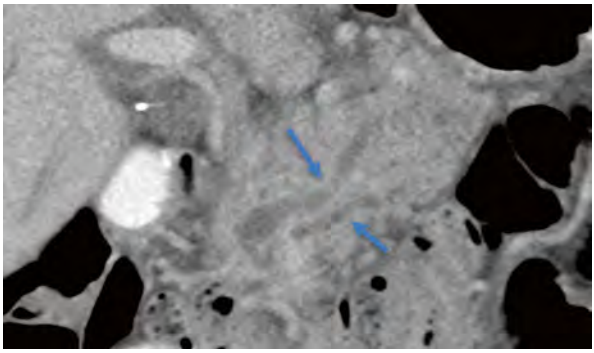

Fig. 4.7 Coronal contrast enhanced CT demonstrating two distinct ducts, the dorsal duct (upper arrow) and the ventral duct (lower arrow)

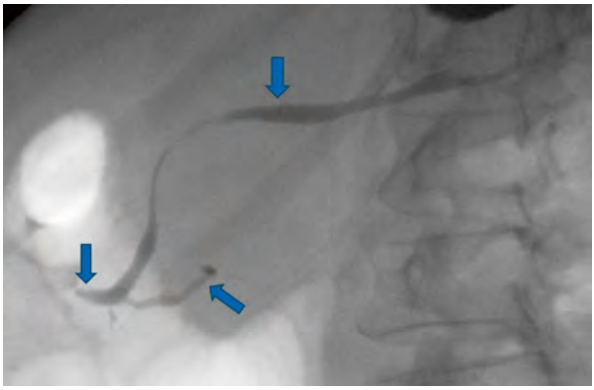

Fig. 4.8 ERCP demonstrating contrast injected into the major papilla resulting in opacification of the common bile duct and ventral pancreatic duct

- MRCP
  - MRCP is the best noninvasive imaging modality for demonstrating pancreas divisum.
  - There will be no communication between the dorsal and ventral ducts (Fig. e4.2).
- ERCP
  - Contrast injection into the major papilla results in opacification of the ventral duct only (Fig. 4.8).
  - Most accurate means of diagnosis; however, it is an invasive procedure with risks including bleeding, pancreatitis, and infection.
- Ultrasound
  - Limited utility due to frequent obscuration of the pancreas by overlying bowel gas.
- Endoscopic ultrasound (EUS)
  - Linear EUS demonstrates high accuracy in the diagnosis of pancreas divisum.
  - Absence of "stack sign."

The stack sign: Parallel orientation of the distal common bile duct, ventral pancreatic duct, and portal vein. Absence of this sign is indicative of pancreas divisum.
  - Presence of "crossed duct sign."
  - The appearance of the dominant dorsal duct crossing the intrapancreatic common bile duct to empty into the minor papilla.
- Annular pancreas

  Abnormal or failed embryologic rotation of the ventral bud and/or rotation of duodenum resulting in a partial ring of tissue around the second part of the duodenum [1].

  CT
  - Pancreatic tissue encircling the second part of the duodenum (Fig. 4.9).

  MRI
  - T1 fat saturation: hypointense bowel contents pass through a relatively hyperintense pancreas (Fig. e4.3).
  - T2 fat saturation: hyperintense bowel contents pass through a relatively hypointense pancreas (Fig. 4.10).

  ERCP
  - Ventral duct completely encircles the duodenum.

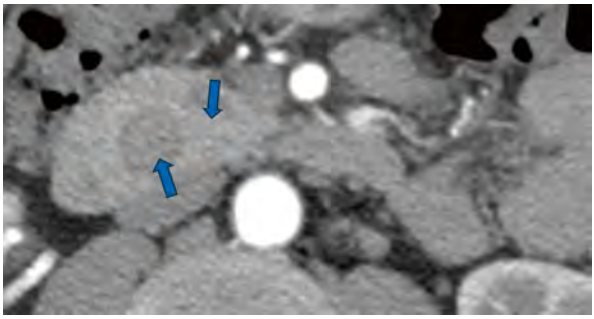

Fig. 4.9 Axial contrast enhanced CT demonstrating the pancreas (right arrow) encasing the hypodense duodenum (left arrow)

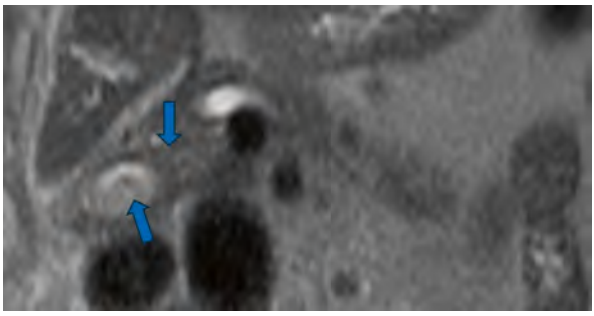

Fig. 4.10 Axial T2 weighted MRI demonstrating the hypointense pancreas (right arrow) encasing the hyperintense duodenum (left arrow)

- Pancreaticobiliary maljunction
  Abnormal junction of the pancreatic duct and the common bile duct outside of the duodenal wall.
  Abnormal junction results in a long common channel extending from high confluence of the pancreatic duct and common bile duct to the duodenum. This results in reflux between the two systems.
  Two types
  - With biliary dilatation (80%)
    - Associated with stricture of the hilar duct and typically more symptomatic.
  - Without biliary dilatation (20%)
    - Difficult to diagnose due to lack of ductal dilation.
    - Main symptom is abdominal pain.

  Ultrasound
  - Transabdominal
    - Dilated common bile duct (Fig. 4.11), nonspecific gallbladder wall thickening (Fig. 4.12).

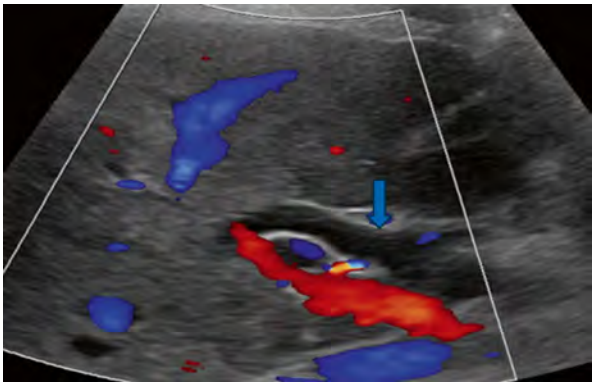

Fig. 4.11 Ultrasound demonstrated a dilated common bile duct (arrow)

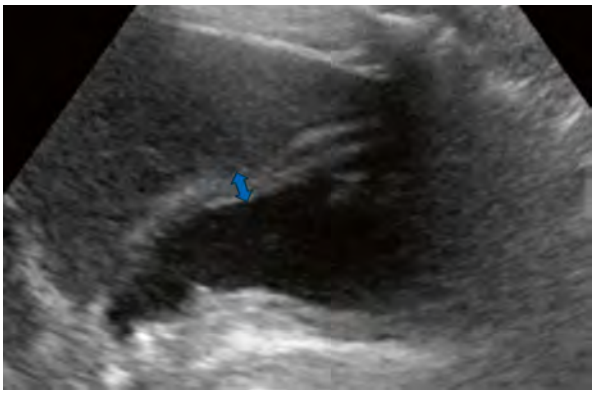

Fig. 4.12 Sagittal ultrasound demonstrating gallbladder wall thickening (arrow)

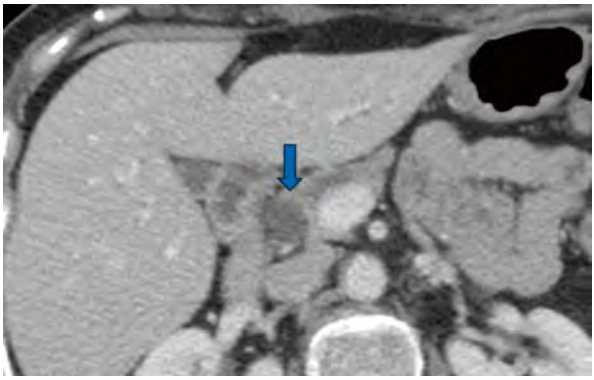

Fig. 4.13 Coronal contrast enhanced CT demonstrating dilated common duct (arrow)

- Endoscopic
  - Can confirm union of pancreatic duct and common bile duct outside of the duodenum.

CT
- Dilated common bile duct (Figs. 4.13 and e4.4).

MRI/MRCP
- Long fluid-filled channel distal to the abnormal high confluence of the pancreatic duct and common bile duct.

ERCP
- Confirms ductal abnormality and lack of normal sphincter of Oddi.
- The major risk of ERCP in pancreaticoduodenal maljunction is pancreatitis, which occurs in 3.5% of patients.
- Additional risks include bleeding, cholangitis, and infection.

Common Pathologies

- **Pancreatitis**
  - An inflammatory reaction of the pancreatic parenchyma due to the release of pancreatic enzymes within the pancreas rather than into the duodenum.
  - There are multiple inciting factors including, but not limited to, biliary obstruction, trauma, medications, and autoimmunity.
  - Diagnosis requires two of three of the following criteria:
    Clinical symptoms of pancreatitis.
    Elevated serum amylase and lipase.
    Imaging features of pancreatitis.
  - **Acute pancreatitis**
    An acute inflammatory process of the pancreas.

The most common cause is an obstructing gallstone lodged within the biliary tree.

The clinical diagnosis of pancreatitis requires two of the following criteria:

- Acute, persistent epigastric pain.
- Lipase/amylase elevation greater than three times the upper normal limit.
  - Accepted laboratory reference values for amylase and lipase
    Amylase: normal range, 19–86 U/L.
    Lipase: 7–59 U/L.
- Features characteristic of acute pancreatitis on ultrasound, CT, or MRI [2].

Ultrasound

- Enlarged, heterogeneously hypoechoic pancreatic parenchyma (Fig. 4.14).

CT

- Enlarged pancreas demonstrating homogeneous enhancement with or without adjacent inflammatory stranding (Fig. 4.15).

MRI

- Enlarged gland with loss of T1 signal. The pancreas is typically the brightest structure on T1-weighted imaging (Fig. 4.16).
- Increased parenchymal signal on T2 imaging (Fig. 4.17).
- T2 sequence will also demonstrate peripancreatic edema and fluid collections.
- Intravenous contrast can be used to assess for pancreatic necrosis and vascular occlusions.
  - Contrast-enhanced MR is equivalent to CT in the assessment of acute pancreatitis.

Revised Atlanta criteria

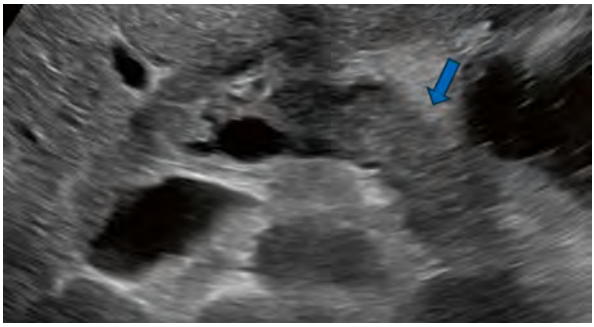

Fig. 4.14 Sagittal ultrasound demonstrating heterogeneously hypoechoic pancreatic parenchyma

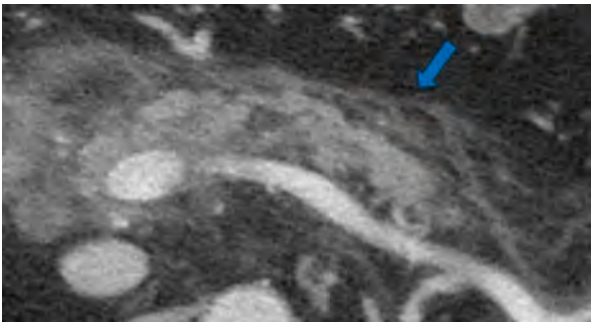

Fig. 4.15 Axial contrast enhanced CT demonstrating pancreas (arrow) with homogenous enhancement with extensive adjacent inflammatory stranding

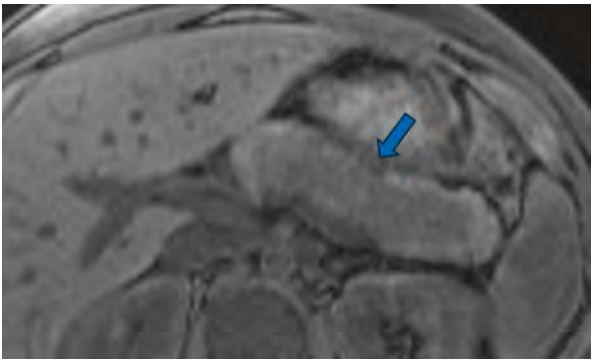

Fig. 4.16 Axial T1 weighted MRI demonstrating an enlarged pancreas (arrow) with loss of the T1 signal

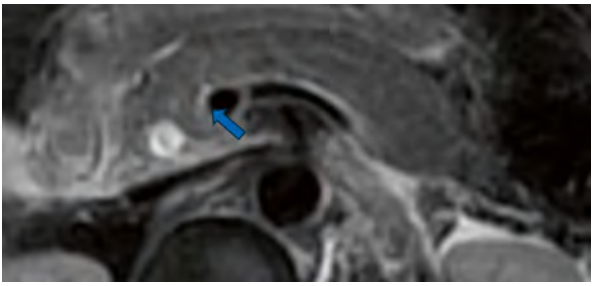

Fig. 4.17 Axial T2 weighted MRI demonstrating an enlarged pancreas with slightly increased T2 signal (arrow)

- Preferred descriptive classification system for the severity of acute pancreatitis.
  - Two phases of acute pancreatitis
    - Early: within the first week.
    - Late: after the first week.
  - Severity
    - Mild: no organ failure.
    - Moderate: organ failure lasting less than 48 h.
    - Severe: organ failure lasting longer than 48 h.

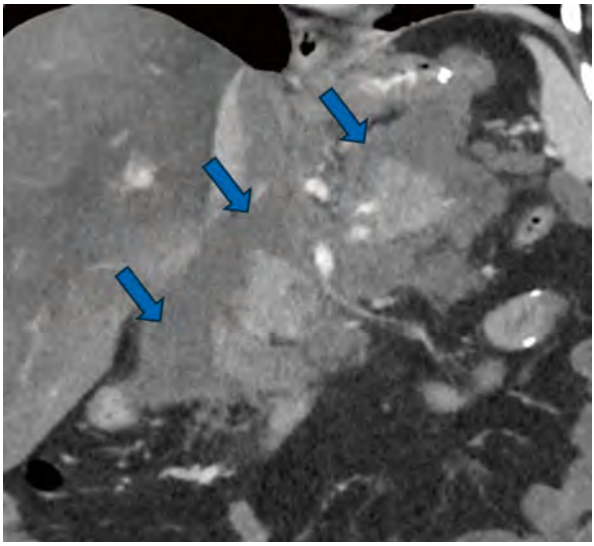

Fig. 4.18 Coronal CT demonstrating a homogeneously hypodense fluid collection without capsule (arrows)

- Types and complications

  Interstitial edematous

  - Acute peripancreatic fluid collection: less than 4 weeks.
    - Nonencapsulated fluid collection.
    - Ultrasound

      Hypoechoic lesion with increased through transmission (Fig. e4.5).
    - CT

      Well-circumscribed, homogeneously hypodense fluid collection without capsule (Fig. 4.18).
    - MRI

      T1 hypointense (Fig. 4.19), T2 hyperintense, nonenhancing lesion (Fig. e4.6).
  - Pseudocyst: greater than 4 weeks
    - Encapsulated fluid collection.
    - Ultrasound

      Well-circumscribed, unilocular anechoic mass associated with posterior acoustic enhancement (Fig. 4.20).
    - CT

      Homogeneously hypodense lesion, which demonstrates simple fluid density (Fig. 4.21).

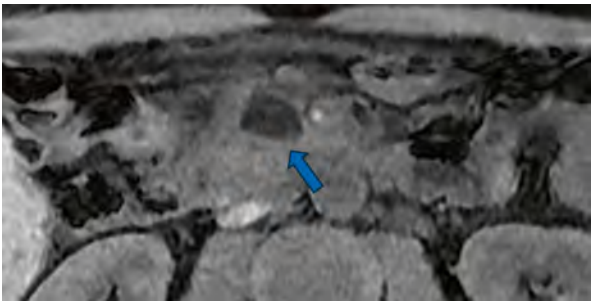

Fig. 4.19 Axial T1 weighted MRI demonstrating a hypointense nonenhancing lesion (arrow)

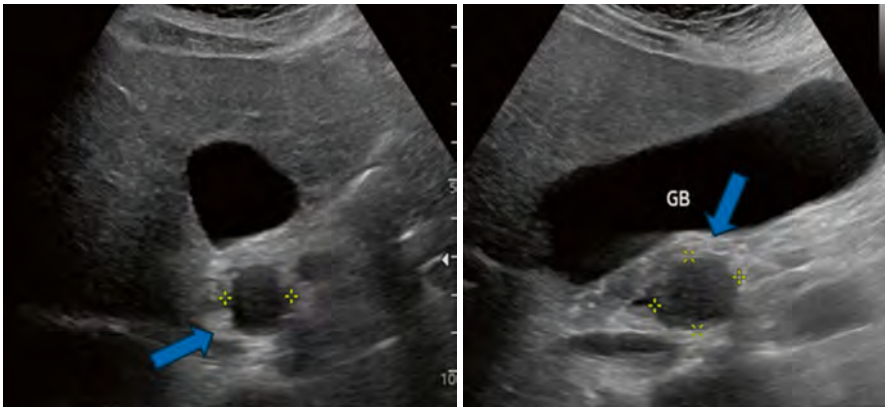

Fig. 4.20 Transverse and sagittal ultrasound demonstrating well circumscribed, unilocular anechoic mass with posterior acoustic enhancement (arrows)

- MRI
  T1 hypointense, T2 hyperintense with an enhancing fibrous capsule (Fig. 4.22).

Necrotizing

- Acute necrotic collection: less than 4 weeks.
  - Nonencapsulated collection of heterogeneous material.
  - Ultrasound
    Ill-defined heterogeneous collection with scattered hyperechoic debris (Fig. 4.23).
  - CT
    Heterogeneous, nonfluid density collection without a defined capsule and no peripheral enhancement (Figs. 4.24 and e4.7).
  - MRI
    T1 heterogeneous, T2 hyperintense fluid containing T2 hypointense material (Fig. 4.25).

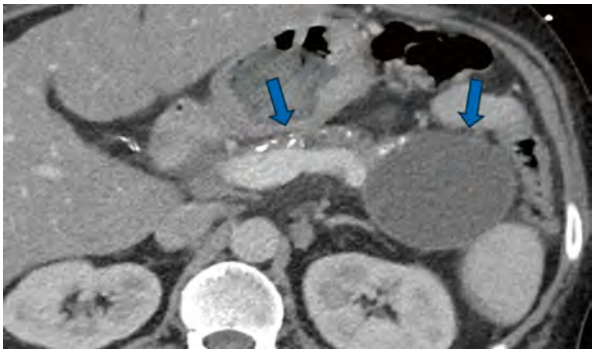

Fig. 4.21 Axial contrast enhanced CT demonstrating a lesion of homogeneous simple fluid density, (right arrow) extending from the pancreas. The pancreas parenchyma demonstrates numerous calcifications (left arrow), likely sequela of chronic pancreatitis

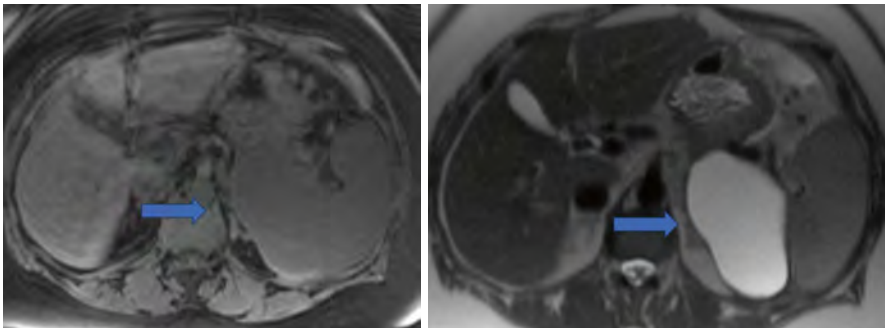

Fig. 4.22 Axial T1 (left image) and T2 weighted images demonstrating a pancreatic pseudocyst. Note the iso to slightly hypointense T1 collection (arrow) and the hyperintense T2 collection (arrow)

- Walled off necrosis: greater than 4 weeks.
  - Encapsulated collection of nonliquified heterogeneous material.
  - Ultrasound
    Round heterogeneous collection with fibrous capsule (Fig. 4.26).
  - CT
    Encapsulated fluid density collection within a region that was previously necrotic tissue (Figs. 4.27 and e4.8).
  - MRI
    MRI is better suited to visualize the necrotic debris. T1 heterogeneous (Fig. 4.28), T2 heterogeneous with a peripherally enhancing capsule (Fig. 4.29).

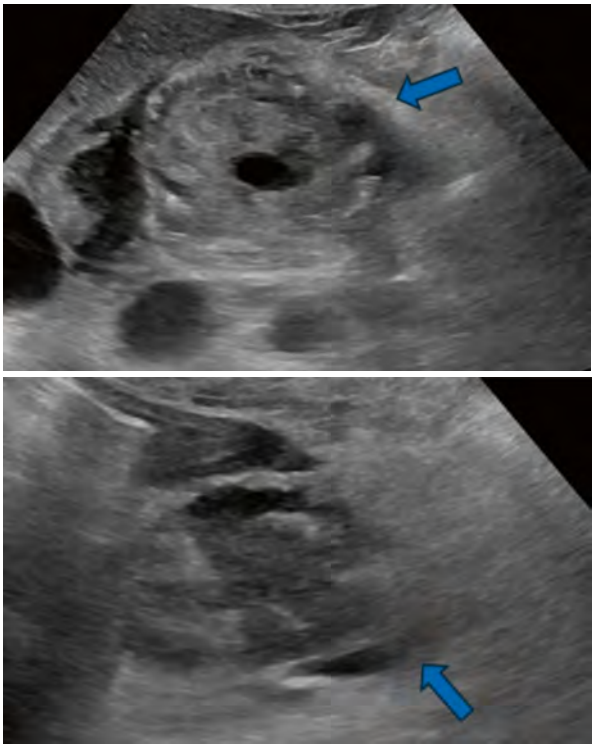

Fig. 4.23 Transverse (left arrow) and sagittal (right arrow) ultrasound demonstrating ill-defined heterogeneous collection with scattered hyperechoic debris

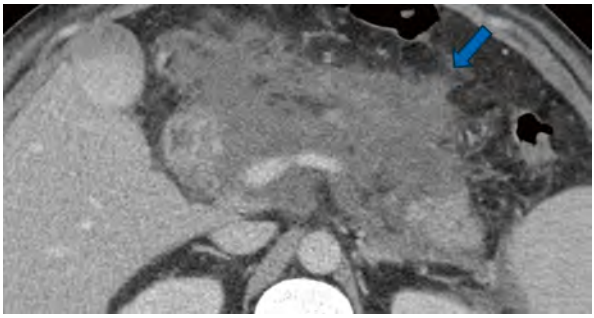

Fig. 4.24 Axial contrast enhanced CT demonstrates a heterogeneous collection without a defined capsule and no peripheral enhancement (arrow)

– **Chronic pancreatitis**

Persistent inflammatory change of the pancreas resulting in fibrosis due to repeated bouts of acute pancreatitis.

The most common cause is prolonged alcohol use.

Ultrasound

- Atrophied pancreatic parenchyma with echogenic foci of calcification and ductal dilatation (Fig. e4.9).

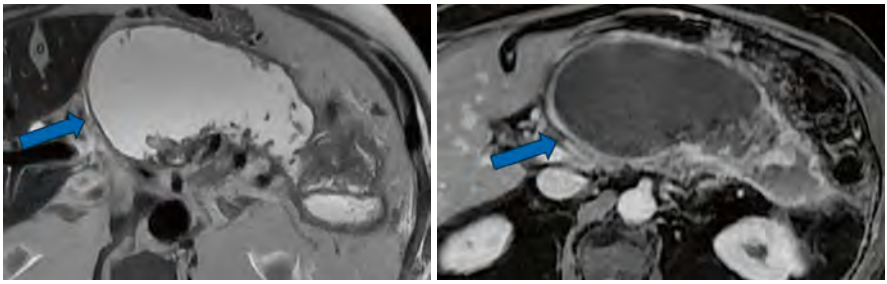

Fig. 4.25 Axial T2 weighted hyperintense collection (left arrow) and axial T1 MRI hyperintense collection (right arrow)

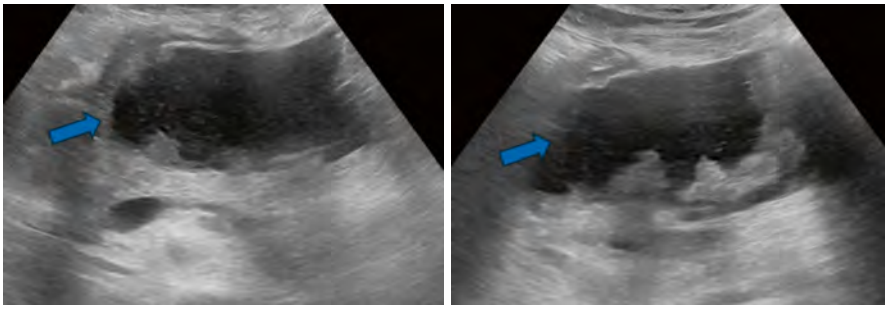

Fig. 4.26 Transverse ultrasound (left arrow) and sagittal ultrasound (right arrow) demonstrating round heterogeneous collection with a surrounding fibrous capsule

CT

- Atrophied pancreatic parenchyma demonstrating variable, multifocal enhancement.
- Scattered coarse calcifications.
  - Calcifications in the distribution of the main pancreatic duct are pathognomonic for chronic pancreatitis [3] (Fig. 4.30).
- Main and side-branch ductal dilatation.

MRI/ERCP

- Dilated pancreatic duct with areas of stricture (Fig. 4.31).
- Delayed contrast enhancement.

– **Autoimmune pancreatitis**

A form of chronic pancreatitis without definitive cause, but commonly associated with elevated levels of IgG4 antibodies.

CT

- Diffuse, sausage-like enlargement of the pancreas with loss of normal parenchymal lobulations and a surrounding low attenuation "halo" (Fig. 4.32) [1].

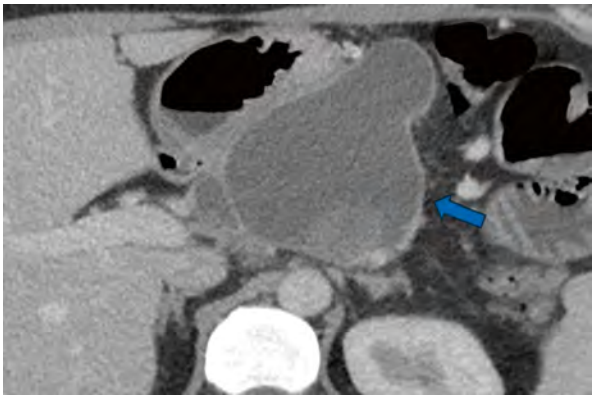

Fig. 4.27 Axial contrast enhanced CT demonstrating fluid density collection. The underlying pancreatic parenchyma was previously necrotic

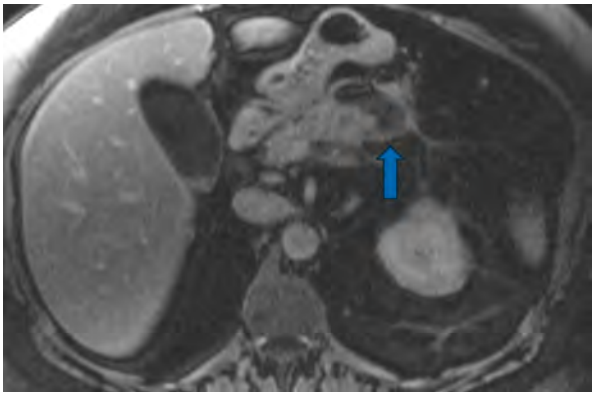

Fig. 4.28 Fat saturated T1 post contrast MRI demonstrating the evolving walled off collection (arrow)

MRI
- Diffuse enlargement with T1 hypointense signal and T2 hyperintense signal (Fig. 4.33).

ERCP/MRCP
- Irregular narrowing of the pancreatic duct with multifocal strictures.

- **Cystic pancreatic lesions**
  - Wide variety of cystic lesions frequently noted incidentally on CT and/or MRI examination.
  - Psuedocyst

    An encapsulated collection of fluid and inflammatory exudate developing greater than 4 weeks following an acute pancreatic fluid collection.

    CT
    - Well-defined homogeneously low attenuation collection surrounded by a thin, enhancing wall [4].

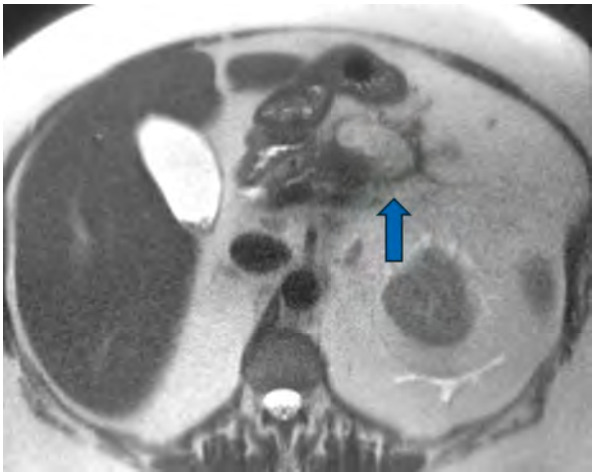

Fig. 4.29 Axial T2 MRI demonstrating the evolving walled off collection (arrow)

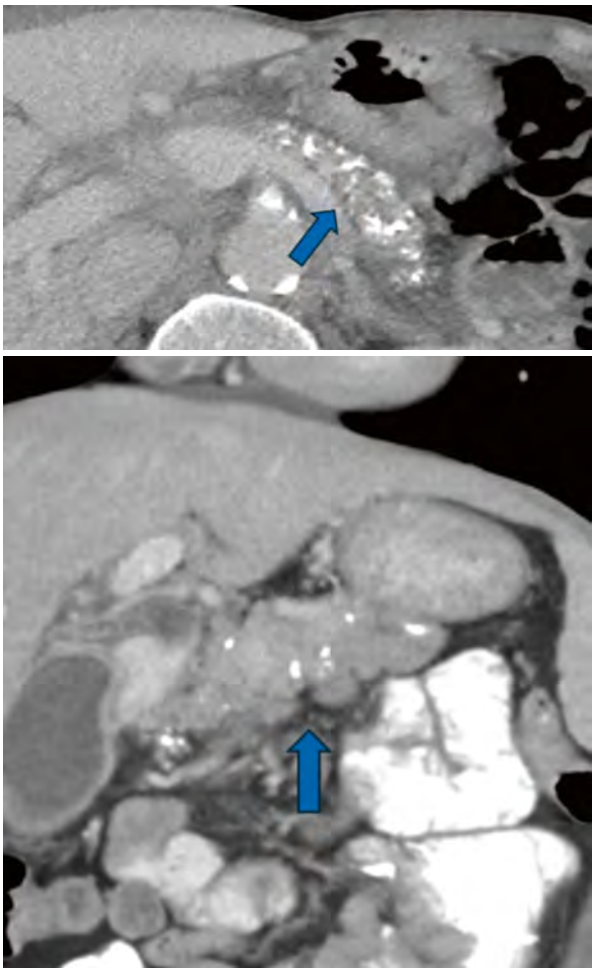

Fig. 4.30 Axial contrast enhanced CT (upper image) and coronal contrast enhanced CT (lower image) demonstrating multiple calcifications within the pancreas (arrows)

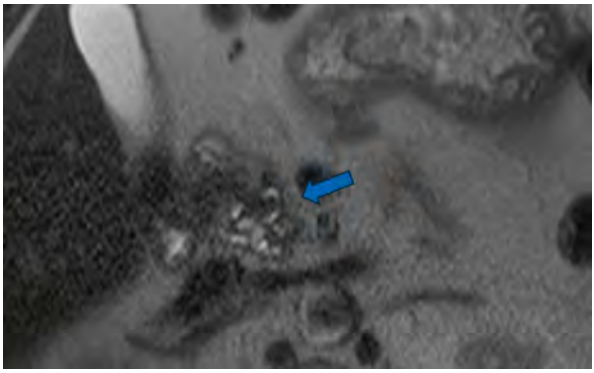

Fig. 4.31 Axial T2 MRI demonstrating multiple calcifications in the pancreatic head (arrow)

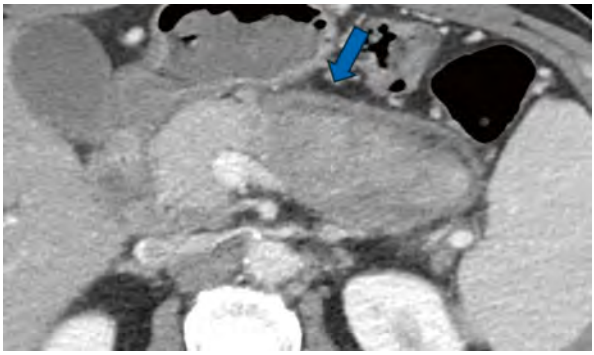

Fig. 4.32 Contrast enhanced axial CT demonstrating diffuse enlargement of the pancreas with a surrounding low attenuation "halo" (arrow)

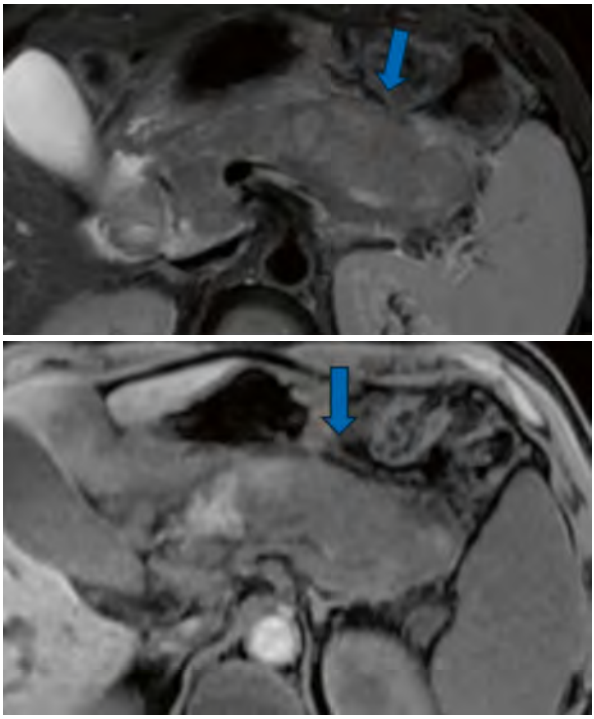

Fig. 4.33 Axial T2 MRI (upper image) demonstrating a hyperintense large pancreas (arrow). Axial T1 MRI (lower image) demonstrating a hypointense large pancreas (arrow)

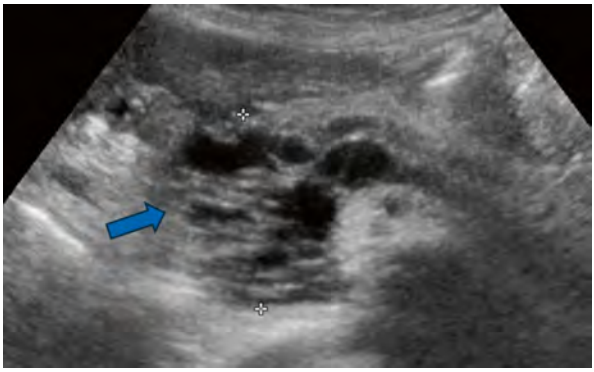

Fig. 4.34 Ultrasound of pancreatic head with numerous small cystic spaces

MRI
- T1 hypointense, T2 hyperintense with a progressively enhancing wall.

– **Pancreatic serous cystadenoma**

Benign solitary, multicystic lesion arising from the centroacinar cells of the exocrine pancreas composed of small proteinaceous cysts.

Commonly associated with a central stellate scar demonstrating calcification [5].

"Grandmother tumor"
- Greater predominance in older women (F:M = 4:1) in the fifth to seventh decade.

Ultrasound
- May appear as a solid mass as numerous, individual cysts are not readily distinguished (Fig. 4.34).
- Can appear hyperechoic with increased posterior acoustic enhancement.

CT
- Heterogeneous, mixed-density lesion made up of small cysts.
- Cluster of hypoattenuating cysts greater than 6 in number.
  – "Bunch of grapes" appearance (Fig. 4.35) [3].
- Central scar with or without calcification (Fig. e4.10).

MRI

T1 hypointense, T2 hyperintense cystic components with T2 hypointense septae and central enhancing scar with calcification (Fig. 4.36).

– **Mucinous cystic neoplasm**

Septated, cystic neoplasm of mucin-producing epithelium and ovarian-like stroma.

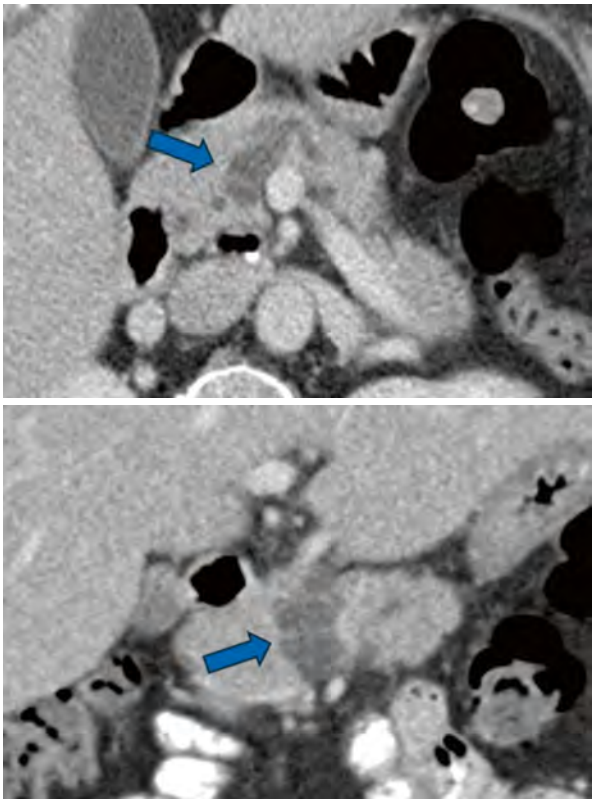

Fig. 4.35 Axial contrast enhanced CT (upper image) and coronal contrast enhanced CT (lower image) demonstrating a lobulated multicystic mass resembling a "bunch of grapes" appearance within the pancreas (arrows)

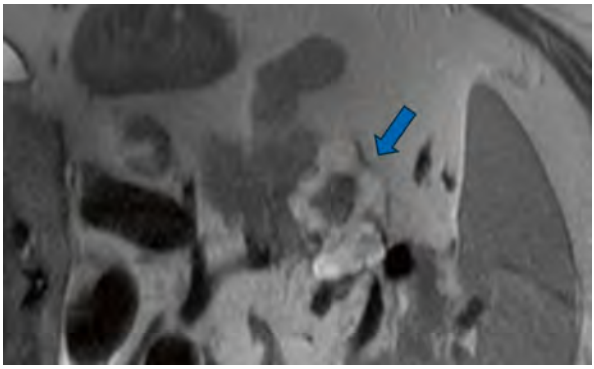

Fig. 4.36 Axial T2 MRI demonstrating a cluster of small cysts within the pancreas and with a central fibrous scar that is of low signal (arrow)

"Mother tumor."
- Predilection for middle-aged women.

Ultrasound
- Limited utility in distinguishing from serous cystadenoma.

CT
- Well-circumscribed, low attenuation cystic lesion with enhancing walls and solid mural nodules (Fig. 4.37).

MRI
- T1 variable, T2 cysts with variable intensity septations with delayed enhancement of a fibrous wall (Fig. 4.38).

– **Solid pseudopapillary tumor**

Benign cystic lesion.
"Daughter tumor."
- Most commonly present in non-white females aged 20s–30s.

Ultrasound
- Large mass with heterogeneous cystic and solid components (Fig. 4.39).

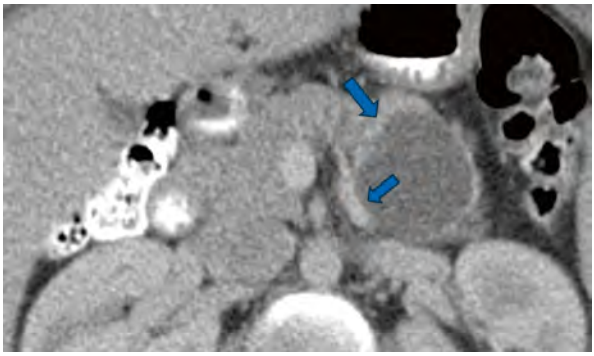

Fig. 4.37 Axial contrast enhanced CT demonstrating a hypodense encapsulated pancreatic tail mass (upper arrow) with inferior mural thickening (lower arrow)

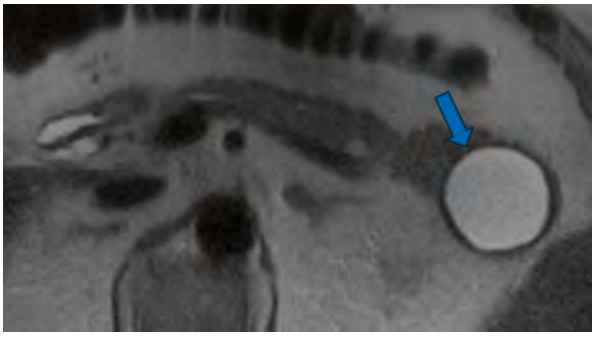

Fig. 4.38 Axial T2 MRI demonstrating hyperintense cystic mass in pancreatic tail with fibrous capsule (arrow)

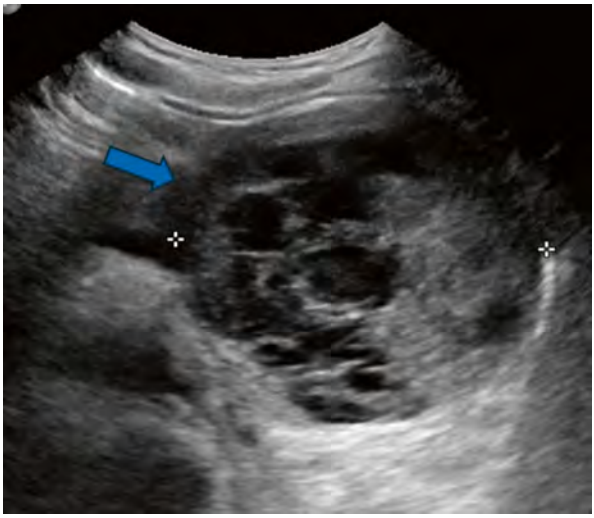

Fig. 4.39 Ultrasound demonstrating a large mass within the pancreas with a heterogeneous appearance, due to its cystic and solid composition

CT
- Well-circumscribed, encapsulated lesion with varying solid and cystic components.
  - Peripheral solid enhancing components with centrally located cystic components (Fig. 4.40).

MRI
- T1 heterogeneous signal, T2 hyperintense signal, progressive heterogeneous enhancement (Figs. 4.41 and e4.11).

– **Intraductal papillary mucinous tumor (IPMT)**

A mucin-producing tumor arising from the epithelial cells of the main pancreatic duct or its side branches.

IPMNs can be associated with ductal dilatation due to significant mucin production.

Greater than 60% are incidentally noted.

Side-branch IPMN:
- Well-circumscribed cystic lesion in communication with the main pancreatic duct.
- Multiple cysts scattered throughout the pancreas are suggestive of the diagnosis.
- Ultrasound
  - Limited utility as the pancreas is frequently obscured by overlying bowel gas (Fig. e4.12).

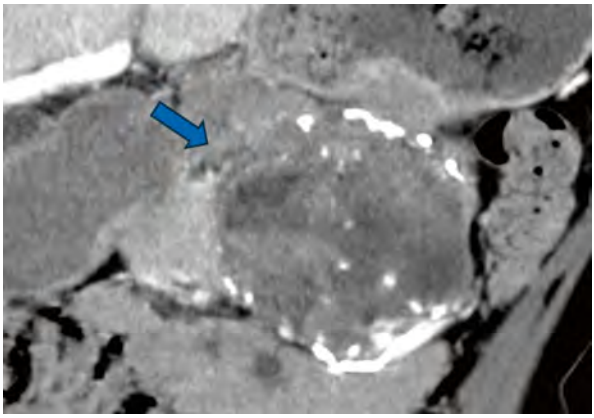

Fig. 4.40 Contrast enhanced coronal CT demonstrating a well encapsulated pancreatic mass with solid and cystic components. Calcifications and enhancing solid areas noted in the periphery, cystic spaces are more centrally located which is typical

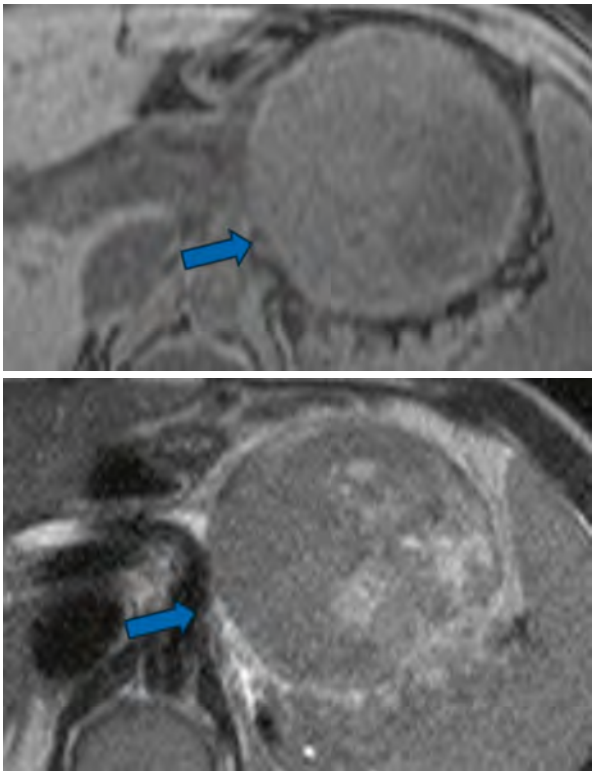

Fig. 4.41 Axial T1 MRI (upper image) heterogeneously hypointense mass (arrow) and axial T2 MRI (lower image) demonstrating a heterogeneously hyperintense mass (arrow)

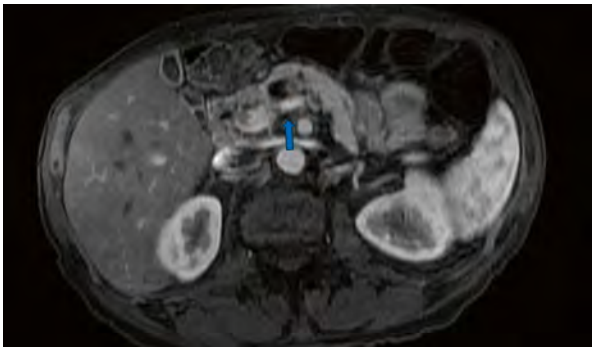

Fig. 4.42 IPMN: Contrast enhanced T1 weighted image demonstrates an enhancing nodule within the cystic mass, consistent with a malignant IPMN (arrow)

    - CT
      - Well-circumscribed hypodense lesion commonly shown to communicate with the main pancreatic duct (Fig. e4.13).
    - MRI
      - T1 hypointense (Fig. e4.13), T2 hyperintense lesion communicating with the main pancreatic duct (Fig. 4.42).
  - **Main duct IPMN**

    Prominent focal or diffuse dilatation of the main pancreatic duct with a "bulging" ampulla filled with mucin.

    Associated with dilatation of the main pancreatic duct greater than or equal to 0.5 cm.

    CT
    - Main pancreatic dilated >0.5 cm and tortuous (Fig. 4.43).
    - There may be an enhancing nodule.

    MRI
    - Segmental T2 hyperintense dilation of the main pancreatic duct (Fig. 4.44).
    - There may be an enhancing nodule.
- **Solid pancreatic epithelial neoplasms**
  - **Pancreatic ductal adenocarcinoma**

    The most common malignant lesion of the exocrine pancreas that arises from the ductal epithelium.

    Ultrasound
    - Usually first-line evaluation for obstructive jaundice.
    - Can indicate level of obstruction, but less sensitive for demonstrating the mass.
    - May show a hypoechoic mass associated with pancreatic ductal dilatation (Fig. 4.45).

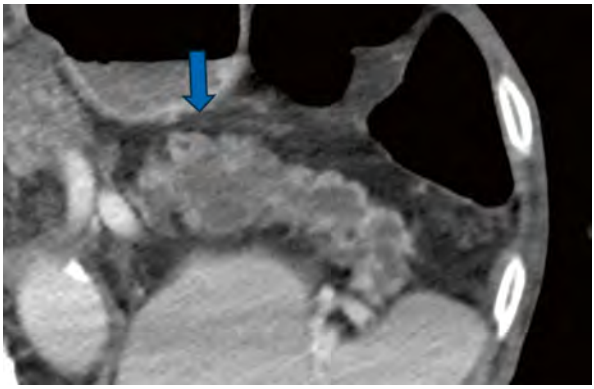

Fig. 4.43 Contrast enhanced axial CT demonstrating diffuse dilatation and tortuosity of the pancreatic duct (arrow)

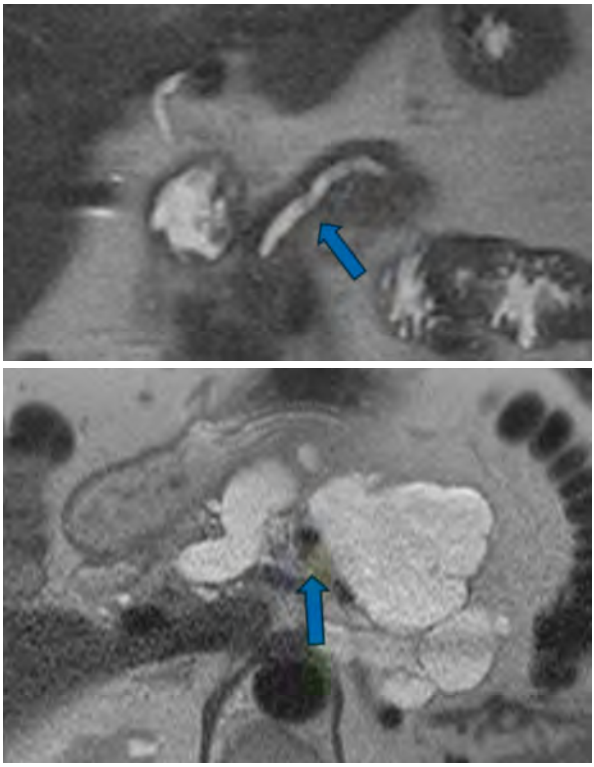

Fig. 4.44 Coronal T2 MRI (upper photo) and Axial T2 MRI (lower photo) demonstrating a dilated hyperintense pancreatic duct

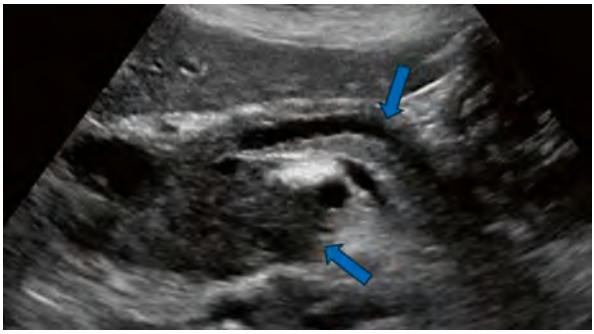

Fig. 4.45 Transverse ultrasound demonstrating a hypoechoic pancreatic mass (left arrow) with a dilated pancreatic duct (right arrow)

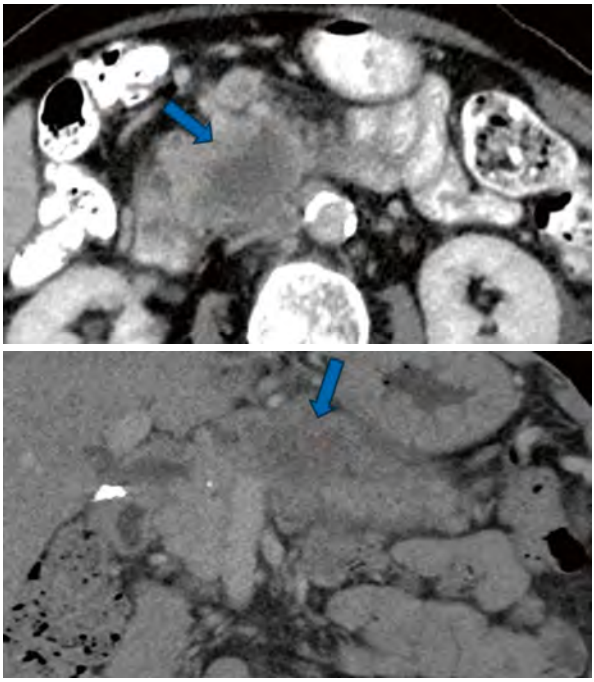

Fig. 4.46 Contrast enhanced axial CT (upper image) and noncontrast coronal CT (lower image) demonstrating a hypodense pancreatic mass with ill defined borders (arrows)

CT

- Hypodense mass with poorly defined margins (Fig. 4.46).
- Commonly demonstrates invasion into the retroperitoneum.
- Obstruction of the main pancreatic duct with pancreatic parenchymal atrophy upstream of the obstructing mass.

MRI

- T1 hypointense, T2 variable intensity (Fig. 4.47).
- Progressive delayed enhancement.

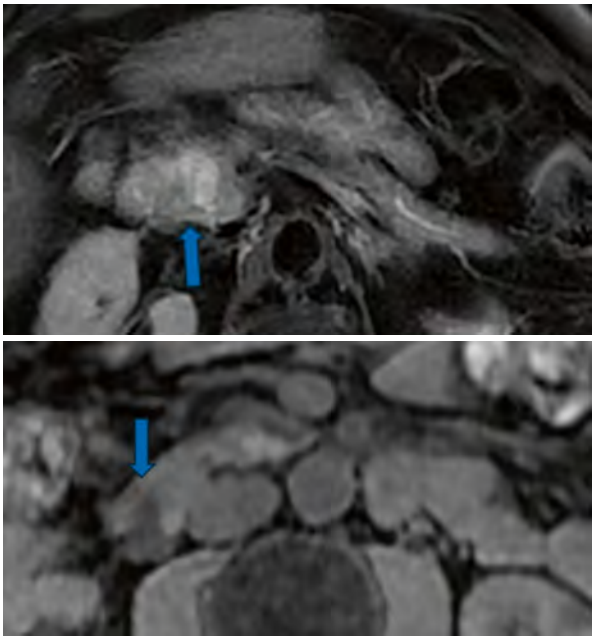

Fig. 4.47 Axial T2 MRI (upper photo) demonstrating a heterogeneously hyperintense pancreatic mass (arrow) and axial T1 MRI (lower photo) demonstrating a hypointense pancreatic mass (arrow)

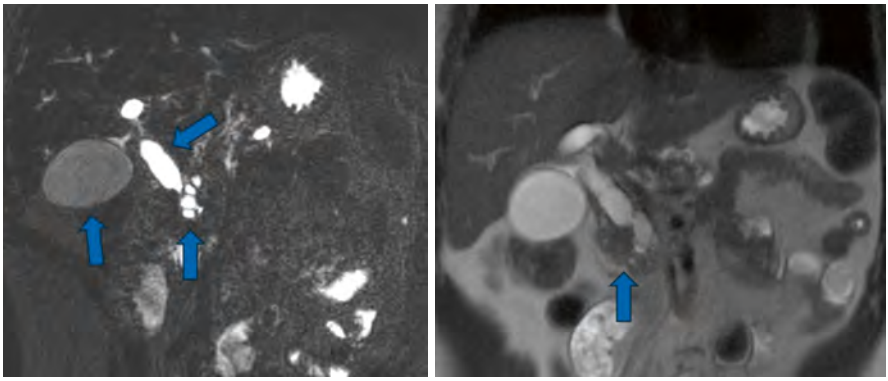

Fig. 4.48 Coronal thick slab MRCP image (left) demonstrates dilatation of the common bile duct and pancreatic duct (arrows) from a pancreatic head mass. Note the dilated gallbladder (arrow). Coronal T2 weighted images demonstrate the low T2 signal mass causing the biliary obstruction (arrow)

MRCP

- Double-duct sign: Obstruction of both the common bile duct and the main pancreatic duct (Fig. 4.48).

– Acinar cell carcinoma

Large, well-circumscribed mass with cystic degeneration.

Endoscopic ultrasound elastography.

- Relatively harder parenchyma compared to surround soft tissue, which demonstrated enhancement and rapid washout with contrast-enhanced EUS.

CT

- Enhancing, predominantly oval and purely solid pancreatic mass that most frequently present with no bile duct dilatation, no visible lymph nodes, no adjacent organ involvement, and larger visible lymph nodes compared to PDA.

MRI

- T1 hypointense, mild T2 heterogeneous hyperintensity without notable contrast enhancement.

– Pancreatic neuroendocrine tumors

Tumors arising from pancreatic endocrine cells.

Insulinoma, gastrinoma, glucagonoma, VIPoma, and somatostatinoma.

Well-circumscribed hypervascular pancreatic masses.

Ultrasound

- Well-defined hypoechoic masses with increased vascularity (Fig. e4.14).
- Best for the identification of small neuroendocrine tumors not well demonstrated on CT or MRI.

CT

- Preferred over MRI for the assessment of vascular invasion and resectability.
- Hypervascular masses that appear prominent on arterial phase imaging (Fig. e4.15).
- Frequently associated with calcifications and larger lesions commonly demonstrate central necrosis (Fig. 4.49).

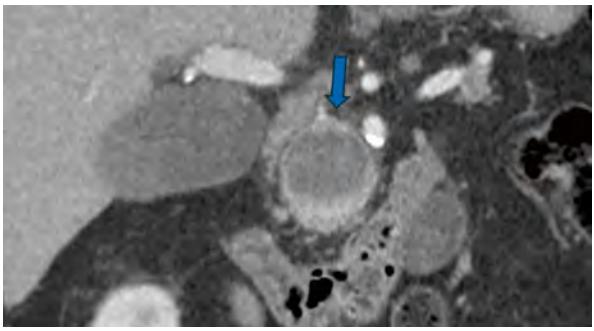

Fig. 4.49 Contrast enhanced coronal CT demonstrating a pancreatic mass (arrow). Note the central necrosis which is commonly seen with larger pancreatic neuroendocrine tumors

MRI

- Compared to normal pancreatic parenchyma, lesions appear T1 hypointense and T2 hyperintense (Fig. e4.16). Additionally, smaller lesions (<2 cm) demonstrate a homogeneous enhancement pattern similar to that seen on CT, while larger lesions (>2 cm) are associated with heterogeneous enhancement with areas of necrosis.

References

1. Boland G. Gastrointestinal imaging: the requisites. 4th ed. Philadelphia, PA: Elsevier Saunders; 2014.
2. Banks P, et al. Classification of acute pancreatitis—2012: revision of the Atlanta classification and definitions by international consensus. Gut. 2013;62:102–11.
3. Sun E, Shi J, Mandell J. Core radiology: a visual approach to diagnostic imaging, vol. 1. 2nd ed. UK, Cambridge University Press; 2021.
4. Thoeni RF. The revised Atlanta classification of acute pancreatitis: its importance for the radiologist and its effect on treatment. Radiology. 2012;262(3):751–64. https://doi.org/10.1148/radiol.11110947.
5. Kim Y, et al. Imaging diagnosis of pancreatic cystic lesions: pseudocyst versus nonpseudocyst. Radiographcis. 2005;25(3):671. https://doi.org/10.1148/rg.253045104.

Spleen

5

Christine Boatright

Optimal Imaging Modalities for Splenic Imaging

Ultrasound (US)

- Ideal for evaluating splenic size or splenic abnormalities, particularly in children.
- Splenic lesions are not well characterized by US, beyond confirmation of cystic versus solid lesions.

CT

- Noncontrast CT is of little value in the evaluation of the spleen beyond splenic size.
- In the arterial phase of contrast-enhanced CT, the spleen will have zonal enhancement, manifest as a zebra-striped appearance.
- There is homogeneous enhancement of the spleen in the portal venous phase.

MRI

- Noncontrast MR is of greater utility for the assessment of the spleen than CT.
- On T2-weighted images, splenic lesions may be detected if hyperintense to the normal tissue.

Supplementary Information The online version contains supplementary material available at https://doi.org/10.1007/978-3-031-76624-4_5.

C. Boatright (✉)
Department of Radiology, University of Kansas Medical Center, Kansas City, KS, USA
e-mail: cboatright@kumc.edu

© The Author(s), under exclusive license to Springer Nature Switzerland AG 2024

T. Catanzano (ed.), *What Radiology Residents Need to Know: Abdominal Radiology*, What Radiology Residents Need to Know,
https://doi.org/10.1007/978-3-031-76624-4_5

- On T1-weighted images, splenic lesions may be detected if hypointense to the normal tissue.
- In the late arterial phase of contrast-enhanced MR, the spleen may display the striped appearance seen on CT.
- In the portal venous phase, homogeneous enhancement is seen.
- MRI is a comprehensive evaluation for parenchymal abnormalities and characterizes splenic lesions by determining cystic versus solid mass as well as enhancement patterns.

Nuclear Medicine

- Important for confirming accessory splenic tissue (splenules) or splenosis such as those within the pancreatic tail or within atypical locations such as within the thorax or pelvis.
- Imaging tracers can include Tc-99m sulfur colloid, among others, depending on study indication.

Splenic Anatomy and Normal Imaging Appearance

Splenic Anatomy

- Located within the left upper abdomen.
- Entirely covered by peritoneum. Peritoneal folds covering the spleen come together to maintain the position of the spleen by forming its suspensory ligaments: phrenicosplenic (Fig. 5.1), gastrosplenic, splenorenal, and splenocolic ligaments.

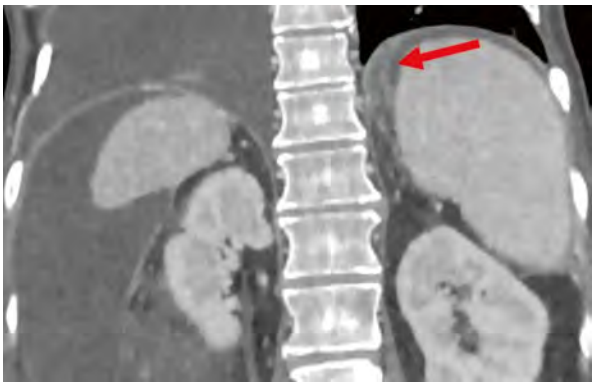

Fig. 5.1 Example of the phrenicosplenic ligament outlined by ascites, the peritoneal fold connecting the spleen to the left hemidiaphragm

Normal Imaging Appearance

- Normal length is less than 13 cm in adults.
- Normal length in children varies by age in months.

US

- Uniform echogenicity with overall homogeneous appearance and mild hypervascularity (Fig. 5.2).
- A normal finding in young children is a heterogeneous appearance with bands of differing echogenicity resembling the zebra-stripe appearance.

CT/MRI

- May have a heterogeneous appearance on early contrast phases described as a tiger- or zebra-stripe appearance on arterial phase.
- Appearance is due to differential blood flow to different parts of the parenchyma, red versus white pulp (Fig. 5.3). Uniform enhancement on portal venous and delayed images (Fig. 5.4). High diffusion signal on high *B*-value diffusion-weighted imaging, similar to the appearance of lymph nodes (Fig. 5.5).

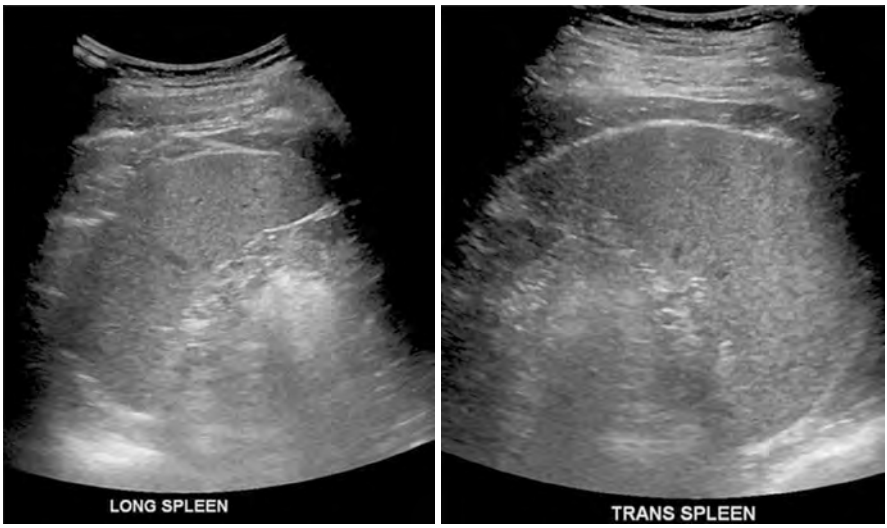

Fig. 5.2 Normal sonographic appearance of the spleen on ultrasound with homogeneous appearance of the parenchyma

Fig. 5.3 Arterial phase CT demonstrating the normal heterogeneous enhancement pattern of the spleen with a *tiger* or *zebra stripe* appearance

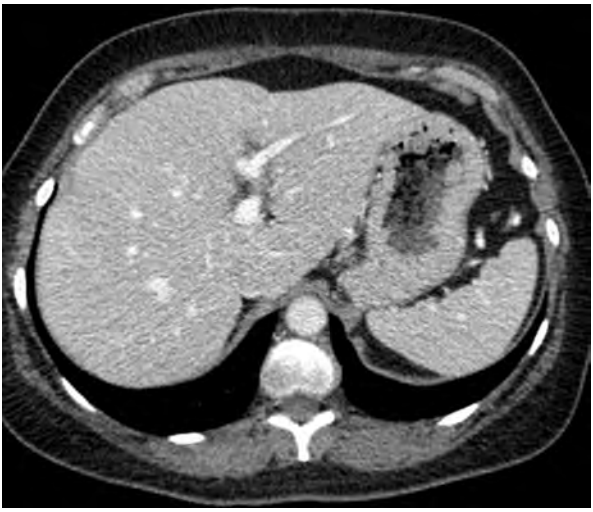

Fig. 5.4 Portal venous phase CT demonstrating the normal, homogeneous enhancement of the splenic parenchyma

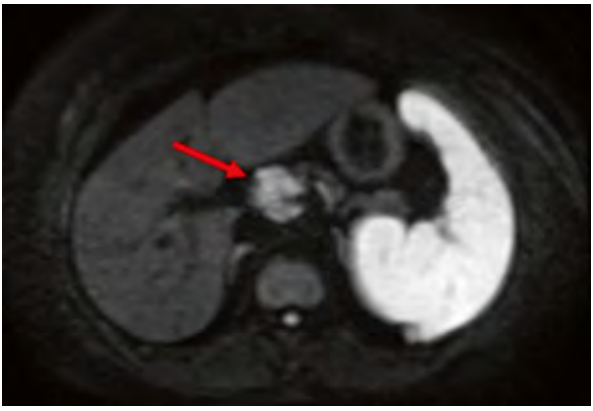

Fig. 5.5 Diffusion-weighted imaging appearance of the spleen on MRI demonstrating the normal, homogeneous high signal intensity on this high *B*-value diffusion sequence, similar to the diffusion signal seen in lymph nodes

Nuclear Medicine

- Depends upon the radiotracer utilized.
- Technetium-99m sulfur colloid (Fig. 5.6): taken up by the reticuloendothelial system of the liver, spleen, and bone marrow.
- 18F-fluorodeoxyglucose (FDG) (Fig. 5.7): mild diffuse uptake throughout the spleen, though typically similar or lower than the hepatic parenchyma.
- Technetium-99m-tagged-heat-damaged red blood cell (RBC) (Fig. 5.8): functional splenic tissue sequesters the damaged RBCs.

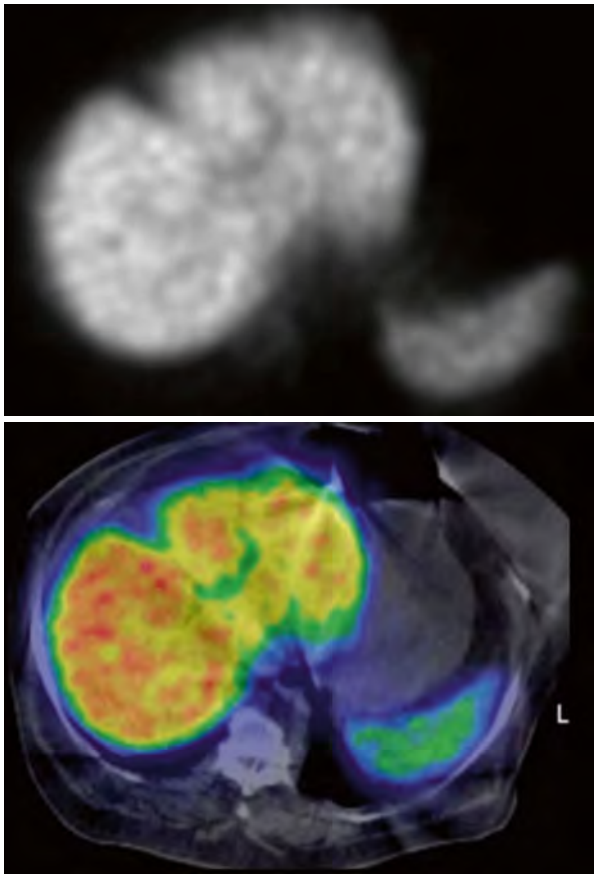

Fig. 5.6 Normal imaging appearance of the spleen on technetium-99m sulfur colloid examination with splenic uptake of the radiotracer though less than that of the liver

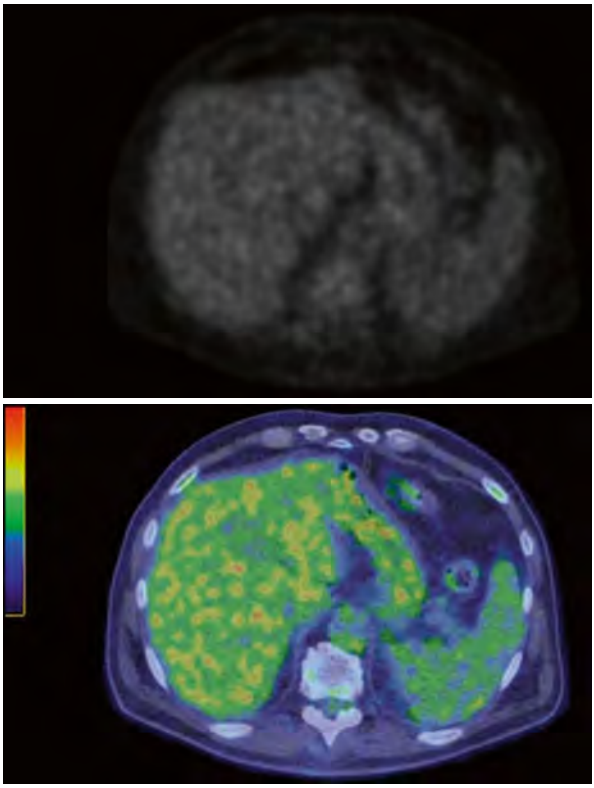

Fig. 5.7 Normal imaging appearance of the spleen on FDG-PET with mild diffuse uptake throughout the spleen, similar or slightly lower than the liver

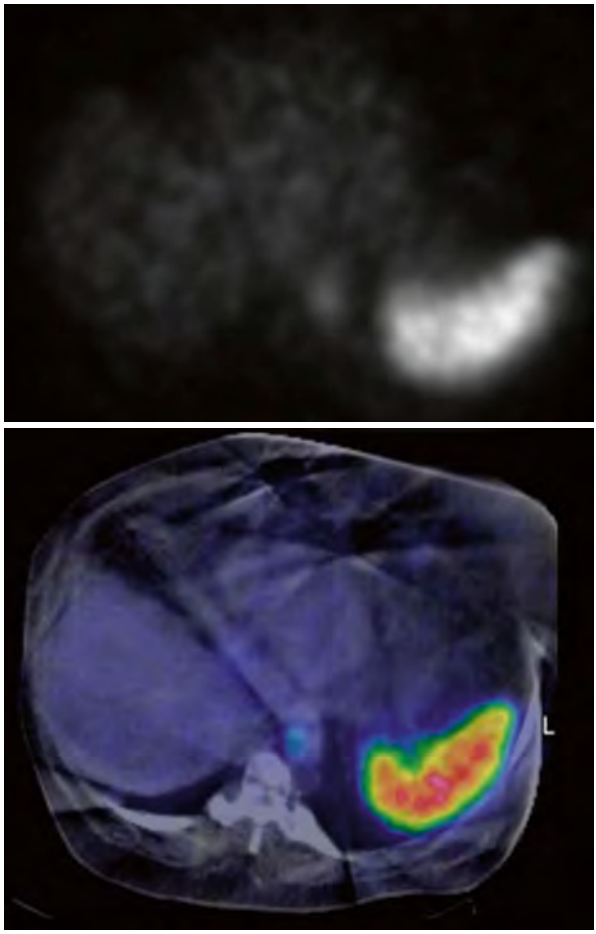

Fig. 5.8 Normal imaging appearance of the spleen on technetium-99m tagged-heat-damaged RBC scan with radiotracer uptake within functioning splenic tissue

Congenital Splenic Findings

Accessory Spleen or Splenule (Fig. 5.9)

- Common, congenital, and often incidental finding.
- Typically rounded mass-like lesion; may be mistaken for a lymph node or mass.
- Of no clinical consequence with the exception of patients with immune thrombocytopenic purpura (ITP); it can cause recurrent symptoms in these patients if not resected.
- May hypertrophy following splenectomy.
- Most often located in the splenic hilum, though can be found within other locations such as adjacent to or within the pancreatic tail (Fig. e5.1).
- **Ultrasound**
  - Well-defined, round or oval mass with similar echogenicity to the spleen.

Fig. 5.9 CT appearance of a splenule, or accessory splenic tissue, with the same enhancement and appearance to the adjacent spleen

  - It may be difficult to visualize on US due to obscuration by bowel gas or poor acoustic windows.
- **CT**
  - Similar in density and enhancement pattern to the spleen.
  - It is typically found in the splenic hilum.
  - More difficult to characterize as an accessory spleen if in an ectopic location such as the pancreas; assess carefully for signal intensity and enhancement similar to the spleen.
- **MR**
  - Similar in intensity and enhancement pattern to the spleen.
  - It is typically found in the splenic hilum.
  - More difficult to characterize as an accessory spleen if in an ectopic location such as the pancreas; assess carefully for attenuation and enhancement similar to the spleen.
- **Nuclear Medicine**
  - Can use technetium-99m sulfur colloid or heat-damaged RBCs in difficult cases (Fig. 5.10).
  - These agents are taken up by the spleen and accessory spleen.

Splenic Cleft

- Appear as prominent lobulations and linear grooves along the contour of the spleen (Fig. 5.11).
- Remnants of splenic lobules in embryonic development. May be mistaken for lacerations in the setting of trauma.

Ultrasound

- The cleft may be difficult to visualize due to acoustic windows and artifact from the air–diaphragm interface.

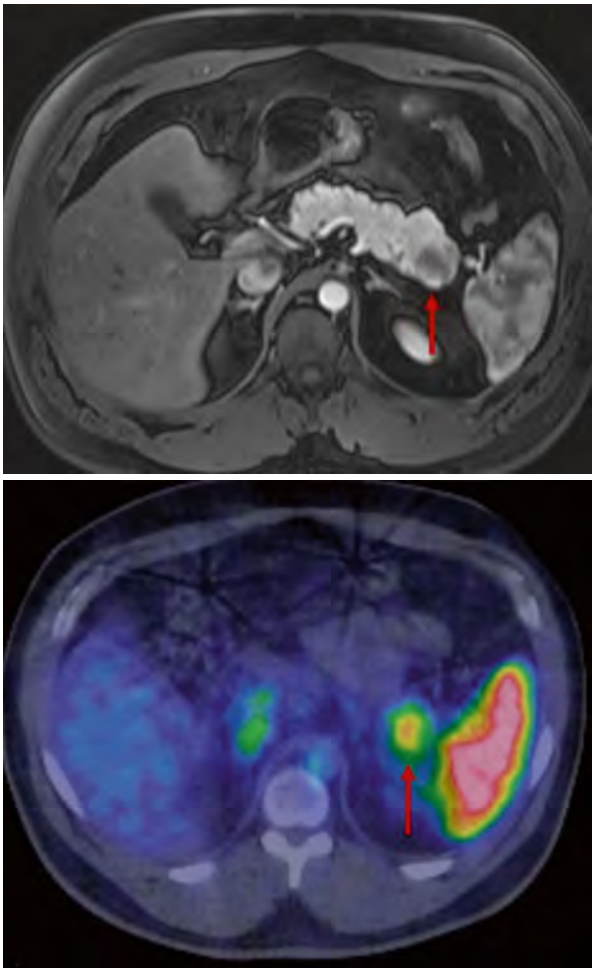

Fig. 5.10 MRI post-contrast image and corresponding Tc-99m-heat damaged RBC scan demonstrating radiotracer uptake within the pancreatic tail confirming intrapancreatic splenule

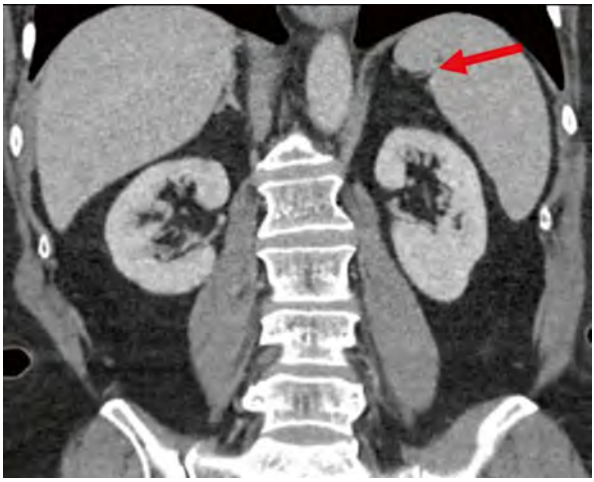

Fig. 5.11 Coronal CT image demonstrating a small linear cleft within the medial aspect of the spleen

- If visible, will appear as a contour deformity with a hypoechoic linear or crescentic area bisecting the splenic tissue.

CT

- The cleft is directly visualized as linear or hypodense area bisecting the spleen.
- If hypodense, it may be mistaken for a splenic laceration in a setting of trauma.
- Coronal images are often the most useful plane for evaluation of a splenic cleft.

MR

- The cleft may be visible as a contour deformity or area of signal abnormality.
- It may be seen on axial or coronal images. It is harder to identify on sagittal images.

Polysplenia

- Congenital syndrome hallmarked by multiple small spleens (Fig. 5.12).
- There is a wide range of other congenital anomalies within the abdomen as well as cardiac anomalies that comprise this syndrome.
- Multiple spleens may be on the right or left side of the abdomen but are always on the same side as the stomach (Fig. e5.2).

Ultrasound

- There may be a dominant spleen.
- Multiple spleens of varying sizes may be seen in the abdomen, although they are most easily characterized as splenic tissue if located in the left upper quadrant.
- Other abnormalities in the polysplenia syndrome may be assessed at the time of the examination, including hepatic abnormalities.

Fig. 5.12 Coronal CT image demonstrating multiple spleens within the left upper quadrant consistent with polysplenia

CT

- Multiple soft-tissue structures are present with the appearance and attenuation of normal splenic tissue.
- They are often in the left upper quadrant but may also be ectopic.
- Enhancement patterns will follow the characteristic splenic pattern described above.
- Associated anomalies such as vascular and osseous findings may be identified on CT.

MR

- They are often in the left upper quadrant but may also be ectopic.
- Enhancement patterns will follow the characteristic splenic pattern described above.
- Small splenic tissue may not be easily detected if there is significant bowel peristalsis, which can degrade the images. Consideration may be given to an antiperistaltic agent for imaging.
- Associated anomalies such as vascular and osseous findings may be identified.

Asplenia

- Congenital absence of the spleen (Fig. 5.13).
- It is nearly always associated with congenital heart defects and a subsequent high mortality rate.
- It is commonly associated with midline position of the liver (Fig. e5.3).

US

- No spleen is present in the left upper quadrant.

Fig. 5.13 CT image of the upper abdomen demonstrating no visible splenic tissue within the normal location of the spleen within the left upper quadrant consistent with asplenia. Notice also a portion of the visualized stomach with the right abdomen instead of the left

- Scanning should include all quadrants of the abdomen to assess for an ectopic ("wandering") spleen if the splenic bed is empty.
- False positives can occur in patients with small spleens (e.g., autoinfarction in the setting of sickle cell disease).

CT

- No splenic tissue is present.
- Associated anomalies such as an interrupted IVC or cardiac anomaly can be detected.

MR

- No splenic tissue is present.
- Ectopic splenic tissue in the pelvis may not be detected if only the abdomen is imaged to keep imaging time down. This will result in a false-positive diagnosis of asplenia.

Trauma

- The spleen is the most common visceral organ to rupture secondary to trauma.
- May present with perisplenic or subcapsular hemorrhage (Fig. 5.14), parenchymal hypoenhancement (Fig. 5.15), or devascularization in extreme cases.
- Treatment varies depending on the severity of the injury and can include
  - Expectant management.
  - Percutaneous embolization.
  - Splenectomy.
- **US**
  - Ultrasound is of limited utility in the assessment of splenic trauma.

Fig. 5.14 Axial CT image of the spleen with heterogeneous perisplenic hematoma consistent with acute traumatic splenic injury

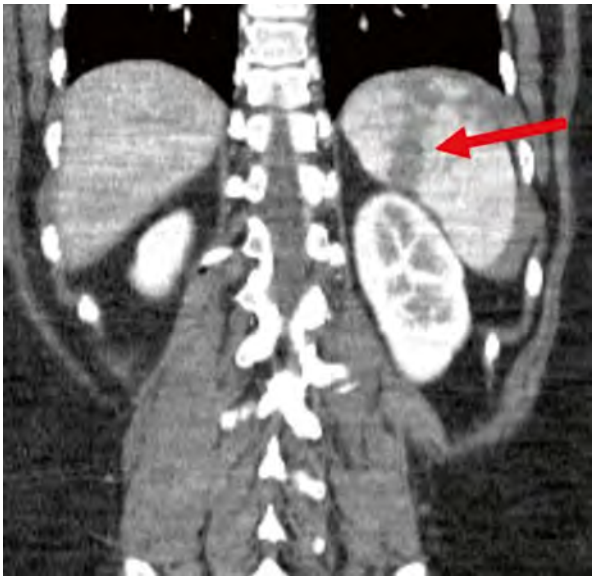

Fig. 5.15 Coronal CT image demonstrating linear hypo-enhancement within the superior aspect of the spleen with perisplenic hemorrhage consistent with acute traumatic splenic injury and laceration

  - It may be used as a screening study in pregnant patients, particularly if there is low suspicion for injury.
- **CT**
  - CT is the study of choice for the assessment of splenic trauma.
  - A grading system was created by the surgical societies to standardize grading and management decisions (Figs. e5.4, e5.5, e5.6, e5.7, e5.8, e5.9, and e5.10).
  - These CT examinations should be performed with intravenous contrast as subtle splenic injuries and active splenic bleeding (contrast extravasation or puddling) cannot be detected on noncontrast examinations.
- **MR**
  - MR may be performed if CT is contraindicated but is not the study of choice due to length of time required for image acquisition.
  - Lacerations may appear as linear signal abnormalities.
  - Acute perisplenic hematomas will be T1 bright.
  - Intravenous contrast extravasation may be seen in active bleeds.

Splenosis

- May occur after splenic trauma/rupture or splenectomy (Fig. 5.16).
- Deposits of splenic tissue within or near the splenectomy bed or within other locations such as the thorax or pelvis (Fig. 5.17).

US

- Imaging findings are similar to polysplenia.

Fig. 5.16 Axial CT image demonstrating small enhancing nodule within the splenic fossa following splenectomy consistent with splenosis

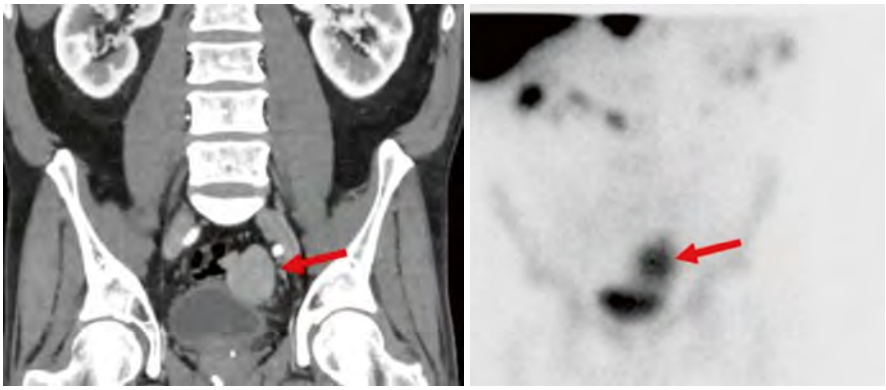

Fig. 5.17 Coronal CT image demonstrating enhancing nodule within the left pelvis adjacent to the urinary bladder. This was confirmed to be splenosis in the setting of prior splenectomy by tracer uptake on technetium-99m-heat-damaged-RBC scan

- The entire abdomen should be interrogated to assess for ectopic locations as splenic tissue in splenosis will often be remote from the splenic bed.
- Detection is often limited due to limited penetration of the ultrasound beam from bowel gas.
- There is a relatively low sensitivity for detection with ultrasound.

CT

- Splenic tissue of varying sizes may be identified throughout the abdomen and pelvis.
- Small deposits may be difficult to identify.
- Intravenous contrast provides increased sensitivity for detection; negative enteric contrast agents will distend bowel and improve detection for surface and inter-loop splenic tissue.

Nuclear Medicine

- Heat-damaged RBC and sulfur colloid examinations can detect splenic tissue.

Infiltrative Disease

- Often difficult to distinguish etiology by imaging appearance alone.
- Clinical history, other imaging findings, and laboratory values are often helpful.

Causes

- Lymphoma or leukemic involvement can present with diffuse splenic enlargement (Fig. 5.18).
- Infectious or inflammatory etiologies can present with diffuse splenic enlargement, such as disseminated histoplasmosis (Fig. 5.19), and may also demonstrate diffusely increased FDG uptake on PET, such as in sarcoidosis (Fig. 5.20).

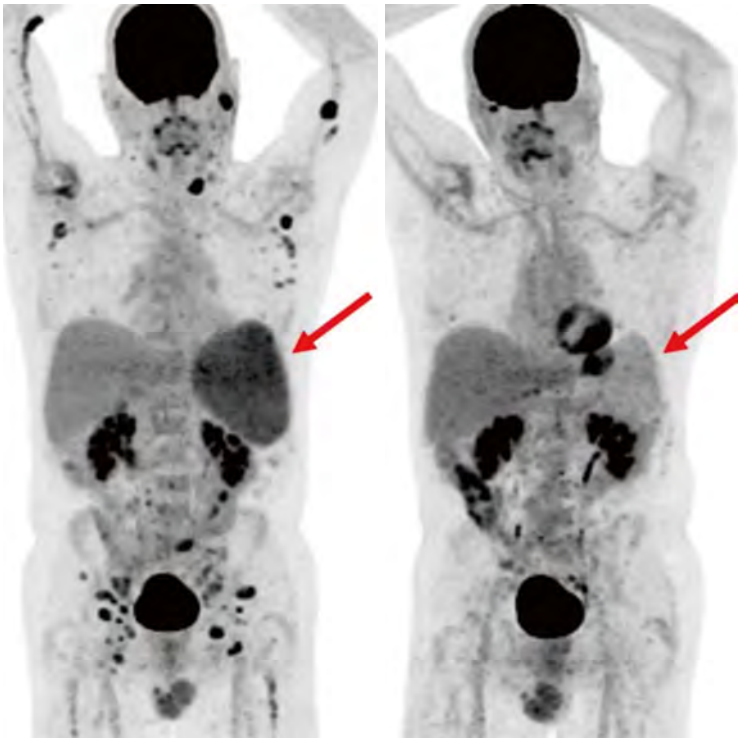

Fig. 5.18 Maximum intensity projection (MIP) images from FDG PET examination demonstrating diffuse uptake of the enlarged spleen on initial examination (left) and decreased size and uptake on the post-treatment examination (right) in a patient with follicular lymphoma consistent with diffuse splenic involvement by lymphoma

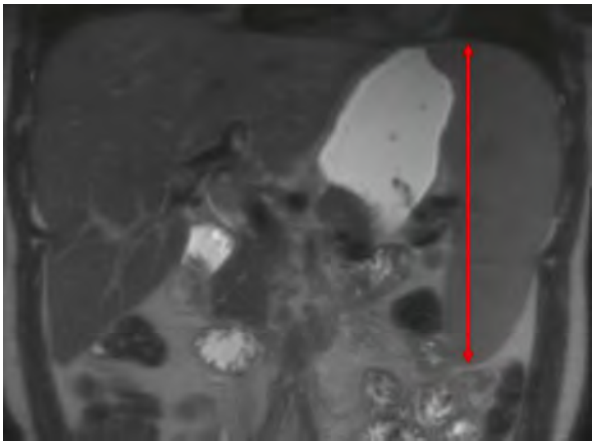

Fig. 5.19 Coronal T2-weighted MR image demonstrating diffuse splenic enlargement, which was new and occurred in the setting of lymphadenopathy and lab values consistent with disseminated histoplasmosis

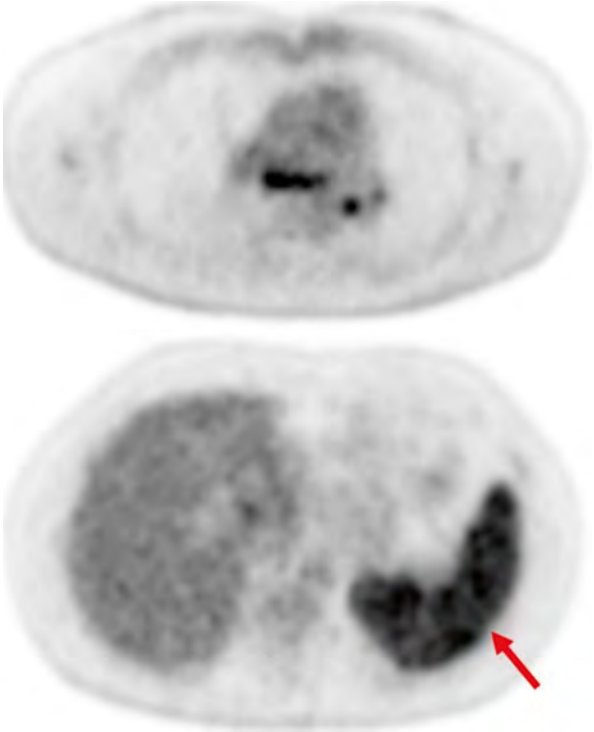

Fig. 5.20 FDG PET images in a patient with known sarcoidosis demonstrates mediastinal and hilar lymphadenopathy as well as diffuse increased FDG uptake throughout the spleen consistent with splenic involvement by sarcoidosis

Splenic Masses

- Variable in appearance depending upon etiology.
- Majority of splenic lesions are benign.
- Solid masses are best characterized on CT or MR, although definitive diagnosis is difficult as imaging findings are nonspecific and can overlap with various entities.

- It is important to distinguish cystic versus solid mass as well as to determine the enhancement pattern.
- **US**
  - Lesions may be hypo- or isoechoic or may be echogenic.
  - Vascularity can be detected with Doppler techniques or intravenous ultrasound microbubble contrast.
  - There are no specific imaging characteristics that can determine the diagnosis.
- **CT**
  - Lesions can be difficult to detect on noncontrast examinations and in the arterial phase of contrast enhancement (obscured by the striped enhancement pattern).
  - Lesions may show early enhancement and fill in (hemangiomas) or may enhance and washout (nonspecific finding).
  - Splenic lesions such as metastatic disease or infection often occur in conjunction with hepatic disease; assess the liver carefully on narrow windows if splenic lesions are detected.
- **MR**
  - Lesions are more easily detected on noncontrast MR than on noncontrast CT; typically seen best on T2-weighted images.
  - Imaging findings are similar to CT and often nonspecific.

Cystic Masses

- True cysts, also called congenital or epithelial cysts, are most often unilocular and are characterized by an epithelial lining (Fig. 5.21).
- Demonstrates no postcontrast enhancement.
- Calcifications are uncommon.

US

- Cysts are anechoic with increased through transmission of the ultrasound beam (posterior acoustic enhancement).
- The wall will be imperceptible.

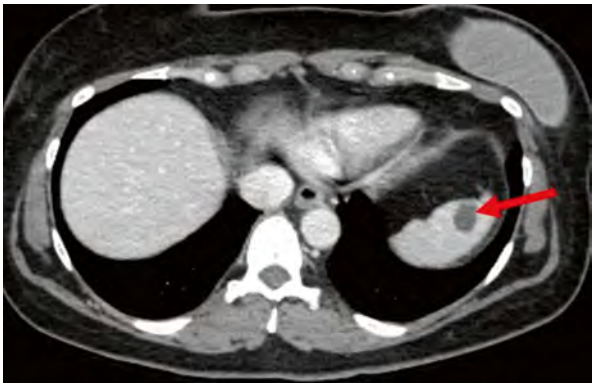

Fig. 5.21 Small unilocular cyst containing simple fluid density on CT consistent with a small splenic epithelial cyst

- Simple epithelial cysts will not contain internal septations or debris unless there has been trauma, hemorrhage, or infection.

CT

- Cysts are water density and low attenuation.
- The wall is imperceptible.
- No enhancement is present.

MR

- Cysts are T1 hypointense and T2 hyperintense.
- The wall is imperceptible.
- No enhancement is present.

Pseudocysts

- These are often seen as sequelae of prior trauma, inflammation, hemorrhage, or infarct.
- Often have a thickened, partially calcified wall and may have internal septations (Fig. 5.22).

Lymphangioma

- This is a benign lymphatic malformation presenting as a unilocular or lobulated, multilocular cyst with partially calcified internal septations (Fig. 5.23).
- May be multifocal or diffusely involve the spleen.

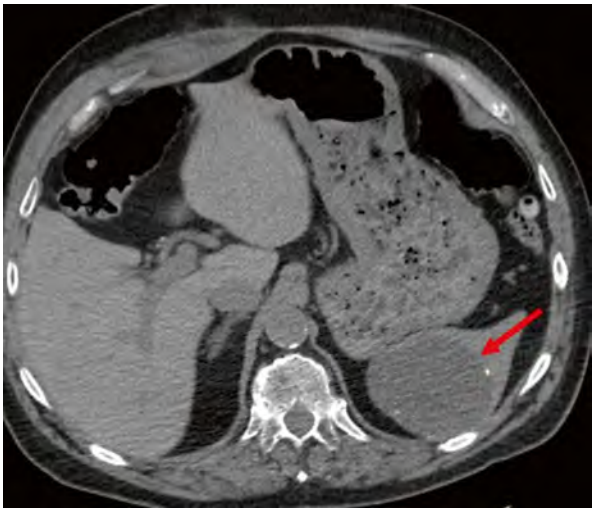

Fig. 5.22 CT image demonstrating a splenic cystic lesion with peripheral calcifications most consistent with a splenic pseudocyst

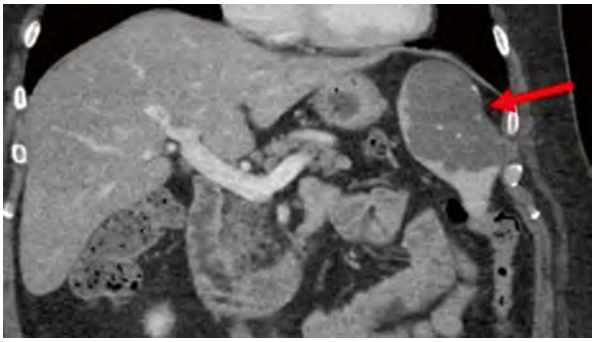

Fig. 5.23 Coronal CT image demonstrating a lymphangioma within the spleen that has intervening septations some of which are partially calcified

Fig. 5.24 Gas and fluid containing collection within the splenic parenchyma consistent with a splenic abscess

- May be indistinguishable from cyst or pseudocyst but lobulated outer contour or the presence of multiple thin internal septations may help distinguish lymphangioma from these other entities.

Infectious Cysts and/or Abscesses

- Hydatid cysts often have multi-organ involvement, wall calcifications, and daughter cysts.
- Abscesses may present as a cystic lesion in the setting of sepsis with or without internal gas (Fig. 5.24).

Solid Masses

- There are many different solid splenic masses with variable imaging appearances on CT or MRI.
- The majority of solid splenic masses are benign.

Hemangioma

- This is the most common benign splenic neoplasm.

US

- Similar appearance to hepatic hemangiomas.
- May be echogenic, although appearance and echogenicity vary.

CT

- Enhancement pattern can vary, though it may exhibit similar enhancement characteristics to hepatic hemangiomas with discontinuous peripheral enhancement early with fill-in on delayed images (Fig. 5.25).

Fig. 5.25 Lobulated mass within the anterior spleen with hypo-enhancement on portal venous phase CT that fades to iso-enhancement on delayed images consistent with a hemangioma

MR

- Will demonstrate T2 hyperintense signal like hemangiomas within the liver.

Hamartoma

- Rare, benign enhancing neoplasm often associated with tuberous sclerosis (Fig. 5.26).
- **CT/MR**
  - Well-defined, hypervascular mass with arterial enhancement and fade to background splenic parenchymal enhancement on more delayed images.

Littoral Cell Angioma

- Rare, benign vascular mass.
- **CT/MR**
  - Often multiple masses with progressive enhancement, hypoenhancing initially and isoenhancing to splenic parenchyma on delayed images (Fig. e5.11).
  - May be indistinguishable from other hypoenhancing masses such as splenic metastasis and often require splenectomy.

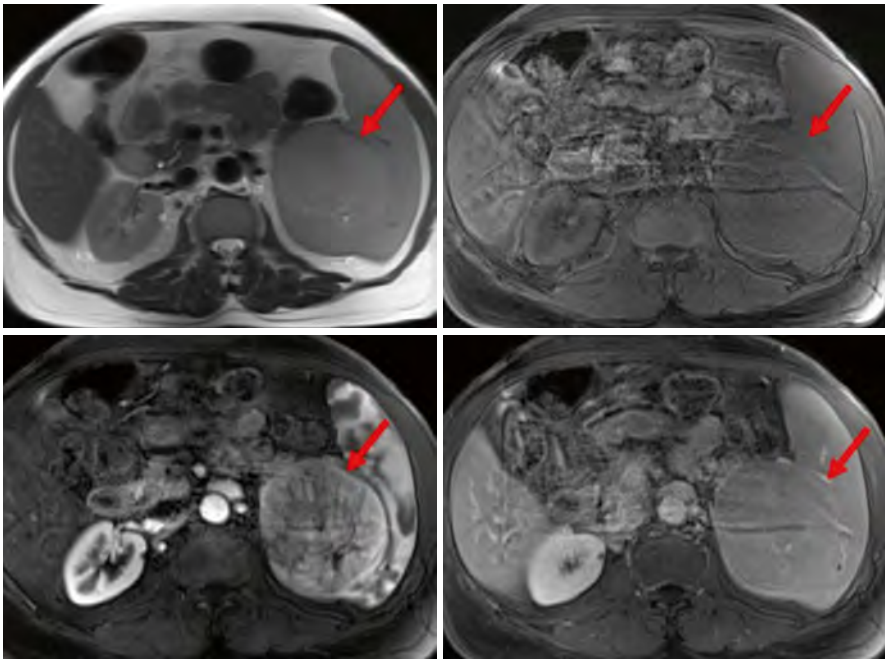

Fig. 5.26 Multiple MR images demonstrating a T1 and T2 isointense mass with early arterial enhancement and iso-enhancement on portal venous phase consistent with a splenic hamartoma

Sclerosing Angiomatoid Nodular Transformation of the Spleen (SANT)

- Benign, often solitary mass with peripheral enhancement early postcontrast and progressive linear bands of enhancement centrally on more delayed images (Fig. 5.27).
- May contain foci of hemosiderin in MRI and often have T2 hypointense bands extending centrally.

Inflammatory or Infectious Nodules

- May manifest as a single mass or multiple tiny masses throughout the spleen and are often hypoenhancing to the splenic parenchyma.
- Etiologies may include sarcoidosis, histoplasmosis, IgG4, etc.

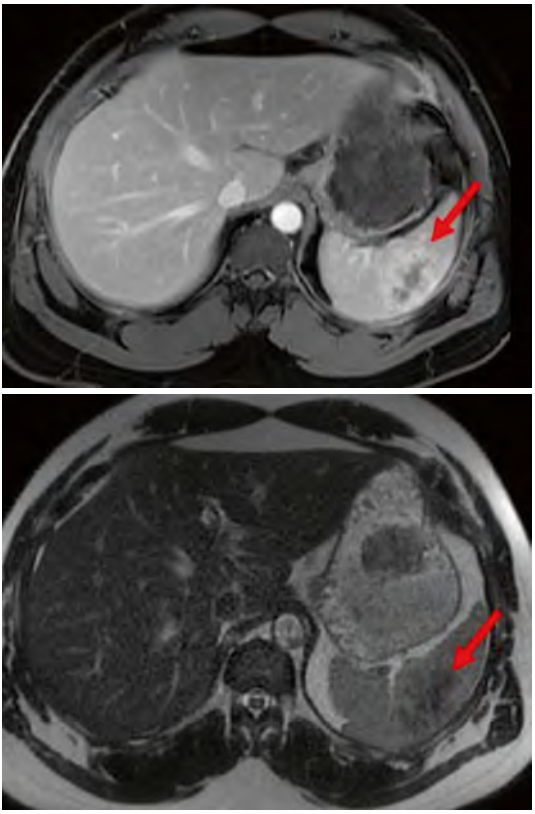

Fig. 5.27 MR images demonstrating a peripherally enhancing mass with T2 hypointense radiating central bands suggestive of sclerosing angiomatoid nodular transformation of the spleen (SANT)

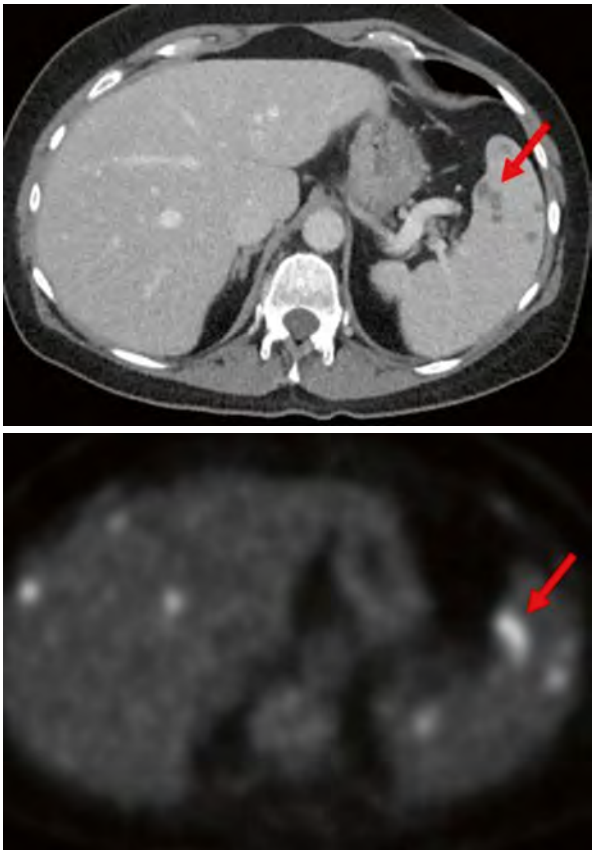

Fig. 5.28 CT and FDG PET images demonstrating hypo-enhancing splenic masses with associated FDG uptake consistent with lymphomatous involvement in this patient with known lymphoma

Malignant Splenic Masses

- Most common malignant neoplasm of the spleen is lymphoma.
  - May present as a single or multiple solid hypoenhancing masses (Fig. 5.28), though may also present as diffuse enlargement/infiltrative disease.
- Splenic metastases are most often seen in the setting of disseminated metastatic disease, though can be isolated and often present as hypoenhancing, solid masses (Fig. 5.29).
- Primary splenic malignancies are very rare such as primary splenic angiosarcomas, which often present with diffuse metastatic disease due to aggressive nature (Fig. 5.30).

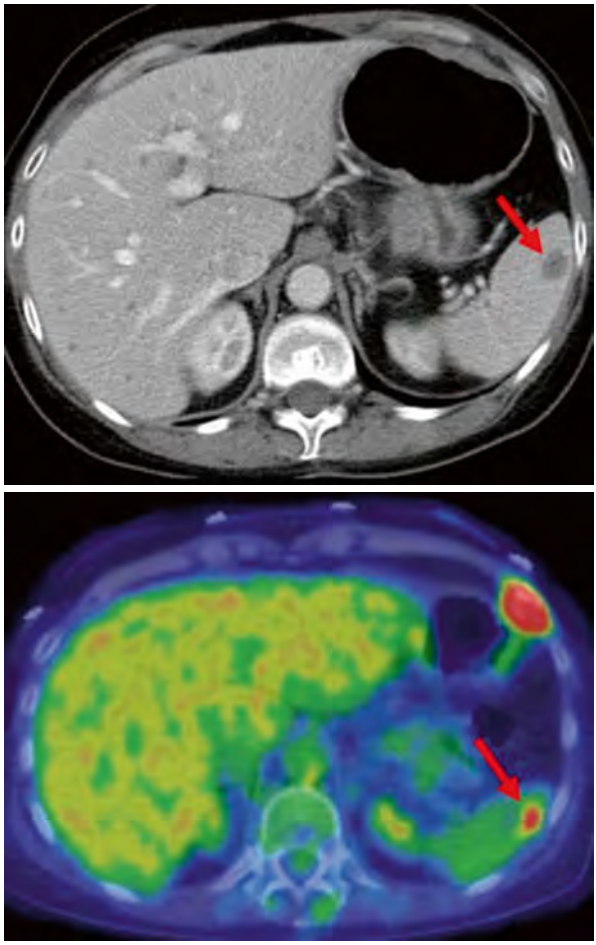

Fig. 5.29 CT and FDG PET/CT images demonstrating small hypermetabolic lesion within the spleen compatible with a metastasis in the setting of known metastatic small cell lung cancer

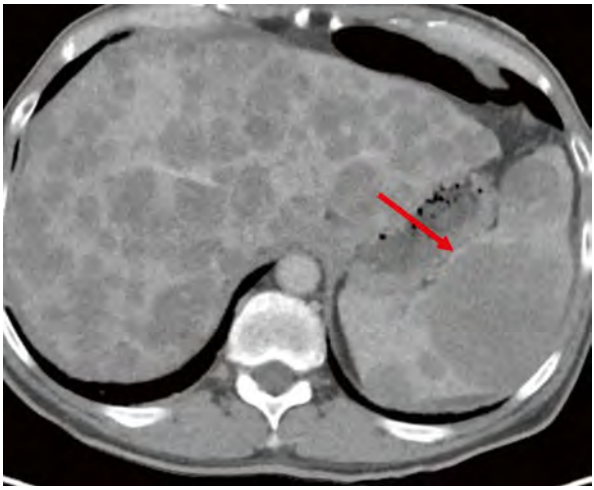

Fig. 5.30 Diffuse hepatic and splenic hypo-enhancing masses in a patient with biopsy-proven metastatic angiosarcoma

Portal Hypertension

- Very common cause of diffuse splenic enlargement.
- May be seen with many causes, including hepatic cirrhosis and portal vein thrombosis.
- Increased pressure of flow within the splenic venous outflow contributes to splenic enlargement.
- **US**
  - Splenomegaly is the most common finding.
  - Perisplenic varices and splenorenal shunts can be detected with color and spectral Doppler imaging.
- **CT**
  - Splenomegaly is the most common finding.
  - Perisplenic varices and splenorenal shunts can be seen on noncontrast and contrast-enhanced examinations.
- **MR**
  - Gamna–Gandy bodies are tiny foci of hemosiderin secondary to tiny, chronic microhemorrhages in the setting of portal hypertension and are best visualized on in- and opposed-phase images on MRI (Fig. 5.31).

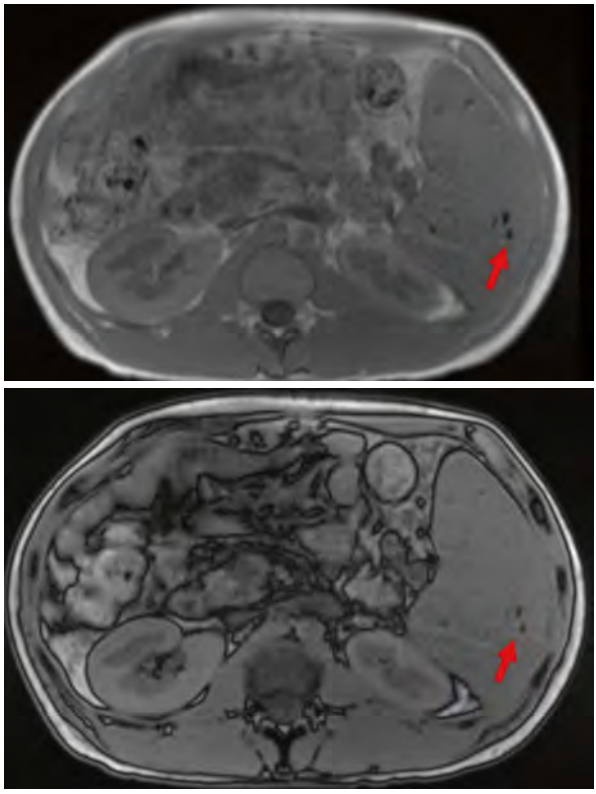

Fig. 5.31 Gamna-gandy bodies on MRI with tiny foci of susceptibility artifact visualized on the in- and opposed-phase imaging corresponding to foci of hemosiderin in the setting of portal hypertension

Embolic and Vascular Disease

- Microabscesses within the spleen occur in the setting of sepsis and known infection with hematogenous spread/seeding to the spleen (Fig. 5.32). They may be from bacterial or fungal organisms, more commonly affecting those in an immunocompromised state.
- **US**
  - Multiple hypoechoic rounded lesions.
  - Avascular appearance due to the small size.
- **CT**
  - Multiple hypodense, nonenhancing rounded lesions in the spleen.
  - Concomitant hepatic microabscesses should be evaluated for.
- **MR**
  - Multiple T1 hypointense, T2 hyperintense rounded lesions in the spleen.
  - No enhancement is demonstrated.
  - May demonstrate perilesional edema and/or restricted diffusion.
  - Hepatic microabscesses are often seen in the setting of splenic microabscesses.

Fig. 5.32 US and CT images demonstrating tiny splenic lesions in the setting of sepsis and known infection consistent with microabscesses

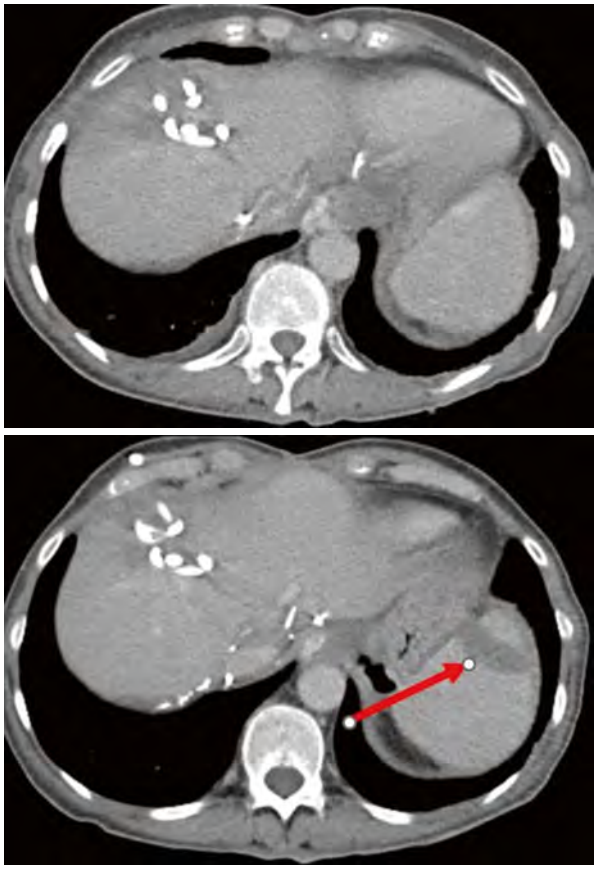

Fig. 5.33 CT images demonstrating a new linear hypo-enhancing region within the anterior spleen consistent with new splenic infarct

- Infarcts often manifest as linear or wedge-shaped areas of hypo-enhancement within the spleen (Fig. 5.33). There are many causes, including torsion, portal hypertension, or embolic sources such as endocarditis.
- **US**
  - Iso- or hypoechoic region of abnormal echotexture. May also be echogenic, depending on the stage of infarct.
- **CT**
  - Often wedge-shaped, peripheral hypoechoic area in the acute phase.
  - May calcify or liquify over time.
- **MR**
  - Often wedge-shaped, T1 hypointense, hypoenhancing area of signal abnormality.
- Auto-infarction of the spleen is associated with sickle cell disease and is the result of multiple episodes of infarction to the spleen, resulting in a small, calcified spleen without significant residual functioning splenic tissue (Fig. 5.34).

Fig. 5.34 CT image demonstrating a tiny, calcified spleen in the setting of sickle cell disease compatible with auto-infarction of the spleen

Further Readings

1. Serafino MD, Verde F, Ferro F, et al. Ultrasonography of the pediatric spleen: a pictorial review. J Ultrasound. 2019;22:503–12.
2. Giambelluca D. The "zebra" spleen. Abdom Radiol. 2019;44:1189–90.
3. Gayer G, Hertz M, Strauss S, Zissin R. Congenital anomalies of the spleen. Semin Ultrasound CT MRI. 2006;27(5):358–69.
4. Elsayes KM, Narra VR, Mukundan G, Lewis JS Jr, Menias CO, Heiken JP. MR imaging of the spleen: spectrum of abnormalities. Radiographics. 2005;25:967–82.
5. Ingle SB, Hinge CR, Patrike S. Epithelial cysts of the spleen: a minireview. World J Gastroenterol. 2014;20:13899–903.
6. Kim N, Auerbach A, Manning MA. Algorithmic approach to the splenic lesion based on radiologic-pathologic correlation. Radiographics. 2022;42:683–701.
7. Ehrlich CP, Papanicolaou N, Treves S, Hurwitz RA, Richards P. Splenic scintigraphy using Tc-99m-labeled heat-denatured red blood cells in pediatric patients: concise communication. J Nucl Med. 1982;23:209–13.
8. Jolepalem P, Balon HR. Application of heat-damaged Tc-99m RBCs in a patient with suspected hepatic metastasis. Radiol Case Rep. 2013;8(1):1–3.
9. Moore EE, Cogbill TH, Jurkovich GJ, Shackford SR, Malangoni MA, Champion HR. Organ injury scaling-spleen and liver (1994 revision). J Trauma. 1995;38(3):323–4.

Adrenal Imaging

6

Anugayathri Jawahar

Adrenal Anatomy

- The adrenal gland, also known as the suprarenal gland, is an important paired endocrine gland.
- It has a dual embryological origin.
  - The adrenal medulla arises from the neural crest tissue in the sympathetic ganglion at the level of the celiac plexus.
  - The adrenal cortex arises from the coelomic mesoderm of the urogenital ridge.
- The embryology of adrenal origin helps understand the location of ectopic adrenal rests in the retroperitoneum, testes, broad ligament, ovaries, and inguinal canal.
- The adrenal cortex has three zones: zona glomerulosa, zona fasciculata, and zona reticularis from outer to inner zones, respectively.
- At birth, the adrenals are approximately one-third the size of the kidneys and predominantly made of the adrenal cortex.
  - The adrenal cortex plays an essential role in synthesizing glucocorticoids, precursor steroids, and sex steroids.
- The adrenals are superior and anteromedial to the kidneys.
  - The right gland is between the liver, inferior vena cava, and right crus of hemidiaphragm.
  - The left gland is between the pancreatic tail and left hemidiaphragm.
- On CT, they typically appear as an inverted "y" or "v" shape (Fig. 6.1a, b).

Supplementary Information The online version contains supplementary material available at https://doi.org/10.1007/978-3-031-76624-4_6.

A. Jawahar (✉)
Department of Radiology, Northwestern University-Feinberg School of Medicine, Chicago, IL, USA
e-mail: anugayathri.jawahar@nm.org

© The Author(s), under exclusive license to Springer Nature Switzerland AG 2024

T. Catanzano (ed.), *What Radiology Residents Need to Know: Abdominal Radiology*, What Radiology Residents Need to Know,
https://doi.org/10.1007/978-3-031-76624-4_6

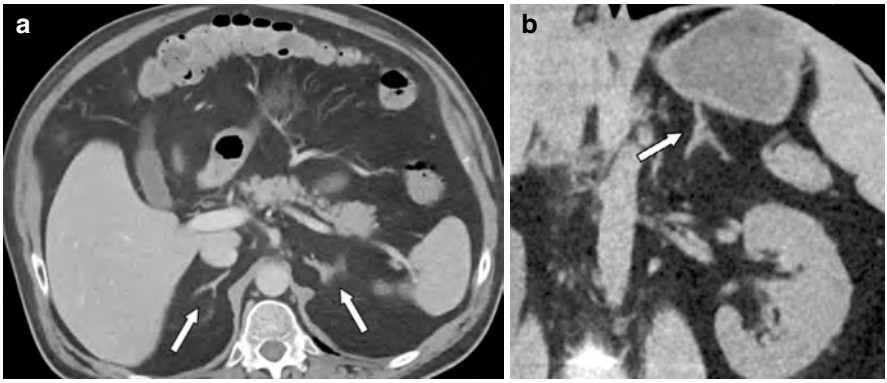

Fig. 6.1 Normal adrenal gland (CT). (**a**) Axial view of unenhanced CT: normal right adrenal gland with inverted "Y"-shaped configuration (arrow). (**b**) Coronal image of the normal left adrenal gland (arrow)

  – In patients with congenital ipsilateral renal agenesis, the adrenal gland has a discoid shape (Fig. e6.1).
- The maximum width of the body of a normal adrenal is less than 1 cm, with each limb less than 0.5 cm and the length less than 4 cm.

Optimal Imaging Modalities for Adrenal Imaging

Ultrasonography (US)

- Adrenal imaging in neonates and infants is ideally performed using US.
- Readily available, no radiation to the patient, cost-effective, and faster reads.
- The limitations are operator dependence, significantly lower sensitivity for adrenal lesions less than 3 cm, and limited ability to differentiate benign from malignant nodules.
- In adults, evaluation might be limited based on patient size and bowel gas.
- The adrenal glands appear as a hypoechoic cortex (owing to the surrounding hyperechoic fat) and an echogenic medulla (Fig. 6.2).
- US is a primary imaging modality for evaluating testicular adrenal rests in patients with congenital adrenal hyperplasia.

Computed Tomography (CT)

- Primary modality of adrenal imaging.
- Increasing detection of incidental adrenal nodules/incidentalomas.
- High temporal and spatial resolution.

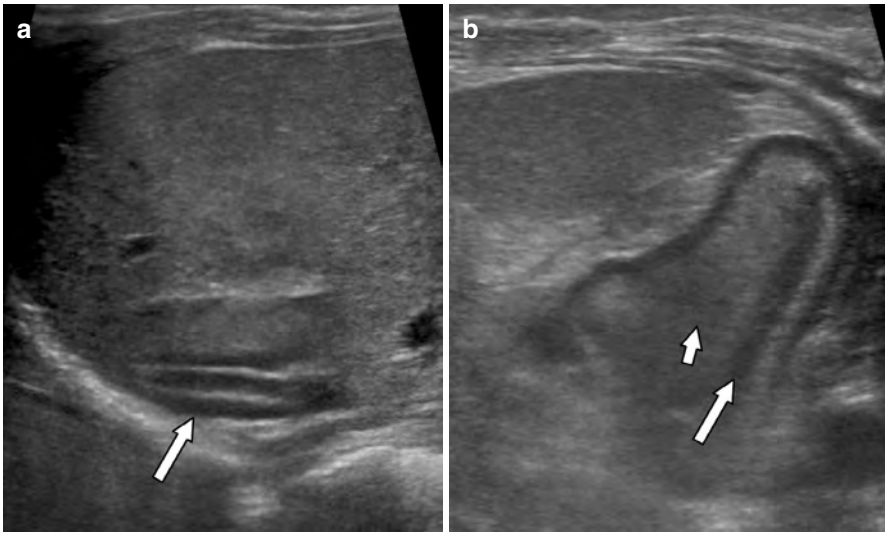

Fig. 6.2 Normal adrenal gland (US). Transverse (**a**) and longitudinal (**b**) images show a hypoechoic adrenal cortex (arrows) with a hyperechoic medulla (arrowhead)

- Unenhanced CT density measurement can help determine benign etiology in most cases.
- In indeterminate cases, contrast-enhanced CT with multiphasic acquisition and density measurements for relative and absolute washout can be used for lesion characterization.
- The CT adrenal washout protocol has a 100% sensitivity for detecting adrenal adenomas in nodules with an attenuation of more than 20 HU.
- Dual-energy CT examinations can help detect lipid-rich adenomas by assessing the reduction in attenuation on low kilovolt peak (kVp) acquisitions with a specificity of 100%, though with only a sensitivity of 50%.

Magnetic Resonance Imaging (MRI)

- High contrast resolution and inherent tissue characterization.
- Normal adrenal gland appears low to intermediate signal intensity on T1- and T2-weighted images.
- Chemical shift imaging (CSI) with in- and out-of-phase images is the most important part of adrenal MRI.
- CSI helps identify intracellular lipids based on the different resonant frequencies of fat and water protons.
- CSI can also be used in quantitative assessment where an adrenal-to-spleen CSI ratio of <0.71 on a 1.5 Tesla MRI scanner represents lipid-rich adenoma.

– The spleen is used as a reference organ for comparison since fatty infiltration does not affect it (Fig. e6.2).

$$\text{CSI ratio} = \frac{\text{Adrenal lesion-to-spleen signal intensity in-phase image}(\text{SIIP})}{\text{Adrenal lesion-to-spleen signal intensity out-of-phase image}(\text{SIOP})}$$

$$\text{Adrenal signal intensity ratio} = \frac{\text{SIIP} - \text{SIOP}}{\text{SIIP}} \times 100$$

- Similarly, the percentage of signal loss on out-of-phase images >16.5% represents lipid-rich adenoma (Fig. e6.2).

Positron Emission Tomography (PET/CT)

- ^{18}F-Fluorodeoxyglucose (FDG) PET is best used to differentiate benign from malignant adrenal lesions.
- The normal adrenal gland is barely visible on FDG PET.
- Combined PET/CT can show the gland with a maximum standardized uptake value (SUV) ranging from 0.95 to 2.46.
- When the adrenal gland's SUVmax is higher than the liver SUVmax, or when the SUVmax is over 3.1, it is suspicious for malignant lesions (Fig. e6.3).

Benign Adrenal Lesions

Adrenal Hyperplasia

- Physiological overgrowth of the adrenal cortex.
- Secondary to prolonged hormonal stimulation in Cushing disease, primary aldosteronism, or ectopic adrenocorticotropic hormone (ACTH) syndrome.
- Congenital adrenal hyperplasia (CAH) is an autosomal-recessive condition where enzyme deficiency causes glucocorticoid deficiency, which in turn causes increased ACTH secretion, resulting in adrenal hyperplasia.
- CAH also causes stimulation of aberrant adrenal rests in the testes, resulting in testicular adrenal rest tumors.
- Medically managed depending on the source of hormonal stimulation.
- "Functioning" adrenal adenomas require adrenalectomy.
- CT is the investigation of choice for identifying hyperplasia and also differentiating these from adenomas.
- Nearly impossible to differentiate hyperplasia from adenoma based on imaging alone.
  – Studies have shown that bilateral or multiple unilateral adrenal nodules or diffuse adrenal thickening favors hyperplasia (Fig. 6.3).

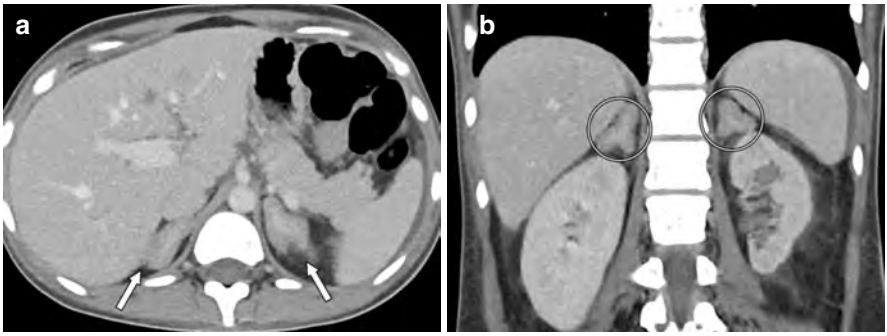

Fig. 6.3 Axial (**a**) and coronal (**b**) images of the contrast-enhanced CT demonstrate uniform thickening of both adrenal glands representing hyperplasia (arrow in **a** and circle in **b**). No discrete nodules are seen. This was a patient with Cushing syndrome due to ectopic adrenocorticotropic hormone secretion (ACTH)

- For testicular adrenal rest tumors (TART), ultrasound is the imaging test of choice.
  - Important to identify the characteristic imaging features to avoid being mistaken for testicular tumors and prevent unnecessary biopsies or orchiectomies.
  - Both occur mainly in a similar age distribution of 20–40 years.
- Ultrasound
  - TART appears as bilateral, lobular, well-demarcated hypoechoic masses within the rete testis.
  - Size ranges from 0.4 to 3.8 cm.
  - They do not show cystic changes or calcifications (Fig. 6.4).

Adrenal Calcification

- Most adrenal calcifications are detected incidentally and are usually benign and unilateral.
- The majority are benign, as in a primary adenoma.
- Less than 20% are seen with pheochromocytoma or malignant tumors like adrenocortical carcinoma and metastases.
- Ancillary findings of malignancy, like associated infiltrative mass, heterogeneity, or local invasion, can be helpful in the evaluation.
- In children, the most common calcified adrenal lesion is neuroblastoma.
- The most common etiology is idiopathic, with other less common causes including adrenal tumors, hemorrhage, or infiltrative disease.
- The adrenal calcifications can be of varying shapes: punctate, coarse, linear/curvilinear, or rim-like (Fig. e6.4).
- Ultrasound
  - Calcifications may be difficult to detect due to adjacent echogenic bowel.

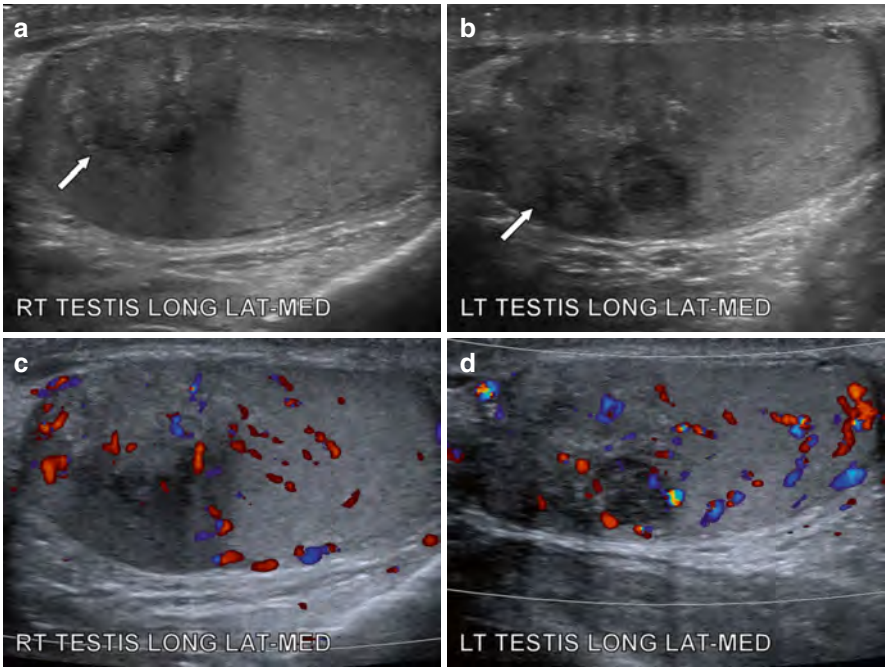

Fig. 6.4 Ultrasound of the scrotum demonstrating eccentric, ill-defined, heterogeneous hyperechoic masses in the mediastinum of both testes [arrow in the right testis (**a**) and left testis (**b**)], with hypovascularity on color Doppler imaging [right testis (**c**) and left testis (**d**)]

  - Appear as echogenic areas with posterior acoustic shadowing (if large).
- CT
  - Calcification is present within the gland.
  - It may be linear or globular and mass-like.
  - No enhancement of the calcification is seen if intravenous contrast is administered.
- MR
  - Calcification can be difficult to detect on MR.
  - Signal loss on T2 from hemosiderin related to old blood products may be present.

Adrenal Hemorrhage

- Adrenal hemorrhage is a rare entity.
- Prevalence of 0.14–1.8% in autopsies.
- It is usually not clinically symptomatic.
- If symptomatic, they present with flank or back pain, shock-like symptoms, or very rarely acute adrenal insufficiency.

- Etiology includes multiple causes, the most common being acute stress like septicemia, shock, recent major surgery, anticoagulation, hemorrhagic diathesis, and blunt trauma.
- A minority of patients can have an underlying adrenal benign or malignant tumor that is bleeding (Fig. 6.5).
- Hemorrhage is attributed to its unique blood supply.
  - Each gland is supplied by three feeding arteries and a single draining vein, which makes it susceptible.
  - Stress causes a rise in catecholamine levels, increasing vascularity, and high epinephrine concentration in the adrenal vein, causing platelet aggregation and vasoconstriction.
- Hemorrhage can cause abrupt enlargement of the gland with a heterogeneous appearance on contrast-enhanced CT mimicking malignancy.
- Lack of necrosis within the parenchyma will favor hemorrhage over malignancy.
- The imaging findings depend on the size and age of the hemorrhage.
- Ultrasound
  - Limited utility in adults due to difficulty visualizing the gland.
  - It is the study of choice for the assessment of adrenal hemorrhage in neonates.
  - The gland will appear enlarged with a mass-like area.
  - Echogenicity will vary depending on the phase of the hemorrhage (echogenic, then heterogeneous, then hypoechoic, then possibly calcified).
- CT

  The main CT finding indicative of adrenal hemorrhage in abdominal trauma is usually adrenal enlargement and periadrenal fat stranding.
  - Acute and subacute hemorrhage: hyperattenuation is observed on CT, with an attenuation between 40 and 60 HU.
  - Periadrenal infiltration or haziness can be seen.
  - Chronic hemorrhage: varying density depending on the evolution of hematoma.
  - Temporal change is key in assessing these hematomas, especially when they are new (Fig. 6.6).
  - They can develop calcifications and pseudocysts.
- MR

  Acute or subacute: hyperintensity is observed on T1- and T2-weighted images of MRI.
  - Periadrenal infiltration or haziness can be seen.
  - Chronic hemorrhage: varying intensity depending on the evolution of hematoma.
  - Temporal change is key in assessing these hematomas, especially when they are new.
  - They can develop calcifications and pseudocysts.

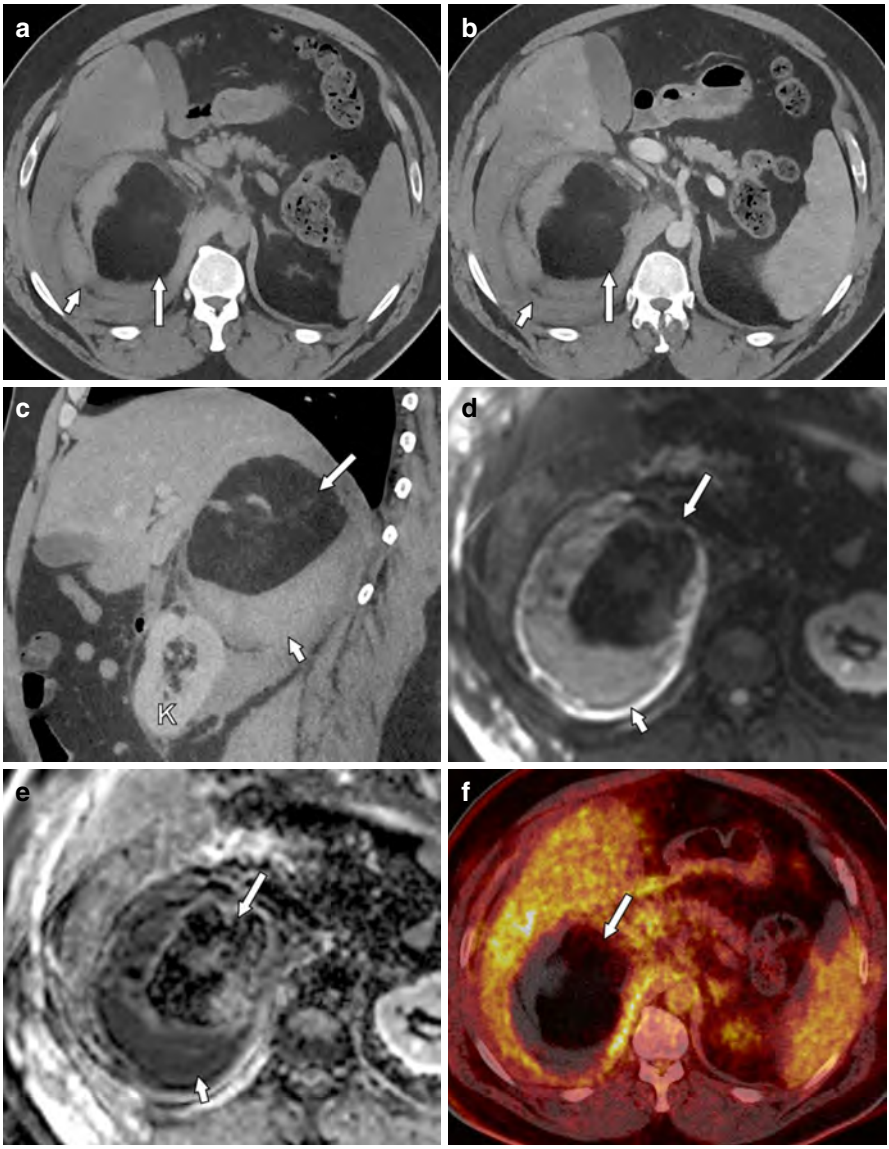

Fig. 6.5 CT of the abdomen in axial precontrast (**a**) and postcontrast phase in axial (**b**), and sagittal planes (**c**). A large expansile heterogeneous fat-density mass is in the suprarenal region with a nonvisualized right adrenal gland (arrows). There is nonenhancing peripheral curvilinear hyperdensity along the posterior and inferior aspect of the mass (arrowheads), representing hemorrhage within the mass. The right kidney is inferiorly displaced (annotation K in **c**). MRI abdomen with diffusion-weighted images, *b*-value of 800 (**d**), and apparent diffusion coefficient (ADC) images (**e**) show restricted diffusion in the peripheral hematoma (arrowhead). PET/CT image (**f**) shows no tracer uptake within the mass (arrow). The mass was resected and reported as lipid-rich adrenal angiomyolipoma with resolving hematoma

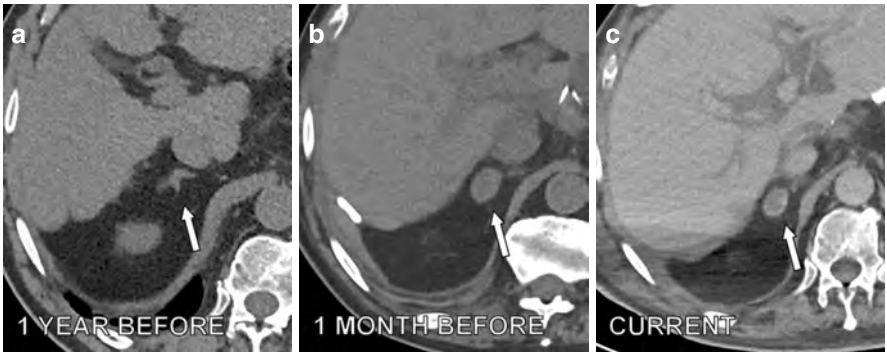

Fig. 6.6 Unenhanced axial CT abdomen shows normal right adrenal gland 1 year prior in (**a**) (arrow), a new hyperdense right adrenal nodule in CT from 1 month prior in (**b**) (arrow) representing hematoma, and the current CT in (**c**) demonstrating heterogeneity of the nodule with central hypodensity and peripheral hyperdensity representing peripheral calcifications from evolving hematoma (arrow). The patient was elderly, had a recent liver transplant, and had a spontaneous hemorrhage in the adrenal gland

Adrenal Cyst

- It is relatively rare, about 0.2%.
- Usually found incidentally on imaging.
- If symptomatic, presents with abdominal pain, abdominal mass, or hypertension.
- Often unilateral, with a slight female predilection.
- They can show minimal enlargement over time, with a median growth rate of 2 mm/year.
- Caused by epithelial or endothelial proliferation, hemorrhage, or parasitic disease and classified accordingly as endothelial (most common; >80% of cysts), epithelial, parasitic, and pseudocysts.
- **CT**
  - Well-defined round or oval hypodense mass with an attenuation of <20 HU.
  - They have thin walls and thin septa <3 mm, when present.
  - The cyst wall and septa may contain calcifications.
  - There is no enhancement with contrast.
- **MRI**
  - Low signal on T1-weighted images, high signal on T2-weighted images.
  - There is no enhancement on postcontrast images.
  - There is no signal loss on in- and out-of-phase images.
  - May be difficult to differentiate from adrenal myelolipoma, which has similar MRI features.

    In such cases, the fat-only image of the Dixon sequence will help differentiate the adrenal cyst from myelolipoma, where the cyst has a low signal, whereas myelolipoma has a high signal on the fat-only Dixon image (Fig. 6.7).

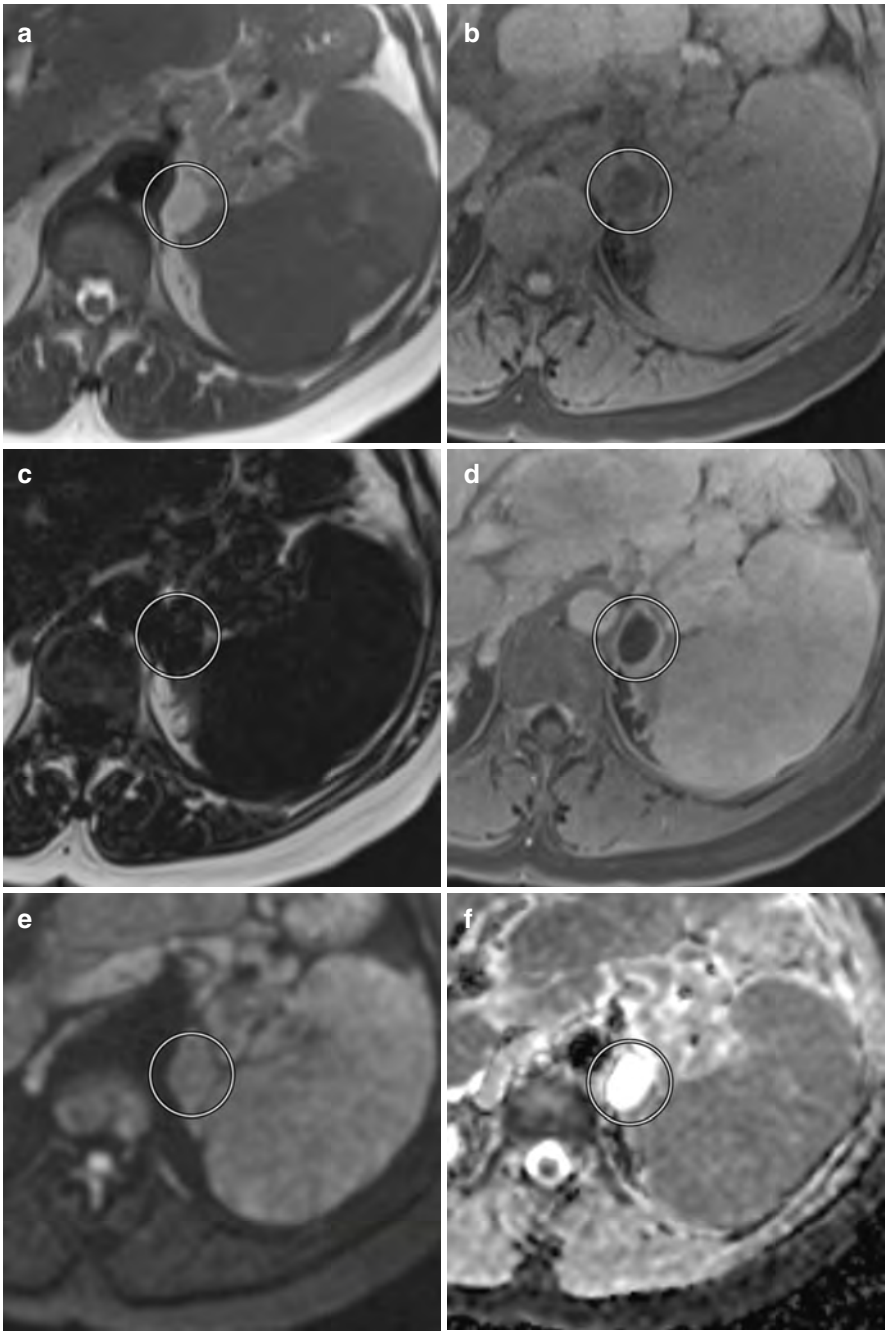

Fig. 6.7 Axial views of the MRI abdomen. The circles show the 1.5 cm left adrenal cyst, which shows a high signal on HASTE (**a**), a low signal on unenhanced water-only Dixon (**b**), and fat-only Dixon (**c**). The lesion does not show enhancement of the lesion, although the uniform thin wall shows enhancement on contrast-enhanced water-only Dixon (**d**). There is no restricted diffusion with a high signal on *b*-800 DWI (**e**) and ADC images (T2-shine through) (**f**)

  - If there are nodular septations with enhancement, cystic adrenal tumors such as pheochromocytoma or adrenal cortical carcinoma should be considered.

Adrenal Masses

- When an adrenal mass is found on imaging, two things need to be determined: whether the nodule is hormonally active and whether it could be malignant.
- While various masses can occur in the adrenal gland, the most common benign mass is adrenocortical adenoma, and the most common malignant mass is adrenocortical carcinoma.

Adrenal Adenoma

- The most common adrenal lesion arising from the adrenal cortex and constitutes 80–90% of all adrenal lesions.
- Incidence of adrenal incidentalomas has increased by 10 times over the past two decades with the increasing use of cross-sectional imaging.
- Most adenomas are incidentally detected and are hormonally inactive.
- Functioning adenomas account for only about 6%, among which the majority are cortical-secreting tumors.
- Functioning and nonfunctioning adenomas appear similar on imaging and cannot be differentiated.
- Atrophy of the contralateral adrenal gland, which might be from pituitary ACTH secretion suppressed by elevated cortisol levels, can suggest that the lesion is functioning.
- Clinical suspicion from symptoms and laboratory tests determine the functionality of adrenal adenomas.
- On imaging, these are typically well-circumscribed homogeneous lesions and usually stable in size or show very slow growth on serial imaging.
  - Normally measure 1–3 cm in size (Fig. e6.5).
- Rarely these adenomas present as large masses with calcifications, hemorrhage, or cystic changes.
- Adenomas can be lipid-rich or lipid-poor depending on the extent of intracytoplasmic microscopic fat.
- There are also adenomas with macroscopic fat, which has to be differentiated from myelolipomas.
- **US**
  - Adenomas can be seen incidentally as well-defined, round, or oval, hypoechoic nodular masses (Fig. 6.8).
- **CT**
  - Lipid-rich adenomas demonstrate an attenuation of ≤10 Hounsfield Units (HU) on unenhanced CT.

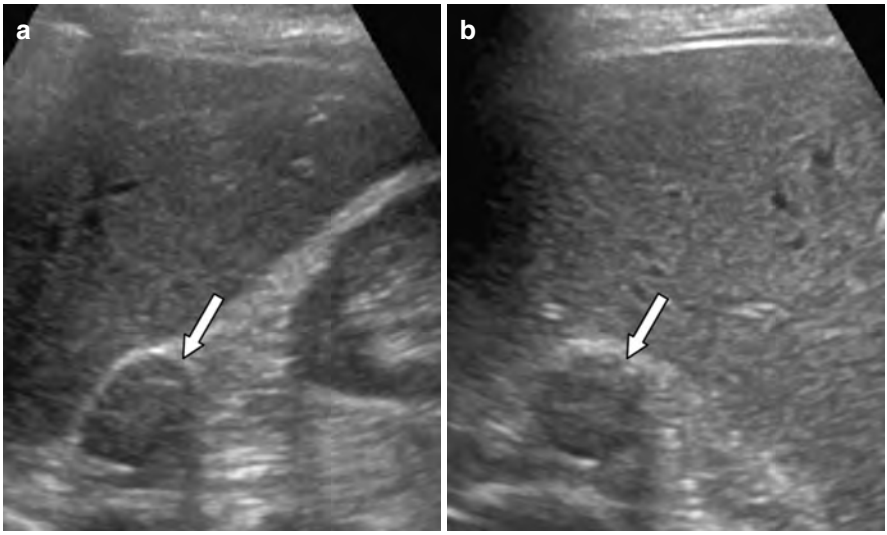

Fig. 6.8 Ultrasound in longitudinal (**a**) and transverse planes (**b**) shows a homogeneous hypoechoic nodule superior to the upper pole of the right kidney (arrows), representing an adrenal nodule

- The attenuation cutoff values ≤10 HU on virtual unenhanced CT are diagnostic of lipid-rich adenoma similar to conventional unenhanced CT.
- Unenhanced CT has a sensitivity of 71–73% and a specificity of 96–98% in detecting adrenal lipid-rich adenomas.

- Indeterminate lesions are diagnosed based on the triphasic adrenal protocol, which includes an unenhanced phase, a 60–90-s enhanced phase, and a 15-min delayed enhanced phase exam with about 120–150 cc of non-iodinated intravenous contrast administration.
  - The attenuation calculated in HU from the ROI placed within the adenoma on the three phases is used to calculate the absolute and relative washout.

$$\text{Absolute washout} = \frac{\text{Enhanced CT @ 60s (HU)} - \text{Delayed CT (HU) @ 15-min}}{\text{Enhanced CT @ 60s (HU)} - \text{Unenhanced CT}} \times 100\%$$

$$\text{Relative washout} = \frac{\text{Enhanced CT @ 60s (HU)} - \text{Delayed CT (HU) @ 15-min}}{\text{Enhanced CT @ 60s (HU)}} \times 100\%$$

- An absolute washout of >60% and/or relative washout of >40% has 100% sensitivity and specificity for an adenoma (Fig. 6.9).

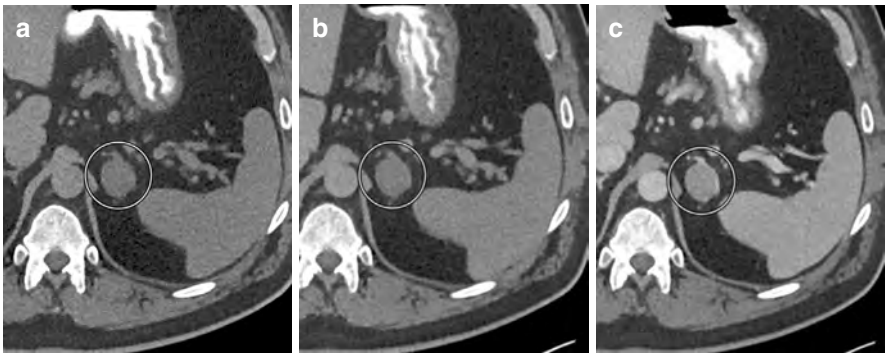

Fig. 6.9 Axial CT adrenal washout protocol showing a left adrenal nodule (circle) measuring attenuation of 18 Hounsfield Units (HU) on unenhanced image (**a**), 62 HU on portal venous phase (**b**), and 18 HU on delayed phase image (**c**). The relative contrast washout was 50%, and the absolute washout was 71%, consistent with an adenoma

- This adrenal washout technique has a sensitivity of 100% and specificity of 98% in detecting adrenal adenomas.
- **MRI**
  - Demonstrates uniform enhancement on postcontrast images unless heterogeneity is due to hemorrhage, calcifications, or cystic changes (Fig. 6.10).
  - Lipid-rich and lipid-poor adenomas contain intracellular fat, demonstrating signal loss on opposed phase images.
  - Adenoma with macroscopic fat will demonstrate signal loss on fat-suppressed images and India Ink artifacts at the interfaces of fat and water.

    While this is similar in imaging to adrenal myelolipoma, the amount of macroscopic fat is markedly less compared to myelolipoma.
  - When there is only a small amount of macroscopic fat, myelolipomatous degeneration within an adrenal adenoma should be considered (Fig. 6.11).
- **PET/CT**
  - Adenomas do not demonstrate FDG uptake on PET/CT.
  - If there is uptake, it is usually less than the liver SUVmax (Fig. e6.6).
- The American College of Radiology (ACR) released white paper guidelines for managing incidental adrenal masses on imaging with recommendations for follow-up and treatment.
  - Incidental adrenal nodules detected on CT or MRI do not need follow-up if they have clear benign imaging features like <10 HU on unenhanced CT, drop in signal on chemical shift MRI, or show stability for over a year.
  - Nodules larger than 1 cm but less than 4 cm might require adrenal washout CT to determine if it is benign or require further testing with PET/CT or biopsy.
  - Nodules larger than 4 cm may require intervention with resection if there is no history of malignancy or biopsy/PET-CT if there is a history of malignancy.

Fig. 6.10 Axial MRI adrenal protocol (**a**–**e**) and axial CT abdomen in portal venous phase (**f**). The arrows point to the left adrenal nodule, which exhibits a low signal on the Half Fourier Single-shot Turbo Spin Echo (HASTE) sequence (**a**) and unenhanced T1-weighted image (**b**). The nodule shows heterogeneous enhancement on the postcontrast image (**c**) with a signal drop on the opposed phase (**d**) relative to the in-phase images (**e**), which is consistent with lipid-rich adenoma. CT shows a heterogeneous hypodense nodule (**f**)

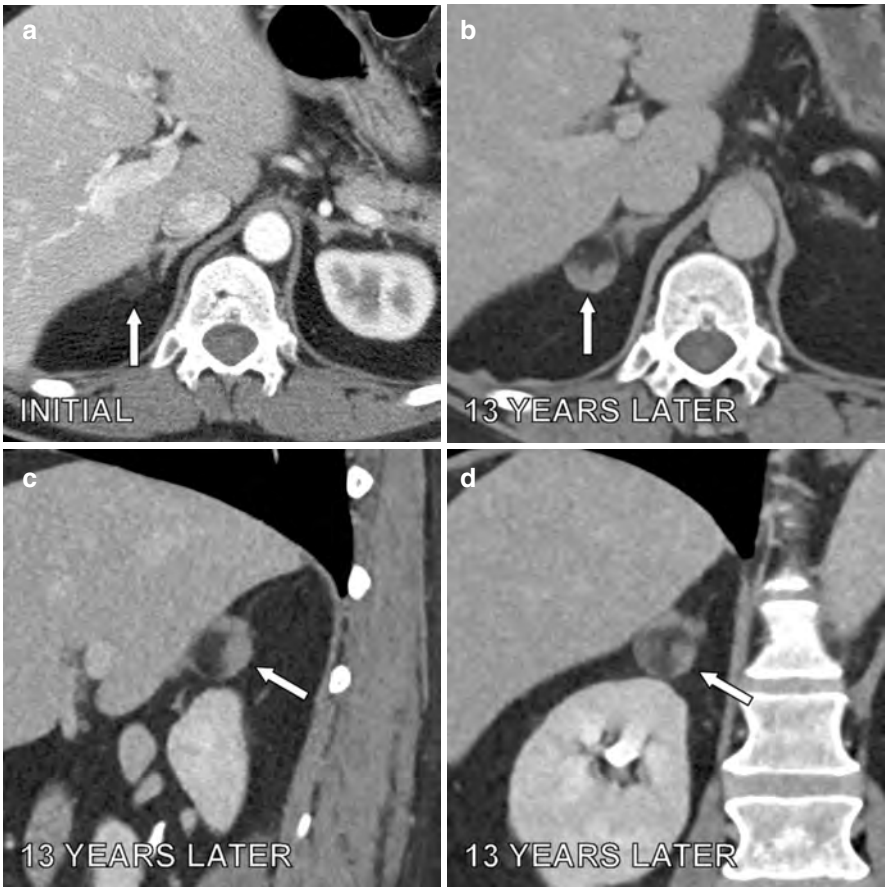

Fig. 6.11 CT abdomen images in axial (**a**, **b**), sagittal (**c**), and coronal planes (**d**) show a 0.8 cm right adrenal fat-density, lipid-rich adenoma (**a**). On the subsequent CT abdomen 13 years later, the nodule demonstrated a heterogeneous nodule that now measures 2.4 cm and with more than 50% fat density (**b**–**d**). Resection was performed with pathology reported as myelolipomatous degeneration of adenoma

- Stability of adrenal nodules >12 months or growth ≤3 mm/year suggests benignity and, most commonly, an adenoma.

Adrenal Myelolipoma

- These are secondary-origin tumors of no specific cortex or medulla histological origin.
- Nonfunctioning benign adrenal tumors with macroscopic fat and myelopoietic cells.

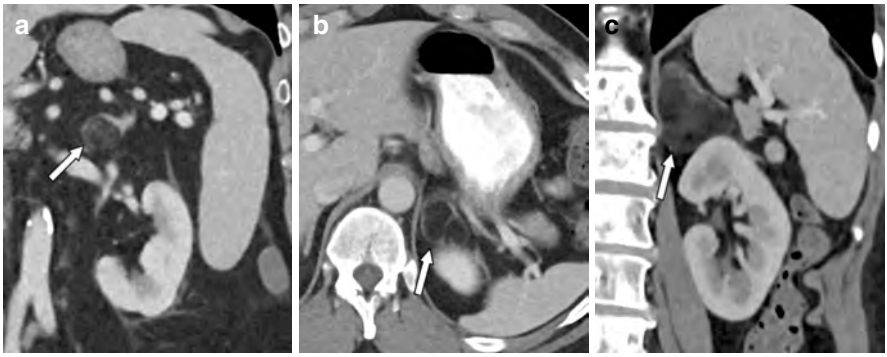

Fig. 6.12 Contrast-enhanced CT of three different sizes and morphological appearances of left adrenal fat-density lesions representing myelolipomas in three different patients (arrows). The lesion in (**a**) has a relatively homogeneous fat density and measures 1.6 cm. The lesion in (**b**) measures 2.7 cm and is homogeneous but has a thin linear hypodensity within the lesion, which appears like a septation. The lesion in (**c**) measures 4.6 cm and has a slightly heterogeneous fat density

- Usually incidentally detected but can rarely present with pressure symptoms or pain.
- **CT**
  - Fat attenuation of less than −30 HU.
  - Can have mild enhancement with contrast due to poor vascularity (Fig. 6.12).
- **MRI**
  - Unlike adenomas, myelolipomas contain macroscopic fat and are best seen with signal loss on fat-saturated MRI sequences.
  - They demonstrate high signal on T1- and T2-weighted images (Fig. 6.13).
- When large, myelolipomas can also cause intratumoral hemorrhage or infarction.
- Due to the risk of hemorrhage, lesions >4 cm are usually surgically resected or undergo adrenalectomy—American Association of Clinical Endocrinologists and American Association of Endocrine Surgery (AACE/AAES) 2009 guidelines.
- Myelolipomas <4 cm do not require follow-up or further testing if there are apparent benign features and without complications.
- The differentials for adrenal myelolipoma on MRI include adenoma with macroscopic fat and adrenal cysts.

Pheochromocytoma

- Pheochromocytomas are the most common tumors arising from the chromaffin cells of the adrenal medulla.
- They produce catecholamines.
- It is usually benign in 90% of cases and most commonly seen in adults.
- Pheochromocytoma Rule of 10: 10% of tumors can be malignant, multiple, bilateral, extra-adrenal, familial, and/or occur in children.

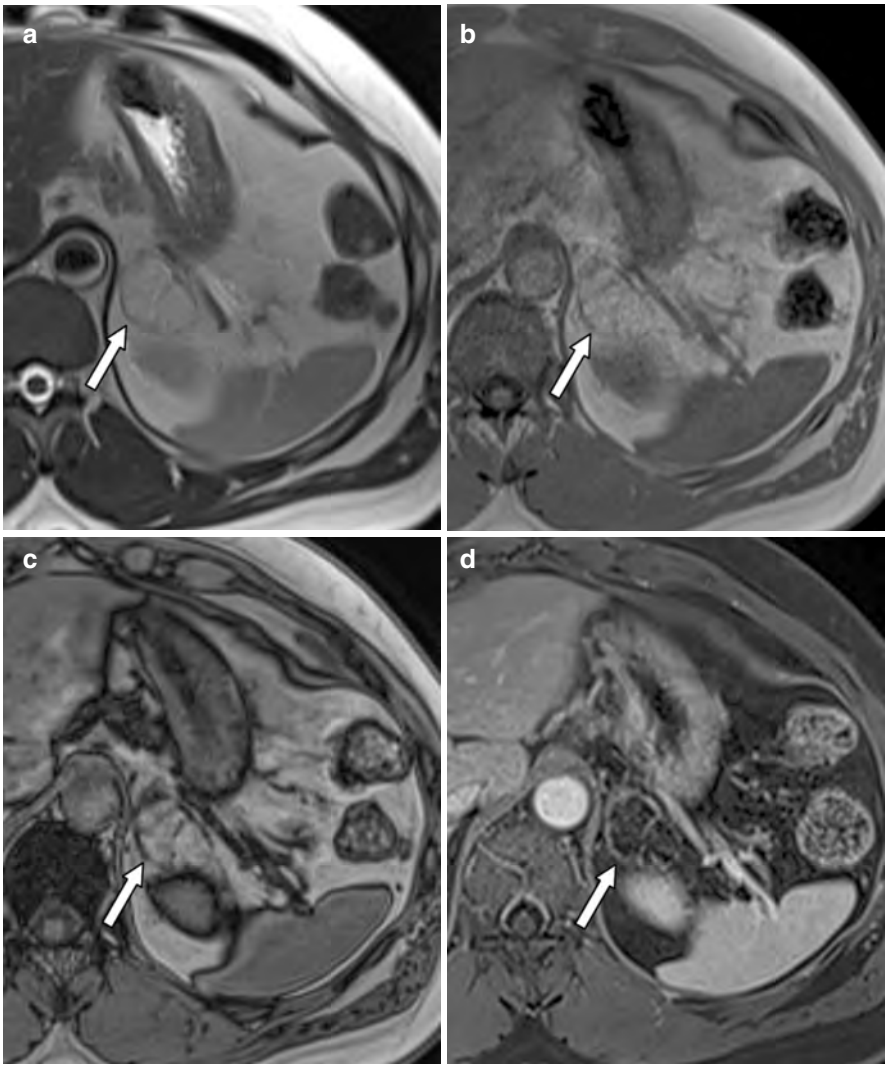

Fig. 6.13 MRI abdomen shows a 2.7 cm left adrenal nodule, which demonstrates a high signal on HASTE sequence (**a**), high signal on in-phase (**b**), and opposed-phase images (**c**), without loss of signal on opposed phase. However, signal loss was on the contrast-enhanced, water-only Dixon sequence (**d**), which has inherent macroscopic fat suppression

- Hereditary syndromes associated with pheochromocytoma include multiple endocrine neoplasia (MEN) syndrome types 2A and 2B, von Hippel–Lindau syndrome, and neurofibromatosis type I.
- Hereditary/familial pheochromocytomas, compared to sporadic ones, are usually small in size, less 24-h urinary metanephrines, and are less symptomatic.

- These tumors are often diagnosed by their typical imaging features, while a few patients can have atypical findings.
- **CT**
  - They are oval, well-circumscribed soft-tissue masses.
  - Attenuation is approximately 40 HU.
  - These show avid homogeneous or heterogeneous enhancement (Fig. 6.14).
- **MRI**
  - These mostly demonstrate high signal on T2-weighted images (light bulb sign).
  - They do not show a signal loss on out-of-phase images due to a lack of substantial intracytoplasmic lipids.
  - They also demonstrate intense enhancement with intravenous contrast (Fig. 6.15).

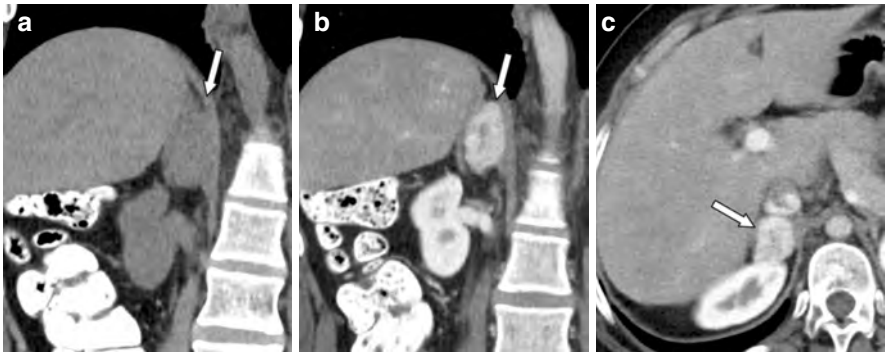

Fig. 6.14 CT abdomen in coronal (**a**, **b**) and axial planes (**c**) shows an incidental 3.7 cm right adrenal nodule (arrows), which is homogeneously hypodense on the precontrast image (**a**) and demonstrates mildly heterogeneous but avid enhancement on the postcontrast images (**b**, **c**)

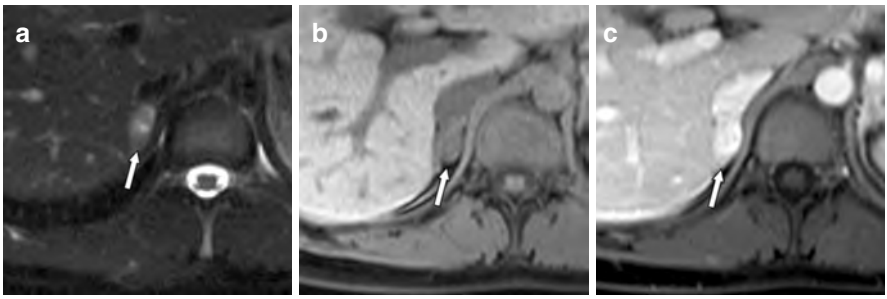

Fig. 6.15 MRI abdomen shows a 1.6 cm heterogeneous hyperintense signal in the right adrenal nodule (arrows) on the fat-suppressed T2-weighted image (**a**), hypointense signal on the unenhanced T1-weighted image (**b**), and intense enhancement on the postcontrast T1-weighted image (**c**). The nodule was resected in lieu of a concurrent renal lesion, and its pathology was reported as pheochromocytoma

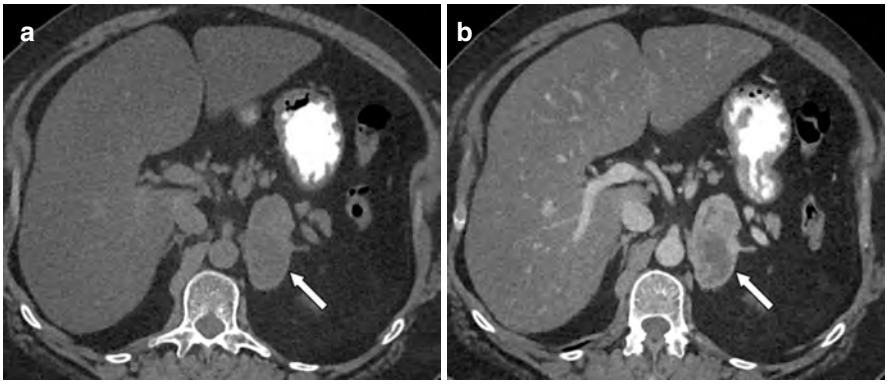

Fig. 6.16 Axial precontrast (**a**) and postcontrast (**b**) images of the CT abdomen show an incidental 7 cm heterogeneous hypodense mass (arrows) with heterogeneous enhancement and multiple small nonenhancing cystic areas. The resected mass was reported on pathology as pheochromocytoma

- Imaging appearances can be variable based on cyst or pseudocyst formation, necrotic features, or hemorrhage (Fig. 6.16).
- While FDG-PET/CT is used for these pheochromocytomas, 131I- or 123I-labeled metaiodobenzylguanidine (MIBG) is a test of choice for extra-adrenal paragangliomas.

Malignant Adrenal Masses

- Evaluation of any incidental adrenal nodule should include size, homogeneity or heterogeneity of nodule, enhancement, contrast washout, radiotracer avidity, and presence of a primary tumor.
- Imaging findings that favor malignant mass include large size (usually >4 cm), size growth compared to priors, irregular margin, infiltrative features, and heterogeneous appearance.
- Smaller adrenal nodules with an absolute washout of <60% or relative washout of <40% are almost always associated with malignancy.

Adrenal Metastasis

- Adrenal metastasis is the most common malignant adrenal tumor, with primary tumors from the lung, breast, bowel, and pancreas.
- Imaging appearances are variable depending on the primary tumor.
  Adrenal metastasis commonly does not show washout on the CT adrenal washout protocol.
  However, metastasis from hypervascular primary tumors like clear cell renal cell carcinoma (RCC), neuroendocrine tumors, hepatocellular carcinoma (HCC), or melanoma will demonstrate a washout of contrast (Fig. e6.7).

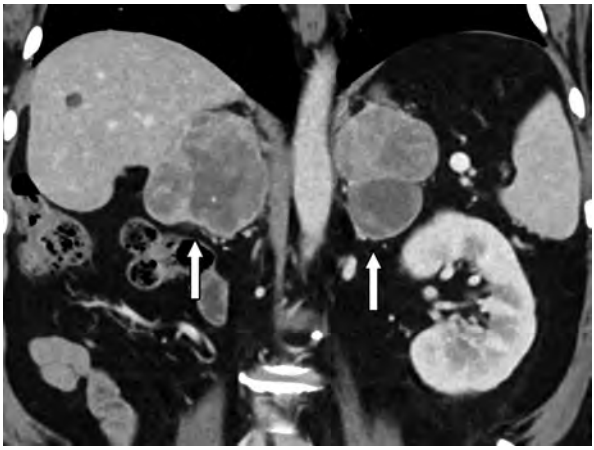

Fig. 6.17 Coronal postcontrast CT abdomen shows large bilateral adrenal masses (arrows) demonstrating heterogeneous enhancement and cystic necrosis. Note the absent right kidney—post right nephrectomy for renal cell carcinoma. The adrenal nodules were reported as metastatic from renal cell carcinoma at pathology

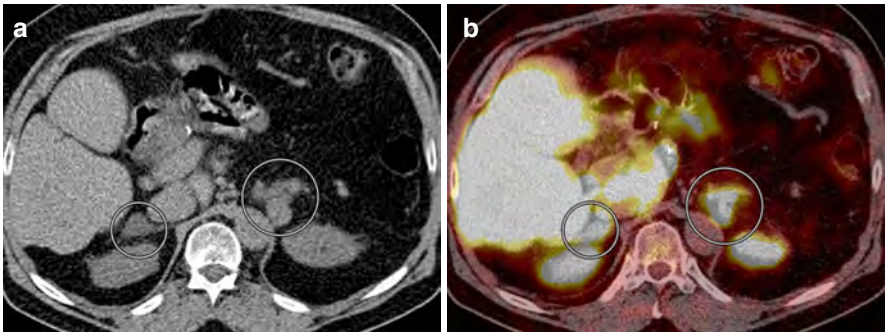

Fig. 6.18 PET/CT images—unenhanced CT (**a**) and fused PET/CT image (**b**). Nodules (circles) are present in both adrenal glands, which demonstrate intense tracer uptake in both adrenal nodules on the PET image (**b**)

- Metastases from clear cell RCC and HCC can contain microscopic fat, which confuses imaging appearance with a differential of a lipid-poor adenoma (Fig. 6.17).
  - Features favoring metastasis: presence or history of a known primary malignancy, multiplicity, and a new hypermetabolic mass on PET/CT (Fig. 6.18), and high signal on T2-weighted images with heterogeneity.
- On CT, these have an attenuation of >10 HU.
- PET/CT helps identify these metastases with high sensitivity and specificity.

Adrenal Cortical Carcinoma

- Hormonally active malignant tumor of the adrenal cortex.
- Bimodal age distribution: first and fourth decades of life.

- Clinically presents with hypertension, Cushing's syndrome, feminization, virilization, or a combination of the above.
- Occasionally, these can present with pain, palpable mass, or symptoms related to mass effect on the adjacent bowel.
- When adrenal nodules demonstrate rapid growth of ≥5 mm/year, adrenal cortical carcinomas should be suspected.
- On imaging, these are typically large masses with a majority of 6 cm or more at presentation.
- Unlike adrenocortical adenomas, these tumors are inhomogeneous on unenhanced CT due to necrosis; few might demonstrate calcifications.
- **CT**
  - They present as heterogeneously enhancing mass with peripheral enhancement or thin enhancing rim seen in a few cases (Fig. 6.19).
  - Adrenal washout CT will demonstrate a relative washout of <40%.
- **MRI**
  - They are usually large heterogeneous masses with nonenhancing central cystic or necrotic areas that appear as high signals on T2-weighted images.
  - They can also have intrinsic high signal on T1-weighted images from intratumoral hemorrhage (Fig. 6.20).
- **PET/CT**
  - These tumors are FDG-avid and can demonstrate heterogeneous uptake with photopenic regions within the tumor corresponding to cystic necrosis or hemorrhage (Fig. e6.8).
  - PET/CT can also evaluate local recurrence or distant metastasis.
- They can present with metastasis. The most common organs are the liver, lungs, and lymph nodes.
- Percutaneous biopsy of adrenal cortical carcinoma is generally avoided, given the risk of tumor seeding [1–31].

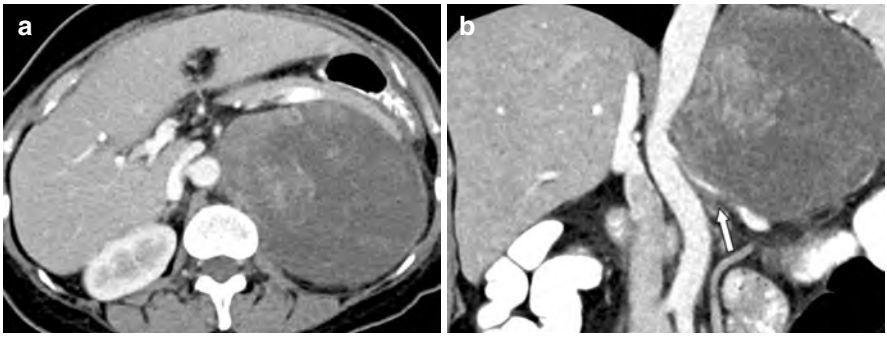

Fig. 6.19 Postcontrast CT abdomen in axial (**a**) and coronal planes (**b**) shows a 12.3 cm left adrenal heterogeneous mass with irregular foci of internal hemorrhage. There is a mass effect on the abdominal aorta, pushing it to the right of the midline and also compressing the left renal artery (arrow in **b**). The resected mass was reported as adrenal cortical carcinoma. The patient succumbed 2 months later from multiorgan failure and obstructive shock

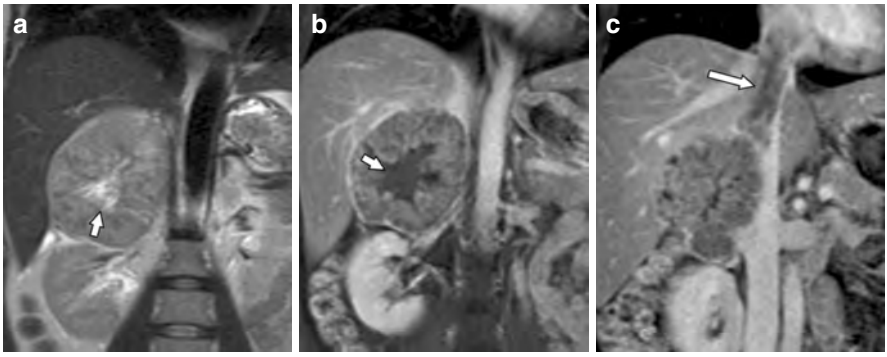

Fig. 6.20 MRI abdomen in the coronal plane shows a large, 11.3 cm, relatively well-defined, heterogeneous solid mass arising from the right adrenal gland. There are central hyperintense areas within the mass on the HASTE sequence (**a**) that do not show enhancement on postcontrast images (arrowheads in **b** and **c**). A similar heterogeneously enhancing tumor thrombus extends from the adrenal mass into the IVC (arrow in **c**)

References

1. Barwick TD, Malhotra A, Webb JA, Savage MO, Reznek RH. Embryology of the adrenal glands and its relevance to diagnostic imaging. Clin Radiol. 2005;60(9):953–9.
2. Deshpande SS, Shetty D, Saifi S. Sonographic appearance of testicular adrenal rest tumour in a patient with congenital adrenal hyperplasia. Pol J Radiol. 2017;82:526–9.
3. Elsayes KM, Mukundan G, Narra VR, Lewis JS Jr, Shirkhoda A, Farooki A, Brown JJ. Adrenal masses: MR imaging features with pathologic correlation. Radiographics. 2004;24(Suppl 1):S73–86.
4. Moore KL, Persaud TVN. The developing human. 6th ed. Philadelphia, PA: Saunders; 1998.
5. Williams PL, Bannister LH, Berry MM, et al. Gray's anatomy. 38th ed. London: Churchill Livingstone; 1995.
6. Panda A, Das CJ, Dhamija E, Kumar R, Gupta AK. Adrenal imaging (Part 1): Imaging techniques and primary cortical lesions. Indian J Endocrinol Metab. 2015;19(1):8–15.
7. John R, Putta T, Simon B, Eapen A, Jebasingh F, Thomas N, Rajaratnam S. Normal adrenal gland thickness on computerized tomography in an Asian Indian adult population. Indian J Radiol Imaging. 2018;28(4):465–9.
8. Wan YL. Ultrasonography of the adrenal gland. J Med Ultrasound. 2007;15(4):213–27.
9. Bracci B, De Santis D, Del Gaudio A, Faugno MC, Romano A, Tarallo M, Zerunian M, Guido G, Polici M, Polidori T, Pucciarelli F, Matarazzo I, Laghi A, Caruso D. Adrenal lesions: a review of imaging. Diagnostics (Basel). 2022;12(9):2171.
10. Badawy M, Gaballah AH, Ganeshan D, Abdelalziz A, Remer EM, Alsabbagh M, Westphalen A, Siddiqui MA, Taffel MT, Itani M, Shaaban AM, Elsayes KM. Adrenal hemorrhage and hemorrhagic masses; diagnostic workup and imaging findings. Br J Radiol. 2021;94(1127):20210753.
11. Nandra G, Duxbury O, Patel P, Patel JH, Patel N, Vlahos I. Technical and interpretive pitfalls in adrenal imaging. Radiographics. 2020;40(4):1041–60.
12. Blake MA, Prakash P, Cronin CG. PET/CT for adrenal assessment. AJR Am J Roentgenol. 2010;195(2):W91–5.
13. Blake MA, Cronin CG, Boland GW. Adrenal imaging. AJR Am J Roentgenol. 2010;194(6):1450–60. https://doi.org/10.2214/AJR.10.4547. Erratum in: AJR Am J Roentgenol. 2012;198(5):1232.

14. Fujiyoshi F, Nakajo M, Kukukura Y, Tsuchimochi S. Characterization of adrenal tumors by chemical shift fast-low angle shot MR imaging: comparison of four methods of quantitative evaluation. AJR. 2003;180:1649–57.
15. Metser U, Miller E, Lerman H, Lievshitz G, Avital S, Even-Sapir E. 18F-FDG PET/CT in the evaluation of adrenal masses. J Nucl Med. 2006;47:32–7.
16. Park SY, Park BK, Park JJ, Kim CK. Differentiation of adrenal hyperplasia from adenoma by use of CT densitometry and percentage washout. AJR Am J Roentgenol. 2016;206(1):106–12.
17. Kenney PJ, Stanley RJ. Calcified adrenal masses. Urol Radiol. 1987;9(1):9–15.
18. Kittithaworn A, Dogra P, Rahimi L, Sandooja R, Bancos I. Etiology, morphology, and outcomes of adrenal calcifications in 540 adult patients—a retrospective single-center study. Eur J Endocrinol. 2023;189(1):K1–6.
19. Lattin GE Jr, Sturgill ED, Tujo CA, Marko J, Sanchez-Maldonado KW, Craig WD, Lack EE. From the radiologic pathology archives: adrenal tumors and tumor-like conditions in the adult: radiologic-pathologic correlation. Radiographics. 2014;34(3):805–29.
20. Chorney E, Rosen A, Lewis S, Wilck E, Simpson W. Radiologic differentiation of adrenal lesions and its impact on patient management. Contemp Diagn Radiol. 2020;43(24):1–5.
21. Panda A, Kumar A, Gamanagatti S, Bhalla AS, Sharma R, Kumar S, et al. Are traumatic bilateral adrenal injuries associated with higher morbidity and mortality?—a prospective observational study. J Trauma Manag Outcomes. 2015;9:1–6.
22. Ebbehoj A, Li D, Kaur RJ, Zhang C, Singh S, Li T, Atkinson E, Achenbach S, Khosla S, Arlt W, Young WF, Rocca WA, Bancos I. Epidemiology of adrenal tumours in Olmsted County, Minnesota, USA: a population-based cohort study. Lancet Diabetes Endocrinol. 2020;8(11):894–902.
23. Johnson PT, Horton KM, Fishman EK. Adrenal mass imaging with multidetector CT: pathologic conditions, pearls, and pitfalls. Radiographics. 2009;29(5):1333–51.
24. Low G, Dhliwayo H, Lomas DJ. Adrenal neoplasms. Clin Radiol. 2012;67(10):988–1000. https://doi.org/10.1016/j.crad.2012.02.005. Epub 2012 Apr 7.
25. Chung R, O'Shea A, Sweeney AT, Mercaldo ND, McDermott S, Blake MA. Hereditary and sporadic pheochromocytoma: comparison of imaging, clinical, and laboratory features. AJR Am J Roentgenol. 2022;219(1):97–109.
26. Yu H, Parakh A, Blake M, McDermott S. Texture analysis as a radiomic marker for differentiating benign from malignant adrenal tumors. J Comput Assist Tomogr. 2020;44(5):766–71.
27. Mayo-Smith WW, Song JH, Boland GL, Francis IR, Israel GM, Mazzaglia PJ, Berland LL, Pandharipande PV. Management of incidental adrenal masses: a white paper of the ACR Incidental Findings Committee. J Am Coll Radiol. 2017;14(8):1038–44.
28. Albano D, Agnello F, Midiri F, Pecoraro G, Bruno A, Alongi P, Toia P, Di Buono G, Agrusa A, Sconfienza LM, Pardo S, La Grutta L, Midiri M, Galia M. Imaging features of adrenal masses. Insights Imaging. 2019;10(1):1.
29. Chung R, Garratt J, Remer EM, Navin P, Blake MA, Taffel MT, Hackett CE, Sharbidre KG, Tu W, Low G, Bara M, Carney BW, Corwin MT, Campbell MJ, Lee JT, Lee CY, Dueber JC, Shehata MA, Caoili EM, Schieda N, Elsayes KM. Adrenal neoplasms: lessons from adrenal multidisciplinary tumor boards. Radiographics. 2023;43(7):e220191.
30. Wang F, Liu J, Zhang R, Bai Y, Li C, Li B, Liu H, Zhang T. CT and MRI of adrenal gland pathologies. Quant Imaging Med Surg. 2018;8(8):853–75.
31. Dogra P, Rivera M, McKenzie TJ, Foster TR, Dy BM, Lyden ML, Young WF, Bancos I. Clinical course and imaging characteristics of benign adrenal cysts: a single-center study of 92 patients. Eur J Endocrinol. 2022;187:429–37.

Genitourinary Diseases

7

Andrew Wentland

Anatomy

- Kidneys
  - Each kidney is typically supplied by a single renal artery that arises from the abdominal aorta.
    Main renal arteries branch into segmental arteries at the renal hilum.
    Accessory renal arteries are common and seen in up to 29% of patients.
  - Each kidney is typically drained by a single renal vein.
    Multiple renal veins are present in 15–30% of patients.
    Each renal vein drains into the inferior vena cava.
    The left renal vein typically courses between the superior mesenteric artery and the aorta.
    The left renal vein has common anatomic variants, including a retroaortic course (in 3% of patients), as well as a circumaortic pattern (in 17% of patients), in which the vein splits and courses both anteriorly and posteriorly to the aorta.

Supplementary Information The online version contains supplementary material available at https://doi.org/10.1007/978-3-031-76624-4_7.

A. Wentland (✉)
Department of Radiology, University of Wisconsin School of Medicine and Public Health, Madison, WI, USA

Department of Medical Physics, University of Wisconsin School of Medicine and Public Health, Madison, WI, USA

Department of Biomedical Engineering, University of Wisconsin School of Medicine and Public Health, Madison, WI, USA
e-mail: alwentland@wisc.edu

© The Author(s), under exclusive license to Springer Nature Switzerland AG 2024

T. Catanzano (ed.), *What Radiology Residents Need to Know: Abdominal Radiology*, What Radiology Residents Need to Know,
https://doi.org/10.1007/978-3-031-76624-4_7

  - In adults, kidney lengths are approximately 11.5–13.3 cm in men and 10.5–12.7 cm in women.
  - Renal anatomy (Fig. 7.1)

    The renal parenchyma is divided into the outer renal cortex and the medulla.

    The medullary pyramids taper to the renal papilla, which transmits urine into the collecting system.

    The collecting system then begins with the minor calyces, which combine to form the major calyces.

    Subsequently, the major calyces form the renal pelvis, which tapers and forms the ureter.
- Ureters
  - The ureters are muscular tubes that deliver urine from the renal pelvis to the urinary bladder.
  - The ureter initially runs along the medial aspect of the psoas muscle, then courses anteriorly to the sacroiliac joint at the level of the common iliac vessel bifurcation, and finally courses anterior to the internal iliac artery down along the pelvic sidewall.
  - The ureter terminates at the posterolateral wall of the urinary bladder.
- Bladder
  - The urinary bladder is an extraperitoneal structure that serves as a reservoir for urine.
  - The urinary bladder anatomically (Fig. 7.2) includes a posterior base (the fundus), the superior dome, anterior apex, and an inferior neck. The trigone is

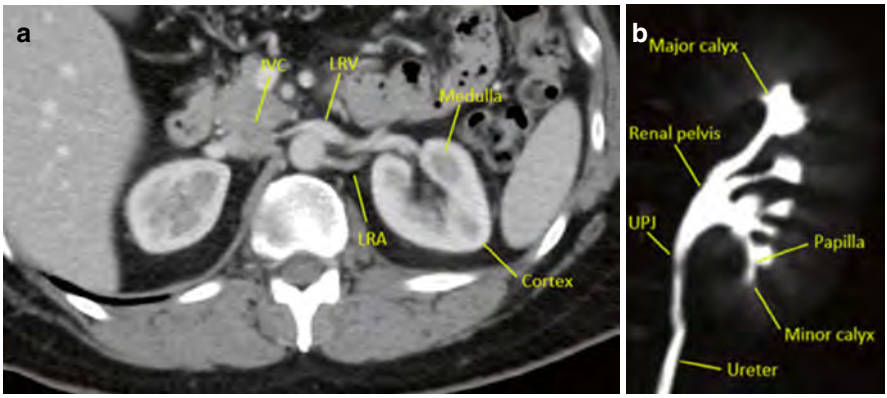

Fig. 7.1 Renal anatomy in a 49-year-old male. Axial contrast-enhanced CT (**a**) demonstrates normal enhancing medullary pyramids and renal cortex. The vasculature of the left kidney is shown with the single left renal artery (LRA), single pre-aortic left renal vein (LRV), and inferior vena cava (IVC). Maximum intensity projection image derived from an excretory phase CT (**b**) demonstrates the normal anatomy of the renal collecting system, with a representative papilla shown; the renal papillae are where the collecting ducts transmit urine into the collecting system. Urine then flows into the minor and then major calyces, which combine to form the renal pelvis. The renal pelvis tapers to the ureteropelvic junction (UPJ) and urine then flows into the ureter

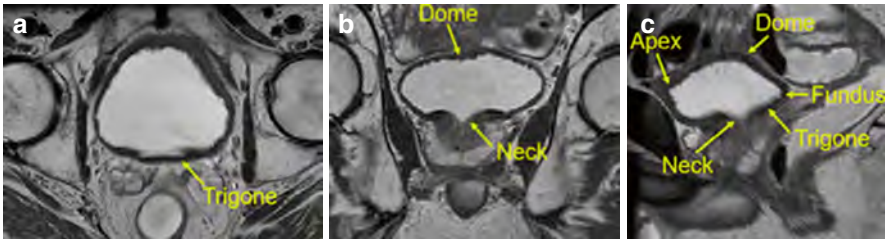

Fig. 7.2 Bladder anatomy labeled on axial (**a**), coronal (**b**), and sagittal (**c**) T2-weighted MR images in a 65-year-old male

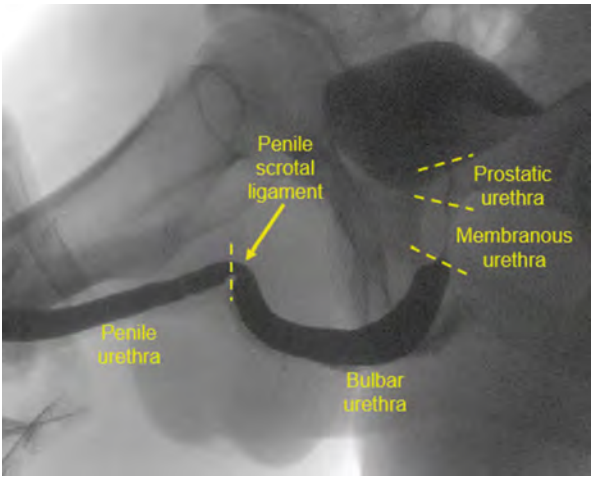

Fig. 7.3 Anatomy of the urethra on a fluoroscopic retrograde urethrogram in a 23-year-old male

a triangular area at the internal surface of the bladder defined by the ureteral orifices and internal urethral meatus.
  - The bladder is predominantly lined by transitional cell epithelium, although the trigone has stratified squamous epithelium.
  - The bladder contracts via the detrusor muscle.
- Urethra
  - The urethra (Fig. 7.3) is a fibromuscular tube that transmits urine from the urinary bladder to the external urethral meatus.
  - The urethra is divided into anterior (penile and bulbar urethra) and posterior (membranous and prostatic urethra) portions.
  - The verumontanum is a structure along the posterior wall of the prostatic urethra. The prostatic utricle opens into the verumontanum.
  - The penile scrotal ligament runs from the pubic bone, laterally around the penis like a sling, and terminates at the scrotal septum.
  - The glands of Littré are mucus-producing glands along the anterior male urethra but are often not seen on imaging except in the setting of urethral stricture or chronic infection.

Congenital Abnormalities

- Multiple congenital abnormalities and anatomic variants of the kidneys exist, which stem from embryologic morphogenesis.
- In utero, the kidneys begin close to one another in the sacral region, and during development are drawn apart as they ascend to the typical adult position near the adrenal glands.
- Renal agenesis
  - Renal agenesis can be unilateral or bilateral, although the latter is incompatible with life.
  - Unilateral renal agenesis occurs in 1 in 2000–3000 births.
  - Unilateral renal agenesis is associated with unicornuate uterus, absence of the ipsilateral epididymis and vas deferens, and a pancake adrenal gland (Fig. e7.1).
  - A pancake adrenal gland occurs when the kidney fails to ascend and push on the adrenal gland—a process that is required to form the standard adreniform shape.
- Structural anomalies occur during the end of kidney development and include persistent fetal lobulation, a hypertrophied column of Bertin, and a dromedary hump.
  - Persistent fetal lobulation is characterized by indentations along the renal contour between the renal pyramids (Fig. 7.4).

    Persistent fetal lobulation is present in approximately 4% of the population. There are no clinical implications of persistent fetal lobulation, although the finding can simulate renal masses or cortical scarring.
  - Hypertrophied column of Bertin, also known as focal cortical hyperplasia, is a region of hypertrophied renal cortex, which is interposed between the renal pyramids and projects into the renal sinus (Fig. 7.5).

    A hypertrophied column of Bertin is typically located in the interpolar region of the kidney.

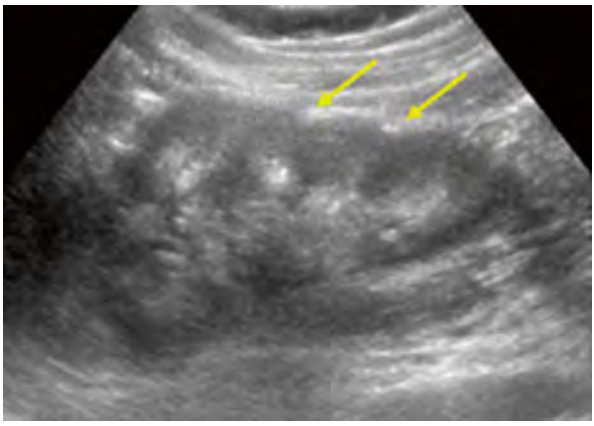

Fig. 7.4 B-mode image of the left kidney in a 43-year-old female demonstrates indentations along the renal contour between the renal pyramids (arrows), consistent with persistent fetal lobulation

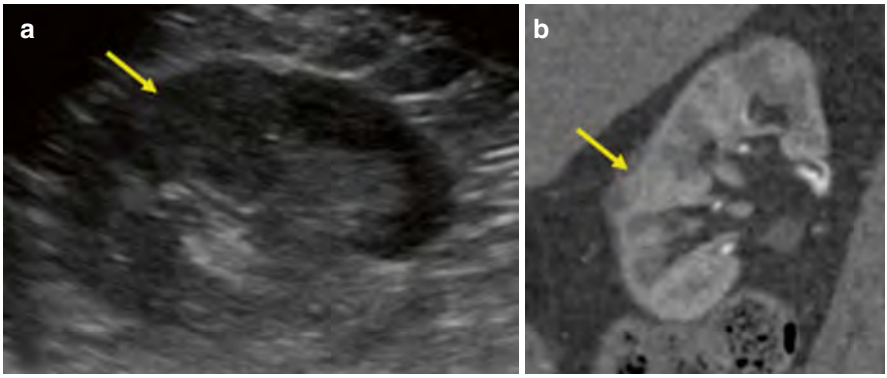

Fig. 7.5 B-mode image (**a**) of the right kidney in a 79-year-old male demonstrates a region of tissue in the interpolar region (arrow) that is interposed between medullary pyramids and that extends into the renal sinus; the structure is of identical echogenicity compared to the renal cortex. Findings are consistent with a hypertrophied column of Bertin. A coronal CT image of the right kidney (**b**) shows a similar region of prominent tissue interposed between medullary pyramids and extending into the renal sinus (arrow), which has similar attenuation compared to the renal cortex

There are no clinical implications associated with a hypertrophied column of Bertin, although this finding can simulate a renal mass.

On imaging, a hypertrophied column of Bertin will be contiguous with cortical renal parenchyma and have similar echogenicity, signal intensity, and attenuation on ultrasound, MRI, and CT, respectively.

– Dromedary hump is a prominent bulge on the lateral contour of the left kidney due to the splenic impression (Fig. e7.2).

Dromedary humps are present in approximately 0.5% of the population.

There are no clinical implications due to the presence of a dromedary hump, although this finding can simulate a renal mass.

On imaging, a dromedary hump will be contiguous with cortical renal parenchyma and have similar echogenicity, signal intensity, and attenuation on ultrasound, MRI, and CT, respectively.

- Fusion anomalies of the kidneys occur during migration of the kidneys cranially during development.
- As the kidneys traverse umbilical arteries, changes in position or fusion of the immature kidneys can occur—resulting in horseshoe kidney.
  – Horseshoe kidney is the fusion of two kidneys (Fig. 7.6), one on each side of the body, and due to this fusion, the ascending fused kidneys are trapped by the inferior mesenteric artery.

Due to the arrest of migration by the inferior mesenteric artery, the kidneys are inferior in location and have an anteriorly facing renal pelvis.

Horseshoe kidneys are found in 0.25% of the population and are twice as common in men than women.

Most patients with horseshoe kidney are asymptomatic.

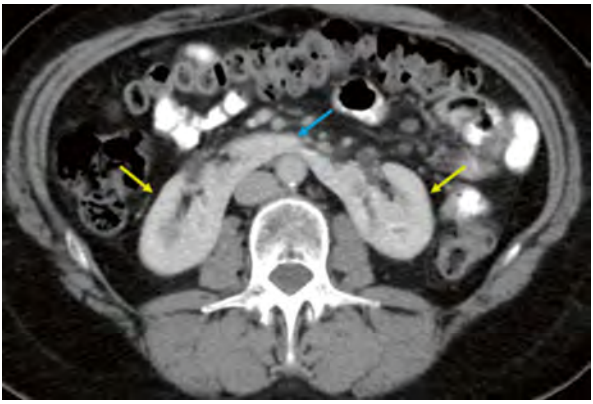

Fig. 7.6 60-year-old female with a horseshoe kidney. A post-contrast axial CT image depicts the bilateral kidneys (yellow arrows) that are connected with a bridge of tissue (blue arrow)

Complications can occur with horseshoe kidney, including ureteropelvic junction obstruction, urolithiasis, renal infection, and a propensity to renal laceration in the setting of blunt abdominal trauma.

Ultrasound can detect horseshoe kidneys and depict the contiguity of the horseshoe isthmus with the inferior poles of each kidney.

CT and MRI can aid in identifying the anatomy of the vasculature and collecting system of the horseshoe kidney.

- Duplication of the collecting systems can also occur due to incomplete fusion of the renal moieties during development.
  - Duplicated collecting systems

    Duplicated, or duplex, collecting systems are common congenital abnormalities resulting from incomplete fusion of the upper and lower renal moieties during development.

    This incomplete fusion results in a spectrum of duplication that can range from duplication of the entire collecting systems and ureters, to the collecting systems and portions of the ureters, to only the collecting systems.

    Duplicated collecting systems are seen in 0.7% of the healthy population and 2–4% of the population presenting with urinary tract symptoms.

    Most patients with duplicated collecting systems are asymptomatic, although patients with complete duplication tend to have symptoms more frequently, such as vesicoureteral reflux, hydronephrosis, and flank pain.

    Fluoroscopy with intravenous pyelography (IVP) can readily depict the extent of collecting system duplication (Fig. e7.3).

    - IVP can depict the drooping lily sign classically associated with duplicated collecting systems, in which the lower renal moiety is inferolaterally displaced due to an obstructed upper pole moiety (Fig. 7.7).

    CT

    - While duplication of the collecting system can be seen in the absence of IV contrast, the phenomenon is most readily seen on excretory phase postcontrast images.

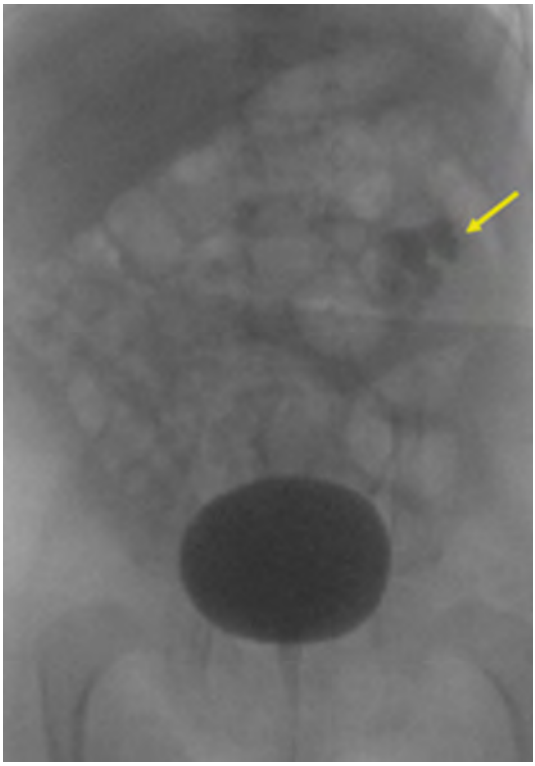

Fig. 7.7 8-month-old male with a duplicated collecting system. Fluoroscopic cystogram demonstrates inferolateral displacement of the left lower moiety, providing a "drooping lily" appearance (arrow)

Renal Trauma

- Renal trauma can be due to blunt injury (particularly due to shearing in the setting of deceleration), penetrating injury, or iatrogenic causes, such as surgery, biopsy, and lithotripsy.
- Patients can present with hematuria, flank pain, and hypotension.
- Renal trauma can be accompanied by avulsion of the renal pedicle with devascularization of the kidney (Fig. 7.8), pseudoaneurysm, arteriovenous fistula, and renal artery transection or dissection.
- The severity of renal trauma is graded using the American Association for the Surgery of Trauma (AAST) renal injury scale. Renal trauma is graded per Fig. 7.9/Fig. e7.4.

Imaging

- Ultrasound
  - Ultrasound has limited utility in evaluating renal parenchymal injury but can be used to detect hemoretroperitoneum.

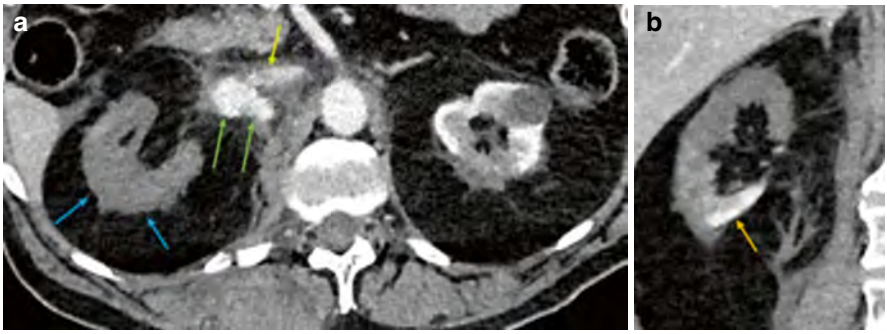

Fig. 7.8 75-year-old male bicyclist versus motor vehicle. Axial CT image in the arterial phase (**a**) demonstrates disruption of the right renal artery (yellow arrow) with resultant extravasation and pseudoaneurysm formation (green arrows). The right kidney is devascularized (blue arrows) and only a small component in the inferior pole remains perfused (orange arrow, **b**)

  - Color and spectral Doppler can be used to assess for patency of the renal arteries and veins.
- CT
  - CT is the modality of choice for acute traumatic renal injury.
  - Noncontrast and arterial phase postcontrast imaging can aid in detecting vascular injury and contrast extravasation.
  - A nephrographic phase (60–90 s postcontrast) is optimal for detecting renal laceration (Fig. 7.10).
  - Delayed/excretory phase imaging is used to assess for collecting system injuries and can also aid in detecting active bleeding, particularly from a venous source that may be slow and thereby missed on arterial phase images.
  - A large perinephric hematoma can cause compression of the renal parenchyma, which may lead to hypertension (Fig. e7.5). This phenomenon is called a Page kidney.
- MR
  - MRI provides excellent ability to depict renal parenchymal injury, and when combined with gadolinium-based contrast agents, can be used to depict vascular injury.
  - Nevertheless, MRI is not typically used for acute renal trauma due to long scan times compared to CT.

Grade	Description	Example
I	• Subcapsular hematoma, and/or • Parenchymal contusion without laceration	
II	• Hematoma confined to Gerota's fascia, or • Renal parenchymal laceration ≤ 1 cm Note: • No urinary extravasation is present	
III	• Renal parenchymal laceration greater than 1 cm without collecting system rupture or urinary extravasation, or • Any vascular injury or active bleeding confined to the perirenal fascia	
IV	• Laceration involving the collecting system with urinary extravasation, or • Laceration of the renal pelvis and/or complete ureteropelvic disruption, or • Segmental renal vein or artery injury, or • Active bleeding beyond Gerota's fascia, or • Segmental or complete kidney infarction due to vessel thrombosis without active bleeding	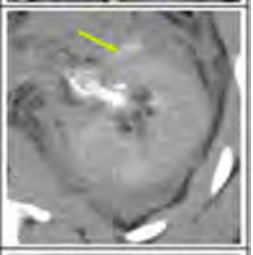
V	• Main renal artery or vein laceration, or • Avulsion of the hilum, or • Devascularized kidney with active bleeding, or • Shattered kidney without identifiable renal parenchyma	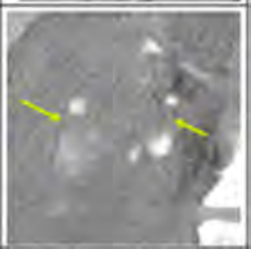

Fig. 7.9 Grade I: 13-year-old male. Axial portal venous phase CT image of the left kidney with a cortical renal contusion. Grade II: 25-year-old male. Axial portal venous phase CT image of the left kidney with a 0.9 cm laceration. Grade III: 20-year-old female. Coronal portal venous phase CT image of the left kidney with a 1.5 cm laceration. Grade IV: 24-year-old male. Axial excretory phase CT image of the left kidney with urinary extravasation. Grade V: 26-year-old female. Coronal portal venous phase CT image of the right kidney, which is shattered without identifiable renal parenchyma

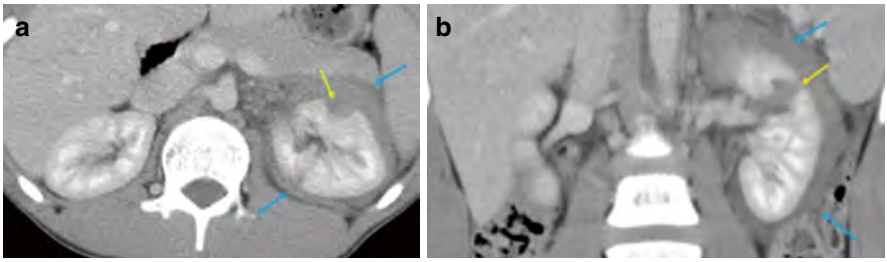

Fig. 7.10 14-year-old male presenting after a motor vehicle collision. Axial (**a**) and coronal (**b**) post-contrast CT images demonstrate a renal laceration >1 cm (yellow arrows) with perinephric blood products (blue arrows). There is no evidence of extension of the laceration to the collecting system or active bleeding beyond Gerota's fascia. Findings are consistent with a grade 3 laceration

Renal Infarct

- Renal infarction has a wide range of causes, including thromboembolism (most common), arterial dissection, vasculitis, renal trauma, iatrogenic causes, and renal vein occlusion.
- Infarcts can be asymptomatic, particularly when small, but patients typically present with flank pain and hematuria.

Imaging

- Ultrasound
  - Ultrasound is not typically used for evaluating renal infarction. When seen, color Doppler will show an absence of blood flow in the affected region.
- CT
  - Renal infarcts appear as peripheral wedge-shaped areas of hypoenhancement in the renal parenchyma (Fig. 7.11).
  - CT angiography may be needed to identify arterial causes of renal infarction, such as arterial dissection or thrombus causing occlusion of the renal artery.

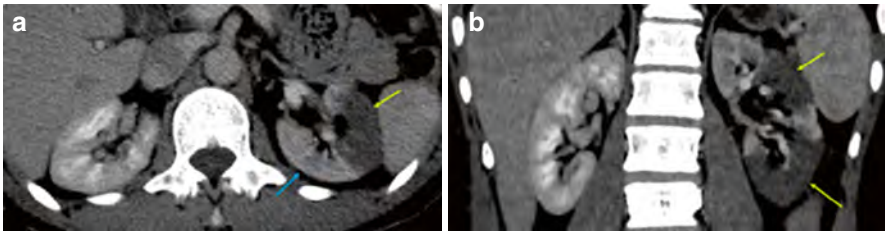

Fig. 7.11 43-year-old male with spontaneous renal artery dissection leading to multifocal infarct of the left kidney. Axial (**a**) and coronal (**b**) post-contrast CT images demonstrate wedge-shaped areas of non-enhancement in the periphery of the left kidney (yellow arrows), consistent with infarcts. The remainder of the left renal parenchyma (blue arrow) is relatively hypoenhancing compared to the right kidney

Renal Papillary Necrosis

- Renal papillary necrosis is defined by necrosis and sloughing of the renal papillary tissue.
- Patients may present with flank pain and hematuria.
- Causes of renal papillary necrosis include diabetes mellitus, analgesia use, pyelonephritis, sickle cell anemia, and urinary obstruction.

Imaging

- Intravenous pyelography and the excretory phase in CT urography demonstrate contrast filling within a necrotic cavity at the renal papilla (Fig. e7.6).
- Small collections of contrast may be present in the papillary regions peripheral to the calyces.
- Sloughed papillae can lead to filling defects in the collecting system.
- Classic signs associated with renal papillary necrosis include "ball on tee," in which contrast fills a central excavation in the papilla leading to a ball on a tee appearance, as well as the lobster claw sign, in which contrast fills into an excavated area around the edge of the papilla.

Infection of the Renal Parenchyma

Renal Abscess

- A renal abscess is an infected collection of fluid typically as a sequela of pyelonephritis.
- Several factors predispose patients to renal abscess, including diabetes mellitus, renal calculi, and ureteral obstruction.
- Patients present with fever, chills, flank pain, and dysuria.

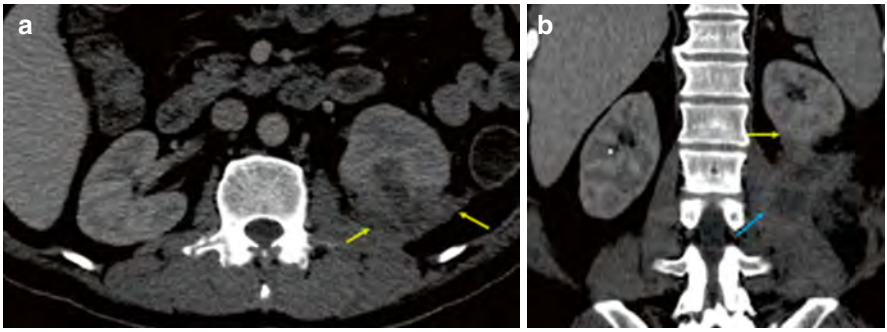

Fig. 7.12 42-year-old male with diabetes mellitus presenting with a left renal abscess. Axial (**a**) and coronal (**b**) post-contrast CT images demonstrate a heterogeneous region of low attenuation in the posterior aspect of the interpolar left kidney (yellow arrows), consistent with an abscess. Phlegmonous material extends into the perirenal space and invades into the left psoas muscle (blue arrow). Subtle heterogeneous enhancement of the renal cortices can be appreciated, consistent with pyelonephritis

- Renal abscess often appears dissimilar to other abscesses in the abdomen, as there is often not a well-defined fluid collection with an enhancing wall.
- Renal abscesses can be difficult to differentiate from a renal mass, and as such comparison to prior imaging and the clinical history may be needed to reach the diagnosis.

Imaging

- Ultrasound
  - Renal abscess on ultrasound is typically seen as a hypoechoic collection within the renal parenchyma.
  - Internal echoes may be present within the collection.
  - The remainder of the renal parenchyma may be hypoechoic due to superimposed pyelonephritis.
- CT
  - CT is the standard modality for evaluating renal abscesses.
  - Renal abscess on CT is seen as a hypoattenuating structure in the renal parenchyma with or without a well-defined wall or pseudocapsule (Fig. 7.12).
  - Gas is sometimes present within the abscess.

Acute Pyelonephritis

- Pyelonephritis is a complicated urinary tract infection involving the renal parenchyma.
- Acute pyelonephritis occurs more commonly in females, with a female:male ratio of 5:1.
- Patients with acute pyelonephritis present with fever, chills, nausea, vomiting, costovertebral angle tenderness, and flank pain.

- Acute pyelonephritis is most commonly secondary to *Escherichia coli*, but can also be due to *Klebsiella*, *Proteus*, *Enterobacter*, and *Pseudomonas*.

Imaging

- Pyelonephritis is ultimately a clinical diagnosis but can have corresponding imaging findings.
- Ultrasound
  - Ultrasound is insensitive to acute pyelonephritis.
  - Ultrasound findings can include decreased vascularity in the cortex on power Doppler images as well as focal and segmental areas of low echogenicity in the cortex.
- CT
  - CT images with contrast demonstrate peripheral areas of wedge-shaped low attenuation in the renal cortex, which can create a striated nephrogram appearance (Fig. 7.13).
- MRI
  - MRI is not typically used to image pyelonephritis but may be useful in pregnant patients.
  - MRI demonstrates intrinsic T1 hypointensity and T2 hyperintensity in peripheral wedge-shaped areas of the cortex.
  - If contrast is administered, these regions will show reduced enhancement.

Emphysematous Pyelonephritis

- Emphysematous pyelonephritis is a severe infection of the kidneys with gas formation within the renal parenchyma.
- Emphysematous pyelonephritis occurs most commonly in females and approximately 90% of patients have diabetes.
- *Escherichia coli*, *Klebsiella pneumonia*, and *Proteus mirabilis* are the most commonly identified organisms.

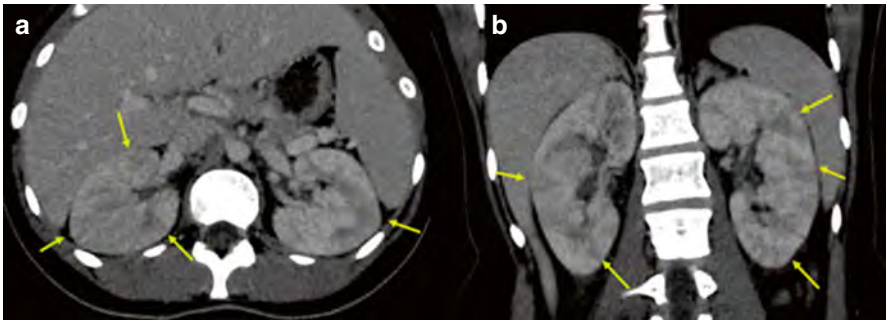

Fig. 7.13 22-year-old female presenting with bilateral flank pain and a known urinary tract infection. Contrast-enhanced axial (**a**) and coronal (**b**) CT images demonstrates intermittent wedge-shaped areas of low attenuation in the bilateral renal cortices, consistent with acute pyelonephritis

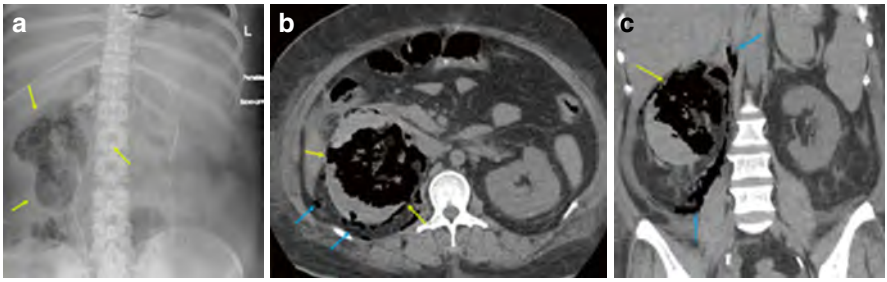

Fig. 7.14 45-year-old diabetic female presenting with high fever and right flank pain. An abdominal radiograph (**a**) demonstrates mottled gas in the expected location of the right kidney (arrows). Subsequent non-contrast CT in the axial (**b**) and coronal (**c**) planes shows extensive gas within the renal parenchyma (yellow arrows) with gas extending into the perinephric space (blue arrows)

- Emphysematous pyelonephritis warrants a prompt call to the referring team and surgical consultation.

Imaging

- Radiograph
  - Radiographs demonstrate mottled gas within the expected location of the renal fossa (Fig. 7.14a).
- Ultrasound
  - Gas may be seen sonographically and will appear as echogenic foci with ring-down artifact, consistent with dirty shadowing.
- CT
  - CT is the best modality for demonstrating the imaging findings of emphysematous pyelonephritis.
  - CT demonstrates focal areas of necrosis in the renal parenchyma with foci of gas and possible gas-fluid levels.
  - Gas may extend into the perinephric space (Fig. 7.14b, c).

Emphysematous Pyelitis

- Emphysematous pyelitis is gas production within the urinary excretory system, typically due to bacterial infection.
- Emphysematous pyelitis is a benign entity, in stark contrast to emphysematous pyelonephritis.
- Emphysematous pyelitis occurs more frequently in females and typically occurs in the setting of diabetes mellitus or urinary obstruction.
- *Escherichia coli*, *Proteus mirabilis*, and *Aerobacter aerogenes* are the most common causative organisms.

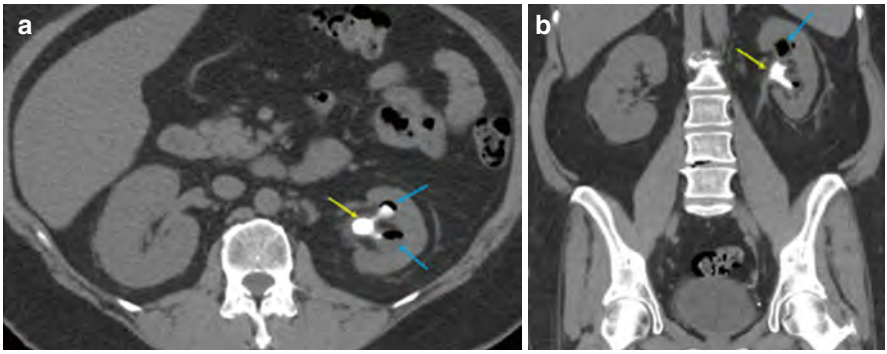

Fig. 7.15 50-year-old female with diabetes presenting with emphysematous pyelitis. Axial (**a**) and coronal (**b**) non-contrast CT images demonstrate a staghorn calculus in the left renal collecting system (yellow arrows) with gas accumulating in the calyces (blue arrows). The urothelium of the collecting system is thickened. No gas extends into the renal parenchyma

Imaging

- Radiograph
  - Radiographs can demonstrate mottled gas within the expected location of the renal collecting system.
- Ultrasound
  - Gas may be seen sonographically and will appear as echogenic foci with ring-down artifact, consistent with dirty shadowing, in the renal collecting system.
- CT
  - CT can clearly depict gas accumulating within the collecting system, frequently with inflammatory changes of the collecting system including surrounding stranding and urothelial thickening (Fig. 7.15).

Xanthogranulomatous Pyelonephritis

- Xanthogranulomatous pyelonephritis is a form of chronic pyelonephritis that can occur secondary to obstruction by infected renal stones.
- Xanthogranulomatous pyelonephritis is a chronic granulomatous disease process that leads to destruction of the renal parenchyma with resulting renal dysfunction.
- Middle-aged females with recurrent urinary tract infections are affected most commonly.
- Patients present with flank pain, fever, anorexia, malaise, and weight loss.
- Urinalysis shows bacteriuria, and most commonly one of several organisms are cultured, including *Escherichia coli*, *Proteus mirabilis*, *Pseudomonas*, *Enterococcus faecalis*, and *Klebsiella*.

Fig. 7.16 56-year-old female with xanthogranulomatous pyelonephritis. An anteroposterior radiograph (**a**) demonstrates an extensive staghorn calculus in the calyces and renal pelvis in the left kidney (arrow). Transabdominal ultrasound (**b**) of the left kidney demonstrates loss of the normal renal architecture with dilatation of the calyces and large shadowing calculi (arrow). Coronal contrast-enhanced CT (**c**) also shows dilatation of the calyces in a multiloculated pattern resembling a bear's paw print (arrows). Large staghorn calculi are again seen

Imaging

- Radiograph
  - Radiographs demonstrate branching staghorn calculi projecting over the renal outline (Fig. 7.16a).
- Ultrasound
  - Ultrasound demonstrates distortion of the kidney with dilatation of the calyces and large shadowing calculi located centrally within the calyces (Fig. 7.16b).
- CT
  - CT imaging shows dilatation of the calyces in a multiloculated pattern reminiscent of a bear's paw print (bear's paw sign) (Fig. 7.16c).
- MRI
  - MR images do not show calculi well, but the large staghorn calculi will predominantly be seen as a dark filling defect on T2-weighted images.
  - T2-weighted images will optimally demonstrate the dilated calyces.

Pyonephrosis

- Pyonephrosis is the term for infected hydronephrosis with suppurative destruction of the renal parenchyma.
- Pyonephrosis is associated with states of immunosuppression and renal failure.
- The diagnosis of pyonephrosis is suspected when patients present with fever and flank pain in combination with the imaging diagnosis of urinary tract obstruction.

Imaging

- Ultrasound
  - On ultrasound, pyonephrosis is depicted as dilatation of the pelvicalyceal system with echogenic debris within the collecting system and possible dirty shadowing secondary to gas.

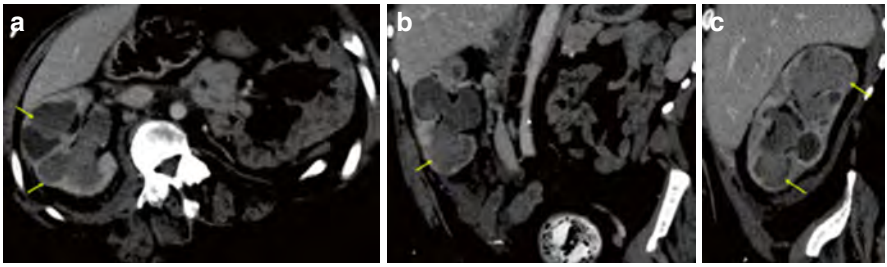

Fig. 7.17 46-year-old female with pyonephrosis. Contrast-enhanced CT in the axial (**a**), coronal (**b**), and sagittal (**c**) planes shows dilatation of the collecting system and high attenuation material layering within the collecting systems (yellow arrows)

- CT
  - CT in the setting of pyonephrosis can show urothelial thickening, hydronephrosis, layering dense material within the collecting system, gas, and perinephric stranding (Fig. 7.17).
- MRI
  - MRI is similar to CT in that hydronephrosis, perinephric inflammation, and urothelial thickening are present.
  - Debris within the collecting system may be challenging to see but when seen is depicted as a filling defect on T2-weighted images or excretory phase post-contrast images.

Benign Renal Neoplasms

Cysts

- Renal cysts are extremely common imaging findings and seen in approximately 40% of all individuals undergoing a CT examination.
- Simple cysts are the most common lesions in the kidney.
- Cysts increase in prevalence with age and typically enlarge over time.
- Renal cysts can have internal complexity, and generally with increasing complexity the risk of a cystic renal malignancy increases in likelihood.
- Complex renal cysts are classified according to the Bosniak classification system (Figs. 7.18 and e7.7).
- Hemorrhagic/proteinaceous cysts are benign lesions that can be difficult to distinguish from a renal neoplasm on unenhanced CT or single-phase postcontrast CT.
- Autosomal-dominant polycystic kidney disease occurs in approximately 0.1% of the population.
  - On imaging (Fig. 7.19), numerous simple and hemorrhagic/proteinaceous cysts are present in the kidneys.
  - The kidneys will progressively enlarge over time.
  - Cysts are also frequently present in the liver, in up to 83% of cases.

Grade	CT Description	MRI Description	CT Example	MRI Example
I	• Well-defined cyst with thin smooth walls (≤2 mm); or • Mass with homogeneous simple fluid (-9 to 20 HU). Note: No septa or calcifications. Walls may enhance.	• Well-defined cyst with thin smooth walls (≤2 mm); or • Mass with homogeneous simple fluid (similar signal intensity compared to cerebrospinal fluid). Note: No septa or calcifications. Walls may enhance.		
II	• Cysts with thin (≤2 mm) and few (1-3) septa, or • Homogeneous hyperattenuating (≥70 HU) lesion on non-contrast CT, or • Homogeneous non-enhancing masses >20 HU, or • Homogeneous masses -9 to 20 HU on non-contrast CT, or • Homogeneous masses 21 to 30 HU on portal venous phase CT, or • Homogeneous hypoattenuating masses too small to characterize. Note: Septa may enhance and have calcifications.	• Cysts with thin (≤2 mm) and few (1-3) septa with any non-enhancing septa and calcifications of any type, or • Homogeneous mass with marked T2 hyperintensity on non-contrast MRI, or • Homogeneous mass with marked T1 hyperintensity (~2.5x normal parenchymal intensity) on non-contrast MRI.	Renal mass CT 51 HU Non-enhancing	Non-contrast T1-weighted
III	• Masses with a minimally thickened (3 mm) enhancing wall, or • Masses with smooth minimal thickening (3 mm) of ≥1 septa, or • Masses with many (≥4) smooth thin (≤2 mm) enhancing septa.	• Masses with a minimally thickened (3 mm) enhancing wall, or • Masses with smooth minimal thickening (3 mm) of ≥1 septa, or • Masses with many (≥4) smooth thin (≤2 mm) enhancing septa, or • Cystic masses that are heterogeneously hyperintense on pre-contrast fat-saturated T1-weighted images.	3 mm	3 mm
III	• Masses with ≥1 enhancing thick (≥4 mm) walls or septa, or • Masses with enhancing irregular (≤3 mm obtusely margined convex protrusion) walls or septa.	• Masses with ≥1 enhancing thick (≥4 mm) walls or septa, or • Masses with enhancing irregular (≤3 mm obtusely margined convex protrusion) walls or septa.	5 mm	4 mm
IV	• Masses with ≥1 enhancing nodules (≥4 mm convex protrusion with obtuse margins or a convex protrusion of any size that has acute margins).	• Masses with ≥1 enhancing nodules (≥4 mm convex protrusion with obtuse margins or a convex protrusion of any size that has acute margins).		

Fig. 7.18 Bosniak v2019 descriptors and examples for CT and MRI. *HU* Hounsfield units

Imaging

- Ultrasound
  - Simple cysts on ultrasound are well-circumscribed, anechoic, and may demonstrate posterior acoustic enhancement (Fig. 7.20).
  - Ultrasound is commonly performed to distinguish between a hemorrhagic/proteinaceous cyst from a renal neoplasm incidentally detected on CT.
  - Hemorrhagic/proteinaceous cysts on ultrasound can be variable in appearance and may be anechoic with posterior acoustic enhancement, similar to a simple cyst.
  - Internal debris may cause the cyst to be hypoechoic with internal echoes rather than anechoic (Fig. e7.8).

    As a result, additional imaging with contrast-enhanced ultrasound or MRI may be needed.
- CT
  - On CT simple cysts are well-circumscribed lesions with thin or imperceptible walls (Fig. e7.9).
  - Simple cysts are of water attenuation—between 0 and 20 Hounsfield units.

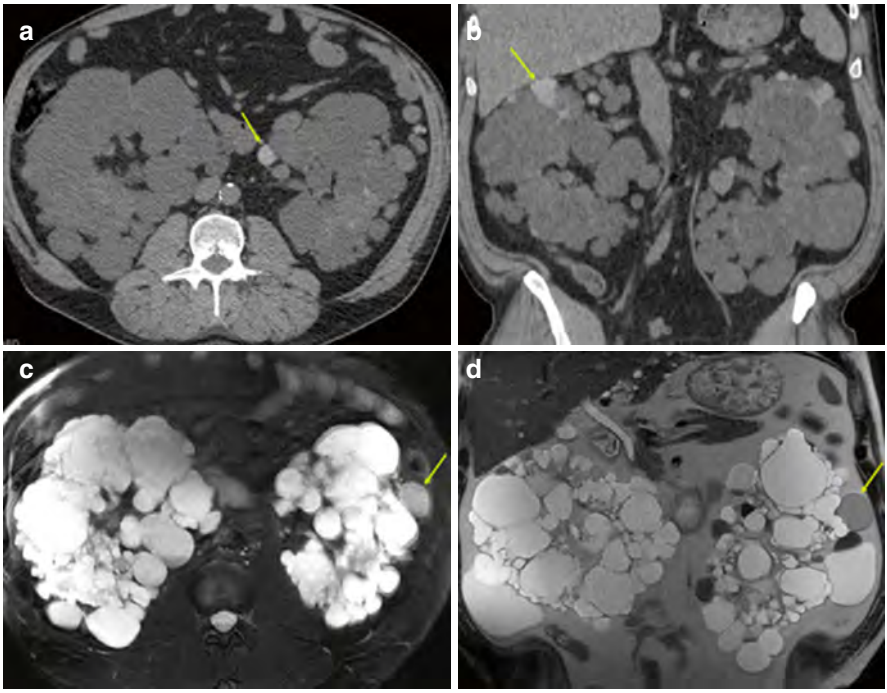

Fig. 7.19 61-year-old male with autosomal dominant polycystic kidney disease. Non-contrast axial (**a**) and coronal (**b**) CT demonstrates innumerable cysts that replace nearly the entirety of the renal parenchyma. Similarly, axial T2-weighted images with fat saturation (**c**) and coronal single-shot fast spin echo images (**d**) also demonstrate innumerable cysts. Some of the cysts are hemorrhagic/proteinaceous in nature and are thereby intrinsically hyperattenuating on non-contrast CT and T2 hypointense on MRI (yellow arrows)

  - The lesions are nonenhancing, with a difference of less than 10–20 Hounsfield units between pre- and postcontrast images.
  - Hemorrhagic/proteinaceous cysts are greater in attenuation than simple cysts, with attenuation >20 Hounsfield units (Fig. 7.21).

    If seen on noncontrast CT or single-phase postcontrast CT, further imaging is needed to differentiate a hemorrhagic/proteinaceous cyst from a renal neoplasm, such as pre- and postcontrast CT, MRI, or ultrasound.
- MRI
  - Simple cysts on MRI are intrinsically T1 hypointense, T2 hyperintense, and without enhancement (Fig. e7.9).
  - Hemorrhagic/proteinaceous cysts on MRI are intrinsically T1 hyperintense, moderately T2 hyperintense, and nonenhancing (Fig. 7.21).

Angiomyolipoma

- Angiomyolipomas are the most common benign solid renal neoplasms.

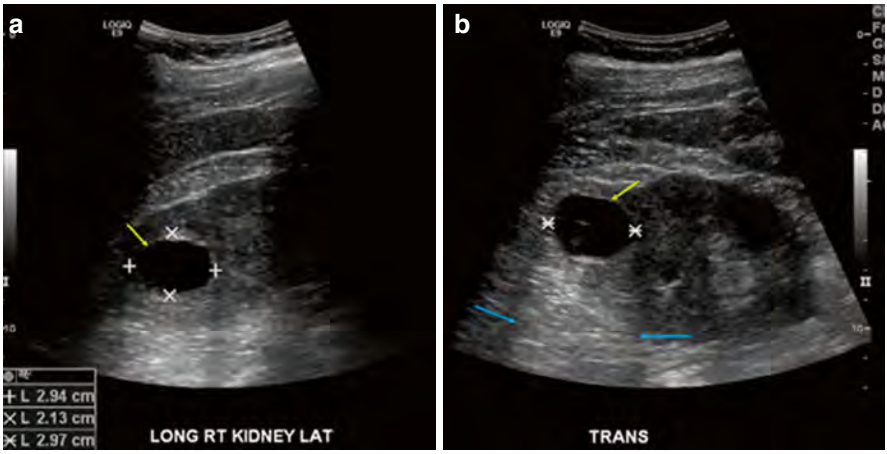

Fig. 7.20 Lateral (**a**) and trans (**b**) B-mode ultrasound images in a 27-year-old male demonstrate an anechoic lesion (yellow arrows) in the superior pole of the right kidney with imperceptible walls and posterior acoustic enhancement (blue arrows)

- Angiomyolipomas occur sporadically but are also associated with the tuberous sclerosis complex.
  - Tuberous sclerosis accounts for approximately 20% of all renal angiomyolipomas.
- Angiomyolipomas are benign neoplasms but are at risk of spontaneous hemorrhage.
- Risk of rupture increases with lesion size, and generally lesions greater than 4 cm are treated surgically or with ablation.

Imaging

- Ultrasound
  - Angiomyolipomas are typically hyperechoic sonographically and demonstrate attenuation of the ultrasound beam posterior to the lesion.
- CT
  - Most angiomyolipomas have gross fat and will have a measurable area of fat within the lesion with an attenuation less than −20 Hounsfield units (Fig. 7.22).
  - Approximately 5% of angiomyolipomas are fat-poor and therefore cannot be reliably distinguished from other renal neoplasms on CT.
- MRI
  - The fat components of angiomyolipomas are isointense to surrounding fat on MRI, and therefore will be hyperintense on T1-weighted images without fat saturation and hypointense on T1-weighted images with fat saturation (Fig. 7.22).
  - In- and out-of-phase imaging may be needed to identify fat within angiomyolipomas, and specifically chemical shift signal intensity loss may aid in identifying a fat-poor angiomyolipoma.

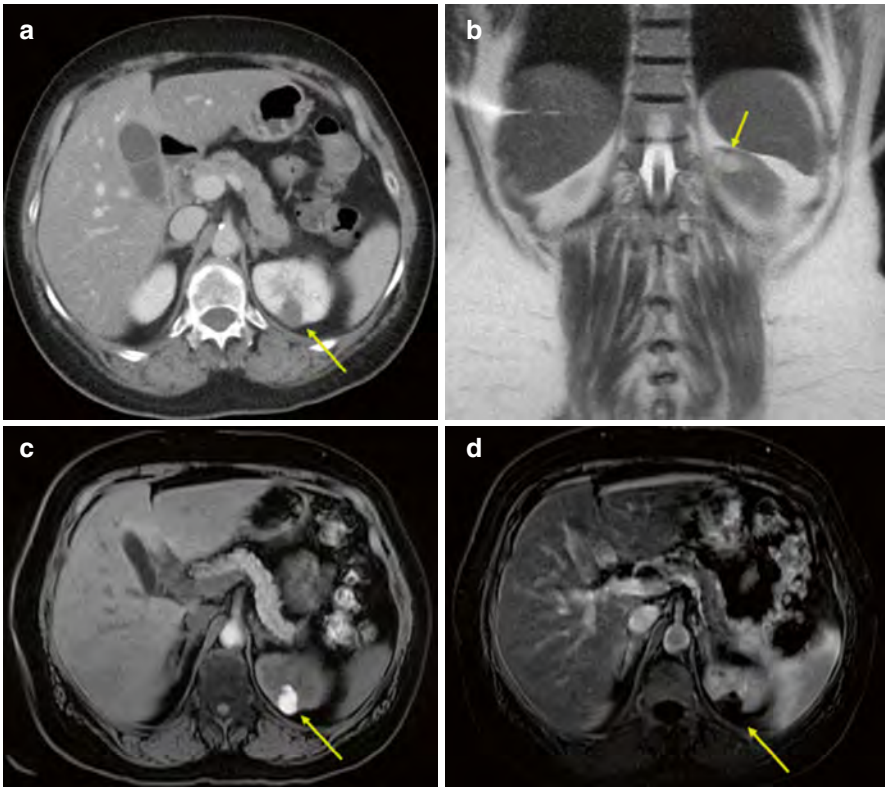

Fig. 7.21 59-year-old female with a hemorrhagic/proteinaceous cyst in the superior pole of the left kidney. On axial portal venous phase post-contrast CT images (**a**) a lesion in the superior pole of the left kidney is seen, with a mean attenuation of 44 Hounsfield units. A coronal single-shot fast spin echo image (**b**) demonstrates that the lesion is moderately T2 hyperintense. The lesion on axial pre-contrast T1-weighted images is intrinsically hyperintense (**c**), and there is no enhancement within the lesion as shown on subtraction images (pre-contrast axial T1-weighted images subtracted from axial portal venous phase post-contrast T1-weighted images) (**d**)

Oncocytoma

- Oncocytomas are benign lesions but can be difficult to distinguish from malignant renal neoplasms, particularly chromophobe renal carcinoma, even on histology.
- Approximately 3–7% of resected renal neoplasms are oncocytomas.
- Oncocytomas are more common in males than females.

Imaging

- Ultrasound
  - Oncocytomas are large masses and are generally isoechoic to the remainder of the renal parenchyma. A central scar may be visible.

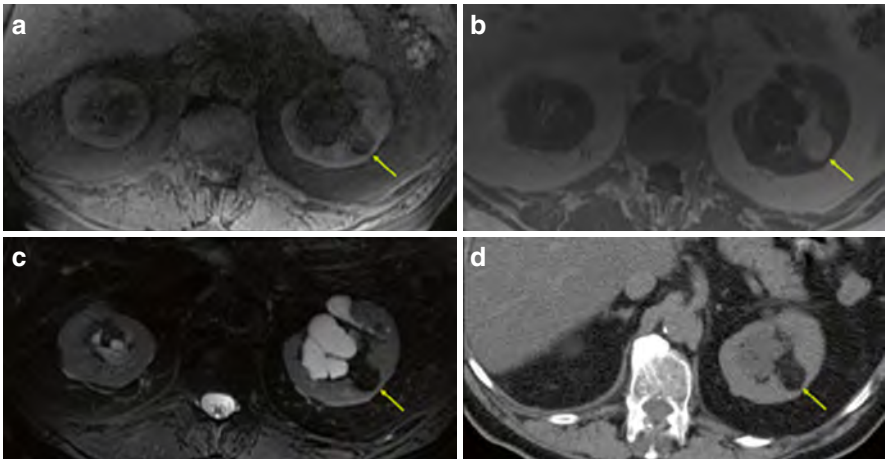

Fig. 7.22 79-year-old male with a left renal angiomyolipoma. The lesion is isointense to retroperitoneal fat on non-contrast T1-weighted images with fat saturation (**a**) and without fat saturation (**b**). The lesion is hypointense on T2-weighted images (**c**). On corresponding axial non-contrast CT images (**d**), the lesion is isoattenuating to retroperitoneal fat, with a mean attenuation of −82 Hounsfield units

- CT
  - Oncocytomas are homogeneous in attenuation when small.
  - However, most oncocytomas are large and are heterogeneous in enhancement (Fig. e7.10).
  - A scar is present in one-third of oncocytomas.
- MRI
  - Most components of large oncocytomas are hyperintense on T2-weighted MRI.
  - Oncocytomas enhance homogeneously when small and heterogeneously when large.
  - Large oncocytomas commonly have a central T2 hypointense nonenhancing scar (Fig. e7.10).

Malignant Renal Neoplasms

Renal Cell Carcinoma

- Renal cell carcinoma originates from the renal cortex.
- In the United States, there are approximately 81,800 cases of renal cell carcinoma per year, with approximately 14,890 deaths.
- Renal cell carcinoma is more common in males than females in a ratio of 2:1.
- These neoplasms typically arise in the sixth to eighth decades of life and are uncommon in individuals less than 40 years of age.

- Risk factors for renal cell carcinoma include smoking, hypertension, obesity, dialysis with acquired polycystic disease of the kidney, occupational exposures such as cadmium, asbestos, and petroleum, heavy use of aspirin, nonsteroidal anti-inflammatory drugs, and acetaminophen, and hereditary kidney cancer syndromes.
- Patients can present with hematuria, flank pain, and/or a palpable mass.
- Major subtypes of renal cell carcinoma include clear cell (~80%), papillary (15%), and chromophobe (5%).
- Risk of metastatic disease is most common with the clear cell subtype, and progressively less common with papillary and chromophobe subtypes, respectively. Furthermore, the risk of metastatic disease is directly proportional to tumor size.
- Paraneoplastic syndromes are relatively common in renal cell carcinoma, occurring in 10–40% of patients.
  - The most common paraneoplastic syndromes include hypercalcemia, hypertension, and polycythemia.

Imaging

- Ultrasound
  - Renal cell carcinoma has a highly variable sonographic appearance and can be hyper-, iso-, or hypoechoic relative to the renal parenchyma.
  - Ultrasound has a limited ability to detect metastatic disease.
  - Contrast-enhanced ultrasound can aid in evaluating an incidentally detected renal lesion on cross-sectional imaging and can differentiate a hemorrhagic/proteinaceous cyst from a renal neoplasm (Fig. 7.23).
- CT
  - CT is commonly used to detect and stage renal cell carcinoma.

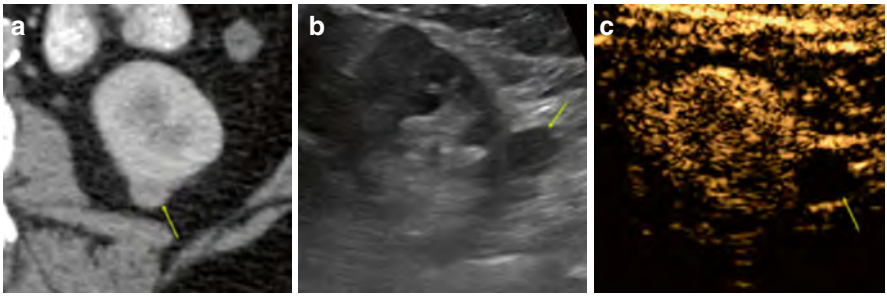

Fig. 7.23 67-year-old female with an incidentally detected lesion in the left kidney. On CT (**a**) a 1.5 × 1.2 cm exophytic lesion was identified in the left kidney. The lesion had a mean attenuation of 70 Hounsfield units. Given that this was a CT with only a portal venous phase, it was indeterminate if this was an enhancing lesion. The patient was taken to ultrasound. On B-mode images (**b**), the lesion was hypoechoic but without posterior acoustic enhancement. Therefore, it was still indeterminate if the lesion was a cyst or solid neoplasm. Contrast-enhanced ultrasound (**c**) was then performed, which confirmed that the lesion was without enhancement and therefore consistent with a hemorrhagic/proteinaceous cyst

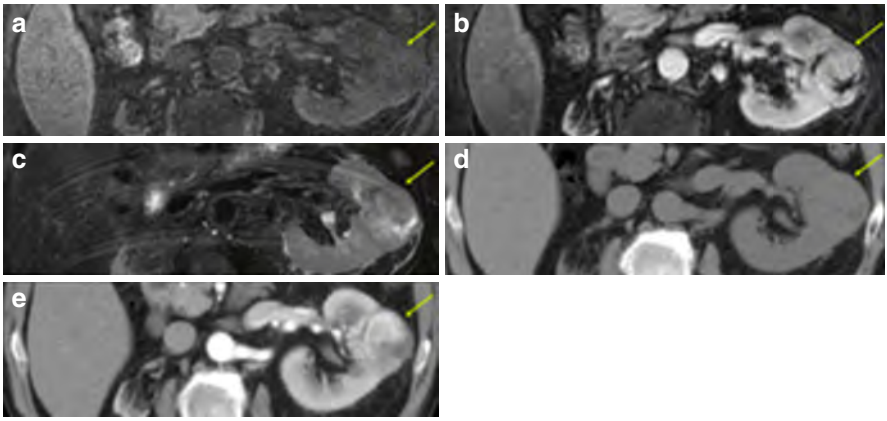

Fig. 7.24 57-year-old male with a grade 3 clear cell renal cell carcinoma centered in the interpolar region of the left kidney. The mass is minimally hypointense to adjacent renal cortex on pre-contrast T1-weighted images with fat saturation and has a mean signal intensity of 141 (**a**). The mass enhances more than renal cortex on arterial phase post-contrast images and has a mean signal intensity of 585 (**b**). The mass is isointense to renal cortex as seen on T2-weighted images with fat saturation (**c**). The mass also demonstrates arterial hyperenhancement on post-contrast axial CT images (**d**, **e**), with a mean attenuation of 37 HU on non-contrast images and 163 HU on post-contrast images

- Renal cell carcinoma is typically between 20 and 70 Hounsfield units on non-contrast images.
- Calcification is present in approximately 30% of renal cell carcinoma.
- It can be challenging to differentiate the subtypes of renal cell carcinoma on CT, but there are some typical features:

  The clear cell subtype is typically the most avidly enhancing among the three major subtypes, particularly on arterial phase imaging, with hyperenhancement relative to the renal cortex (Fig. 7.24).

  The papillary subtype is typically minimally enhancing, particularly relative to the renal cortex (Fig. e7.11).

  Chromophobe renal cell carcinomas are also hypoenhancing relative to the renal parenchyma but often enhance more than papillary renal cell carcinoma and less than clear cell renal cell carcinoma (Fig. 7.25).
- Invasion of the mass into the renal vein occurs in up to 9% of cases.
- Metastases from renal cell carcinoma, particularly the clear cell subtype, are typically arterially enhancing.

• MR
  - MRI is also excellent in the detection and staging of renal cell carcinoma.
  - Scoring systems have been developed, such as the clear cell likelihood score, which utilize the pattern of T2 intensity and enhancement on corticomedullary phase postcontrast T1-weighted images to determine the likelihood that a renal mass is the clear cell subtype.

Fig. 7.25 30-year-old female with a chromophobe renal cell carcinoma centered in the interpolar region of the right kidney. The mass is relatively isointense to adjacent renal cortex on pre-contrast T1-weighted images with fat saturation and has a mean signal intensity of 245 (**a**). The mass enhances less than renal cortex on arterial phase post-contrast images and has a mean signal intensity of 961 (**b**). The mass is mildly hypointense to renal cortex on T2-weighted images with fat saturation (**c**). The mass demonstrates mild enhancement on pre- and post-contrast axial CT images (**d**, **e**), with a mean attenuation of 32 and 65 HU, respectively, albeit to a lesser extent than the adjacent renal cortex

However, the clear cell likelihood scoring system has not been widely adopted in clinical practice.

  - The clear cell subtype is typically arterially hyperenhancing on corticomedullary phase images and is T2 iso- to hyperintense (Fig. 7.24).
  - The papillary subtype is often hypointense on T2-weighted images and hypoenhancing relative to the renal cortex (Fig. e7.11).
  - Chromophobe renal cell carcinoma is often isointense on T2-weighted images and shows moderate enhancement relative to the renal cortex (Fig. 7.25).
  - MRI can also identify invasion of the mass into the vasculature and can aid in differentiating between bland and tumor thrombus (Fig. 7.26).
- Nuclear medicine
  - FDG PET/CT is not commonly used for renal cell carcinoma, as the primary mass can be masked given that the radiotracer is excreted through the kidneys.
  - Furthermore, renal cell carcinoma has variable FDG radiotracer avidity (Fig. e7.12).

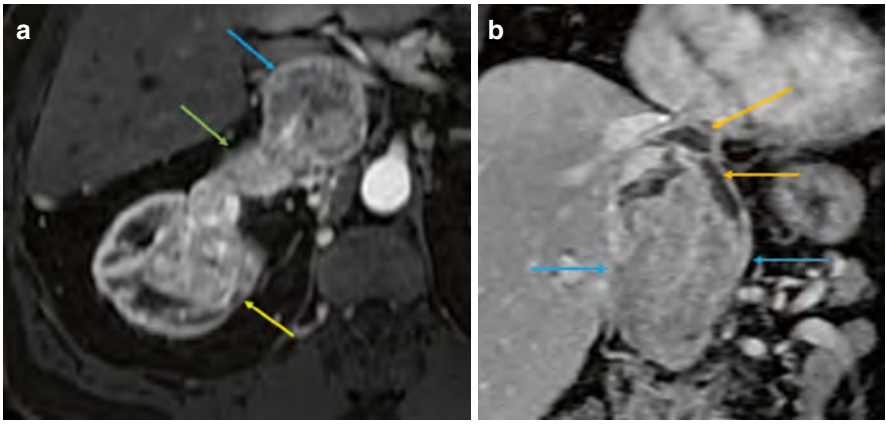

Fig. 7.26 71-year-old male with clear cell renal cell carcinoma. Post-contrast T1-weighted images in the axial (**a**) and (**b**) coronal planes demonstrate a mass arising from the right kidney (yellow arrow). The mass invades into the right renal vein with resulting tumor thrombus (green arrow). The tumor thrombus extends into the inferior vena cava (blue arrows) to the level of the hepatic veins. Superimposed bland thrombus (orange arrows) is appreciated, as this component of the thrombus is non-enhancing

Obstruction/Renal Enlargements

Hydronephrosis/Hydroureteronephrosis

- Hydronephrosis is defined as dilatation of the urinary collecting system, which includes the calyces, infundibula, and renal pelvis.
- Hydroureteronephrosis is hydronephrosis along with dilatation of the ureter (i.e., hydroureter).
- Hydronephrosis and hydroureteronephrosis can be due to
  - A stone.
  - Malignancy with the urinary tract.
  - Malignancy outside the urinary tract causing external compression of the tract.
  - Retroperitoneal fibrosis.

Imaging

- Ultrasound
  - Ultrasound is commonly used to evaluate for hydronephrosis.
  - Sonographically, hydronephrosis appears as dilatation of the pelvicalyceal system (Fig. 7.27).
  - Thinning of the renal cortex implies chronic hydronephrosis.
  - Hydroureter is challenging to identify sonographically as the ureters are deep within the body and often obscured sonographically due to beam attenuation and overlying bowel.

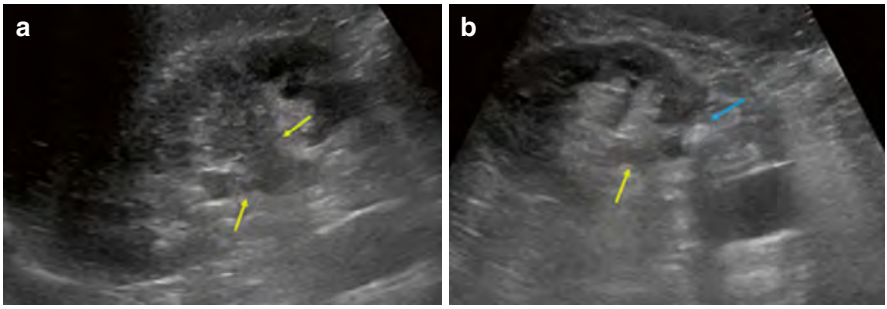

Fig. 7.27 60-year-old male with right-sided flank pain. B-mode ultrasound shows mild hydronephrosis (**a**, **b**) as hypoechoic dilatation of the renal pelvis and calyces (yellow arrows). A 1.2 cm ureteropelvic junction stone (blue arrow) is seen as the etiology of hydronephrosis (**b**)

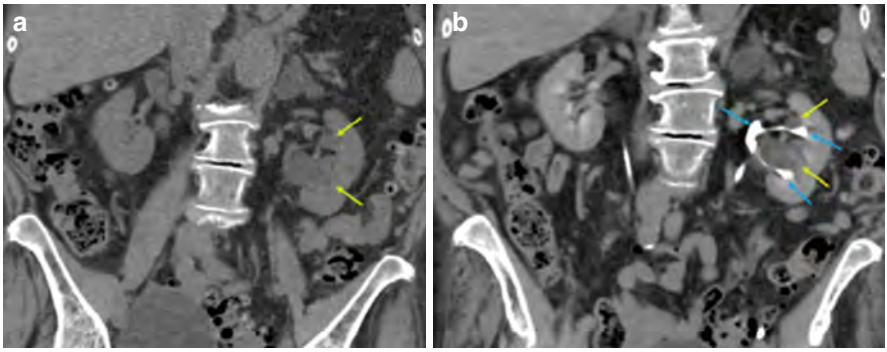

Fig. 7.28 80-year-old female with renal sinus cysts in the left kidney. On non-contrast coronal CT (**a**) cystic structures are visualized in the renal hilum (yellow arrows). These structures were strongly suspected to represent renal sinus cysts, particularly given that no cause of hydronephrosis was identified. The referring urology team wanted confirmation, so CT urography was performed. Coronal excretory phase CT urography images (**b**) redemonstrated the cystic structures (yellows arrows), which did not fill with contrast. The opacified calyces and infundibula (blue arrows) coursed around these cystic structures, thus confirming that the lesions were renal sinus cysts

- CT
  - CT readily shows hydronephrosis and hydroureteronephrosis and can typically identify the etiology of the urinary tract obstruction.
  - Renal sinus cysts can be difficult to distinguish from hydronephrosis. If needed, CT urography with an excretory phase of imaging can be used to distinguish renal sinus cysts with hydronephrosis (Fig. 7.28).
- MRI
  - MRI also readily shows hydronephrosis and hydroureteronephrosis as T2 hyperintense dilated spaces.
  - MRI can identify masses or retroperitoneal fibrosis as etiologies of hydronephrosis and hydroureteronephrosis, but identification of an obstructing stone can be challenging.

Renal Vein Thrombosis

- Thrombus within the renal vein can be bland thrombus or tumor thrombus. Tumor thrombus is discussed under the "Renal Cell Carcinoma" section.
- Bland renal vein thrombus can occur in hypercoagulable states, such as nephrotic syndrome, patients with a history of malignancy, systemic lupus erythematosus, or amyloidosis.
- Patients present with flank pain, hematuria, and acute kidney injury.

Imaging

- Ultrasound
  - Ultrasound can potentially visualize thrombus within the renal vein lumen, but ultrasound is not the preferred imaging modality due to low sensitivity.
  - Occlusive thrombus can lead to enlargement of the kidney on grayscale imaging.
  - Doppler imaging can show reversed arterial diastolic flow and/or an absence of venous flow.
- CT
  - Thrombus on CT is seen as a filling defect within the renal vein, typically on portal venous phase images (Fig. 7.29).
  - The ipsilateral kidney can be enlarged with perinephric stranding.
  - The ipsilateral kidney may have absent or delayed enhancement, particularly when the thrombus is occlusive (Fig. 7.30).
- MRI
  - Thrombus on MRI is seen as a filling defect within the renal vein, typically seen best on T1-weighted postcontrast images in the portal venous phase (Fig. 7.31).
  - The thrombus may be intrinsically T1 hyperintense.
  - Similar to CT, occlusive thrombus may show enlargement of the ipsilateral kidney with perinephric stranding, best seen on T2-weighted images.
  - The kidney may be hypo- or nonenhancing on postcontrast images.

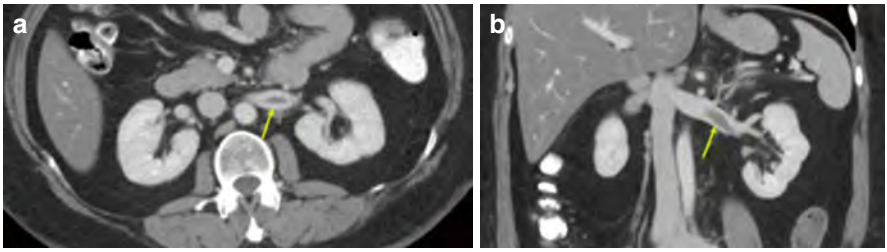

Fig. 7.29 58-year-old female with a history of uterine carcinosarcoma. Post-contrast axial (**a**) and coronal (**b**) CT images demonstrates non-occlusive thrombus in the left renal vein (yellow arrows)

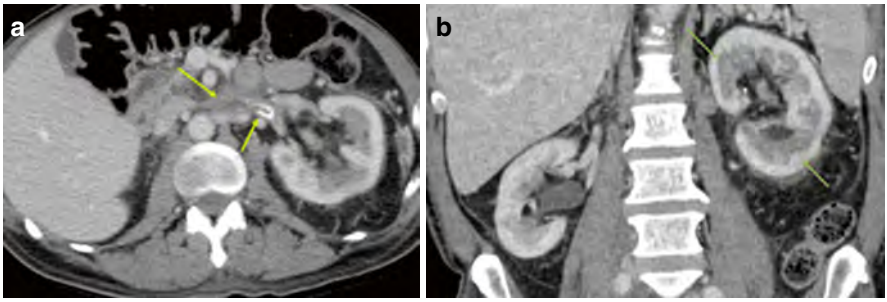

Fig. 7.30 63-year-old male with chronic left renal vein thrombus. Axial (**a**) and coronal (**b**) portal venous phase CT images demonstrate a partially occlusive thrombus within the left renal vein (yellow arrows). The enhancement of the left kidney is mildly delayed, given the increased corticomedullary differentiation of the left kidney compared to the right kidney (green arrows). There is mild edema surrounding the left kidney due to the chronic venous obstruction

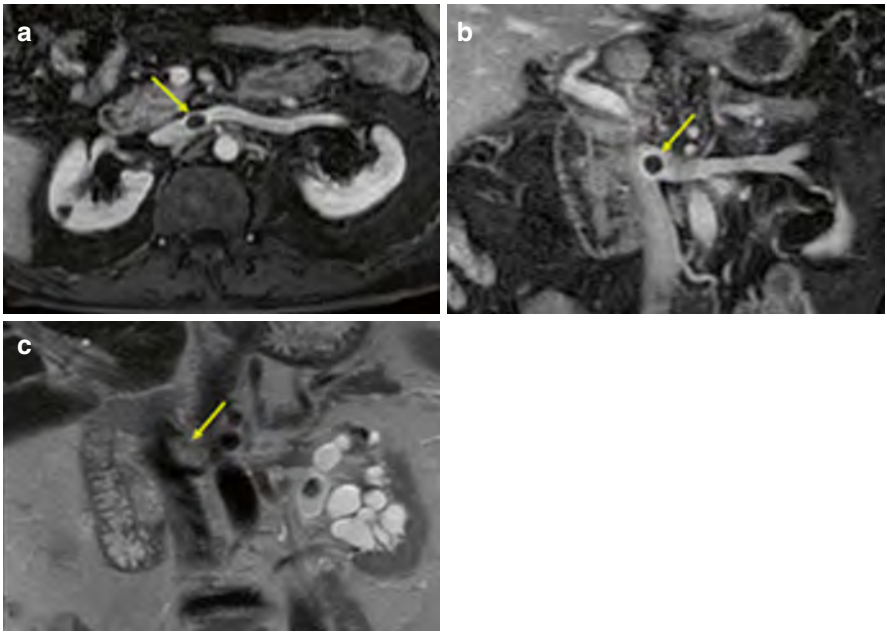

Fig. 7.31 93-year-old male with focal bland thrombus of the left renal vein. Axial (**a**) and coronal (**b**) post-contrast T1-weighted images demonstrate a small area of non-enhancement at the terminus of the left renal vein (arrows), consistent with thrombus. Thrombus can also be appreciated on coronal single-shot fast spin echo images (**c**), but is less conspicuous compared to post-contrast images

Stone Disease

- Urolithiasis is the umbrella term for a stone along the urinary tract, and therefore includes nephrolithiasis (stones within the kidneys, specifically the calyces), ureterolithiasis (stones within the ureters), and bladder calculi.
- The majority (~80%) of uroliths are calcium stones, including predominantly calcium oxalate and less commonly calcium phosphate.
  - Other stone types include uric acid, struvite, medication (such as indinavir), and cystine stones.
- Risk factors for urolithiasis include
  - Dehydration.
  - Congenital urinary tract abnormalities such as a duplicated collecting system or horseshoe kidney.
  - Urinary tract infections.
  - Hypercalciuria.
  - Hyperoxaluria.
- Patients with stones can present acutely with flank pain, particularly when a stone is migrating into the ureters and/or causing urinary tract obstruction.
- Microscopic or gross hematuria is frequently present in those with urolithiasis, although hematuria can be absent in ~15% of patients.
- Urinary tract obstruction due to stones is discussed in "the Hydronephrosis/Hydroureteronephrosis" section.

Imaging

- Radiopaque stone types include calcium oxalate, calcium phosphate, struvite, and cystine.
- Radiolucent stone types include uric acid and medication stones.
- Radiograph
  - Radiographs are commonly used for the initial detection of stones or follow-up of known stones.
  - Small stones may be difficult to identify radiographically, particularly due to overlapping structures such as the bowel.
- Ultrasound
  - Ultrasound can identify nephrolithiasis as well as bladder calculi, but the identification of ureterolithiasis is challenging sonographically, as the ureters are deep within the body and often obscured due to beam attenuation and overlying bowel.
  - Stones on ultrasound appear as echogenic structures with posterior acoustic shadowing and twinkle artifact on color Doppler (Fig. 7.32a).
  - Ultrasound has reduced sensitivity for stones <3 mm.
- CT
  - CT is the best imaging modality for the identification of stones, with sensitivity >94% and specificity >97%.
  - Stones appear as hyperattenuating structures within the urinary tract (Fig. 7.32b).

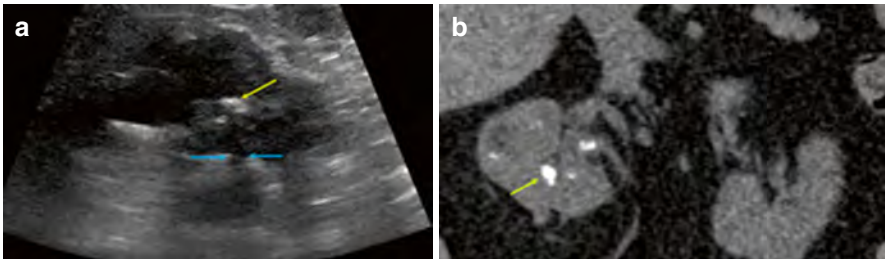

Fig. 7.32 57-year-old female with known urolithiasis. A stone is present in the right kidney, which is echogenic (yellow arrow) with posterior acoustic shadowing (blue arrows) on ultrasound (**a**). The stone (yellow arrow) is markedly hyperattenuating on coronal non-contrast CT (**b**) with a mean attenuation of 434 Hounsfield units

  - Calcium oxalate and calcium phosphate stones are typically between 400 and 600 Hounsfield units, whereas struvite, uric acid, and cystine stones are typically lower in attenuation.
  - Indinavir stones are radiolucent and may only be detected as a filling defect on excretory phase CT urography images.
- MRI
  - Stones are not well visualized on MRI, and typically appear as a void on T1- and T2-weighted images.

Medullary Nephrocalcinosis

- Medullary nephrocalcinosis is the deposition of calcium in the renal medulla.
- There are numerous causes of medullary nephrocalcinosis, including
  - Hyperparathyroidism.
  - Type 1 renal tubular acidosis.
  - Hypervitaminosis D.
  - Sarcoidosis.
  - Hyper- and hypothyroidism.
  - Milk-alkali syndrome.

Imaging

- Ultrasound
  - Grayscale ultrasound demonstrates markedly echogenic medullary pyramids in the setting of medullary nephrocalcinosis (Fig. 7.33a).
- CT
  - Medullary nephrocalcinosis on CT appears as hyperattenuating medullary pyramids (Fig. 7.33b).

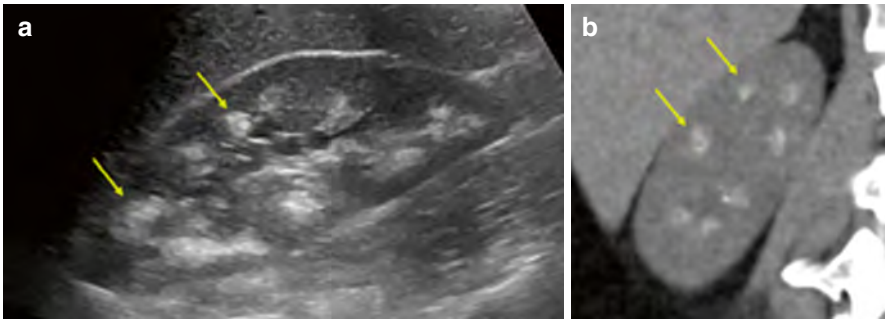

Fig. 7.33 31-year-old female with medullary nephrocalcinosis. Ultrasound images (**a**) demonstrate a markedly echogenic appearance of the medullary pyramids. Similarly, coronal non-contrast CT (**b**) demonstrates hyperattenuating calcifications in the medullary pyramids

Cancer of the Collecting System and Ureter

- Similar to bladder cancer (discussed below), the majority of cancers of the collecting system and ureters are urothelial cell carcinoma, also known as transitional cell carcinoma.
- Urothelial malignancy of the collecting system and ureter is up to 50× less frequent than urothelial malignancy of the bladder.
- Urothelial malignancy of the collecting system and ureter is more common in men and typically seen in the seventh decade.

Imaging

- CT urography is the standard imaging method for identifying malignancy within the collecting systems and ureters.
  - CT urography classically consists of three image phases (Fig. 7.34), including the noncontrast, nephrographic, and excretory phases:

    Noncontrast images are acquired to evaluate for stones and also to establish a baseline for potential tumor enhancement on subsequent postcontrast CT phases.

    The nephrographic phase is acquired 90–100 s after the intravenous administration of iodinated contrast. This phase allows for the identification of renal masses as well as enhancing urothelial masses.

    An excretory phase is acquired 5–10 min after the initial contrast injection. At this phase, contrast has been excreted into the renal collecting system and allows for the identification of filling defects within the collecting systems, ureters, and bladder.
  - CT urography with a split-bolus technique has been developed to reduce radiation dose. The split-bolus technique is acquired in two phases (Fig. 7.35), including a noncontrast and combined nephrographic and excretory phase:

    Noncontrast images are acquired as noted above for three-phase CT urography.

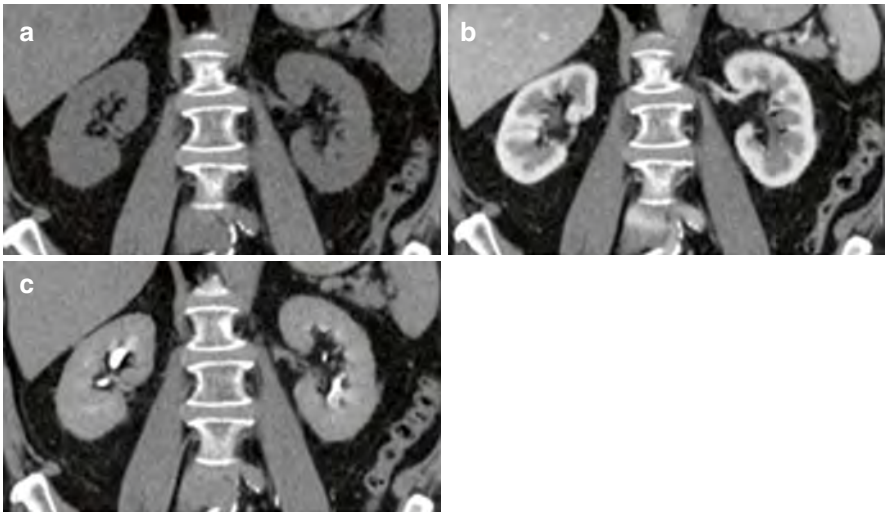

Fig. 7.34 69-year-old male presenting with microscopic hematuria. 3-phase CT urography was performed, with images acquired in the non-contrast (**a**), nephrographic (**b**), and excretory (**c**) phases. No abnormality was found to explain the patient's hematuria

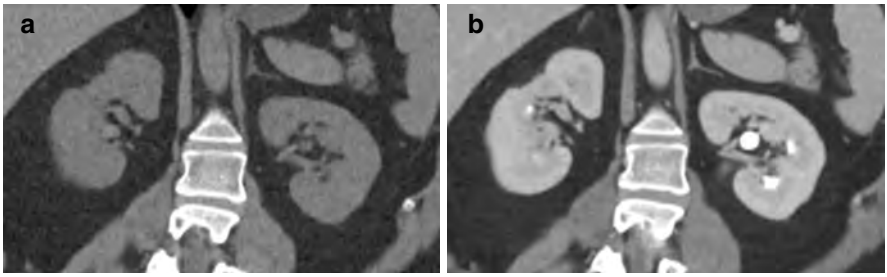

Fig. 7.35 35-year-old male presenting with microscopic hematuria. Split-bolus CT urography was performed, with images acquired in the non-contrast (**a**) and combined nephrographic/excretory (**b**) phases. No abnormality was found to explain the patient's hematuria

For postcontrast images, a portion of the contrast bolus is injected (for example, half), and no images are then acquired. After approximately 10 min, the remainder of the contrast bolus is injected. Images are then acquired 90–100 s later. Therefore, the first bolus is now excreted by the kidneys, providing excretory phase information, and the second bolus is providing nephrographic phase information.

– The use of three-phase versus split-bolus CT urography is often a matter of institutional preference, with some institutions exclusively using one technique or the other, and some institutions using the latter for younger patients given the lower radiation dose.

- Urothelial malignancies will enhance on nephrographic phase images and will be readily identified as filling defects on excretory phase images (Fig. e7.13).

Bladder Infection

- Cystitis is inflammation of the urinary bladder.
- Cystitis is typically due to bacterial urinary tract infection, frequently *Escherichia coli*, although tuberculosis can also be a causative agent.
- Other causes of cystitis include fungal and parasitic infectious agents, chemotherapy agents such as cyclophosphamide, and radiation.
- Cystitis is much more common in females than males, likely due to the shorter urethra and the proximity of the urethra to the anus.

Imaging

- Ultrasound, CT, and MRI show similar findings in the setting of cystitis (Fig. 7.36).
- The bladder wall may be thickened, greater than 3 mm when the bladder is well distended and greater than 5 mm when the bladder is non-distended.
- The bladder wall may be hyperemic on color Doppler ultrasound or hyperenhancing on postcontrast CT and MRI.
- Pericystic stranding can be seen on CT and MRI.
- Debris may layer dependently within the bladder lumen.

Chronic Bladder Outlet Obstruction

- Chronic bladder outlet obstruction is most commonly seen in elderly men secondary to prostate enlargement but can also be due to a distal urinary tract mass, urethral stricture, or congenital urethral valves.
- Patients present with urinary frequency and urgency, urinary retention, and urinary discomfort.

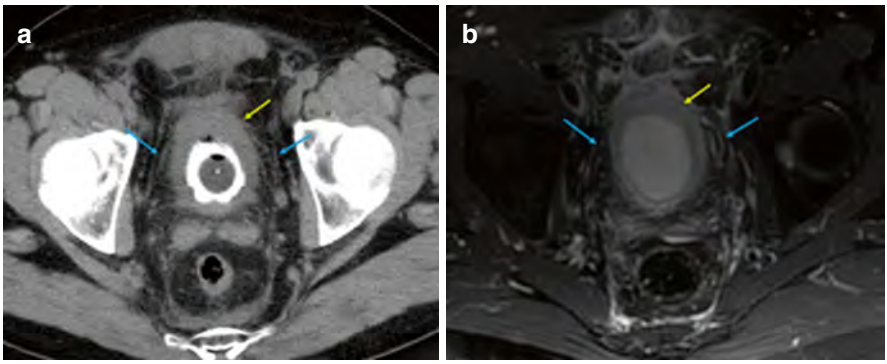

Fig. 7.36 56-year-old male with cystitis. Axial CT cystogram (**a**) and axial T2-weighted MR images with fat saturation (**b**) demonstrate marked thickening of the bladder wall (yellow arrows) with marked pericystic stranding (blue arrows)

Imaging

- Ultrasound, CT, and MRI show similar findings in the setting of chronic bladder outlet obstruction:
  - Bladder wall thickening.
  - Bladder wall trabeculations.
  - Bladder diverticula.
- When chronic bladder outlet obstruction is due to enlargement of the prostate, the enlarged prostate ± median lobe hypertrophy into the bladder base will be seen (Fig. 7.37).

Bladder Cancer

- Urothelial carcinoma is also called transitional cell carcinoma.
- It accounts for up to 95% of bladder cancers.
- Squamous cell carcinoma is the next most common subtype, while adenocarcinoma and small cell carcinoma are rare.
- Patients with bladder cancer often present with hematuria.
- Patients can also present with dysuria as well as urinary frequency and urgency.
- Numerous entities mimic bladder cancer, most commonly thrombus within the bladder lumen as thrombus can be similarly lobulated and/or mass-like (Fig. 7.38).

Imaging

- Ultrasound
  - Ultrasound has a limited role in imaging of bladder cancer.

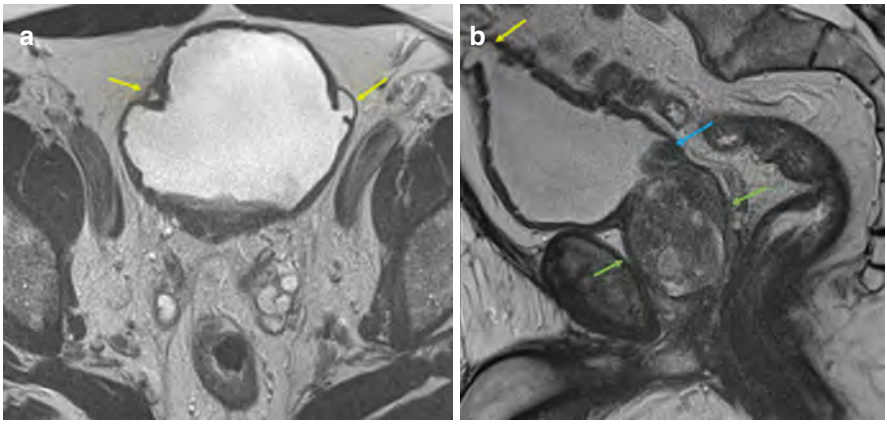

Fig. 7.37 69-year-old male with chronic bladder outlet obstruction and presenting with urinary frequency and urgency. T2-weighted MR images in the axial (**a**) and sagittal (**b**) planes demonstrate bladder diverticula (yellow arrows), enlargement of the prostate (green arrows), and median lobe hypertrophy of the bladder into the bladder base (blue arrow)

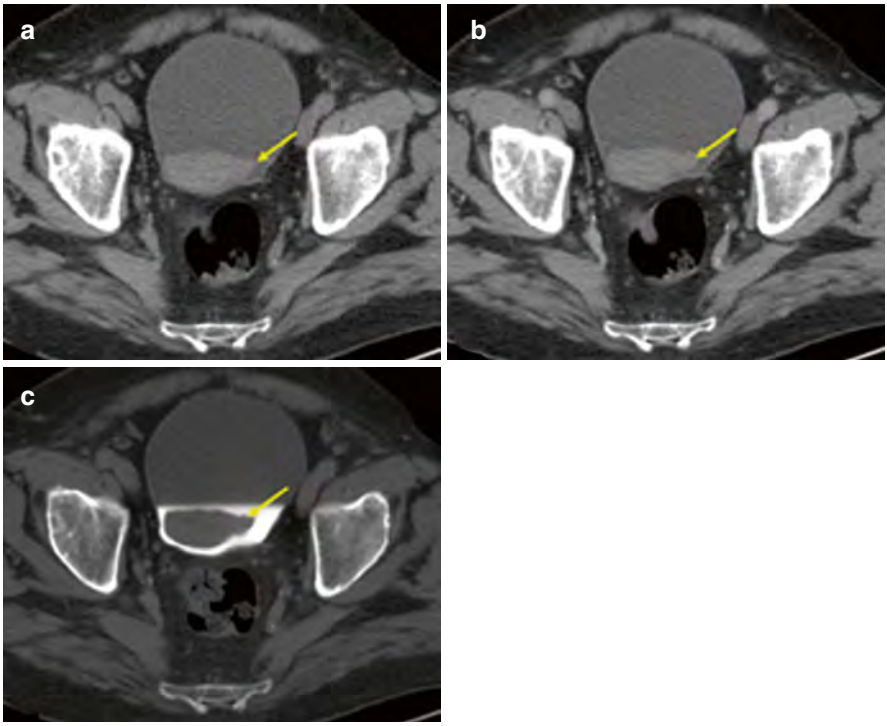

Fig. 7.38 75-year-old male with a suspected bladder mass. Axial CT urography images in the non-contrast (**a**), nephrographic (**b**), and excretory (**c**) phases demonstrate a lobulated mass dependently within the bladder. The mass has a mean attenuation of 43 Hounsfield units on non-contrast images and 47 Hounsfield units on nephrographic and excretory post-contrast images and is therefore indicative of bladder thrombus. Thrombus was confirmed on cystoscopy

  - While a mass within the bladder lumen ± internal vascularity can be identified sonographically (Fig. 7.39), the identification of metastatic disease is limited with ultrasound.
- CT
  - Bladder cancer can appear as a focal region of bladder wall thickening versus a mass that protrudes into the bladder lumen (Fig. 7.40).
  - The mass can extend beyond the bladder wall and invade into the surrounding pelvic structures.
  - Bladder cancer can have small calcifications.
- MRI
  - MRI is excellent at identifying bladder cancer and locally staging the mass.
  - The identification of muscle invasion by the primary tumor is possible with MRI (muscle invasion differentiates a stage T1 tumor from a stage T2 tumor).
  - The MRI parameters for bladder cancer staging have been incorporated into VI-RADS (Vesical Imaging-Reporting and Data System), although the VI-RADS system is not yet widely adopted.

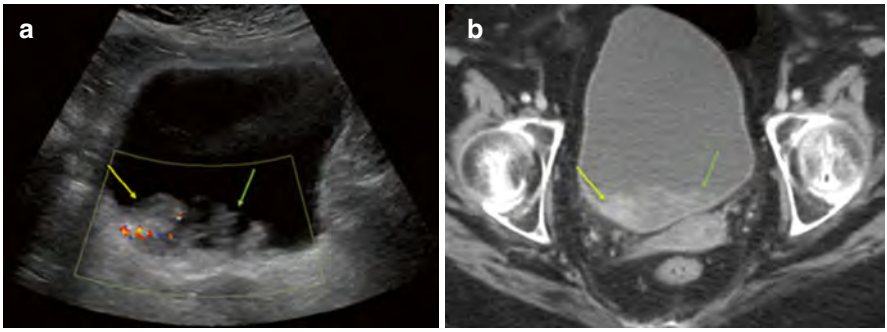

Fig. 7.39 71-year-old female presenting with hematuria. Color Doppler image of the bladder (**a**) demonstrates a focal mass along the right posterolateral aspect of the bladder (yellow arrow) with internal vascularity along with adjacent thrombus (green arrow). Similarly, an axial contrast-enhanced CT (**b**) demonstrates the mass along the right posterolateral aspect of the bladder (yellow arrow) with adjacent thrombus (green arrow). On CT, it can be difficult to distinguish between a neoplasm and thrombus within the bladder if only a single phase is acquired

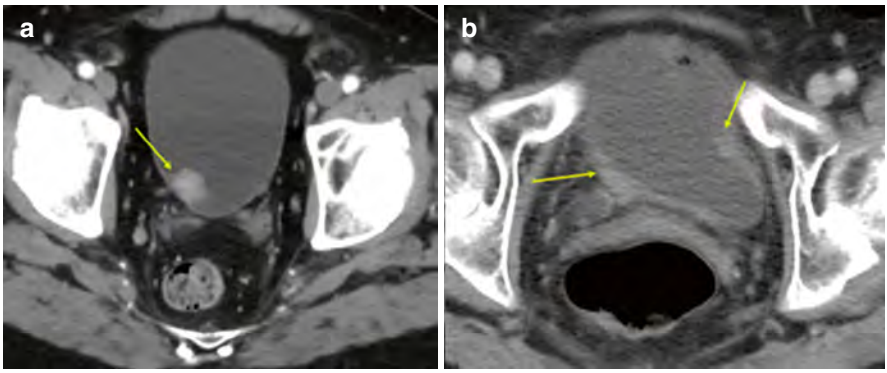

Fig. 7.40 Contrast-enhanced axial CT images in a 73-year-old male showing a protruding mass within the bladder (**a**) as well as a 77-year-old female with two areas of focal wall thickening of the urinary bladder wall (**b**). Both patients were found to have high-grade urothelial carcinoma

- Local staging of bladder cancer with muscular invasion is traditionally diagnosed under cystoscopy by urologists.
- On MRI, bladder cancer appears as slightly T2 hyperintense compared to muscle and demonstrates enhancement on postcontrast T1-weighted images (Fig. e7.14).

Ureterocele

- A ureteroceles is a congenital dilatation of the terminal aspect of the ureter.
- Ureteroceles can be intravesical or extravesical in location.
- Extravesical ureteroceles are associated with duplicated collecting systems.

Imaging

- A ureterocele appears similar on ultrasound, CT, and MRI, and is seen as a cystic structure near the ureterovesical junction (Fig. 7.41).

Bladder Rupture

- Bladder rupture can occur in the setting of marked trauma, particularly high-speed motor vehicle collisions with associated pelvic fractures in most cases.
- Patients may present with hematuria, abdominal pain, and difficulty with micturition.
- Bladder rupture can be intraperitoneal or extraperitoneal depending on the location of injury.
- Extraperitoneal injury is more common, accounting for 60% of cases.
  - Intraperitoneal rupture is treated surgically, whereas extraperitoneal rupture is treated with a urinary catheter.

Imaging

- CT
  - CT cystogram is the standard means of diagnosing bladder rupture.
  - In CT cystography, water-soluble contrast is administered into the bladder via a bladder catheter.
  - Extravasation of contrast from the bladder aids in diagnosing bladder injury.
  - The location of extravasated contrast can identify the injury as intraperitoneal (Fig. 7.42) or extraperitoneal (Fig. 7.43).

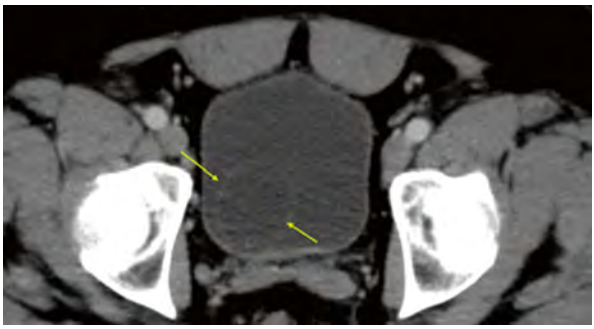

Fig. 7.41 46-year-old male with a subtle cystic structure in the right posterolateral bladder (yellow arrows), consistent with an intravesical ureterocele

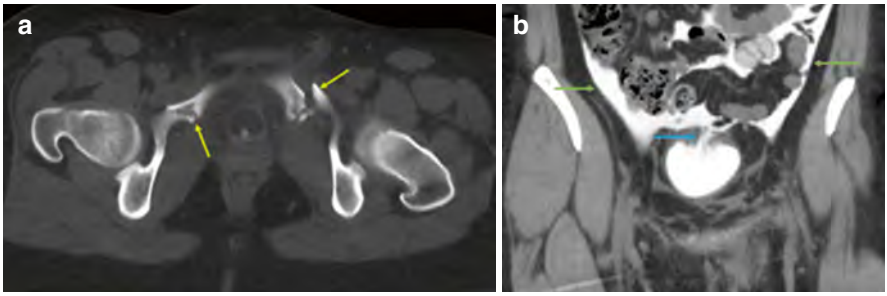

Fig. 7.42 26-year-old female presenting after a high-speed motor vehicle collision that resulted in intraperitoneal bladder rupture. Axial (**a**) and coronal (**b**) CT cystogram shows multiple pelvic fractures including bilateral inferior pubic rami fractures (yellow arrows). Furthermore, contrast infused into the bladder extravasates through the bladder dome (blue arrow) and accumulates in the intraperitoneal cavity (green arrows)

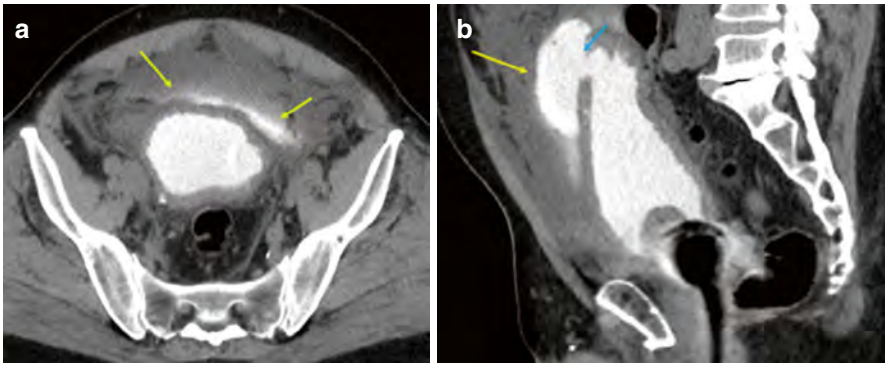

Fig. 7.43 65-year-old male presenting after a motor vehicle collision with multiple pelvic fractures (not shown) that resulted in extraperitoneal bladder rupture. Axial (**a**) and coronal (**b**) CT cystogram shows extravasation of contrast into the space of Retzius (yellow arrows), which is extraperitoneal in location. The defect in the bladder wall anteriorly can be seen (blue arrow)

Urethra

Urethral Trauma

- Urethral injury is common in adults with pelvic fractures, occurring in up to 24% of individuals.
  - Strictures may result from urethral injury.
- Urethral injury can be anterior (penile/bulbar urethra) or posterior (membranous/prostatic urethra).
  - Anterior injuries occur due to direct trauma, such as straddle injury.
  - Posterior injuries occur due to crushing forces of the urethra against the pelvis.

- Patients can present with blood products at the penile meatus, difficulty voiding, scrotal/perineal ecchymosis or hematoma, and concomitant pelvic fracture.
- Injury is classified per the Goldman classification system:
  - Type 1: stretching of the posterior urethra.
  - Type 2: injury to the posterior urethra above the urogenital diaphragm.
  - Type 3: membranous urethra injury with extension to the proximal bulbous urethra.
  - Type 4: injury to the bladder base with extension into the proximal urethra.
  - Type 5: isolated anterior urethral injury.
- Imaging
  - Imaging is used to identify and stage the urethral injury.
  - Fluoroscopy

    Voiding cystourethrography is used to evaluate the posterior urethra, whereas retrograde urethrography is used to evaluate the anterior urethra.
    - Imaging can demonstrate disruption of the urethra via discontinuity along the course of the urethra with resultant extravasation of contrast (Fig. 7.44).
    - Stricturing of the urethra can result from trauma. Obstruction to urine flow by the urethral strictures can result in the filling of the glands of Littré (Fig. e7.15).
  - CT

    CT cystography can be performed but is better suited for bladder injury and is less sensitive for urethral injury.

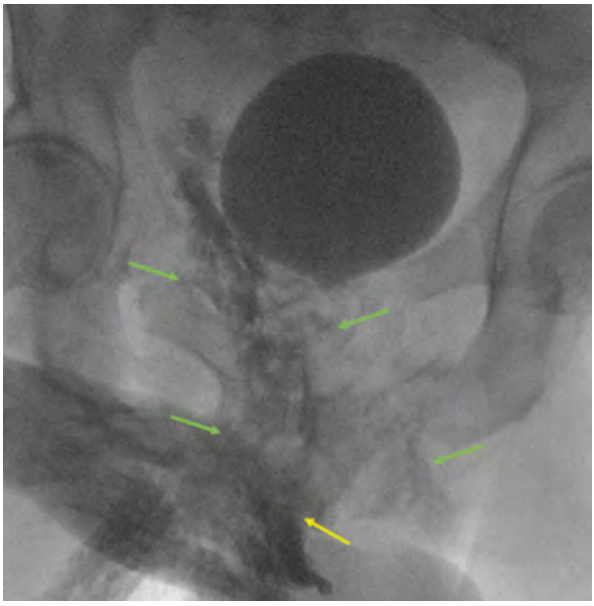

Fig. 7.44 62-year-old male presenting with crush injury. Retrograde urethrogram demonstrates complete disruption of the anterior urethra (yellow arrow), with marked extravasation of contrast into the surrounding tissues (green arrows)

Urethral Diverticulum

- Urethral diverticulum is a focal outpouching of the urethral mucosa.
- Urethral diverticula have a prevalence of 1–5% in women and are rare in men.
- Urethral diverticula occur typically between the ages of 20 and 60 years.
- Patients typically present with urinary incontinence, dysuria, dyspareunia, and/or a vaginal mass.
- Delayed diagnosis can lead to urethral stone formation, malignancy, and recurrent urinary tract infections.
- Risk factors include female gender, pelvic trauma, and periurethral interventions.

Imaging

- Urethral diverticulum is seen as a cystic lesion that arises from the posterolateral aspect of the distal urethra and that wraps around the distal urethra.
- Voiding cystourethrography (Fig. 7.45).
  - Considered the imaging modality of choice prior to the general adoption of MRI.
  - The bladder is filled with contrast following catheterization and fluoroscopic images are obtained both during the filling phase as well as the voiding phase.

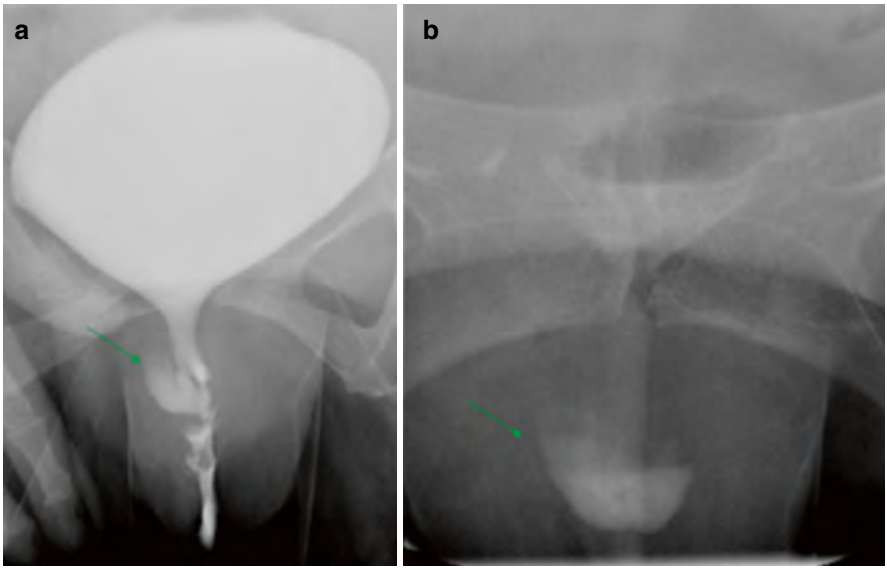

Fig. 7.45 64-year-old female with a urethral diverticulum. During the filling phase of a voiding cystourethrography fluoroscopic study (**a**) a diverticulum fills with contrast along the posterior aspect of the mid urethra (green arrow). Following voiding (**b**), the diverticulum retains contrast (green arrow)

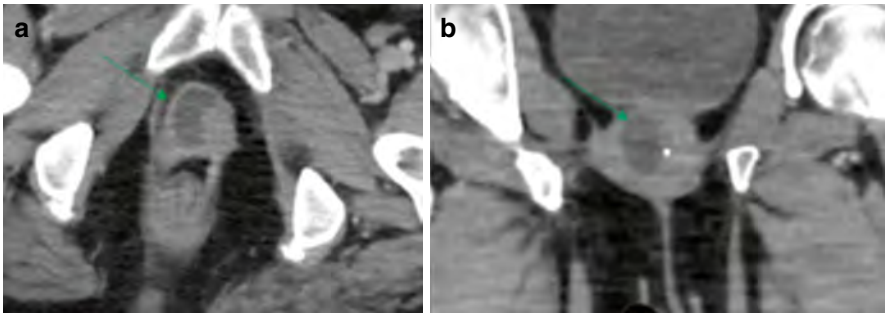

Fig. 7.46 63-year-old female with a urethral diverticulum. Axial (**a**) and coronal (**b**) contrast-enhanced CT images demonstrate a hypoattenuating structure with a mean attenuation of 11 HU that partially encompasses the urethra, consistent with a urethral diverticulum

  - A urethral diverticulum will fill with contrast during the filling phase, and typically retain contrast following the voiding phase.
- CT (Fig. 7.46)
  - CT is somewhat limited in evaluating structures of the female pelvis due to poor contrast resolution particularly in the setting of beam hardening from the pelvic bones.
  - Urethral diverticulum is a cystic structure that partially envelopes the urethra at the level of the pubic symphysis.
  - If large enough, the structure will have a mean attenuation consistent with fluid (0–20 HU), although debris within the diverticulum can lead to a higher mean attenuation.
  - Identification of a neoplasm associated with the diverticulum can be challenging on CT, particularly when small.
- MRI (Fig. e7.16)
  - MRI is generally considered the imaging study of choice.
  - T2-weighted images show a hyperintense cystic structure that partially circumscribes the urethra.
  - Gadolinium-based contrast agents can be used to detect inflammation of the diverticulum, such as wall thickening and hyperenhancement, as well as neoplasms that arise within the diverticulum.

    The diverticulum on delayed postcontrast imaging fills with contrast. Postcontrast imaging aids in differentiating a diverticulum from a periurethral cyst, including Skene duct cyst or other cyst in the vaginal wall.

Urethral Infection

- Urethritis occurs most frequently in men with a history of sexually transmitted infections.
- Patients present with purulent urethral discharge and dysuria.
- Complications include urethral strictures, abscess, and fistula.

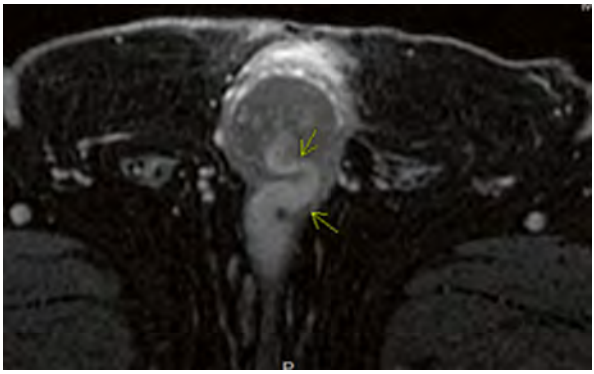

Fig. 7.47 58-year-old male with a history of sexually transmitted infections. Axial post-contrast MRI through the penis demonstrates stricturing and tortuosity of the penile urethra (arrows)

Imaging

- Retrograde urethrography and voiding cystourethrography are commonly performed for the evaluation of urethral stricture, which can demonstrate stricturing of the urethra and potential filling of the glands of Littré.
- MRI can also visualize urethral stricture and tortuosity of the urethra (Fig. 7.47).

Conclusion

This introductory chapter serves as a foundation for the role of imaging in identifying diseases of the urinary tract. The chapter includes basic imaging anatomy of the structures along the urinary tract. Furthermore, the chapter describes the most common disease processes of the urinary tract with their associated imaging findings. It should be noted that rare disease processes, and rare presentations of common disease processes, were not included in this chapter. Nevertheless, with a focus on the basic anatomy and diseases of the urinary tract, along with representative images of these diseases, readers are well-equipped to navigate their first rotation in abdominal radiology.

Further Readings

1. Urban BA, Ratner LE, Fishman EK. Three-dimensional volume-rendered CT angiography of the renal arteries and veins: normal anatomy, variants, and clinical applications. Radiographics. 2001;21(2):373–86; questionnaire 549–55.
2. Gulas E, Wysiadecki G, Cecot T, Majos A, Stefanczyk L, Topol M, et al. Accessory (multiple) renal arteries—differences in frequency according to population, visualizing techniques and stage of morphological development. Vascular. 2016;24(5):531–7.
3. Cheong B, Muthupillai R, Rubin MF, Flamm SD. Normal values for renal length and volume as measured by magnetic resonance imaging. Clin J Am Soc Nephrol. 2007;2(1):38–45.
4. Potenta SE, D'Agostino R, Sternberg KM, Tatsumi K, Perusse K. CT urography for evaluation of the ureter. Radiographics. 2015;35(3):709–26.

5. Houat AP, Guimaraes CTS, Takahashi MS, Rodi GP, Gasparetto TPD, Blasbalg R, et al. Congenital anomalies of the upper urinary tract: a comprehensive review. Radiographics. 2021;41(5):E165.
6. Laurichesse Delmas H, Kohler M, Doray B, Lemery D, Francannet C, Quistrebert J, et al. Congenital unilateral renal agenesis: prevalence, prenatal diagnosis, associated anomalies. Data from two birth-defect registries. Birth Defects Res. 2017;109(15):1204–11.
7. Harrison LH Jr, Flye MW, Seigler HF. Incidence of anatomical variants in renal vasculature in the presence of normal renal function. Ann Surg. 1978;188(1):83–9.
8. Shah HU, Ojili V. Multimodality imaging spectrum of complications of horseshoe kidney. Indian J Radiol Imaging. 2017;27(2):133–40.
9. O'Brien J, Buckley O, Doody O, Ward E, Persaud T, Torreggiani W. Imaging of horseshoe kidneys and their complications. J Med Imaging Radiat Oncol. 2008;52(3):216–26.
10. Glodny B, Petersen J, Hofmann KJ, Schenk C, Herwig R, Trieb T, et al. Kidney fusion anomalies revisited: clinical and radiological analysis of 209 cases of crossed fused ectopia and horseshoe kidney. BJU Int. 2009;103(2):224–35.
11. Schiappacasse G, Aguirre J, Soffia P, Silva CS, Zilleruelo N. CT findings of the main pathological conditions associated with horseshoe kidneys. Br J Radiol. 2015;88(1045):20140456.
12. Raj GV, Auge BK, Assimos D, Preminger GM. Metabolic abnormalities associated with renal calculi in patients with horseshoe kidneys. J Endourol. 2004;18(2):157–61.
13. Gay SB, Armistead JP, Weber ME, Williamson BR. Left infrarenal region: anatomic variants, pathologic conditions, and diagnostic pitfalls. Radiographics. 1991;11(4):549–70.
14. Hartman GW, Hodson CJ. The duplex kidney and related abnormalities. Clin Radiol. 1969;20(4):387–400.
15. Callahan MJ. The drooping lily sign. Radiology. 2001;219(1):226–8.
16. Chien LC, Herr KD, Archer-Arroyo K, Vakil M, Hanna TN. Review of multimodality imaging of renal trauma. Radiol Clin North Am. 2020;58(5):965–79.
17. Kozar RA, Crandall M, Shanmuganathan K, Zarzaur BL, Coburn M, Cribari C, et al. Organ injury scaling 2018 update: spleen, liver, and kidney. J Trauma Acute Care Surg. 2018;85(6):1119–22.
18. Kawashima A, Sandler CM, Corl FM, West OC, Tamm EP, Fishman EK, et al. Imaging of renal trauma: a comprehensive review. Radiographics. 2001;21(3):557–74.
19. Lee YJ, Oh SN, Rha SE, Byun JY. Renal trauma. Radiol Clin North Am. 2007;45(3):581–92, ix.
20. Dopson SJ, Jayakumar S, Velez JC. Page kidney as a rare cause of hypertension: case report and review of the literature. Am J Kidney Dis. 2009;54(2):334–9.
21. Urban BA, Fishman EK. Tailored helical CT evaluation of acute abdomen. Radiographics. 2000;20(3):725–49.
22. Kawashima A, Sandler CM, Ernst RD, Tamm EP, Goldman SM, Fishman EK. CT evaluation of renovascular disease. Radiographics. 2000;20(5):1321–40.
23. Jung DC, Kim SH, Jung SI, Hwang SI, Kim SH. Renal papillary necrosis: review and comparison of findings at multi-detector row CT and intravenous urography. Radiographics. 2006;26(6):1827–36.
24. Dyer RB, Chen MY, Zagoria RJ. Classic signs in uroradiology. Radiographics. 2004;24(Suppl 1):S247–80.
25. Yen DH, Hu SC, Tsai J, Kao WF, Chern CH, Wang LM, et al. Renal abscess: early diagnosis and treatment. Am J Emerg Med. 1999;17(2):192–7.
26. Kawashima A, Sandler CM, Ernst RD, Goldman SM, Raval B, Fishman EK. Renal inflammatory disease: the current role of CT. Crit Rev Diagn Imaging. 1997;38(5):369–415.
27. Foxman B, Klemstine KL, Brown PD. Acute pyelonephritis in US hospitals in 1997: hospitalization and in-hospital mortality. Ann Epidemiol. 2003;13(2):144–50.
28. Fairley KF, Carson NE, Gutch RC, Leighton P, Grounds AD, Laird EC, et al. Site of infection in acute urinary-tract infection in general practice. Lancet. 1971;2(7725):615–8.
29. Czaja CA, Scholes D, Hooton TM, Stamm WE. Population-based epidemiologic analysis of acute pyelonephritis. Clin Infect Dis. 2007;45(3):273–80.

30. Craig WD, Wagner BJ, Travis MD. Pyelonephritis: radiologic-pathologic review. Radiographics. 2008;28(1):255–77; quiz 327–8.
31. Johnson PT, Horton KM, Fishman EK. Optimizing detectability of renal pathology with MDCT: protocols, pearls, and pitfalls. AJR Am J Roentgenol. 2010;194(4):1001–12.
32. Woodward S, Elsayes KM, Akhtar AL. Imaging of emphysematous pyelonephritis: self-assessment module. AJR Am J Roentgenol. 2010;194(6 Suppl):S70–2.
33. Xing ZX, Yang H, Zhang W, Wang Y, Wang CS, Chen T, et al. Point-of-care ultrasound for the early diagnosis of emphysematous pyelonephritis: a case report and literature review. World J Clin Cases. 2021;9(11):2584–94.
34. Parsons MA, Harris SC, Longstaff AJ, Grainger RG. Xanthogranulomatous pyelonephritis: a pathological, clinical and aetiological analysis of 87 cases. Diagn Histopathol. 1983;6(3–4):203–19.
35. Chuang CK, Lai MK, Chang PL, Huang MH, Chu SH, Wu CJ, et al. Xanthogranulomatous pyelonephritis: experience in 36 cases. J Urol. 1992;147(2):333–6.
36. Goodman M, Curry T, Russell T. Xanthogranulomatous pyelonephritis (XGP): a local disease with systemic manifestations. Report of 23 patients and review of the literature. Medicine (Baltimore). 1979;58(2):171–81.
37. Wagenlehner FME, Bjerklund Johansen TE, Cai T, Koves B, Kranz J, Pilatz A, et al. Epidemiology, definition and treatment of complicated urinary tract infections. Nat Rev Urol. 2020;17(10):586–600.
38. Tamburrini S, Lugara M, Iannuzzi M, Cesaro E, De Simone F, Del Biondo D, et al. Pyonephrosis ultrasound and computed tomography features: a pictorial review. Diagnostics (Basel). 2021;11(2):331.
39. Carrim ZI, Murchison JT. The prevalence of simple renal and hepatic cysts detected by spiral computed tomography. Clin Radiol. 2003;58(8):626–9.
40. Clayman RV, Surya V, Miller RP, Reinke DB, Fraley EE. Pursuit of the renal mass. Is ultrasound enough? Am J Med. 1984;77(2):218–23.
41. Terada N, Ichioka K, Matsuta Y, Okubo K, Yoshimura K, Arai Y. The natural history of simple renal cysts. J Urol. 2002;167(1):21–3.
42. Wentland AL, Nystrom J, Lubner MG, Mao L, Abel EJ, Pickhardt PJ. Natural history of simple renal cysts: longitudinal CT-based evaluation. Abdom Radiol (NY). 2022;47(3):1124–32.
43. Silverman SG, Pedrosa I, Ellis JH, Hindman NM, Schieda N, Smith AD, et al. Bosniak classification of cystic renal masses, version 2019: an update proposal and needs assessment. Radiology. 2019;292(2):475–88.
44. Jonisch AI, Rubinowitz AN, Mutalik PG, Israel GM. Can high-attenuation renal cysts be differentiated from renal cell carcinoma at unenhanced CT? Radiology. 2007;243(2):445–50.
45. Gabow PA. Autosomal dominant polycystic kidney disease. N Engl J Med. 1993;329(5):332–42.
46. Odedra D, Sabongui S, Khalili K, Schieda N, Pei Y, Krishna S. Autosomal dominant polycystic kidney disease: role of imaging in diagnosis and management. Radiographics. 2023;43(1):e220126.
47. Bae KT, Zhu F, Chapman AB, Torres VE, Grantham JJ, Guay-Woodford LM, et al. Magnetic resonance imaging evaluation of hepatic cysts in early autosomal-dominant polycystic kidney disease: the Consortium for Radiologic Imaging Studies of Polycystic Kidney Disease cohort. Clin J Am Soc Nephrol. 2006;1(1):64–9.
48. Umeoka S, Koyama T, Miki Y, Akai M, Tsutsui K, Togashi K. Pictorial review of tuberous sclerosis in various organs. Radiographics. 2008;28(7):e32.
49. Logue LG, Acker RE, Sienko AE. Best cases from the AFIP: angiomyolipomas in tuberous sclerosis. Radiographics. 2003;23(1):241–6.
50. Wang C, Li X, Peng L, Gou X, Fan J. An update on recent developments in rupture of renal angiomyolipoma. Medicine (Baltimore). 2018;97(16):e0497.
51. Kotis A, Lisgos F, Karatapanis S. Ultrasound and CT imaging assessment of renal angiomyolipoma. BMJ Case Rep. 2010;2010:bcr0120102624.

52. Park BK. Renal angiomyolipoma: radiologic classification and imaging features according to the amount of fat. AJR Am J Roentgenol. 2017;209(4):826–35.
53. Shetty AS, Sipe AL, Zulfiqar M, Tsai R, Raptis DA, Raptis CA, et al. In-phase and opposed-phase imaging: applications of chemical shift and magnetic susceptibility in the chest and abdomen. Radiographics. 2019;39(1):115–35.
54. Mirkheshti N, Farrukh N, Legesse T, Rowe SP, Gordetsky J, Hussain A. Renal oncocytoma: a challenging diagnosis. Curr Opin Oncol. 2022;34(3):243–52.
55. Mauermann J, de Martino M, Waldert M, Haitel A, Klingler HC, Remzi M, et al. Gender differences in benign renal masses. World J Urol. 2013;31(5):1051–7.
56. Prasad SR, Surabhi VR, Menias CO, Raut AA, Chintapalli KN. Benign renal neoplasms in adults: cross-sectional imaging findings. AJR Am J Roentgenol. 2008;190(1):158–64.
57. Siegel RL, Miller KD, Wagle NS, Jemal A. Cancer statistics, 2023. CA Cancer J Clin. 2023;73(1):17–48.
58. Thompson RH, Ordonez MA, Iasonos A, Secin FP, Guillonneau B, Russo P, et al. Renal cell carcinoma in young and old patients—is there a difference? J Urol. 2008;180(4):1262–6; discussion 6.
59. Siemer S, Hack M, Lehmann J, Becker F, Stockle M. Outcome of renal tumors in young adults. J Urol. 2006;175(4):1240–3; discussion 3–4.
60. Cumberbatch MG, Rota M, Catto JW, La Vecchia C. The role of tobacco smoke in bladder and kidney carcinogenesis: a comparison of exposures and meta-analysis of incidence and mortality risks. Eur Urol. 2016;70(3):458–66.
61. Hidayat K, Du X, Zou SY, Shi BM. Blood pressure and kidney cancer risk: meta-analysis of prospective studies. J Hypertens. 2017;35(7):1333–44.
62. Adams KF, Leitzmann MF, Albanes D, Kipnis V, Moore SC, Schatzkin A, et al. Body size and renal cell cancer incidence in a large US cohort study. Am J Epidemiol. 2008;168(3):268–77.
63. Brennan JF, Stilmant MM, Babayan RK, Siroky MB. Acquired renal cystic disease: implications for the urologist. Br J Urol. 1991;67(4):342–8.
64. Mandel JS, McLaughlin JK, Schlehofer B, Mellemgaard A, Helmert U, Lindblad P, et al. International renal-cell cancer study. IV. Occupation. Int J Cancer. 1995;61(5):601–5.
65. Maclure M. Asbestos and renal adenocarcinoma: a case-control study. Environ Res. 1987;42(2):353–61.
66. McLaughlin JK, Blot WJ, Mehl ES, Stewart PA, Venable FS, Fraumeni JF Jr. Petroleum-related employment and renal cell cancer. J Occup Med. 1985;27(9):672–4.
67. Cho E, Curhan G, Hankinson SE, Kantoff P, Atkins MB, Stampfer M, et al. Prospective evaluation of analgesic use and risk of renal cell cancer. Arch Intern Med. 2011;171(16):1487–93.
68. Hereditary Kidney Cancer Syndromes (PDQ(R)): Patient Version. PDQ Cancer Information Summaries. Bethesda, MD; 2002.
69. Ng CS, Wood CG, Silverman PM, Tannir NM, Tamboli P, Sandler CM. Renal cell carcinoma: diagnosis, staging, and surveillance. AJR Am J Roentgenol. 2008;191(4):1220–32.
70. Shanks JH. Pathology of renal cell carcinoma: recent developments. Clin Oncol (R Coll Radiol). 1999;11(4):263–8.
71. Bostwick DG, Eble JN. Diagnosis and classification of renal cell carcinoma. Urol Clin North Am. 1999;26(3):627–35.
72. Monda SM, Lui HT, Pratsinis MA, Chandrasekar T, Evans CP, Dall'Era MA. The metastatic risk of renal cell carcinoma by primary tumor size and subtype. Eur Urol Open Sci. 2023;52:137–44.
73. Palapattu GS, Kristo B, Rajfer J. Paraneoplastic syndromes in urologic malignancy: the many faces of renal cell carcinoma. Rev Urol. 2002;4(4):163–70.
74. Sheth S, Scatarige JC, Horton KM, Corl FM, Fishman EK. Current concepts in the diagnosis and management of renal cell carcinoma: role of multidetector CT and three-dimensional CT. Radiographics. 2001;21 Spec No:S237–54.
75. Kim JK, Kim TK, Ahn HJ, Kim CS, Kim KR, Cho KS. Differentiation of subtypes of renal cell carcinoma on helical CT scans. AJR Am J Roentgenol. 2002;178(6):1499–506.

76. Marko J, Craig R, Nguyen A, Udager AM, Wolfman DJ. Chromophobe renal cell carcinoma with radiologic-pathologic correlation. Radiographics. 2021;41(5):1408–19.
77. Hoehn W, Hermanek P. Invasion of veins in renal cell carcinoma—frequency, correlation and prognosis. Eur Urol. 1983;9(5):276–80.
78. Pedrosa I, Cadeddu JA. How we do it: managing the indeterminate renal mass with the MRI clear cell likelihood score. Radiology. 2022;302(2):256–69.
79. Quencer KB, Friedman T, Sheth R, Oklu R. Tumor thrombus: incidence, imaging, prognosis and treatment. Cardiovasc Diagn Ther. 2017;7(Suppl 3):S165–S77.
80. Liu Y. The place of FDG PET/CT in renal cell carcinoma: value and limitations. Front Oncol. 2016;6:201.
81. Farber NJ, Kim CJ, Modi PK, Hon JD, Sadimin ET, Singer EA. Renal cell carcinoma: the search for a reliable biomarker. Transl Cancer Res. 2017;6(3):620–32.
82. Cai PY, Lee RS. Ureteropelvic junction obstruction/hydronephrosis. Urol Clin North Am. 2023;50(3):361–9.
83. Asghar M, Ahmed K, Shah SS, Siddique MK, Dasgupta P, Khan MS. Renal vein thrombosis. Eur J Vasc Endovasc Surg. 2007;34(2):217–23.
84. Lieske JC, Rule AD, Krambeck AE, Williams JC, Bergstralh EJ, Mehta RA, et al. Stone composition as a function of age and sex. Clin J Am Soc Nephrol. 2014;9(12):2141–6.
85. Press SM, Smith AD. Incidence of negative hematuria in patients with acute urinary lithiasis presenting to the emergency room with flank pain. Urology. 1995;45(5):753–7.
86. Fowler KA, Locken JA, Duchesne JH, Williamson MR. US for detecting renal calculi with nonenhanced CT as a reference standard. Radiology. 2002;222(1):109–13.
87. Fulgham PF, Assimos DG, Pearle MS, Preminger GM. Clinical effectiveness protocols for imaging in the management of ureteral calculous disease: AUA technology assessment. J Urol. 2013;189(4):1203–13.
88. Saw KC, McAteer JA, Monga AG, Chua GT, Lingeman JE, Williams JC Jr. Helical CT of urinary calculi: effect of stone composition, stone size, and scan collimation. AJR Am J Roentgenol. 2000;175(2):329–32.
89. Cheng PM, Moin P, Dunn MD, Boswell WD, Duddalwar VA. What the radiologist needs to know about urolithiasis: Part 1—Pathogenesis, types, assessment, and variant anatomy. AJR Am J Roentgenol. 2012;198(6):W540–7.
90. Sayer JA, Carr G, Simmons NL. Nephrocalcinosis: molecular insights into calcium precipitation within the kidney. Clin Sci (Lond). 2004;106(6):549–61.
91. Leder RA, Dunnick NR. Transitional cell carcinoma of the pelvicalices and ureter. AJR Am J Roentgenol. 1990;155(4):713–22.
92. Browne RF, Meehan CP, Colville J, Power R, Torreggiani WC. Transitional cell carcinoma of the upper urinary tract: spectrum of imaging findings. Radiographics. 2005;25(6):1609–27.
93. Vikram R, Sandler CM, Ng CS. Imaging and staging of transitional cell carcinoma: Part 2, Upper urinary tract. AJR Am J Roentgenol. 2009;192(6):1488–93.
94. Foxman B. Urinary tract infection syndromes: occurrence, recurrence, bacteriology, risk factors, and disease burden. Infect Dis Clin N Am. 2014;28(1):1–13.
95. El-Ghar MA, Farg H, Sharaf DE, El-Diasty T. CT and MRI in urinary tract infections: a spectrum of different imaging findings. Medicina (Kaunas). 2021;57(1):32.
96. Taylor BC, Wilt TJ, Fink HA, Lambert LC, Marshall LM, Hoffman AR, et al. Prevalence, severity, and health correlates of lower urinary tract symptoms among older men: the MrOS study. Urology. 2006;68(4):804–9.
97. Pelucchi C, Bosetti C, Negri E, Malvezzi M, La Vecchia C. Mechanisms of disease: the epidemiology of bladder cancer. Nat Clin Pract Urol. 2006;3(6):327–40.
98. Wentland AL, Desser TS, Troxell ML, Kamaya A. Bladder cancer and its mimics: a sonographic pictorial review with CT/MR and histologic correlation. Abdom Radiol (NY). 2019;44(12):3827–42.
99. Vikram R, Sandler CM, Ng CS. Imaging and staging of transitional cell carcinoma: Part 1, Lower urinary tract. AJR Am J Roentgenol. 2009;192(6):1481–7.

100. Panebianco V, Narumi Y, Altun E, Bochner BH, Efstathiou JA, Hafeez S, et al. Multiparametric magnetic resonance imaging for bladder cancer: development of VI-RADS (Vesical Imaging-Reporting And Data System). Eur Urol. 2018;74(3):294–306.
101. Berrocal T, Lopez-Pereira P, Arjonilla A, Gutierrez J. Anomalies of the distal ureter, bladder, and urethra in children: embryologic, radiologic, and pathologic features. Radiographics. 2002;22(5):1139–64.
102. Ramchandani P, Buckler PM. Imaging of genitourinary trauma. AJR Am J Roentgenol. 2009;192(6):1514–23.
103. Gomez RG, Ceballos L, Coburn M, Corriere JN Jr, Dixon CM, Lobel B, et al. Consensus statement on bladder injuries. BJU Int. 2004;94(1):27–32.
104. Brandes S, Borrelli J Jr. Pelvic fracture and associated urologic injuries. World J Surg. 2001;25(12):1578–87.
105. Lumen N, Kuehhas FE, Djakovic N, Kitrey ND, Serafetinidis E, Sharma DM, et al. Review of the current management of lower urinary tract injuries by the EAU Trauma Guidelines Panel. Eur Urol. 2015;67(5):925–9.
106. Morey AF, Brandes S, Dugi DD III, Armstrong JH, Breyer BN, Broghammer JA, et al. Urotrauma: AUA guideline. J Urol. 2014;192(2):327–35.
107. Koraitim MM. Pelvic fracture urethral injuries: evaluation of various methods of management. J Urol. 1996;156(4):1288–91.
108. Bjurlin MA, Fantus RJ, Mellett MM, Goble SM. Genitourinary injuries in pelvic fracture morbidity and mortality using the National Trauma Data Bank. J Trauma. 2009;67(5):1033–9.
109. Goldman SM, Sandler CM, Corriere JN Jr, McGuire EJ. Blunt urethral trauma: a unified, anatomical mechanical classification. J Urol. 1997;157(1):85–9.
110. Ingram MD, Watson SG, Skippage PL, Patel U. Urethral injuries after pelvic trauma: evaluation with urethrography. Radiographics. 2008;28(6):1631–43.
111. Foley CL, Greenwell TJ, Gardiner RA. Urethral diverticula in females. BJU Int. 2011;108(Suppl 2):20–3.
112. Burrows LJ, Howden NL, Meyn L, Weber AM. Surgical procedures for urethral diverticula in women in the United States, 1979–1997. Int Urogynecol J Pelvic Floor Dysfunct. 2005;16(2):158–61.
113. Martensson O, Duchek M. Translabial ultrasonography with pulsed colour-Doppler in the diagnosis of female urethral diverticula. Scand J Urol Nephrol. 1994;28(1):101–4.
114. Kadian YS, Rattan KN, Singh M, Kajal P. Congenital anterior urethral diverticulum in children: a case report and review. ISRN Surg. 2011;2011:120307.
115. Alphs HH, Meeks JJ, Casey JT, Gonzalez CM. Surgical reconstruction of the male urethral diverticulum. Urology. 2010;76(2):471–5.
116. Romanzi LJ, Groutz A, Blaivas JG. Urethral diverticulum in women: diverse presentations resulting in diagnostic delay and mismanagement. J Urol. 2000;164(2):428–33.
117. Morton HC, Hilton P. Urethral injury associated with minimally invasive mid-urethral sling procedures for the treatment of stress urinary incontinence: a case series and systematic literature search. BJOG. 2009;116(8):1120–6.
118. Kawashima A, Sandler CM, Wasserman NF, LeRoy AJ, King BF Jr, Goldman SM. Imaging of urethral disease: a pictorial review. Radiographics. 2004;24(Suppl 1):S195–216.

Gastric Disorders

8

Tara Catanzano

Gastric Anatomy

- The stomach is a muscular organ and is composed of the mucosa, submucosa, muscularis, and serosal surfaces.
- The stomach is divided into gastric fundus, body, antrum, and pylorus (schematic Figs. 8.1, 8.2, 8.3, and 8.4).
- Shares fascial planes with
  - Spleen (gastrosplenic and splenorenal ligaments) (see Fig. e8.1).
  - Transverse colon (transverse mesocolon) (see Fig. e8.2).
  - Liver (gastrohepatic ligaments) (see Fig. e8.3).
- Posterior to the stomach is the foramen of Winslow and the lesser sac; anterior to the stomach is the greater omentum (Figs. 8.5, 8.6, and 8.7).

Optimal Studies for Gastric Imaging

Assessment of Catheter Positioning

- Appropriate positioning of gastric tubes—oro- or nasogastric tube; gastrostomy (G tube); and gastrojejunal (G-J) tube—are essential for both proper function and patient safety.
- Therefore, radiologists must be aware of the expected locations of these devices, as well as signs of malpositioning and dysfunction.

Supplementary Information The online version contains supplementary material available at https://doi.org/10.1007/978-3-031-76624-4_8.

T. Catanzano (✉)
Department of Radiology, UMass Chan-Baystate, Springfield, MA, USA
e-mail: Tara.catanzano@bhs.org

© The Author(s), under exclusive license to Springer Nature Switzerland AG 2024

T. Catanzano (ed.), *What Radiology Residents Need to Know: Abdominal Radiology*, What Radiology Residents Need to Know,
https://doi.org/10.1007/978-3-031-76624-4_8

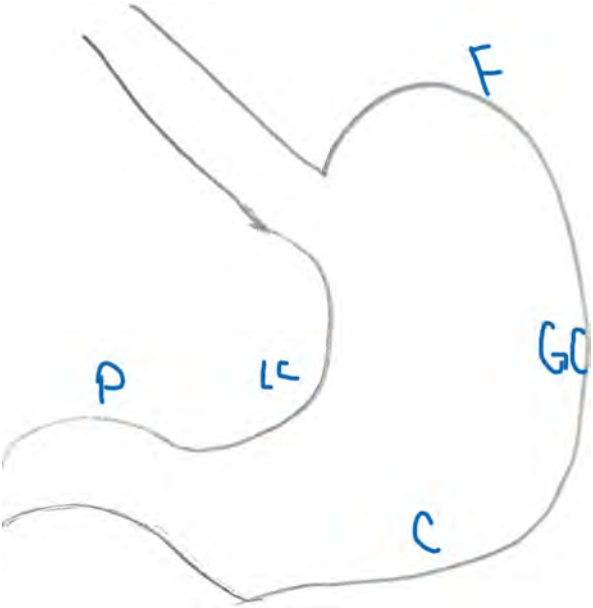

Fig. 8.1 Schematic of the stomach. *F* fundus, *GC* greater curve, *C* cardia, *LC* lesser curve, *P* pylrous

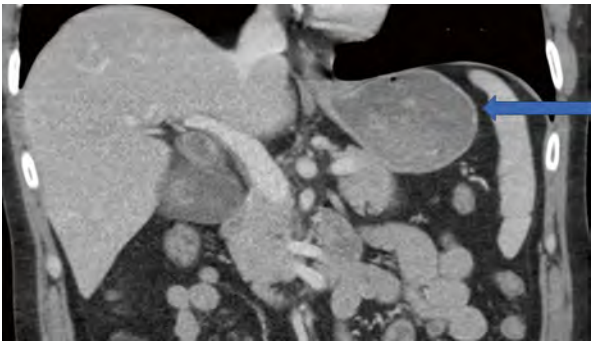

Fig. 8.2 Coronal contrast enhanced CT demonstrating a normal gastric fundus (arrow)

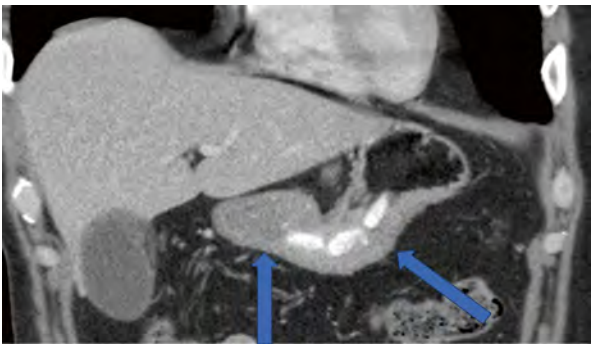

Fig. 8.3 Coronal contrast enhanced CT demonstrating a normal gastric body (right arrow) and antrum (left arrow)

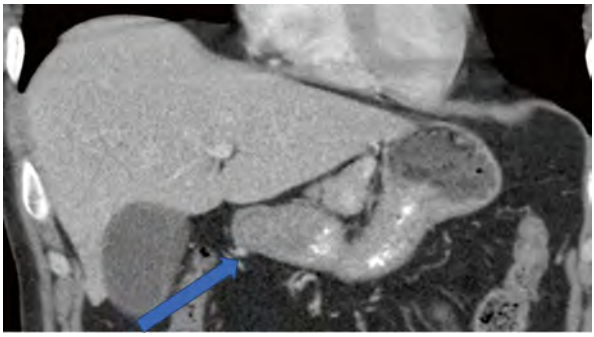

Fig. 8.4 Coronal contrast enhanced CT demonstrating a normal pyloric region

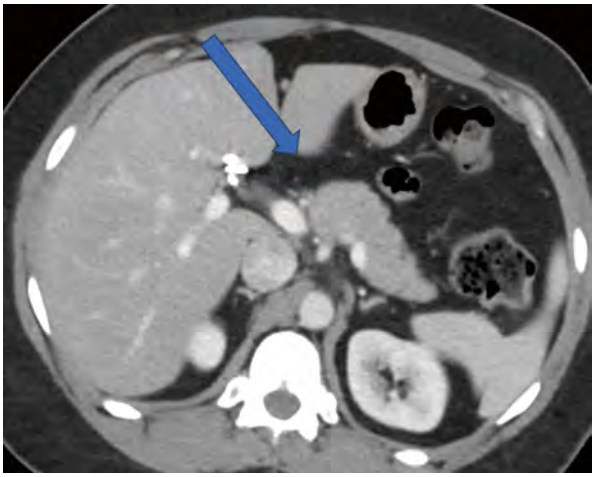

Fig. 8.5 Axial contrast enhanced CT demonstrating the foramen of Winslow (arrow)

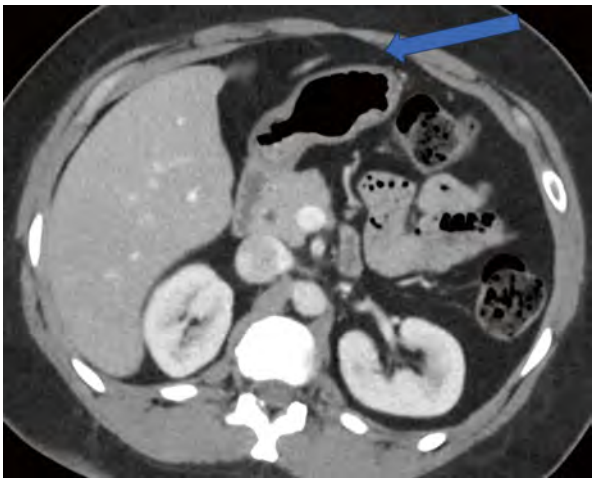

Fig. 8.6 Axial contrast enhanced CT demonstrating the location of the greater omentum (arrow)

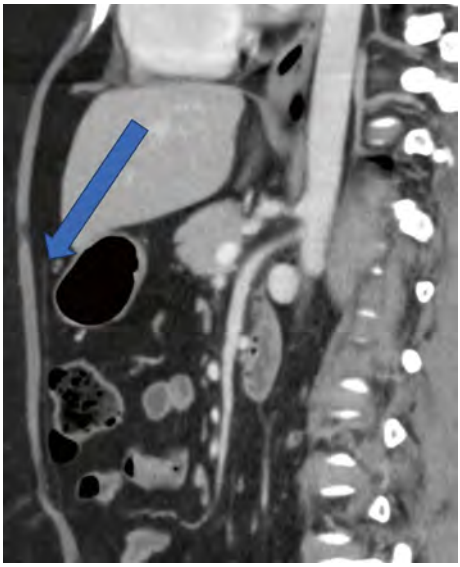

Fig. 8.7 Sagittal image demonstrating the location of the greater omentum anterior to the stomach (arrow)

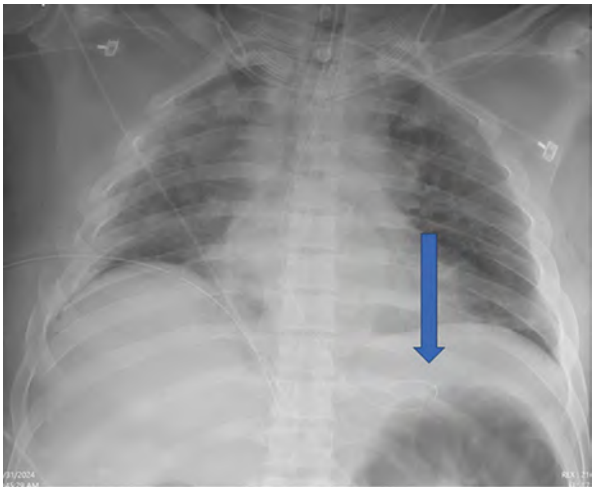

Fig. 8.8 Frontal chest xray demonstrating an appropriately positioned enteric tube with the tip and sideport below the left diaphragm in the stomach (arrow). Note the apparent "break" in the line representing the sidehole

Enteric Tube

Correct Position

- An enteric tube should terminate in the stomach, with the sideport (if present), also below the diaphragm and within the stomach (Fig. 8.8): tip and sideport should be below the left hemidiaphragm (Fig. e8.4).

- The sideport can be recognized by a short "break" in the radiodense line of the tube (Fig. 8.8). A chest X-ray centered low on the chest and upper abdomen or a KUB (frontal view of the abdomen) are the study of choice to assess positioning.
- Highest confidence if the stomach is air-filled and tip can be seen in the region of gastric body.

Abnormal Positions

- Malpositioned enteric tubes may be coiled in the pharynx (with no catheter seen on a well-centered film), the airway, or the esophagus (Figs. 8.9, 8.10, and 8.11).
- Complications vary depending upon the location of the malpositioned line and include airway compromise, pneumonitis (if the catheter is used for feeding without confirmation of positioning), and esophageal reflux with the potential for aspiration pneumonitis/pneumonia.
- Catheters may be difficult to advance beyond a hiatal hernia, which can increase the risk of reflux or perforation.
- Tube positioning may be confirmed by injecting contrast under fluoroscopic guidance, although this is rarely necessary.
- More commonly, fluoroscopy is used to guide placement of an enteric tube if it cannot be successfully placed at the bedside, most commonly a result of anatomic or surgical anomalies such as a hiatal hernia or fundoplication.

Fig. 8.9 Frontal chest X-ray of a malpositioned enteric tube which is coiled in the upper esophagus with the tip directed cranially (arrow)

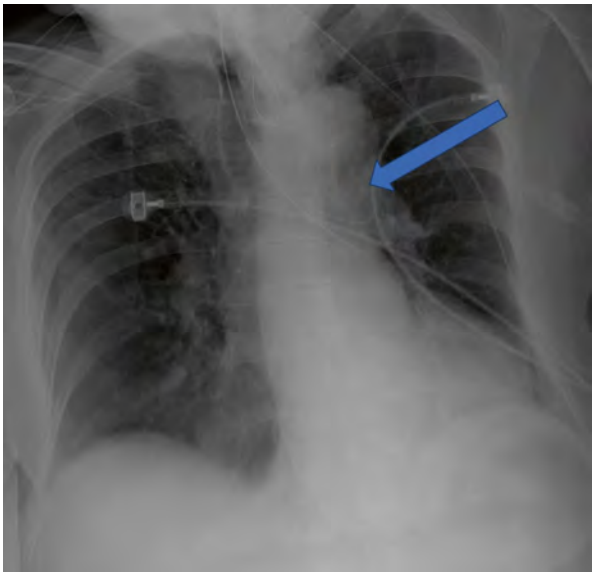

Fig. 8.10 Frontal chest X-ray demonstrating a malpositioned enteric tube with the tip in the left mainstem bronchus (arrow)

Fig. 8.11 Frontal chest X-ray demonstrating a malpositioned enteric tube which enters the right mainstem bronchus, coils, then crosses the carina to enter the left mainstem bronchus (arrow)

Gastrostomy Tube

- The most common complications of a G-tube are dislodgement and malpositioning outside of the gastric lumen.
- Occasionally, low position of a gastric tube or balloon overinflation can cause a functional gastric outlet obstruction (Fig. 8.12).
- Radiographs play a limited role in assessing G-tube positioning as the precise location is difficult to ascertain and extraluminal positioning cannot be easily assessed even after contrast material is injected through the catheter at the time of X-ray acquisition.
- Many institutions have moved to obtaining both frontal and lateral images of the abdomen following G-tube injection to improve the detection of extraluminal positioning, although there is still limited ability to detect subtle extraluminal contrast extravasation (Figs. 8.13 and 8.14).
- When only a frontal view is obtained, the radiologist must rely on the location and morphology of the contrast to determine if it is within or external to the stomach; once rugal folds are visible, luminal positioning can be confirmed (Fig. 8.15).
- Gastrostomy tube positioning can be confirmed by injection of contrast under intermittent fluoroscopy.

Fig. 8.12 Frontal fluoroscopic image demonstrating injection of a G-J tube. Note the low positioning of the gastric balloon near the gastric antrum (arrow)

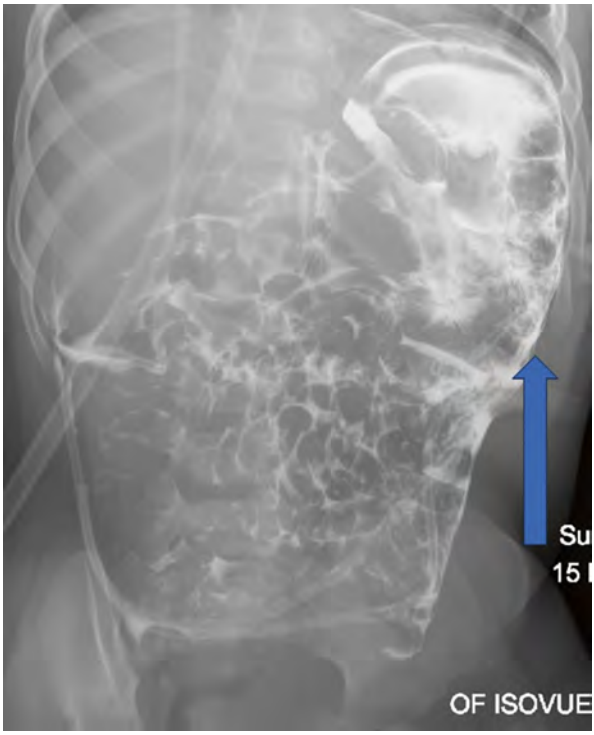

Fig. 8.13 Frontal view of an abdomen following injection of a gastrostomy tube. Note that that position of the tube is obscured on this single view which demonstrates contrast extravasation into the peritoneum (arrow) indicating extraluminal G-tube positioning

Fig. 8.14 Frontal view of an abdomen following injection of a gastrostomy tube in the same patient as Fig. 8.13. Note the contrast collecting in the subdiaphragmatic space (arrow)

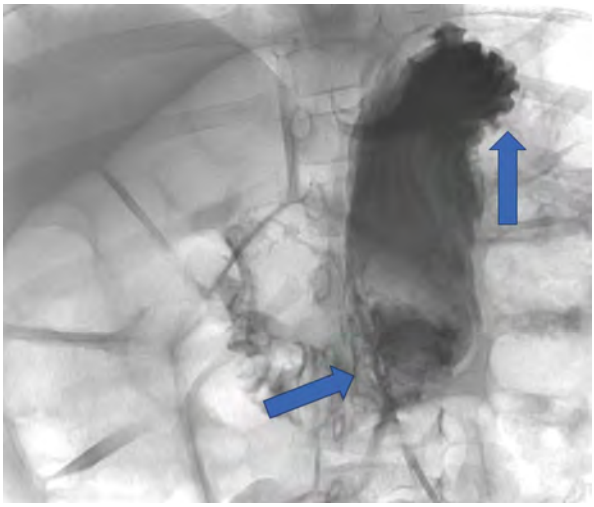

Fig. 8.15 Frontal fluoroscopic view from a G-tube injection confirming intraluminal positioning of the catheter. Note the contrast outlining rugal folds (arrow), confirming intraluminal positioning

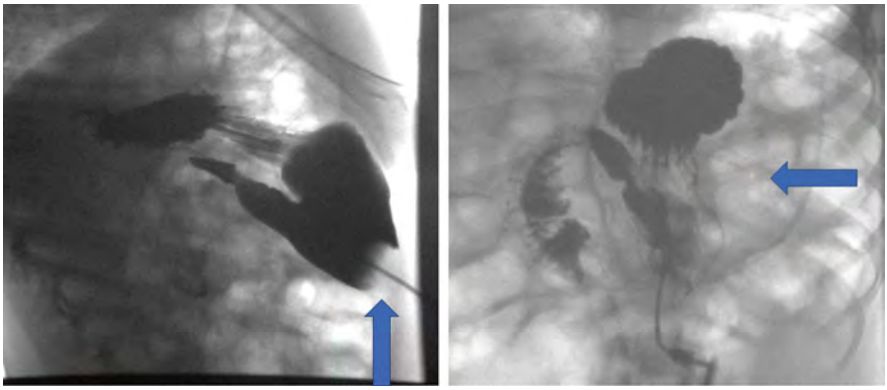

Fig. 8.16 Images taken from a fluoroscopic G-tube injection. The left image is obtained in the lateral position. Note the balloon outlined by injected contrast (arrow). Frontal supine positioning (right image) demonstrates rugal folds (arrow), confirming intraluminal positioning

- Contrast should be seen around the catheter and outline rugal folds (Fig. e8.5).
- Extraluminal leakage of contrast in different positions must be carefully assessed (Fig. 8.16 and e8.6).
- Grossly malpositioned tube will be seen directly outside of the gastric lumen (Fig. 8.17).
- Less displaced or undersized G tubes identified by leakage of the injected contrast (Fig. 8.18).

Gastrojejunostomy Tube

Correct Position

- The gastrostomy tube and balloon should be within the region of the gastric body/antrum (see Fig. e8.7).

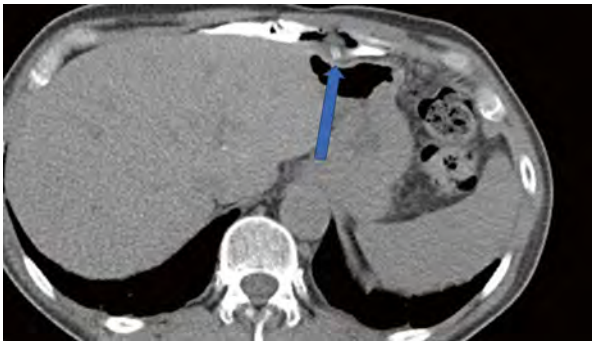

Fig. 8.17 Axial CT without intravenous contrast and with enteric contrast injected through a G-tube. Not the balloon of the g-tube is outside of the gastric wall (arrow) and injected contrast freely spills into the peritoneum in this malpositioned tube

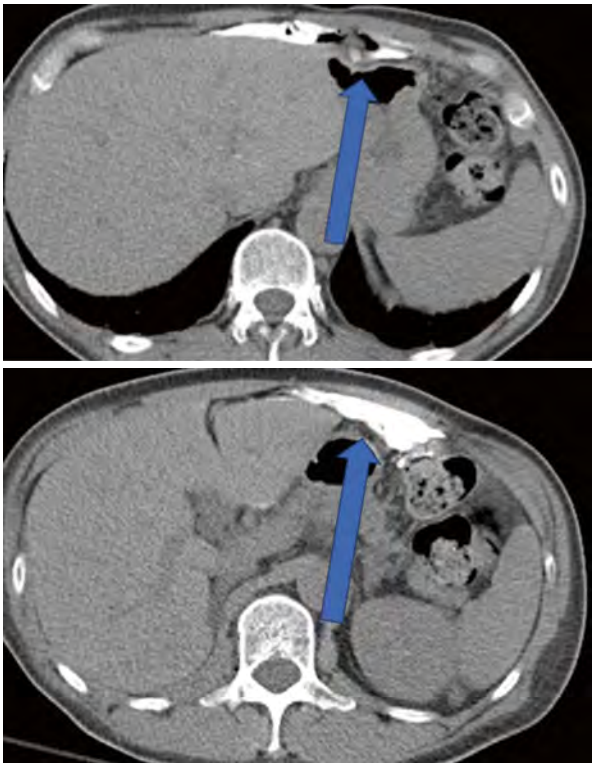

Fig. 8.18 Axial CT image without intravenous contrast and with enteric contrast injected through a G-tube demonstrating free contrast spill into the periteonum (arrow)

- The jejunostomy component should have the tip in the left abdomen, beyond the expected location of the duodenal-jejunal junction (Fig. 8.19).

Abnormal Positions

- Difficult to accurately assess on radiographs unless the entire tube is within the stomach (Fig. 8.20).
- Contrast injected through the catheter may more accurately depict positioning, particularly for the jejunal component (unless confirmed by opacification of a jejunal loop; Fig. e8.8).

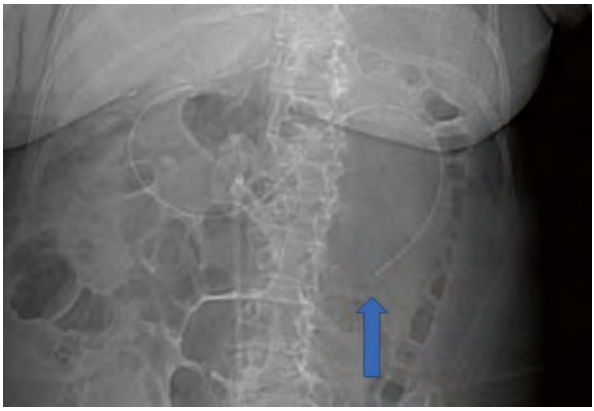

Fig. 8.19 Frontal view of the abdomen demonstrating a normally positioned gastro-jejunostomy tube. Note the tip of the jejunal component in the left upper quadrant (arrow)

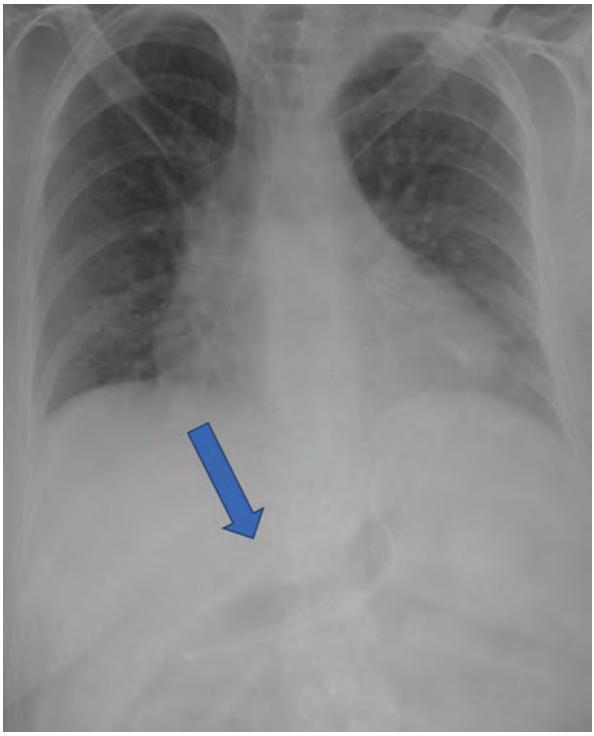

Fig. 8.20 Frontal view of the chest demonstrating a clearly malpositioned G-J tube with the entire catheter looped in the stomach (arrow)

Gastric Diverticula

- Outpouchings from the stomach that contain all parts of the gastric wall.
- Characteristically communicate with the lumen and are most commonly found arising from the gastric fundus posteriorly.
- When contrast filled, they are easy to diagnose; however, can mimic other processes, such as malignant gastrointestinal stromal tumors (GIST), when collapsed.
- Necrotic GIST tumors may also communicate with the lumen, but this tumor is typically large and mostly exophytic with a substantial heterogeneously enhancing, soft-tissue component. A diverticulum should have a very thin wall, without significant solid components.

Imaging

- Fluoroscopy
  - Fills with administered barium, but not visible prior to enteric contrast administration.
  - Due to the characteristic posterior location, oblique or lateral positioning is required to visualize the diverticulum.
- CT
  - Non-distended, gastric diverticula may mimic a mass such as a GIST tumor (Fig. e8.9), lymph node, accessory spleen, or peritoneal implant.
  - Lesion location and clear communication with the gastric lumen in the absence of a mass-like component are the key to diagnosis (Fig. 8.21). See Fig. e8.9. Supplemental information.

Gastritis/Emphysematous Gastritis

- Causes include caustic ingestion, early ulcer disease, infiltrative diseases such as Menetrier's, *H. pylori*, or other bacterial infection.
- Imaging findings of inflammation are nonspecific.
- Mucosal lesions may be below the resolution of imaging, and endoscopy may be required for diagnosis.
- Emphysematous gastritis typically results from an ischemic event, often related to hypotension or an embolic event, and demonstrates a characteristic appearance due to gas formation within the gastric wall.
- This condition typically arises from ischemic states and may be the result of systemic hypotension or embolic events.

Imaging

- Radiographs
  - Gastric wall thickening may be apparent on radiographs, though it often is subtle (Fig. 8.22).

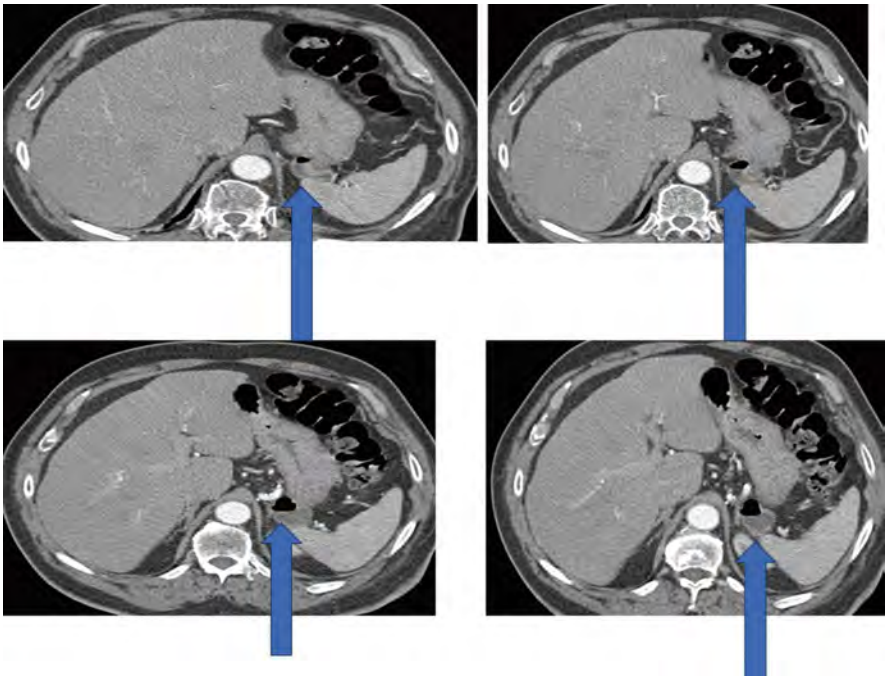

Fig. 8.21 Axial contrast enhanced CT demonstrating an air and fluid containing structure arising from the postero-superior gastric fundus and communicating with the lumen (arrow). This is a classic appearance for a gastric diverticulum

  - Not apparent until the inflammation/infection becomes transmural and causes wall thickening.
  - Wall thickening is best appreciated when there is air within the stomach, and the stomach is slightly displaced away from the spleen.
  - Emphysematous gastritis is characterized by round or linear foci of air outlining the stomach (Fig. 8.23).
  - Air within the submucosa or wall of the stomach can be difficult to distinguish from intraluminal air.
- Fluoroscopy
  - Gastritis related to peptic ulcer disease presents a spectrum of findings, ranging from early mucosal erosions to frank ulceration and potential perforation.
  - Erosions are often subtle and best seen with double-contrast upper GI technique (barium to coat the stomach and an effervescent agent to provide mucosal relief).
  - Fluoroscopy has no role in the evaluation of emphysematous gastritis.
- Computed tomography
  - Limited role in the evaluation of gastritis since the mucosal surface of the stomach is below the resolution of CT, and the stomach is often not distended on routine CT imaging.

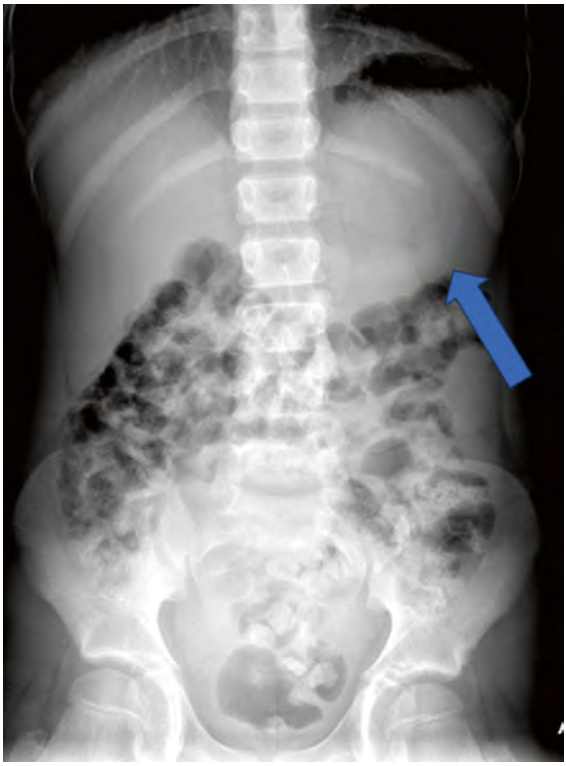

Fig. 8.22 Frontal radiograph of the abdomen demonstrating very subtle gastric wall thickening (arrow), which is difficult to detect on radiographs

- As gastritis progresses to involve the wall, there is resultant wall thickening (Fig. 8.24), and often adjacent fat stranding.
- Overcalling gastric wall thickening when it is absent is more common than recognizing it when present due to underdistension of the muscular gastric wall. Emphysematous gastritis is more readily recognized as foci of air within the gastric wall (Fig. 8.25).
- Air may also track into the short gastric veins draining the stomach (Fig. e8.10).

Trauma

- Gastric trauma is relatively uncommon, with the majority arising iatrogenically as a result of endoscopy, endoscopic biopsy, or rarely chronic enteric catheter placement. Less commonly a result of direct trauma; even more uncommonly may arise from blunt abdominal trauma.
- May also be injured during gastrostomy/gastrojejunostomy placement with findings often related to leakage of air and fluid/gastric contents from the stomach into the surrounding structures and tissue planes.

An important pearl is that free abdominal air confined to the upper abdomen is most often the result of proximal bowel (gastric/duodenal) perforation.

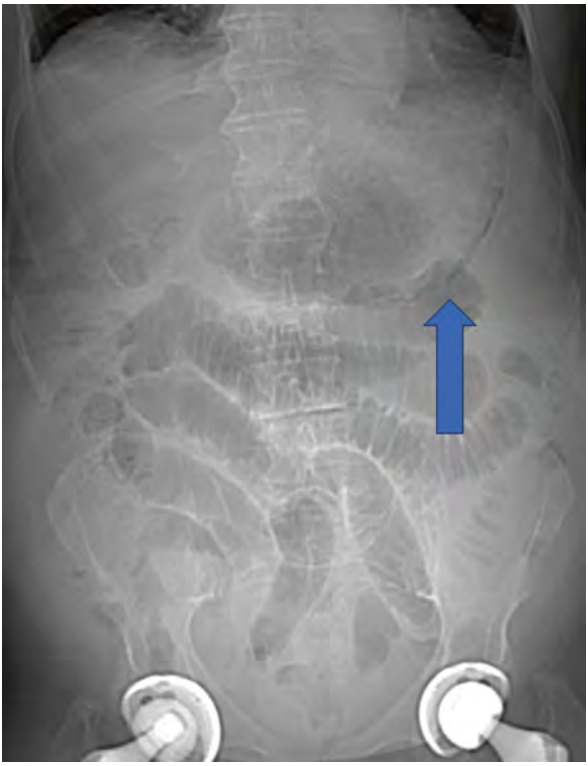

Fig. 8.23 Frontal radiograph of the abdomen demonstrating air within the gastric wall (arrow) consistent with emphysematous gastritis

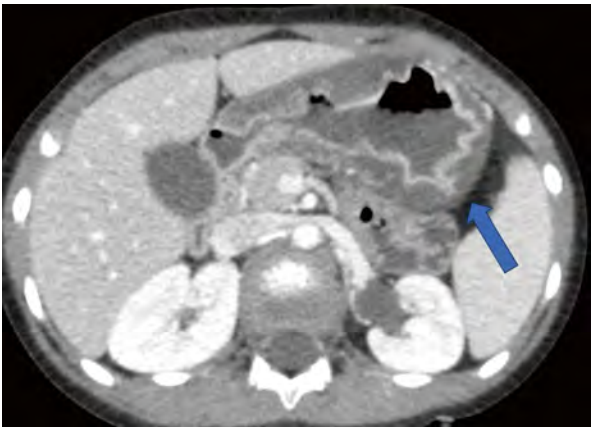

Fig. 8.24 Axial contrast enhanced CT of the stomach demonstrates diffuse wall thickening and edema within the wall (arrow) in a patient with advanced gastritis

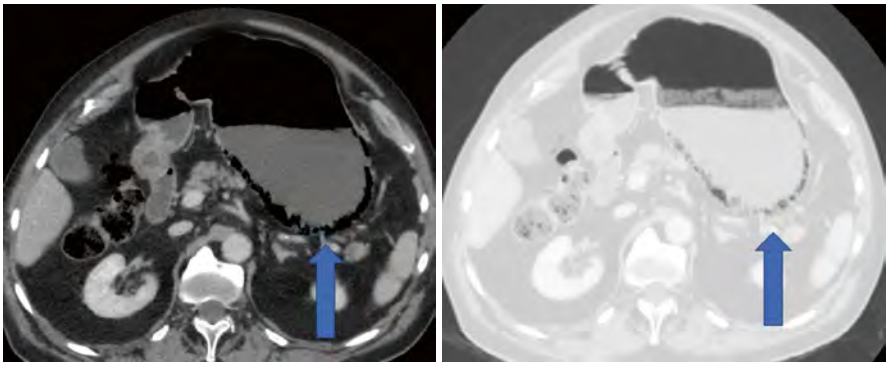

Fig. 8.25 Axial contrast enhanced CT images in a body window (left) and lung window (right) demonstrating air within the gastric wall (arrows) in a patient with emphysematous gastritis

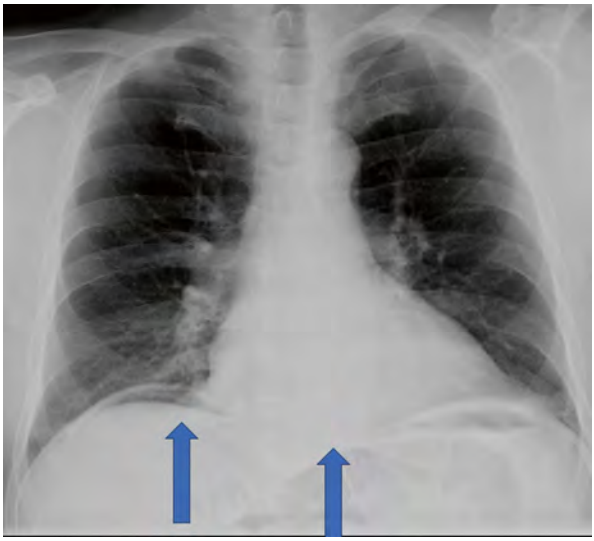

Fig. 8.26 Frontal radiograph of the chest demonstrating the continuous diaphragm sign. Note the lucencies beneath the diaphragms consistent with free intraperitoneal air (left arrow). The left and right diaphragm appears continuous (right arrow)

Imaging

- Radiographs
  - In frank gastric perforation, pneumoperitoneum may be seen.
  - The *continuous diaphragm sign*, *football sign*, and *air surrounding the liver* can all be signs of free air.
  - The *continuous diaphragm sign* is seen on an erect chest radiograph where it appears that both the right and left hemidiaphragms are connected as one (Fig. 8.26).
  - The *football sign* is seen on a supine radiograph where there is a football-shaped air collection, often in the midline of the abdomen, which represents the collection of the extraluminal air (Fig. 8.27).

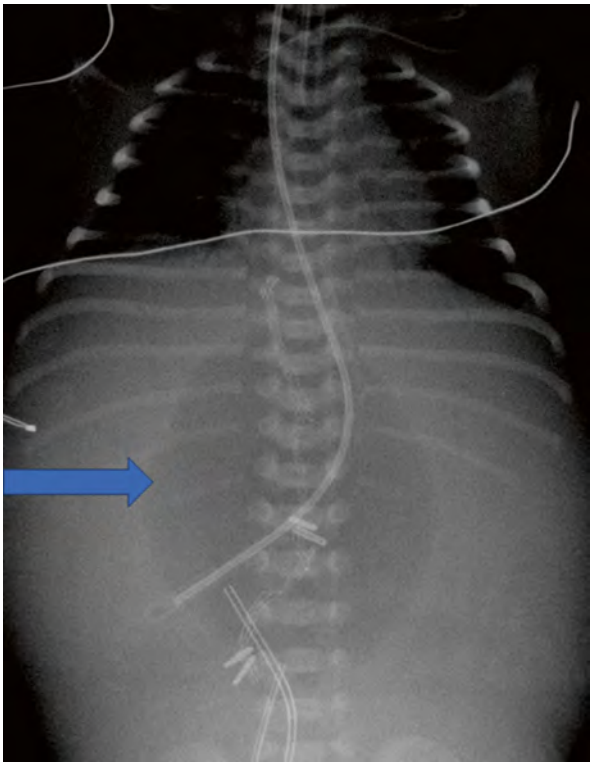

Fig. 8.27 Frontal view of the abdomen in a pediatric patient demonstrating the football sign of free air (arrow). Note how the free intraperitoneal air accumulates in the central abdomen and is shaped like an American football

  - *Rigler's sign* (air outlining the bowel wall) is less likely to be seen in gastric perforation given the expected location of air in the upper abdomen in an upper GI perforation (Fig. 8.28).
  - One pearl to be aware of is that patients must be positioned appropriately (erect for the continuous diaphragm sign, supine for the football sign, and right side up decubitus position) for several minutes prior to obtaining a film to allow enough air to move into a visible location.
- Fluoroscopy
  - Limited role in the evaluation of gastric trauma.
  - Extravasation of water-soluble contrast material confirms the diagnosis of perforation. Barium is not used if there is concern for a perforation.
- Computed tomography
  - *Indirect* signs include perigastric stranding/fluid and/or free air (Fig. e8.11).
  - *Direct* evidence of gastric perforation is less frequently seen than indirect indicators of perforation.
  - Enteric contrast extravasation from the stomach is clear evidence of a perforation (Fig. 8.29; see Fig. e8.12).
  - The location of the perforation is dependent upon the cause; for example, gastric ulcers tend to perforate anteriorly in the distal stomach.

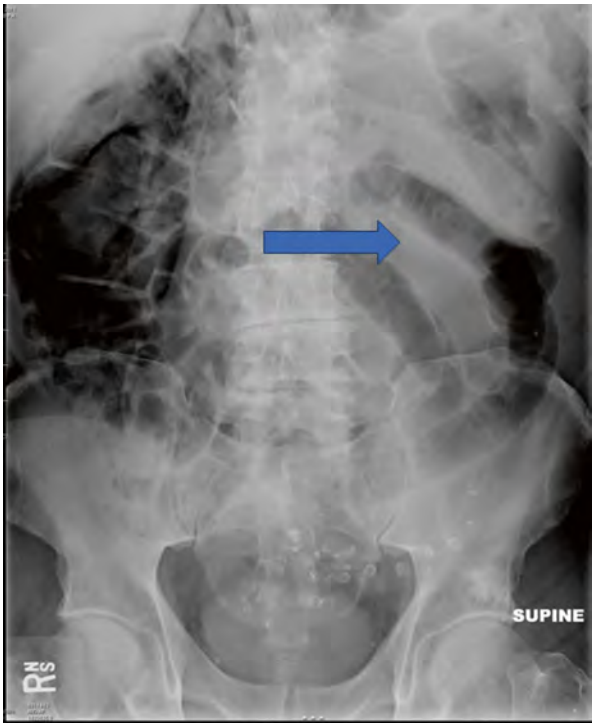

Fig. 8.28 Frontal view of the abdomen demonstrating Rigler's sign (arrow) of free intraperitoneal air. Note how both the inner and outer walls of the bowl are visible due to outlining by air within and outside of the lumen due to the pneumoperitoneum

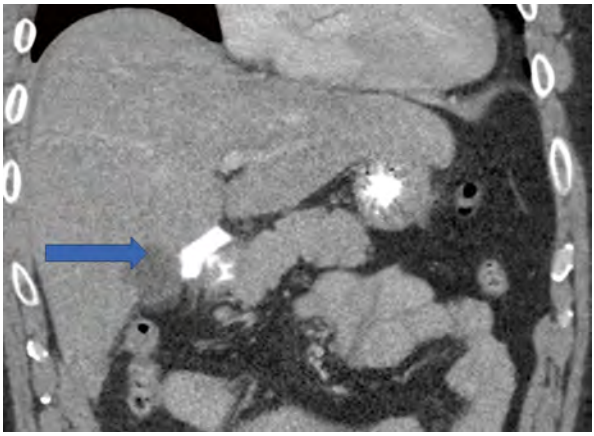

Fig. 8.29 Coronal contrast enhanced CT with oral and intravenous contrast. Contrast extravasates through a perforated gastric ulcer to enter the subhepatic space (arrow)

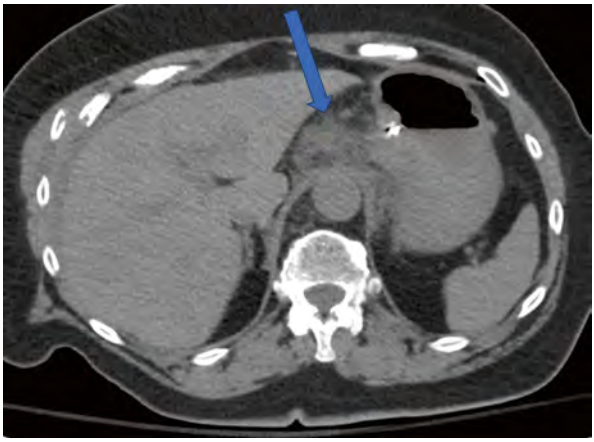

Fig. 8.30 Axial noncontrast CT demonstrates stranding in the perigastric fat (arrow) in this patient with trauma, indicating a gastric injury

- In blunt trauma, injury is often more subtle and may appear as stranding or fluid in the perigastric fat or as a vascular blush from vascular injury (Fig. 8.30).

Volvulus

- Gastric volvulus results from malpositioning of the stomach, typically within a hiatal hernia sac.
- Malpositioning in and of itself does not indicate a volvulus, it is a predisposing risk factor.
- Organoaxial volvulus—the stomach twists along its long axis while the gastroesophageal junction and pylorus remain normally positioned (Fig. 8.31).
- Mesenteroaxial volvulus—the stomach flips along its short axis such that the body sits above the level of the gastric fundus (Fig. 8.32).

Imaging

- Radiographs
  - Useful for findings suggesting gastric outlet obstruction; such as a fluid or air distended, dilated stomach with disproportionate lack of air within distal bowel loops (Fig. 8.33).
  - If the gastric wall has become ischemic from the vascular compromise, pneumatosis within the wall may be visible and there is often thinning of the wall.
  - The type of volvulus is difficult to ascertain on radiographs alone and typically requires additional fluoroscopic or CT imaging.
- Fluoroscopy
  - Single-contrast upper GI examination may be diagnostic, assuming that a sufficient amount of enteric contrast can be administered to opacity the stomach adequately.
  - For organoaxial volvulus, the stomach will be rotated along its long axis.

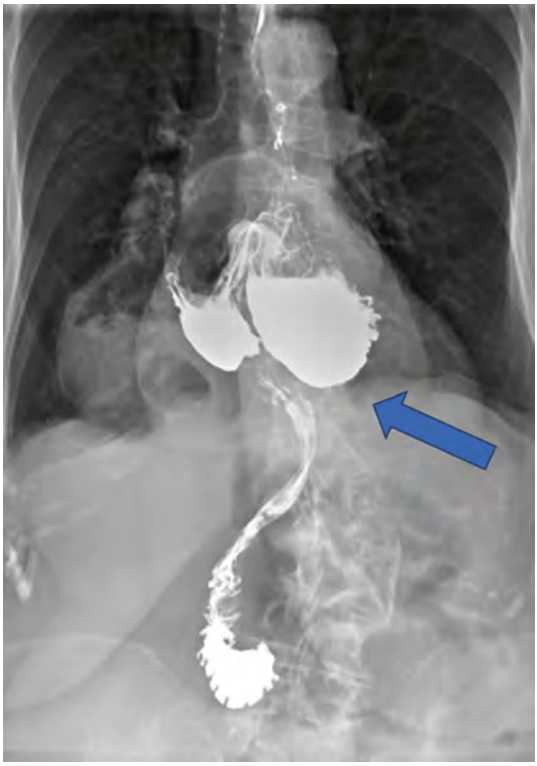

Fig. 8.31 Frontal image from an upper GI examination demonstrating the gastric fundus below the body

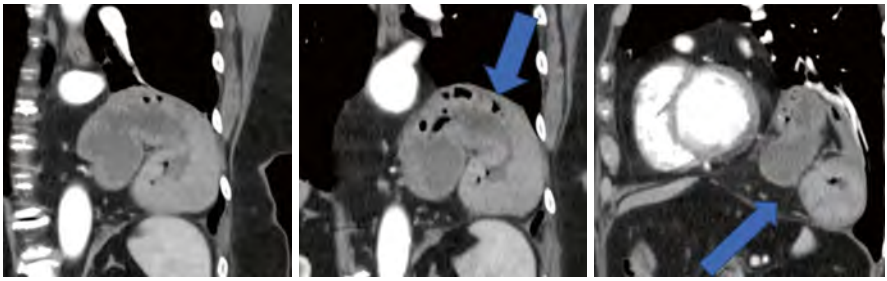

Fig. 8.32 Sagittal contrast enhanced CT images demonstrate a mesenteroaxial volvulus with the body above the level of the gastric fundus (arrows)

  - Atlantoaxial volvulus, the stomach will be inverted with the body above the level of the fundus (Fig. e8.13).
- Computed tomography
  - Rapid diagnostic test.
  - Enteric contrast, while helpful, is not essential given that the stomach is typically fluid filled due to the outlet obstruction.
  - Diagnosis may be difficult, particularly if the stomach is completely obstructed and the wall is thinned.

Fig. 8.33 Frontal chest radiograph demonstrating the dilated stomach within a large hiatal hernia sack (arrow) in this patient with a gastric obstruction due to a gastric volvulus

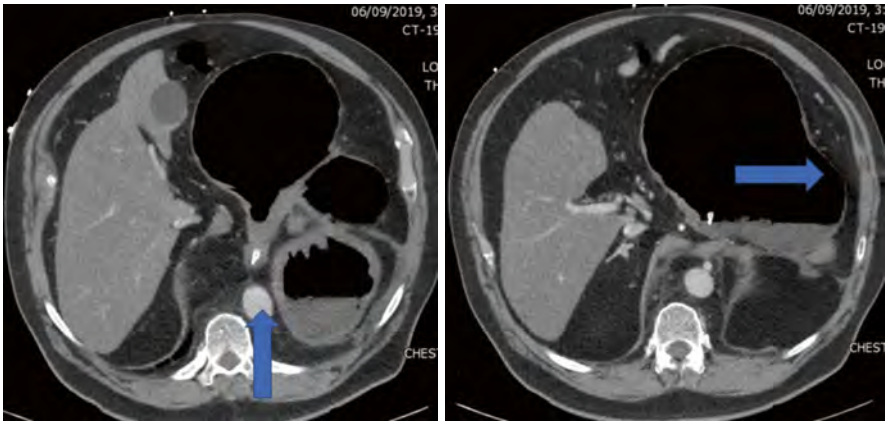

Fig. 8.34 Axial CT images in a patient with a gastric volvulus (left arrow) demonstrating gastric wall thinning (right arrow), which is a sign of gastric wall ischemia

- If there is gastric wall ischemic, there may be gastric wall thinning (Fig. 8.34), pneumatosis, and air in gastric and portal veins (Fig. 8.35).
- Complete or near-complete gastric outlet obstruction, particularly if the stomach is contained within a hiatal hernia suggests the diagnosis.
- Malpositioning of the gastric components as noted above confirms the diagnosis.

Ulcer Disease

- Gastric ulcers can result from *Helicobacter pylori* infection, stress response, medication, and chronic trauma.

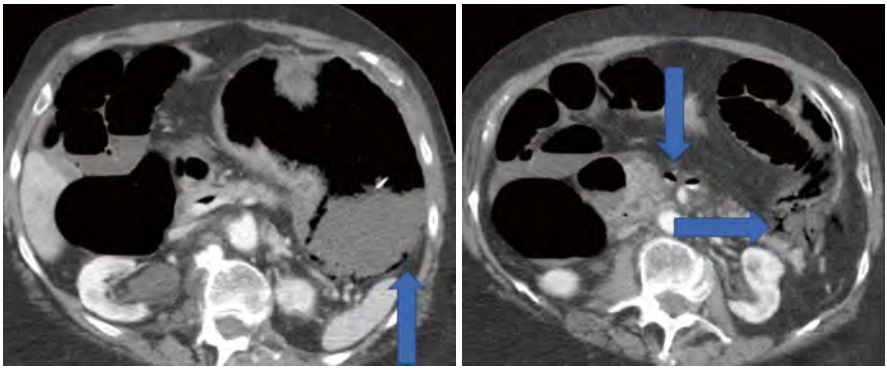

Fig. 8.35 Axial contrast enhanced CT demonstrating gastric wall pneumatosis (left arrow) and air in the gastric and portal veins (right arrows) in this patient with gastric ischemia

- Ulcerated benign and malignant neoplasms may also be considered as a source of ulcer disease as the clinical presentation may be similar.
- Spectrum from superficial mucosal ulceration to involvement of the mucosa, with extension into the muscular wall.
- Full thickness involvement potentially resulting in perforation through the wall and serosa into the peritoneum can occur.

Imaging

- Radiographs
  - Limited value unless perforation has occurred.
  - In ulcer perforation, free air may be detected, often on an upright chest radiograph (Fig. 8.36).
  - Decubitus views of the abdomen may be necessary to confirm small amounts of pneumoperitoneum (Fig. 8.37).
- Fluoroscopy
  - Double-contrast technique (barium and effervescent agent) is optimal since erosions may be subtle and difficult to detect.
  - Erosions appear as filling defects in the contrast column, best seen when contrast is flowing across the mucosa.
  - As erosions progress into ulcers, the crater becomes deeper and may fill with contrast when dependent.
  - An ulcer will appear as a filling defect when in mucosal relief.
  - It is important to differentiate benign from malignant ulcers.
  - Features of benign ulcers are:

    Location along the lesser curve, often in the body/antrum.
    Outpouching of the ulcer crater beyond the gastric wall.
    Smooth, round, deep crater.
    Smooth ulcer mound and smooth gastric folds radiating to the crater.
    Hampton's line—thin, lucent line at collar of ulcer.

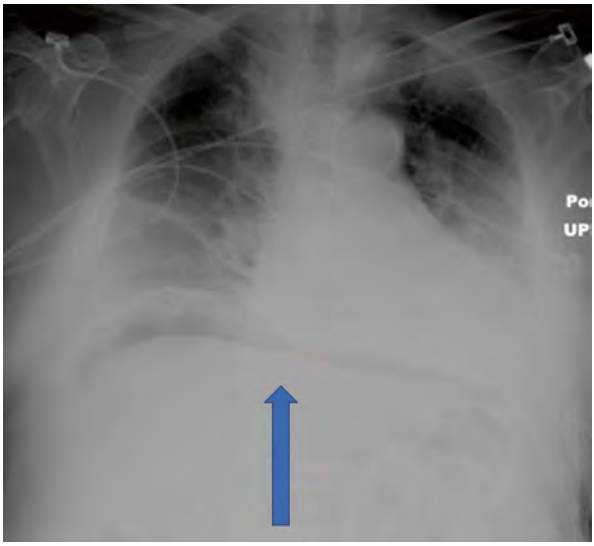

Fig. 8.36 Frontal chest radiograph demonstrating free intraperitoneal air (arrow) in a patient with ulcer perforation

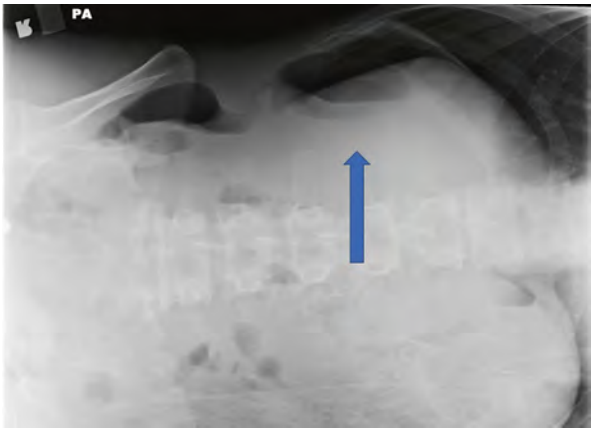

Fig. 8.37 Decubitus view of the abdomen demonstrating free intraperitoneal air rising over the liver (arrow)

- Features of malignant ulcers are:
  Location along the greater curve.
  No protrusion beyond gastric wall.
  Irregular, shallow crater.
  Irregular, nodular mound with gastric folds that do not reach the ulcer margin.
  Carman meniscus sign—lenticular barium collection with the inner margin convex toward the lumen.

- Computed tomography
  - Good gastric distension with positive (barium or non-ionic contrast) or negative (water or Volumen) contrast agents is required.

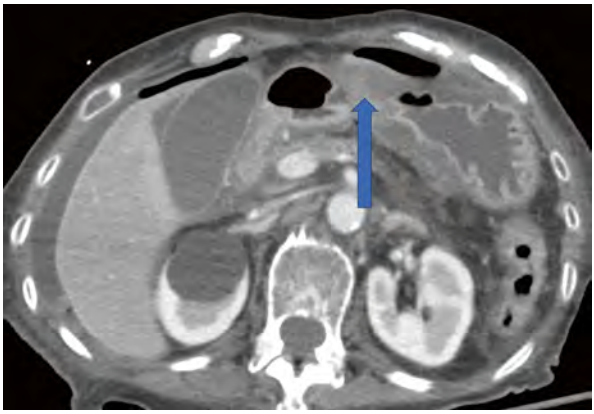

Fig. 8.38 Axial contrast enhanced CT demonstrating free fluid and pneumoperitoneum (arrow) adjacent to the stomach in this patient with a perforated gastric ulcer

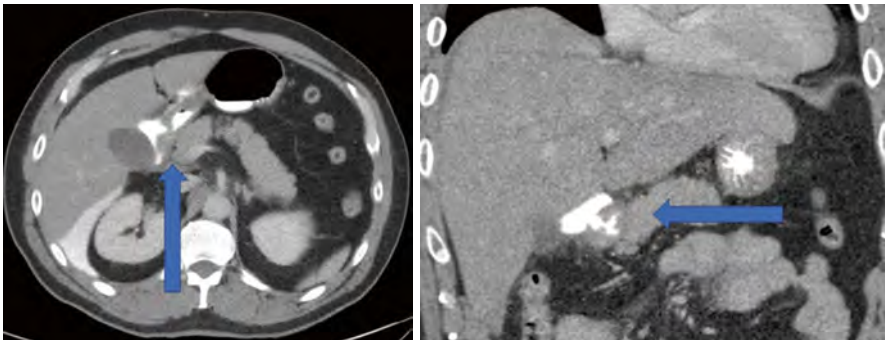

Fig. 8.39 Axial contrast enhanced CT demonstrating free spill of enteric contrast from a perforated gastric ulcer (arrows). In the right image, the ulcer crater is directly visualized spilling enteric contrast

- Some institutions will administer an effervescent agent immediately before scan acquisition to improve gastric distension.
- Superficial ulcerations are below the resolution of CT.
- Enteric contrast may be seen to extend into the ulcer crater, often a subtle finding.
- Indirect findings of perforation include perigastric fat stranding/fluid and pneumoperitoneum may become apparent (Fig. 8.38).
- Perforation is confirmed if oral contrast extravasates (Fig. 8.39).
- Look carefully for an associated mass as malignant ulcers and ulcerated masses may be mistaken for benign ulcer.

Gastric Surgery

- Gastric surgery may be performed for a variety of indications, including trauma, ulcer disease, oncological conditions, and elective.
- Elective indications are most commonly related to weight loss procedures and will be the focus of this section.

Gastric (Lap) Band

- Gastric bands are devices that are placed around the gastroesophageal fundus to regulate the amount of food consumed.
- The band is fluid filled and the degree of GE junction compression can be regulated by adding to or removing liquid from the band, typically performed under fluoroscopic guidance.
- Commonly encountered complications include band slippage, band loosening, and gastric erosions.

Imaging

- Radiographs
  - The *phi angle* of the band is assessed to determine appropriate placement.
  - *Phi angle*—an angle from the top of the long axis of the band and along the vertical component of the thoracic spine (Figs. 8.40 and 8.41).
  - Normal bands have an angle of 4–58°.
  - Bands with *phi angles* outside of this range are considered to have slipped.

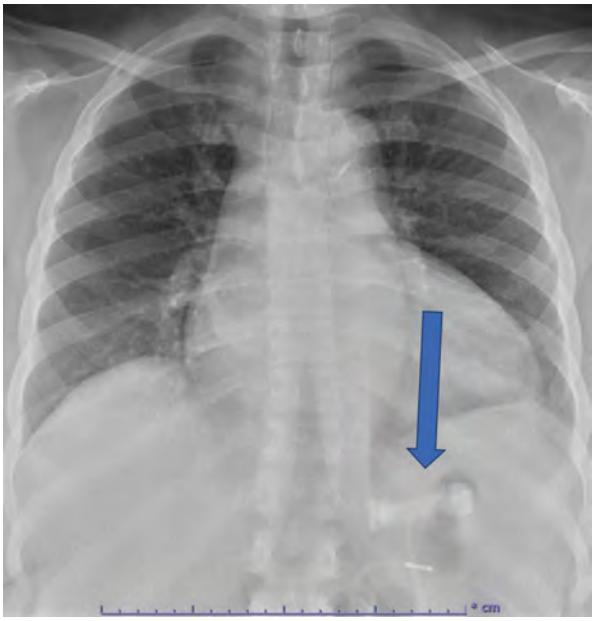

Fig. 8.40 Frontal view of the chest demonstrating a gastric band (arrow). Note that the band is slightly horizontal in position, suggesting it is not in appropriate position

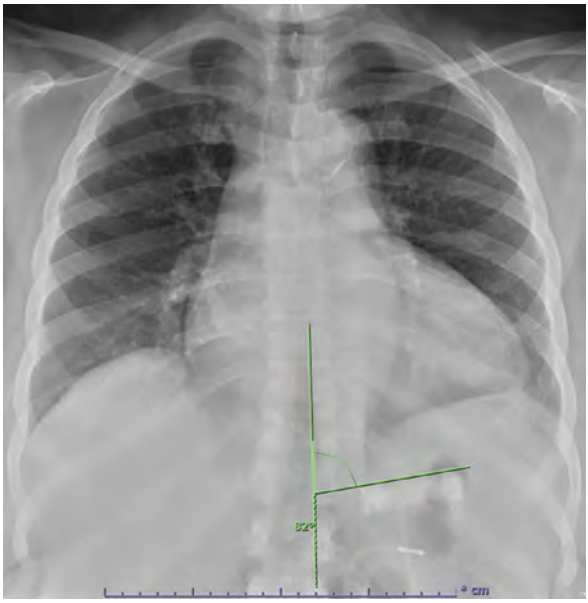

Fig. 8.41 Frontal view of the chest in the same patient as Fig. 8.43. Note the abnormal phi angle, which is measured as shown

- Fluoroscopy
  - The *Phi angle* can be assessed on the scout image from the study.
  - Tight bands—contrast slowly passes through the esophagus and into the stomach (Fig. 8.42).
  - Slipped bands—greater than expected amount of contrast material within the gastric fundus.
  - Band erosion—contrast extravasation can be seen.

Gastric Roux en Y Bypass

- Division of the stomach into a small pouch (the reservoir) and a larger excluded segment.
- Excluded segment empties normally into the duodenum as the biliopancreatic limb (Fig. 8.43).
- The pouch is anastomosed to the roux limb of the jejunum (alimentary limb).
- Alimentary limb is placed in an ante-gastric and ante-colic location.
- The two limbs are connected by a side-to-side anastomosis.
- Marginal ulcers can occur near the pouch-enteric anastomosis and may result from reflux of gastric acid or due to an ischemic event.
- One of the most significant early complications is a leak, which can occur at any of the anastomotic sites.
- Another complication is a gastro-gastric fistula, which may result in failure of continued weight loss, or even weight gain. This fistula may result from failure of the staple line between the gastric pouch and the excluded stomach.

Fig. 8.42 Fluoroscopic image demonstrating contrast passing through a tight gastric band. Note the narrowing of the stomach at the level of the band (arrow)

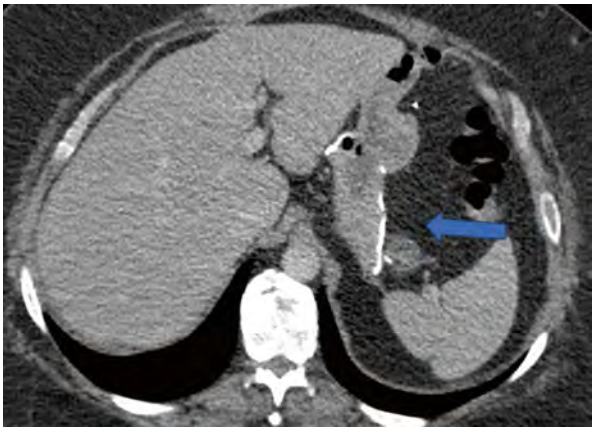

Fig. 8.43 Axial CT image demonstrating the staple line of the bypass

Imaging

- Fluoroscopy
  - Intact bypass will have the esophagus and pouch empty freely and quickly into the roux limb.
  - No contrast within the excluded stomach.
  - Contrast will pass into proximal small bowel and beyond the jejunojejunal anastomosis without hold up (Fig. 8.44 images).
  - Stenosis at the surgical anastomosis—contrast will not pass through anastomosis or will pass through very slowly.
  - Marginal ulcers will appear as a fixed contrast collection with adjacent fold thickening (Fig. 8.45).
  - Anastomotic leak—extravasation of contrast material from the lumen into the peritoneum (Fig. 8.46).
  - Gastro-gastric fistula—extension of enteric contrast from the gastric pouch into the excluded segment, which should not opacify if the anastomosis is intact (Fig. 8.47).
- Computed tomography
  - Gastro-gastric fistulas may be seen on CT if enteric contrast is administered.
  - Contrast within the excluded segment may be detected.
  - More commonly seen are findings of small bowel obstruction related to the small bowel limbs of the surgery.

Fig. 8.44 Image from an upper GI demonstrating the normal anatomy of a gastric bypass (arrow)

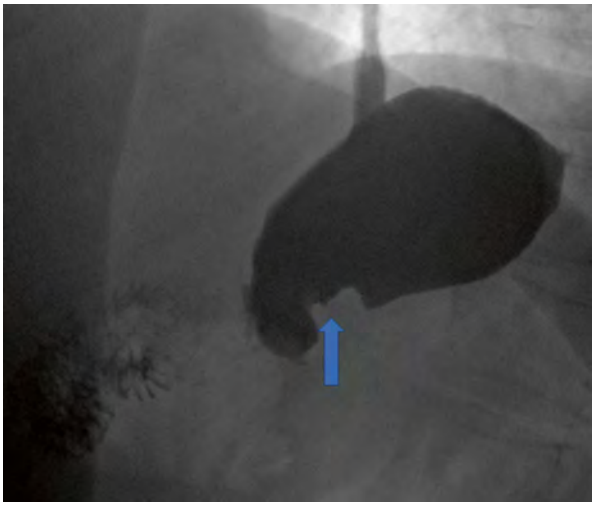

Fig. 8.45 Image from an upper GI demonstrating a marginal ulcer (arrow)

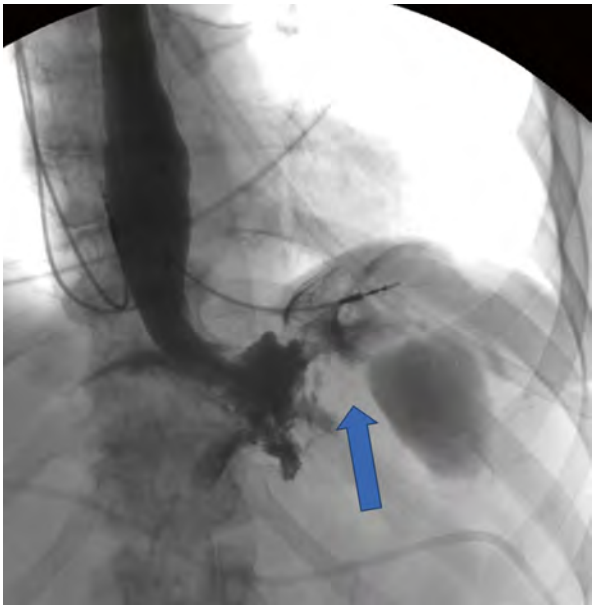

Fig. 8.46 Image from an upper GI demonstrating an anastamotic leak. Note the free spill of contrast from the disrupted anastamotic site (arrow)

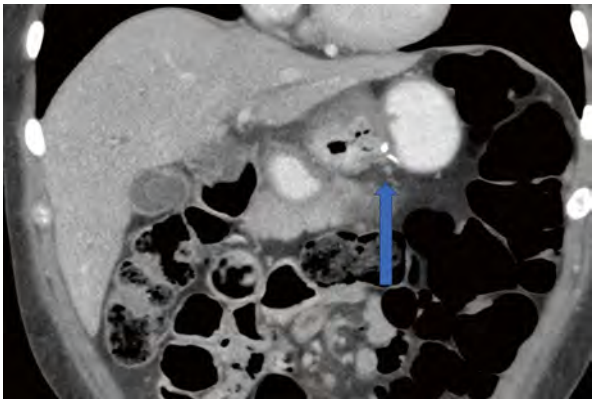

Fig. 8.47 Coronal contrast enhanced CT with oral and intravenous contrast demonstrating opacification of both the gastric pouch and the excluded segment (arrow), consistent with a gastro-gastric fistula

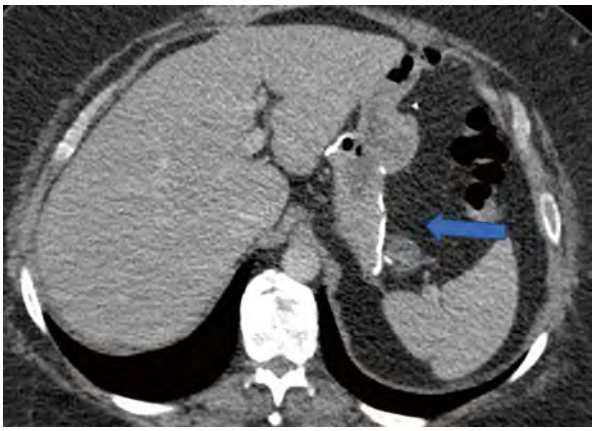

Fig. 8.48 Axial CT demonstrating the elongated stomach with the staple line along the curvature consistent with a gastric sleeve

Sleeve Gastrectomy

In a sleeve gastrectomy, approximately 75% of the stomach is removed, decreasing gastric capacity and absorptive area. The gastric remnant appears like a tube as the stomach is divided along its long axis. Complications include leak from the staple line and stenosis.

Imaging

- Fluoroscopy
  - Gastric leaks are identified by extravasation of contrast material from the remnant stomach.
  - Stenosis is suggested when there is slow or delayed emptying from the gastric remnant. Focal narrowing at the gastric egress may also be seen.
- Computed tomography
  - The stomach is elongated with multiple clips along the stomach where the partitioning occurs (Fig. 8.48).

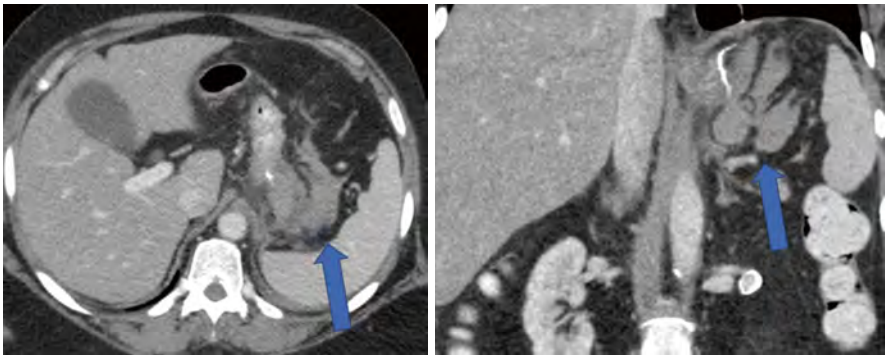

Fig. 8.49 Axial (left image) and coronal CT images demonstrating hemorrhage and fluid around the anastamotic site (arrows) consistent with a post-operative leak

- Free air, perigastric fluid, and contrast extravasation suggest a diagnosis of postoperative leak (Fig. 8.49).
- Gastric outlet obstruction due to edema or stenosis at the anastomotic sites may present as a dilated stomach with an air fluid level or a fluid/contrast level.

Infiltrative Diseases

- Infiltrative diseases of the stomach (benign and malignant) include amyloidosis, sarcoidosis, lymphoma, and metastatic disease (often breast). Regardless of the cause, the imaging findings are similar for these disorders and include gastric wall and rugal fold thickening.

Imaging

- **Radiographs**
  - Gastric wall or rugal fold thickening (rarely) can be seen on radiographs (Fig. 8.50), often in thin individuals or children, and appears as a soft tissue density outlined by air within the gastric lumen and perigastric fat or air within the transverse colon (inferior).
  - Gastric wall thickening appears as a soft tissue density outlined by air within the gastric lumen and perigastric fat or air within the transverse colon (inferior).
- **Fluoroscopy**
  - Gastric lumen may be decreased in size due to the wall thickening. Gastric fold thickening can be seen as serpiginous filling defects within a contrast-distended stomach.
- **Computed tomography**
  - Gastric wall thickening can be difficult to assess on CT (Fig. 8.51). It is more likely to be over-called when the stomach is underdistended (false positive).
  - Focal and diffuse areas of wall thickening can both be identified.

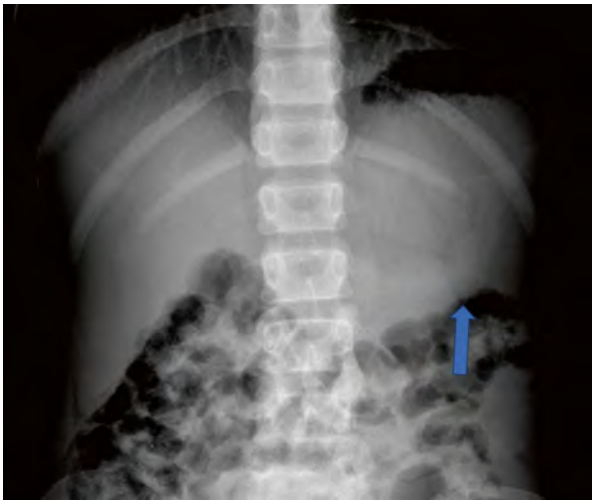

Fig. 8.50 Frontal radiograph of the stomach demonstrating subtle thickened rugal folds (arrow)

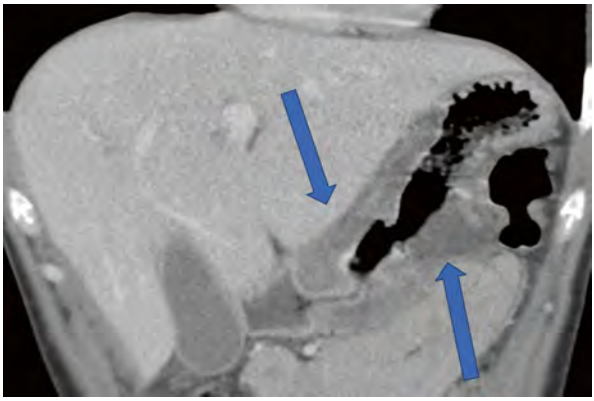

Fig. 8.51 Coronal contrast enhanced CT image demonstrating diffuse circumferential gastric wall thickening (arrow)

– Rugal wall thickening can be directly visualized as serpiginous thickened soft-tissue areas extending into the submucosa.

Masses

Benign Gastric Masses

- There are several benign masses that can affect the stomach, most frequently leiomyomas.
- Masses can be submucosal, mucosal, intramural, or subserosal.
- Imaging appearances will vary depending on cell type and location.

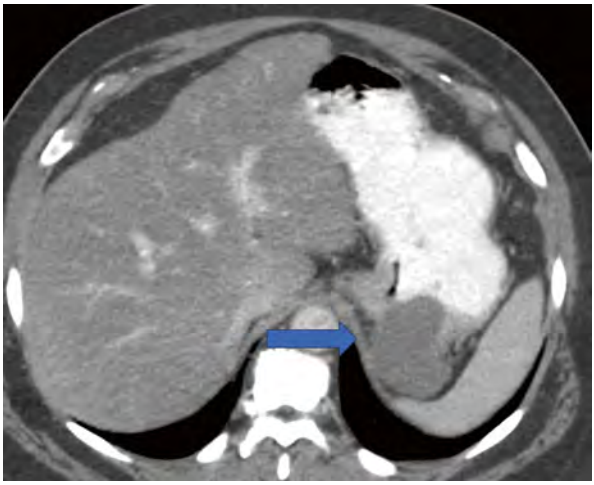

Fig. 8.52 Axial contrast enhanced CT image demonstrating a mass at the gastric fundus (arrow), which is predominantly homogeneous anteriorly but slightly heterogeneous posteriorly

Imaging

- Fluoroscopy: Masses will present as filling defects (if mucosal), or as lumen deforming areas that deform the contrast-filled lumen.
- Computed tomography
  - Masses can be homo- or heterogeneous in appearance depending upon the composition (Fig. 8.52).
  - Enhancement is variable depending upon tumor type.

Malignant Gastric Masses

- Malignant gastric masses may be primary or metastatic tumors.
- Gastrointestinal stromal tumor (GIST) has increased in prevalence in recent years.
  - It is most common in the gastric fundus.
  - Heterogeneous appearance, often with necrosis.
  - Tends to arise exophytically.
- Neoplastic gastric disease may present as a focal mass, multiple masses, focal wall. Thickening, diffuse wall thickening, or may present with gastric outlet obstruction.
- Risk factors include gastric ulcers, *H. pylori* infection, and smoking.

Imaging

- Fluoroscopy
  - Present as filling defects (if mucosal), or as lumen deforming areas that deform the contrast filled lumen.
  - Mucosal ulceration and ulceration of the mass/gastric wall may be visualized.
  - If the tumor is infiltrative (e.g., scirrhous carcinoma), the stomach will not optimally distend and will appear relatively fixed in morphology.

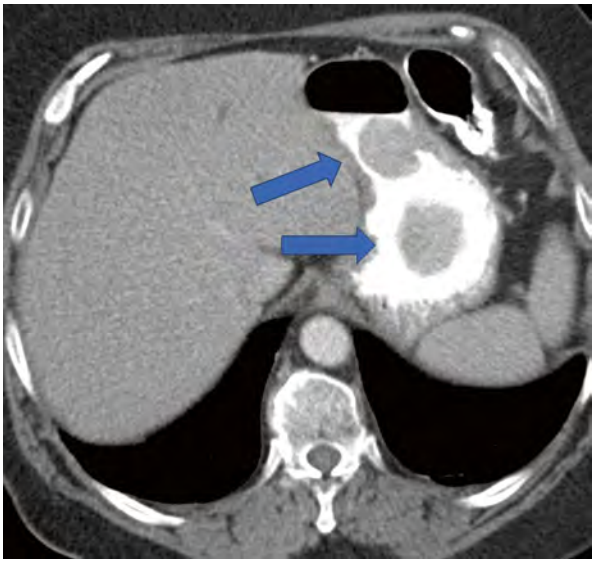

Fig. 8.53 Axial contrast enhanced CT demonstrating intraluminal polypoid gastric masses (arrows) surrounded by enteric contrast material in this patient with metastatic renal cell cancer

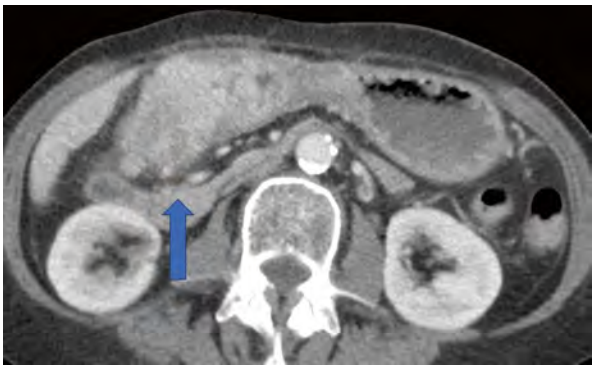

Fig. 8.54 Axial contrast enhanced CT demonstrating a circumferential mass in the gastric antrum (arrow) with fluid distending the more proximal stomach

- Computed tomography
  - Masses can be homo- or heterogeneous in appearance depending upon the composition.
  - Areas of necrosis may be present.
  - May present as focal or diffuse wall thickening (Figs. e8.14 and e8.15).
  - Polypoid masses can be seen, particularly in metastatic disease (Fig. 8.53).
  - Gastric cancers can cause gastric outlet obstruction (Figs. 8.54 and 8.55).
  - GIST tumors are often exophytic (Fig. 8.56).
  - Mural or intraluminal masses can be hard to detect on CT if the stomach is not distended, which is often the case on CT (Fig. 8.57).
  - If there is high suspicion of a gastric mass, an effervescent agent may be given immediately before scanning to distend the stomach.

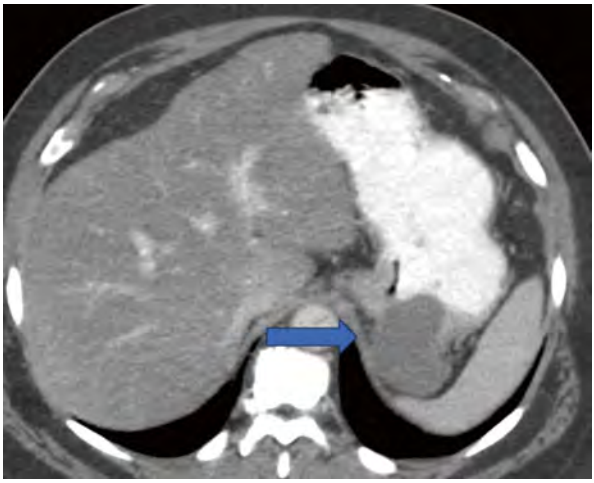

Fig. 8.55 Coronal CT images in the same patient as Fig. 8.57 demonstrating the markedly fluid distended stomach in this patient with gastric cancer due to delayed transit of enteric contents across the mass (arrow)

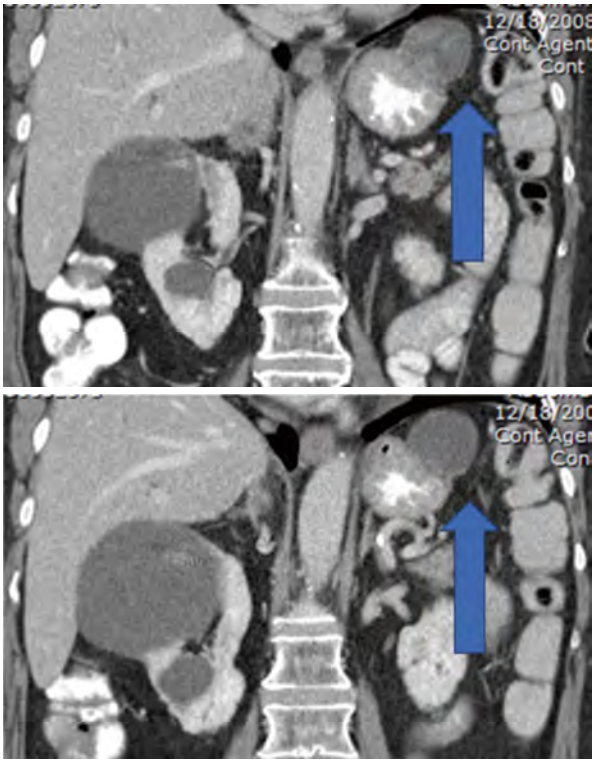

Fig. 8.56 Coronal contrast enhanced CT images demonstrating a heterogeneous exophytic mass at the gastric fundus (arrows) consistent with a GIST tumor

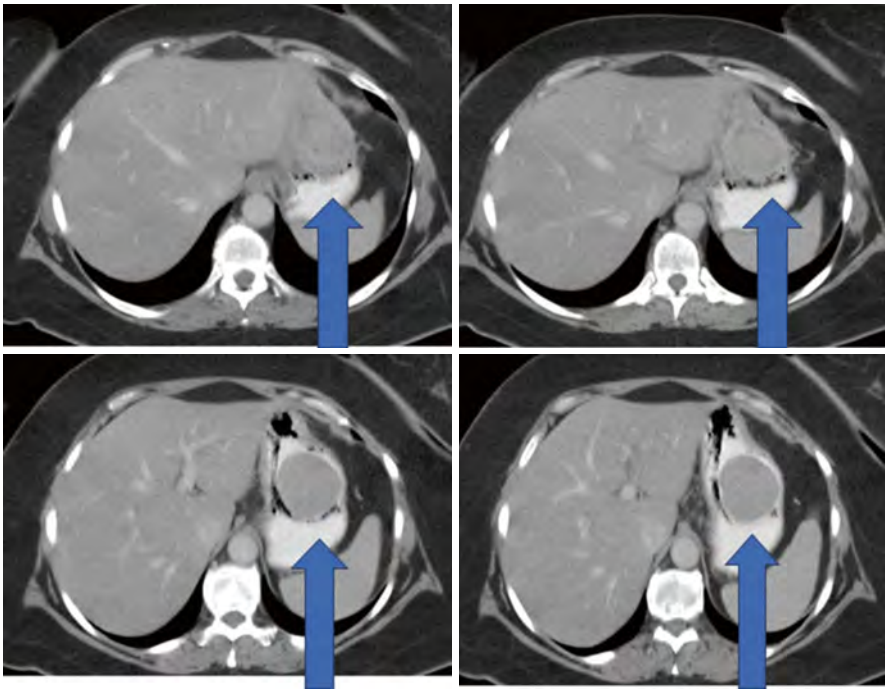

Fig. 8.57 Axial contrast enhanced CT images in a patient with a gastric mass (arrows). Note how difficult it is to visualize the mass in the top images where the stomach is underdistended in comparison to the bottom images where the mass is nicely outlined by enteric contrast in a distended stomach

- MRI
  - Limited role in the evaluation of gastric masses, may be performed for local staging.
  - May be used for the evaluation of hepatic metastases.

Acknowledgments All illustrations were created by Shae McHugh.

Further Readings

1. Boland G. Gastrointestinal imaging: the requisites. 4th ed. Elsevier Health Sciences; 2013.
2. Webb RW, Brant WE, Major NM. Fundamentals of body CT. 5th ed. Elsevier Health Sciences; 2019.
3. Roth CG, Naringrekar H, Deshmukh S. Fundamentals of body MRI, Fundamentals of radiology. 2nd ed. Elsevier Health Sciences; 2016.

Small Bowel Imaging

9

Edward Lawrence

Introduction

- Multiple imaging modalities will be useful for the assessment of small bowel; however, computed tomography (CT) has taken the central role for small bowel evaluation in many settings [1, 2, 3].
- Other modalities, including radiographs, ultrasound, and magnetic resonance imaging, can also be useful.
- Key pathological processes that occur in the small bowel include enteritis, bowel masses, obstruction, mesenteric ischemia, and trauma.
- Many pathological processes in the small bowel (e.g., enteritis, enteropathy) will present with abnormal wall thickening and enhancement.
  - Targetoid enhancement, often suggesting central submucosal edema, will point toward an inflammatory or infectious cause, while bowel wall thinning and hypoenhancement will raise concern for underlying ischemia.
  - Wall thickening that is irregular and with soft-tissue enhancement throughout may be more suggestive of an underlying neoplastic or malignant process.
- Crohn's disease causes characteristic skip lesions of small bowel wall thickening, often involving the terminal ileum.
  - Associated penetrating disease causes a variety of complications, including fistula and abscess.

Supplementary Information The online version contains supplementary material available at https://doi.org/10.1007/978-3-031-76624-4_9.

E. Lawrence (✉)
Department of Radiology, University of Wisconsin-Madison School of Medicine and Public Health, Madison, WI, USA

Department of Radiology, University of Galway, Galway, Ireland
e-mail: elawrence@uwhealth.org

© The Author(s), under exclusive license to Springer Nature Switzerland AG 2024

T. Catanzano (ed.), *What Radiology Residents Need to Know: Abdominal Radiology*, What Radiology Residents Need to Know,
https://doi.org/10.1007/978-3-031-76624-4_9

- While overlap between different small bowel masses exists, many will have a few characteristic features that can assist with the differential diagnosis and underlying concern for a malignant versus benign process.
  - Wall thickening and bowel mass often require clinical correlation and, possibly, tissue sampling for confident diagnosis.
- Small bowel obstructions can range from partial to high grade.
  - While obstructions can be identified on radiographs, CT is useful to evaluate for the underlying cause and possible complications.
  - Closed-loop obstructions represent an emergent process given the combined proximal and distal obstruction (creating the "closed loop") with risk for bowel ischemia due to vascular compromise.
  - Mesenteric ischemia represents another emergent small bowel diagnosis and can be divided into those caused by inflow arterial occlusion versus outflow venous obstruction.
  - In cases of closed-loop obstruction and mesenteric ischemia, key features to identify include bowel wall hypoenhancement/thinning as well as associated pneumatosis or portal venous gas that suggest underlying bowel ischemia/necrosis.
- Traumatic injuries to the small bowel and mesentery are relatively rare but can be easily missed and typically require surgical management if present.
  - Disruption of the bowel wall, focal mesenteric hematoma, and active mesenteric bleeding are specific findings.

Optimal Imaging Studies for Small Bowel Imaging

- Appearance of the small bowel will depend on segment and imaging modality.
- Bowel wall is made of multiple layers (outer serosa → muscularis → submucosa → inner mucosa).
- The small bowel comprises the duodenum, jejunum, and ileum.
  - The duodenum is C-shaped and begins with the duodenal bulb (to the right of the spinal column) and ends with the ligament of Treitz (where it becomes the jejunum) in the left upper quadrant.
  - Clinically, it is considered part of the upper gastrointestinal tract and frequently discussed with the stomach (e.g., the upper GI fluoroscopic evaluation).
  - The jejunum is located in the left upper abdomen and often has a more "feathery" appearance to its folds (Fig. 9.1).
  - The ileum lies in the lower abdomen and connects to the cecum as the terminal ileum in the right lower quadrant through the ileocecal valve.
- Arterial supply for the jejunum and ileum from the superior mesenteric artery and venous drainage to the superior mesenteric vein.

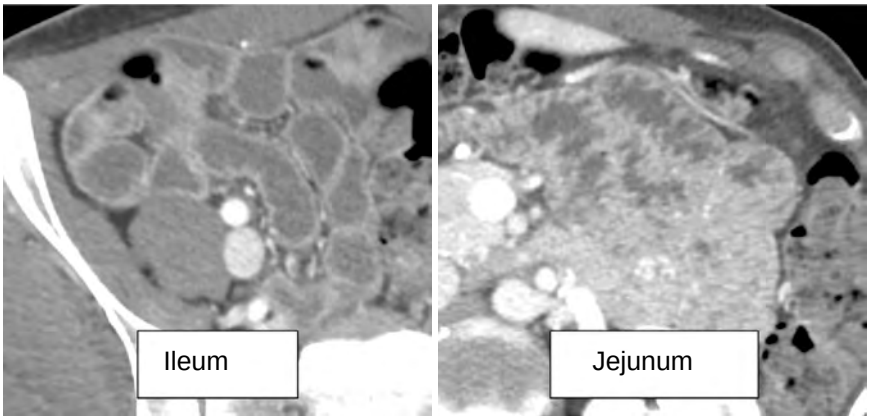

Fig. 9.1 Ileal versus jejunal folds. The jejunum is located in the left upper abdomen and will have a more 'feathery' appearance to its folds. In contrast, the ileum is primarily in the lower abdomen and has a smoother appearance of the bowel wall

Radiographs

- Basic imaging appearance (Fig. 9.2)
  - On radiographs, the jejunal valvulae conniventes and ileal folds of the small bowel are closer together and completely encircle the bowel lumen, which contrasts with the incomplete haustral folds of the colon.
  - The small bowel is also often more central and will have liquid or gaseous contents, which contrasts the solid feces that may be seen in the colon.
- Radiographs have limited sensitivity or utility for most small bowel pathologies.
- May have a role in the evaluation of small bowel obstruction, ileus, foreign object ingestion (Fig. e9.1), and pneumoperitoneum (on upright view) (Fig. 9.3).

Fluoroscopy

- On small bowel fluoroscopy, evaluation of the bowel wall, diameter, and fold size will depend on the degree of luminal distension and barium coating [4].
- Historically small bowel enteroclysis was used for the evaluation of small bowel (including strictures, masses, and luminal abnormalities); however, it is infrequently used in current practice given its invasive nature (requires catheter placement and direct contrast injection into the small bowel) and the increased use of CT and MRI.
- Small bowel follow-through (Fig. 9.4)
  - Involves per oral administration of contrast and intermittent fluoroscopic/radiographic evaluation as the contrast transits the small bowel (often lasting between 30–180 min).

Fig. 9.2 26-yo with chronic constipation. Supine abdominal radiograph demonstrates some of the characteristic features of small bowel versus colon, including the wider haustral fold of the colon (arrow) seen near the splenic flexure, stool within the ascending/transverse colon (arrowheads), and more central small bowel loops with encircling small bowel folds (dashed arrow)

Fig. 9.3 Pneumoperitoneum on upright AXR. 32-yo initially presenting with acute uncomplicated diverticulitis on CT (not shown). Increased abdominal pain 1 day later. Upright abdominal radiograph demonstrates new pneumoperitoneum, seen as curvilinear lucencies (air) underlying the diaphragm (arrows). Perforated diverticulitis was confirmed surgically

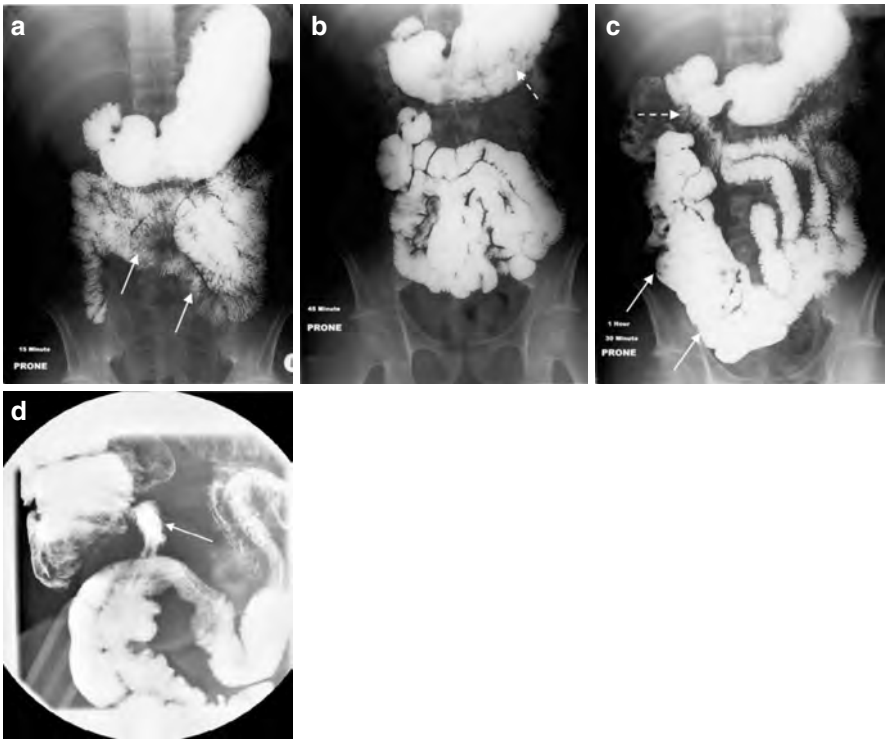

Fig. 9.4 Example small bowel follow-through. 30-yo with nausea, vomiting, and abdominal pain. Multiple abdominal radiographs were obtained at 15 min (**a**), 45 min (**b**), and 1 h 30 min (**c**) after contrast administration. Contrast is initially seen in the jejunum (arrows in **a**) with subsequent normal transit into the ileum (arrows in **c**). Mild thickening of the gastric and duodenal folds was noted (dashed arrows), felt to suggest a possible mild underlying gastritis/duodenitis, but the remaining small bowel was normal. (**d**) Spot full exposure fluoroscopic images may also be obtained, such as in this case where an image of the right lower quadrant was completed centered on the normal terminal ileum (arrow), using compression by a paddle held by the radiologist to push other bowel out of the way

CT

- Often primary modality for bowel imaging given its rapid acquisition, noninvasiveness, diagnostic performance, and broad accessibility in most healthcare environments.
- On CT, the appearance of the small bowel depends heavily on the presence or absence of intravenous and oral contrast.
  - Positive oral contrast (Fig. 9.5) can assist with delineating bowel from other intraperitoneal structures (e.g., masses, abscesses).

    It assists with delineation of the presence and severity of small bowel obstruction.

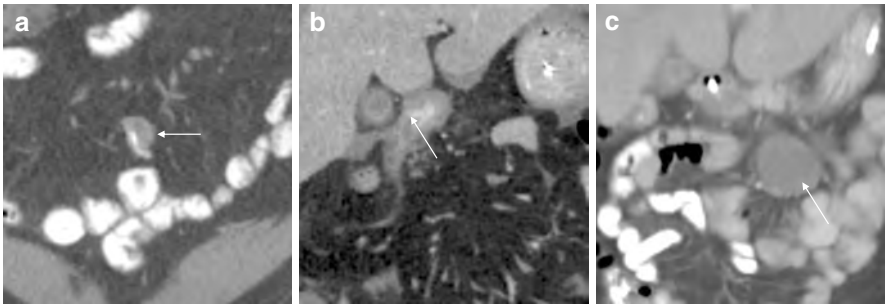

Fig. 9.5 Examples of diagnostic utility of positive oral contrast. (**a**) Coronal image from a CT with IV and oral contrast demonstrates a subtle small distal ileal lesion (arrow) that was found to be neuroendocrine tumor on resection. (**b**) Positive oral contrast can be seen extending into a duodenal ulceration (arrow) and was also noted to be extraluminal (not shown) in this patient with perforated peptic ulcer disease. (**c**) A rounded hypoattenuating mesenteric mass (arrow) is easier to delineate given the positive oral contrast in the surrounding bowel (found to be a desmoid tumor on biopsy)

  Possible downsides include increased preparation time to account for contrast drinking and possible obscuration of luminal-sided bowel wall enhancement.
- Intravenous contrast is necessary to assess for abnormalities in enhancement and is very helpful in identifying abnormal wall thickening or masses, particularly in underdistended bowel.
- Negative oral contrast can be used for combined optimized luminal distension and evaluation of wall thickening/enhancement (i.e., CT enterography).

Ultrasound

- Used more commonly in pediatric patients.
- In adults, can be used in specific settings (e.g., appendicitis, IBD follow-up) or findings seen incidentally on other examinations.
- Bowel has a multilayered appearance ("signature") on US with alternating hyperechoic and hypoechoic layers (Fig. 9.6).
- Advantages
  - Low cost, no radiation.
  - Dynamic study that can evaluate compression and change over time.
  - Ability to use Doppler for vascular evaluation.
- Disadvantages
  - User dependence.
  - Technical limitations (shadowing from gas, body habitus).

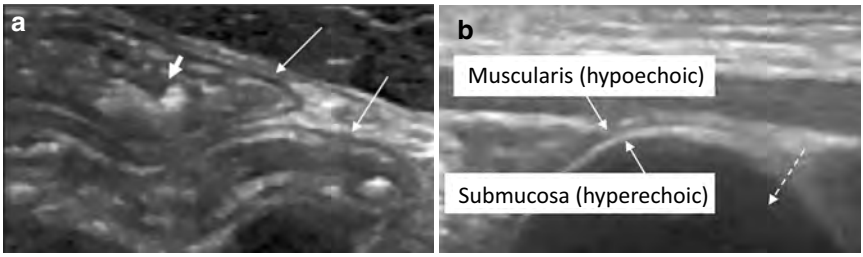

Fig. 9.6 US bowel basics. The key to identifying bowel on ultrasound is to look for the 'bowel signature' caused by the layers of the bowel wall (two bowel loops denoted by arrows in **a**). In practice, typically a dark black (hypoechoic) line is seen surrounding a white (hyperechoic) line, created by the muscularis and submucosa layers, respectively. Luminal contents can be hypoechoic (if fluid, dashed arrow in **b**), heterogeneously echogenic (if stool, arrowhead in **b**), or shadowing (if air filled)

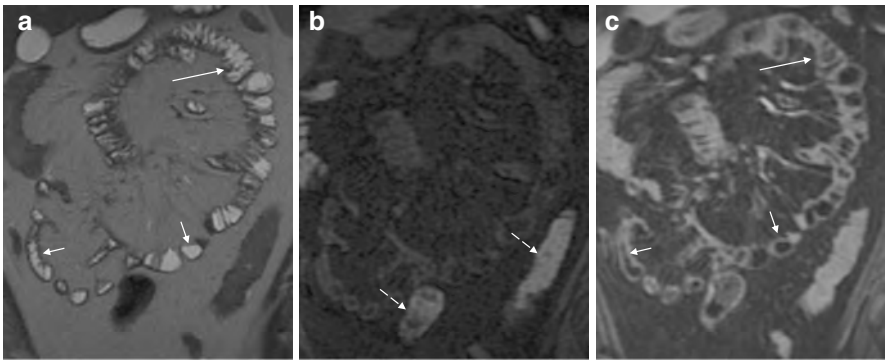

Fig. 9.7 Example MR enterography images. A T2-weighted singleshot fast spin echo (**a**), pre-contrast T1-weighted (**b**), and post-contrast T1-weighted coronal series is typically acquired. Negative oral contrast is given to the patient prior to the scan with the goal of causing fluid distension of the small bowel loops (arrows in **a**). Stool, more often seen in the colon, will appear as inherently T1-hyperintense on pre-contrast images (dashed arrows), which needs to be distinguished from true enhancement, such as seen in the small bowel wall on post-contrast T1 (arrows in **c**). No evidence of inflammatory bowel disease was noted

MRI

- Small bowel evaluation is often difficult on standard MRI given luminal under-distension, bowel peristalsis, and susceptibility artifact from gas.
- MR enterography utilizes negative oral contrast to distend the lumen. Frequently also utilizes IV glucagon administration to limit bowel peristalsis.
- Comparable features to CT but with possible additional diagnostic capabilities to assess wall edema (through T2-weighted sequences ± diffusion-weighted sequences) and dynamic peristalsis (Fig. 9.7).

Infection (Enteritis)

General imaging features of small bowel infection and inflammation:

- **CT**
  - Wall thickening is a key finding to suspect enteritis and will depend on contrast used (Fig. 9.8).
  - In general, the wall should be <1–2 mm when adequately distended (diameter 2–3 cm).
  - Targetoid enhancement with stratified enhancement of the serosal and luminal sides and central hypoattenuation (often due to submucosal edema) favors a benign process and is often seen in infection (Fig. 9.9).
  - Greater lengths of involvement, particularly diffuse thickening, also may favor enteritis.
  - Secondary inflammatory features (stranding, fluid) are often present.
- **MRI**
  - Similar features to CT (i.e., wall thickening and surrounding inflammation).
  - Wall thickening will often demonstrate T2-hyperintensity due to associated edema in the wall.
  - Surrounding inflammation may be seen as T2-hyperintense fluid around the bowel loops (Fig. e9.2).
- **Radiograph/fluoroscopy**
  - Limited sensitivity.

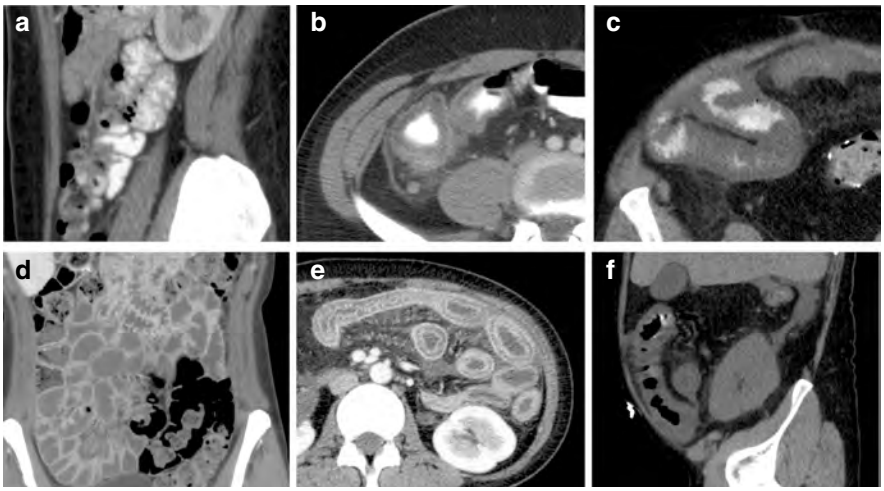

Fig. 9.8 Example images of normal and thickened small bowel depending on contrast type present. (**a**) Normal small bowel with IV and oral contrast. (**b**) Thickened small bowel with IV and oral contrast. (**c**) Thickened small bowel with oral and without IV contrast. (**d**) Normal small bowel with IV and without oral contrast. (**e**) Thickened small bowel with IV and without oral contrast. (**f**) Thickened small bowel without IV nor oral contrast

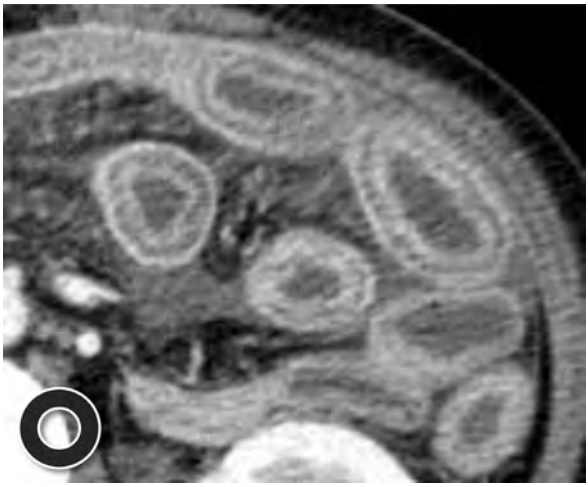

Fig. 9.9 Targetoid enhancement represents stratified enhancement of the serosal and luminal bowel sides with relative central hypoattenutation. The hypoattenuation is often due to submucosal edema and favors a benign, often infectious, process. Rarely the hypoattenuation can represent hemorrhage

  - May see secondary reactive ileus (mildly dilated small bowel in the region of the inflammation and enteritis).
  - On fluoroscopy, fold thickening may be the predominant identified abnormality.
- On imaging, features of infectious enteritis overlap with other noninfectious etiologies such as radiation enteritis, portal enteropathy, medication-induced angioedema, and vasculitis.

Infectious Enteritis

- Background
  - Associated clinical history (including travel history, if relevant) may be important for diagnosis.
  - Pathogens can include bacterial, viral, fungal, and parasitic.
- Imaging features
  - **CT**

    Studies may be normal or demonstrate nonspecific wall thickening, fold thickening, or small bowel inflammation.
  - **MRI**

    Similar features to CT.
  - **Radiograph/fluoroscopy**

    Limited sensitivity

    May see reactive ileus and possibly fold thickening (better seen on fluoroscopy).
  - Specific pathogens

    Yersinia enterocolitica (Gram-negative bacteria) and tuberculosis (especially in immunocompromised individuals) can result in distal ileal

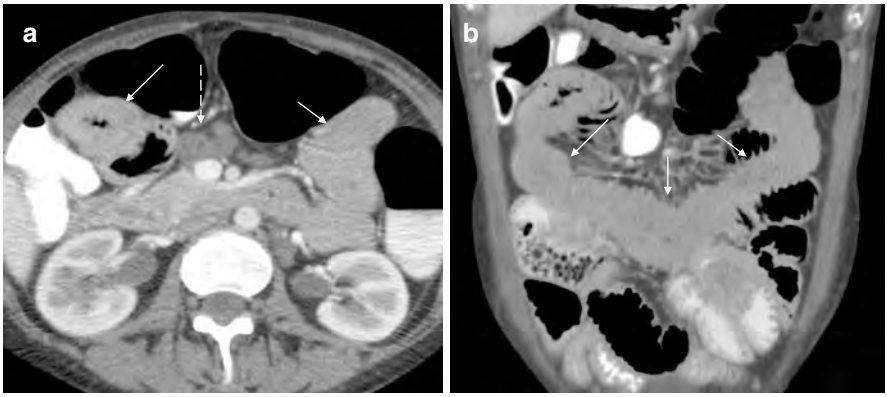

Fig. 9.10 42-yo with confirmed Whipple's disease. Axial (**a**) and coronal (**b**) CT images with IV and oral contrast demonstrates diffuse proximal small bowel thickening, mostly in the jejunum (arrows) as well as low attenuation central mesenteric lymphadenopathy (dashed arrow in **a**). (Case provided by Dr. Perry J Pickhardt, UW-Madison)

inflammation that could mimic Crohn's disease on imaging and appendicitis clinically.

Whipple's disease is a rare bacterial infection (*Tropheryma whippeli*) that can cause enteritis as well as affect the joints and CNS.

- Classically causes low attenuation proximal mesenteric adenopathy as well as proximal small bowel fold thickening (Fig. 9.10).

Scleroderma/Systemic Sclerosis

- Background
  - Autoimmune connective tissue disease, marked by collagen deposition, fibrosis, and soft-tissue calcification.
  - Most common sites of disease involvement include joint arthropathy, lungs, and GI tract (esophagus > small bowel > colon).
- Imaging features
  - **CT/MRI**

    In addition to wall thickening and surrounding stranding, features may include luminal dilatation and reduced peristalsis/impaired transit ("pseudo-obstruction").

    Associated pneumatosis cystoides intestinalis has also been reported and is better seen on CT than MRI.
  - **Radiographs/fluoroscopy**

    Can have associated luminal dilatation and reduced peristalsis ("pseudo-obstruction").

Classic "hidebound" appearance of the jejunum due to crowding of the valvulae conniventes resulting in closely spaced fold without significant fold thickening.
Associated pneumatosis cystoides intestinalis has also been reported.

Celiac Disease

- Background
  - Also known as nontropical sprue and gluten-sensitive enteropathy.
  - Presentation can range from vague abdominal complaints to iron-deficiency anemia, steatorrhea, weight loss, and diarrhea.
  - Primary treatment is a gluten-free diet with consideration for corticosteroid treatment, if necessary.
  - One rare but worrisome possible complication is small bowel T-cell lymphoma.
- Imaging features
  - **CT/MRI**
    Primarily involves the duodenum and jejunum.
    In addition to standard features of enteritis, may also see jejunal and ileal fold reversal where there is loss of the normal "fluffy" jejunal fold due to inflammation and destruction and resultant hypertrophy and increased thickening of the ileal folds to compensate for the decreased absorption in the jejunum.
    May see associated pneumatosis intestinalis, intussusception, and (rarely) cavitating mesenteric lymph nodes.
  - **Radiographs/fluoroscopy**
    Radiographs have limited sensitivity.
    Classic findings on fluoroscopy.
    - Jejunal and ileal fold reversal where there is loss of the normal "fluffy" jejunal fold due to inflammation and destruction and resultant hypertrophy and increased thickening of the ileal folds to compensate for the decreased absorption in the jejunum.
    - Cast-like, featureless jejunum (moulage sign) due to the destruction of the underlying jejunal folds.

    May see associated pneumatosis intestinalis.

Radiation Enteritis

- Background
  - Inflammatory response to radiation, often in the pelvis, that can be seen both acutely and chronically.
  - Establishing the associated prior history of radiation is often key to confident diagnosis.

Common history might include radiation treatment for cervical, uterine, prostate, colorectal, or pancreatic cancer.

- Imaging features
  - **CT/MRI**
    Wall thickening (including targetoid enhancement, submucosal edema) and associated stranding/fluid (Fig. 9.11).
    Key clue is wall thickening/inflammation that is regional (in the area of prior radiation) and may not involve a single segment or vascular territory.
    Can see associated luminal narrowing, including chronic stricture in severe cases, possibly with upstream small bowel obstruction (Fig. 9.12).
  - **Radiographs/fluoroscopy**
    Limited or nonspecific findings on radiograph.
    Fluoroscopy may demonstrate areas of regionally located and discontinuous wall thickening with or without associated area of luminal narrowing (stricture).
    In the setting of stricture there may be upstream dilated bowel with or without findings of a true small bowel obstruction (described later in the chapter).

Other Causes/Mimics of Enteritis

- Portal enteropathy (Fig. 9.13).
  - **CT/MRI**
    Diffuse, edematous bowel wall thickening seen in the setting of cirrhosis and portal hypertension.

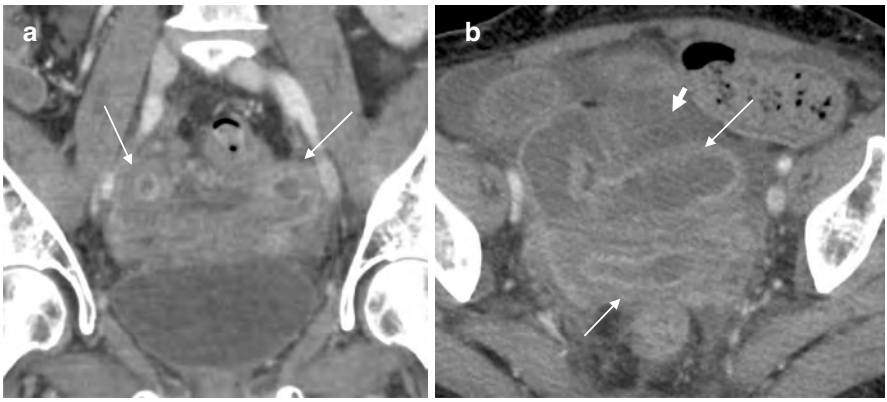

Fig. 9.11 Acute radiation enteritis. 59-yo status post chemoradiation for anal cancer who presented with acute abdominal pain. Coronal (**a**) and axial (**b**) CT images with IV contrast demonstrate thickened loops of small bowel (arrows) with primarily luminal sided enhancement and associated free fluid in the pelvis (arrowhead). A key clue for radiation enteritis is regional wall thickening corresponding to the area of prior radiation treatment (in this case the pelvis)

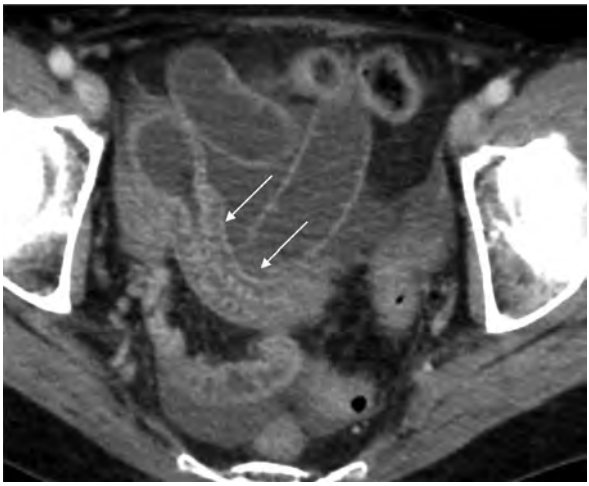

Fig. 9.12 Chronic radiation enteritis (complicated by stricture and SBO). Axial CT image with regional small bowel wall thickening in the pelvis, including a segment with severe luminal narrowing (arrows) and resultant upstream fluid filled, dilated small bowel. Small volume free fluid is also noted in the pelvis. Many of the findings of chronic radiation enteritis are similar to its acute counterpart, except for the development of chronic strictures (as in this case) that predisposes to small bowel obstruction, often recurrent

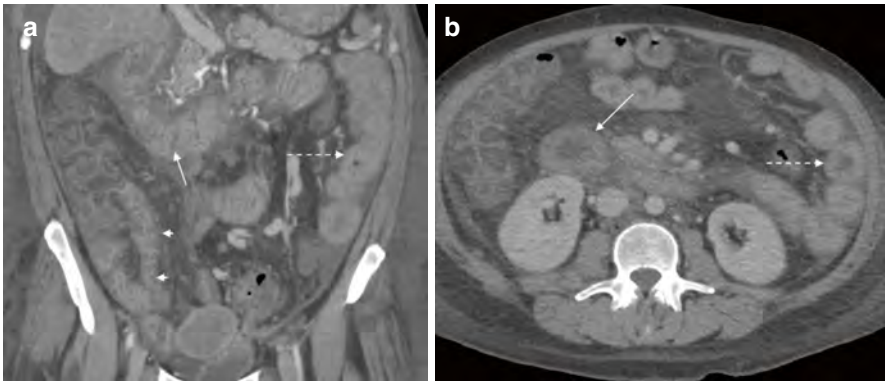

Fig. 9.13 Portal enteropathy in a 44-yo with history of alcoholic cirrhosis. Coronal (**a**) and axial (**b**) images from a CT with IV contrast demonstrates diffuse thickening of the visualized small bowel, including duodenum (arrow), jejunum (dashed arrow), and ileum (arrowhead). Portal enteropathy is often seen diffusely and associated with thickening of the colon as well as ascites (as in this case)

Associated findings.
- Cirrhotic liver with surface nodularity, caudate hypertrophy, fissural widening, and segmental redistribution.
- Portosystemic collateral vessels, including recannulated paraumbilical vein, splenorenal shunt, and gastroesophageal varices.
- Ascites with disorganized peritoneal fluid that can range from trace perihepatic ascites to large-volume ascites throughout the peritoneal cavity.

May see associated colonic wall thickening (portal colopathy).
Often seen on surveillance CT or MRI obtained to screen for hepatocellular carcinoma in cirrhotic patients.

– **Radiograph/fluoroscopy**
Limited utility
May seen general findings of cirrhosis including hepatosplenomegaly as well as features of ascites with diffusely increased density in the abdomen and associated decrease in ability to detect the soft-tissue shadows.

- Medication-induced angioedema
  – Background
  Most commonly blood pressure medications (ACE-inhibitors, angiotensin II receptor blockers, Ca^{2+} channel blockers) or chemotherapeutic agents (bevacizumab, imatinib).
  Symptoms and imaging findings will typically resolve after stopping the causal medication.
  Acquired and hereditary intestinal angioedema is also rarely seen with similar findings.
  – Imaging features (Fig. 9.14)
  Primarily on CT and, less commonly, MRI.
  Long segment (>10 cm) edematous wall thickening, often with associated mild mesenteric edema and possibly with small-volume ascites.
- Vasculitis
  – Background

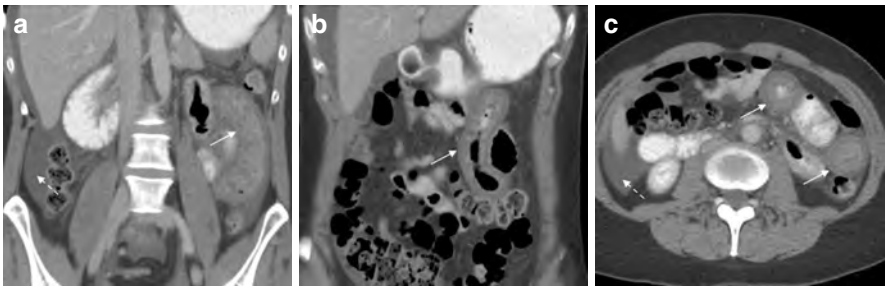

Fig. 9.14 Medication-induced angioedema. 47-yo with history of hypertension with new abdominal pain after recently starting lisinopril. Coronal (**a**, **b**) and axial (**c**) CT images obtained with IV and oral contrast demonstrate long segment, targetoid thickening of proximal small bowel loops in the left abdomen (arrow). Associated ascites is also noted (dashed arrow in **a**, **c**). The patient's symptoms resolved a few weeks after stopping the medication

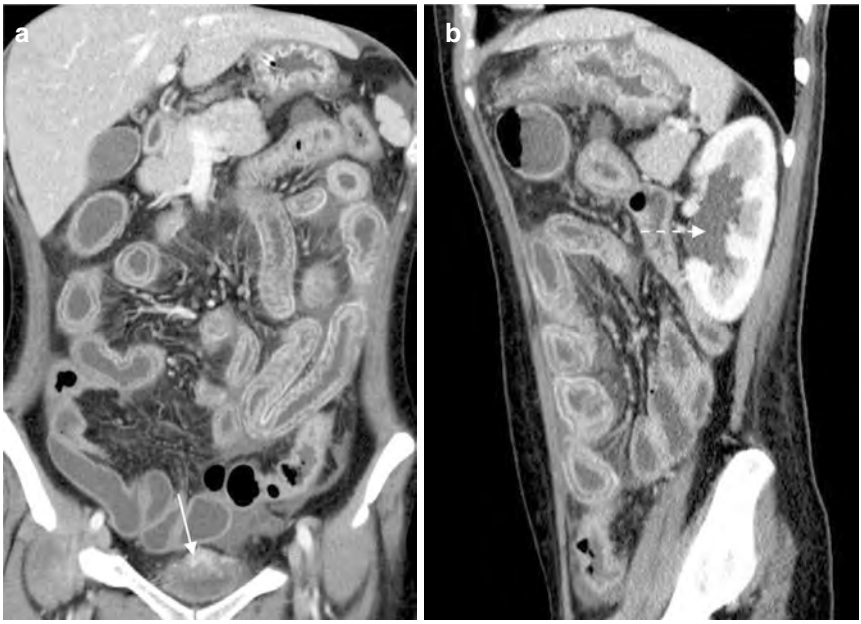

Fig. 9.15 Small bowel vasculitis. Coronal (**a**) and sagittal (**b**) CT images with IV contrast in a 20-yo demonstrate diffuse targetoid small bowel wall thickening, particularly in the jejunum. Hydronephrosis (dashed arrow) and plaque-like thickening along the bladder dome (arrow) were also seen. In addition to the classic 'targetoid' edematous enhancement often seen with small bowel vasculitis, the involvement of other organ systems (particularly the urinary system) is also a common feature of many vasculopathies

Many vasculopathies can involve the small bowel (e.g., Henoch–Schonlein purpura, systemic lupus erythematosus, microscopic polyangiitis).

– Imaging features

CT/MRI

- Wall thickening is often targetoid or with features of hemorrhage and may have associated corkscrew appearance of the underlying vessels.
- Thickening can either be diffuse or multifocal with intervening areas of normal bowel.
- The presence of associated urinary findings (hydronephrosis, cystitis, nodular bladder/ureteral wall thickening) may help with diagnosis as many vasculopathies involve both systems (Fig. 9.15).
- Medium- or large-vessel vasculitis is more likely to have imaging findings similar to mesenteric ischemia (see ischemia section).

Radiograph/fluoroscopy

- Limited utility in current practice.
- On fluoroscopy may see wall thickening that can be either diffuse or multifocal with intervening normal bowel.

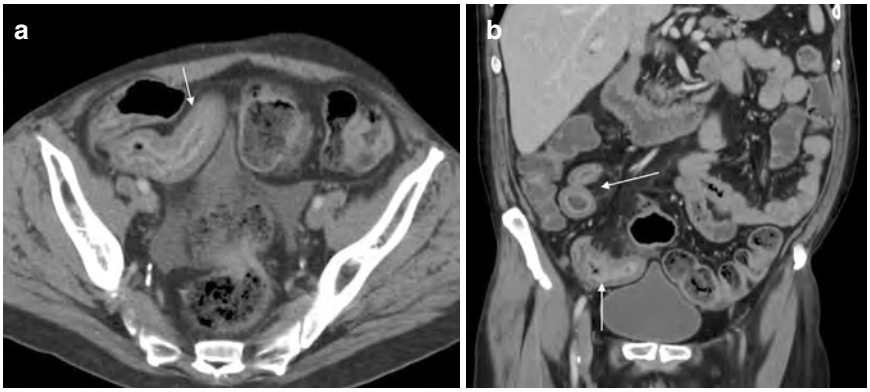

Fig. 9.16 Graft versus host disease (GVHD) in a 58-yo with history of lymphoma status post bone marrow transplant. Axial (**a**) and coronal CT images with IV contrast demonstrate targetoid segmental thickening in the distal ileum (arrows) with associated ascites (**b**). The imaging findings are non-specific; however, in a patient with recent bone marrow transplantation GVHD would be a concern. The patient was subsequently diagnosed with steroid refractory GVHD

- Graft-versus-host disease (GVHD)
  - Background
    GVHD can affect the GI tract throughout its entirety.
    Small bowel involvement may be diffuse as well as possible colonic involvement.
    Should be considered in the differential diagnosis for bowel wall thickening in a patient with prior bone marrow transplantation.
  - Imaging features (Fig. 9.16)
    Primarily seen on CT or, less commonly, MR enterography.
    - Wall thickening (commonly with mucosal-sided hyperenhancement) as well as possible fat stranding and engorgement of the vasa recta.
- Foreign body perforation
  - Background
    Common causes include fishbone or grill bristle.
    Differential considerations include small bowel diverticulitis and perforated adenocarcinoma.
    Correlate with recent corresponding ingestion of a possible foreign body source.
  - Imaging features
    CT/MRI
    - More often seen with CT, especially given the common presentation with acute abdominal pain (Fig. 9.17).
    - Focal small bowel wall thickening and surrounding stranding.
    - Evidence of a foreign body (such as fishbone or metallic grill bristle) that is often seen as a linear hyperdense object that is either external to or traversing through the bowel wall.

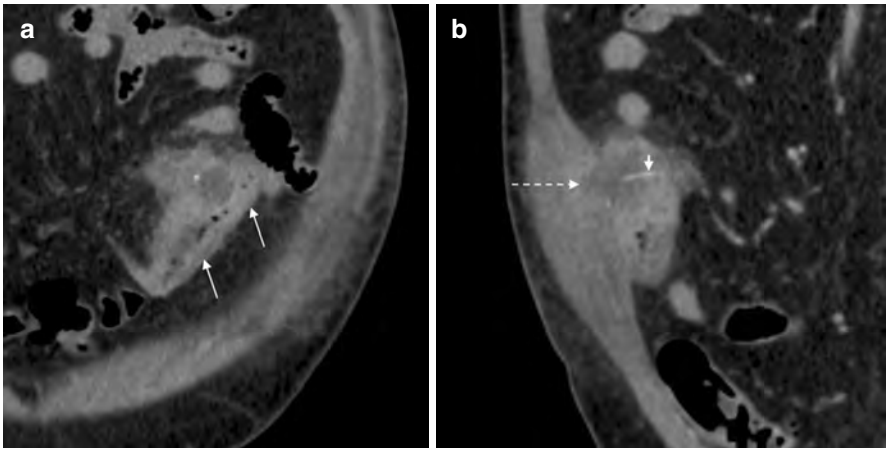

Fig. 9.17 (**a**, **b**) Foreign body (fishbone) small bowel perforation. Coronal and sagittal magnified CT images with IV contrast demonstrate a focally thickened short segment of small bowel (arrows) with adjacent small abscess (dashed arrow) and surrounding inflammation extending into the overlying abdominal wall. Best seen on the sagittal view, there is a radiopaque linear foreign body (arrowhead) that has perforated through the bowel wall and extends into the abscess

    - Often will demonstrate small collection/abscess associated with the extraluminal part of the foreign body.
    - In rare cases can cause frank perforation (demonstrated by free fluid/free air).

    Radiograph/fluoroscopy
    - Fluoroscopic evaluation would be rare, particularly given the typical acute presentation.
    - Radiographs offer limited sensitivity.
    - In rare case may be able to see the foreign object (although typically too small to easily see on radiographs).
    - Could see pneumoperitoneum, in the setting of perforation, or air-fluid level, in the setting of adjacent abscess.
- Small bowel diverticulitis
  - Rare compared to colonic diverticulitis.
  - Imaging features

    CT/MRI (Fig. 9.18)
    - Typically evaluated with CT given the acute presentation.
    - Inflamed outpouching of the bowel with wall thickening, surrounding stranding.
    - Can be mistaken for an abscess. Features that may allow for differentiation:
      - Connection with the bowel lumen
      - Multilayered appearance of the diverticular wall (versus the inflammatory wall of an abscess)
      - Presence of other small bowel diverticula

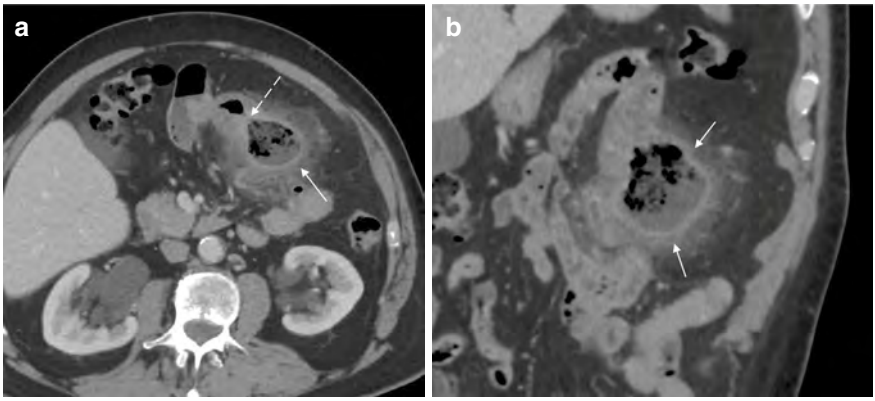

Fig. 9.18 Small bowel diverticulitis. Axial (**a**) and coronal (**b**) CT images with IV contrast demonstrating a large ovoid structure (arrows) with peripheral wall and filled with fecalized contents. Key findings to suggest this is an inflamed diverticulum, include the small connection between the structure and adjacent jejunum (dashed arrow) as well as the 'bowel signature' of the peripheral wall with enhancement along the luminal side

Radiograph/fluoroscopy

- Limited utility.

- Gastrointestinal bleeding
  - Background

    Many causes of gastrointestinal bleeding will occur in the colon (e.g., diverticular bleed) or in the stomach (e.g., gastric ulcer).

    Small bowel causes of bleeding are less common, but clinically important to identify on imaging as they can be difficult to evaluate endoscopically.

    Possible etiologies in the small bowel include tumor, vascular anomalies (e.g., angioectasia, arteriovenous malformations), trauma, and Meckel's diverticulum.
  - Imaging acquisition

    CT angiogram (CTA) is the study of choice for evaluation. CTA involves a specialized contrast injection and image acquisition to optimize evaluation of the arterial vessels.

    When the concern is for active bleeding, a multiphase CTA is ideally performed, including a noncontrast phase, arterial phase, and some type of delayed phase.
  - Imaging features

    CT (Fig. e9.3)

    - CTA is optimal, although evidence of active bleeding can also be seen on a routine portal venous phase CT.
    - Classic CTA findings of active GI bleeding include a focus of luminal high attenuation (contrast) on the arterial phase that was absent on the noncontrast phase and which demonstrates enlargement and redistribution in the bowel lumen on delayed phase.

- On a single portal venous phase, only the delayed phase findings of extravasated contrast in the bowel lumen will be seen.

MRI

- In very rare cases (e.g., severe CT contrast allergy) could consider MRA to assess for bleeding; however, given study length, cost, and challenges with bowel evaluation, it would be a second-line evaluation.
- On a multiphase MRA, the findings would be similar with focus of contrast (hyperintensity) on postcontrast arterial T1-weighted imaging with further enlargement and redistribution on the delayed phases.

Inflammatory Bowel Disease

Crohn's Disease Background

- Can involve any segment of the bowel from mouth to anal canal.
- Small bowel involvement is common, particularly of the terminal ileum (Fig. 9.19).
- Classic features on imaging include skip lesions, mesenteric-sided thickening/fibrosis, pseudo-sacculations, and mesenteric fatty proliferation [5].
- Complications can include stricture, bowel obstruction, fistula, and abscess.

Imaging Assessment of IBD

- **CT**
  - Acute/emergent evaluation will typically involve standard CT with contrast (portal venous phase) with or without positive oral contrast.
  - Acute evaluation focused on acute complications (e.g., abscess, fistula, obstruction).
  - Outpatient, nonemergent evaluation will use CT enterography.
  - Advantages of CT/MR enterography over endoscopy and fluoroscopy include better evaluation of the bowel wall and for extraintestinal complication.
  - Uses negative oral contrast (fluid distension of the bowel lumen for better assessment of the wall).
- **MRI**
  - Not used in the acute setting. Outpatient evaluation will utilize MR enterography.
  - MR enterography uses negative oral contrast to optimize fluid distension of the bowel lumen for better assessment of the wall and possibly with IV glucagon (antiperistalsis agent) for MR to decrease artifact related to bowel motion.
- **Ultrasound**
  - May be utilized in some centers for surveillance of disease (particularly with pediatric patients).

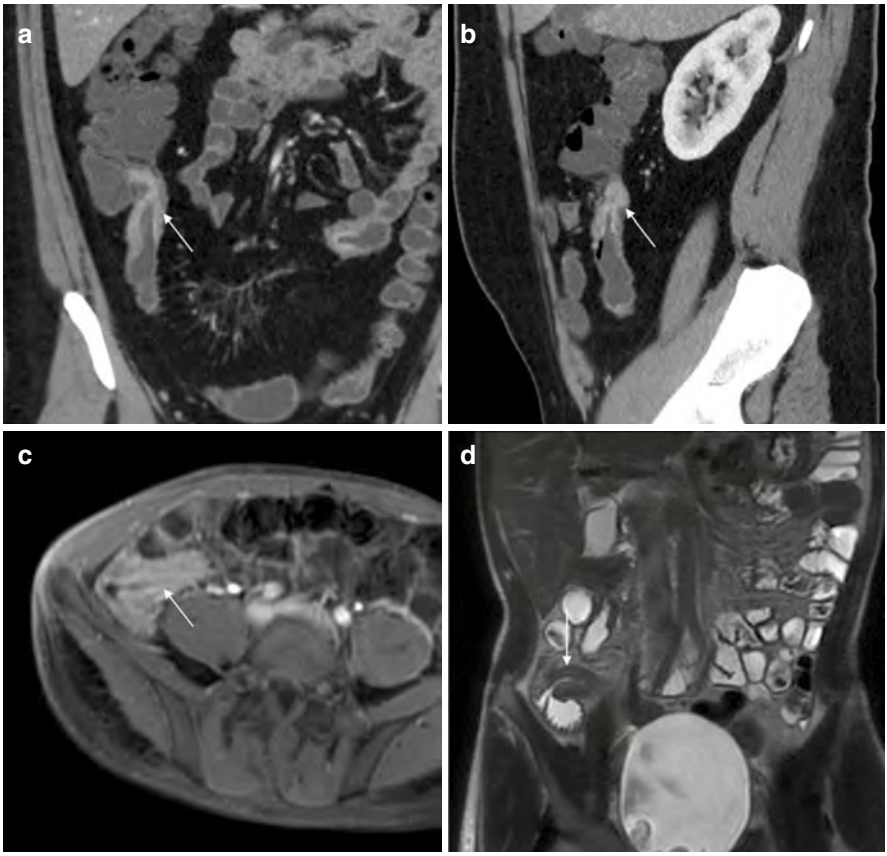

Fig. 9.19 Terminal ileum thickening in Crohn's disease. (**a**, **b**) 25-yo with initial diagnosis of Crohn's disease and terminal ileal thickening (arrow) seen on coronal (**a**) and sagittal (**b**) images from CT enterography. (**c**, **d**) 22-yo underwent MR enterography for initial diagnosis of Crohn's disease. Terminal ileum thickening (arrow) seen on axial post-contrast T1-weighted image (**c**) and coronal T2 single shot fast spin echo image (**d**)

- **Fluoroscopy**
  - Historically was used in this setting; however, now infrequently used in modern practice (preference given to CT or MR enterography).
  - Could consider in practice areas with limited access to CT or MRI.

Basic Imaging Features

- **CT/MRI**
  - Wall thickening (Fig. 9.20)

    Segmental thickening can be circumferential or asymmetric.

Fig. 9.20 Crohn's disease: wall thickening (skip lesions, asymmetric thickening, pseudo-sacculations). Coronal (**a**) and axial (**b**) CT enterography images from a patient with Crohn's disease demonstrate some of characteristic features including asymmetric wall thickening (arrow), skip lesions (two different lesions seen on **a** and **b**). (**c**) A different patient with Crohn's disease demonstrating pseudo-sacculations (dashed arrow)

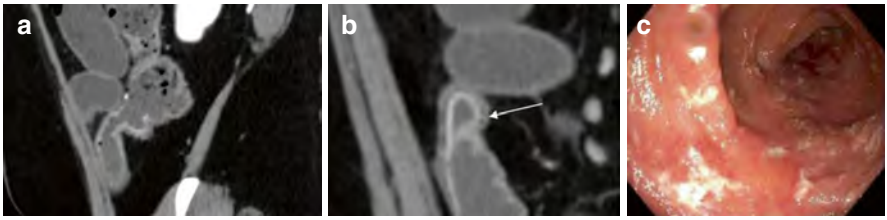

Fig. 9.21 32-yo with history of Crohn's disease, status post ileocecectomy 13 years ago. (**a**, **b**) Magnified CT images demonstrate active inflammation at the neo-terminal ileum, including focal submucosal enhancement (arrow), which is a CT feature that has been shown to correlate with active ulceration on endoscopy/pathology. (**c**) Subsequent colonoscopy demonstrated moderate congestion, acute inflammation, and ulceration

Skip lesions (multiple areas of segmental thickening with intervening normal bowel).

Areas of asymmetric thickening can be associated with pseudo-sacculation of the antimesenteric side.

– Wall hyperenhancement

Stratified enhancement includes enhancement primarily of the inner aspect (bilaminar) or combination of both the inner and outer wall (trilaminar or "targetoid") (Fig. e9.4) and can be due to acute inflammation (e.g., submucosal edema) or chronic changes (e.g., fibrosis, intramural fat deposition).

While homogeneous enhancement is more common, can see areas of ulceration with associated disruption of the mucosal-sided enhancement or focal submucosal enhancement (relatively specific for active Crohn's disease) (Fig. 9.21).

– Mesenteric fatty proliferation and vasa recta engorgement.

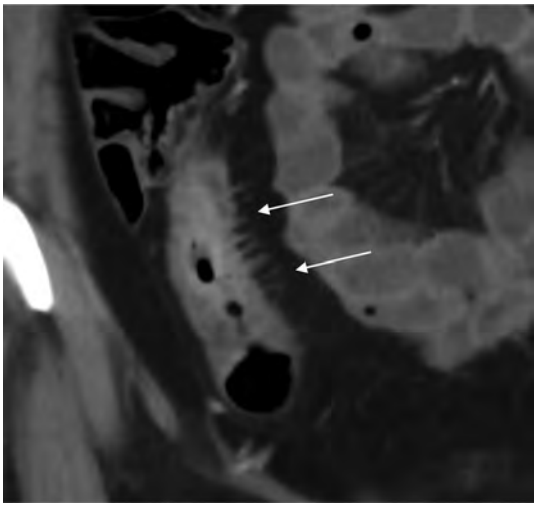

Fig. 9.22 Coronal CT image with IV contrast demonstrates the 'comb sign' (arrows), which is secondary to engorgement of the vasa recta associated with a segment of inflamed/thickened small bowel

Fibrofatty proliferation (i.e., "creeping fat") due to mesenteric fat hypertrophy adjacent to diseased bowel segments, resulting in displacement/spreading of the vessels and other structures.

Associated engorgement of the draining and feeding vessels (vasa recta) is also seen (i.e., "comb sign") (Fig. 9.22).

- **Fluoroscopy**
  - Mucosal ulcers on small bowel follow-through

    Can be shallow or deep.

    Multiple ulcers can give a cobblestone appearance due to longitudinal fissures and ulcers with "islands" or "stones" of retained mucosa.
  - Thickened folds.
  - Widely separated small bowel loops due to intervening fibrofatty proliferation.
  - Pseudo-sacculation due to contraction on the side of the ulceration and inflammation with dilatation and sacculation on the opposite, often antimesenteric, side.
  - Segmental area of luminal narrow due to the underlying stricture or spasm ("string sign").

Complications

- **CT/MRI**
  - Fistula

    Simple fistulas connect two structures and are named by the structures connected (enteroenteric, enterocutaneous, enterocolonic, etc.).

Fig. 9.23 Crohn's disease: simple fistulas. 20-yo with Crohn's disease complicated by multiple fistulas. (**a**) Axial CT image demonstrating perianal soft tissue thickening surrounding a tract of gas/fluid (arrow) consistent with perianal fistula. (**b**) Sagittal CT image with IV and oral contrast from a few years later demonstrates development of an enterocutaneous fistula as demonstrated by a linear area of oral contrast extending outside the bowel lumen (arrow) with continuation of a soft tissue tract to the cutaneous surface (dashed arrow). (**c**) Coronal CT image from a different patient with inflamed fistulous tract (arrow) connecting the terminal ileum (dashed arrow) and appendix (arrowhead)

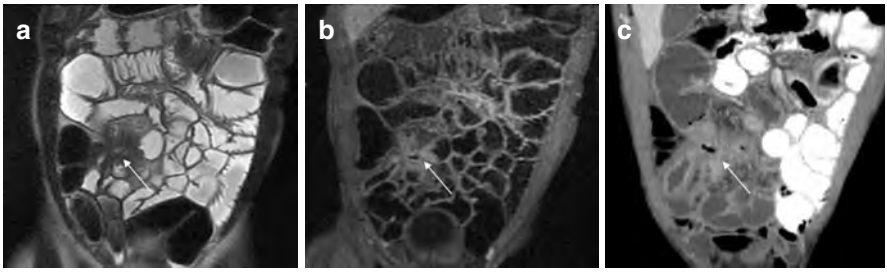

Fig. 9.24 Crohn's disease: complex fistula. Single shot fast spin echo (SSFSE) image (**a**), post-contrast T1-weighted image (**b**), and coronal CT enterography image (**c**) from the same patient demonstrates a complex fistula in the right abdomen with a stellate area of T2 dark (arrow in **a**) and enhancing (arrow in **b**, **c**) soft tissue surrounded by multiple loops of inflamed and tethered distal ileum (including the neo-terminal ileum). A small focus of gas can be seen centrally within the fistula on CT

Imaging demonstrates tubular soft tissue/enhancement connecting the two structures and possibly with associated air along the tract (Fig. 9.23).

Complex fistulas involve more than one fistulous connection and can lead to a star-shaped appearance of clustered bowel from combined fistulization and tethering (Fig. 9.24).

A sinus tract is a blind-ending tract arising from transmural penetration without connection to another structure.

Perianal fistula is a common and sometimes presenting complication of Crohn's disease (Fig. e9.5).

– Abscess

  Fluid collection with rim enhancement. Can be related to the underlying fistula/sinus tract (Fig. 9.25).

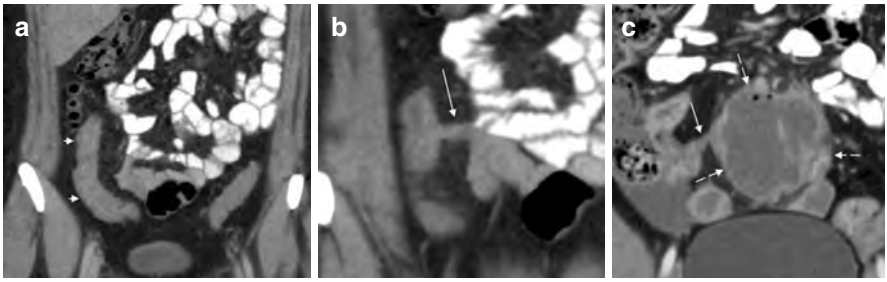

Fig. 9.25 Crohn's disease: sinus tract with eventual abscess. Coronal (**a**) and magnified coronal (**b**) images from a CT obtained with IV and oral contrast, in a 24-yo who initially presented with abdominal pain, demonstrate thickening of the terminal ileum (arrowheads) and adjacent tubular soft tissue tract extending medially (arrow), highly suspicious for sinus tract. Particularly given the presence of the sinus tract, the suspected diagnosis of Crohn's disease was raised. (**c**) Patient represented 2 months later with new abdominal pain and was found to have a fluid collection with few foci of gas and peripheral enhancing rim, consistent with abscess (dashed arrows), at the end of the prior sinus tract (arrow) on a follow-up CT with IV and oral contrast

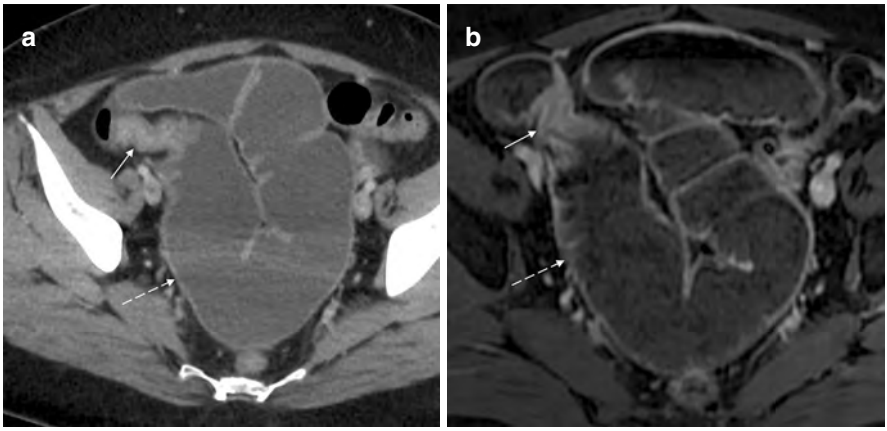

Fig. 9.26 Crohn's disease: stricture and SBO. CT enterography (**a**) and MR enterography post-contrast T1 (**b**) axial images from the same patient obtained 2 weeks apart demonstrate a short segment area of wall thickening and severe luminal narrowing (arrows) with upstream dilated small bowel (dashed arrows). These findings are consistent with fibrostenotic stricture and associated (recurrent partial) small bowel obstruction. Although areas of IBD-related luminal narrowing should always be described, a true stricture is best characterized in the setting of upstream dilatation

Inflammatory mass (defined as focal mesenteric inflammation without discrete fluid collection or wall).

– Stricture

  Bowel segment with focal luminal narrowing (>50% loss) and upstream dilatation or obstruction (Fig. 9.26).

  Look for penetrating disease (e.g., fistula, abscess, inflammatory mass), if stricture is present, as the two are often present simultaneously.

- **Fluoroscopy**
  - Fistula
    Seen as a tract of contrast extending from the small bowel.
    May see contrast fill or opacify the connected structure, such as adjacent colon, or collect in an adjacent abscess.
  - Abscess
    Primarily only seen on fluoroscopy if there is an associated active fistula connecting the bowel and abscess.
  - Stricture
    Seen as the "string sign."
    May see upstream obstruction or bowel dilatation.

Obstruction

Background

- Small bowel obstruction (SBO) is a common cause of acute abdominal pain and is a leading cause of emergency general surgery procedures.
- Imaging plays a very important role regarding triaging patients who may require emergent surgical management and defining the underlying cause.

Basic Imaging Features of SBO

- Dilated (3 cm or greater) small bowel loops with minimal air in the distal small bowel/colon.
- **Radiographs**
  - Multiple air-fluid levels on upright radiograph.
  - Uneven levels ("fighting loops") increase suspicion and are related to the underlying pressure that builds up in the obstructed and partially fluid-filled small bowel.
  - On supine radiographs, multiple dilated gas-filled loops of small bowel (often seen in the central abdomen) (Fig. 9.27).
  - Key diagnostic consideration is adynamic ileus, which will typically be more diffuse and often involve both dilatation of small bowel and colon (Fig. 9.28).
  - Differentiating between a partial small bowel obstruction and ileus can be difficult on imaging.
- **CT**
  - CT is highly sensitive for the presence of small bowel obstruction.
    This accuracy, as well as limitations in the accuracy of radiographs and limited ability to diagnose other conditions that can cause an acute abdomen, has resulted in the increased use of CT in the setting of suspected small bowel obstruction.

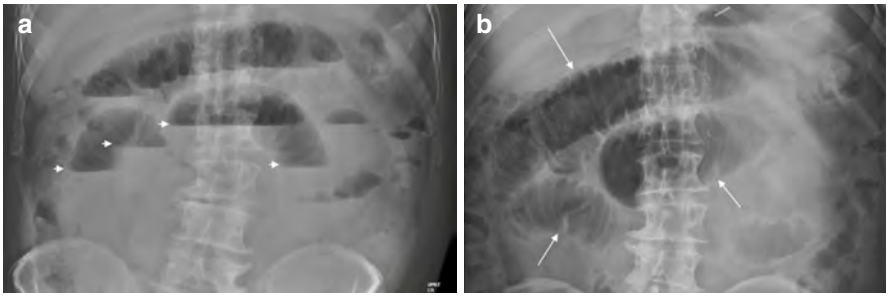

Fig. 9.27 SBO on radiographs. Upright (**a**) and supine (**b**) AP abdominal radiographs demonstrate some of the characteristic features of small bowel obstruction, including 'fighting loops' with differential air-fluid levels on upright (arrowheads) as well as dilated air/fluid filled small bowel (arrows) with relative decompression of the colon along the periphery

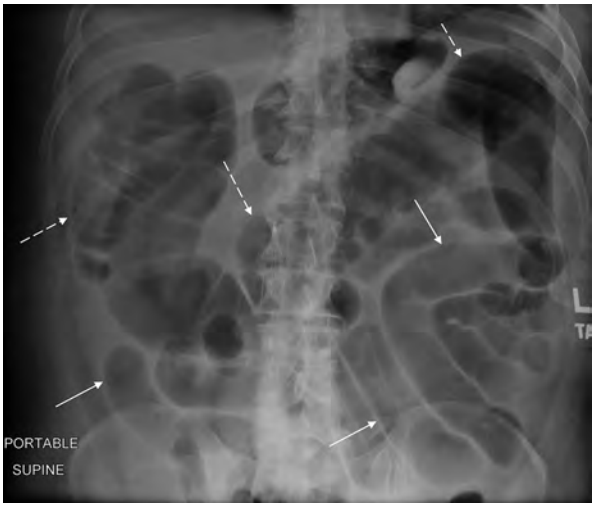

Fig. 9.28 Post-operative ileus on radiographs. Supine portable radiograph demonstrates gaseous dilatation of both small bowel (arrows), measuring up to 3.3 cm, and colon (dashed arrows), measuring up to 6.7 cm in a 68-yo patient who had recently underwent open bladder repair and placement of suprapubic catheter 3 days ago. Ileus was managed non-operatively and resolved prior to discharge

  - In addition to identifying the presence of SBO, CT can also identify the transition point/source of obstruction (Fig. 9.29).
  - Most common cause of obstruction is postoperative adhesion.
  - Small bowel feces sign: area of fecal material and locules of gas (giving the appearance of colonic stool) seen in SBO, often at the transition point.
    Correlates positively with partial SBO (Fig. 9.30).
- Water soluble contrast challenge [6]
  - Study involves the bedside administration of water-soluble contrast (e.g., Omnipaque, Gastrografin) through a nasogastric tube with subsequent radiographs to track transit (most commonly at 8 and 24 h).
  - Successful transit of contrast into the colon by 24 h has shown strong correlation with successful nonsurgical management of SBO (Fig. 9.31).

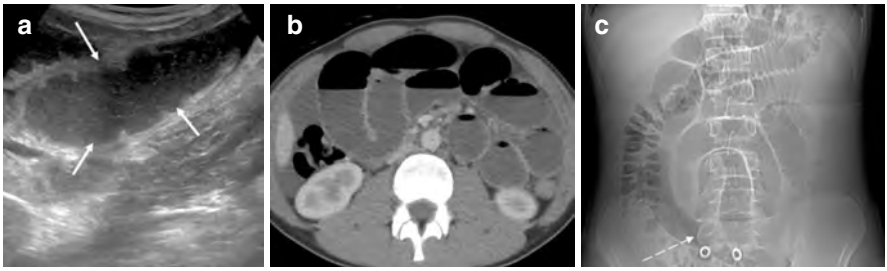

Fig. 9.29 SBO caused by ingested foreign body in a teenager presenting with abdominal pain. Initial ultrasound (**a**) demonstrated dilated, fluid filled small bowel (arrows). Subsequent CT with IV contrast (**b**, axial) with multiple dilated fluid and air-filled small bowel with relative colonic decompression. (**c**) CT scout image demonstrates dilated gas filled small bowel with a rounded density projecting over the midpelvis (dashed arrow) as the probable obstructive cause, which was found to be an ingested foam ball on surgical extraction

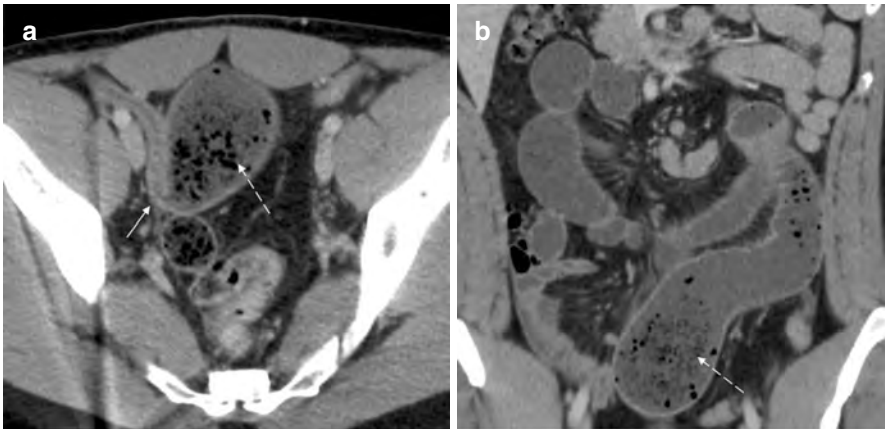

Fig. 9.30 25-yo with suspected adhesive, partial small bowel obstruction on CT. Axial (**a**) and coronal (**b**) CT images, obtained with IV and oral contrast, demonstrate dilated small bowel with focal transition point in the right pelvis (arrow). An associated small bowel 'feces sign', with fecalized material seen in the small bowel upstream to the obstruction, was noted (dashed arrow). This finding correlates positively with a partial obstruction

  - May have a therapeutic benefit due to the hyperosmolar nature of the administered oral contrast (controversial).
  - Once implemented, this can potentially replace the need for a fluoroscopic small bowel follow-through.

Complicated SBO

- **CT/MRI**
  - Gallstone ileus

Fig. 9.31 Successful water-soluble contrast challenge. Abdominal radiograph in the same patient as Fig. 9.30, which was obtained 8 h after the bedside administration of water-soluble contrast (as part of the WSC challenge). XR demonstrates successful transit of contrast into the colon with a small amount of contrast in the terminal ileum and some persistent mildly dilated small bowel loops. This type of 'successful' WSC challenge has been shown to accurately predict success of non-operative management, which was true in this case

Classic Rigler's triad: pneumobilia, small bowel obstruction, migrated gallstone seen in the small bowel lumen (Fig. 9.32).

Initial erosion of a gallstone into the small bowel (cholecystoduodenal fistula) (Fig. e9.6) and downstream transit resulting in eventual SBO.

– Hernia related

  Can be related to a variety of hernias (ventral, parastomal, umbilical, inguinal, femoral) (Fig. 9.33).

  May require surgical intervention if herniated bowel is nonreducible or incarcerated.

– Intussusception

  In pediatrics, intussusception without lead point mass is more common.

  In adults, the presence of an intussusception resulting in SBO should cause concern for underlying lead point mass (Fig. 9.34).

  Transient enteroenteric intussusception is commonly seen incidentally on CT and will not be associated with upstream dilatation or obstruction.

– Closed-loop SBO

  Surgical emergency due to vascular compromise of the involved bowel (due to both afferent and efferent obstruction).

  Key features

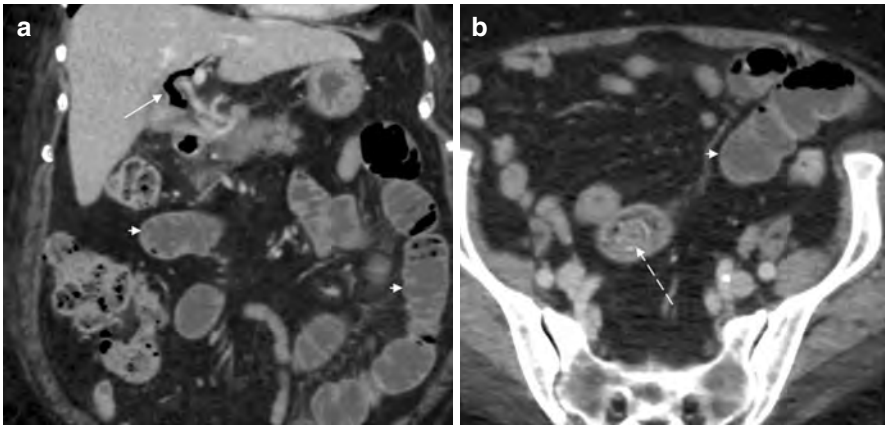

Fig. 9.32 73-yo with gallstone ileus. Coronal (**a**) and axial (**b**) CT images with IV contrast demonstrate the classic triad of gallstone ileus: pneumobilia (arrow), dilated small bowel (arrowheads), and obstructing/migrated gallstone, seen in this case as a rounded intraluminal structure with concentric hyperattenuating rings (dashed arrow)

Fig. 9.33 Hernia related small bowel obstructions. (**a**–**c**) Coronal (**a**), sagittal (**b**), and magnified axial (**c**) images from a CT with IV contrast in a 56-yo with abdominal pain demonstrate a SBO with transition point associated with the neck of a small umbilical hernia (arrows). Dilated fluid filled small bowel loop was seen in the hernia sac with normal enhancement and wall thickness; however, associated fluid in the hernia sac (arrowhead in **b**) and non-reducible on examination would raise concern for incarceration and risk for bowel compromise. (**d**–**f**) Coronal (**d**) and magnified axial (**e**, **f**) images from a CT with IV contrast in an 81-yo with abdominal and left groin pain demonstrate a SBO with transition point in the left groin (arrow in **d**). Differentiating an inguinal from femoral hernia can be difficult on imaging; however, positioning of the hernia lateral to the pubic tubercle (demarcated by arrowhead) and compression of the femoral vein (dashed arrow), both of which were present in this case, are more suggestive of femoral. Femoral hernia was confirmed in intraoperatively

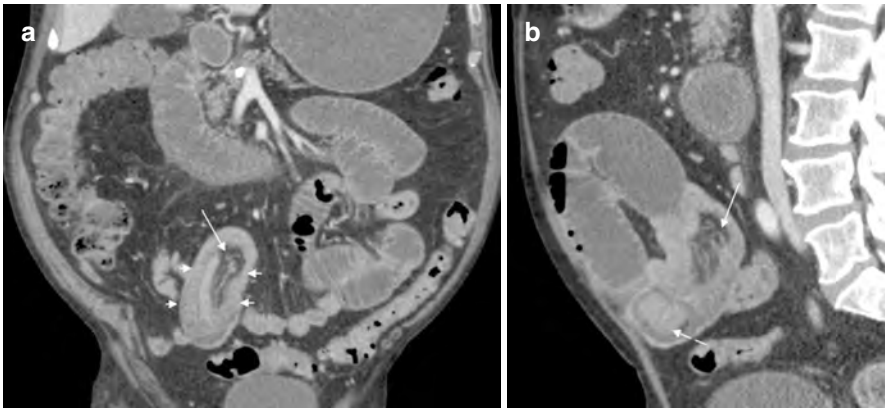

Fig. 9.34 71-yo with intussusception and small bowel obstruction due to lead point bowel mass. Coronal (**a**) and sagittal (**b**) images from a CT with IV contrast demonstrate characteristics features of intussusception including a central area of mesenteric fat and vessels centrally (arrows) within the lumen of the small bowel with thickening at the periphery, due in part to the presence of two layers of bowel wall (arrowheads in **a**). Upstream fluid filled small bowel is noted, consistent with small bowel obstruction. Additionally, there is a subtle rounded enhancing soft tissue mass at the lead point of the intussusception (dashed arrow), pathologically proven to be metastatic melanoma on small bowel resection

    - Two adjacent transition points with intervening dilated (and often fluid-filled SB).
    - U-shaped or balloons on a string appearance of the bowel loops.
    - Narrowed or whirl sign of the associated mesenteric vessels.
    - Focal edema in the associated mesentery (Fig. 9.35).

    Can be due to adhesions or internal hernia (Fig. 9.36).
- **Radiographs**
  - Abdominal radiographs have very limited sensitivity or specificity for complex small bowel obstructions.
  - Gallstone ileus

    Rarely may see pneumobilia and rounded obstructing leadpoint/gallstone.
  - Hernia related

    Rarely may see bowel gas within the herniated loop, such as within the groin region for an inguinal or femoral hernia.
  - Intussusception

    May see a rounded opacity at the site of obstruction, with upstream gas-filled dilated bowel, caused by the intussusecipiens (i.e., intussuscepting portion of bowel).
  - Closed-loop obstruction

    Lack of small bowel gas on radiograph can suggest possible high-grade or closed-loop obstruction, although this has limited specificity as a paucity of small bowel gas can also be seen due to variation in normal bowel distension or due to obscuration from overlying soft tissue as well as the presence of ascites.

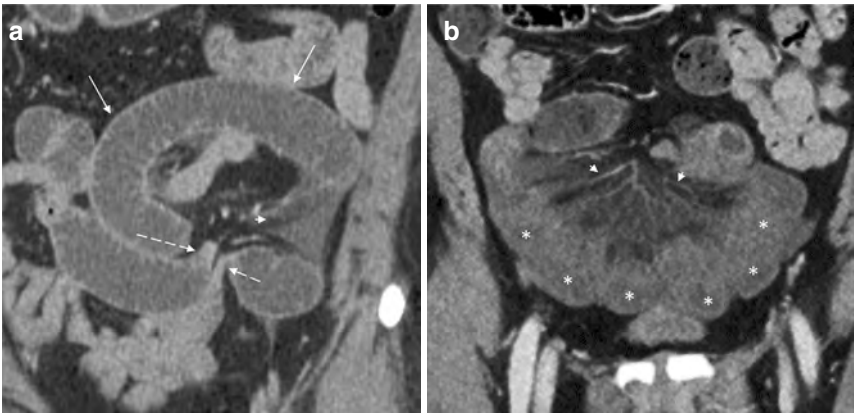

Fig. 9.35 Closed loop obstruction. (**a**) Coronal CT image with IV contrast demonstrates some of the characteristic features of closed loop obstruction, such as (1) C-shaped fluid filled small bowel loop (arrows), (2) two immediately adjacent transition points (dashed arrows), and associated mesenteric edema (arrowhead). (**b**) Coronal CT image with IV contrast in a different patient with closed loop obstruction demonstrates radiating small bowel loops (arrows), with central mesenteric edema and the stretched mesenteric vessels (arrowheads) leading toward a central point ('balloons-on-a-string' sign). The small bowel walls are somewhat indistinct due to edematous thickening and possible associated hypo enhancement

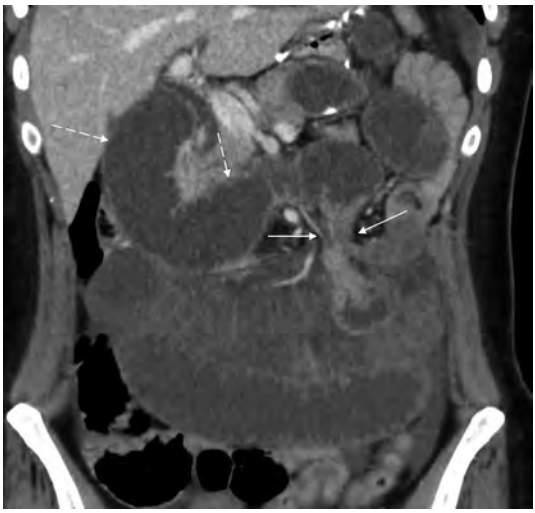

Fig. 9.36 Closed loop obstruction from internal hernia. 43-yo with history of Roux-en-Y gastric bypass, presented with acute onset severe abdominal pain. Coronal image from a CT with IV contrast demonstrated features of closed loop obstruction due to herniation of small bowel through a mesenteric defect next to the jejunojejunostomy (arrows) with resultant dilated fluid filled small bowel in the central abdomen. Upstream dilatation of the biliopancreatic limb was also present (dashed arrows)

Tumors

Key Diagnostic Features

- Location is a key characteristic to assist with differential (Fig. 9.37)
  - Mucosa/submucosa—adenoma, hamartoma, lipoma, adenocarcinoma, and metastatic disease.
  - Serosal—neuroendocrine tumor, endometriosis, and metastatic disease.
  - Exophytic—gastrointestinal stromal tumor.
  - Proximal—adenocarcinoma (duodenum, proximal jejunum).
  - Distal—lymphoma and neuroendocrine tumor (ileum).
- Additional characteristics include homogeneous versus heterogeneous enhancement; calcifications; solitary or multiple; and associated abnormalities (e.g., lymphadenopathy, metastatic disease).

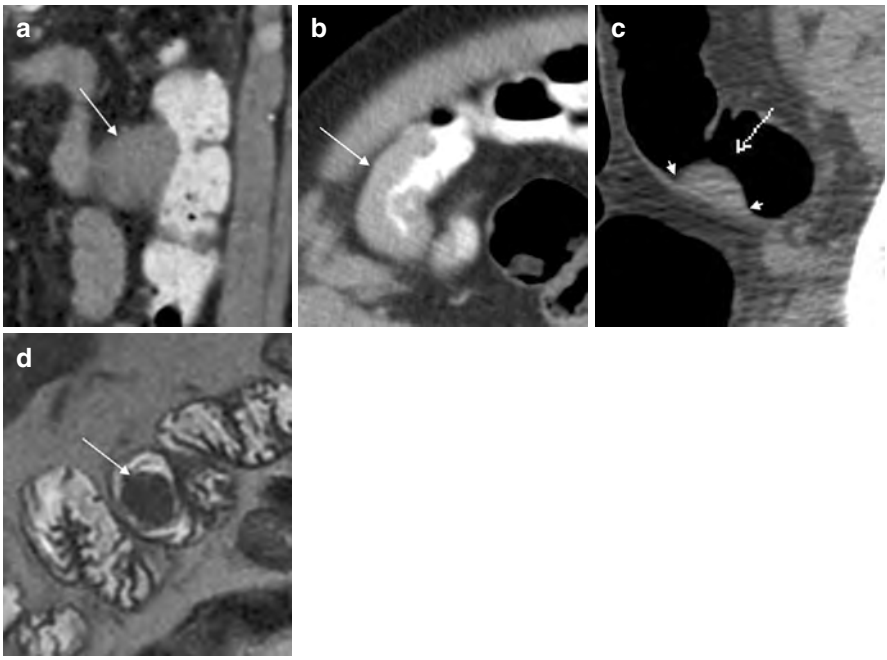

Fig. 9.37 Bowel mass locations. (**a**) CT with oral contrast image demonstrates an exophytic small bowel mass (arrow), well seen given the distension of the adjacent bowel with oral contrast. (**b**) CT with oral contrast demonstrates irregular mass-like thickening of the bowel wall, suggesting a possible intramural mass (arrow). (**c**) Submucosal mass is seen within a gas filled loop of small bowel. Notice the flat angle between the bowel wall and the mass (arrowheads) giving it a 'ball under the rug' like appearance. (**d**) Magnified single shot fast spin echo (SSFSE) image demonstrates a rounded intraluminal mass (arrow) surrounded by hyperintense fluid in the bowel lumen

Benign Small Bowel Masses

- Hamartoma
  - Can be seen in isolation or associated with polyposis syndromes (e.g., Peutz–Jager).
  - Small risk of malignant potential.
  - Peutz–Jager: autosomal-dominant; carries increased risk of intestinal adenocarcinoma as well as other nongastrointestinal tumors (Fig. 9.38).
  - Imaging features

    CT/MRI
    - Polypoid, enhancing soft-tissue mass often either located in the lumen or mucosal/submucosal.
    - No aggressive features or findings of invasion.
    - Can be solitary or multiple (polyposis).
    - Depending on luminal distension may not be well seen on imaging.

    Fluoroscopy
    - Smooth intraluminal filling defect(s).
- Adenoma
  - Usually solitary (Fig. 9.39); multiple in polyposis syndromes (e.g., familial adenomatous polyposis).
  - Carries risk of eventual malignant degeneration.
  - Most common location is in the duodenum.
  - Imaging features

    CT/MRI
    - Polypoid, enhancing soft-tissue mass often either located in the lumen or mucosal/submucosal.
    - No aggressive features or findings of invasion.

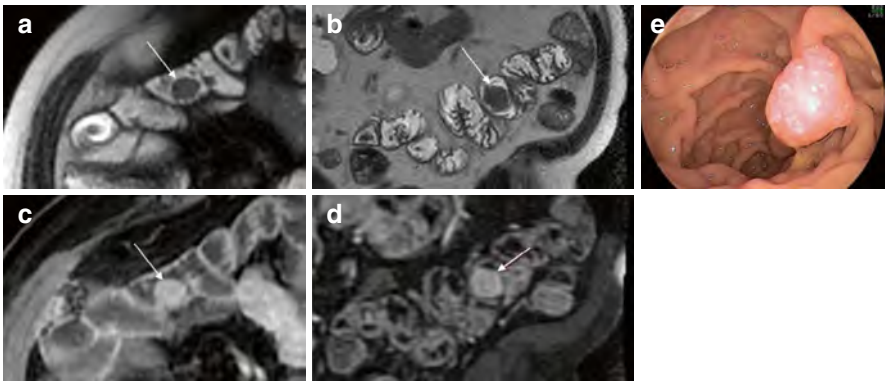

Fig. 9.38 Abdominopelvic MRI demonstrates multiple mucosal hamartomatous polyps in a patient with Peutz-Jager. T2-weighted (**a**), single shot fast spin echo (**b**), and post-contrast T1 (**c**, **d**) demonstrate two different luminal masses, both demonstrating intermediate T2 signal and post-contrast enhancement (arrows). (**e**) Endoscopic image of one of the polyps

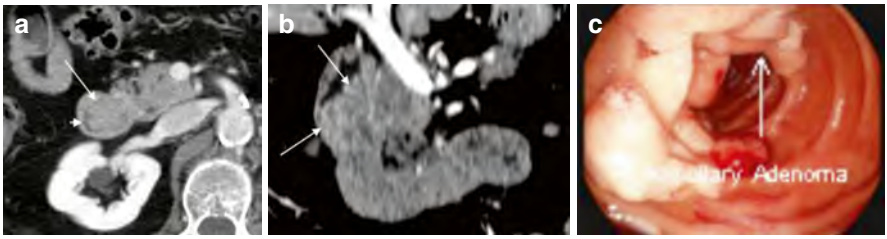

Fig. 9.39 69-yo with polypoid duodenal/ampullary mass; found to be adenoma on biopsy. (**a**) Axial CT image with IV contrast demonstrates a subtle area of nodular soft tissue (arrow) that appears to be in the duodenal lumen, given the cleft of fluid (arrowhead) seen around the lateral and posterior margins. (**b**) Reformatted coronal image redemonstrates abnormal nodular soft tissue (arrows) in the region of the ampulla. Endoscopy was recommended and subsequently performed, confirming the presence of a lobular, smooth soft tissue mass (**c**) that was found to be a benign adenoma on biopsy

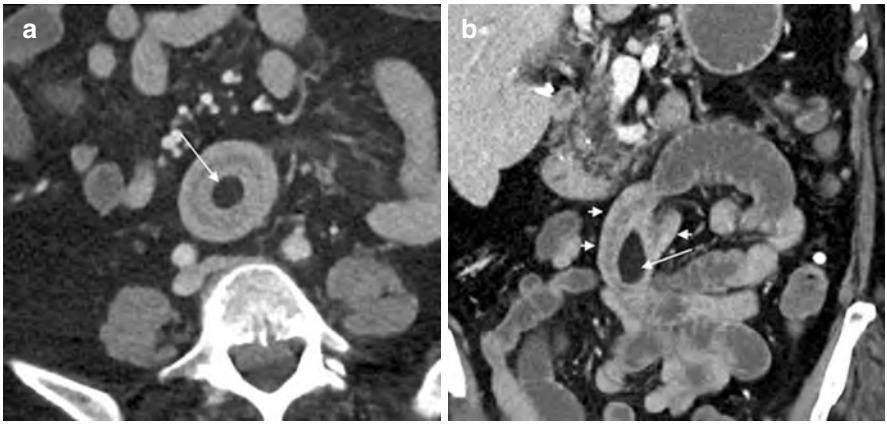

Fig. 9.40 Small bowel lipoma, causing intussusception. Axial (**a**) and coronal (**b**) CT image with IV contrast demonstrate a short segment intussusception (arrowheads) with central fat density lenticular mass (arrow), consistent with a benign lipoma, that is the lead point for intussusception. Small bowel lipomas are often either sub-mucosal or pedunculated in location. The axial image demonstrates the classic target appearance of intussusception

    - Can be solitary or multiple (polyposis).
    - Depending on luminal distension may not be well seen on imaging.

    Fluoroscopy
    - Smooth intraluminal filling defect(s).

- Lipoma
  - Fat density mass on imaging, arising in the submucosa or pedunculated.
  - No malignant potential.
  - Many are asymptomatic, although can be a cause of intussusception and/or intermittent obstruction (Fig. 9.40).
  - Imaging features

CT/MRI
- Smooth fat density mass.
- CT: negative attenuation consistent with macroscopic fat.
- MRI: demonstrates high signal on non-fat-saturated T1 and T2 with loss of signal on fat-saturated images due to its macroscopic fat.
- No aggressive features or enhancing soft tissue.

Fluoroscopy
- Smooth intraluminal filling defect.
- Fat density may be difficult to identify fluoroscopically.

Malignant Small Bowel Masses

- Adenocarcinoma
  - Heterogeneous soft-tissue enhancement, short-segment thickening or focal mass.
  - Usually seen in the proximal jejunum or duodenum (Fig. 9.41).
  - Primarily endophytic/luminal, but can have exophytic invasion and associated metastatic disease.
  - Imaging features

    CT/MRI
    - Enhancing soft-tissue mass, often with heterogeneous enhancement.
    - When small will often be seen as a plaque-like, flat mass along the luminal side; however, as they get larger will see evidence of extension outside of the bowel and possible invasion of adjacent structures.
    - Can be difficult to see in decompressed bowel so the administration of oral contrast, either positive or negative, may assist with identification.
- Neuroendocrine (Fig. 9.42)
  - Can occur anywhere but most often ileal.
  - Can range from well-differentiated tumor to poorly differentiated cancer.

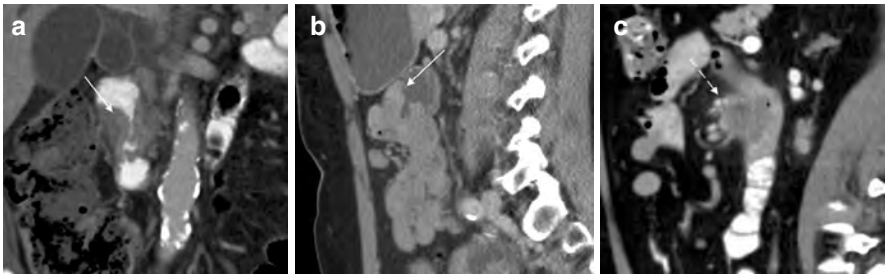

Fig. 9.41 Three examples of small bowel adenocarcinoma, all in the duodenum/jejunum. Coronal (**a**) and sagittal (**b**, **c**) images from three different patients demonstrating proximal small bowel masses. Each mass demonstrates an irregular appearance. The masses in the first two patient are more circumferential and luminal (arrow), while the mass in the third patient (**c**) is partially exophytic (dashed arrow)

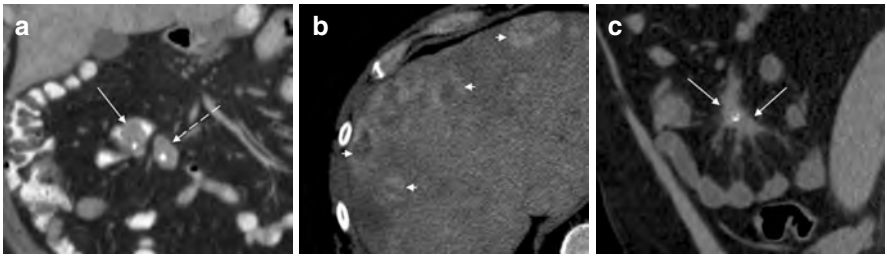

Fig. 9.42 Ileal neuroendocrine tumor. (**a**, **b**) CT coronal and axial images from a patient with metastatic neuroendocrine tumor with primary partially luminal and partially exophytic ileal soft tissue mass (arrow), adjacent mesenteric metastatic lymphadenopathy (dashed arrow), and liver metastases (arrowheads). (**c**) Coronal image from a non-contrast CT, in a different patient, demonstrates the classic calcified spiculated mesenteric metastasis (arrows), biopsy proven to be a neuroendocrine metastasis

- "Carcinoid" syndrome
  A set of symptoms, including flushing, diarrhea, and wheezing that occur due to secretion of serotonin.
  Only present in the setting of liver metastases.
- Imaging findings
  CT/MRI
  - May not see primary mass, but may demonstrate arterial hyperenhancement if present.
  - Often more homogeneously enhancing, particularly when small.
  - Classic finding is calcified, spiculated mesenteric lymph node metastases.
  - Liver metastases are also common and can be seen both with well-differentiated and poorly differentiated subtypes.

  Fluoroscopy
  - Utility limited by the inability to see metastatic disease and the often distal location of the primary tumor.
  - Primary mass could be seen as distal small bowel filling defect.

- Lymphoma
  - Bowel involvement can be primary or a component of more diffuse disease.
  - Diffuse large B-cell and follicular subtypes are the most likely to involve the small bowel.
  - Imaging features
    CT/MRI
    - Irregular wall thickening of the small bowel.
    - Often with multiple sites of disease, including multifocal bowel involvement and associated lymphadenopathy as well as possibly solid organ involvement.
    - Degree of enhancement and wall thickening is often greater than other tumors.

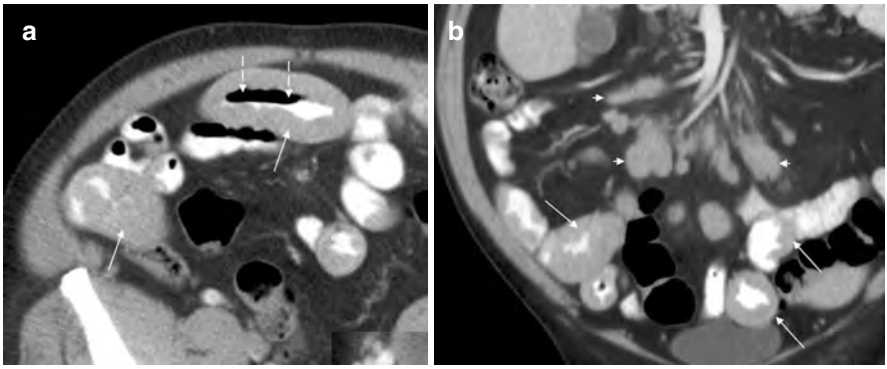

Fig. 9.43 Small bowel lymphoma. Axial (**a**) and coronal CT images with oral and IV contrast show multifocal irregular soft tissue small bowel wall thickening (arrows). One loop demonstrates the classic aneurysmal dilatation of the bowel lumen (dashed arrows), which is characteristic for bowel lymphoma given the associated disruption of the muscularis layer. Associated mesenteric lymphadenopathy is also supportive (arrowheads) (**b**). Subsequent biopsy was consistent with MALT lymphoma

    - Aneurysmal dilatation of the lumen, without associated obstruction, is classic (due to malignant infiltration into the muscular layers of the bowel wall).
  - MALT lymphoma: subtype arising from the mucosa-assisted lymphoid tissue (MALT) that tends to be more indolent, with similar imaging findings (Fig. 9.43).
- Post-transplant lymphoproliferative disease (PTLD)
  - Imaging findings

    CT/MRI: similar imaging findings to bowel lymphoma, except more likely to have associated ulceration and can result in perforation (Fig. e9.7).
  - PTLD is an uncommon complication of transplantation (common sites include the allograft and bowel involvement).
- GIST
  - Imaging findings

    CT/MRI: exophytic heterogeneous mass (often has calcifications and/or necrosis) (Fig. 9.44).
  - Benign more common than malignant but has "malignant potential" so surgical excision is the preferred treatment.
- Metastatic disease
  - Common sources include lung cancer, melanoma, and breast cancer.
  - Direct invasion can occur from colorectal cancer and ovarian cancer.
  - Imaging findings

    CT/MRI:
    - Given the possibility of hematological spread can be luminal, intramural, or serosal.

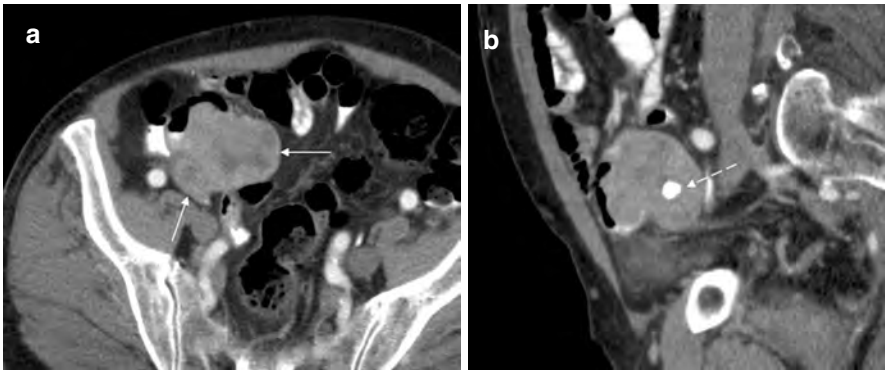

Fig. 9.44 Small bowel GIST. Axial (**a**) and sagittal (**b**) CT images with IV and oral contrast demonstrate an exophytic, heterogenous attenuating (enhancing) soft tissue mass (arrows, **a**) with rounded calcification (dashed arrow, **b**). Small bowel GIST can also demonstrate necrotic components

- Overall findings are nonspecific and could be solitary or multifocal bowel masses or irregular short-segment wall thickening.

Trauma

Background

- Given an increasing trend toward nonoperative management of solid organ injuries (depending on severity), there is a greater emphasis on the detection of bowel or mesenteric injuries since if present these might necessitate surgical management.
- Bowel and mesenteric injuries can be very difficult to detect on CT with low sensitivity and variable specificity of many of the findings.
- In recent years, a majority of trauma imaging occurs with only intravenous contrast (i.e., without oral or rectal contrast).
- However, if there is a high level of suspicion for bowel injury, oral contrast can be especially helpful either as part of the initial trauma work-up or during a subsequent follow-up scan.

Bowel Injury

- Imaging findings
  - **CT**

    The most common findings include wall thickening, hyper-/hypo-enhancement.

    Discrete bowel wall discontinuity is one of the most specific signs of bowel injury but is uncommonly seen (Fig. 9.45).

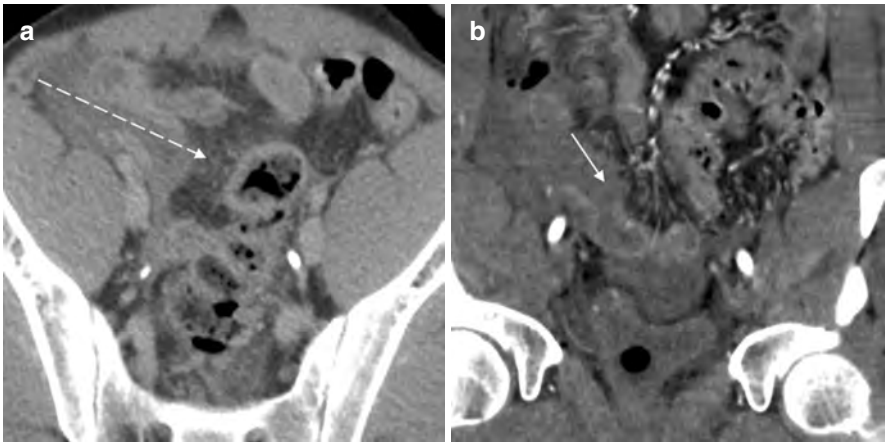

Fig. 9.45 Small bowel penetrating traumatic injuries in a 26-yo presented after multiple gunshot wounds. Axial (**a**) and oblique coronal (**b**) delayed CTA images demonstrate penetrating injuries into the abdomen, including transmural injury to the distal ileum (Trajectory traversing the bowel shown on **a**). Focal discontinuity and adjacent pelvic free fluid shown in **b** (arrow)

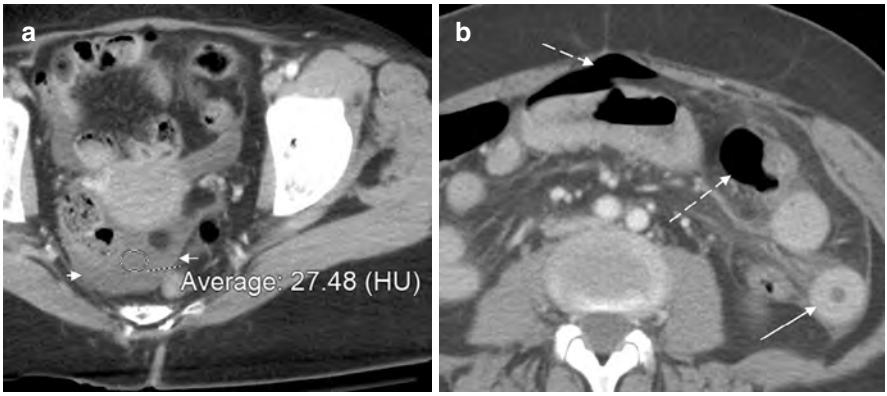

Fig. 9.46 Small bowel blunt traumatic injury. 58-yo presents after MVC with seatbelt sign, abdominal tenderness on exam. (**a**, **b**) Axial CT images with IV and without oral contrast demonstrates hemoperitoneum (best seen in the pelvis, arrowheads) as well as pneumoperitoneum (dashed arrows) localized around a thickened loop of proximal jejunum (arrow) in the upper abdomen. Associated mesenteric fluid. Transmural jejunal injury (30 cm from the ligament of Treitz) found intraoperatively

When oral contrast is administered, the presence of extraluminal contrast is also specific for bowel injury, although this also has a relatively low sensitivity.

Pneumoperitoneum, or extraluminal gas, is suspicious for bowel injury in the setting of blunt trauma (Fig. 9.46); however, in the setting of penetrating trauma, it is a nonspecific finding.

- **MRI**
  Limited use in the setting of acute trauma.
- **Radiographs**
  Suboptimal for trauma evaluation and, therefore, abdominal radiographs are not typically recommended or obtained for the work-up of trauma.
  If obtained, findings might include pneumoperitoneum as well as possibly metallic foreign bodies, especially in the setting of penetrating trauma.

Mesenteric Bleed

- CT findings
  - Hemoperitoneum, without obvious solid organ injury, raises suspicion for underlying bowel and/or mesenteric injury (Fig. 9.46). Blood products will typically have an attenuation above simple fluid (i.e. >15 HU), although the actual value can depend on a variety of factors such as age of blood products and location of hemorrhage.
  - Mesenteric hematoma is a distinct entity from hemoperitoneum and is seen as a triangular-/angular-shaped area of hemorrhage contained within the mesentery. If present, this should raise a high level of suspicion for associated bowel/mesenteric injury (Fig. 9.47).
  - If significant vascular injury is present, there may be changes in the downstream bowel with abnormal enhancement and associated wall thickening or thinning (Fig. 9.48).

Fig. 9.47 Mesenteric hematoma. CT axial image with IV contrast demonstrates a triangular shaped collection of high density fluid in the mesentery (arrow) consistent with a mesenteric hematoma. This finding as well as the associated small bowel wall thickening (arrowhead) and free air (dashed arrow) is highly concerning for bowel and mesenteric injury. A rent in the jejunal mesentery with active bleeding and associated transmural bowel injury was seen intraoperatively

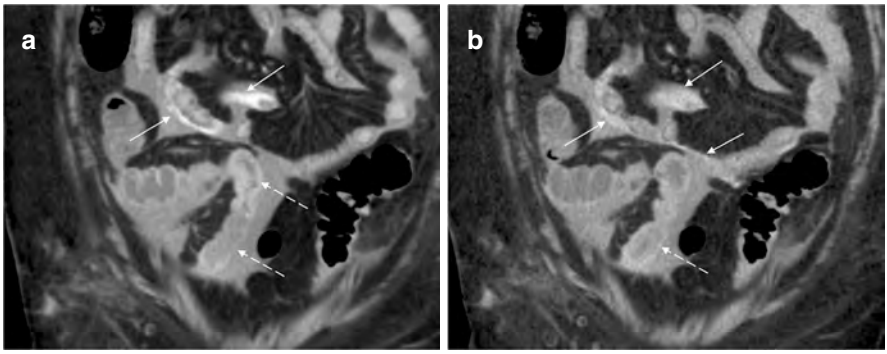

Fig. 9.48 Active mesenteric bleeding after motor vehicle collision. Coronal images from the arterial (**a**) and delayed (**b**) phase of a CT angiograph demonstrates extensive hemoperitoneum and mesenteric blood with an area of extravasated contrast (arrows) the expands and redistributes on delayed phase (arrows), consistent with active mesenteric bleeding. Adjacent thickening and hypo- or hyper-enhancing bowel was seen (dashed arrows). Intraoperatively, active bleeding from an ileal branch of the ileocolic artery was found and 30 cm of small bowel had to be resected due to mesenteric avulsion

Ischemia

Background

- Dominant vascularity to/from small bowel is through the superior mesenteric artery (SMA) and superior mesenteric vein (SMV).
- Main categories include arterial (embolic and thrombotic) and venous mesenteric ischemia.
- Ideal imaging includes multiphase contrast-enhanced CT. Oral contrast is not utilized to optimize evaluation of bowel wall enhancement.

CT/MRI

- Common imaging features
  - Can initially include hyperenhancement and thickening with progression to hypoenhancement/nonenhancement and thinning.
  - Bowel wall pneumatosis and portal venous gas are suspicious for significant bowel ischemia (Fig. 9.49).
  - Eventually ischemia can lead to perforation.
- Specific imaging features of arterial ischemia
  - Leads to lack of inflow to the small bowel, resulting in hypo- or nonenhancing bowel and a relative lack of associated edematous finding (Fig. 9.50).
  - Key feature is evidence of occluded feeding arteries (best seen with CTA) (Fig. 9.51).

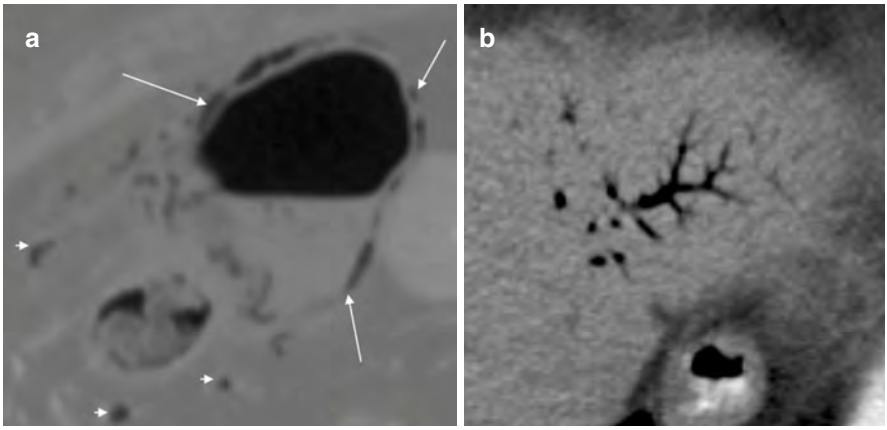

Fig. 9.49 Pneumatosis and portal venous gas in the setting of acute mesenteric ischemia. (**a**) Magnified axial CT image that has been windowed to accentuate air demonstrates pneumatosis as linear gas along the periphery of the bowel circumferentially (arrows). Venous gas in the draining veins (arrowheads) surrounding the cecum and terminal ileum is also seen. (**b**) Portal venous gas in the same patient is seen as branching, linear gas in the peripheral liver

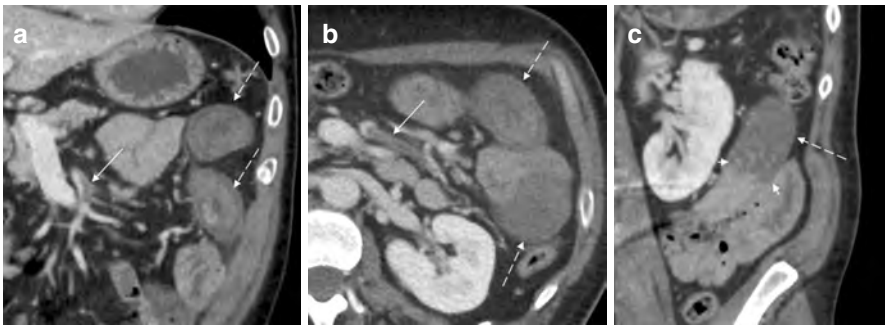

Fig. 9.50 Arterial small bowel mesenteric ischemia. Coronal (**a**, **c**) and axial (**b**) images from a CT angiogram in a 47-yo presenting with acute abdominal pain. Focal occlusion of jejunal SMA branches (arrow in **a**, **b**) is seen, likely embolic given the more distal location. Multiple downstream loops of abnormal small bowel are seen in the left abdomen, with circumferential thickening and varying degrees of hypo enhancement (dashed arrows), which is highly concerning for ischemic bowel when seen. A clear demarcation between the normally and hypo enhancing bowel is shown in **c** (arrowheads). The patient underwent successful emergent open endarterectomy and no bowel resection was required

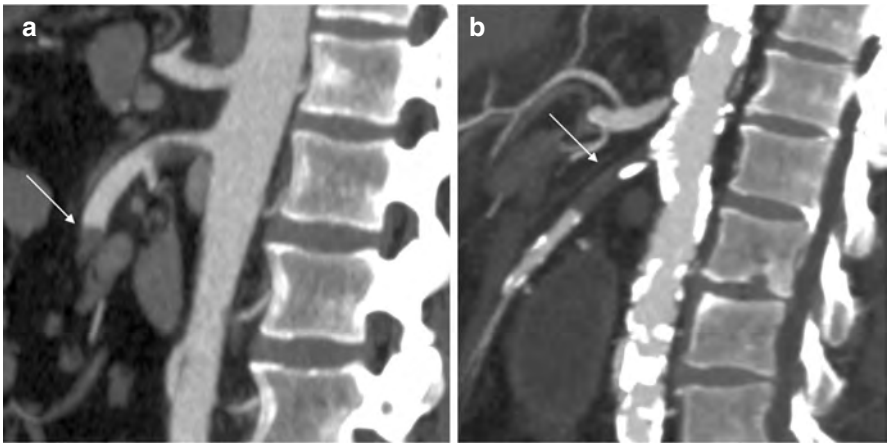

Fig. 9.51 Embolic versus thrombotic arterial occlusion. (**a**) Sagittal MIP from a CT angiograph demonstrates an embolic occlusion (arrow) of the SMA a few centimeters from the origin. Partial narrowing at the origin is also seen. (**b**) Sagittal MIP for a CT angiograph in a different patient demonstrates thrombotic occlusion starting at the SMA origin and extending for a few centimeters (arrow). Extensive background calcified atherosclerotic plaque is seen throughout the abdominal aorta and extending to the SMA

Embolic arterial mesenteric ischemia often occurs more distally and at branch points.
Thrombotic arterial mesenteric ischemia often occurs close to the origin of the SMA.
Embolic cause is more likely.

- Specific imaging features of venous ischemia
  - Often caused by massive thrombus within the superior mesenteric (and possibly portal) venous system, given the relatively robust collaterals available.
  - Venous ischemia is more likely to be associated with signs of congestion, including mesenteric edema and edematous (targetoid) bowel wall thickening (Fig. 9.52).
  - Thickening of the bowel wall is often present, at least initially.
- Complications of ischemia
  - Perforation: persistent or severe ischemia can result in necrosis and subsequent perforation of the bowel wall.
  - Fistulization: ischemia, possibly accompanied with reperfusion, can result in fistulation between adjacent bowel loops secondary to breakdown of the intervening wall (Fig. 9.53).

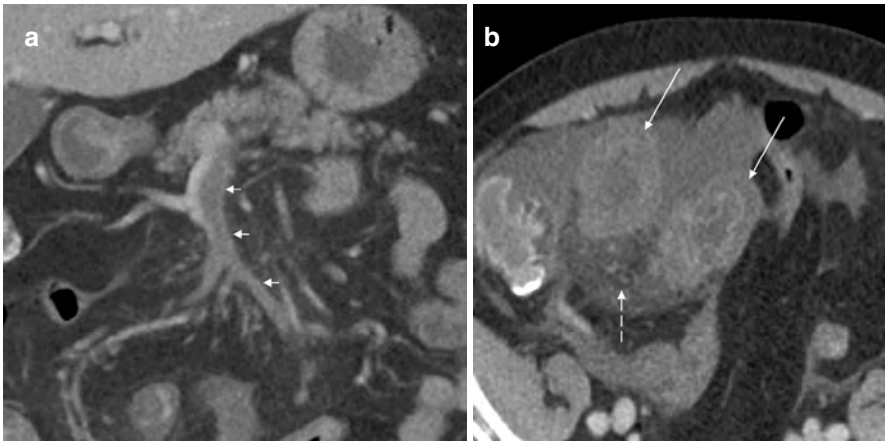

Fig. 9.52 Venous mesenteric ischemia. Coronal (**a**) and axial (**b**) CT images with IV contrast in a 65-yo with history of bilateral lung transplantation, presented acutely with SMV thrombus and associated venous mesenteric ischemia. (**a**) Extensive occlusive clot in seen in the SMV (arrowheads). (**b**) Classic congestive features of venous ischemia, due to 'outflow obstruction' were noted in the bowel, including edematous, thickened bowel wall (arrows) with associated mesenteric congestion (dashed arrow) and ascites. The patient was successfully managed nonsurgically with anticoagulation

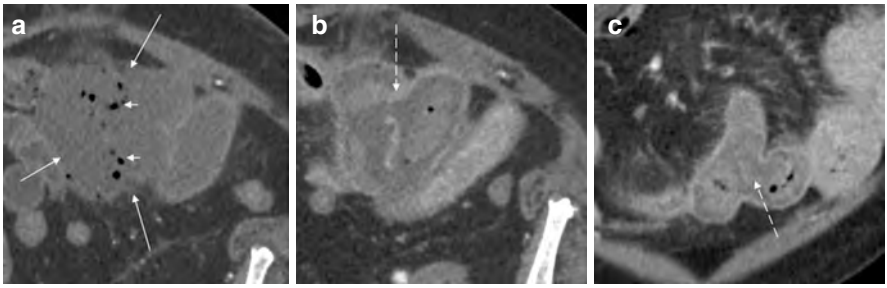

Fig. 9.53 Enteroenteric fistula that developed as a complication to chronic mesenteric ischemia after revascularization. (**a**) Arterial phase CT image from CT angiogram, obtained due to suspicion for chronic mesenteric ischemia, demonstrated a cluster of abnormal small bowel loops in the anterior abdomen, including hypo enhancing and indistinct walls (arrows) as well as associated pneumatosis (arrowheads). (**b**, **c**) Axial and coronal portal venous phase CT images from a follow-up study obtained after revascularization demonstrates improved enhancement of the majority of the bowel wall but with multiple fistulous connections between the adjacent loops (dashed arrows)

References

1. Webb RW, Brant WE. Fundamentals of body CT. 5th ed. Philadelphia: Elsevier/Saunders; 2020.
2. Pickhardt PJ, Arluk GM. Atlas of gastrointestinal imaging: radiologic-endoscopic correlation. 1st ed. Philadelphia: Elsevier/Saunders; 2007.
3. Macari M, Megibow AJ, Balthazar EJ. A pattern approach to the abnormal small bowel: observations at MDCT and CT enterography. Am J Roentgenol. 2007;188:1344–55.
4. Levine MS, Ramchandani P, Rubesin SE. Practical fluoroscopy of the GI and GU tracts. 1st ed. Cambridge: Cambridge University Press; 2012.
5. Guglielmo FF, et al. Small bowel Crohn disease at CT and MR enterography: imaging atlas and glossary of terms. Radiographics. 2020;40:354–75.
6. Lawrence EM, Pickhardt PJ. Evaluating suspected small bowel obstruction with the water-soluble contrast challenge. Br J Radiol. 2022;95(1130):20210791.

The Colon and Appendix

10

Anugayathri Jawahar

Optimal Imaging Studies for the Colon and Appendix

Radiographs

- Abdominal radiographs are often performed on an adult patient presenting to the emergency room with bloating, abdominal distension, and abdominal pain.
- Other common indications related to the colon include assessing the evolution of partial bowel obstructions, retained foreign bodies (Fig. e10.1), and assessing colonic stool burden (Fig. 10.1).
- Radiographs are usually performed as a single-view anteroposterior (AP) view of the supine abdomen for most indications. However, other views, such as upright and lateral decubitus, can be obtained in patients suspected of pneumoperitoneum (Figs. e10.2 and e10.3).
- Radiographs have high specificity for pneumoperitoneum but have low sensitivity, especially when the pneumoperitoneum is small. On the contrary, CT has a high sensitivity for pneumoperitoneum.
- Radiographs are lower-cost examinations with reduced radiation doses compared to CT.
- **Limitation**: Although reduced radiation, these are avoided in pregnant patients.

Supplementary Information The online version contains supplementary material available at https://doi.org/10.1007/978-3-031-76624-4_10.

A. Jawahar (✉)
Department of Radiology, Northwestern University-Feinberg School of Medicine, Chicago, IL, USA

© The Author(s), under exclusive license to Springer Nature Switzerland AG 2024

T. Catanzano (ed.), *What Radiology Residents Need to Know: Abdominal Radiology*, What Radiology Residents Need to Know,
https://doi.org/10.1007/978-3-031-76624-4_10

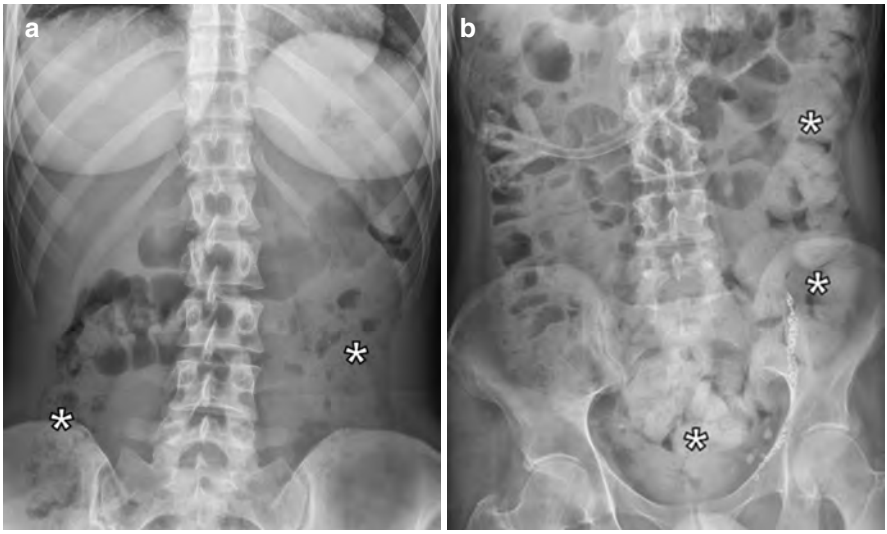

Fig. 10.1 (**a**, **b**) AP radiographs of the abdomen and pelvis performed in patients with constipation to assess stool burden. The images demonstrate moderate to large stool burden within the colonic loops (*)

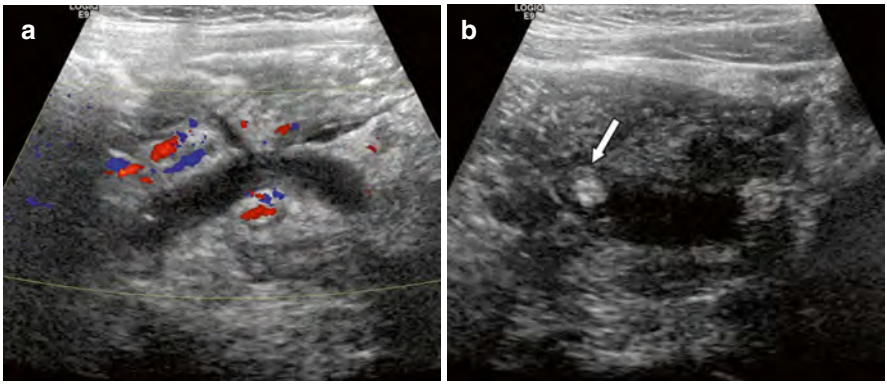

Fig. 10.2 Focused ultrasound images of the right lower abdomen in a patient with acute appendicitis. (**a**) Shows a color Doppler image, which shows a dilated appendix with surrounding hyperechoic fat and increased vascularity on Doppler images. (**b**) Shows a focal hyperechogenicity within the dilated appendix (arrow), representing appendicolith

Ultrasonography (US)

- It is the first imaging exam recommended by the ACR appropriateness criteria in pregnant patients and children with suspected appendicitis (Fig. 10.2) and in cases of acute right upper abdominal pain when biliary etiology is suspected.
- **Advantages**: No ionizing radiation, lower cost than cross-sectional imaging, faster turnaround time, and broader availability.

- **Limitations**: Operative dependence, suboptimal images in patients with a high body mass index, and increased bowel gas obscuring the organ of interest. Particularly in cases of acute appendicitis, the US is limited in patients with variant locations of the appendix. The operator-dependent visualization rate of the appendix on ultrasound ranges from 40% to 89%.

Fluoroscopy

- Contrast enema is performed by injecting barium or water-soluble contrast into the rectum using a rectal tube.
- The procedure can be done as a single or double contrast depending on the indication.
- A single-contrast enema with water-soluble contrast has been performed for recent postoperative patients concerned with anastomotic leaks and patients with suspected colonic fistula or perforation (Fig. e10.4).
- A double-contrast enema is performed with thin barium injected through the rectal tube, followed by air insufflation (Fig. 10.3). It is usually performed for colonic mucosal or luminal pathologies like polyps, diverticula, tumors, and inflammatory diseases (Fig. e10.5).
- Bowel preparation with the patient drinking clear liquids the day before the exam and drinking magnesium citrate the previous day is essential for a good quality exam.

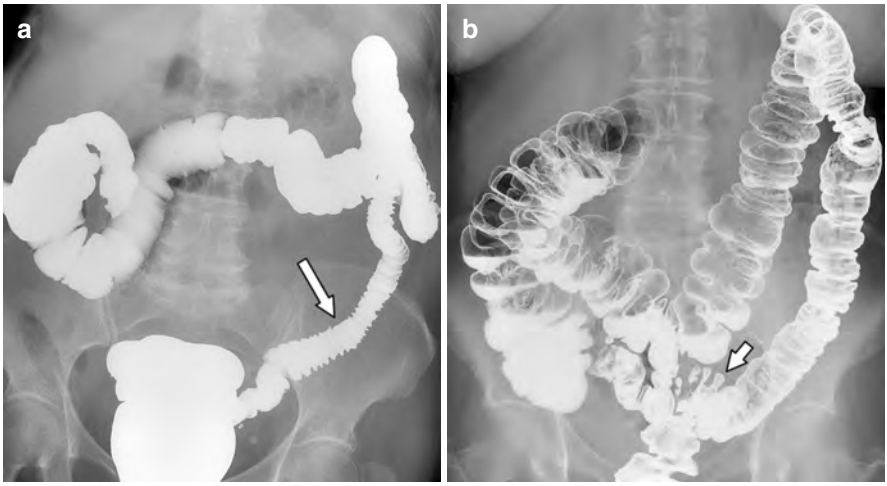

Fig. 10.3 Double-contrast barium enema images with initial oral contrast instilled through a rectal tube that opacifies the rectum and colonic loops reaching the cecum (**a**). The arrow in (**a**) shows a closely spaced haustral pattern in the sigmoid colon, representing a thickened colonic wall in patients with chronic diverticulosis. The left image shows air pumped through the rectum, contrasting a barium-coated wall with an air-filled lumen (**b**). The arrowhead in (**b**) shows focal outpouching/diverticula of the sigmoid colon

- Allergy to iodinated contrast must be confirmed before performing single-contrast enema examinations with water-soluble iodinated contrast. If necessary, pre-medication has to be performed if mild to moderate allergy. If there is a history of anaphylaxis, alternative imaging investigation should be considered.
- Relative contraindications to the use of a retention rectal tube are pelvic radiation, active colitis, suspected rectovaginal fistula, and history of anal canal surgery.
- **Advantages**: Inexpensive and simple exams.
- **Limitation**: The colon is evaluated only from the mucosal side of the colon without evaluating the pathologies that might involve the wall or extracolonic origin if present.

CT

- CT for the abdomen and pelvis has different protocols depending on the clinical indication and can be performed with or without oral contrast and with or without intravenous (IV) contrast.
- American College of Radiology (ACR) appropriateness criteria recommend CT abdomen and pelvis with intravenous contrast as the usually appropriate first exam to be ordered for any patient with acute nonlocalized abdominal pain, right lower or left lower quadrant abdominal pain.
- CT abdomen and pelvis with IV contrast and/or oral contrast is the exam that is commonly performed in investigation for gastrointestinal pathologies. The exam is performed in the portal venous phase at 60–80 s after intravenous injection of 100–120 cc of low-osmolarity iodinated contrast.
- In case of suspected gastrointestinal bleeding, the exam is performed in precontrast, arterial phase (20–35 s delay), and portal venous phase to identify hemorrhagic blood products on precontrast and arterial or venous source of a bleeding vessel on the postcontrast images (Fig. e10.6).
- In case of abdominal trauma, a delayed phase of 3–5 min post-injection is added to identify any slow flow bleeds.
- **Advantages of CT**: Highly accurate, widely available, short examination time, not operator-dependent, and requires no sedation in pediatric patients.
- **Limitations**: Risks of ionizing radiation, especially in children and pregnant patients, requiring IV contrast material, and more expensive.

CT Colonography (CTC)

- CTC is the exam recommended by the ACR appropriateness criteria for colorectal cancer screening. The current guidelines also recommend CTC performed every 5 years as an acceptable alternative screening method for colorectal cancers.
- CTC, or virtual colonoscopy, is a minimally invasive imaging technique to evaluate the colon and has been approved by the U.S. Food and Drug Administration (FDA) for colorectal cancer screening since 2006.

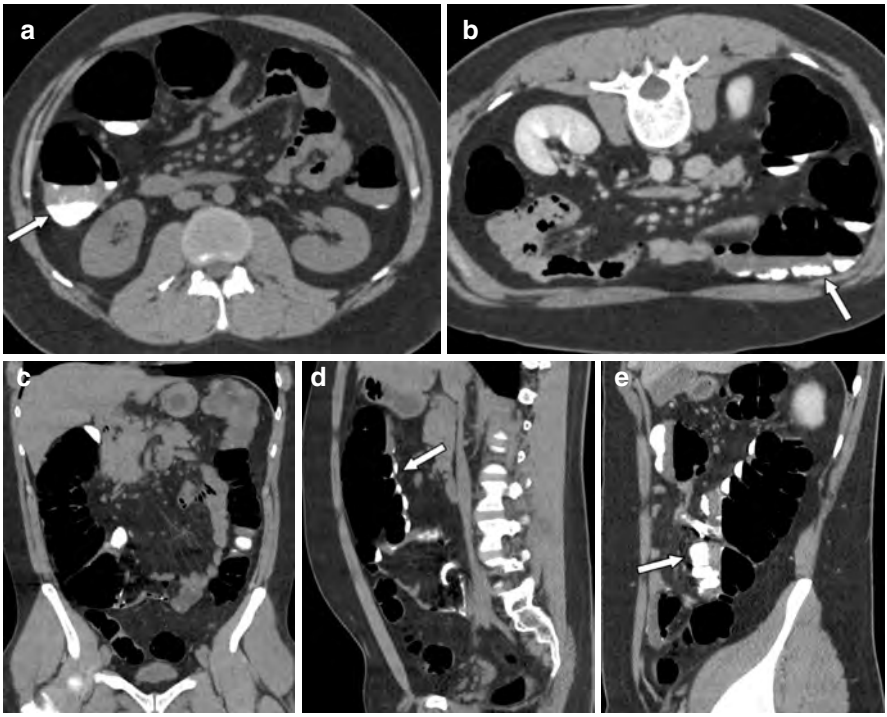

Fig. 10.4 CT colonography: axial images of the abdomen after colonic distention with oral contrast and air insufflated through a rectal tube with the patient in a supine position (axial, **a**, and sagittal, **d**) and a prone position (axial, **b**, and sagittal, **e**) with oral contrast layering in the dependent portions of the colon (arrows). The mid-abdominal coronal image (**c**) shows an air-distended colon

- CTC is performed with multidetector CT (MDCT), using thinner sections in single breath hold, 2D, and 3D reconstructions, improving the detection of colorectal polyps (Fig. 10.4).
- **Advantages of CTC**
  - Procedure-related advantages: No risk of bleeding, no interruption of therapeutic anticoagulation regimen in patients with gastrointestinal bleeding, almost negligible risk of perforation, and no sedation required.
  - Interpretation-related advantages: Evaluation of colonic mucosal abnormality, along with extracolonic structures.
- **Limitations of CTC**: Radiation exposure, incidental extracolonic findings on CTC necessitating further diagnostic workup for potentially benign findings, and a small percentage of complications associated with CTC procedure detailed below.
- **Complications with CTC**: There is minimal risk of complications; however, it is not insignificant.
  - Risk of perforation with colonic gas insufflation (0.04%).

  - Vasovagal episodes.
  - Side effects related to antispasmolytic agents used for the procedure to reduce bowel peristalsis—blurry vision (patients are advised not to drive until symptoms subside).
  - IV contrast-related allergic reactions.
  - Infection (mean frequency of 4.4% due to translocation of gastrointestinal flora).
- **CT Colonography Reporting and Data System (C-RADS)**
  - It is an initiative of the American College of Radiology to standardize the reporting of CTC findings.
  - The latest version is v2023.
  - Like other RADS systems, the C-RADS helps standardize the terminology or lesion descriptors and classification of CTC findings, as well as provides guidelines for treatment and prognosis.

MRI

- The role of MRI is limited to fewer specific indications such as appendicitis in children and pregnant patients (Fig. e10.7), inflammatory bowel disease, Crohn's disease, and ulcerative colitis, and in the initial staging and follow-up of rectal cancers.
- **Advantages**: Higher spatial and contrast resolution, accurate diagnosis, and follow-up of multiple lesions, particularly in inflammatory bowel disease. Lack of ionizing radiation and preferred examination modality in pregnant women and few pediatric patients when ultrasound is negative or equivocal; most cases can be performed without sedation, especially in adults, with diagnostic accuracy similar to CT.
- **Limitations**: Susceptibility artifact from bowel gas and its motility/peristalsis, high cost, and reduced availability. The length of the examination may require IV contrast examination, which has limited availability and requires sedation, especially in pediatric patients. It is also more expensive than ultrasound or CT.
- MRI is a reasonable alternative to CT, as the ALARA principle suggests, with comparable sensitivity and specificity.

PET/CT

- PET/CT can evaluate colorectal malignancy for primary and metastatic tumors, primarily for preoperative staging and postoperative surveillance for recurrence.
- It can also be used in inflammatory bowel disease to differentiate acute/active inflammation versus chronic fibrotic processes or malignancy by assessing metabolic activity, which plays a significant role in its management.

The Appendix

- The normal appendix arises from the cecum near the ileocecal valve in the right lower abdomen, at the junction between the lateral and middle thirds of the right spinoumbilical line/McBurney's point (Fig. 10.5).
- The appendix is variable, ranging from 6 to 15 cm in length, with an average length of about 7.6 cm and a diameter of less than 6 mm.
- However, the appendix is mobile and can be seen in variable locations about the cecum, like retrocecal, pelvic, subileal, subcecal, preileal, postileal, and paracecal locations; the most common being retrocecal locations accounting for about 60% of variant locations (Fig. 10.6).
- The appendix may rarely be seen in the right inguinal canal when called an Amyand hernia (Figs. 10.7 and e10.8), and when seen in the femoral canal, it is called a De Garengeot hernia. It is imperative to remember that in patients with situs inversus and congenital malrotation of the gut, patients have the appendix in the left lower abdomen.

Appendicitis

- Acute right lower quadrant pain is one of the most common presenting complaints for emergency room admissions, and acute appendicitis is the most common cause of acute surgical abdominal emergencies in adults and children.

Fig. 10.5 (**a**, **b**) Coronal CT images of the abdomen and pelvis showing normal caliber appendix in normal anatomic position (arrows) in two different patients

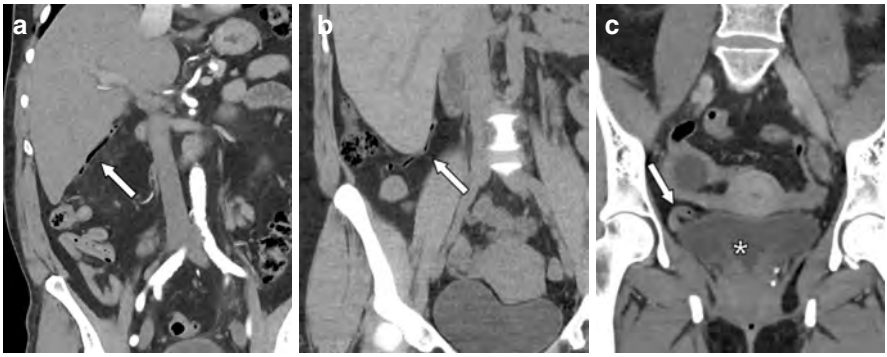

Fig. 10.6 Coronal CT images of the abdomen and pelvis demonstrating variant positions of the appendix. (**a**) Tip of appendix along the medial and inferior margin of the right lobe of the liver (arrow). (**b**) Appendix tip at the inferior tip of the right lobe of the liver (arrow). (**c**) Appendix (arrow) in the right hemipelvis abutting the right superior bladder wall (*)

Fig. 10.7 MRI images of the pelvis with axial post-contrast T1-weighted image (**a**), coronal STIR (**b**), and sagittal T2-weighted image (**c**) show right Amyand hernia in which the inguinal hernia contains the uninflamed appendix (arrows)

- Acute appendicitis is a clinical imaging diagnosis. Clinical suspicion is based on clinical history and physical examination findings, supported by laboratory findings, including elevated white count, C-reactive protein, and imaging findings.

Imaging of Acute Appendicitis

- **Ultrasound**
  - It is the preferred and initial imaging modality in children with suspected appendicitis. CT or MRI can be performed in select cases when ultrasound is limited or equivocal.
  - Ultrasound with graded compression examination of the appendix has a sensitivity of 89%, specificity of 97%, and 87–96% accuracy.
  - A combination of transabdominal ultrasound (TAS) and transvaginal ultrasonography (TVUS) can also be performed in patients with suspected appendicitis. The sensitivity and specificity of TAS for diagnosis of appendicitis are 75–90% and 93%, respectively, whereas combining TVUS with TAS had a

sensitivity of 97%, specificity of 91%, positive predictive value of 92%, and negative predictive value of 97%. However, the combined ultrasound has the limitation of time required for dual exams, operator-dependence requiring proficiency in performing both techniques.

- **Sonographic diagnosis of acute appendicitis** (Fig. 10.2)
  - Maximum outer diameter of >6 mm.
  - Noncompressible appendix.
  - Blind-ending loop.
  - Inflamed hyperechoic periappendiceal fat.
  - Effacement of the echogenic submucosal layer.
  - Periappendiceal fluid.
  - Presence of an appendicolith.
- Sonographic findings of gangrenous appendicitis include loss of normal mural stratification, loss of normal echogenic submucosal layer reflectivity, and abnormally echogenic periappendiceal fat.
- Doppler examination is usually performed with preset parameters of wall filter and pulse repetition frequency, and Doppler gain is optimized for detecting low-volume flow in the appendicular artery. With appendicitis, there is inflammatory hyperemia resulting from increased vascularity within the appendix and mesoappendix.
- Ultrasound shear wave elastography has been described in the literature to differentiate between normal and inflamed appendix. US elastography had the advantage of quantifying tissue elasticity. The inflamed appendix had a higher median elastic modulus (>12.5 kPa) value than the normal appendix and had a sensitivity of 93% and specificity of 100%.

CT

- CT is often performed as the first investigation in the emergency department and in cases where equivocal ultrasound cases occur.
- The sensitivity and specificity of CT in diagnosing acute appendicitis is ~90%, and the accuracy is reported at 93–99%.
- CT has reduced the negative appendectomy rates from 15–20% to 2–12%.
- **CT signs of acute appendicitis** are the same as sonographic signs described above, including appendix diameter >6 mm, mucosal hyperenhancement, and periappendiceal inflammation, enlarged mesenteric nodes in the right lower abdomen (Figs. 10.8 and 10.9)
  - Secondary signs of appendicitis include the “arrowhead sign” with focal thickening of the cecal apex, resulting in arrowhead-shaped contrast in the cecum.
  - Periappendiceal fat stranding and wall hyperemia on CT increase the confidence in diagnosing acute appendicitis when the size of the appendix is borderline and other secondary signs like appendiceal wall thickening and absence of intraluminal air are present. There is a well-established association between periappendiceal fat inflammation and appendicitis.

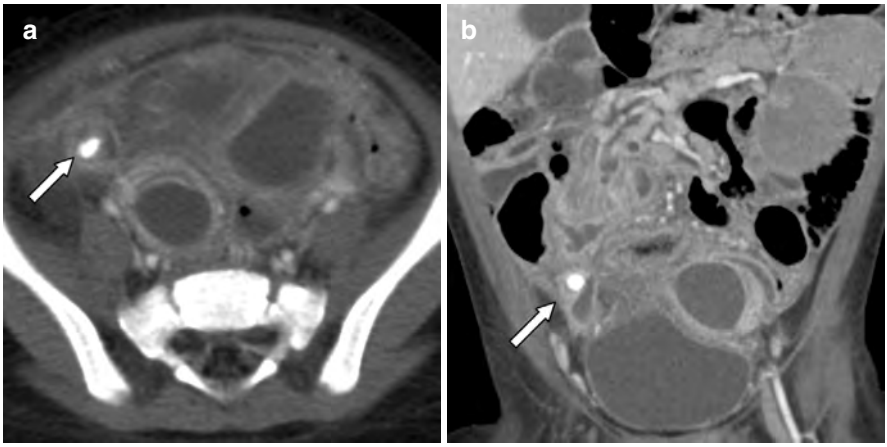

Fig. 10.8 Axial (**a**) and coronal (**b**) CT images of the abdomen and pelvis in an 18-month-old child show a dilated appendix with wall thickening and an appendicolith (arrows). There are secondary inflammatory changes in the adjacent small bowel loops, which are dilated. Operative and pathological findings confirmed acute appendicitis

- MRI will demonstrate similar findings of acute appendicitis, similar to CT (Fig. e10.9).
- **Borderline or equivocal appendicitis** is when the maximum diameter of the appendix is between 6 and 8 mm or when the diameter is abnormal but without periappendiceal inflammatory findings. These borderline cases must be carefully evaluated for additional sonographic findings like the intramural flow on Doppler; periappendiceal inflammatory findings can be used to be certain of the presence/absence of acute appendicitis. This can help reduce the unnecessary surgery in the case of a normal appendix based on the additional supportive findings and/or also reduce the unplanned readmission after appendectomy in children or adults due to a normal appendix being removed and further search for abdominal pain evaluated.
- **Atypical forms of appendicitis** include tip appendicitis, where only the tip of the appendix is inflamed while the rest of the appendix is normal in caliber; stump appendicitis in patients who had a partial appendectomy with >5 cm of residual appendiceal stump, which is inflamed; and appendicitis without leucocytosis.
- **Complications of appendicitis**
  - Perforated appendix
  - Appendiceal abscess
  - Peritonitis
  - Pylephlebitis, pyelothrombosis
  - Hydroureteronephrosis
  - Bowel obstruction
- **Perforated appendicitis**: CT is commonly used for diagnosing perforated appendicitis with a high specificity of over 90% even if one of the following CT signs is present and each sign individually has a specificity of >95%. The CT

Fig. 10.9 Acute appendicitis in different extents of inflammation. Axial and coronal images of patient 1 with uncomplicated acute appendicitis (**a**, **b**) show a mildly dilated appendix with wall thickening and periappendiceal fat stranding (arrow). Axial and coronal images of patient 2 with complicated appendicitis (**c**, **d**) similarly show a dilated appendix with significant wall thickening, mucosal hyperenhancement, mild periappendiceal fat stranding, and appendicolith (arrow). There was focal wall discontinuity along its medial margin concerning perforation (arrowhead). The patient underwent appendectomy with ileocecectomy, and pathology was reported as acute appendicitis with appendicolith, focal necrosis, and perforation

signs indicating a perforated appendix are a discontinuous wall in the presence of an obstructing appendicolith, periappendiceal abscess, extraluminal air, and/or extraluminal appendicolith. The determination of perforation has an impact on management decisions (Figs. 10.10 and e10.10).

- Differentiating primary from secondary appendicitis is vital for management decisions. Secondary or reactive appendicitis can be caused by infectious or inflammatory processes in the terminal ileum, cecum, ascending colon, or acute gynecological process.
- Similarly, not all dilated appendix is appendicitis and need to be differentiated from appendiceal mucinous neoplasm or other appendiceal tumors.
- Oral contrast or stool within the appendix supports evidence of a nonobstructed appendix.
- **Differential diagnosis of appendicitis**: Terminal ileitis, pelvic inflammatory disease, mesenteric adenitis, infectious colitis, typhlitis, epiploic appendagitis, and small bowel diverticulitis.
- **Management of appendicitis**
  - Acute appendicitis with classic clinical and imaging features is treated with emergent appendectomy.
  - Complicated appendicitis is treated with appendectomy and perioperative intravenous antibiotic coverage, particularly in perforated appendicitis. However, in cases with an appendicular abscess, preoperative intravenous antibiotics with abscess drainage are usually performed under ultrasound or CT guidance while delaying surgery to reduce the mortality associated with the emergent appendectomy in that subset of patients (Ochsner-Sherren regime).
  - Equivocal appendicitis is managed with laparoscopy.

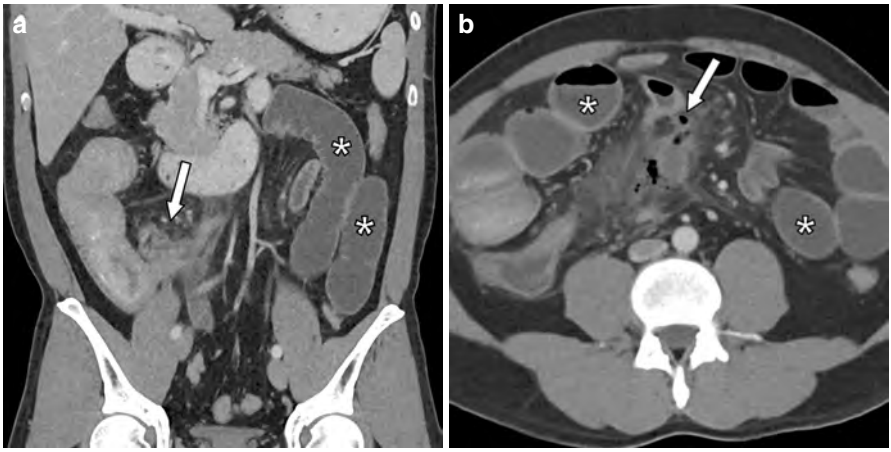

Fig. 10.10 Coronal (**a**) and axial (**b**) images of the abdomen and pelvis show an ill-defined appendix with significant periappendiceal fat stranding and a trace amount of free fluid (arrow in **a**). There were also pockets of free intraperitoneal air and free fluid surrounding these air pockets (arrow in **b**), representing phlegmon from perforated appendicitis. Note the mildly dilated, fluid-filled small bowel loops (* in **a** and **b**), secondary to inflammatory changes in the distal ileum adjacent to the inflamed appendix

Appendiceal Tumors

- Appendiceal tumors are one of the less common gastrointestinal tumors.
- These are usually benign and few malignant tumors.
- Most are epithelial tumors, of which epithelial adenocarcinoma is the most common and includes mucinous and nonmucinous subtypes, followed by goblet cell adenocarcinoma and neuroendocrine tumors. Among neuroendocrine tumors, carcinoids are common; however, they are usually incidental at appendectomy.
- A few less common benign tumors include adenoma, gastrointestinal stromal tumor (GIST), and leiomyoma.
- All malignant appendiceal tumors with local extension undergo right hemicolectomy with lymphadenectomy with/without cytoreductive surgery with hyperthermic intraperitoneal chemotherapy (HIPEC), depending on peritoneal involvement. The only exception is low-grade mucinous neoplasms, which undergo a simple appendectomy when confined to the appendix.

Mucinous Epithelial Tumors

- Mucocele is now called mucinous neoplasms of the appendix, which account for 70% of epithelial tumors of the appendix.
- Appendiceal mucocele terminology describes the appendiceal lumen distended with mucin. However, if the diameter of the mucoceles is greater than 2 cm, it most likely represents a tumor (Fig. 10.11).
- Mucinous neoplasms of the appendix can be benign or malignant and are classified into four types based on cellular atypia: adenoma, low-grade and high-grade appendiceal mucinous neoplasm, and mucinous adenocarcinoma (Figs. e10.11, e10.12, and e10.13).

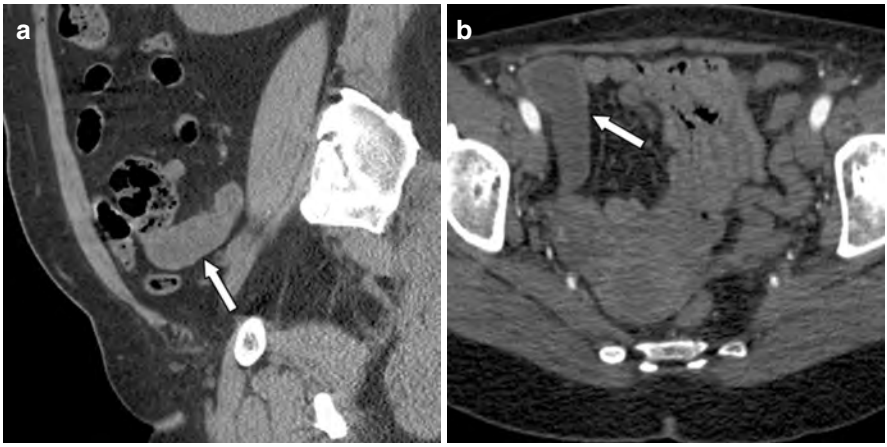

Fig. 10.11 Sagittal (**a**) and axial (**b**) images of the abdomen and pelvis showed an incidental dilated appendix measuring 3.4 cm in diameter with fluid attenuation (arrows). There were no surrounding inflammatory changes. The appendectomy specimen was reported as low-grade appendiceal mucinous neoplasm

- Mucinous cystadenocarcinoma is the most common, clinically significant tumor of the appendix.
- Mucinous appendiceal adenocarcinoma presents as nodular mural thickening of the appendix or soft-tissue attenuation with coarse calcifications (Fig. 10.12).
- They can sometimes present as secondary acute appendicitis (Fig. 10.13).
- Owing to the risk of malignant degeneration, these mucinous tumors are always surgically resected, and surgery involves appendectomy, cecal resection, and right hemicolectomy with careful attention to avoid spillage of mucin. Hence, a high index of suspicion is required while diagnosing mucinous appendiceal neoplasms.

Nonmucinous (Colonic-Type) Adenocarcinoma

- These are commonly seen in older men in their 60s–70s.
- They often clinically present with acute appendicitis symptoms.
- These tumors have an infiltrative mass-like presentation without mucocele formation.
- Periappendiceal fat stranding is common in cases of diffuse appendiceal mural thickening, either due to the tumor extending outside the appendix wall or from superimposed acute appendicitis, which is not an uncommon clinical presentation (Fig. 10.14).
- The presence of distant visceral metastases to the liver and lung or regional/distant lymphadenopathy suggests a non-mucinous tumor.

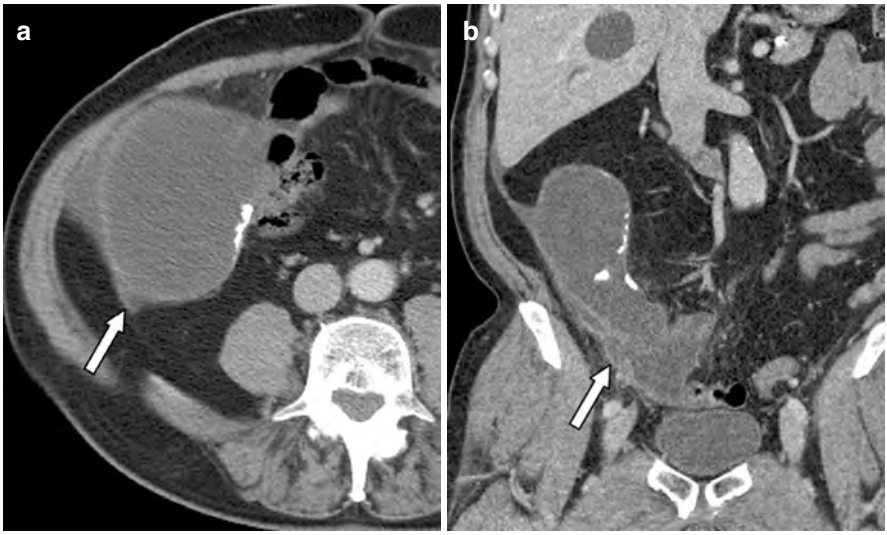

Fig. 10.12 Axial (**a**) and coronal (**b**) CT images of the abdomen and pelvis in a 37-year-old woman with a prior appendicitis history. Images showed a 6 cm, dilated, fluid-filled tubular structure (arrow) with peripheral calcifications in the irregular wall. There is infiltration of the adjacent cecum (arrowhead in **a**). Surgical resection showed well-differentiated mucinous adenocarcinoma

Fig. 10.13 CT images of the abdomen and pelvis in a 59-year-old man are shown at two-time intervals. Top images: axial (**a**), coronal (**b**), and sagittal (**c**) images at initial presentation when the patient had dilated, fluid-filled appendix with small appendicolith, enhancing wall and surrounding fat stranding, consistent with acute appendicitis. Since the patient had undergone cardiac bypass graft surgery and was on a double platelet regimen, emergent appendectomy was deferred, and the patient was managed medically. Follow-up CT was performed 8 months later for planning elective appendectomy, which is shown in the bottom images: axial (**d**), coronal (**e**), and sagittal (**f**) CT images. There was a dilated and tortuous appendix with fluid density, significantly increased in size compared to baseline CT, and absent inflammatory findings. An appendectomy was performed and reported as low-grade mucinous neoplasm

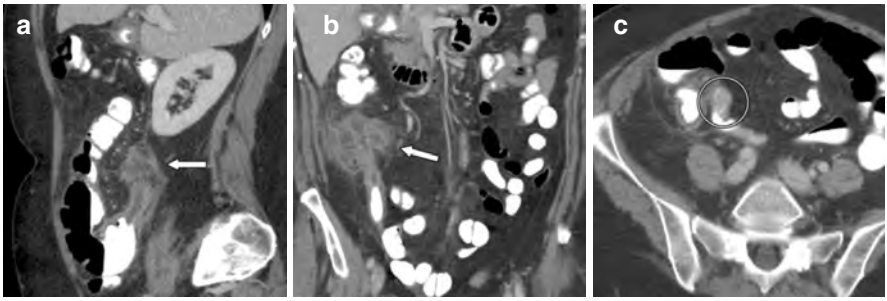

Fig. 10.14 Sagittal (**a**), coronal (**b**), and axial (**c**) CT images of the abdomen and pelvis show a dilated appendix with irregular wall thickening, inflammation, and abscess (arrows) with a soft-tissue nodule at the base of the appendix (circle in **c**). Right hemicolectomy was performed, and pathology was reported as acute appendicitis with appendix adenocarcinoma and concurrent neuroendocrine tumor of the terminal ileum

Appendiceal Lymphoma

- Primary appendiceal lymphomas are rare, with an estimated prevalence of about 0.0015% of all appendectomy specimens.
- These have a peak incidence in middle-aged adults, unlike other appendiceal tumors.
- They are almost always B-cell tumors.
- Clinical presentation is usually of acute appendicitis symptoms.
- They present as markedly enlarged appendix with a preserved shape; however, they present with classic aneurysmal luminal dilation (Fig. 10.15).
- Regional lymphadenopathy can be seen if the appendix is involved secondarily.
- Management changes if the appendix involvement is primary or secondary. Primary lymphoma is treated with surgical resection, with/without chemotherapy and radiation therapy. Whereas secondary appendiceal involvement is treated with chemotherapy.

Appendiceal Neuroendocrine Tumors

- Appendiceal neuroendocrine tumors (NET) are common in young females in the fourth decade of life.
- These tumors are usually hard to diagnose due to their small size.
- When visualized, it commonly presents as small localized enhancing masses within the distal third or tip of the appendix without inflammatory findings (Fig. 10.16).
- The masses can have calcifications and regional lymphadenopathy.
- Rarely can have hepatic metastasis at presentation.
- Cross-sectional imaging with CT abdomen and pelvis is recommended in patients who have NET diagnosed at appendectomy, particularly if tumors are >2 cm, have positive margins, or have carcinoid syndrome.

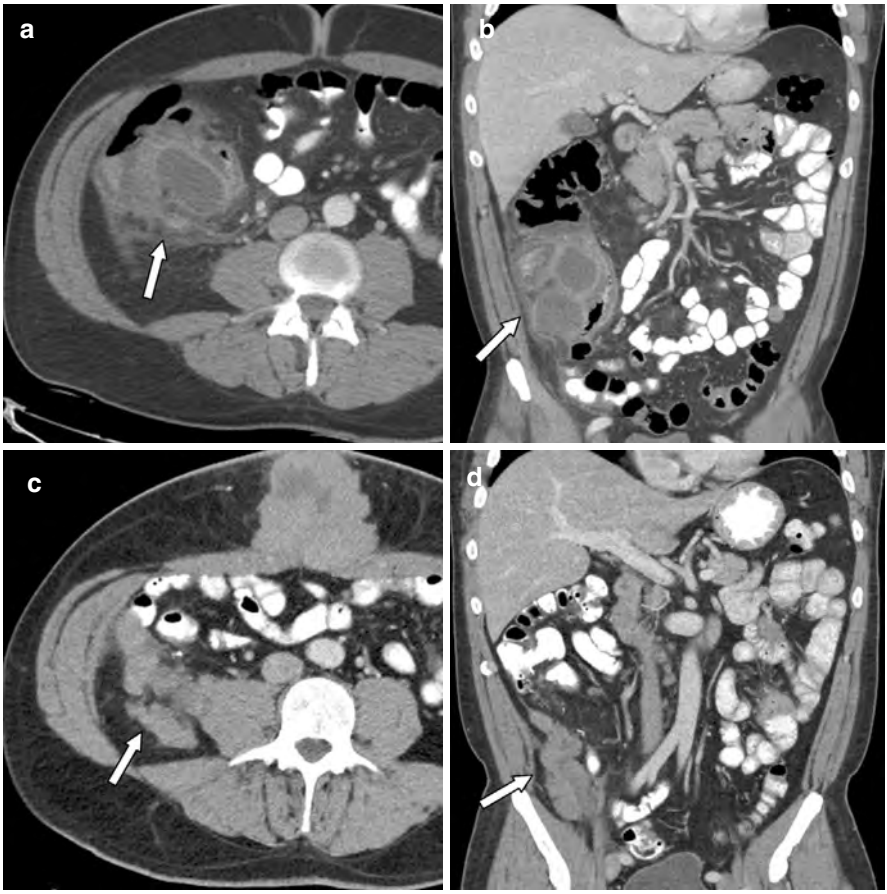

Fig. 10.15 CT images of the abdomen and pelvis in a 40-year-old man at initial presentation in the top images: axial (**a**), coronal (**b**), which showed an irregular, thick-walled fluid collection with surrounding inflammatory changes in the right lower abdomen (arrows). A normal appendix was not identified. It was reported as perforated acute appendicitis with abscess. The patient underwent laparoscopic appendectomy, which was reported as acute appendicitis with perforation and abscess. Six months later, the patient presented with a palpable mass at the umbilicus/laparoscopic port site. CT in the borrow row: axial (**c**) and coronal (**d**) images showed irregular soft-tissue masses at the appendectomy site and right retroperitoneum (arrows) and a large 6.1 cm irregular soft-tissue mass at the laparoscopic port site (arrowhead in **c**). Tissue sampling of the umbilical site mass was reported as B-cell lymphoma. The patient expired 6 months without a response to chemotherapy

- For well-differentiated appendiceal NET, 111-In Octreotide scan has higher sensitivity, whereas 18-F FDG PET-CT has higher sensitivity in poorly differentiated tumors.
- Management depends on the size of the tumor and whether it is confined to the appendix or metastatic at presentation. Tumors <1 cm in size confined within the appendix are usually managed with simple appendectomy. Whereas tumors of

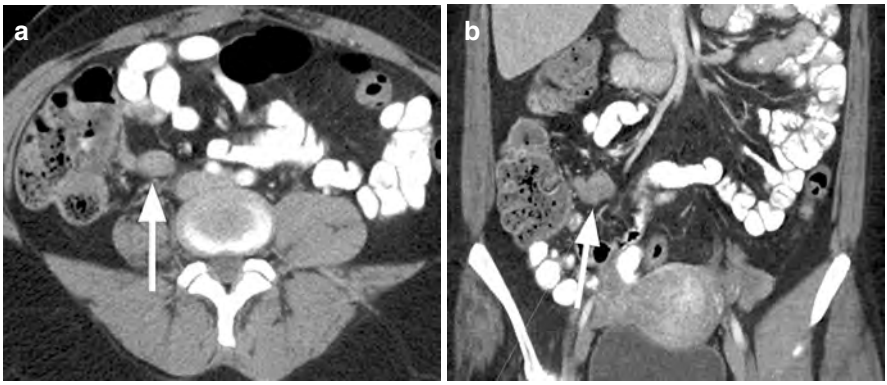

Fig. 10.16 Axial (**a**) and coronal (**b**) CT images of the abdomen and pelvis show lobulated and dilated appendix with soft-tissue density (arrows). No fluid density or surrounding inflammatory changes were noted. Appendectomy was reported as a neuroendocrine tumor of the appendix

any size that extend beyond the wall are treated with right hemicolectomy and regional lymphadenectomy with imaging follow-up, and somatostatin therapy is added for those with metastasis.

Pseudomyxoma Peritonei

- Mucin in low-grade and high-grade appendiceal mucinous neoplasms can dissect through the wall and perforate, predisposing to pseudomyxoma peritonei. It usually represents high-grade disease.
- Pseudomyxoma peritonei is a clinical syndrome caused by mucus within the cystic masses or free mucus within the peritoneal cavity, usually from mucin-producing neoplasms.
- Most pseudomyxoma peritonei is caused by mucinous appendiceal tumors, with other causes of gastrointestinal or reproductive origin.
- The most common site of metastasis of appendiceal neoplasm is the peritoneum, which depends on the histological type and presence of appendiceal perforation.

Imaging

- **US**
  - US helps to differentiate pseudomyxoma multiseptated cystic masses from ascites.
- **CT**
  - Present as low attenuation masses with characteristic scalloping edges of the liver (Fig. 10.17).
  - Loculated ascites, calcifications, and septations within these mucinous masses represent advanced disease.

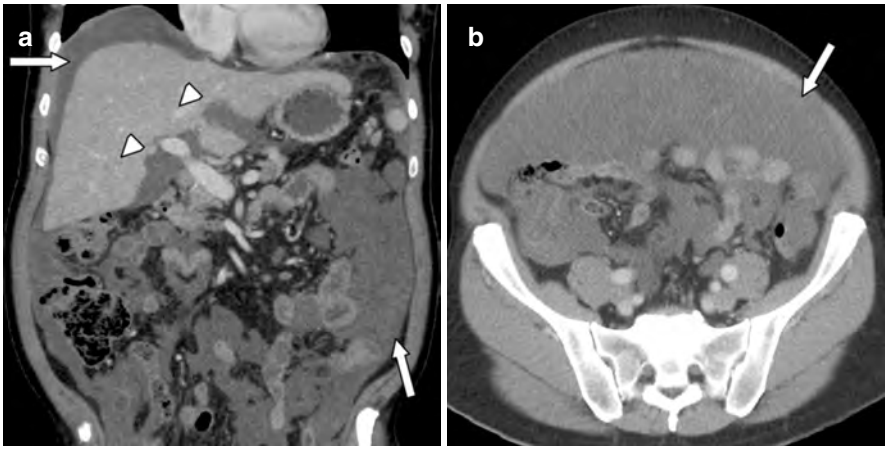

Fig. 10.17 Coronal (**a**) and axial (**b**) images of the abdomen show moderate volume, low attenuation fluid in the intraperitoneal spaces, omentum, and mesentery (arrows in **a** and **b**). There is mild scalloping of the medial margin of the right lobe of the liver (arrowheads in a). Sampling of the peritoneal fluid was reported as metastatic mucinous adenocarcinoma consistent with pseudomyxoma peritonei

  - The peritoneal cancer index (PCI) is calculated preoperatively by imaging, but the final assessment is performed using a laparotomy.
  - PCI is an assessment of the extent and volume of peritoneal disease.
  - It is a systematic assessment performed by dividing the abdomen into nine sites and the small bowel into four parts. Each site is assessed for tumor deposit, and scoring is based on tumor size.
  - Lesion size (LS) scores are as follows: LS-0 is absence of tumor at that site; LS-1 is deposits that are <0.5 cm; LS-2 are deposits that are 0.5–5.0 cm; and LS-3 are >5 cm in diameter.
  - PCI score ranges from 0 to a maximum score of 39.
- **MRI**
  - Multiloculated masses with hyperintense signal on T2-weighted images with variable signal intensity on T1-weighted images, depending on the mucin concentration and hemorrhagic content, cause high signal intensity on precontrast T1-weighted images.
  - Though the septations and wall demonstrate enhancement in postcontrast images, the mucinous components do not enhance owing to lack of vascularity. However, gadolinium absorption in the extracellular space can mimic enhancement in a few situations when there is a delayed phase.
  - DWI can help identify solid nodules within these mucinous masses.
- **PET/CT**: Limited use due to limited metabolic activity from limited cellularity.
- **Management**: Cytoreductive surgery with palliative chemotherapy.

Colonic Disorders

- Colonic anatomy helps in understanding the etiologies of common colonic pathology.
- The cecum and ascending colon have variable mesentery lengths, making the cecum more prone to twisting, resulting in volvulus. Similarly, the sigmoid colon has a long sigmoid mesocolon with a narrow attachment to the posterior abdominal wall, making it prone to sigmoid volvulus.
- The descending colon is retroperitoneal in location, and the rectosigmoid junction lies in the extraperitoneal pelvis.
- The ascending colon is supplied by the right colic branches of the superior mesenteric artery and vein (SMA and SMV), and the transverse colon, including the radiologic hepatic and splenic flexures, is supplied by the middle colic branches of SMA and SMV. The descending colon is supplied by the inferior mesenteric artery and vein (IMA and IMV). This is a reason why colon cancers almost always metastasize to the liver.
- The rectum has dual blood supply from mesenteric vessels (superior rectal branch of IMA and IMV), and systemic vessels (middle and inferior rectal branches in internal iliac artery and vein). The dual supply is the reason why rectal cancer metastasizes via mesenteric vessels to the liver and through the systemic circulation to the lungs, etc. (imaging book).
- Acute colitis can have various causes, including infection, inflammation (Crohn's disease and ulcerative colitis), ischemia, neutropenia, toxins, and radiation.
- **CT**
  - It is the best diagnostic method for diagnosing infectious colitis.
  - Although not specific, the classic CT signs of colitis include colonic wall thickening >4 mm, pericolic fat stranding, the "halo sign" from submucosal edema, and hyperenhancement of the mucosa from hyperemia (Fig. 10.18).
  - A few of these signs can also be seen with other conditions like colonic malignancies, diverticulitis, and portal hypertension.
  - Colitis presents with symmetric and segmental mural thickening, which has to be differentiated from asymmetric and focal wall thickening, as seen with colorectal adenocarcinomas or endometriosis implants in the colonic wall (Fig. 10.19).
  - Colonic wall enhancement can have a target appearance due to the stratification of the bowel wall layers: hyperenhancement of the mucosa with a relatively decreased enhancement of the submucosa and serosa. Although this is nonspecific, portal hypertension and right heart failure, which can cause impaired venous drainage, can have the halo sign or target sign.
  - Other ancillary imaging signs include fatty infiltration and dilated mesenteric vessels due to hyperemia and serous fluid leakage, ascites, and mesenteric lymph node enlargement >5 mm in short axis.
  - "Accordion sign" is due to marked thickening of the colonic haustral folds.

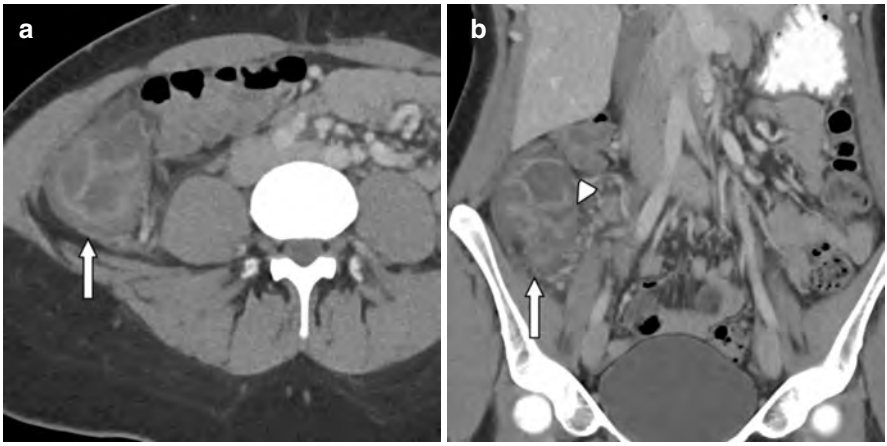

Fig. 10.18 Axial (**a**) and coronal (**b**) CT images of the abdomen and pelvis in a patient with fever and right abdominal pain. The images show edematous thickening of the ascending colonic wall (arrows) with mild surrounding fat stranding, trace-free fluid, and prominent mesenteric nodes (arrowhead). Findings were consistent with acute ascending colitis. The laboratory tests, including culture results, confirmed bacterial etiology, indicating infectious colitis

Fig. 10.19 Coronal (**a**), sagittal (**b**), and axial (**c**) CT images of the abdomen and pelvis in a patient with fever, diarrhea, and abdominal pain show long segment circumferential thickening of the descending colon with surrounding pericolonic fat stranding (arrows) representing acute infectious colitis

Infectious Colitis

- The most common cause of infectious colitis is bacterial infection. Other causes include viral, fungal, and parasitic infections.
- Few rare viral infections, particularly underlying chronic conditions, can cause colitis. For example, monkeypox proctitis is more common in HIV patients (Fig. 10.20).
- Clinical presentation and acuity of symptoms vary depending on the pathogen. Hence, laboratory and serological tests are important in the diagnosis.

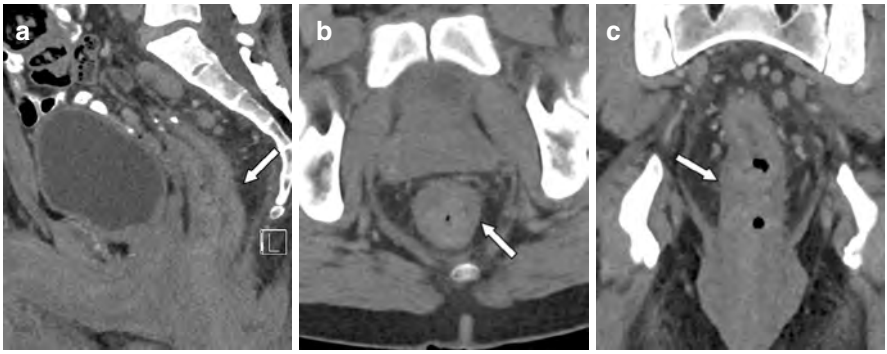

Fig. 10.20 Sagittal (**a**), axial (**b**), and coronal (**c**) CT images of the pelvis in a 43-year-old male patient with HIV show uniform circumferential thickening of the rectal wall. Serological tests were positive for the monkeypox virus. The patient was treated for monkeypox proctitis

- **Pseudomembranous colitis**: This form of colitis is caused by *Clostridium difficile* infection, almost always exclusively from long-term broad-spectrum antibiotic use (Fig. 10.21).

Inflammatory Bowel Disease

- Inflammatory bowel disease (Crohn's disease and ulcerative colitis) is one of the common causes of bowel wall thickening.
- **Crohn's disease (CD)**
  - It occurs in young patients in their 20s, usually with bloody mucoid diarrhea. The patients typically have a positive family history.
  - It can affect the entire digestive tract, anywhere from mouth to anus.
  - Hallmarks of CD are significant bowel wall thickening >10 mm, transmural involvement, asymmetric discontinuous involvement with skipped lesions, and other signs like sinus tracts, fistulae, abscesses, ascites, and "comb sign," which favor the diagnosis (Fig. 10.22) (Table 10.1).
- **Ulcerative colitis (UC)**
  - The epidemiology and clinical presentation are similar to CD.
  - UC is known for its association with primary sclerosing cholangitis.
  - Unique features that differentiate UC from CD are its exclusive, retrograde, continuous involvement of the colon, with the left colon more frequently involved, less than 10 mm wall thickening, unlike CD, predominant involvement of mucosa and submucosa in comparison to transmural involvement by CD and hence no fistula or abscess formation (Fig. 10.23) (Table 10.1).
- **Stercoral colitis**
  - It is an inflammatory colitis resulting from increased intraluminal pressure within the rectum or colon due to impacted stool.

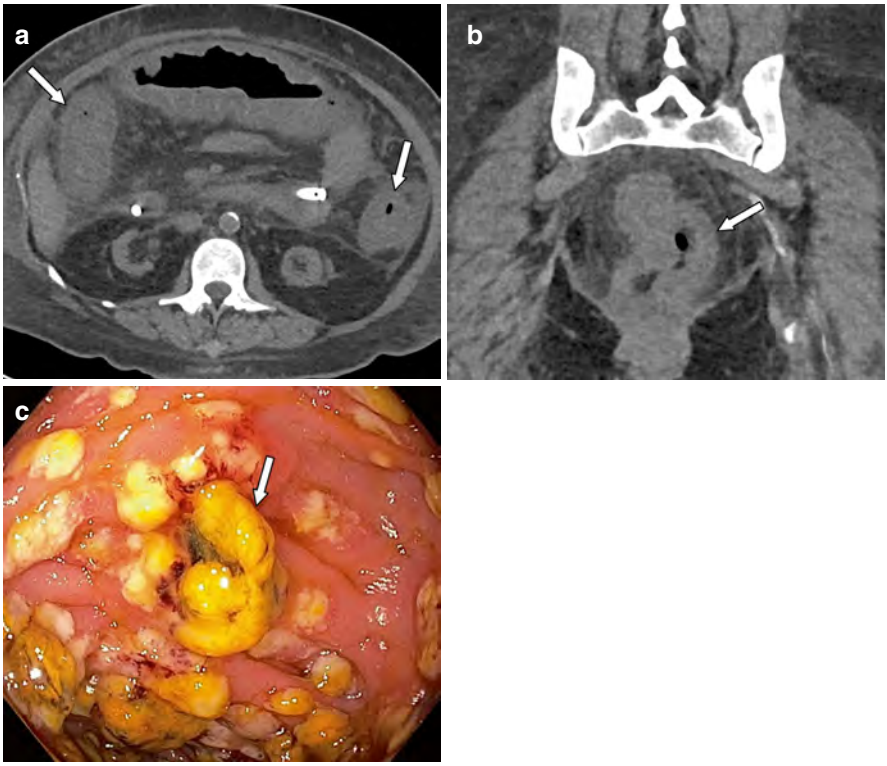

Fig. 10.21 Axial (**a**) and coronal (**b**) CT images of the abdomen and pelvis in a 40-year-old woman with a history of pancreas and kidney transplant presenting with abdominal pain and diarrhea. The images show diffuse colonic and rectal wall thickening (arrows in **a** and **b**) with surrounding fat stranding and trace ascites. The findings represented pancolitis. A colonoscopy (**c**) was performed, which showed severe edematous, erythematous, friable, and ulcerated mucosa with pseudomembranes throughout the rectum and colon consistent with severe *Clostridium difficile* colitis, confirmed with serological tests

- Common predisposing factors include chronic constipation, advanced age, and medical comorbidities leading to physical inactivity.
- **CT**: Dilated colon with impacted stool and surrounding inflammatory findings, including colonic wall thickening, surrounding fat stranding, and free fluid (Fig. e10.14).
- Perforation is the most common and dreaded complication, and when it occurs, the mortality rate is as high as 32–57% (Fig. 10.24).
- Other complications include prolonged pressure leading to vascular compromise, ischemia, and ulceration.

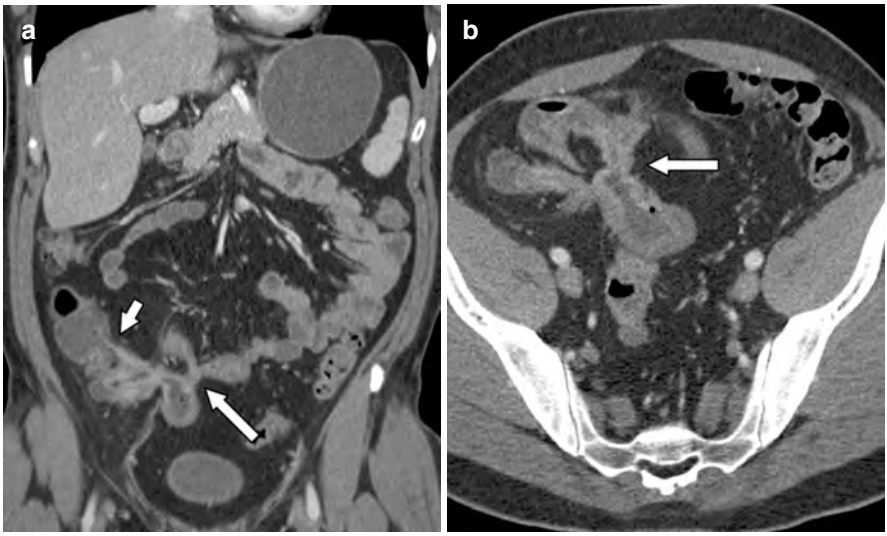

Fig. 10.22 Coronal (**a**) and axial (**b**) CT images of the abdomen and pelvis in a patient with known Crohn's disease. The images show long segment distal and terminal ileal thickening involving the ileocecal junction (arrowhead in **a**) with multiple focal areas of narrowing/strictures, mucosal hyperenhancement, and enteroenteric fistula between adjacent ileal loops in the lower abdomen (arrow in **a** and **b**)

Table 10.1 Differentiating various colonic pathologies by pattern of involvement

Diagnosis	Part of the colon commonly involved	Length of segment involvement	Other features
Ulcerative colitis	Rectum	Long segment or pancolitis	Contiguous involvement extending proximally from the rectum
Crohn's disease	Terminal ileum, perirectal involvement also seen	Variable length, segmental involvement	Skipped areas
Infectious colitis	Any part	Long segment or pancolitis	Laboratory and serological tests
Typhilitis	Cecum and ascending colon	Moderate length	Neutropenic patients
Ischemic colitis	Splenic flexure or sigmoid colon; spares rectum	Segmental involvement	Atherosclerotic disease and diabetes mellitus
Diverticulitis	Sigmoid-most common; spares rectum	Segmental involvement	When chronic, they cause myochosis which causes hypertrophy of the circular muscle layer, shortening of the taeniae, and luminal narrowing
Colon cancer	Any part	Short segment	Soft-tissue density mass, nodal metastasis, hepatic and liver metastasis

Diverticulitis

- Acute colonic diverticulitis, which results from inflammation of the colonic diverticula, is a common cause of abdominal pain in the elderly.

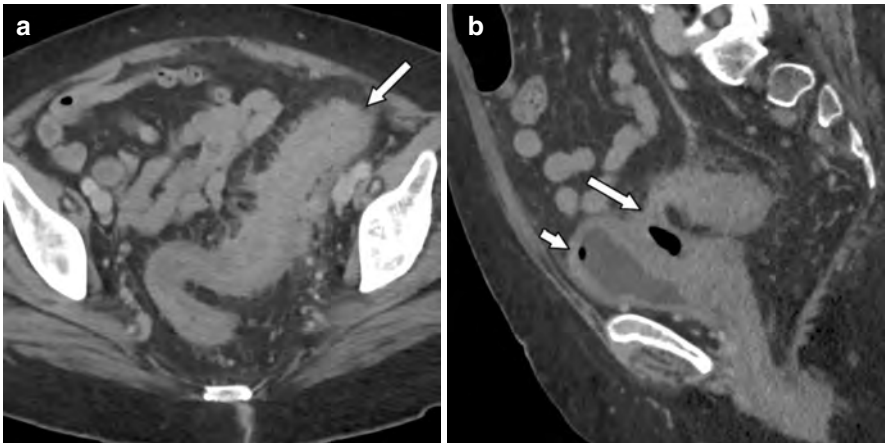

Fig. 10.23 Axial (**a**) and sagittal (**b**) CT images of the pelvis in a patient with a known history of ulcerative colitis show a long segment circumferential thickening of the sigmoid colon with pericolonic fat stranding and mesenteric engorgement (arrow in **a**), representing acute sigmoid colitis. There is curvilinear soft tissue extending from the sigmoid colon to the vaginal vault and posterior wall of the bladder (arrow in **b**) and with a tiny pocket of air within the bladder (arrowhead in **b**). These represent the colo-vaginal and colovesical fistula from complicated sigmoid colitis

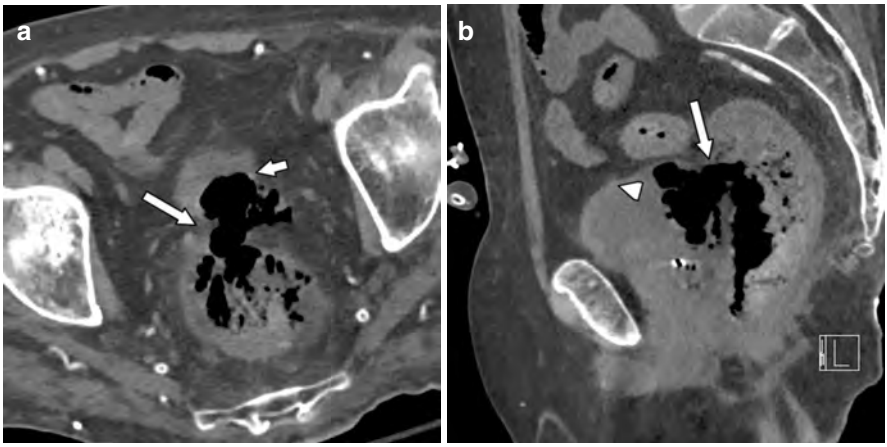

Fig. 10.24 Axial (**a**) and sagittal (**b**) CT images of the pelvis show moderate stool burden in the rectum with wall thickening and minimal perirectal fat stranding representing stercoral colitis. Extraluminal air from the anterior wall of the rectum (arrows) extends into the bladder (arrowheads) from the perforation of stercoral colitis

- CT is the best imaging test to diagnose acute diverticulitis and rule out other causes of abdominal pain, with a sensitivity of 79–99%.
- Descending and sigmoid colon are the most common affected sites (Table 10.1).
- Acute diverticulitis occurs when it gets obstructed by feces, food particles, or inflammation.

Fig. 10.25 Axial (**a**), sagittal (**b**), and coronal (**c**) CT images of the abdomen and pelvis show signs of inflammation including focal pericolic fat stranding and mesenteric engorgement surrounding descending colonic diverticula (arrows), consistent with acute uncomplicated diverticulitis

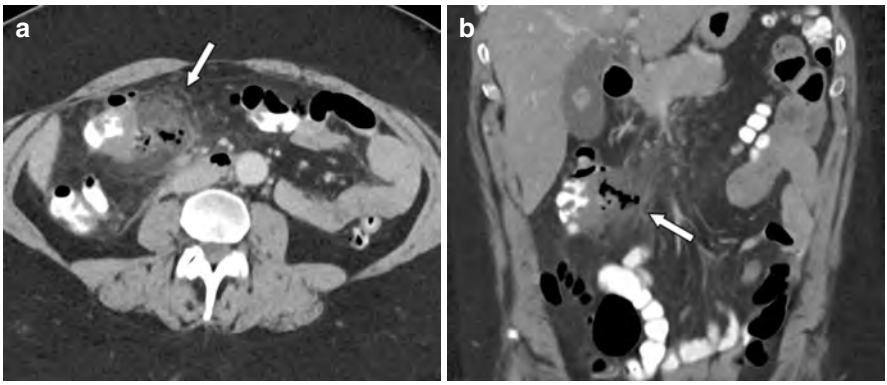

Fig. 10.26 Axial (**a**) and coronal (**b**) CT images of the abdomen and pelvis show focal segmental colonic wall thickening and significant surrounding fat stranding surrounding an ascending colonic diverticulum (arrow in **a**). There is focal free intraperitoneal air within the fat stranding (arrow in **b**). Findings represent acute perforated diverticulitis. Incidental note of a gallstone

- **Imaging**: **CT**
  - Diverticula appear as small, air-filled sacculations protruding outward from the colonic wall within the involved segment and with signs of inflammation, including focal colonic wall thickening, pericolic fat stranding, and/or phlegmon (Fig. 10.25).
  - None or a few small, nonenlarged nodes.
- It is imperative to differentiate an occult colon cancer that may mimic diverticulitis with pericolonic fat infiltration.
- A colonoscopy is usually not performed on a patient during an acute episode of inflammation. It is done 6–8 weeks after an acute incident.
- **Complicated diverticulitis**: Complications of acute diverticulitis include abscess, dissemination of infection through the superior mesenteric vein and portal vein into the liver with hepatic abscess, adjacent small bowel obstruction from adhesions, fistulas with adjacent organs when untreated, perforation (Figs. 10.26 and e10.15) or lower gastrointestinal bleed (Fig. 10.27).

Fig. 10.27 Axial CT images of the abdomen in noncontrast (**a**), arterial phase (**b**), portal venous phase (**c**), and sagittal image in arterial (**d**) are shown in a 71-year-old woman with complaints of melena. There is a curvilinear hyperdensity on the arterial phase image, which was not present in the noncontrast image (**a**), representing active contrast extravasation in the distal transverse colon (arrow in **b** and **d**), which is persistent but less intense in the portal venous phase (arrow in **c**). The patient underwent a colonoscopy and was found to have fresh blood in the sigmoid colon and rectum without active bleeding during the procedure. The patient was monitored for hemoglobin and discharged home in stable condition

- Management depends on whether the disease is localized or complicated.
  - Localized uncomplicated diverticulitis: medical management with intravenous antibiotics and anti-inflammatory medications.
  - Diverticular abscess: CT or US-guided percutaneous drainage.
  - Perforation: emergency surgery with segmental resection and anastomosis.
- **Segmental Colitis Associated with Diverticula (SCAD)**
  - SCAD is a kind of chronic inflammation involving the interdiverticular mucosa of the colon with relative sparing of the diverticular orifices.
  - It most commonly involves the sigmoid colon with relative sparing of the right colon.
  - Diagnosis is primarily based on endoscopic and pathological findings since the imaging findings resemble inflammatory bowel disease.
  - CT: Significant colonic wall thickening, more pronounced than the surrounding inflammatory findings (Fig. 10.28).

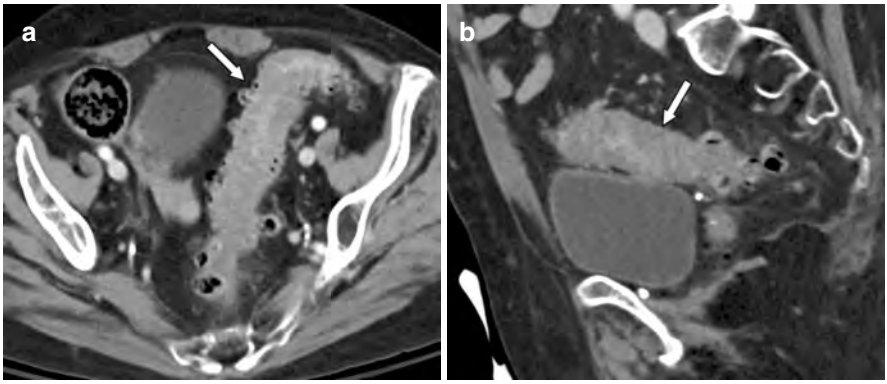

Fig. 10.28 Coronal (**a**) and axial (**b**) CT images of the pelvis in a patient with chronic lower abdominal pain show segmental circumferential wall thickening of the sigmoid colon with diverticulosis. There were no inflammatory findings to suggest acute colitis. Findings are consistent with segmental colitis associated with diverticulosis (SCAD)

  - Management: Antibiotics with the addition of mesalamine and corticosteroids for patients unresponsive to antibiotics. Intractable cases can be treated with surgical resection.

Epiploic Appendagitis

- Epiploic appendages are subserosal pockets of fat extending off the colonic surface. Twisting and infarction of these appendages result in clinical symptoms that mimic diverticulitis or appendicitis.
- It is a rare self-limiting cause of abdominal pain and mimics acute diverticulitis or acute appendicitis in clinical presentation and examination, depending on the laterality of pain.
- **Imaging**: **CT**
  - Characteristic imaging appearance with an oval, fat-density structure seen along the colon with a high-density rim and punctate central hyperdense dot representing the thrombosed vascular pedicle (Fig. 10.29).
  - Surrounding inflammatory fat stranding and focal peritoneal thickening can be present.
  - Findings are classically around the colonic circumference, predominantly along the anti-mesenteric margins or anterior aspect of the sigmoid and descending colon.
  - In chronic cases, they can calcify and detach, forming an intraperitoneal loose body.
- These are managed with nonsteroidal anti-inflammatory drugs (NSAIDs) as it is self-limiting.
- The importance of correct identification is that it mimics appendicitis or diverticulitis, thereby avoiding unnecessary surgery.

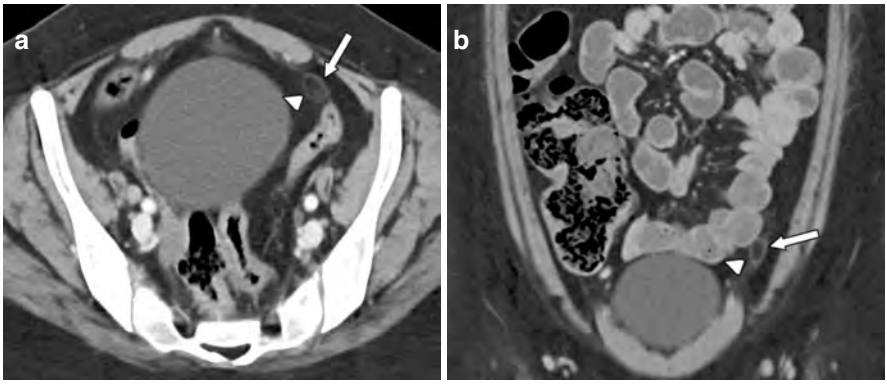

Fig. 10.29 Axial (**a**) and coronal (**b**) CT images of the abdomen and pelvis in a patient with left lower abdominal pain show an oval fat-density lesion along the anti-mesenteric border of the distal descending colon (arrows in **a** and **b**) and mild surrounding fat stranding (arrowhead in **b**). There is a subtle central hyperdense focus within the lesion (arrowhead in **a**). Findings are consistent with epiploic appendagitis

Ischemia

- Ischemic colitis usually occurs in the elderly after 60 years of age.
- The most common risk factors include atherosclerotic vascular disease and non-insulin-dependent diabetes mellitus (Table 10.1).
- Atherosclerotic vascular disease can be embolic or atheromatous in origin, with the left colon and sigmoid the most commonly involved in the watershed areas (SMA and IMA meet each other at the splenic flexure and sigmoid).
- It can be from acute occlusion from embolism/thrombosis or chronic decreased blood supply to the colon.
- The vascular insult is classified into two types: ischemic or reperfusion injury.
- Diagnosis is based on clinical suspicion, serological, imaging, endoscopic, and pathological findings.
- Timely diagnosis is crucial and imaging plays a key role.

Imaging

- Given the acuity and morbidity associated with ischemic colitis, CT is the primary and best modality to evaluate patients with suspicion of ischemic colitis.
  - Ultrasound is nonspecific and operator-dependent.
  - MRI is time-consuming and limited utility in patients with acute severe pain who cannot remain still in the scanner.
- **Abdominal radiograph**
  - Thumbprinting-gas-filled colon with rounded densities along the wall resulting from the edematous colonic wall.
  - Other signs include pneumatosis, portal venous gas, and megacolon.

- **CT**
  - First-line imaging modality for diagnosing mesenteric ischemia.
  - Early reversible stage: submucosal edema, mucosal enhancement, and marked pericolic inflammatory signs (Fig. 10.30).
  - Late irreversible stage: decreased or absent wall enhancement representing transmural infarction, sometimes dense wall on noncontrast images, and pneumatosis coli (Fig. e10.16).
  - The chronic phase can also present with loss of haustral folds and strictures.
  - Other imaging findings include shaggy mesentery with pericolic fluid.
  - CT signs of acute mesenteric ischemia include bowel wall thinning, diminished or absent mural enhancement when the etiology is arterial embolism or thrombosis (constitutes ~80% of acute mesenteric ischemia). Whereas, with mesenteric venous thrombosis (~5–20%), there is significant bowel wall thickening, mural stratification, mesenteric stranding, and edema (Fig. 10.30).
  - Nonocclusive mesenteric ischemia (NOMI) is a term used when no occlusive etiology is identified, and mesenteric ischemia is presumed to be due to vasoconstriction or spasm to preserve cardiac or nervous system blood flow. CT angiography usually shows a beaded appearance of the SMA and features of CT hypoperfusion complex—mural hyperenhancement, renal and adrenal hyperenhancement.
- **CT report should ideally include the following details in the report**
  - Type of vascular insult (ischemia/reperfusion).
  - Segment of the colon involved.
  - Extent of damage (long segment/multiple segments).
  - Phase of ischemia (acute/subacute/chronic).

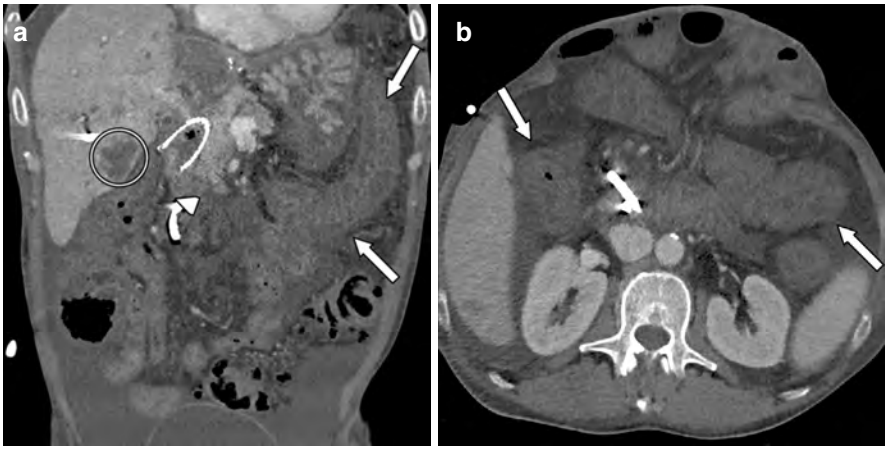

Fig. 10.30 Coronal (**a**) and axial (**b**) CT images of the abdomen and pelvis in a 64-year-old male patient with a history of cholangiocarcinoma presenting with abdominal pain. Images show diffusely hypoenhancing and thickened colonic wall involving ascending to the transverse colon (arrows in **a** and **b**). An occlusive superior mesenteric vein thrombus (arrowhead in **a**) caused ischemic colitis of the involved segments in the distribution. There was a small volume of ascites. Note the hypodense metastatic liver lesion in the right lobe of the liver (circle in **a**)

- **Management**
  - In contrast to popular belief, 85% of cases improve within 1–2 days following conservative management, like bowel rest and IV fluids, and it resolves within 1–2 weeks.
  - Surgical management is restricted to the excision of irreversibly necrosed intestine to limit the complications of sepsis, stricture, and protein-losing enteropathy.

Trauma and Colonic Perforation

- Gastrointestinal perforation is one of the common medical emergencies, which is associated with significant mortality rates of 30–50%.
- The etiology of colonic perforation includes prior surgery, trauma, and foreign bodies (Fig. e10.17). However, malignancy is the most common cause of about 36% of colorectal perforations.
- Colonic perforations usually have a slower protracted course with secondary bacterial peritonitis or abscesses. Also, perforation into the retroperitoneal space is present late.
- **CT**: It is a crucial investigation in hemodynamically stable patients, and CT helps localize the site of colonic rupture and complications of perforation.
- **Imaging findings** (Fig. e10.17)
  - Colonic wall discontinuity.
  - Concentrated extraluminal gas and/or oral contrast close to the bowel wall.
  - Pericolonic fat stranding.
  - Ancillary findings
    - Bowel wall thickening
    - Abnormal bowel wall enhancement
    - Fecal impaction
    - Ischemia
    - Foreign bodies
    - Free fluid
- It is important to differentiate contained versus free perforation as the latter requires emergent surgery.
- Appendiceal perforation has been discussed above in the appendicitis section. Unlike colonic perforation, if present, the free air is usually minimal, about 1–2 mL.
- Pneumoperitoneum in suspected perforation is best evaluated with high sensitivity in lung window settings on CT. However, there is limited specificity since intraperitoneal and retroperitoneal air can be present from other causes like peritoneal lavage and mechanical ventilation.
- Unlike gastric/duodenal and small bowel perforations, the amount of free air from colonic perforation can be variable and sometimes helps localize the perforation site.
- Similarly, the location of free air can be a clue to the site of perforation as well. With colonic perforations, free air is commonly seen in the pelvis, mesenteric folds, and retroperitoneal space.

Obstruction

- Large bowel obstructions (LBO) are way less common than small bowel obstructions and account for 2–4% of surgical admissions.
- LBO are usually from mechanical obstruction and associated with a high risk of perforation and peritonitis, resulting in high morbidity of 42–46% and mortality rates of 13–19%.
- Common causes of LBO include colon cancer (60–80%), volvulus (11–15%), and fecal impaction.
- Imaging investigation starts with an abdominal radiograph, which has a sensitivity of 84% and a specificity of 72% due to its limited ability to differentiate obstruction from pseudo-obstruction. In such cases, CT of the abdomen and pelvis is performed.
- **Imaging findings**
  - Dilated colonic loops proximal to a transition point and decompressed colon distal to the transition point.
  - The cecum is usually the most dilated colonic part.
  - The transition point can be a malignant mass that presents as asymmetric, short-segment colonic wall thickening and/or enhancing soft-tissue mass, causing shouldering at the site of obstruction (Fig. 10.31).
- **Volvulus**
  - Colonic volvulus accounts for 10–15% of all LBO causes.
  - Sigmoid volvulus (60–75%) is more common than cecal volvulus (25–40%), with other less common volvulus involving transverse colon and splenic flexure.
  - Though an abdominal radiograph is usually the initial imaging exam performed, CT is the standard diagnostic modality.
  - **Cecal volvulus**

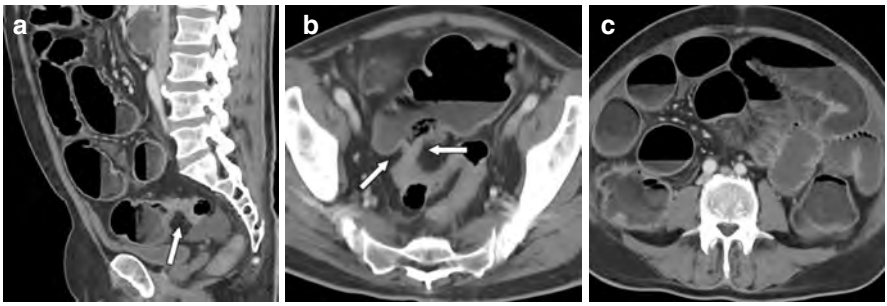

Fig. 10.31 Sagittal (**a**) and axial (**b**, **c**) images of CT abdomen and pelvis in a 50-year-old man with a history of treated sigmoid adenocarcinoma, presented with abdominal pain and constipation. The images show multiple dilated colonic and distal small bowel loops with air-fluid levels. There is an abrupt transition point at the irregular stricture in the treated sigmoid colon (arrows in **a** and **b**). Findings represent colonic obstruction from stricture in the sigmoid colon

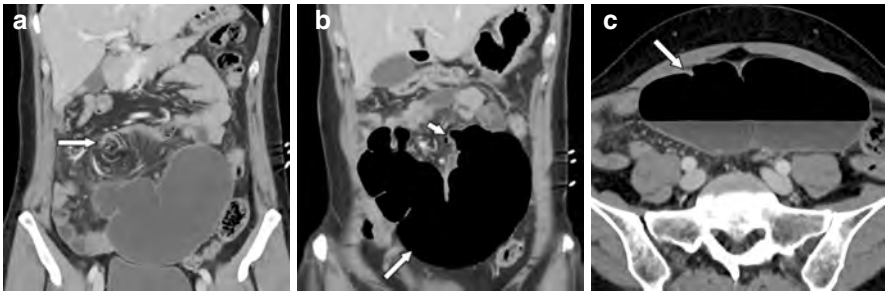

Fig. 10.32 Coronal CT images of the abdomen and pelvis in different slices (**a**, **b**), and axial (**c**) images in a 46-year-old woman show dilated cecum with an air-fluid level measuring 7.1 cm and in a horizontal orientation in the lower abdomen (arrows in **b** and **c**). The appendix is air-filled (arrowhead in **b**). Swirling of the mesentery noted (arrow in **a**). CT findings were consistent with the operative report—cecal bascule

Commonly associated with congenital anomalies like problems with fixation of the right colon/increased motility of the right colon.

Types: axial and bascule

- **Cecal bascule**: a rare type of cecal volvulus where the cecum folds on itself in an anteromedial direction (Fig. 10.32).
- Less likely to strangulate, unlike other types of cecal volvulus.

Imaging findings (Fig. e10.18)

- Arises in the right lower quadrant of the abdomen.
- Extends to left upper quadrant or epigastric region.
- Preserved haustral pattern.
- Distal colon is decompressed.
- Small bowel is dilated.

Management

- Resection is required in patients with nonviable or perforated bowel.
- If the colon is viable, nonoperative procedures can be used.
- Endoscopic reduction is not recommended, unlike sigmoid volvulus.

– **Sigmoid volvulus**

Imaging

- Arises in the left lower quadrant of the abdomen/pelvis.
- Extends to the right upper quadrant.
- Ahaustral appearance.
- Dilated ascending, transverse, and descending colon resulting from obstruction by the volvulus (Fig. e10.18).

Recurrence is common with sigmoid volvulus, as high as 84%.

Management

- Rigid or flexible sigmoidoscopy is performed first to depict sigmoid viability and allow initial detorsion and decompression.
- Sigmoidectomy is only performed when endoscopic detorsion is not possible or nonviable/perforated colon.

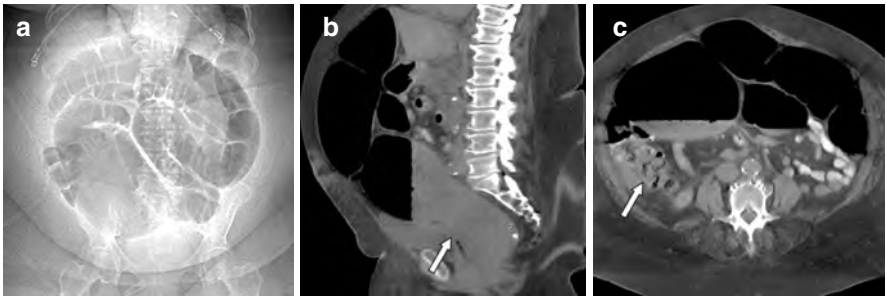

Fig. 10.33 Scanogram image (**a**), sagittal (**b**), and axial (**c**) images of CT abdomen and pelvis in a 70-year-old woman with abdominal pain and distention. Images show multiple, air-filled, dilated colonic loops involving transverse colon to rectum without a transition point or obstructive etiology representing pseudo-obstruction. Air-fluid levels were noted within the dilated sigmoid colon (arrow in **b**). Stool noted in the non-dilated ascending colon (arrow in **c**)

- Differential diagnosis and closer mimicker are colonic pseudo-obstruction, also known as Ogilvie syndrome.
- **Colonic pseudo-obstruction**
  - Also known as Ogilvie syndrome.
  - Acute colon dilatation is due to altered autonomic innervation without a mechanical obstruction.
  - A few causes include a history of surgery, metabolic derangements, cardiac and neurological diseases, medications, and systemic infections.
  - **Imaging findings differentiating from LBO**

    Dilation only involves portions of the colon, frequently up to the splenic flexure. In acute inflammatory processes like appendicitis or cholecystitis, a dilated colon involves only the ascending colon and hepatic flexure, resulting in a "colon cut-off sign."

    In cases with diffuse dilation, the relative cecal size helps differentiate LBO from pseudo-obstruction. In contrast, the cecal diameter in the latter is less than the rest of the dilated colon (Figs. 10.33 and e10.19).

    The extensive distension can lead to ischemia and perforation despite the absence of mechanical obstruction.

Neoplasm (Including Rectal Cancer)

- Colorectal adenocarcinoma is the most common gastrointestinal malignancy and one of the significant causes of mortality and morbidity in the world.
- Optical colonoscopy remains the gold standard for screening and diagnostic purposes of colorectal malignancy detection. However, CTC is a valuable complementary diagnostic tool for colonoscopy. It has widened the possibility of screening for colorectal malignancies, particularly for patients who cannot undergo screening colonoscopy for various reasons.

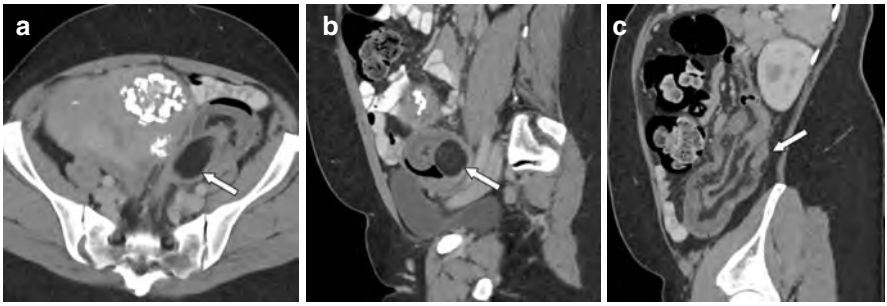

Fig. 10.34 Axial (**a**) and sagittal (**b**, **c**) images of CT abdomen and pelvis show bowel-within-bowel configuration (arrow in **c**) involving the sigmoid colon representing intussusception with a lead point from a submucosal lipoma (arrow in **a** and **b**), which was later resected

- Screening of colon cancer includes fecal occult blood tests and colonoscopy. Alternatively, CTC can be used as a screening modality for colon cancer.
- CTC has good sensitivity for detecting T3-T4 grade colonic tumors, increasing the accuracy of detection.
- However, MRI has higher sensitivity and accuracy and is the standard for staging colorectal tumors and guiding therapy in these patients.

Colonic Masses

- Colorectal masses include a variety of benign and malignant masses.
- Benign masses include colonic polyps-adenomatous versus hyperplastic polyps, submucosal tumors like lipoma (Fig. 10.34), lymphangioma, and rare ones like leiomyoma and hemangioma.
- **Villous adenomas**
  - Villous colonic lesions are benign but have the potential to be malignant and hence detected on imaging or colonoscopy. Hence, it is essential to know the different imaging appearances of these villous adenomas.
  - The risk of malignancy depends on the adenomatous polyp size (>10 mm in size adenomas of any histology), histopathology (>25% villous component on histology), and severity of epithelial dysplasia (high-grade dysplasia on histology). For example, polyps >2 cm in size have >40% risk of being malignant (Fig. 10.35).
  - Patients with hereditary polyposis or colorectal cancer syndromes have an increased risk of developing villous adenomas and cancer at younger age. For example, patients with familial adenomatosis polyposis (FAP) have almost 100% risk of developing colorectal cancer and 4–12% lifetime risk of developing duodenal adenocarcinoma. Similarly, hereditary nonpolyposis colorectal cancer (HNPCC) had an 80% chance of developing colon cancer.
  - **Imaging**

    Most commonly seen in the rectum and rectosigmoid colon.

    Large, lobulated, or frond-like appearance, usually larger than 2–3 cm in size (Fig. e10.20).

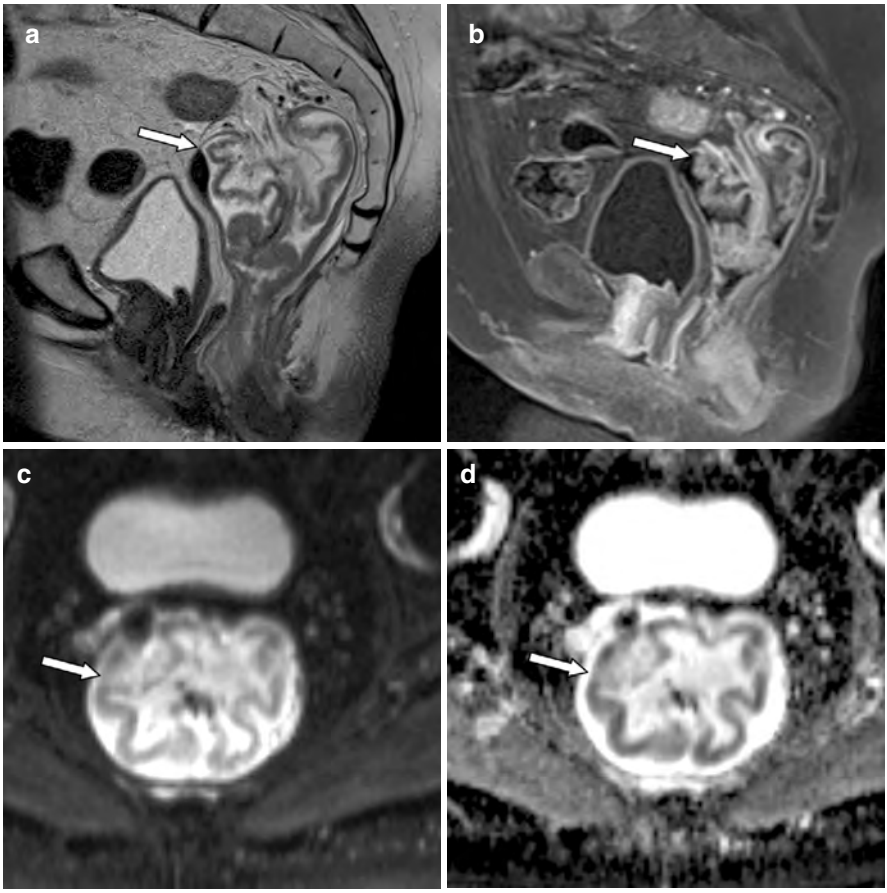

Fig. 10.35 MRI images of the pelvis in sagittal T2-weighted image (**a**), sagittal postcontrast T1-weighted image (**b**), axial DWI (**c**), and axial ADC (**d**) images show a large heterogeneous, predominantly T2 hyperintense polypoidal mass in the proximal and mid rectum (arrow in **a**). The T2 hyperintense portions of the mass do not show enhancement or restricted diffusion and represent mucinous contents. The solid portions of the mass enhance with restricted diffusion (arrows in **b**–**d**). The resected mass pathology was reported as mucinous adenocarcinoma

MRI: The polyps have a thick peripheral T2 hyperintense layer due to mucinous coating or high cellularity, but overall have heterogeneous T2 intermediate to high signal, low signal on T1-weighted images, and heterogeneous enhancement (Fig. 10.36).

- **Management**: Given the risk of malignancy, these are usually surgically resected.

- **Colon cancers**
  - Adenocarcinomas are the most common type of colorectal malignancy, with less common mucinous and signet-ring cell carcinomas (Table 10.1).
  - Most tumors occur in the rectosigmoid (55%), followed by cecum and ascending colon (20%).

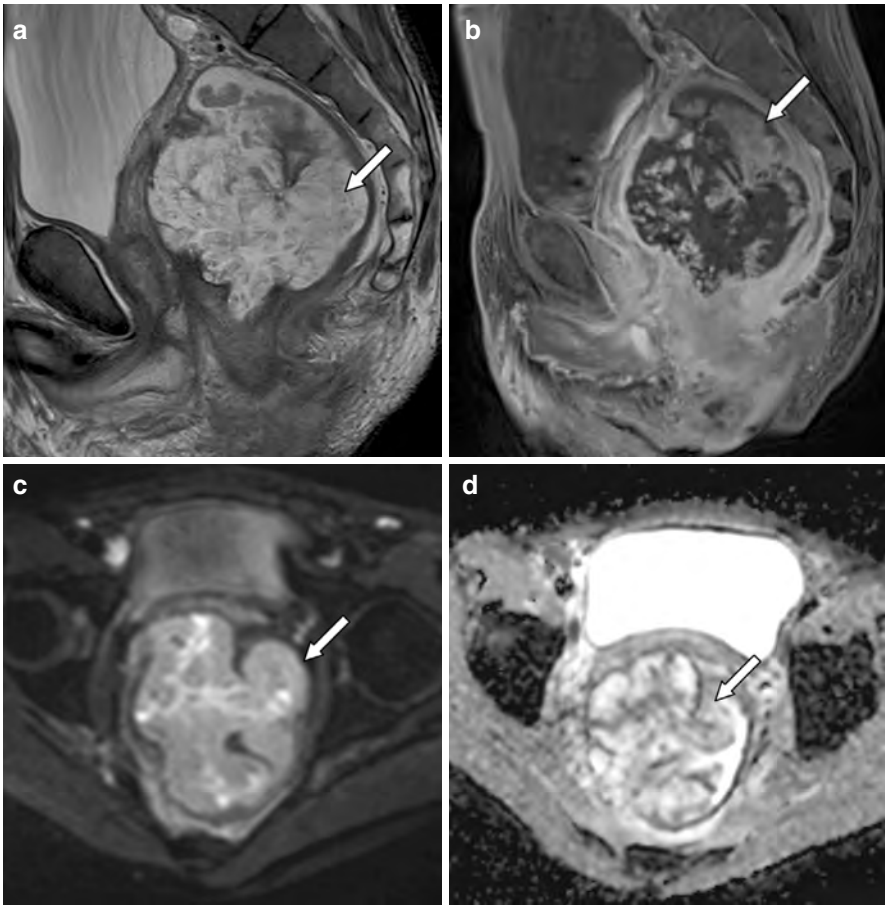

Fig. 10.36 MRI images of the pelvis in sagittal T2-weighted image (**a**), sagittal postcontrast T1-weighted image (**b**), axial DWI (**c**), and ADC (**d**) show an 8.1 cm, polypoid mass with heterogeneous T2 signal, peripheral enhancement and restricted diffusion, arising from the rectosigmoid and projecting intraluminally into the mid rectum (arrows). There was fluid surrounding the mass in the rectum. There were no signs of colonic obstruction despite the size of the mass. The resected mass was reported as a rectal tubulovillous adenoma

- Most recurrences (85%) occur within the first 3 years after surgery. Hence, the post-treatment surveillances are focused on these initial 3 years.
- **Staging**: CT chest, abdomen, and pelvis. The abdomen and pelvis are in the arterial and portal venous phase, covering the chest and abdomen to identify liver metastases. The recommendations are based on ACR appropriateness criteria and NCCN guidelines.
- **Imaging findings**

  Short-segment asymmetric/eccentric colonic wall thickening (Figs. 10.37 and 10.38) or enhancing soft-tissue colonic mass (Fig. 10.39).

  Luminal narrowing at the site of the tumor (Fig. 10.39).

  Invasion into adjacent organs (Fig. 10.40).

Fig. 10.37 Coronal (**a**) and axial (**b**) CT images of the abdomen and pelvis in a 58-year-old woman show focal irregular circumferential thickening of the mid-descending colon (arrows). Mild irregularity of the wall beyond the serosa was seen along the anterior margin (arrowhead in **b**). There were no obstructive signs. Colonoscopy (**c**) showed asymmetric thickened, erythematous, and ulcerated colonic mucosa, later biopsy-proven as moderately differentiated adenocarcinoma

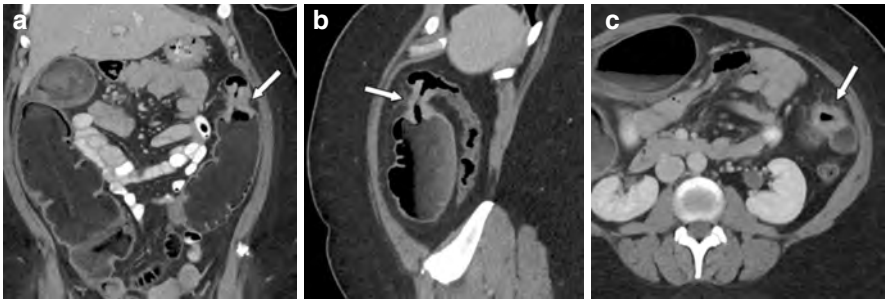

Fig. 10.38 Coronal (**a**), sagittal (**b**), and axial (**c**) images of CT abdomen and pelvis in a 45-year-old woman show short-segment irregular narrowing and thickening at the sigmoid flexure (arrows). The short segment of the abnormal bowel wall involved is well-demarcated (arrows in **a** and **b**). There is minimal pericolonic fat stranding (**c**). This was biopsied and reported as invasive adenocarcinoma

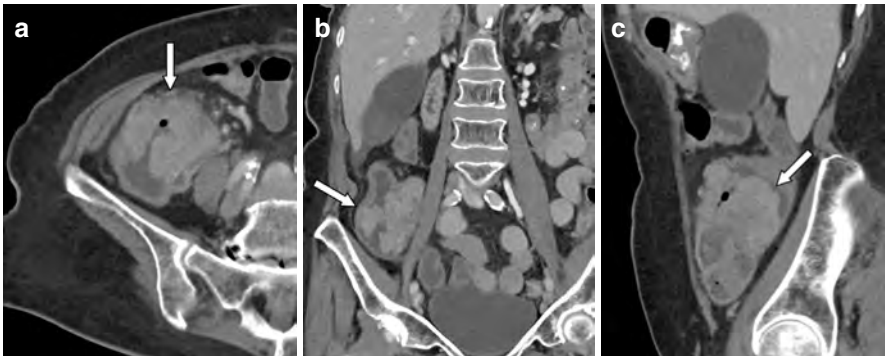

Fig. 10.39 Axial (**a**), coronal (**b**), and sagittal (**c**) CT images of the abdomen and pelvis show a 5.1 cm lobulated, irregular, heterogeneously enhancing mass in the cecum (arrows). The patient underwent a right hemicolectomy, and the pathology was reported as cecal adenocarcinoma

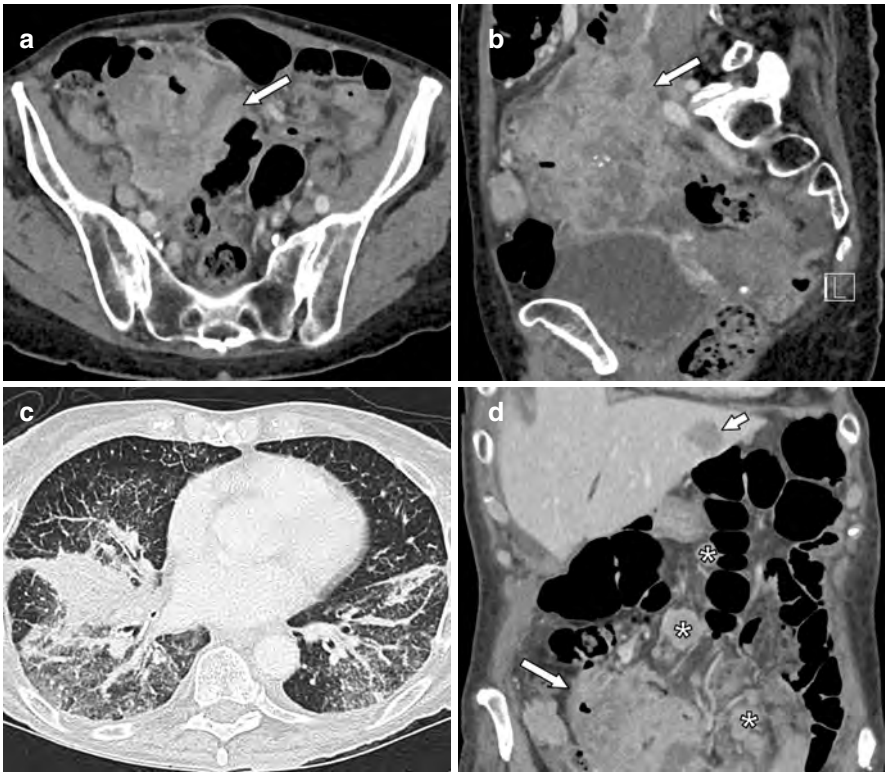

Fig. 10.40 Top row: axial (**a**) and sagittal (**b**) CT images of the pelvis in a 77-year-old woman with weight loss and cough. CT showed a large, irregular, infiltrative heterogeneous mass from the cecum with cystic areas representing necrosis (arrows). The mass infiltrates the adjacent colonic loops. The mass was biopsied and reported as invasive adenocarcinoma. Bottom row: axial chest CT in lung window (**c**) shows a large irregular mass in the superior right lower lobe along the fissure with nodular interstitial thickening and punctate pulmonary nodules representing metastasis. Coronal CT of the abdomen (**d**) shows portions of the colonic mass (arrow), multiple enlarged mesenteric lymph nodes (*), and an irregular hypodense left hepatic lobe metastatic lesion (arrow)

Metastases—most common is liver (Fig. 10.40).
Ascites.
Carcinomatosis with peritoneal nodules.
Colonic obstruction—colon cancer is the most common cause of LBO, accounting for 60–80% of LBO cases.
Nodal staging: Nodes that are >1 cm in size predict nodal metastasis, although size is not the ideal indicator given that benign nodes can be larger than 1 cm (Fig. e10.21).
PET/CT can be useful in preoperative staging, particularly in assessing nodal metastasis using the metabolic activity in the nodes and liver metastasis (accuracy of 99%) and in the postoperative surveillance for recurrence.

- **Management**
  Resectable cancer: colectomy with en bloc removal of regional lymph nodes.
  Unresectable cancer (medically or surgically inoperable tumors): neoadjuvant treatment.

- **Rectal cancers**
  - Tumors occurring in the 15 cm length of the bowel loop from the anal verge are rectal tumors.
  - Most commonly, adenocarcinoma, with other less common types being mucinous tumors. When distal rectal tumor pathology is reported as squamous cell carcinoma, they are treated as anal cancers.
  - Mucinous tumors are usually higher grade at presentation and have a higher metastatic tendency.
  - **Staging**: MRI pelvis is recommended for primary diagnosis, and T and N of TNM staging of rectal tumors based on ACR appropriateness criteria and NCCN guidelines and follow-up of treated rectal and anal tumors.
  - **Follow-up imaging**: MRI of the pelvis is recommended for post-treatment follow-up of the primary tumor. However, CT or PET/CT can be performed depending on the clinical suspicion.
  - **Imaging findings**
    Polypoidal, rectal thickening or solid mass with T2 intermediate signal (Fig. e10.22).
    Spiculation of mesorectal fat when the tumor extends outside the lamina propria (Fig. 10.41).
    Invasion into adjacent organs with or without fistula (Figs. 10.42 and e10.23).
    Nodal metastasis with regional nodes being mesorectal and internal iliac nodes. Mesorectal nodes are the first and most common nodes involved, usually within 5 cm of the primary tumor (Fig. 10.43).
  - MRI structured reporting for rectal cancers
    Structured reporting is vital for standardization and good quality reports as the descriptors and staging are used in deciding patient management and follow-up.
    The structured reporting template created and proposed by the Society of Abdominal Radiology (SAR) was adopted by the National Accreditation Program for Rectal Cancer (NAPRC).
    Things to remember when using the SAR reporting template:
    - The template only applies to rectal adenocarcinomas with a biopsy-proven malignancy before imaging.
    - The template does not apply to squamous cell carcinoma histology of tumors as the distal rectal squamous cell carcinomas should be staged as anal cancers.
    - If there is no biopsy report available before pelvic MRI, the MR report conclusion should mention that the staging may not be applicable if cancer is not reported at resection.

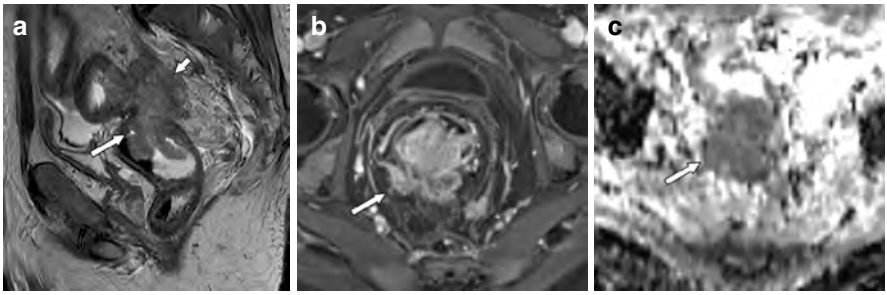

Fig. 10.41 MRI images of the pelvis in sagittal T2-weighted image (**a**), axial postcontrast T1-weighted image (**b**), and axial ADC (**c**) show an irregular T2 hypointense, enhancing mass with restricted diffusion in the rectosigmoid (arrows) extending outside the bowel wall into the presacral soft tissues (arrowhead in **a**). The mass was a stage T3d N+ rectal tumor by imaging grading

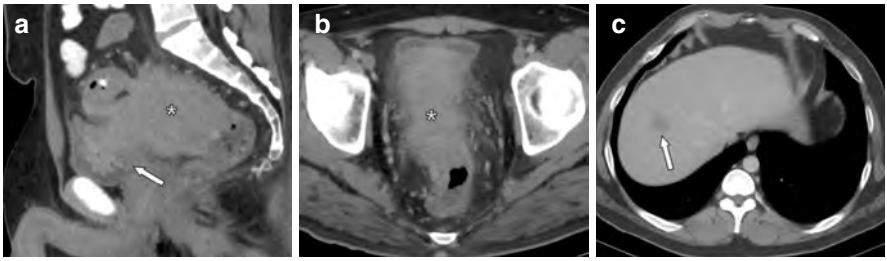

Fig. 10.42 Sagittal (**a**) and axial (**b**) CT images of the pelvis and axial CT of the abdomen (**c**) in a 30-year-old man with pelvic pain show a large infiltrative mass in the rectosigmoid (*), fistulizing into the urinary bladder anteriorly (arrow in **a**). There was an irregular hypodense lesion in segment 8 of the right lobe liver (arrow in **c**), which was later biopsy-proved to be metastasis. Biopsy of the mass was reported as an invasive, high-grade adenocarcinoma

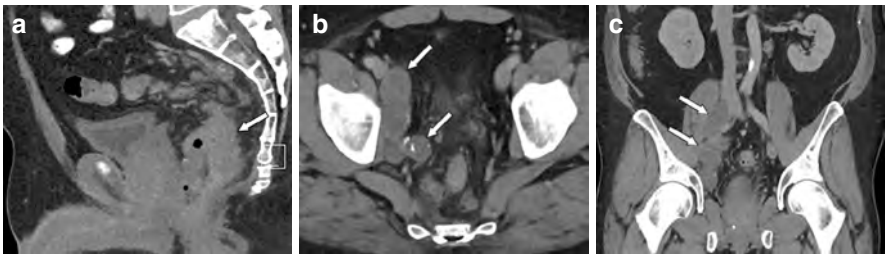

Fig. 10.43 Sagittal (**a**), axial (**b**), and coronal (**c**) CT images of the abdomen and pelvis show rectal wall thickening (arrow in **a**), which was biopsy proven to be rectal adenocarcinoma. Multiple enlarged hypodense metastatic lymph nodes are along the right internal iliac, obturator (arrows in **b**), and external and common iliac nodes (arrows in **c**)

- If rectal adenocarcinoma is reported on a resected polyp, the template may be used with modification/abbreviation.

The rectal cancer reporting template is listed in Table 10.2.

– **Management**

Tumor in the upper rectum: surgery—low anterior resection (LAR) with total mesorectal resection.

Tumors in the distal rectum: depending on the local extension, sphincter-sparing surgeries or abdominoperineal resection (APR) are chosen.

- **Colonic lymphoma**
  - Primary lymphomas of the gastrointestinal (GI) tract are rare, reported as 6–12% of GI lymphomas, and usually involve only one site.
  - It commonly affects the cecum and rectum.
  - Most low-grade primary GI lymphomas arise from mucosa-associated lymphoid tissue (MALT), also known as MALT lymphomas or large B-cell lymphomas.
  - Differentiating from primary versus secondary involvement of GI lymphomas: With primary GI lymphomas:

    No lymphadenopathy in the chest or superficial palpable lymph nodes.

Table 10.2 MRI pelvis structured reporting of rectal cancers

Descriptors	MRI findings
Morphology	Polyp, annular, partly annular Solid, mucinous, mixed
Location	Upper-mid-distal rectum based on tumor distance from anal verge Distance of lower border of tumor from anorectal junction in cm Circumferential location in o'clock position Relationship to anterior peritoneal reflection
Size	Size in cm (craniocaudal length)
cT stage	Based on the depth of rectal wall invasion T1 or T2: contained by muscularis propria (distinction between T1 and T2 are based on endoscopic results) T3: extending outside the rectal wall T3ab: ≤5 mm mesorectal invasion T3cd: >5 mm mesorectal invasion T4a: invasion into peritoneum T4b: invasion into adjacent structures or organs
Mesorectal fascia (MRF)	Free or involved (≤1 mm distance between tumor and MRF)
Extramural vascular invasion (EMVI)	Negative or positive (tumor signal extending within vessel)
cN stage	cN0: No suspicious regional nodes cN1: 1–3 suspicious regional nodes cN2: ≥4 suspicious regional nodes
Tumor deposits	Tumor deposits in the mesorectum
Pelvic metastasis (M)	Any nonregional nodes: common iliac, external iliac, inguinal Distant metastasis within the pelvis

"c" prefix indicates pretreatment clinical stage

"y" prefix is used to indicate tumors after neoadjuvant treatment in clinical and pathological staging (e.g., ycTNM or ypTNM)

"p" prefix is used to indicate final TNM stage at pathology after surgical resection

Any involved lymph node is usually confined to the drainage area.
No involvement of the liver or spleen.
White blood count is normal.

– **Imaging**

They can present in different forms:
- Polypoid masses.
- Circumferential thickening, with or without ulceration.
- Cavitary mass involving the mesentery.
- Mucosal nodularity and fold thickening.
- Intussusception can occur with cecal involvement (Fig. 10.44).
- Rare forms: strictures, ulcerative mass with fistula formation, aneurysmal dilation.

Differentiation from colonic adenocarcinoma: GI lymphoma has.
- Well-defined margins with preserved fat planes.
- No invasion into adjacent structures.

Staging
- I—tumor confined to GI tract and multiple noncontiguous lesions.
- II—tumor extends into the abdominal cavity
  – II1—local nodal involvement.
  – II2—distant nodal involvement.
- III—penetration into adjacent tissue or organs.
- IV—disseminated extranodal involvement with supradiaphragmatic nodal involvement.

- **Anal cancers**
  – Relatively uncommon tumors of the GI tract with a reported incidence of <2%.
  – Almost always squamous cell carcinomas, with the most common risk factor being human papillomavirus (HPV) types 16 and 18 infection. The other significant risk factor is homosexual men with HIV infection.
  – Imaging is crucial, mainly to differentiate anal from rectal tumors.

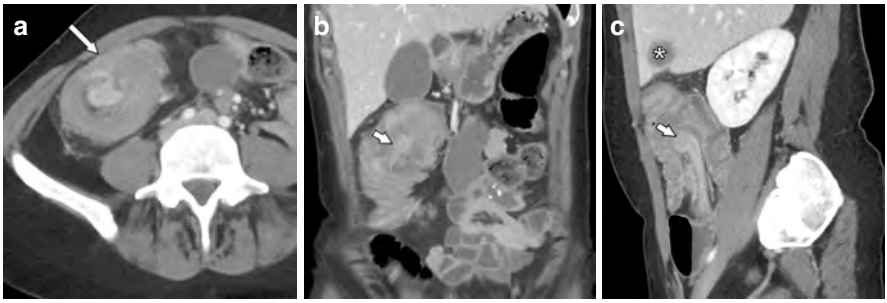

Fig. 10.44 Axial (**a**), coronal (**b**), and sagittal (**c**) CT images of the abdomen and pelvis in a 40-year-old woman show a short segment of ascending colon demonstrating marked colonic wall thickening measuring 1.8 cm in thickness but without luminal narrowing (arrow in **a**). This segment also has colo-colic intussusception (arrowhead in **b** and **c**). A biopsy of the colonic wall was reported as diffuse large B-cell lymphoma

– The dentate line marks the delineation of columnar epithelium in the rectum from squamous epithelium in the anal canal.
– **Imaging**

  MRI is the gold standard for imaging of anal cancers, for preoperative staging, and posttreatment follow-up.

  Lobulated intraluminal or extramural infiltrative mass with intermediate to high signal on T2W images and isointense to hypointense on T1W images (Fig. e10.24).

  It tends to spread circumferentially (Fig. 10.45).

  Usually located within 1.5 cm from the anal verge and seen along the anterior wall of the anal canal.

Fig. 10.45 A 32-year-old man with a history of HIV. MRI images of the pelvis in sagittal T2-weighted image (**a**), sagittal postcontrast T1-weighted image (**b**), axial postcontrast T1-weighted image (**c**), and axial ADC (**d**) show mass with thick hypoenhancing wall and central necrosis arising from the anal canal extending into the distal rectum (arrows). There is peripheral restricted diffusion in the solid portions of the mass (arrow in **d**). The mass was resected and reported as HPV-mediated, invasive, moderately differentiated squamous cell carcinoma

T-staging is primarily based on the size of the lesion rather than the depth of invasion.

- T1: <2 cm in greatest dimension.
- T2: 2–5 cm.
- T3: >5 cm.
- T4: invading adjacent structures like the vagina, urethra, bladder, and prostate (Fig. 10.46).

Direct invasion into the rectal wall, perianal skin, subcutaneous soft tissues, and sphincter is not considered a T4 disease (Fig. e10.25).

Regional lymph nodal involvement: inguinal and external iliac nodes.

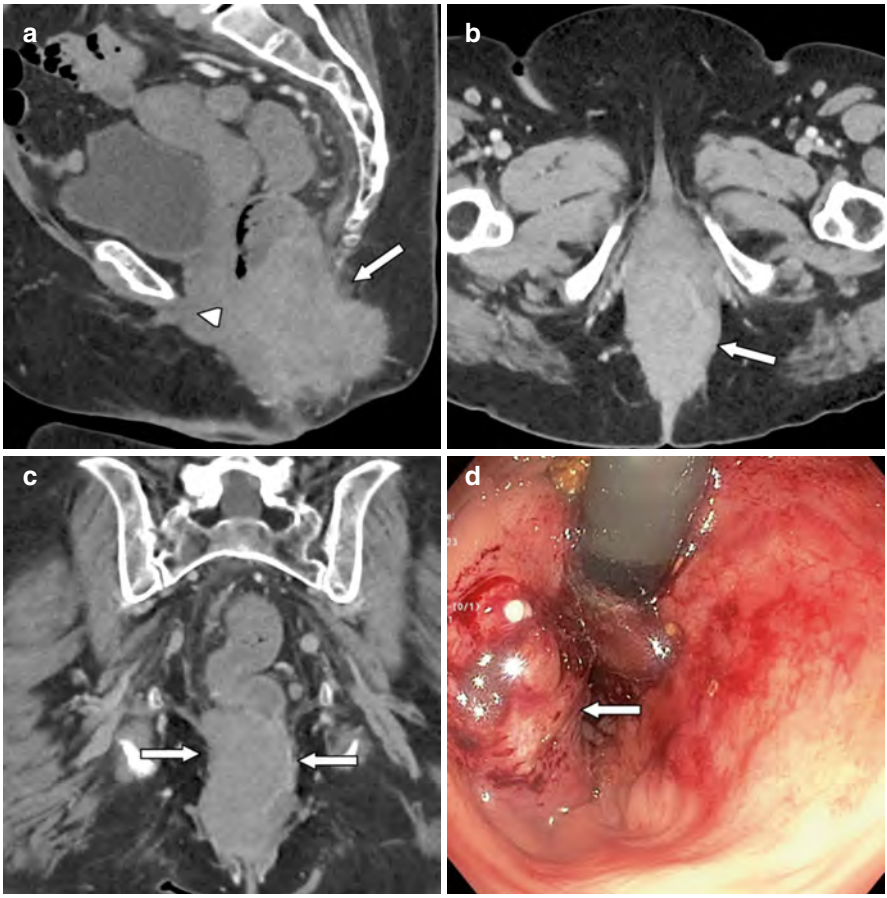

Fig. 10.46 Sagittal (**a**), axial (**b**), and coronal (**c**) CT images of the pelvis in a 75-year-old female patient with rectal bleeding. The images show an 8.8 cm anal canal mass involving the distal rectum (arrow in **a**), invading the distal vagina (arrowhead in **a**) and infiltrating the levator ani muscles (arrow in **b** and **c**). Flexible sigmoidoscopy (**d**) showed a nonobstructive friable mass in the distal rectum and proximal aspect of the dentate line (arrow in **d**). The resected mass pathology was reported as HPV-positive, invasive, moderately differentiated squamous cell carcinoma involving anorectal junction

Post-treatment imaging assessment of treatment response: decreased tumor size with reduced signal intensity on T2-weighted images is considered a positive treatment response.

– **Management**

Chemoradiation is the standard treatment and serves to preserve the sphincter complex.

Salvage surgery with APR is reserved only for unresponsive to treatment patients.

Recurrences are common, with up to 35% having locoregional or metastatic relapse despite combination treatment.

Post-treatment follow-up imaging is done with an MRI of the pelvis [1–35].

References

1. Jaremko JL, Crockett A, Rucker D, Magnus KG. Incidence and significance of inconclusive results in ultrasound for appendicitis in children and teenagers. Can Assoc Radiol. 2011;62:197–202.
2. Swenson DW, Ayyala RS, Sams C, Lee EY. Practical imaging strategies for acute appendicitis in children. AJR Am J Roentgenol. 2018;211:901–9.
3. Partain KN, Patel A, Travers C, McCracken CE, Loewen J, et al. Secondary signs may improve the diagnostic accuracy of equivocal ultrasounds for suspected appendicitis in children. J Pediatr Surg. 2016;51(10):1655–60.
4. Zhang H, Liao M, Chen J, Zhu D, Byanju S. Ultrasound, computed tomography or magnetic resonance imaging: which is preferred for acute appendicitis in children? A meta-analysis. Pediatr Radiol. 2017;47:186–96.
5. Ceresoli M, Zucchi A, Allievi N, Harbi A, Pisano M, et al. Acute appendicitis: epidemiology, treatment and outcomes-analysis of 16544 consecutive cases. World J Gastrointest Surg. 2016;8(10):693–9.
6. McGrath B, Buckius MT, Grim R, Bell T, Ahuja V. Economics of appendicitis: cost trend analysis of laparoscopic versus open appendectomy from 1998 t0 2008. J Surg Res. 2011;171(2):e161–8.
7. Bucklius MT, McGrath B, Monk J, Grim R, Bell T, Ahuja V. Changing epidemiology of acute appendicitis in the United States: study period 1993-2008. J Surg Res. 2012;175:185–90.
8. Estey A, Poonai N, Lim R. Appendix not seen: the predictive value of secondary inflammatory sonographic signs. Pediatr Emerg Care. 2013;29:435–9.
9. Thoeni RF, Cello JP. CT imaging of colitis. Radiology. 2006;240(3):623–38.
10. Maddu KK, Mittal P, Shuaib W, Tewari A, Ibraheem O, Khosa F. Colorectal emergencies and related complications: a comprehensive imaging review—imaging of colitis and complications. AJR Am J Roentgenol. 2014;203(6):1205–16.
11. Gajendran M, Loganathan P, Jimenez G, Catinella AP, Ng N, Umapathy C, Ziade N, Hashash JG. A comprehensive review and update on ulcerative colitis. Dis Mon. 2019;65(12):100851.
12. Zisman TL, Rubin DT. Colorectal cancer and dysplasia in inflammatory bowel disease. World J Gastroenterol. 2008;14(17):2662–9.
13. Barral M, Boudiaf M, Dohan A, Hoeffel C, Camus M, Pautrat K, Fishman EK, Cohen S, Soyer P. MDCT of acute colitis in adults: an update in current imaging features. Diagn Interv Imaging. 2015;96(2):133–49.

14. Olson MC, Bach CR, Wells ML, Andrews JC, Khandelwal A, Welle CL, Fidler JL. Imaging of bowel ischemia: an update, from the AJR Special Series on Emergency Radiology. AJR Am J Roentgenol. 2023;220(2):173–85.
15. Pouli S, Kozana A, Papakitsou I, Daskalogiannaki M, Raissaki M. Gastrointestinal perforation: clinical and MDCT clues for identification of etiology. Insights Imaging. 2020;11(1):31.
16. Singh JP, Steward MJ, Booth TC, Mukhtar H, Murray D. Evolution of imaging for abdominal perforation. Ann R Coll Surg Engl. 2010;92(3):182–8.
17. Pickhardt PJ, Yee J, Johnson CD. CT colonography: over two decades from discovery to practice. Abdom Radiol (NY). 2018;43(3):517–22.
18. Schonberger M, Lefere P, Dachman AH. Pearls and pitfalls of interpretation in CT colonography. Can Assoc Radiol J. 2020;71(2):140–8.
19. Poletti PA, Botsikas D, Becker M, Picarra M, Rutschmann OT, Buchs NC, Zaidi H, Platon A. Suspicion of appendicitis in pregnant women: emergency evaluation by sonography and low-dose CT with oral contrast. Eur Radiol. 2019;29(1):345–52.
20. Pickhardt PJ, Levy AD, Rohrmann CA Jr, Kende AI. Primary neoplasms of the appendix: radiologic spectrum of disease with pathologic correlation. Radiographics. 2003;23(3):645–62. https://doi.org/10.1148/rg.233025134. Erratum in: Radiographics. 2003 Sep–Oct;23(5):1340.
21. O'Connor OJ, McDermott S, Slattery J, Sahani D, Blake MA. The use of PET-CT in the assessment of patients with colorectal carcinoma. Int J Surg Oncol. 2011;2011:846512.
22. Jaffe T, Thompson WM. Large-bowel obstruction in the adult: classic radiographic and CT findings, etiology, and mimics. Radiology. 2015;275(3):651–63.
23. Somwaru AS, Philips S. Imaging of uncommon causes of large-bowel obstruction. AJR Am J Roentgenol. 2017;209(5):W277–86.
24. Choi JS, Lim JS, Kim H, Choi JY, Kim MJ, Kim NK, Kim KW. Colonic pseudoobstruction: CT findings. AJR Am J Roentgenol. 2008;190(6):1521–6.
25. Sun P, Li X, Wang L, Wang R, Du X. Enhanced computed tomography imaging features predict tumor grade in pseudomyxoma peritonei. Quant Imaging Med Surg. 2022;12(4):2321–31.
26. Leonards LM, Pahwa A, Patel MK, Petersen J, Nguyen MJ, Jude CM. Neoplasms of the appendix: pictorial review with clinical and pathologic correlation. Radiographics. 2017;37(4):1059–83.
27. Wei PK, Gupta M, Tsai LL, Lee KS, Jaramillo AM, Smith MP, LeGout JD, Shenoy-Bhangle AS. Spectrum of MRI features of mucin-producing neoplasms in the abdomen and pelvis. Radiographics. 2022;42(2):469–86.
28. Aherne EA, Fenlon HM, Shields CJ, Mulsow JJ, Cronin CG. What the radiologist should know about treatment of peritoneal malignancy. AJR Am J Roentgenol. 2017;208(3):531–43.
29. Flor N, Maconi G, Cornalba G, Pickhardt PJ. The current role of radiologic and endoscopic imaging in the diagnosis and follow-up of colonic diverticular disease. AJR Am J Roentgenol. 2016;207(1):15–24.
30. Minordi LM, Larosa L, Berte G, Pecere S, Manfredi R. CT of the acute colonic diverticulitis: a pictorial essay. Diagn Interv Radiol. 2020;26(6):546–51.
31. Wortman JR, Dhyani M, Ali SM, Scholz FJ. Pearls and pitfalls in multimodality imaging of colonic volvulus. Radiographics. 2020;40(4):1039–40.
32. Li ZH, You DY, Gao DP, Yang GJ, Dong XX, Zhang DF, Ding YY. Role of CT scan in differentiating the type of colorectal cancer. Onco Targets Ther. 2017;10:2297–303.
33. Kim H, Kim JH, Lim JS, Choi JY, Chung YE, Park MS, Kim MJ, Kim KW, Kim SK. MRI findings of rectal submucosal tumors. Korean J Radiol. 2011;12(4):487–98.
34. Mang T, Lefere P. Chapter 19: Benign diseases of the colon and rectum (incl. CT colonography). In: Hodler J, Kubik-Huch RA, von Schulthess GK, editors. Diseases of the abdomen and pelvis 2018–2021: diagnostic imaging—IDKD book. Cham: Springer; 2018.
35. Iyer RB, Silverman PM, DuBrow RA, Charnsangavej C. Imaging in the diagnosis, staging, and follow-up of colorectal cancer. AJR Am J Roentgenol. 2002;179(1):3–13.

Artificial Intelligence (AI) in Abdominal Imaging

11

Florence X. Doo

Key Points

- Artificial intelligence (AI) is poised to transform diagnostic radiology, with increasing integration into clinical workflows.
- As radiology subspecialists, abdominal radiologists should have a basic understanding of AI applications.
- AI-enabled image interpretation has the potential to improve diagnostic accuracy, workflow efficiency, and accessibility of imaging expertise. This chapter will provide an overview of AI, current applications in abdominal imaging, and future directions.

Basic AI Core Concepts

- A**rtificial intelligence (AI)**
  - A field of computer science focused on creating systems capable of performing tasks that require human intelligence.
  - AI encompasses a range of technologies, from simple automated processes to complex machine learning (ML) models.
  - For instance, AI in radiology can be used as a flexible term, ranging from large language models (LLMs) and chatbots, to deep learning models (DL), which can automatically detect abnormalities in X-ray images (Fig. 11.1).

F. X. Doo (✉)
Department of Diagnostic Radiology and Nuclear Medicine, University of Maryland School of Medicine, Baltimore, MD, USA

University of Maryland-Institute for Health Computing (UM-IHC), University of Maryland, North Bethesda, MD, USA
e-mail: fdoo@som.umaryland.edu

© The Author(s), under exclusive license to Springer Nature Switzerland AG 2024

T. Catanzano (ed.), *What Radiology Residents Need to Know: Abdominal Radiology*, What Radiology Residents Need to Know,
https://doi.org/10.1007/978-3-031-76624-4_11

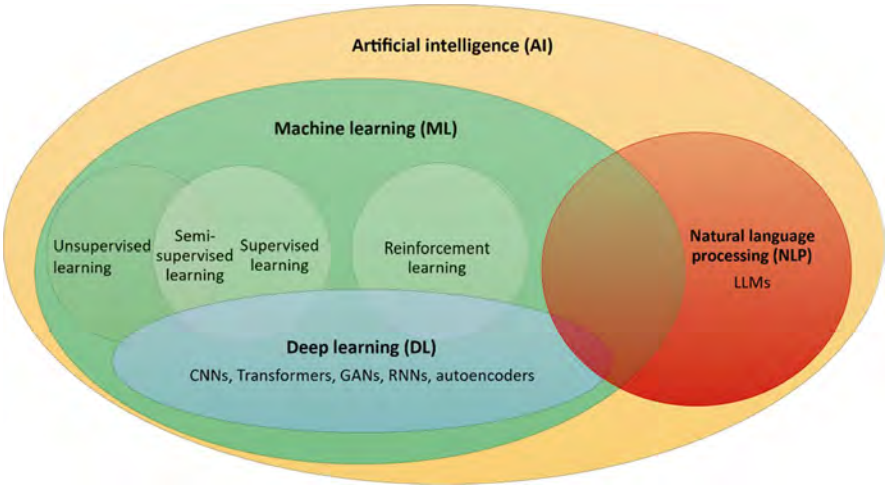

Fig. 11.1 A high-level overview of artificial intelligence terms and related concepts

- **Machine learning (ML)**
  - A core component of AI where algorithms learn from large datasets, identifying patterns and making decisions.
  - In abdominal imaging, ML algorithms can learn from thousands of CT scans to identify common patterns associated with diseases like liver cirrhosis.
  - Supervised learning: An algorithm learns from labeled training datasets, mapping inputs to desired outputs.

    Example: An AI model developed for detecting kidney stones on ultrasound images is trained with images already labeled with known diagnoses such as "with kidney stone" or "without kidney stone."
  - Unsupervised learning: Involves training AI models on data without labeled outcomes, helping to identify hidden patterns.

    Example: Clustering pixels on noncontrast CT scans into different abdominal organ types based on intensity values and spatial relationships, without using pre-labeled organ segmentation maps.
  - Semi-supervised learning: Combination of labeled and unlabeled data during training.

    Example: Detecting liver lesions on CT using a small set of labeled scans and a large pool of unlabeled scans.
  - Reinforcement learning: An area of ML where algorithms learn to make decisions by trial and error, receiving feedback to improve performance.

    Example: An AI agent that adjusts CT reconstruction parameters (filter, iterative strength, etc.) in a simulated environment to maximize a reward function based on diagnostic image quality and reconstruction time. The agent learns the optimal parameters to reconstruct diagnostic quality CT images in the shortest time.

  - Transfer learning: Leverages knowledge gained from one task and applies it to a new related task.
    Example: Using a model trained to detect adult renal cysts, then fine-tuning it to detect pediatric renal cysts.
- **Deep learning**
  - A subset of ML based on artificial neural networks, particularly effective in image recognition.
  - Deep learning algorithms have been used to differentiate between benign and malignant tumors in MRI scans by learning from vast datasets of annotated images.
  - Convolutional neural networks (CNNs)
    CNNs are commonly used for medical image analysis.
    They apply convolutional filters to extract hierarchical feature representations.
    CNNs are effective for tasks like image classification and object detection.
  - Transformers
    Transformers are attention-based deep learning models.
    They analyze relationships between inputs using attention mechanisms rather than convolutional operations.
    Transformers are gaining popularity in medical imaging to integrate multimodal data.
  - Generative adversarial networks (GANs)
    GANs contain a generator and discriminator network.
    The generator creates synthetic data to fool the discriminator.
    GANs can be used to generate synthetic medical images.
  - Recurrent neural networks (RNNs)
    RNNs process sequence data by passing information across sequence steps.
    They are useful for analyzing data like time-series images or clinical reports.
  - Autoencoders
    Autoencoders compress inputs into a lower-dimensional latent space then reconstruct inputs.
    They are used for tasks like medical image denoising and compression.
- **Natural language processing (NLP)**
  - A technology that enables computers to understand, interpret, and generate human language.
  - In radiology, NLP can extract relevant information from radiology reports to aid in decision-making or populate structured reports.
  - Large language models (LLMs)
    Advanced NLP models capable of understanding, generating, and interacting with human language at a sophisticated level.
    LLMs are an emerging technology.
    They can generate detailed radiology report summaries or answer basic clinical queries.
    There are technical limitations including reproducibility and accuracy.

Specific AI Applications in Abdominal Imaging

Noninterpretive AI Applications

- Noninterpretive AI enhances aspects of radiological practice other than direct image interpretation (Fig. 11.2, orange box and arrows).
- Image acquisition and preprocessing (optimization)
  - Image quality enhancement: Can denoise and improve image acquisition, or adjust parameters based on patient-specific data.
  - MRI/CT protocol selection: Recommends optimal imaging protocols based on patient-specific data.
- Workflow and operational efficiency
  - Practice staffing: Automates employee scheduling.
  - Worklist management: Fair list distribution based on modality, complexity, and pace.
  - Patient scheduling and management: Predicts no-shows and optimizes appointment schedules.
  - Billing automation: Automatic billing correction and coding.
  - Radiology report optimization: Use NLP for efficient report generation and data extraction.
- Triage and follow-up
  - Acute/urgent case triage: Identifies critical findings for prioritized review (e.g., pneumoperitoneum on CT).
  - Automated follow-up recommendations: Suggests follow-up studies based on initial findings.

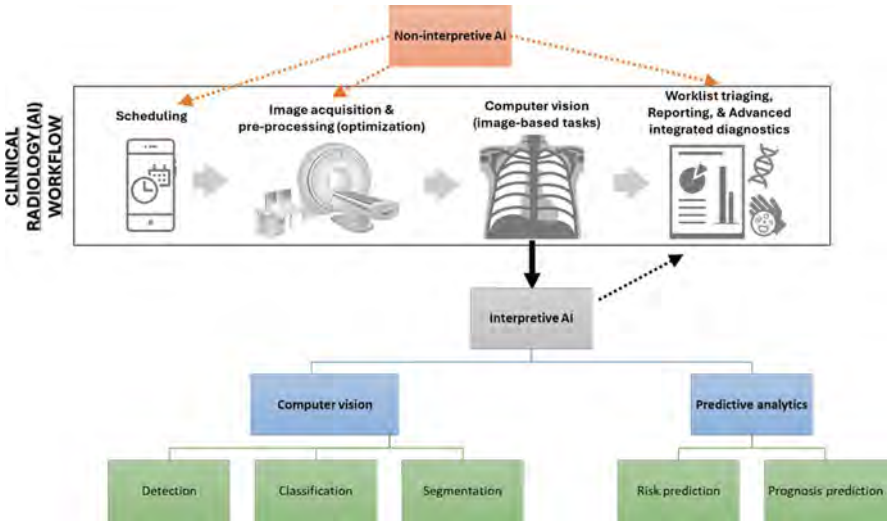

Fig. 11.2 Applications of AI in the clinical radiology workflow, subdivided into both the noninterpretive and interpretive domains

Interpretive AI Applications

- Interpretive AI directly assists in the interpretation of medical images (Fig. 11.3, gray boxes and blue/green subheadings).
- It involves computer vision, a field of AI that trains computers to interpret and understand visual information from digital images.
- Computer vision in radiology
  - Utilizes algorithms to detect, segment, and characterize abnormalities in imaging data (Fig. 11.3).
  - Lesion detection

    AI does well in narrow applications, such as in detecting lesions like polyps on CT colonography.

    These algorithms analyze imaging characteristics on the pixel level.

    Studies often gauge accuracy in comparison to "ground truth" datasets and/or experienced radiologists.
  - Disease classification

    AI tools aid in classifying and staging pathologies into predefined categories such as fatty liver disease, fibrosis, and cirrhosis.

    Some tools are able to analyze texture and density metrics, providing quantitative assessments that support diagnostic decisions.
  - Segmentation

    Delineate structures, such as abdominal organs or lesions on image, which can assist radiologists in rapidly identifying and assessing organs such as the liver, kidneys, and pancreas, or can also one step in more complex multimodality model development.

    Treatment response assessment and recurrence monitoring
    - With specialized instance segmentation, AI can automatically track changes in both images and reports across multiple reports over time.
    - It can help expedite care for example with automatic RECIST measurements in cancer workups.
- Predictive analytics

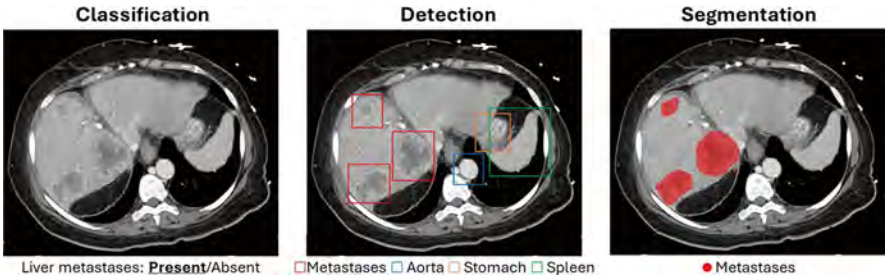

Fig. 11.3 Examples of three main types of interpretive AI, using liver metastases: classification, detection, and segmentation

- Employs statistical models and machine learning techniques to predict outcomes based on imaging findings.
- Outcomes include prognosis, recurrence risk, and therapy response.
- Can use "radiomics," defined as high-throughput extraction of quantitative imaging features that are imperceptible to the human eye.
- Some examples are given below

  Risk prediction
  - Pancreatic cancer risk assessment: Using imaging features from abdominal CT or MRI, AI algorithms can identify subtle changes in the pancreas that may indicate early stages of pancreatic cancer or precancerous lesions, assisting in early detection and intervention.

  Bowel disease activity: In conditions like Crohn's disease and ulcerative colitis, AI models can use features to assist in assessing disease extent, activity, and response to therapy by analyzing bowel wall thickening, contrast enhancement patterns, and other features.
- Prognosis prediction

  Liver disease progression
  - AI models analyze liver imaging from CT or MRI to predict the progression of diseases like cirrhosis or nonalcoholic fatty liver disease (NAFLD).
  - They may assess factors like liver volume, texture, and fat distribution to predict the likelihood of disease advancement or the risk of developing liver-related complications.

  Prostate cancer: Can help in identifying aggressive prostate cancer by analyzing the tumor's shape, edge sharpness, and texture, which can guide biopsy and treatment decisions.

Assessing Abdominal AI Applications

Clinical Evaluation

- When evaluating AI tools for radiological applications, understanding and weighing the statistical metrics of sensitivity, specificity, PPV, and NPV is crucial (Fig. 11.4).
- These metrics provide insight into the tool's diagnostic accuracy and its utility in clinical practice.
- Prevalence
  - How common or frequent something is in a given population.
  - Typically expressed as the proportion or percentage of individuals affected by a condition.
  - In clinically evaluating an AI system, higher prevalence of a condition can increase the number of true positives (TP) and false negatives (FN) and the results of a confusion matrix.

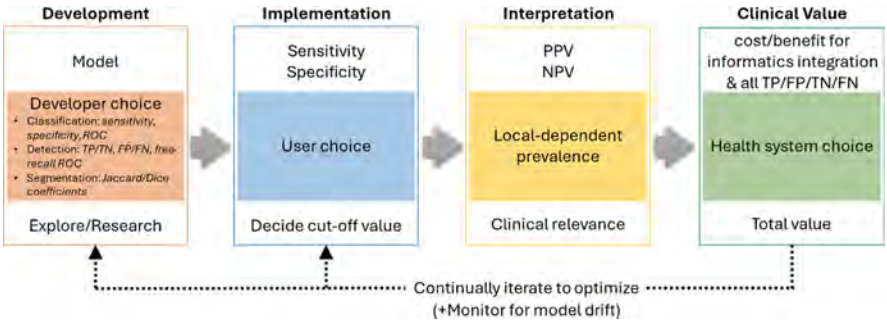

Fig. 11.4 Process diagram explaining clinical evaluation of AI in radiology, and associated relevant statistics for decision-making

  - Therefore, it is important to know local prevalence of the disease in your practice setting, to properly clinically evaluate an AI tool.
  - For example, higher prevalence of liver lesions in the study population can increase the number of true positive lesion detections and false negative missed lesions.
- Sensitivity
  - Measures the tool's ability to correctly identify positive cases (e.g., detecting a tumor).
  - High sensitivity is crucial in situations where missing a pathology could have serious implications, especially in initial screening or in acute conditions where missing a diagnosis could lead to harm.
  - Example: Detecting liver lesions on MRI with a high sensitivity rate.
- Specificity
  - Assesses the tool's ability to correctly identify negative cases.
  - High specificity reduces false positives, important where overdiagnosis can lead to unnecessary interventions (follow-ups or treatments).
  - Example: CT colonography AI showing a high specificity in excluding non-polypoid structures.
- Positive predictive value (PPV)
  - The probability that subjects with a positive screening test truly have the disease.
  - Higher PPV means fewer false positives.
  - In settings where the consequences of false positives are significant (e.g., invasive follow-up procedures), high PPV is desirable.
  - Example: AI used in prostate MRI with a high PPV for detecting clinically significant cancer.
- Negative predictive value (NPV)
  - The probability that subjects with a negative screening test truly do not have the disease.
  - High NPV is crucial in ensuring that diseases are not missed.

  - Example: Pulmonary embolism detection algorithm demonstrating high NPV in ruling out pulmonary embolism.
- Integration with PACS/RIS and medical informatics
  - Workflow compatibility and integration

    A team of IT and clinical radiologists should work together to test a short predefined pilot on local real-time deployment.

    Seamless integration of AI tools with existing Picture Archiving and Communication Systems (PACS) and Radiology Information Systems (RIS) should ensure that AI aids rather than hinders the radiology workflow.
  - Model drift and monitoring

    Continuous monitoring of AI tool performance is necessary to identify and address any model drift, ensuring sustained accuracy over time.
- Balancing these metrics in decision-making, to continually optimize.
  - Local prevalence consideration: As discussed earlier, disease prevalence directly affects predictive value (PPV and NPV).

    In low prevalence conditions, even a test with high sensitivity and specificity can have a low PPV.
  - Context-specific evaluation

    The importance of each metric varies based on clinical context.

    For instance, in cancer screening, high sensitivity (to catch as many true cases as possible) might be prioritized over high specificity.
  - Cost–benefit analysis

    Weigh the cost of false positives (unnecessary treatments, anxiety) against false negatives (missed diagnoses).

    In some cases, the cost of additional confirmatory testing may justify an AI tool with lower specificity but high sensitivity (Fig. 11.5a).

Extra: "Advanced" AI statistical concepts used in AI development, for additional reading (Fig. 11.5b):

- Classification (diagnosis) models
  - Should report both threshold-dependent (i.e., sensitivity, specificity) and threshold-independent metrics (receiver operating characteristic curve, ROC).
  - ROC curve

    The ROC curve plots the true positive rate (how often the tool correctly identifies liver lesions) against the false-positive rate (how often it incorrectly flags healthy tissue as a lesion).

    In abdominal imaging, an ROC curve might be used to evaluate an AI tool designed for detecting liver lesions on CT scans.

    If an AI tool has an AUC close to 1, it is excellent at distinguishing between patients with and without liver lesions.

    An AUC closer to 0.5 might indicate that the tool is no better than random chance at detecting lesions.

    Threshold ("cut off") setting

a

- Sens = Sensitivity
- Spec = Specificity
- Prev = prevalence
- # = total number of cases evaluated

		"Real" Ground truth (depends on local population)		
		Positive (prevalence)	**Negative** (1-prevalence)	**Predictive value**
AI prediction result	**Positive**	**True positive (TP) =** Sens*Prev*#	**False positive (FP) =** (1-Spec)*(1-Prev)*#	**PPV (precision)** TP/(TP+FP)
	Negative	**False negative (FN) =** (1-Sens)*Prev*#	**True negative (TN) =** Spec*(1-Prev)*#	**NPV** TN/(TN+FN)
		Sensitivity (TP/TP+FN)	**Specificity** (TN/TP+FP)	**Accuracy** (TP+TN) / (TP+TN+FP+FN)

b

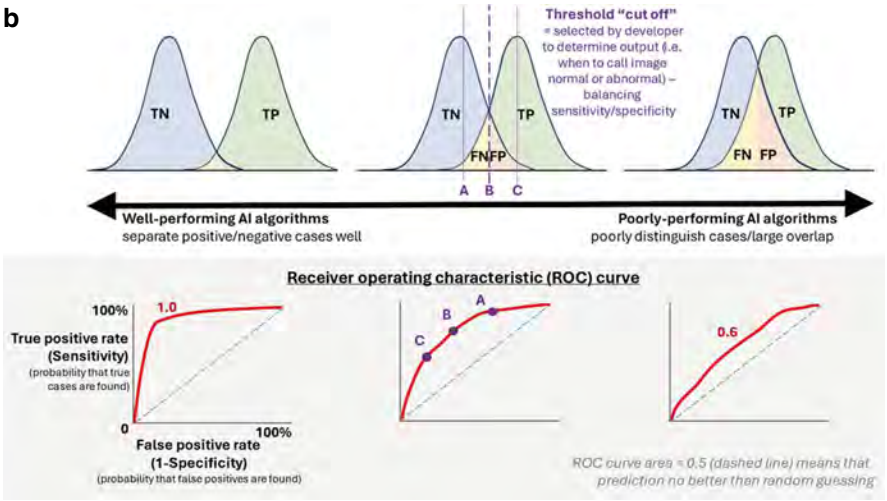

Fig. 11.5 (**a**) A confusion matrix inclusive of the mathematical definitions of sensitivity, specificity, positive predictive value, negative predictive value, and accuracy. (**b**) Distinguishing well-performing AI algorithms from poorly performing AI algorithms, using a receiver operative characteristic (ROC) curve

    - A developer can vary the threshold, which adjusts the AI tool's sensitivity (and specificity) for identifying lesions.
    - A lower threshold might detect more lesions (higher sensitivity) but also increase false positives, while a higher threshold could reduce false positives but miss smaller lesions.
- Detection algorithms
  - Should report both patient-level classification metrics (i.e., true positive and negative, false positive and negative) and also trade-offs between sensitivity and false-positive rate such as with a free-response ROC analysis.
  - Free-response ROC (FROC) analysis

Evaluates detection tasks where there are multiple possible targets per image (e.g., lesions) by plotting the fraction of targets detected against the average number of false alarms per image at multiple decision thresholds.
Provides a more nuanced measure of detection accuracy than regular ROC analysis.
In an abdominal CT scan study evaluating detection of liver lesions, radiologists would set multiple confidence thresholds for calling a lesion present (e.g., 50%, 70%, 90% confidence), then plot the fraction of actual lesions detected (sensitivity) vs. the average number of false-positive lesions marked per scan at each threshold to generate the FROC curve.

- Segmentation algorithms
  - Should report voxel-level metrics such as Jaccard/Dice coefficients and absolute volume differences.
  - Jaccard/Dice coefficients
    These are measures of the similarity between two sample sets.
    Basically, this compares ratio of the size of the datasets' intersection divided by the size of their union, providing a statistic between 0 and 1 indicating the degree of overlap.
    In abdominal imaging, they might be used to compare the segmentation of an organ (like the liver) by an AI tool versus a human expert.
    A high Dice or Jaccard score indicates that the AI tool's segmentation closely matches the expert's segmentation.

Business/Financial Implications

- The integration of AI in abdominal imaging has significant business and financial implications for radiology practices, extending beyond mere revenue generation.
- A comprehensive understanding of these factors is essential to make an informed decision about investing in AI technology purchases.
- Improved patient throughput
  - Streamlining workflow: AI tools can
    Expedite image analysis and radiology reporting.
    Improve patient scheduling and protocol section, to increase the number of patients imaged per day, boosting throughput and revenue.
  - Reducing operational costs: AI-driven improvements in image quality and accuracy can reduce the need for repeat scans from suboptimal imaging, saving time and resources.
  - Enhanced decision support
    AI tools can provide radiologists and referring physicians with more precise, quantitative data, aiding in clinical decision-making and potentially leading to better patient outcomes.
    May also improve referrals when a practice offers state-of-the-art AI-assisted imaging services from clinicians seeking advanced diagnostic support.

- Patient safety and medicolegal risk mitigation
  - Radiation dose optimization: AI algorithms can optimize scan parameters to minimize radiation exposure while maintaining image quality, appealing to patient safety concerns.
  - Contrast dose reduction: AI can assist in achieving diagnostic quality images with lower doses of contrast, reducing the risk of contrast-induced nephropathy and other complications.
  - Medicolegal risk mitigation

    Directly, can reduce errors which enhances patient safety and reduces risk of patient harm.

    Secondarily can potentially lower the risk of litigation due to misdiagnosis or delayed diagnosis.
- New billing opportunities
  - Additional services: AI can enable radiology practices to offer advanced services (e.g., quantitative image analysis such as liver fat quantification, or detailed volumetric analysis), which can represent additional billable services.
  - Reimbursement for AI-assisted procedures: Some AI applications may qualify for additional reimbursement under certain conditions, adding a revenue stream.
- Balancing these factors in decision-making
  - Initial investment vs. long-term savings: The cost of integrating AI tools should be weighed against potential long-term savings from increased efficiency, additional revenue streams, and reduced medicolegal risks.
  - Operational efficiency gains: Efficiency improvements, while hard to quantify monetarily, can lead to significant cost savings over time.

Challenges, Considerations, and Future Directions

- Diversity and bias
  - Training data quality and diversity

    Models should be trained on good-quality, diverse datasets to reduce bias and improve the accuracy and applicability (generalizability) of AI tools across different patient populations.

    Datasets should encompass a wide range of variations, including pathologies and patient demographics.
- Transparency and the "black box"
  - Algorithm transparency: More research is needed to ensure that AI algorithms are transparent and understandable to users, to facilitate trust and effective utilization.
- Ethical and legal aspects
  - Data privacy: Patient confidentiality and compliance with data protection regulations like HIPAA is crucial when implementing AI tools that process patient data.

- Liability (misdiagnoses, etc.): Currently, the legal responsibility in cases of diagnostic errors involving AI tools remains to be determined.
- Sustainability and resource management

  AI (and radiology informatics in general) has a growing environmental impact, including its significant energy consumption and associated greenhouse gas emissions.

  Radiologists should be aware of resource stewardship, including energy source choices and understanding water for cooling data centers, to minimize environmental footprint and promote sustainable practices.

- Future directions
  - Interdisciplinary collaboration to advance AI: Fostering collaboration between radiologists, data scientists, and software engineers to drive innovation and ensure that AI tools meet clinical needs effectively.

    Multiorgan, multimodal algorithms
    - Currently, there are many "narrow" applications of AI that focus on single-task solutions (i.e., such as detecting prostate cancer).
    - Developing and refining sophisticated algorithms for multiorgan evaluation across various imaging modalities (CT, MRI, PET) and data modalities (voice, text, imaging) can streamline complex disease evaluations, such as comprehensive metastatic workups in cancer patients.

    Personalized medicine: AI can be leveraged to tailor diagnostics and treatment plans to individual patient characteristics and disease profiles.

    Generative AI and large language models (LLMs): Many innovative applications in diagnostic imaging are being actively explored, including report generation, patient education, and population data analysis.
  - Governance

    There are ongoing efforts throughout various practice settings, to establish robust governance structures to oversee the deployment and use of AI in radiology.

    This includes creating policies for ethical AI use, auditing AI systems for fairness and accuracy, and ensuring that AI applications adhere to regulatory and professional standards.

Conclusion

As algorithms continue to mature, abdominal imagers must develop an understanding of AI principles to guide appropriate integration into clinical practice. Collaboration between community participants, physicians, and computer scientists is critical to ensure that AI systems align with the values of patients, radiologists, and referring physicians.

Further Readings

1. Hosny A, Parmar C, Quackenbush J, Schwartz LH, Aerts HJWL. Artificial intelligence in radiology. Nat Rev Cancer. 2018;18:500–10. https://doi.org/10.1038/s41568-018-0016-5.
2. Rubin DL. Artificial intelligence in imaging: the radiologist's role. J Am Coll Radiol. 2019;16:1309–17. https://doi.org/10.1016/j.jacr.2019.05.036.
3. Perchik JD, Rothenberg SA, Tridandapani S, Perchik LM, Smith AD. Artificial intelligence in body imaging: an overview of commercially available tools. Semin Roentgenol. 2023;58:196–202. https://doi.org/10.1053/j.ro.2023.02.007.
4. Hadjiiski L, Cha K, Chan H-P, Drukker K, Morra L, Näppi JJ, et al. AAPM task group report 273: Recommendations on best practices for AI and machine learning for computer-aided diagnosis in medical imaging. Med Phys. 2023;50:e1–24. https://doi.org/10.1002/mp.16188.
5. Oka A, Ishimura N, Ishihara S. A new dawn for the use of artificial intelligence in gastroenterology, hepatology and pancreatology. Diagnostics. 2021;11:1719. https://doi.org/10.3390/diagnostics11091719.
6. Gandhi D, Garg T, Patel L, Elkassem AA, Bansal V, Smith A. Artificial intelligence in gastrointestinal and hepatic imaging: past, present and future scopes. Clin Imaging. 2022;87:43–53. https://doi.org/10.1016/j.clinimag.2022.04.007.
7. Baydoun A, Jia AY, Zaorsky NG, Kashani R, Rao S, Shoag JE, et al. Artificial intelligence applications in prostate cancer. Prostate Cancer Prostatic Dis. 2023:1–9. https://doi.org/10.1038/s41391-023-00684-0.
8. Park SH, Han K, Jang HY, Park JE, Lee J-G, Kim DW, et al. Methods for clinical evaluation of artificial intelligence algorithms for medical diagnosis. Radiology. 2023;306:20–31. https://doi.org/10.1148/radiol.220182.
9. Cheng PM, Montagnon E, Yamashita R, Pan I, Cadrin-Chênevert A, Perdigón Romero F, Chartrand G, Kadoury S, Tang A. Deep learning: an update for radiologists. Radiographics. 2021;41(5):1427–45. https://doi.org/10.1148/rg.2021200210.
10. Omoumi P, Ducarouge A, Tournier A, Harvey H, Kahn CE, Louvet-de Verchère F, et al. To buy or not to buy—evaluating commercial AI solutions in radiology (the ECLAIR guidelines). Eur Radiol. 2021;31:3786–96. https://doi.org/10.1007/s00330-020-07684-x.
11. Doo FX, Vosshenrich J, Cook TS, Moy L, Almeida EP, Woolen SA, et al. Environmental sustainability and artificial intelligence in radiology: a double-edged sword. Radiology. 2024;310:e232030.

Index

A
Abdominal imaging
  American College of Radiology, 32
  central tenants, 31, 32
  computed tomography, 22, 28, 29
  fluoroscopy, 12, 14, 16
  magnetic resonance imaging, 29, 31
  plain films, 1–6
  templated reporting, 32, 33
  ultrasound, 18, 20, 21
Acinar cell carcinoma, 113
Acute cholecystitis, 79–82
Acute pyelonephritis, 180, 181
Adenocarcinoma, 287
Adenoma, 71, 72, 285
Adenomyomatosis, 82, 83
Adrenal adenoma, 155–159
Adrenal calcifications, 149, 150
Adrenal cortical carcinoma, 164–166
Adrenal cyst, 153–155
Adrenal gland, 48
Adrenal hemorrhage, 150–153
Adrenal hyperplasia, 148–150
Adrenal imaging
  anatomy, 145, 146
  benign adrenal lesions
    adrenal calcifications, 149, 150
    adrenal cyst, 153–155
    adrenal hemorrhage, 150–153
    adrenal hyperplasia, 148–150
  mass
    adenoma, 155–159
    cortical carcinoma, 164–166
    malignant, 163
    metastasis, 163, 164
    myelolipomas, 159–161
    pheochromocytomas, 160, 162, 163
  optimal imaging
    computed tomography, 146
    magnetic resonance imaging, 147, 148
    positron emission tomography, 148
    ultrasonography, 146, 147
Adrenal metastasis, 163, 164
Adrenal myelolipomas, 159–161
Amiodarone toxicity, 76
Amyand hernia, 305
Anal cancers, 341–344
Angiomyolipomas, 187, 188
Appendiceal lymphomas, 314, 315
Appendiceal tumors, 311–316
Appendicitis, 306–310
Appendix
  acute appendicitis, 306–310
  amyand hernia, 305
  appendiceal tumors, 311–316
  locations, 305
  McBurney's point, 305
  optimal imaging, 299–306
  pseudomyxoma peritonei, 316, 317
  spinoumbilical line, 305
Artificial intelligence (AI)
  business/financial implications, 356, 357
  challenges, considerations, and future directions, 357, 358
  clinical evaluation
    classification, 354, 355
    decision-making, 354, 355
    detection algorithms, 355, 356
    NPV, 353
    PACS/RIS and medical informatics, 354
    PPV, 353
    prevalence, 352, 353
    process diagram, 352, 353

© The Editor(s) (if applicable) and The Author(s), under exclusive license to Springer Nature Switzerland AG 2024

T. Catanzano (ed.), *What Radiology Residents Need to Know: Abdominal Radiology*, What Radiology Residents Need to Know,
https://doi.org/10.1007/978-3-031-76624-4

Artificial intelligence (AI) (*cont.*)
segmentation algorithms, 356
sensitivity, 353
specificity, 353
definition, 347
high-level overview, 348
interpretive domain
computer vision, 351
predictive analytics, 352
types, 351
non-interpretive domain, 350
Asplenia, 127, 128
Atherosclerotic vascular disease, 327
Autoencoders, 349
Autoimmune pancreatitis, 101

B
Barium enema, 41
Biliary system, 63, 64
Black box, 357
Bladder, 43, 51
anatomy, 170
cancer, 203–205
chronic bladder outlet obstruction, 202, 203
infection, 202
rupture, 206
ureterocele, 205
Bones, 53, 55
Bowel disease activity, 352
Bowel injury, 290–292
Business/financial implications, 356, 357

C
Carcinoid syndrome, 288
Cecal volvulus, 330
Celiac disease, 263
Cholangiocarcinoma (CCA), 73–76
Cholangitis, 85
Cholelithiasis, 78–80
Chronic bladder outlet obstruction, 202, 203
Chronic cholecystitis, 82
Cirrhosis, 77
Colon, 41
acute colitis, 318, 319
anatomy, 318
ascending, 318
descending, 318
IBD
Crohn's disease, 320, 322
diverticulitis, 322, 324–326
epiploic appendagitis, 326, 327
stercoral colitis, 320, 323
ulcerative colitis, 320, 323
infectious colitis, 319–321
ischemia, 327–329
neoplasm, 332–344
obstruction, 330–332
optimal imaging, 299–306
pathologies, 322
trauma and perforation, 329
Colonic lymphoma, 340, 341
Colonic volvulus, 330
Common bile duct (CBD), 63
Computer vision, 351
Congenital adrenal hyperplasia (CAH), 148
Context-specific evaluation, 354
Convolutional neural networks (CNNs), 349
Cost-benefit analysis, 354
Crohn's disease (CD), 320, 322

D
Data privacy, 357
Deep learning, 349
Detection algorithms, 355, 356
Diffuse liver disease
amiodarone toxicity, 76
cirrhosis, 77
iron overload, 77
liver transplant appearance, 77
pseudocirrhosis, 77
steatosis, 74, 76
Dromedary hump, 173
Duodenum, 254
Duodenum/small bowel, 40

E
Embolic disease, 142, 143
Emphysematous gastritis, 228–230
Emphysematous pyelitis, 182, 183
Emphysematous pyelonephritis, 181, 182
Enteric tube, 220, 221
Epiploic appendagitis, 326, 327
Esophagus, 38
Ethical and legal aspects, 357

F
Focal liver lesions
diffuse liver disease
amiodarone toxicity, 76
cirrhosis, 77
iron overload, 77
liver transplant appearance, 77
pseudocirrhosis, 77
steatosis, 74, 76

hepatic cysts, 68
solid liver masses
adenoma, 71, 72
CCA, 73–76
FNH, 69–71
HCC, 72–74
hemangiomas, 68, 69
metastatic disease, 72, 73
Focal nodular hyperplasia (FNH), 69–71
Foreign body perforation, 268, 269
Free-response ROC (FROC) analysis, 355, 356

G
Gallbladder, 42, 48, 64
acute cholecystitis, 79–82
adenomyomatosis, 82, 83
anatomy, 77
cancer, 83, 84
cholangiocarcinoma, 85
cholangiopathy, 84, 85
cholangitis, 85
cholecystectomy, 85, 86
cholelithiasis, 78–80
chronic cholecystitis, 82
gangrenous cholecystitis, 82, 83
PSC, 85
Gangrenous cholecystitis, 82, 83
Gastric disorders
anatomy, 217
benign gastric masses, 248
catheter positioning, 217
emphysematous gastritis, 228–230
enteric tube, 220, 221
gastric diverticula, 228
gastrojejunostomy tube, 225
gastrostomy tube, 223, 225
infiltrative diseases, 247, 248
malignant gastric masses, 249, 250, 252
surgery
bands, 241, 242
Roux en Y bypass, 242, 244
sleeve gastrectomy, 246, 247
trauma, 230, 232, 233, 235
ulcer disease, 237–240
volvulus, 235, 237
Gastric diverticula, 228
Gastric trauma, 230, 232, 233, 235
Gastric volvulus, 235, 237
Gastrointestinal bleeding, 270, 271
Gastrointestinal stromal tumor (GIST), 289
Gastrojejunostomy tube, 225
Gastrostomy tube, 223, 225
Generative adversarial networks (GANs), 349
Genitourinary diseases, *see* Kidneys
Governance, 358
Graft versus host disease (GVHD), 268

H
Hamartoma, 285
Hemangiomas, 68, 69
Hepatic cysts, 68
Hepatobiliary imaging
assessment, 64–66
biliary system, 63, 64
blood supply, 61, 62
diffuse liver disease, 74, 76–78
focal liver lesions (*see* Focal liver lesions)
gallbladder, 64
acute cholecystitis, 79–82
adenomyomatosis, 82, 83
anatomy, 77
cancer, 83, 84
cholangiocarcinoma, 85
cholangiopathy, 84
cholangitis, 85
cholecystectomy, 85, 86
choledocholithiasis, 84, 85
cholelithiasis, 78–80
chronic cholecystitis, 82
gangrenous cholecystitis, 82, 83
PSC, 85
liver, 61, 62
images, 65–68
lobes, 62, 63
segments, 63
Hepatobiliary iminodiacetic acid (HIDA), 65
Hepatocellular carcinoma (HCC), 72–74
Hydronephrosis, 194, 195
Hydroureteronephrosis, 194, 195
Hypertrophied column of Bertin, 172

I
Ileum, 254
Image acquisition, 350
Infiltrative disease, 131
Inflammatory bowel disease (IBD)
colon
Crohn's disease, 320, 322
diverticulitis, 322, 324–326
epiploic appendagitis, 326, 327
stercoral colitis, 320, 323
ulcerative colitis, 320, 323
complications, 274, 275, 277
Crohn's disease, 271
imaging assessment, 271, 272
imaging features, 272, 274

Intraductal papillary mucinous tumor (IPMT), 108, 110
Intravenous pyelography (IVP), 174
Iron overload, 77
Ischemia, 293, 295
Ischemic colitis, 327–329

J
Jaccard/Dice coefficients, 356
Jejunum, 254

K
Kidneys, 42, 48, 54
  anatomy, 169, 170
  benign renal neoplasms
    angiomyolipomas, 187, 188
    cysts, 185–187
    oncocytomas, 189, 190
  congenital abnormalities, 172–174
  malignant renal neoplasms, 190–193
  obstruction/renal enlargements
    hydronephrosis/hydroureteronephrosis, 194, 195
    medullary nephrocalcinosis, 199
    renal vein thrombosis, 196
    stone disease, 198, 199
  renal infarction, 178
  renal papillary necrosis, 179
  renal parenchyma
    abscess, 179, 180
    acute pyelonephritis, 180, 181
    emphysematous pyelitis, 182, 183
    emphysematous pyelonephritis, 181, 182
    pyonephrosis, 184, 185
    xanthogranulomatous pyelonephritis, 183, 184
  renal trauma, 175, 176

L
Large bowel obstructions (LBO), 330–332
Large language models (LLMs), 349, 358
Lesion detection, 351
Liability, 358
Lipoma, 286
Littoral cell angioma, 137
Liver, 42, 46, 54, 61, 62
Liver disease progression, 352
Lungs, 54
Lymphangioma, 134
Lymph nodes, 53
Lymphoma, 288

M
Machine learning (ML), 348, 349
Medullary nephrocalcinosis, 199
Mesenteric bleeding, 292–293
Mesenteric ischemia, 254, 295
Metastatic disease, 289
Monkeypox proctitis, 319
Mucinous cystic neoplasm, 105
Mucinous epithelial tumors, 311–313
Mucosa-assisted lymphoid tissue (MALT), 289
Multi-modal algorithms, 358
Multi-organ evaluation, 358

N
Natural language processing (NLP), 349
Negative predictive value (NPV), 353
Neuroendocrine, 287
Neuroendocrine tumors (NET), 114, 163, 258, 284, 288, 311, 314, 316
  appendix, 314, 316
Nonmucinous (colonic-type) adenocarcinoma, 312, 314
Nonocclusive mesenteric ischemia (NOMI), 328
Nuclear medicine, 64–66

O
Obstruction/renal enlargements
  hydronephrosis/hydroureteronephrosis, 194, 195
  medullary nephrocalcinosis, 199
  renal vein thrombosis, 196
  stone disease, 198, 199
Ogilvie syndrome, 332
Oncocytomas, 189, 190

P
Pancreas, 42
  acute pancreatitis, 94–99
  anatomy/function, 87
  autoimmune pancreatitis, 101
  chronic pancreatitis, 100, 101
  cystic pancreatic lesions
    IPMT, 108, 110
    mucinous cystic neoplasm, 105
    psuedocyst, 102
    serous cystadenoma, 105
    solid pseudopapillary tumor, 107
  imaging modalities, 87, 89–94
  solid pancreatic epithelial neoplasms, 110, 112, 114, 115

Pancreatic ductal adenocarcinoma, 110, 112, 114, 115
Pancreatic neuroendocrine tumors, 114, 115
Patient safety, 357
Patient scheduling, 350
Peritoneal cancer index (PCI), 317
Peritoneum, 51
Persistent fetal lobulation, 172
Personalized medicine, 358
Pheochromocytomas, 160, 162, 163
Polysplenia, 126, 127
Portal hypertension, 141–143
Positive predictive value (PPV), 353
Post-transplant lymphoproliferative disease (PTLD), 289
Predictive Analytics, 351, 352
Primary sclerosing cholangitis (PSC), 85
Prostate cancer, 352
Pseudocirrhosis, 77
Pseudomembranous colitis, 320
Pseudomyxoma peritonei, 316, 317
Pyonephrosis, 184, 185

Q
Quality improvement/quality control (QI/QC), 36, 41, 46

R
Radiomics, 352
Receiver operative characteristic (ROC) curve, 355
Rectal cancers, 338–340
Recurrent neural networks (RNNs), 349
Reinforcement learning, 348
Renal abscess, 179, 180
Renal cell carcinoma, 190–193
Renal cysts, 185–187
Renal infarction, 178
Renal papillary necrosis, 179
Renal parenchyma
  abscess, 179, 180
  acute pyelonephritis, 180, 181
  emphysematous pyelitis, 182, 183
  emphysematous pyelonephritis, 181, 182
  pyonephrosis, 184, 185
  xanthogranulomatous pyelonephritis, 183, 184
Renal trauma, 175, 176
Renal vein thrombosis, 196
Resource management, 358
Risk mitigation, 357
Risk prediction, 352
Roux en Y bypass, 242, 244

S
Scleroderma/systemic sclerosis, 262, 263
Sclerosing angiomatoid nodular transformation of the spleen (SANT), 138
Search patterns
  abdominal plain film, 36, 37
  CT, 46, 48, 50, 51, 53
  fluoroscopy, 38, 41
  MRI, 54, 57–59
  ultrasound, 41–43
Segmentation algorithms, 356
Semi-supervised learning, 348
Sigmoid volvulus, 331
Small bowel
  infection
    celiac disease, 263
    diverticulitis, 269
    foreign body perforation, 268, 269
    gastrointestinal bleeding, 270, 271
    GVHD, 268
    imaging features, 260, 261
    infectious enteritis, 261, 262
    medication-induced angioedema, 266
    portal enteropathy, 264, 266
    radiation enteritis, 263, 264
    scleroderma/systemic sclerosis, 262, 263
    vasculitis, 267
  inflammatory bowel disease, 271, 273–277
  ischemia, 293, 295
  obstruction, 277, 279, 280, 282
  optimal imaging, 254, 255, 258
  overview, 253, 254
  trauma, 290, 292
  tumors
    benign small bowel masses, 285–287
    diagnostic features, 284
    malignant small bowel masses, 287–290
Small bowel diverticulitis, 269
Small bowel obstruction (SBO)
  complication, 280, 282
  imaging features, 277, 279
  overview, 277
Solid liver masses
  adenoma, 71, 72
  CCA, 73–76
  FNH, 69–71
  HCC, 72–74
  hemangiomas, 68, 69
  metastatic disease, 72, 73
Solid pancreatic epithelial neoplasms, 110, 112, 114, 115
Solid pseudopapillary tumor, 107

Spleen, 42, 50, 54
anatomy, 118
congenital finding
accessory spleen or splenule, 123, 124
asplenia, 127, 128
cleft, 124, 126
polysplenia, 126, 127
infiltrative disease, 131
masses, 132, 133
cysts, 133
hamartoma, 137
hemangiomas, 136
infectious cysts and abscesses, 135
inflammatory/infectious nodules, 138
littoral cell angioma, 137
lymphangioma, 134
malignant, 139
pseudocysts, 134
SANT, 138
solid, 135
normal imaging appearance, 119, 121
optimal imaging modalities, 117, 118
portal hypertension, 141–143
trauma, 128–131
Steatosis, 74, 76
Stercoral colitis, 320, 323
Stomach, 38
Stone disease, 198, 199
Supervised Learning, 348
Sustainability, 358

T
Testicular adrenal rest tumors (TART), 149
Training data quality and diversity, 357
Transfer learning, 349
Transparency, 357
Trauma, 128–131

U
Ulcerative colitis (UC), 320, 323
Ulcer disease, 237–240
Unsupervised Learning, 348
Ureters, 170, 200
imaging, 200, 201
Urethra
anatomy, 171
diverticulum, 209, 210
infection, 210, 211
trauma, 207, 208
Urethral diverticulum, 209, 210
Urethral trauma, 207, 208
Urolithiasis, 198

V
Vascular disease, 142, 143
Vasculature, 43
Vessels, 53
Villous adenomas, 333–335

W
Workflow and operational efficiency, 350
Worrisome cysts, 68

X
Xanthogranulomatous pyelonephritis, 183, 184